

# The impact of food processing on physicochemical and nutritional properties of foods

**Edited by**

Hao Jiang, Shaojin Wang, Baoguo Xu and  
Yuanyuan Shan

**Published in**

Frontiers in Nutrition



## FRONTIERS EBOOK COPYRIGHT STATEMENT

The copyright in the text of individual articles in this ebook is the property of their respective authors or their respective institutions or funders. The copyright in graphics and images within each article may be subject to copyright of other parties. In both cases this is subject to a license granted to Frontiers.

The compilation of articles constituting this ebook is the property of Frontiers.

Each article within this ebook, and the ebook itself, are published under the most recent version of the Creative Commons CC-BY licence. The version current at the date of publication of this ebook is CC-BY 4.0. If the CC-BY licence is updated, the licence granted by Frontiers is automatically updated to the new version.

When exercising any right under the CC-BY licence, Frontiers must be attributed as the original publisher of the article or ebook, as applicable.

Authors have the responsibility of ensuring that any graphics or other materials which are the property of others may be included in the CC-BY licence, but this should be checked before relying on the CC-BY licence to reproduce those materials. Any copyright notices relating to those materials must be complied with.

Copyright and source acknowledgement notices may not be removed and must be displayed in any copy, derivative work or partial copy which includes the elements in question.

All copyright, and all rights therein, are protected by national and international copyright laws. The above represents a summary only. For further information please read Frontiers' Conditions for Website Use and Copyright Statement, and the applicable CC-BY licence.

ISSN 1664-8714  
ISBN 978-2-8325-2451-0  
DOI 10.3389/978-2-8325-2451-0

## About Frontiers

Frontiers is more than just an open access publisher of scholarly articles: it is a pioneering approach to the world of academia, radically improving the way scholarly research is managed. The grand vision of Frontiers is a world where all people have an equal opportunity to seek, share and generate knowledge. Frontiers provides immediate and permanent online open access to all its publications, but this alone is not enough to realize our grand goals.

## Frontiers journal series

The Frontiers journal series is a multi-tier and interdisciplinary set of open-access, online journals, promising a paradigm shift from the current review, selection and dissemination processes in academic publishing. All Frontiers journals are driven by researchers for researchers; therefore, they constitute a service to the scholarly community. At the same time, the *Frontiers journal series* operates on a revolutionary invention, the tiered publishing system, initially addressing specific communities of scholars, and gradually climbing up to broader public understanding, thus serving the interests of the lay society, too.

## Dedication to quality

Each Frontiers article is a landmark of the highest quality, thanks to genuinely collaborative interactions between authors and review editors, who include some of the world's best academicians. Research must be certified by peers before entering a stream of knowledge that may eventually reach the public - and shape society; therefore, Frontiers only applies the most rigorous and unbiased reviews. Frontiers revolutionizes research publishing by freely delivering the most outstanding research, evaluated with no bias from both the academic and social point of view. By applying the most advanced information technologies, Frontiers is catapulting scholarly publishing into a new generation.

## What are Frontiers Research Topics?

Frontiers Research Topics are very popular trademarks of the *Frontiers journals series*: they are collections of at least ten articles, all centered on a particular subject. With their unique mix of varied contributions from Original Research to Review Articles, Frontiers Research Topics unify the most influential researchers, the latest key findings and historical advances in a hot research area.

Find out more on how to host your own Frontiers Research Topic or contribute to one as an author by contacting the Frontiers editorial office: [frontiersin.org/about/contact](https://frontiersin.org/about/contact)



# The impact of food processing on physicochemical and nutritional properties of foods

## Topic editors

Hao Jiang — Northwest A&F University, China

Shaojin Wang — Northwest A&F University, Yangling, China

Baoguo Xu — Jiangsu University, China

Yuanyuan Shan — Northwest A&F University, China

## Citation

Jiang, H., Wang, S., Xu, B., Shan, Y., eds. (2023). *The impact of food processing on physicochemical and nutritional properties of foods*. Lausanne: Frontiers Media SA.  
doi: 10.3389/978-2-8325-2451-0

## Table of contents

- 05 **Effects of different proteins and maltodextrin combinations as wall material on the characteristics of *Cornus officinalis* flavonoids microcapsules**  
Mengyue Zhao, Weiwei Cao, Linlin Li, Aiqing Ren, Yuan Ang, Junliang Chen, Bhesh Bhandari, Zhe Wang, Xing Ren, Guangyue Ren and Xu Duan
- 16 **Flavor properties of Chinese noodles processed by dielectric drying**  
Qian Lin, Aiqing Ren, Rui Liu, Yanan Xing, Xiuzhu Yu and Hao Jiang
- 30 **Ozone treatment promotes physicochemical properties and antioxidant capacity of fresh-cut red pitaya based on phenolic metabolism**  
Chen Li, Shan Wang, Jiayi Wang, Zhaohui Wu, Yaping Xu and Zhaoxia Wu
- 44 **Investigating on the influence mechanism of sausage of sea bass on calcium absorption and transport based on Caco-2 cell monolayer model**  
Zhongqiang Wang, Ranzhuo Ma, Zhihui Jia, Peng Lin, Zhenhua Zhao, Wei Wang, Shumin Yi, Xuepeng Li and Jianrong Li
- 62 **Effects of spray drying, freeze drying, and vacuum drying on physicochemical and nutritional properties of protein peptide powder from salted duck egg white**  
Tianyin Du, Jicheng Xu, Shengnan Zhu, Xinjun Yao, Jun Guo and Weiqiao Lv
- 72 **Effects of different cooking methods on volatile flavor compounds, nutritional constituents, and antioxidant activities of *Clitocybe squamulosa***  
Hui Yuan, Lijing Xu, Mingchang Chang, Junlong Meng, Cuiping Feng, Xueran Geng, Yanfen Cheng and Zongqi Liu
- 86 **Reduction of oil uptake in vacuum fried *Pleurotus eryngii* chips via ultrasound assisted pretreatment**  
Aiqing Ren, Zhenzhen Cao, Xiaoxian Tang, Zhenhua Duan, Xu Duan and Xiangyong Meng
- 98 **Corner coil heating mode improves the matrix uniformity of cooked rice in an induction heating cooker**  
Jinxi Kong, Jinxuan Tao, Shanlin Fu, Ya Wen, Siming Zhao and Binjia Zhang
- 108 **Physicochemical properties and gel-forming ability changes of duck myofibrillar protein induced by hydroxyl radical oxidizing systems**  
Xueshen Zhu, Xiandong Shi, Shaohua Liu, Ying Gu, Junya Liu, Qingquan Fu and Renlei Wang
- 120 **Combining e-nose and e-tongue for improved recognition of instant starch noodles seasonings**  
Rong Ma, Huishan Shen, Hao Cheng, Guoquan Zhang and Jianmei Zheng

- 130 **Storage stability of texture, organoleptic, and biological properties of goat milk yogurt fermented with probiotic bacteria**  
Yaling Yang, Ruyue Zhang, Fuxin Zhang, Bini Wang and Yufang Liu
- 144 **Analysis of sucrose addition on the physicochemical properties of blueberry wine in the main fermentation**  
Junbo Liu, Qian Wang, Liping Weng, Ligen Zou, Huiyan Jiang, Jing Qiu and Jiafei Fu
- 152 **High gelatinous salted duck egg white protein powder gel: Physicochemical, microstructure and techno-functional properties**  
Xinjun Yao, Jicheng Xu, Yu Xun, Tianyin Du, Mengqi Huang and Jun Guo
- 160 **Drying sea buckthorn berries (*Hippophae rhamnoides* L.): Effects of different drying methods on drying kinetics, physicochemical properties, and microstructure**  
Zhihua Geng, Lichun Zhu, Jun Wang, Xianlong Yu, Mengqing Li, Wenxin Yang, Bin Hu, Qian Zhang and Xuhai Yang
- 171 **Effect of sodium bicarbonate on the physicochemical properties of fermented rice flour and quality characteristics of fermented semi-dried rice noodles**  
Wen Xiao, Yuqin Ding, Ying Cheng, Sili Xu and Lizhong Lin
- 183 **Enzyme inactivation induced by thermal stabilization in highland barley and impact on lipid oxidation and aroma profiles**  
Qianna Zheng, Zheng Wang, Feiyang Xiong and Guoquan Zhang



## OPEN ACCESS

## EDITED BY

Hao Jiang,  
Northwest A&F University, China

## REVIEWED BY

Yuntao Liu,  
Sichuan Agricultural University, China  
Weiqiao Lv,  
China Agricultural University, China  
Haizhen Mo,  
Henan Institute of Science and  
Technology, China  
Wenhao Li,  
Northwest A&F University, China

## \*CORRESPONDENCE

Weiwei Cao  
caoweiwei@haust.edu.cn  
Aiqing Ren  
renaiqing@126.com  
Xu Duan  
duanxu\_dx@163.com

## SPECIALTY SECTION

This article was submitted to  
Nutrition and Food Science  
Technology,  
a section of the journal  
Frontiers in Nutrition

RECEIVED 31 July 2022

ACCEPTED 23 August 2022

PUBLISHED 14 September 2022

## CITATION

Zhao M, Cao W, Li L, Ren A, Ang Y,  
Chen J, Bhandari B, Wang Z, Ren X,  
Ren G and Duan X (2022) Effects of  
different proteins and maltodextrin  
combinations as wall material on the  
characteristics of *Cornus officinalis*  
flavonoids microcapsules.  
*Front. Nutr.* 9:1007863.  
doi: 10.3389/fnut.2022.1007863

## COPYRIGHT

© 2022 Zhao, Cao, Li, Ren, Ang, Chen,  
Bhandari, Wang, Ren, Ren and Duan.  
This is an open-access article  
distributed under the terms of the  
Creative Commons Attribution License  
(CC BY). The use, distribution or  
reproduction in other forums is  
permitted, provided the original  
author(s) and the copyright owner(s)  
are credited and that the original  
publication in this journal is cited, in  
accordance with accepted academic  
practice. No use, distribution or  
reproduction is permitted which does  
not comply with these terms.

# Effects of different proteins and maltodextrin combinations as wall material on the characteristics of *Cornus officinalis* flavonoids microcapsules

Mengyue Zhao<sup>1</sup>, Weiwei Cao<sup>1\*</sup>, Linlin Li<sup>1</sup>, Aiqing Ren<sup>2\*</sup>,  
Yuan Ang<sup>1</sup>, Junliang Chen<sup>1</sup>, Bhesh Bhandari<sup>3</sup>, Zhe Wang<sup>1</sup>,  
Xing Ren<sup>1</sup>, Guangyue Ren<sup>1</sup> and Xu Duan<sup>1\*</sup>

<sup>1</sup>Department of Food Sciences and Engineering, College of Food and Bioengineering, Henan University of Science and Technology, Luoyang, China, <sup>2</sup>Department of Food Science, Institute of Food Research, Hezhou University, Hezhou, China, <sup>3</sup>Department of ARC Dairy Innovation Hub, School of Agriculture and Food Sciences, The University of Queensland, Brisbane, QLD, Australia

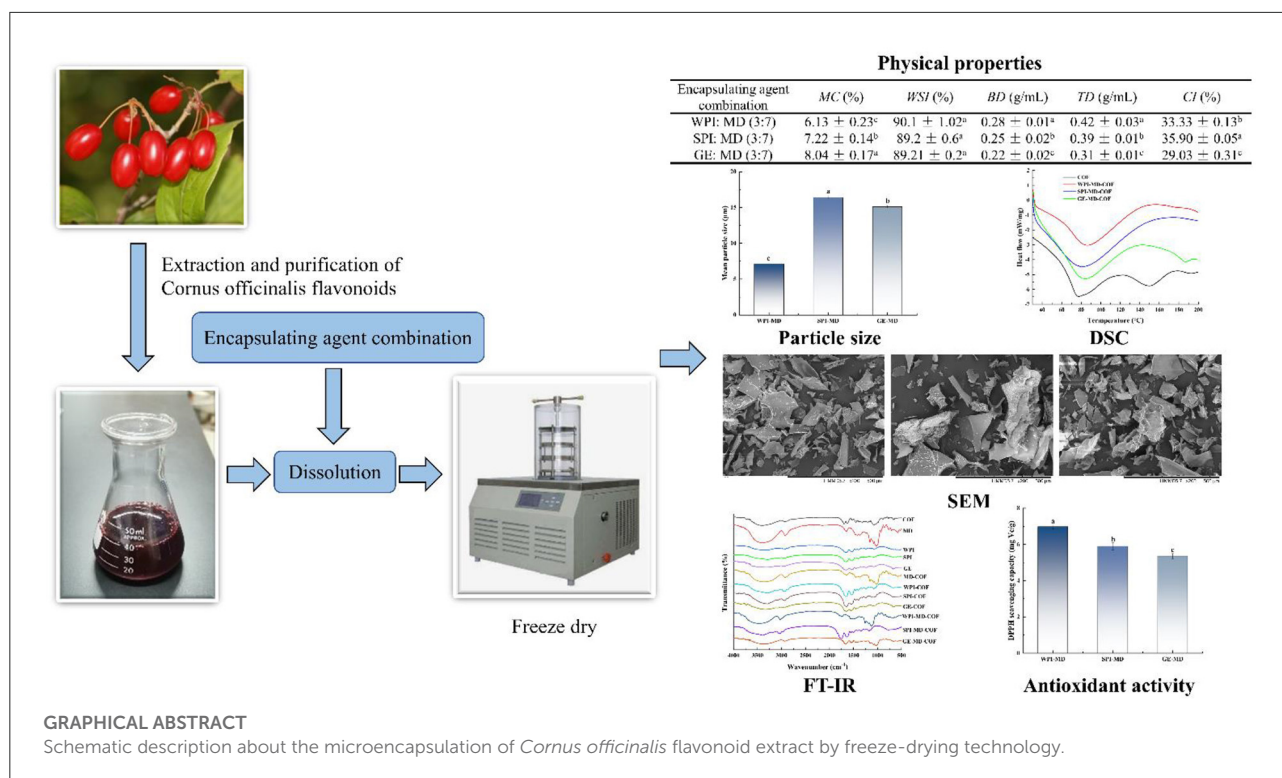
The flavonoids in *Cornus officinalis* (CO) have various pharmacological activities, however, the flavonoid instability limits its application in food and pharmaceutical industries. In this study, *Cornus officinalis* flavonoid (COF) microcapsules were prepared by using a combination of whey isolate protein (WPI), soy isolate protein (SPI), gelatin (GE), and maltodextrin (MD) as wall materials, respectively. Meanwhile, the encapsulation efficiency, solubility, color, particle size, thermal stability and microstructure as well as the antioxidant capacity of microcapsules were assessed. When the protein/MD ratio was 3:7, three kinds of combined wall materials realized high encapsulation efficiency (96.32–98.24%) and water solubility index (89.20–90.10%). Compared with other wall material combinations, the microcapsules with WPI-MD wall ratio at 3:7 had lower particle size (7.17 μm), lower moisture content (6.13%), higher encapsulation efficiency (98.24%), better water solubility index (90.1%), higher thermal stability (86.00°C), brightness L\* (67.84) and higher 1,1-diphenyl-2-picrylhydrazyl (DPPH) scavenging capacity (6.98 mgVc/g), and better flowability. Results suggested that WPI and MD could be better wall materials applied in encapsulating COF.

## KEYWORDS

*Cornus officinalis* flavonoids, microcapsules, protein, maltodextrin, quality

## Introduction

*Cornus officinalis* (CO) is known as the genus *Cornus* L, belonging to the Cornaceae family, which is a kind of traditional Chinese medicine and food homology (1). CO is mainly distributed in China, South Korea, and Japan (2). CO tastes sour and astringent, and is often used to improve liver and kidney function. Many studies have shown that CO is rich in flavonoids, pentacyclic triterpenoids, iridoid glycosides, and other



compounds, which is often used for nourishing the liver and kidneys (3). Flavonoids are the second main components of CO (221.3 mg/10 g) (4), which can be divided into quercetin, kaempferol, rutin, and naringin according to their structure types. Modern pharmaceutical studies have proved that flavonoids have various biological activities such as antioxidant (5), antibacterial (1), hypoglycemic (6), and antiatherosclerosis (7) activities. However, flavonoids are sensitive to light, heat, and food processing conditions, so the application of *Cornus officinalis* flavonoids (COF) in food industry is limited (8). Simulated human gastrointestinal digestion studies demonstrated COF has poor stability in the gastrointestinal tract and is easily degraded. Intestinal digestion resulted in a substantial decrease in the content and antioxidant activity of the fruit extracts, which limits its physiological activity *in vivo* (9). Therefore, it is crucial to protect COF from unfavorable conditions.

Microencapsulation is a common technology to encapsulate bioactive compounds into microcapsules or nanoparticles, which can prevent the encapsulated substance from contacting external environment, effectively protect biological activity, improve storage stability, and conceal the bitter taste (10). Various studies on the methods of encapsulating bioactive compounds have been studied, including spray drying (SD), spray freeze drying, freeze drying (FD), complex coalescence, and electrospraying (11). Among them, FD could make microcapsules dried by sublimation under high vacuum conditions and lower temperature. FD is deemed a suitable

method for encapsulating bioactive compounds sensitive to heat and oxygen (11, 12). At present, natural biopolymers commonly used for embedding flavonoid compounds contain starch, maltodextrin, acacia gum, whey protein isolate, soy protein isolate, gelatin, and protein-polysaccharide combination (13). However, encapsulation products prepared by different coated wall materials have different physicochemical properties. Although a variety of natural biological polymers used for encapsulating flavonoids have been reported, microcapsules fabricated with single coating wall always has several limitations such as low antioxidant capacity (14), poor encapsulation efficiency (15), and unsatisfactory solubility. However, microcapsules prepared by protein-polysaccharide combination as wall materials show many advantages on encapsulation efficiency (EE) and stability. For example, the EE of curcumin encapsulated by coconut whey powder and gum Arabic was higher than that of curcumin encapsulated by single coconut whey powder (16); Hu et al. (17) showed that citrus flavone microcapsules prepared by whey protein concentrate and acacia gum complex had better retention efficiency after 3 months storage than that prepared by single acacia gum. Previous studies reported that the EE of cornelian cherry (*Cornus mas* L.) polyphenols encapsulated by  $\beta$ -cyclodextrin was 65.62% (18), however, protein-polysaccharide combination as better wall material to enhance the EE and stability of COF is scarcely reported.

Maltodextrin (MD) is a type of hydrolyzed starch with good solubility and low viscosity. Whey protein isolate (WPI)



is a good carrier of bioactive substances because of its good emulsification, gelling, and thickening (19). SPI is a type of gel type, which is easily biodegradable and in high nutritional value. Gelatin (GE) is a hydrolyzed protein with good biocompatibility and high stability (14). The combined wall materials can greatly improve the physical properties of microcapsule products. However, the study on COF microcapsules prepared by MD and the above different protein combination has not been reported.

In this study, the combination of different proteins (WPI, SPI, GE) and MD were used to encapsulate COF. The effects of different combinations on the EE, particle size, thermodynamic behavior, structure, and microstructure of microcapsule products were investigated. This study is aimed to screen the best combination of protein and maltodextrin as wall material for encapsulating COF and expand its application in functional food industry.

## Materials and methods

### Materials

*Cornus officinalis* was purchased from Xixia County, Henan Province. CO was dried using a microwave freeze dryer (MFD) developed by Lujie et al. (20). Fresh *Cornus* fruit was frozen at  $-25^{\circ}\text{C}$  for at least 8 h. The drying chamber pressure was set at  $-100$  Pa, and cold trap temperature was  $-40^{\circ}\text{C}$ . The power of microwave was set at 1 W/g. During the drying process, the temperature of the material was detected by an infrared thermal imager. Drying lasted until the dry basis moisture content of the material reached 0.09 g/g dry weight. The dried material was crushed and passed through a 60-mesh sieve and stored at  $-25^{\circ}\text{C}$ .

Maltodextrin, rutin and 1,1-diphenyl-2-picrylhydrazyl (DPPH) were purchased from Shanghai Yuan ye Biological Co., Ltd., China. SPI was purchased from Dezhou Gu Shen Protein Technology Biology Co., Ltd., in Dezhou, China. WPI was purchased from Hilmar Corporation, California, USA. GE was purchased from Henan Bo yang Biotechnology Technology Co., Ltd., in Zhou Kou, China. The other reagents were of analytical grade.

### Ultrasonic extraction of COF

*Cornus officinalis* flavonoids was extracted by using an ultrasonic machine according to Wu et al. (21) with slight modification. CO powder (100 g) was added with 70% ethanol (1:15, w/v) and sonicated 3 times at  $50^{\circ}\text{C}$  with ultrasonic power of 300 W for 30 min each time. The filtrate was mixed and centrifuged, and the supernatant was concentrated by a rotary evaporator, and then stored at  $4^{\circ}\text{C}$ .

Flavonoids were purified by the method that Ismail et al. (22) reported with appropriate modifications. First, AB-8 resin was soaked in anhydrous ethanol for 24 h, and the column was wet-loaded. The elution process continued until the effluent was free of white turbidity, and AB-8 resin was washed with distilled water for 1 h. After decompression concentration, the extract was diluted with the appropriate amount of water and then eluted repeatedly with distilled water to remove impurities such as protein and sugar. Then the flavonoids were eluted with ethanol solution (40%), and the eluent was concentrated and freeze-dried to obtain COF.

### Determination of COF

The aluminum chloride method was used to determine the content of total flavonoids (23). The diluted flavonoid extract (1 ml) was mixed with 4 ml 70% ethanol solution in a 10 ml volumetric flask, the reagents of 0.3 ml 5%  $\text{NaNO}_2$  solution and 0.3 ml 10%  $\text{Al}(\text{NO}_3)_3$  solution were further added and shaken for 6 min, and finally 2 ml 4%  $\text{NaOH}$  solution was added. After 15 min, the absorbance was measured at 510 nm. The content of flavonoids (mg/g) in the extract was calculated according to rutin standard curve.

### Preparation and characterization of microcapsules

WPI, SPI, GE, and MD powders were dispersed in distilled water at different ratios of 2:3, 3:7 and 1:3 (w/w) at  $40^{\circ}\text{C}$  and the mixed carrier solution concentration of 10% (w/w) was obtained. The solution was stirred at  $350 \pm 25$  rpm/min for 2 h. The core material solution was added at a core-wall ratio of 1:9 (w/w) and stirred for 10 min. A high-pressure homogenizer (A25, Shanghai OUHOR Mechanical Equipment Co., Ltd., Shanghai, China) was used for homogenization at 10,000 rpm/min for 1 min. To obtain dry powder samples, the obtained mixtures were freeze-dried (LGJ-10D, Beijing Science Instrument Co., Ltd., Beijing, China).

### Determination of physical properties of microcapsules

#### EE

EE refers to the mass ratio of encapsulated core material to total core material in microcapsule samples (24). The contents of surface flavonoids and total flavonoids in microcapsules were determined according to the method that Hu et al. (17) reported, and EE was calculated according to formula (1):

$$EE (\%) = \frac{TFC - SFC}{TFC} \times 100 \quad (1)$$

### Moisture content (MC)

Water content is an important property of powder, which is closely related to its water activity, fluidity, stability, viscosity and microbial growth (25). Microcapsule samples (5 g) were dried in an oven at 70°C until constant weight ( $M_t$ ), the moisture content (MC) was calculated according to formula (2), where  $M_0$  is the initial weight of microcapsule sample:

$$MC (\%) = \frac{M_0 - M_t}{M_0} \times 100 \quad (2)$$

### Water solubility index (WSI)

The solubility was measured according to the method of Boyano Orozco et al. (26), with some modifications. Microcapsule samples were dispersed in distilled water, magnetically stirred at room temperature for 30 min, and immediately centrifuged at 5,000 rpm/min for 10 min. The supernatant was collected and transferred to a pre-weighed Petri dish for drying at 105°C. The water solubility index was calculated according to formula (3):

$$WSI (\%) = \frac{\text{Weight of the sample in the supernatant}}{\text{Weight of the sample in the solution}} \quad (3)$$

### Density and flowability

The bulk density (BD) and tap density (TD) were obtained by measuring the volume of 1 g microcapsule sample in a 10 ml measuring cylinder, and the fluidity of the microcapsule sample was assessed according to Carr's index (CI) (27). The calculation formula was as follows (4):

$$CI (\%) = \frac{\text{Tapped density} - \text{Bulk density}}{\text{Tapped density}} \quad (4)$$

### Color

Color difference meter (Xrite color i5, X-Rite of America, Michigan, USA) was used to determine the color of microcapsule samples, where  $L^*$  represents brightness (0 = black, 100 = white),  $a^*$  represents red index ( $-a^*$  is green,  $+a^*$  is red),  $b^*$  represents yellow index ( $-b^*$  is blue,  $+b^*$  is yellow), Chroma =  $(a^2 + b^2)^{0.5}$ . Each sample was determined three times.

### Determination of particle size

The preparation of the sample solution referred to Yu et al. (28), with some modifications. A certain amount of microcapsule powder was dispersed in ultrapure water, and placed in laser particle size analyzer (LA-960, HORIBA, Tokyo, Japan) to determine the particle size of microcapsule powder.

### Differential scanning calorimetry (DSC)

Differential scanning calorimetry can be used to analyze the thermal behavior of microcapsules and wall materials. Powder samples were determined by differential scanning calorimeter (Switzerland METTLER-TOLEDO, Zurich, Switzerland). Samples (3–5 mg) were placed in the crucible for DSC analysis at a nitrogen flow rate of 100 ml/min and a temperature rise rate of 10°C/min, ranging from 30°C to 300°C (29).

### Fourier transform infrared spectrometer (FT-IR)

FT-IR (VERTEX70, German BRUKER Company, Karlsruhe, German) was used to measure the chemical structure of raw materials and microcapsule powders at room temperature. The powder samples were mixed with the dried KBr at a ratio of 1:100 for measurement. The scanning range was 4,000–400  $\text{cm}^{-1}$  and the spectral resolution was 4  $\text{cm}^{-1}$  (30).

### Scanning electron microscopy (SEM)

The structural characteristics of microcapsules affect their physical and chemical properties and influence the ability of polymer wall material to protect core material (31). SEM (TM3030Plus, Hitachi High-Tech Corporation, Tokyo, Japan) was used to observe the surface micromorphology of microcapsules. The microcapsule powder was gently placed on the sample table and affixed with conductive tape, and the morphology of the microcapsule was photographed and observed in appropriate field of vision.

### Antioxidant activity

The DPPH radical scavenging ability of microcapsules was determined by ultraviolet spectrophotometry. Sample (200  $\mu\text{l}$ ) was added to 3.8 ml DPPH solution ( $6 \times 10^{-5}$  mol/L), and kept in the dark for 30 min. The absorbance was measured at 517 nm, and the results were calculated based on vitamin C standard curve Equation 5,  $A_0$  and  $A_t$  were the absorbance of DPPH solution and the absorbance of sample mixed with DPPH solution, respectively.

$$\text{DPPH radical scavenging efficiency (\%)} = \frac{A_0 - A_t}{A_0} \times 100 \quad (5)$$

TABLE 1 Effect of protein/MD ratios on EE of COF.

Wall material composition	Protein/MD ratio	EE (%)
WPI: MD	2:3	93.29 ± 0.41 <sup>e</sup>
SPI: MD		93.44 ± 0.56 <sup>e</sup>
GE: MD		93.63 ± 0.45 <sup>e</sup>
WPI: MD	3:7	98.24 ± 0.48 <sup>a</sup>
SPI: MD		97.82 ± 0.31 <sup>b</sup>
GE: MD		96.32 ± 0.54 <sup>c</sup>
WPI: MD	1:3	97.8 ± 0.44 <sup>b</sup>
SPI: MD		96.3 ± 0.35 <sup>c</sup>
GE: MD		95.4 ± 0.31 <sup>d</sup>

Values are displayed as mean ± standard deviation. Different letters in the same column indicate significant differences ( $P < 0.05$ ).

## Results and discussion

### EE

In this study, three proteins were combined with MD to form wall materials at different protein/MD ratios (2:3, 3:7, 1:3), respectively. The effects of different protein/MD ratios on EE are shown in Table 1. The EE of microcapsules with different protein/MD ratios ranged from 93.44 to 98.27%, suggesting that these wall material compositions could realize satisfactory encapsulation. However, when the protein/MD ratio was 3:7, the EE value was higher than the other ratios. Clearly, the ratio of protein/MD as wall materials significantly influenced the EE of COF. When the ratio was 3:7, COF are better encapsulated in the wall material. The EE at the protein/MD ratio of 1:3 was lower than that at the ratio of 3:7. This could be due to the fact that the higher content of MD and the lower protein content was not favorable for enhancing EE. Therefore, the EE of COF was closely related to the wall material composition. The wall material composition induced different film-forming properties, which might contribute to the effect of encapsulating flavonoids. Similarly, Fredes et al. (32) prepared Maqui Juice microencapsulation using SPI and MD mixture as wall material, and EE of Maqui Juice by SD and FD could reach 92.5 and 93.0%, respectively. Norkaew et al. (33) also found that the EE of anthocyanins microcapsules with protein and MD as wall material almost reached 100%, which provided better protection for anthocyanins. Due to the higher EE at protein/MD ratio of 3:7, this ratio of 3:7 was selected to perform the following experiments.

### Physical properties

Table 2 shows the results of MC, WSI, BD, TD, and CI of COF microencapsulation at the protein/MD ratio of 3:7.

MC is an important index to measure the stability of powder products, which is related to drying efficiency, glass transition temperature, fluidity, storage stability, and so on (34). In addition, microcapsules in low moisture content are not prone to mildew and degradation, and can increase the stability of COF storage. In general, dry foods with MC between 4 and 10% have good storage stability (35). In our study, MC with different wall formulations ranged from 6.13 to 8.04%, which was conducive to maintain the stability of microcapsules during storage. GE-MD formulation had the highest MC (8.04%), while WPI-MD formulation had the lowest MC (6.13%) (Table 2), and protein types significantly affected the MC of microcapsules. The MC differences of microencapsulated sample might be related to differential affinity of proteins and water and different diffusion coefficients of water through the wall material.

Water solubility index is a crucial factor to evaluate powder product as food ingredients, because those with poor solubility are not easy to further process and have low economic benefits. The results showed that all the microcapsules were in high solubility, which ranged from 89.2 to 90.1% (Table 2), but different wall material compositions had no significant discrepancy on the WSI of microcapsules ( $P < 0.05$ ). Flavonoids were in low solubility, while the protein-polysaccharide mixture as wall material improved the solubility of COF. The high WSI of microcapsules were caused by that wall materials in high solubility and high content of MD was favorable for the solubility of core material (27).

The BD can reflect the gap size between powder particles, which is an essential parameter for assessing the texture. The BD of microcapsule powder is related to molecular weight of the wall material. The heavier material accommodates the less spaces between the particles, resulting in higher BD (36). As shown in Table 2, the BD of microcapsules prepared under different conditions ranged from 0.22 to 0.28 g/ml. The type of wall material has a significant effect on BD ( $P < 0.05$ ). WPI combined with MD displayed a higher BD than the other two formulations, which may be caused by that WPI and MD combination was conducive to the formation of a more dense structure, resulting in a higher volume density. Higher BD indicates a lower amount of air in the powder void, which can prevent the oxidation of microcapsules so that the quality and preservation of microcapsule products can be guaranteed. For measuring TD, the space between particles is reduced due to the application of external force. The TD of the three types of microencapsulation ranged from 0.31 to 0.42 g/ml. The ratio of protein/MD had a significant effect on TD ( $P < 0.05$ ). The microcapsule prepared by WPI-MD had higher TD and particles density, which indicated that a larger number of powder may be stored in smaller containers, which can reduce the air space of powder and oxidation of microcapsules to maintain the quality and stability of microcapsules (10). CI can be used to represent the free flow characteristics of powder. It can be seen from Table 2 that the CI is within the range of 30.67–35.9,

TABLE 2 Physical properties of microcapsules.

Encapsulating agent combination	MC (%)	WSI (%)	BD (g/ml)	TD (g/ml)	CI (%)
WPI: MD (3:7)	6.13 ± 0.23 <sup>c</sup>	90.10 ± 1.02 <sup>a</sup>	0.28 ± 0.01 <sup>a</sup>	0.42 ± 0.03 <sup>a</sup>	33.33 ± 0.13 <sup>b</sup>
SPI: MD (3:7)	7.22 ± 0.14 <sup>b</sup>	89.20 ± 0.60 <sup>a</sup>	0.25 ± 0.02 <sup>b</sup>	0.39 ± 0.01 <sup>b</sup>	35.90 ± 0.05 <sup>a</sup>
GE: MD (3:7)	8.04 ± 0.17 <sup>a</sup>	89.21 ± 0.20 <sup>a</sup>	0.22 ± 0.02 <sup>c</sup>	0.31 ± 0.01 <sup>c</sup>	29.03 ± 0.31 <sup>c</sup>

Values are displayed as mean ± standard deviation. Data with different superscript letters in the same column are significantly different ( $P < 0.05$ ).

indicating that these microcapsules have good fluidity. These results suggested that the combination of wall materials had a significant effect on the physical properties of microcapsules ( $P < 0.05$ ).

## Color

Table 3 shows the color parameters of microcapsules with different wall material composition. The COF without encapsulation was red, and the freeze-dried powder prepared with WPI-MD and GE-MD was pink, but the powder prepared with SPI-MD was light pink. There were significant differences in  $L^*$ ,  $a^*$ ,  $b^*$  of COF microcapsules with different wall material ( $P < 0.05$ ). Compared with the unencapsulated COF powder, the  $L^*$  of microcapsule powder was significantly increased, the  $a^*$  was significantly reduced, but the value of  $b^*$  had no change. The changes of  $L^*$  and  $a^*$  values were mainly due to the types of wall materials, which could mask the color of flavonoids. COF microcapsules powder prepared by WPI-MD and GE-MD were brighter than that prepared by SPI-MD, as the amount of COF exposed on their surface was less. Total color difference ( $\Delta E$ ) between control and microcapsule samples was also evaluated. There were significant differences between COF and microcapsules with different protein/MD combinations ( $P < 0.05$ ). The  $\Delta E$  order of microcapsules prepared by the three kinds of wall materials was as follows: GE-MD (27.11) > WPI-MD (25.33) > SPI-MD (23.57). High  $\Delta E$  values indicated that the color change of microcapsules greatly increased, compared to unencapsulated COF.

## Particle size

Particle size is an important parameter to evaluate the quality of microcapsule products. The smaller the particle size is, the easier the encapsulated bioactive compounds are to release (37). The average particle size of microcapsules with different wall materials formulations is shown in Figure 1, ranging from 7.17 to 16.4  $\mu\text{m}$ . The particle size was significantly affected by the wall material ( $P < 0.05$ ). The microcapsule particle size was related to the molecular size of wall material. Different wall material mixed with COF possessed different structures and

interaction force, which further influenced the particle size of microcapsules. Among the particles prepared with the three formulations, WPI-MD produced the smallest particles, which implied that WPI-MD-COF complex formed microcapsules with smaller structure. It can be seen that WPI-MD showed good encapsulating ability to form microcapsules. The particle size was also related to BD. The smaller the particle size is, the greater the BD is. It can be seen from Table 2 that the larger BD of microcapsules prepared with WPI-MD corresponded with the particle size.

## DSC analysis

The thermal stability of microcapsule studied by DSC are shown in Figure 2. As can be observed, the thermal properties of microcapsules largely depended on the wall composition. COF powder showed endothermic peaks at 76°C and 150°C, which could be the denature and decomposition temperature of flavonoids, respectively. The COF loaded microcapsules showed the endothermic peaks (79.04°C–86.00°C) compared to single COF endothermic peak at 76°C, which implied that encapsulation changed the glass transition temperature of COF. This phenomenon suggests that the microencapsulation makes COF endothermic peaks shift to higher temperature, due to the interaction of COF and the wall material to increase the stability of the COF. In addition, the endothermic peak of COF at 150°C disappeared, which suggested that COF was embedded into the microcapsules. Microcapsules can maintain the stability of core material from heat treatment. Adsare et al. (16) also have obtained similar thermal behavior of curcumin microencapsulation using coconut milk whey and GA as wall material.

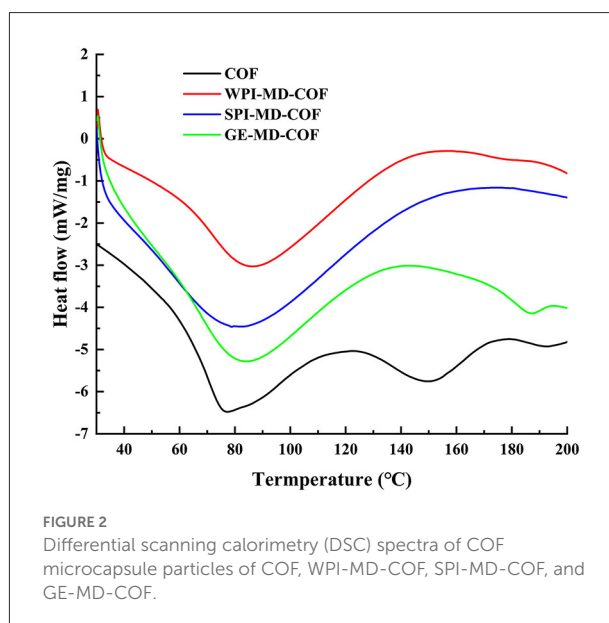
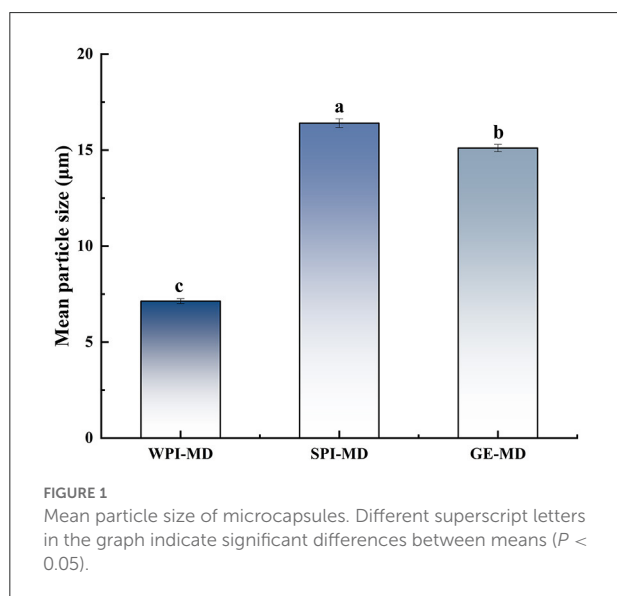
## FT-IR study

The infrared spectrum can be used to analyze whether new functional groups and chemical bonds are introduced into flavonoids microcapsules. The infrared spectra of wall materials, core materials, and microcapsules are shown in Figure 3. The infrared spectrum of COF (Figure 3) showed a broad and strong peak formed by intermolecular hydrogen bonding at 3,408

TABLE 3 Color parameters of microcapsules.

Wall material composition	Color			
	L*	a*	b*	ΔE
COF	44.43 ± 0.33 <sup>a</sup>	20.35 ± 0.7 <sup>a</sup>	4.74 ± 0.43 <sup>b</sup>	
WPI: MD (3:7)	67.84 ± 0.26 <sup>b</sup>	10.75 ± 0.12 <sup>b</sup>	3.48 ± 0.15 <sup>c</sup>	25.33 ± 0.67 <sup>b</sup>
SPI: MD (3:7)	64.20 ± 0.35 <sup>c</sup>	7.53 ± 0.17 <sup>c</sup>	5.30 ± 0.56 <sup>a</sup>	23.57 ± 0.92 <sup>c</sup>
GE: MD (3:7)	69.53 ± 0.67 <sup>a</sup>	10.11 ± 0.53 <sup>b</sup>	4.48 ± 0.13 <sup>b</sup>	27.11 ± 1.06 <sup>a</sup>

Values are displayed as mean ± standard deviation. Different letters indicate significant ( $P < 0.05$ ) differences between columns. The \* symbol indicates the color attribute in table notes.



$\text{cm}^{-1}$ , which proved existence of phenolic hydroxy groups, and the broad peak shape might be due to more hydroxyl groups on the flavonoid molecule (38); Meanwhile, asymmetric bending vibration peaks of  $-\text{CH}_2$  and  $-\text{CH}_3$  for COF were observed at  $2,931 \text{ cm}^{-1}$  and  $1,316 \text{ cm}^{-1}$ , which proved more hydrogens on the saturated carbon. The peaks at  $1,698 \text{ cm}^{-1}$  and  $1,634 \text{ cm}^{-1}$  of COF were related to  $\text{C}=\text{O}$  and  $\text{C}=\text{C}$  stretching vibrational peaks, respectively. The infrared spectra of COF microcapsules prepared with different formulas were similar, and the specific peak of COF was retained, but the hydroxyl stretching vibration peak ( $3,288\text{--}3,383 \text{ cm}^{-1}$ ) shifted to low wavenumbers, indicating that hydrogen bond formed between COF and wall material (39). Compared with individual MD and COF, the spectra of MD-COF mixture showed that the bands at  $3,400 \text{ cm}^{-1}$  of MD and  $1,652 \text{ cm}^{-1}$  of COF were shifted to lower wavenumbers, and the band at  $1,081 \text{ cm}^{-1}$  disappeared, which suggested there was interaction between MD and COF. After three kinds of proteins were individually mixed with COF, the hydroxyl stretching vibration peaks of COF were shifted to lower wavenumbers,  $\text{C}=\text{O}$  of WPI, SPI and GE moved from  $1,651 \text{ cm}^{-1}$ ,  $1,652 \text{ cm}^{-1}$  and  $1,652 \text{ cm}^{-1}$  to  $1,653 \text{ cm}^{-1}$ ,  $1,646$

$\text{cm}^{-1}$  and  $1,646 \text{ cm}^{-1}$ , respectively. Besides, the bands of N-H bending at  $1,395 \text{ cm}^{-1}$ ,  $1,456 \text{ cm}^{-1}$ ,  $1,396 \text{ cm}^{-1}$  of WPI, SPI, and GE disappeared. The shifting in the amide region could confirm the interaction between COF and protein molecules with electrostatic forces (14).

Comparing the spectra of COF microcapsules prepared with combined wall materials, it was found that a strong  $\text{C}=\text{O}$  bond stretching vibration peak was formed in the three types of microcapsules at  $1,652 \text{ cm}^{-1}$ , indicating that there was interaction between the wall material and COF (40). The spectra of microcapsules prepared by WPI-MD, SPI-MD, and GE-MD mixture indicated shifting of the hydroxyl peaks from  $3,408 \text{ cm}^{-1}$  of COF to  $3,360$ ,  $3,361$ , and  $3,358 \text{ cm}^{-1}$ , respectively, but the shift of the hydroxyl peaks was slight compared with their individual protein-COF mixture, due to the MD incorporation. Besides, during the formation of flavonoid microcapsules, the peak shifted from  $1,453 \text{ cm}^{-1}$  of COF to  $1,454$  (WPI-MD-COF),  $1,455$  (SPI-MD-COF) and  $1,457$  (GE-MD-COF)  $\text{cm}^{-1}$  and the peak width of microcapsules narrowed. Compared with the COF spectra, the characteristic peaks of the three microcapsules at



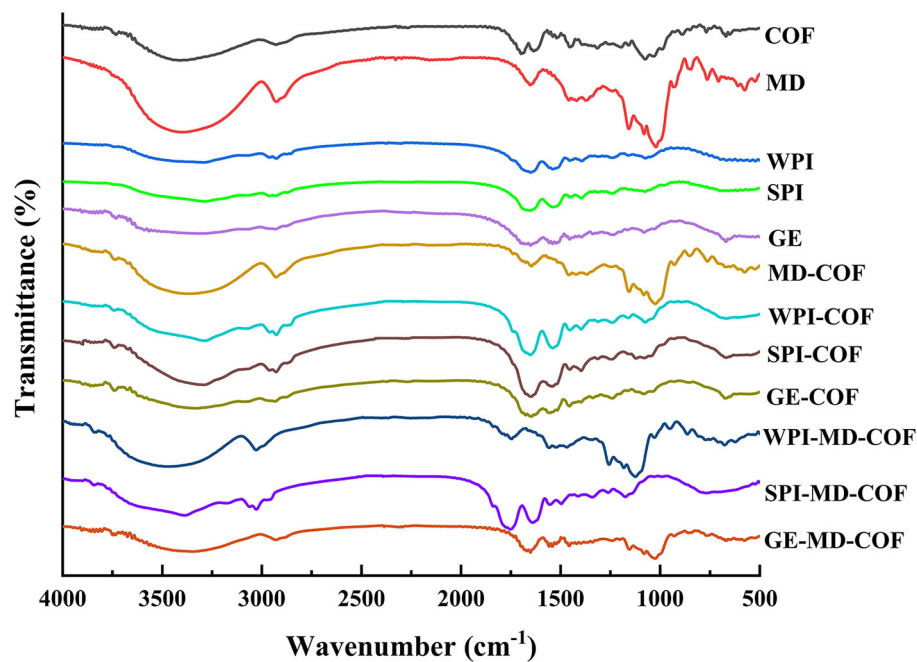


FIGURE 3  
Infrared spectra of COF, MD, protein, protein-COF, and microcapsules.

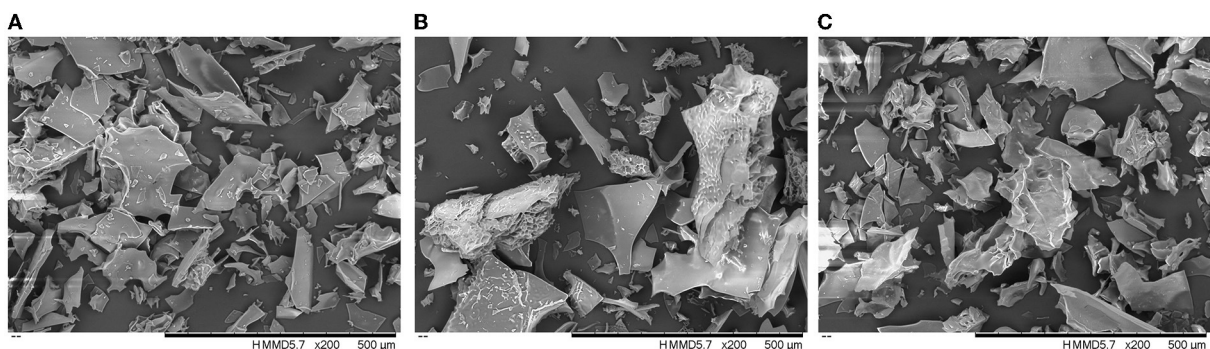


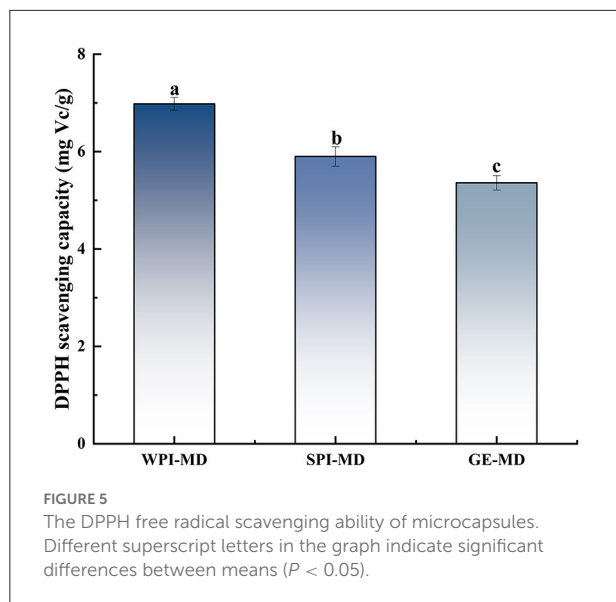
FIGURE 4  
Scanning electron microscopy (SEM) of WPI-MD-COF (A), SPI-MD-COF (B), and GE-MD-COF (C) microcapsules.

1,075  $\text{cm}^{-1}$  and 1,315  $\text{cm}^{-1}$  disappeared, indicating that the COF was encapsulated in the microcapsules. The FT-TR results also supported the differences on DSC spectra of COF and COF microcapsules, which confirmed the interaction between the wall material and the core material, providing the evidences on successfully encapsulating COF.

## Microcapsule morphology

The morphology of microcapsule powder with different formulations is shown in Figure 4. The surface of microcapsules

presented flake structures of different sizes, which was a common feature of FD particles. The microcapsules showed changes in surface microstructure due to the different wall composition (41). Microcapsules prepared with WPI-MD and GE-MD formulations showed glassy structures and smooth surfaces, whereas microcapsules prepared with SPI-MD mixture had irregular shapes and porous surfaces. This was due to the formation of ice crystals during the pre-freezing process of the microencapsulated mixture, which further underwent the sublimation of water vapor and the formation of irregular porous pores. The formed ice crystals at pre-freezing stage destroyed the original



structure of wall materials, and caused solute polymerization, contributing to the structure change of different wall materials under MFD condition. The water sublimation rate of COF microcapsules during MFD process was also affected by wall materials, which led to the morphology differences among different COF microcapsules. These changes destroyed the original structure of the material and changed the physical properties of microcapsules (42, 43). Similar glassy results were observed on the morphology of anthocyanin encapsulated by MD and GA using freeze-drying techniques (44).

## Antioxidant activity

The DPPH radical scavenging ability of microcapsules with different wall material formulations is illustrated in Figure 5. The results revealed that the EE with different wall materials showed different antioxidant ability, and the DPPH radical scavenging ability of COF microcapsules prepared with three protein-polysaccharide mixtures ranged from 5.36 mg Vc/g to 6.98 mg Vc/g. Results showed that the mixture of WPI-MD (3:7) had the highest DPPH free radical scavenging ability, and the mixture of GE-MD (3:7) had the lowest DPPH radical scavenging ability. These results were consistent with the same trend in EE, suggesting that COF in microcapsules played a main role in exhibiting DPPH radical scavenging ability. Moser et al. (45) also proved that anthocyanins encapsulated by WPI-MD wall combinations exerted high DPPH radical scavenging ability (8.6 mmol Trolox/100 g).

## Conclusions

In this study, protein (WPI, SPI, and GE) and MD was both used as wall material to prepare COF microcapsules by FD. The effect of the wall material formulation on characteristics of COF microcapsules was explored. The EE of COF microcapsules at protein/MD ratio of 3:7 was higher than the other ratios. The variety of proteins significantly affected the characteristics of microcapsules. Compared with free COF, microencapsulation can improve thermal stability of COF. FT-IR showed that flavonoids were successfully encapsulated in the wall materials. The microstructure of all the microcapsules exhibited irregular lamellar structure. COF microcapsules prepared by WPI-MD showed higher DPPH scavenging ability. Among the three wall material formulations, WPI-MD mixture displayed more advantages on its application into food industry. This study provided more evidences for developing COF microcapsules as functional food. In future, more researches on investigating controlled release of COF microcapsules in specific food should be further carried out.

## Data availability statement

The original contributions presented in the study are included in the article/supplementary material, further inquiries can be directed to the corresponding author/s.

## Author contributions

XD, AR, and WC: conceptualization. XD, GR, and LL: methodology. MZ: investigation and writing—original draft preparation. MZ, XR, and YA: software. MZ, YA, and ZW: data curation. XD and WC: writing—review and editing. GR, JC, and BB: supervision. XD, AR, and GR: funding acquisition. All authors contributed to the article and approved the submitted manuscript.

## Funding

We acknowledge the financial support from National Natural Science Foundation of China (Contract Nos. 32172352 and 31972207), National Natural Science Foundation of China Regional Fund Project (Contract No. 32160573), Key Scientific Research Projects of Institutions of Higher Learning of Henan (Contract No. 22A550005), Key Science and Technology Program of Henan Province (Contract No. 222102520011), Young Teacher Funding Program of the Henan Higher School (Contract No. 2020GGJS072), Guangxi Natural Science Foundation of China (Contract No. 2020GXNSFAA259093), and Special Program for the Introduction of Foreign Intelligence

in Henan Province (Foreign Experts Project) (Contract No. HNGD2021040), all of which enabled us to carry out this study.

## Conflict of interest

The authors declare that the research was conducted in the absence of any commercial or financial relationships that could be construed as a potential conflict of interest.

## References

- Xie XY, Wang R, Shi YP. Chemical constituents from the fruits of *Cornus officinalis*. *Biochem Syst Ecol.* (2012) 45:120–3. doi: 10.1016/j.bse.2012.07.025
- Peng Z, Wang Y, He J, Zhang J, Pan X, Ye X, et al. Chemical constituents and their antioxidant and anti-inflammatory activities from edible *Cornus officinalis* fruits. *Eur Food Res Technol.* (2022) 248:1003–10. doi: 10.1007/s00217-021-03940-6
- Szczepaniak OM, Kobus-Cisowska J, Kusek W, Przeor M. Functional properties of Cornelian cherry (*Cornus mas* L.): a comprehensive review. *Eur Food Res Technol.* (2019) 245:2071–87. doi: 10.1007/s00217-019-03313-0
- Pawlowska AM, Camangi F, Braca A. Quali-quantitative analysis of flavonoids of *Cornus mas* L. (Cornaceae) fruits. *Food Chem.* (2010) 119:1257–61. doi: 10.1016/j.foodchem.2009.07.063
- Li M, Pare PW, Zhang J, Kang T, Zhang Z, Yang D, et al. Antioxidant capacity connection with phenolic and flavonoid content in Chinese medicinal herbs. *Rec Nat Prod.* (2018) 12:239–50. doi: 10.25135/rnp.24.17.08.138
- Jayaprakasam B, Olson LK, Schutski RE, Tai M-H, Nair MG. Amelioration of obesity and glucose intolerance in high-fat-fed C57BL/6 mice by anthocyanins and ursolic acid in Cornelian cherry (*Cornus mas*). *J Agric Food Chem.* (2006) 54:243–8. doi: 10.1021/jf0520342
- Hosseinpour-Jaghdani F, Shomali T, Gholipour-Shahraki S, Rahimi-Madiseh M, Rafieian-Kopaei M. *Cornus mas*: a review on traditional uses and pharmacological properties. *J Complement Integr Med.* (2017) 14:20160137. doi: 10.1515/jcim-2016-0137
- Nijveldt RJ, Van Nood E, Van Hoorn DE, Boelens PG, Van Norren K, Van Leeuwen PA. Flavonoids: a review of probable mechanisms of action and potential applications. *Am J Clin Nutr.* (2001) 74:418–25. doi: 10.1093/ajcn/74.4.418
- David L, Danciu V, Moldovan B, Filip A. Effects of *in vitro* gastrointestinal digestion on the antioxidant capacity and anthocyanin content of Cornelian cherry fruit extract. *Antioxidants.* (2019) 8:114. doi: 10.3390/antiox8050114
- Osamede Airouyuwa J, Kaewmanee T. Microencapsulation of *Moringa oleifera* leaf extracts with vegetable protein as wall materials. *Food Sci Technol Int.* (2019) 25:533–43. doi: 10.1177/1082013219842469
- Corrêa-Filho LC, Moldão-Martins M, Alves VD. Advances in the application of microcapsules as carriers of functional compounds for food products. *Appl Sci.* (2019) 9:571. doi: 10.3390/app9030571
- Yamashita C, Chung MMS, Dos Santos C, Mayer CRM, Moraes ICF, Branco IG. Microencapsulation of an anthocyanin-rich blackberry (*Rubus* spp) by-product extract by freeze-drying. *LWT.* (2017) 84:256–62. doi: 10.1016/j.lwt.2017.05.063
- Yinbin L, Wu L, Weng M, Tang B, Lai P, Chen J. Effect of different encapsulating agent combinations on physicochemical properties and stability of microcapsules loaded with phenolics of plum (*Prunus salicina* lindl). *Powder Technol.* (2018) 340:459–64. doi: 10.1016/j.powtec.2018.09.049
- Mansour M, Salah M, Xu X. Effect of microencapsulation using soy protein isolate and gum Arabic as wall material on red raspberry anthocyanin stability, characterization, and simulated gastrointestinal conditions. *Ultrason Sonochem.* (2020) 63:104927. doi: 10.1016/j.ultrasonch.2019.104927
- Hu Y, Kou G, Chen Q, Li Y, Zhou Z. Protection and delivery of mandarin (*Citrus reticulata* Blanco) peel extracts by encapsulation of whey protein concentrate nanoparticles. *LWT.* (2019) 99:24–33. doi: 10.1016/j.lwt.2018.09.044
- Adsare SR, Annapure US. Microencapsulation of curcumin using coconut milk whey and gum Arabic. *J Food Eng.* (2021) 298:110502. doi: 10.1016/j.jfoodeng.2021.110502
- Hu Y, Li Y, Zhang W, Kou G, Zhou Z. Physical stability and antioxidant activity of citrus flavonoids in Arabic gum-stabilized microcapsules: modulation of whey protein concentrate. *Food Hydrocoll.* (2018) 77:588–97. doi: 10.1016/j.foodhyd.2017.10.037
- Popović BM, Blagojević B, Latković D, Cetojević-Simin D, Kucharska AZ, Parisi F, et al. A one step enhanced extraction and encapsulation system of cornelian cherry (*Cornus mas* L.) polyphenols and iridoids with  $\beta$ -cyclodextrin. *LWT.* (2021) 141:110884. doi: 10.1016/j.lwt.2021.110884
- Souza AL, Hidalgo-Chávez DW, Pontes SM, Gomes FS, Cabral LM, Tonon RV. Microencapsulation by spray drying of a lycopene-rich tomato concentrate: characterization and stability. *LWT.* (2018) 91:286–92. doi: 10.1016/j.lwt.2018.01.053
- Lujie Z, Xu D, Weiwei C, Xing R, Guangyue R, Panpan L, et al. Effects of different drying methods on the characterization, dissolution rate and antioxidant activity of ursolic acid-loaded chitosan nanoparticles. *Foods.* (2021) 10:2470. doi: 10.3390/foods10102470
- Wu Z, Wang W, He F, Li D, Wang D. Simultaneous enrichment and separation of four flavonoids from *Zanthoxylum bungeanum* leaves by ultrasound-assisted extraction and macroporous resins with evaluation of antioxidant activities. *J Food Sci.* (2018) 83:2109–18. doi: 10.1111/1750-3841.14282
- Ismail BB, Yusuf HL, Pu Y, Zhao H, Guo M, Liu D. Ultrasound-assisted adsorption/desorption for the enrichment and purification of flavonoids from baobab (*Adansonia digitata*) fruit pulp. *Ultrason Sonochem.* (2020) 65:104980. doi: 10.1016/j.ultrasonch.2020.104980
- Rouphael Y, Bernardi J, Cardarelli M, Bernardo L, Kane D, Colla G, et al. Phenolic compounds and sesquiterpene lactones profile in leaves of nineteen artichoke cultivars. *J Agric Food Chem.* (2016) 64:8540–8. doi: 10.1021/acs.jafc.6b03856
- Mahdavi SA, Jafari SM, Assadpoor E, Dehnad D. Microencapsulation optimization of natural anthocyanins with maltodextrin, gum Arabic and gelatin. *Int J Biol Macromol.* (2016) 85:379–85. doi: 10.1016/j.ijbiomac.2016.01.011
- Mahdi AA, Mohammed JK, Al-Ansi W, Ghaleb AD, Al-Maqtari QA, Ma M, et al. Microencapsulation of fingered citron extract with gum Arabic, modified starch, whey protein, and maltodextrin using spray drying. *Int J Biol Macromol.* (2020) 152:1125–34. doi: 10.1016/j.ijbiomac.2019.10.201
- Boyano-Orozco L, Gallardo-Velázquez T, Meza-Márquez OG, Osorio-Revilla G. Microencapsulation of rambutan peel extract by spray drying. *Foods.* (2020) 9:899. doi: 10.3390/foods9070899
- Navarro-Flores MJ, Ventura-Canseco LMC, Meza-Gordillo R, Ayora-Talavera TDR, Abud-Archila M. Spray drying encapsulation of a native plant extract rich in phenolic compounds with combinations of maltodextrin and non-conventional wall materials. *J Food Sci Technol.* (2020) 57:4111–22. doi: 10.1007/s13197-020-04447-w
- Yu Y, Lv Y. Degradation kinetic of anthocyanins from rose (*Rosa rugosa*) as prepared by microencapsulation in freeze-drying and spray-drying. *Int J Food Prop.* (2019) 22:2009–21. doi: 10.1080/10942912.2019.1701011
- Shao P, Xuan S, Wu W, Qu L. Encapsulation efficiency and controlled release of *Ganoderma lucidum* polysaccharide microcapsules by spray drying using different combinations of wall materials. *Int J Biol Macromol.* (2019) 125:962–9. doi: 10.1016/j.ijbiomac.2018.12.153
- Li D, Zhu M, Liu X, Wang Y, Cheng J. Insight into the effect of microcapsule technology on the processing stability of mulberry polyphenols. *LWT.* (2020) 126:109144. doi: 10.1016/j.lwt.2020.109144
- Flores FP, Singh RK, Kong F. Physical and storage properties of spray-dried blueberry pomace extract with whey protein isolate as wall material. *J Food Eng.* (2014) 137:1–6. doi: 10.1016/j.jfoodeng.2014.03.034

## Publisher's note

All claims expressed in this article are solely those of the authors and do not necessarily represent those of their affiliated organizations, or those of the publisher, the editors and the reviewers. Any product that may be evaluated in this article, or claim that may be made by its manufacturer, is not guaranteed or endorsed by the publisher.

32. Fredes C, Becerra C, Parada J, Robert P. The microencapsulation of maqui (*Aristotelia chilensis* (Mol) Stuntz) juice by spray-drying and freeze-drying produces powders with similar anthocyanin stability and bioaccessibility. *Molecules*. (2018) 23:1227. doi: 10.3390/molecules23051227
33. Norkaew O, Thitisut P, Mahatheeranont S, Pawin B, Sookwong P, Yodpitak S, et al. Effect of wall materials on some physicochemical properties and release characteristics of encapsulated black rice anthocyanin microcapsules. *Food Chem.* (2019) 294:493–502. doi: 10.1016/j.foodchem.2019.05.086
34. Mohammed NK, Alhelli AM, Meor Hussin AS. Influence of different combinations of wall materials on encapsulation of *Nigella sativa* oil by spray dryer. *J Food Process Eng.* (2021) 44:e13639. doi: 10.1111/jfpe.13639
35. Santana AA, Cano-Higuita DM, De Oliveira RA, Telis VR. Influence of different combinations of wall materials on the microencapsulation of Jussara pulp (*Euterpe edulis*) by spray drying. *Food Chem.* (2016) 212:1–9. doi: 10.1016/j.foodchem.2016.05.148
36. Ferrari CC, Germer SPM, Alvim ID, Vissotto FZ, De Aguirre JM. Influence of carrier agents on the physicochemical properties of blackberry powder produced by spray drying. *Int J Food Sci Technol.* (2012) 47:1237–45. doi: 10.1111/j.1365-2621.2012.02964.x
37. Nogueira GE, Fakhouri FM, De Oliveira RA. Incorporation of spray dried and freeze dried blackberry particles in edible films: morphology, stability to pH, sterilization and biodegradation. *Food Packag Shelf Life.* (2019) 20:100313. doi: 10.1016/j.fpsl.2019.100313
38. Zakaria I, Ahmat N, Jaafar FM, Widyawaruyanti A. Flavonoids with antiplasmodial and cytotoxic activities of *Macaranga triloba*. *Fitoterapia.* (2012) 83:968–72. doi: 10.1016/j.fitote.2012.04.020
39. Xie Y, Zhou H, Qian H. Effect of addition of peach gum on physicochemical properties of gelatin-based microcapsule. *J Food Biochem.* (2006) 30:302–12. doi: 10.1111/j.1745-4514.2006.00061.x
40. Lee YK, Chang YH. Microencapsulation of a maca leaf polyphenol extract in mixture of maltodextrin and neutral polysaccharides extracted from maca roots. *Int J Biol Macromol.* (2020) 150:546–58. doi: 10.1016/j.ijbiomac.2020.02.091
41. Ezhilarasi P, Indrani D, Jena BS, Anandharamakrishnan C. Freeze drying technique for microencapsulation of *Garcinia* fruit extract and its effect on bread quality. *J Food Eng.* (2013) 117:513–20. doi: 10.1016/j.jfoodeng.2013.01.009
42. Kuck LS, Noreña CPZ. Microencapsulation of grape (*Vitis labrusca* var. Bordo) skin phenolic extract using gum Arabic, polydextrose, and partially hydrolyzed guar gum as encapsulating agents. *Food Chem.* (2016) 194:569–76. doi: 10.1016/j.foodchem.2015.08.066
43. Mazuco RA, Cardoso PMM, Bindaco ÉS, Scherer R, Castilho RO, Faraco AaG, et al. Maltodextrin and gum Arabic-based microencapsulation methods for anthocyanin preservation in Juçara palm (*Euterpe edulis* Martius) fruit pulp. *Plant Foods Hum Nutr.* (2018) 73:209–15. doi: 10.1007/s11130-018-0676-z
44. Mahdavee Khazaei K, Jafari SM, Ghorbani M, Hemmati Kakhki A. Application of maltodextrin and gum Arabic in microencapsulation of saffron petal's anthocyanins and evaluating their storage stability and color. *Carbohydr Polym.* (2014) 105:57–62. doi: 10.1016/j.carbpol.2014.01.042
45. Moser P, Telis VRN, De Andrade Neves N, García-Romero E, Gómez-Alonso S, Hermosín-Gutiérrez I. Storage stability of phenolic compounds in powdered BRS Violeta grape juice microencapsulated with protein and maltodextrin blends. *Food Chem.* (2017) 214:308–18. doi: 10.1016/j.foodchem.2016.07.081



## OPEN ACCESS

## EDITED BY

Junxiang Zhu,  
Qingdao Agricultural University, China

## REVIEWED BY

Mingquan Huang,  
Beijing Technology and Business  
University, China  
Majid Mohammadhosseini,  
Islamic Azad University, Shahrood, Iran

## \*CORRESPONDENCE

Hao Jiang  
jh1812@163.com;  
jh1812@nwafu.edu.cn

## SPECIALTY SECTION

This article was submitted to  
Nutrition and Food Science  
Technology,  
a section of the journal  
Frontiers in Nutrition

RECEIVED 31 July 2022

ACCEPTED 15 September 2022

PUBLISHED 29 September 2022

## CITATION

Lin Q, Ren A, Liu R, Xing Y, Yu X and  
Jiang H (2022) Flavor properties  
of Chinese noodles processed by  
dielectric drying.  
*Front. Nutr.* 9:1007997.  
doi: 10.3389/fnut.2022.1007997

## COPYRIGHT

© 2022 Lin, Ren, Liu, Xing, Yu and  
Jiang. This is an open-access article  
distributed under the terms of the  
[Creative Commons Attribution License](#)  
(CC BY). The use, distribution or  
reproduction in other forums is  
permitted, provided the original  
author(s) and the copyright owner(s)  
are credited and that the original  
publication in this journal is cited, in  
accordance with accepted academic  
practice. No use, distribution or  
reproduction is permitted which does  
not comply with these terms.

# Flavor properties of Chinese noodles processed by dielectric drying

Qian Lin<sup>1</sup>, Aiqing Ren<sup>2</sup>, Rui Liu<sup>3</sup>, Yanan Xing<sup>3</sup>, Xiuzhu Yu<sup>1</sup> and  
Hao Jiang<sup>1,4\*</sup>

<sup>1</sup>College of Food Science and Engineering, Northwest A&F University, Yangling, China, <sup>2</sup>Institute of Food Research, Hezhou University, Guangxi, China, <sup>3</sup>Cereal Industrial Technology Academy, Hebei Jinshahe Flour and Noodle Group/Hebei Cereal Food Processing Technology Innovation Centre, Xingtai, China, <sup>4</sup>Engineering Research Center of Grain and Oil Functionalized Processing, Universities of Shaanxi Province, Yangling, China

Volatile organic compounds (VOCs) significantly impact food flavor. In this work, Electron nose (E-nose), head space solid phase microextraction-gas chromatography-mass spectrometry (HS-SPME-GC-MS), and head space-gas chromatography-ion mobility spectrometry (HS-GC-IMS) techniques were applied to analyze different drying effects: microwave, hot air, and radio frequency on the aroma of Chinese noodles. E-nose analysis suggests that aromatic differences are mainly from broad range-methane. HS-SPME-GC-MS and HS-GC-IMS identified 47 and 26 VOCs in the fresh and dried noodles, respectively. The VOCs in the dried noodles were mainly aldehydes, alcohols, and esters. Drying significantly reduced the types of VOCs in Chinese dried noodles. Microwave dried noodles exhibited the strongest aroma after the shortest time of treatment, suggesting microwave drying may be the best drying method for noodles. Using aromatic analysis, this paper provides useful information for understanding the flavor of flour products and offers new ideas for drying noodles.

## KEYWORDS

Chinese dried noodles, volatile compounds, E-nose, HS-GC-MS, HS-GC-IMS

## Introduction

Wheat is one of the three most widely consumed crops in the world. Asian countries make about 12% of the world's wheat into noodles (1). As a traditional staple food, Chinese dried noodles are widely eaten in many Asian countries because of their easy preservation, convenient consumption, and high nutritional value. Existing studies have analyzed an impressive array of factors associated with Chinese dried noodles: physical and chemical properties; quality improvement; evaluation methods; and changes in storage (2). However, the aromatic characteristics of Chinese dry noodles and the effects of these changes on product quality characteristics are rarely discussed.



Drying is a key step in Chinese dried noodles manufacturing, prolonging the shelf-life of foods. In addition, the volume and weight of dehydrated food reduce the cost of processing, packaging, and transporting. There are some disadvantages to the hot air (HA) drying process, such as slow heat transfer, long running time, high energy consumption, reduced nutrition, and mitigated taste, among other things (3). The current research directions for Chinese dried noodles are mainly to optimize the drying parameters (4) and change the noodle recipe to improve the quality and enrich the flavor of Chinese dried noodles. To reduce the loss of flavor during drying and to overcome the disadvantages of HA drying, it has become necessary to research new drying methods in addition to the two directions mentioned above.

Microwave (MW, 2450 MHz) drying—a subset of dielectric dehydration technology—uses electromagnetic radiation for rapid heating and drying (5). Dielectric heating absorbs electromagnetic waves and converts them into heat energy, a process that greatly improves heating efficiency. Carvalho et al. (6) reduced the drying time of HA drying malt by 95 percent using MW drying. MW drying can not only save energy but also better retain the aromatic components of food materials (7). Pongpichaiudom and Songsermpong (8) compared the quality of the noodles in terms of cooking quality, textural characteristics, and color. The results showed that MW dried noodles have good attributes, including minimal cooking losses. However, there is a paucity of research on the flavor of MW dried noodles. MW drying does have some inherent shortcomings, including uneven heating and limited penetration depth. These issues are a result of the uneven distribution of the electromagnetic field in the heating bin and the uneven distribution of water in the target material. Some methods have been suggested to overcome these drawbacks. Shen et al. (9) proposed a method that combined ventilation convection with MW heating to achieve an even distribution of temperature and water content, thus improving the uniformity of drying.

A low frequency electromagnetic drying called radio frequency (RF, 27 MHz) is an alternative to MW that addresses some of these more pressing issues (10). Compared with MW drying, RF drying has many advantages, such as good heating uniformity, significant penetration depth because of its longer wavelengths, stable product temperature control, and high cost-effectiveness. Jiang et al. (11) dried strawberries using RF to prove the advantages of RF drying on drying rate and nutrient retention. Wang et al. (12) also proved the potential of RF technology in the drying uniformity and quality of agricultural products by drying nuts. During these experiments, RF was less efficient than MW because of the lower frequency. Compared to HA drying, RF exhibited a poorer drying uniformity because of overheating in corners, edges, and centers, although RF

performed far better than MW in terms of uniformity (13). Because RF drying performs far better than MW in terms of uniformity and other aspects, RF is now applied to many aspects of food preparation. Zhang et al. (14) demonstrated that RF heated meat batters were significantly harder, chewier, and gummier. Zhang et al. (15) testified that RF drying gives food a new texture, such as crispy and chewy. However, there is a large gap in the application of RF drying to noodles, especially the effect of dielectric on the flavor of dried noodles has rarely been reported.

Aroma is one of the most important indicators of food quality, while volatile organic compounds (VOCs) are the most important factors impacting flavor (16). To date, two analytical methods (sensory analysis and instrumental analysis) have been used to analyze VOCs in food products. In contrast to subjective sensory analysis, instrumental analysis can be used to explore VOCs at the molecular level. The electronic nose (E-nose) is an aroma detection system that provides fast sensory information on food. E-nose allows efficient, cost-effective, and non-destructive identification of food products. It has been used in a wide range of applications such as freshness and spoilage assessment, classification, and adulteration identification of food products (17, 18). Headspace solid-phase microextraction-gas chromatography-mass spectrometry (HS-SPME-GC-MS) is a technique that combines enrichment extraction with separation and detection for the qualitative and quantitative detection of VOCs in food products (19). It has been widely used in food analysis, such as traceability analysis and identification of species and VOCs in food and oil processing (20). headspace-gas chromatography-ion mobility spectrometry (HS-GC-IMS) is of interest because it combines the high sensitivity of gas chromatography with the fast response time of ion mobility spectrometry. HS-GC-IMS has been applied to the monitoring of food processing and the assessment of aroma changes during food storage (21). Yet limited research exists on the effects of different drying methods on the flavor of Chinese dried noodles. To improve the understanding, this study analyzed different drying techniques—including HA, MW, and RF—on noodles and the flavor thereof. E-nose, HS-SPME-GC-MS, and HS-GC-IMS were used to detect VOCs in Chinese dried noodles.

## Materials and methods

### Samples

Flour was provided by the Hebei Jinshahe flour industry group. The flour had a moisture content of  $13.04\% \pm 0.12$  (w.b.) and protein content of 12.78%. The edible salt used in noodles comes from the local supermarket (Yangling, Shaanxi). The phenethyl acetate was purchased from Sigma-Aldrich (73747, St. Louis, MO, USA). All chemical reagents used in this study are analytical grade.

## Preparation of fresh noodles

Two hundred gram flour, 1% salt, and 30% water are mixed using a dough mixer (KMM760, Kenwood, London, UK) for 4 min. After mixing, the dough was calendered on the experimental noodle machine (BJM-6, Deqing Baijie Electric Appliance Co., Ltd, Huzhou, Zhejiang, China). The calendering process includes several steps: 1.5 mm axial spacing calendering three times, including direct calendering once, and folded calendering twice. The materials were then placed in a self-sealing bag and allowed to incubate for 30 min. After incubation, noodles were passed through the noodle machine for four times to get noodles with a width of 2 mm and a thickness of 1 mm.

## Drying treatment

### Microwave drying

Twenty-five gram of fresh noodles samples were hung on the noodles rack and placed in a commercial microwave oven (MM823ESJ-SA, Midea Group, Guangdong, China). Samples were dried at 500 W power for 4 min with a heating intensity of 20 W/g. After removal from the oven, samples were placed in the dryer and immediately cooled to room temperature.

### Hot air drying

Hundred gram of fresh noodles samples were hung on the drying rack and placed in the drying oven (GZX-9023MBE, Shanghai Boxun Industrial Co., LTD. Medical Equipment Factory, Shanghai, China). Referring to the method of Zhang et al. (4) and optimization, the drying process was split into three stages: pre-drying, main drying, and final drying. Pre-drying lasts for 40 min at 25°C; the main drying takes 140 min at 45°C, and the final drying lasts 60 min at 30°C.

### Radio frequency drying

Three hundred grams of fresh samples were placed in a plastic container (300 × 220 × 60 mm). This container sat in the center of the RF equipment, which was set to 27.12 MHz and 6 KW (SO6B, Streffield International, Wokingham, UK). The distance between the plates was 110 mm. The heating lasted 120 min, and the heating intensity was 20 W/g. During the heating process, the six-channel optical fiber temperature sensor system (HQ-FTS-D120, Xi'an Haier Technology Co., Ltd., Xi'an, China) was used to measure the sample temperature with an accuracy of ± 0.5 °C. The optical fiber sensor was set at the four corners of the sample surface and the core of the sample.

## Determination of moisture content

During the drying process, the drying curve is measured by weight analysis. The weight was recorded after the sample was removed from the drying chamber. Moisture loss was assessed

at 30 s, 30, and 20 min intervals during MW, HA, and RF drying respectively. The weight change was recorded until the weight difference between the two measurements was less than 0.1 g. Consider this as the termination point. After each drying experiment, the dried noodles were heated at 105°C in a dryer until complete desiccation to calibrate the moisture content, ensuring the accuracy of the experimental data.

The moisture content (1) and drying rate (2) of the sample is calculated as follows:

$$\text{Moisture content} = (M_t - M_d)/M_d \quad (1)$$

$$\text{Drying rate} = \frac{M_{t+dt} - M_t}{dt} \quad (2)$$

$M_t$  and  $M_{t+dt}$  was the mass of material (g) at drying time  $t$  and  $t + dt$ , respectively; and  $M_d$  was the absolute dry mass of the material (g).

## Electron nose analysis

The E-nose analysis was carried out using E-nose equipment with a sensor array system (Airsense Analytics GmbH., Schwerin, Germany). The system is composed of ten metal oxide semiconductors with different chemical compositions and thicknesses. These were used to determine the flavor of the Chinese dried noodles treated by different drying methods. Weighed 3 g sample into a 20 mL headspace bottle. After equilibration at 25°C for 24 h, an electronic nose probe was inserted and the air at the top is sampled. The headspace of the bottle was gradually absorbed and replaced by clean air. The volatile gas was transmitted to the detector at a constant rate for 60 s until the sensor signal reached a stable value. Cleaned the detector with clean air between each sample for 300 s, or until the sensor signal returned to baseline. Each sample was measured at least 10 times.

## Headspace solid phase microextraction-gas chromatography-mass spectrometry

According to the method described by Zhao et al. (17) the HS-GC-MS instrument was used for sample analysis, but with a slight modification. The Chinese dried noodles (2 g) were weighed and put into a 20 mL headspace bottle. Then, added 15 µL of phenyl ethyl acetate as an internal standard (final concentration  $4.09 \times 10^4$  µg/L). Sealed the bottle and allowed an incubation period of 15 min. Afterward, a solid-phase micro-extraction sampler with a carboxen/divinylbenzene/polydimethylsiloxane (CAR/DVB/PDMS) fiber (Supelco Ltd., Pennsylvania, PA, USA) was used to extract the VOCs in the headspace for 20 min at 40°C. The sampler was inserted into the gas chromatograph injector and

thermally desorbed at 250°C for 3 min in split free injection mode. Identification and quantitative analysis were performed using the Gas chromatography-Mass Spectrometer Ultra system (QP2010, Shimadzu, Kyoto, Japan). Used the DB-1 MX capillary column (60 m × 0.25 mm × 0.25 μm) for separation. The injection port temperature was 250°C and the injection occurred in non-shunt mode. Helium (≥99.999%) was used as a carrier gas at a constant flow rate of 1 mL/min. The programmed temperature was set to 40°C for 3 min. Following this period, the temperature increased by 4°C/min to 120°C. Then, the temperature grew by 6°C/min to 240°C, where it held constant for 12 min. The mass spectrum conditions sustained an interface temperature of 280°C. The ion source temperature was 230°C. The full scanning range was  $m/z$  50–500. The names and related information for different volatile chemical components were determined by searching the mass spectrometry computer data system and matching the standard mass spectrometry database. The retention indices of each initially characterized substance were used and compared to the retention indices of the corresponding substances reported in the literature for further characterization. The expected concentration of each chemical component was obtained by the internal standard method.

## Headspace-gas chromatography-ion mobility spectrometry

Based on Guo et al. (22) the Agilent 490 Gas chromatograph (Agilent Technologies, Palo Alto, CA, USA) and IMS instrument (FlavourSpec®, Gesellschaft für Analytische Sensorsysteme mbH, Dortmund, Germany) were used for sample analysis, but with slight modification. Noodles (2.0 g) were placed in a 20 mL headspace glass sampling bottle. Then added 15 μL phenylethyl acetate as an internal standard (final concentration  $4.09 \times 10^4$  μg/L). Subsequently, these samples were incubated at 60°C for 15 min. After incubation, the automatic injection device (CTC Analytics AG, Zwingen, Switzerland) injected 500 μL of top air into the syringe (85°C, no shunt mode). Then, the sample was driven into the MTX-5 capillary column (15 m × 0.53 mm) with a nitrogen flow (≥99.999%) under isothermal conditions of 60°C. IMS instrument was used to complete the analysis. The % samples followed a standard progression: 2 mL/min for 2 min; 10 mL/min for 8 min; 100 mL/min for 10 min; 100 mL/min for 5 min. The flow of bleaching gas (nitrogen) in the bleaching pipe was 150 mL/min. All analyses were repeated 3 times. VOCs were identified by comparing RI and the standard drift time (the time in milliseconds taken for ions to reach the collector through the drift tube) in the GC-IMS library.

## Data analysis

The obtained data were analyzed by Excel (version 2016, Microsoft, Redmond, WA, USA), and the charts were drawn

by Origin software (version 2019b, Microcal Inc., Massachusetts, MA, USA). The E-nose data were processed by E-nose software (Winmuster 1.6.2.5, Aisense Analytics GmbH, Schwerin, Germany). GC-MS and GC-IMS used the built-in software database to determine the names and relevant information of different volatile chemical components.

## Results and discussion

### Moisture content

Results showed that the total drying times of MW, HA, and RF were 4, 240, and 120 min, respectively (Figure 1). HA drying could be divided into three stages: pre-drying, main, and final. Pre-drying evaporates part of the water on the surface of wet noodles in order to fix the tissues and avoid the noodles' deformation. The main drying stage had the highest drying temperature and removed moisture from the noodles quickly. This stage allowed for the rapid removal of moisture from the surface of the noodles. If the drying rate is too rapid, the surface of the wet noodles will shrink, rendering the noodles dry outside and wet inside. The main function of the final drying stage was to balance the differences in moisture and temperature inside and outside of the noodles and to eliminate the various internal stresses caused by the drying and shrinking of the noodles.

The drying rate of dielectric drying methods (MW and RF) was significantly higher than that of HA drying. This was due to different energy transfer modes. For HA drying, external heat flux was applied to the product surface, resulting in slow heat penetration from the product surface to the interior. MW and RF drying caused the internal and surface temperature of the material to rise rapidly and synchronously (23). Therefore, the drying rate of MW and RF was significantly higher than that of HA drying. The frequency of MW was higher than that of RF, which means MW exhibits a greater heating rate. Among all drying methods under the same heating intensity, MW drying had the highest drying rate.

The moisture content of Chinese dried noodles in all drying methods gradually decreased as the drying process. The lack of a constant drying period in all methods was probably due to the low thickness of the Chinese dried noodles not providing a constant amount of moisture, indicating that the drying process is mainly controlled by the diffusion of moisture. With advanced and efficient drying technology, MW and RF, especially MW, could shorten the drying time by 98% compared to HA.

### E-nose analysis

E-nose analysis reported the real-time response value of each sensor, which changes gradually with time. The responses of 10 sensors to these samples showed different characteristics. According to Figure 2, drying changed the content and types of VOCs in fresh noodles. Most of the sensors for fresh

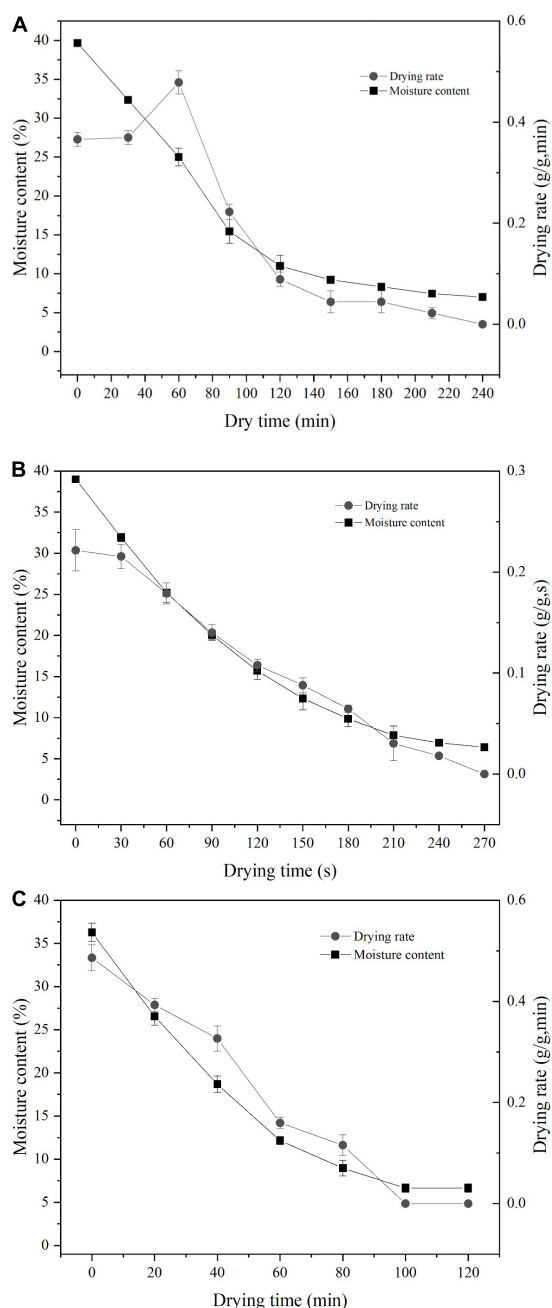


**FIGURE 1**  
Effects of different drying methods on noodle drying curve and drying rate curve. (A) HA, (B) MW, and (C) RF.

noodles seem to display stronger signals than they do for dried noodles, indicating that the smell of fresh noodles is the most complex. For dried noodles, W1W (mainly sensitive to terpene compounds) and W1S (broad range-methane) had the highest response values. Comparing noodles dried by different methods, the signal difference between W1W and W1S sensors was the strongest. This suggested that the differences in basic noodle

flavor mainly come from inorganic sulfides, alcohols, aldehydes, and ketones. During the drying process, the Maillard reaction between sugars, proteins, and amino acids continues, resulting in a large number of heterocyclic compounds, such as furans. These compounds enhanced the signal of W1C (aromatic ring, benzene) and affected the flavor of noodles, giving dry noodles a burnt flavor and sweetness.

In order to evaluate the difference of VOCs in each sample, the E-nose response data set was analyzed by principal component analysis (PCA) (**Figure 2B**). The spatial regions of these samples showed that the flavor of fresh and dried noodles varied in significant ways. The cumulative contribution rate of the first two principal components accounted for 95.2% of the total variance, indicating that these alone were sufficient to reflect the original multi-index information. Principal factor 1 (PC1) explained 80.3% of the variance in the data, and principal factor 2 (PC2) explained 14.9% of the variance. HA and RF dried noodles data were located in the negative region of PC1. According to the **Figure 2B**, W3C (mainly sensitive to aromatic ammonia), W5C (mainly sensitive to an alkane, aromatics, and small polar compounds), and W1C sensors were distributed in the negative region of PC1, which indicates that aromatic compounds contributed more to HA dried noodles and RF dried noodles than other types of VOCs. Fresh noodles and MW dried noodles were located in the positive area of PC1. W5S (mainly sensitive to nitrous oxides), W6S (mainly sensitive to hydrocarbons), W5C (mainly sensitive to an alkane, aromatics, and small polar compounds), W1S, W1W, W2S (mainly sensitive to most alcohols, aldehydes, and ketones), W2W (mainly sensitive to aromatics and organic sulfides) and W3S (mainly sensitive to long-chain alkanes) sensors were distributed in the positive area of PC1. Fresh noodles and MW dried samples contained more sulfur compounds, broad-spectrum methyl compounds (aldehydes, ketones), and broad-spectrum alcohols, indicating that MW has the best flavor retention. This finding was consistent with the results of radar map generation. The E-nose response results highlighted the great flavor differences between samples that experienced different drying methods. But this method was limited in its ability to identify specific compounds that affect characteristic flavor. Volatiles and aromatic active compounds needed to be further studied to determine the impact of each drying method on key aromatic compounds—which ultimately result in flavor variations.

## Chromatography-mass spectrometry analysis

The composition and content of the VOCs formed under different drying regimes were measured using HS-SPME-GC-MS. According to the retention index, retention time, and mass spectral data of standard compounds and the MS library,

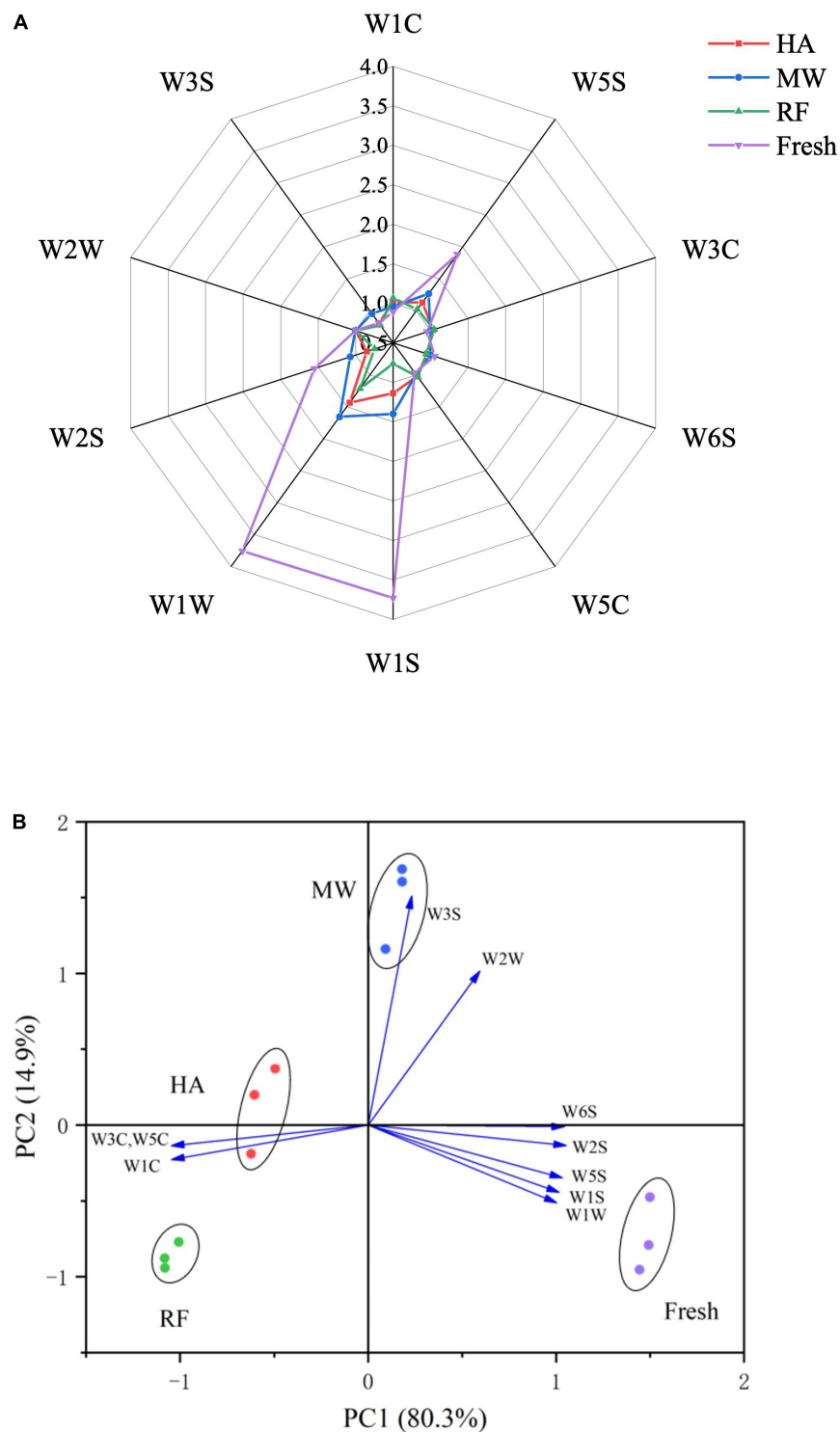


FIGURE 2

E-nose analysis. (A) Radar map of fresh and dried noodles. (B) Principal component analysis of fresh noodles and dry noodles.

a total of 47 VOCs were identified in fresh noodles and noodles dried by three methods (Table 1). These VOCs could be divided into seven categories: 11 kinds of aldehydes, 8

kinds of alcohols, 7 kinds of ketones, 4 kinds of esters, 10 kinds of hydrocarbons, 6 kinds of acids, and 1 kind of furan. The main composition of wheat noodles was consistent



TABLE 1 Comparisons of the detected VOCs in fresh and Chinese dried noodles by HS-SPME-GC-MS.

No	Compounds name	CAS	Formula	Molecular weight	RI	Estimated concentration (µg/kg fresh noodles)			
						Fresh	MW	HA	RF
Aldehydes									
1	Acetaldehyde	75-07-0	C <sub>2</sub> H <sub>4</sub> O	44.05	408	7.49	–	–	–
2	Paraldehyde	513-86-0	C <sub>6</sub> H <sub>12</sub> O <sub>3</sub>	132.16	717	14.89	–	–	–
3	Hexanal	66-25-1	C <sub>6</sub> H <sub>12</sub> O	100.16	806	79.14	1579.21	1230.81	247.12
4	Pentanal	110-62-3	C <sub>5</sub> H <sub>10</sub> O	86.13	707	3.83	169.70	–	–
5	Heptaldehyde	111-71-7	C <sub>7</sub> H <sub>14</sub> O	114.19	905	–	–	–	10.27
6	1-Nonanal	124-19-6	C <sub>9</sub> H <sub>18</sub> O	142.24	1104	–	329.56	263.93	107.19
7	(2E)-2-Nonenal	18829-56-6	C <sub>9</sub> H <sub>16</sub> O	140.22	1112	6.55	–	196.99	102.28
8	4-Octadecenal	56554-98-4	C <sub>18</sub> H <sub>34</sub> O	266.46	1766	–	45.21	–	–
9	Decanal	112-31-2	C <sub>10</sub> H <sub>20</sub> O	156.27	1204	9.13	263.29	149.63	80.10
10	Pentadecanal	2765-11-9	C <sub>15</sub> H <sub>30</sub> O	226.40	1701	5.37	–	–	8.86
11	(Z)-Hexadec-9-enal	56219-04-6	C <sub>16</sub> H <sub>30</sub> O	238.41	1808	–	–	–	7.37
Alcohols									
12	Ethanol	64-17-5	C <sub>2</sub> H <sub>6</sub> O	46.07	463	29.25	439.94	439.35	312.43
13	1-Penten-3-ol	616-25-1	C <sub>5</sub> H <sub>10</sub> O	86.13	671	16.91	–	–	–
14	1-Pentanol	71-41-0	C <sub>5</sub> H <sub>12</sub> O	88.15	761	154.31	411.35	69.46	–
15	1-Hexanol	111-27-3	C <sub>6</sub> H <sub>14</sub> O	102.17	860	380.64	200.72	–	–
16	2-Hydroxycineole	18679-48-6	C <sub>10</sub> H <sub>18</sub> O <sub>2</sub>	170.25	1247	8.92	84.03	38.51	12.80
17	1-Octen-3-ol	3391-86-4	C <sub>8</sub> H <sub>16</sub> O	128.21	969	45.54	–	–	–
18	3,5-Octadien-2-ol	69668-82-2	C <sub>8</sub> H <sub>14</sub> O	126.2	1385	42.85	–	–	–
19	Phenethyl-1-alcohol	60-12-8	C <sub>8</sub> H <sub>10</sub> O	122.16	1934	9.18	–	–	–
Ketones									
20	5-Methyl-2-hexanone	110-12-3	C <sub>7</sub> H <sub>14</sub> O	114.19	789	–	171.65	80.60	53.74
21	2-Heptanone	110-43-0	C <sub>7</sub> H <sub>14</sub> O	114.19	853	27.76	–	–	–
22	3-Methyl-3-buten-2-one	814-78-8	C <sub>5</sub> H <sub>8</sub> O	84.12	797	25.34	–	–	–
23	2-Methyl-4-heptanon	626-33-5	C <sub>8</sub> H <sub>16</sub> O	128.21	888	–	454.70	113.58	–
24	2-Octanone	111-13-7	C <sub>8</sub> H <sub>16</sub> O	128.21	952	5.14	–	–	–
25	Geranylacetone	3796-70-1	C <sub>13</sub> H <sub>22</sub> O	194.31	1420	–	88.71	18.04	30.30
26	3,5-Octadiene-2-one	38284-27-4	C <sub>8</sub> H <sub>12</sub> O	124.18	968	6.81	–	–	–
Esters									
27	2-Amino-propionic acid ethyl ester	17344-99-9	C <sub>5</sub> H <sub>11</sub> NO <sub>2</sub>	117.15	1097	282.15	416.62	148.56	60.13
28	Isobutyl formate	542-55-2	C <sub>5</sub> H <sub>10</sub> O <sub>2</sub>	102.13	718	–	1491.38	–	–
29	(E)-2-Hexenyl hexanoate	53398-86-0	C <sub>12</sub> H <sub>22</sub> O <sub>2</sub>	198.30	1389	7.66	–	–	–
30	Dibutyl phthalate	84-74-2	C <sub>16</sub> H <sub>22</sub> O <sub>4</sub>	278.34	2037	13.54	175.44	–	24.41
Hydrocarbons									
31	Pentane	109-66-0	C <sub>5</sub> H <sub>12</sub>	72.15	518	479.35	5319.61	–	–
32	2-Methylpentane	107-83-5	C <sub>6</sub> H <sub>14</sub>	86.18	554	5.25	115.05	–	9.25
33	3-Methylpentane	96-14-0	C <sub>6</sub> H <sub>14</sub>	86.18	554	37.79	52.11	35.64	6.59
34	Hexane	110-54-3	C <sub>6</sub> H <sub>14</sub>	86.18	618	–	–	431.55	125.22
35	Heneicosane	629-94-7	C <sub>21</sub> H <sub>44</sub>	296.57	2109	11.39	63.47	–	–
36	Eicosane	112-95-8	C <sub>20</sub> H <sub>42</sub>	282.55	2008	–	–	11.96	6.25
37	Hentriacontanone	630-04-6	C <sub>31</sub> H <sub>64</sub>	436.84	3103	7.11	–	9.72	–
38	Dodecane	112-40-3	C <sub>12</sub> H <sub>26</sub>	170.33	1214	9.23	70.24	–	–
39	Tetradecane	629-59-4	C <sub>14</sub> H <sub>30</sub>	198.39	1413	7.81	61.95	46.77	–
40	Dipentene	5989-27-5	C <sub>10</sub> H <sub>16</sub>	136.23	1018	14.40	60.69	21.92	–
Acids									
41	Hexanoic acid	142-62-1	C <sub>6</sub> H <sub>12</sub> O <sub>2</sub>	116.16	974	34.99	72.94	49.29	24.36
42	Acetic acid	64-19-7	C <sub>2</sub> H <sub>4</sub> O <sub>2</sub>	60.05	576	–	–	102.01	17.00
43	Octanoic acid	124-07-2	C <sub>8</sub> H <sub>16</sub> O <sub>2</sub>	144.21	1173	–	46.50	–	5.16
44	Nonanoic acid	112-05-0	C <sub>9</sub> H <sub>18</sub> O <sub>2</sub>	158.24	1272	–	41.94	14.59	5.89
45	Decanoic acid	112-37-8	C <sub>10</sub> H <sub>20</sub> O <sub>2</sub>	172.26	1471	–	–	19.51	–
46	Tridecanlic acid	638-53-9	C <sub>13</sub> H <sub>26</sub> O <sub>2</sub>	214.34	1681	–	–	–	9.90
Furan									
47	2-Pentylfuran	3777-69-3	C <sub>9</sub> H <sub>14</sub> O	138.21	1040	10.18	81.12	21.99	11.93

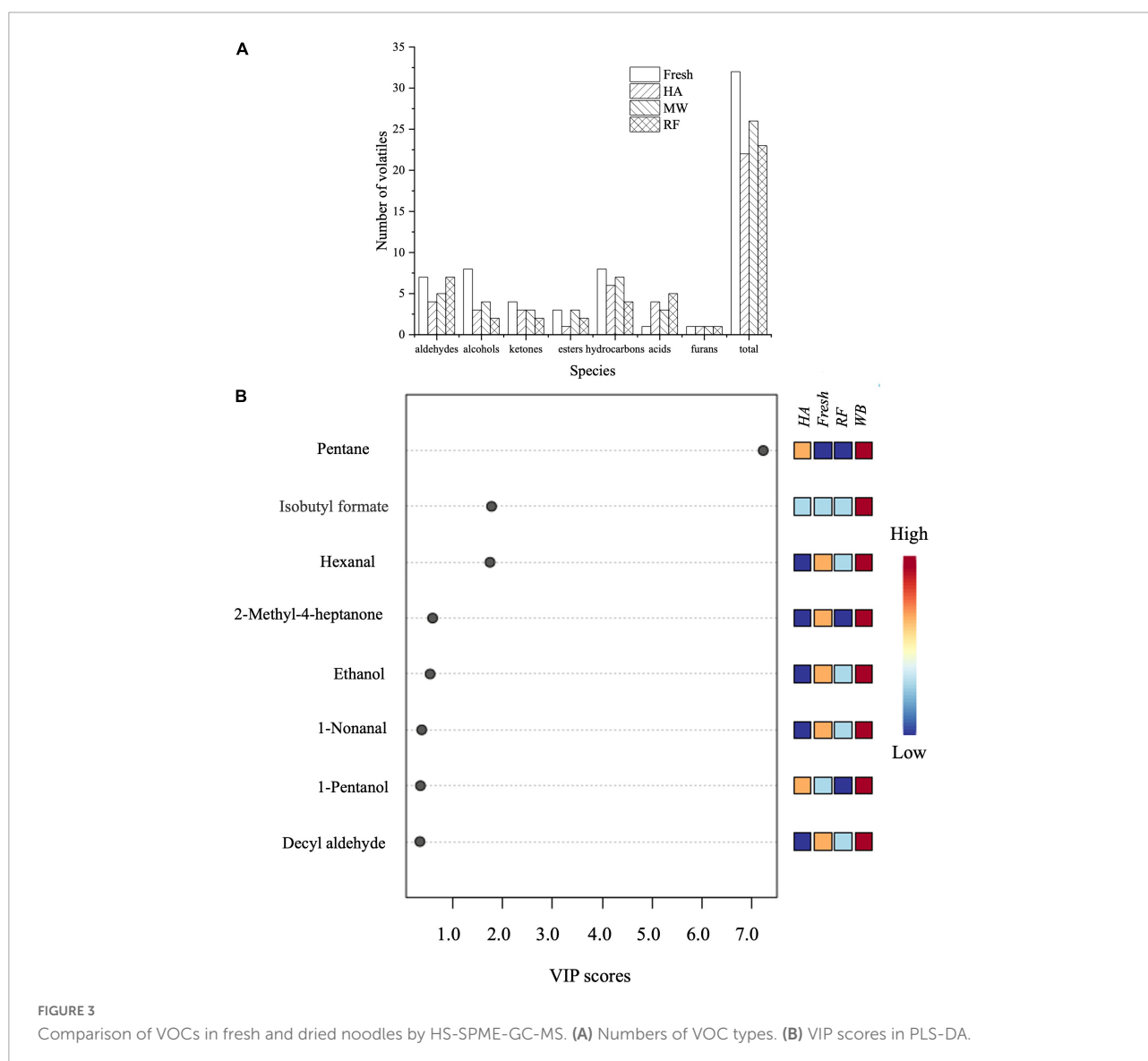
MW, microwave dried noodles; HA, hot air dried noodles; RF, radio frequency dried noodles.

with a previous study on the VOCs analysis of noodles (24).

The quantity of VOCs in fresh noodles differs from VOCs in dried noodles (Figure 3). There were 32 kinds of VOCs in fresh noodles (including three esters, seven aldehydes, eight alcohols, four ketones, eight hydrocarbons, one acid, and one furan). There were 22 VOCs in HA dried noodles, including one ester, four aldehydes, three alcohols, three ketones, six hydrocarbons, four acids, and one furan. MW dried noodles contained 26 VOCs, including three esters, five aldehydes, four alcohols, three ketones, seven hydrocarbons, three acids, and one furan. RF dried noodles contained 23 kinds of VOCs, including two esters, seven aldehydes, two alcohols, two ketones, four hydrocarbons, five acids, and one furan. Data showed that the type of drying treatment significantly altered the types of VOCs in noodles. Acids increased after HA, MW, and RF drying. The variety

of furan did not change after drying but their concentration increased. All other substances showed a decreasing trend in species after drying. In addition, some substances disappeared completely after drying by different methods (e.g., acetaldehyde and paraldehyde). This suggests that drying can effectively eliminate the grassy odor present in fresh noodles. Nonanal, moreover, can only be detected after drying. Nonanal added a pleasant floral and fruity fragrance to the noodles and made the dried noodles more flavorful.

Using the PLS-DA, which provided a value for VIP, a total of 8 differential marker flavor substances were selected from 60 volatile substances. These substances might be what caused the significant flavor difference between differently dried noodles. As shown in Figure 3B, among these eight VOCs, there were three aldehydes (hexanal, 1-nonanal, and decyl aldehyde), one ester (isobutyl formate), two hydrocarbons



(2-methyl-4-heptanon, and pentane), and two alcohols (ethanol, and 1-pentanol). Consistent with the results of Zhang et al. (25), changes in aldehydes during drying had a great impact on flavor. The lipoxygenase oxidation of unsaturated fatty acids by lipoxygenase was a major pathway for the formation of aldehydes (26). Minimal increase in aldehydes after RF drying of fresh noodles. Probably because the maximum temperature of RF drying was 90°C and lipoxygenase was inactivated at 80 and 90°C for holding times above 3 min (27), thus inhibiting the production of aldehydes.

Esters also contributed to a large extent to the noodles. The content of ester compounds produced during MW drying was higher than the content produced in HA and RF drying. It is noteworthy that isobutyl formate, which produces a fruity flavor, was detected in the MW dried noodles and was not detected in any of the other noodle samples. Generally, esters were one of the degradation products of unsaturated fatty acids that occur late in the oxidation process (28). Most of the esters formed by short chain acids provided a fruity flavor. Esters formed by long chain acids offered a light greasy flavor. Unlike MW, HA drying significantly reduced the content of esters detected, and no new esters were formed. In addition, alcohol compounds revealed an inverse trend with drying. Drying significantly reduced the type and content of alcohol substances. These substances played an auxiliary role in the overall flavor composition of Chinese dried noodles. Compared with other kinds of compounds, hydrocarbon compounds did not alter significantly between fresh and dried noodles. Hydrocarbon compounds provide a limited contribution to the flavor quality of the noodles.

Changes in flavor substances were caused by lipid degradation and oxidation, Maillard reactions, and enzymatic reactions (29). Aldehydes, alcohols, and esters were the main VOCs that create noodle flavor differences. A comparison of flavor substances across the drying methods revealed that the aroma of MW dried noodles was the strongest. Different drying methods had different water loss rates. In addition, drying process time and temperature affect flavor variation. High temperature inhibited the oxidative decomposition of unsaturated fatty acids and affected the formation of aldehydes (30). The MW method took only 4 min, less than 2% of the HA drying time. This was relevant as long exposure to heat treatment adversely impacts noodle flavor.

## Chromatography-ion mobility spectrometry analysis

### Identification of volatile organic compounds by chromatography-ion mobility spectrometry

Volatile organic compounds in fresh and dried noodles were analyzed by HS-GC-IMS. HS-GC-IMS and HS-SPME-GC-MS exhibited different VOCs identification capabilities. Chen et al. (31) proved that HS-SPME-GC-MS was more sensitive to

pyrazines, while HS-GC-IMS measured aldehydes and ketones more accurately. Using topographic map derivation, created a difference map to identify VOCs changes. Each point area showed a different retention time (*y*-axis), relative drift time (*x*-axis), and signal strength. The redder the area, the greater the signal strength. The bluer the area, the smaller the signal strength (Figure 4). Based on the National Institute of Standards and Technology library, VOCs were identified by comparing the corresponding retention index and drift time.

After the noodles dry, most of the red signals appeared in the retention time range below 200 s, and the drift time is 1.0–1.5. The results showed that a large number of VOCs were formed during drying. Considering that signal separation was mainly related to polarity—and the retention time of polar compounds is concentrated in the range of 100–200 s—this result indicated that drying may contribute to the formation of polar compounds. In addition, RF dried noodles samples displayed a blue signal in the 100–400 s, which was significantly higher than MW drying and HA drying. RF samples displayed a red signal lower than that of MW and HA samples. This showed that RF drying had the worst flavor retention of the three drying methods, a finding which is consistent with the results of GC-MS.

Head space-gas chromatography-ion mobility spectrometry detected 51 areas, 40 of which were identified; the other 11 areas were not confirmed. It was worth noting that 14 chemicals existed in the form of monomers and dimers [heptanal, 1-pentanol, 2-butanone, 2-methyl-butanal, 2-methylbutanol, (*E*)-2-pentenal, (*E*)-2-heptenal, 2-hexenal, 3-methyl-butanal, ethyl acetate, hexanal, *n*-hexanol, *n*-nonanal and pentanal]. Twenty-six kinds of VOCs were identified in both fresh and dried noodles (Table 2). These included 6 alcohols, 13 aldehydes, 3 ketones, 2 esters, and 1 compound containing sulfur. It should be noted that the content of VOCs in dimer form is often lower than that of monomer form, indicating that the stability of the dimer form is inferior to that of monomer form. It could be that the dissociation transition of dimer monomer was more likely to occur than the degradation of monomer during the drying process (32).

### Comparison of volatile organic compounds fingerprints of samples

The complete VOCs of the fresh and dried noodles in three different ways could be obtained by fingerprint and VOCs differences could be compared intuitively and quantitatively. It could be seen from Figure 4B that the main VOCs flavor substance of fresh noodles are concentrated in region A. These VOCs were used to distinguish the flavor differences between samples. Main substances included five alcohols (1-penten-3-ol, 2-butanol, *n*-hexanol, 2-methylbutanol and 1-pentanol) and five aldehydes ((*E*)-2-heptenal, (*E*)-2-pentena, (*E*)-2-octenal, phenylacetaldehyde and heptanal). Shahidi et al. (33) pointed out that most alcohols, except ethanol, were the result of lipid

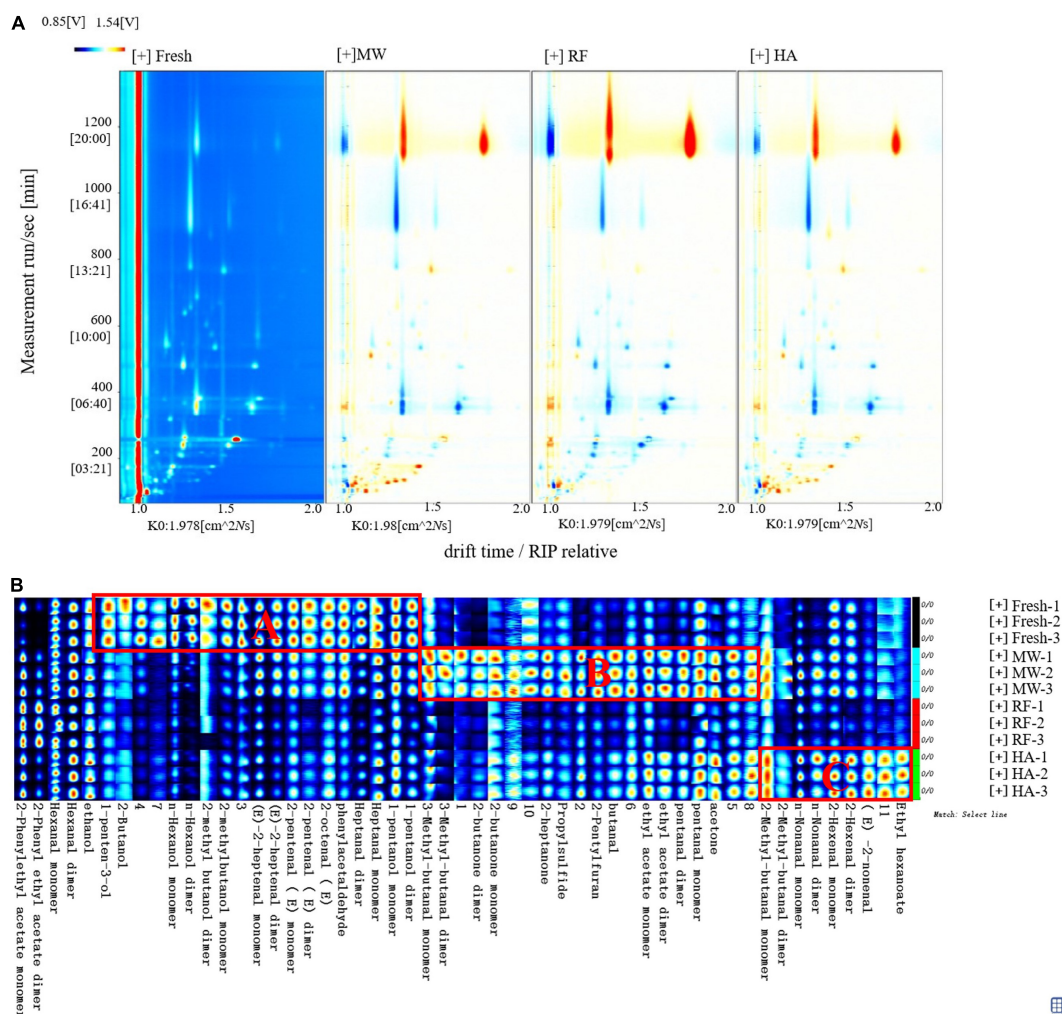


FIGURE 4

Comparison of VOCs in fresh and dried noodles by GC-IMS. (A) Topographic plots of Noodle drying. (B) The fingerprint of volatile organic compounds in fresh and dried noodles.

oxidation. Unsaturated alcohol was one of the main flavor substances in cereal products, which had been detected in dried noodles. However, alcohol compounds had less effect on the taste of noodles than aldehydes and had a synergistic effect on the overall taste of noodles. The main formation pathway of aldehydes was the oxidative decomposition of unsaturated fatty acids (e.g., oleic acid, linoleic acid, and linolenic acid) by hydroperoxide isomerase and lipoxygenase. Some aldehydes were also produced by the oxidative degradation of esters. The detection concentration of aldehydes was high, which will produce a pleasant smell, such as grass and fruit. Similar to the results of Li et al. (34), aldehydes contributed greatly to noodle flavor, more so than other compounds do; aldehydes were likely the main flavor contributor in noodles.

Different drying methods highlighted differences in alcohols, aldehydes, and ketones. Similar VOCs were found

in MW and HA dried samples. The substances in area C can represent VOCs that were characteristic of HA dried noodles. These substances included four aldehydes [2-methylbutyraldehyde, nonanal, hexanal, and (E)-2-nonenal] and one ester (ethyl caproate). Compared with fresh noodles, HA dried noodles possessed a less significant amount of alcohol, which was lost due to vaporization during the drying process (35). The structure of enols was generally unstable and easy to isomerize into stable carbonyl compounds (36), which changed the types of aldehydes present during HA drying. Aldehydes had high reactivity, which was one of the reasons for the volatile flavor during drying. During HA drying, short chain lower aldehydes are transformed into higher fatty aldehydes above C8. These fatty aldehydes have a stronger aroma of oil, nuts, grass, and fruit (37). In dried noodles, certain kinds of aldehydes increased significantly, which was consistent with the results

TABLE 2 Head space-gas chromatography-ion mobility spectrometry integration parameters of volatile compounds in fresh and Chinese dried noodles.

No.	Compound	CAS	Formula	Molecular weight	RI	Rt[sec]	Dt[RIP rel]	Peak volume (a. u.)			
								Fresh	MW	HA	RF
Aldehydes											
1	Butanal	123-72-8	C <sub>4</sub> H <sub>8</sub> O	72.10	590.40	133.81	1.29	154.21	635.13	388.12	116.25
2	3-Methyl-butanal monomer	590-86-3	C <sub>5</sub> H <sub>10</sub> O	86.10	645.40	157.84	1.17	1195.75	1754.21	938.56	682.47
3	3-Methyl-butanal dimer	590-86-3	C <sub>5</sub> H <sub>10</sub> O	86.10	646.00	158.11	1.40	147.94	528.09	114.22	58.42
4	2-Methyl-butanal monomer	96-17-3	C <sub>5</sub> H <sub>10</sub> O	86.10	668.30	167.83	1.18	415.22	627.82	637.94	496.59
5	2-Methyl-butanal dimer	96-17-3	C <sub>5</sub> H <sub>10</sub> O	86.10	666.40	167.02	1.38	76.85	211.79	182.63	84.66
6	Pentanal monomer	110-62-3	C <sub>5</sub> H <sub>10</sub> O	86.10	691.40	178.90	1.19	1366.84	1838.61	1686.40	1143.18
7	Pentanal dimer	110-62-3	C <sub>5</sub> H <sub>10</sub> O	86.10	690.00	177.82	1.42	680.70	1878.67	1186.09	294.06
8	(E)-2-Pentenal monomer	1576-87-0	C <sub>5</sub> H <sub>8</sub> O	84.10	744.10	221.02	1.10	492.27	426.12	338.76	215.81
9	(E)-2-pentenal dimer	1576-87-0	C <sub>5</sub> H <sub>8</sub> O	84.10	743.50	220.50	1.36	113.01	62.45	49.66	19.62
10	Hexanal monomer	66-25-1	C <sub>6</sub> H <sub>12</sub> O	100.20	789.00	258.25	1.26	3307.85	3120.62	3029.02	3152.21
11	Hexanal dimer	66-25-1	C <sub>6</sub> H <sub>12</sub> O	100.20	789.00	258.25	1.56	7939.69	9223.81	9274.95	5084.26
12	2-Hexenal monomer	505-57-7	C <sub>6</sub> H <sub>10</sub> O	98.10	845.00	320.01	1.18	628.45	623.39	696.85	333.35
13	2-Hexenal dimer	505-57-7	C <sub>6</sub> H <sub>10</sub> O	98.10	843.10	317.85	1.51	128.01	130.11	168.72	51.51
14	Heptanal monomer	111-71-7	C <sub>7</sub> H <sub>14</sub> O	114.20	898.90	383.95	1.34	2336.14	1726.92	1539.99	902.74
15	Heptanal dimer	111-71-7	C <sub>7</sub> H <sub>14</sub> O	114.20	897.10	380.70	1.68	1349.68	764.49	614.27	175.68
16	(E)-2-Heptenal monomer	18829-55-5	C <sub>7</sub> H <sub>12</sub> O	112.20	954.50	482.69	1.25	2762.68	2754.50	1903.04	1457.92
17	(E)-2-Heptenal dimer	18829-55-5	C <sub>7</sub> H <sub>12</sub> O	112.20	953.10	480.05	1.66	1169.65	980.76	502.38	234.51
18	<i>n</i> -Nonanal monomer	124-19-6	C <sub>9</sub> H <sub>18</sub> O	142.20	1105.10	768.70	1.48	1370.32	2848.27	3365.48	2498.12
19	<i>n</i> -Nonanal dimer	124-19-6	C <sub>9</sub> H <sub>18</sub> O	142.20	1105.40	769.36	1.94	103.90	328.02	464.48	247.60
20	Phenylacetaldehyde	122-78-1	C <sub>8</sub> H <sub>8</sub> O	120.20	1039.00	639.90	1.26	431.94	438.08	230.48	205.82
21	(E)-2-octenal	2548-87-0	C <sub>8</sub> H <sub>14</sub> O	126.20	1064.70	690.10	1.33	492.29	390.20	380.40	264.10
22	(E) -2-nonenal	18829-56-6	C <sub>9</sub> H <sub>16</sub> O	140.20	1161.00	877.60	1.40	239.30	347.66	642.96	268.71
Alcohols											
23	Ethanol	64-17-5	C <sub>2</sub> H <sub>6</sub> O	46.10	513.10	100.06	1.05	4890.46	4400.35	5114.11	4273.30
24	2-Butanol	78-92-2	C <sub>4</sub> H <sub>10</sub> O	74.10	590.70	133.94	1.15	340.68	129.59	129.96	90.07
25	1-Penten-3-ol	616-25-1	C <sub>5</sub> H <sub>10</sub> O	86.10	685.00	175.12	0.94	719.18	411.18	375.57	283.77
26	2-Methylbutanol monomer	137-32-6	C <sub>5</sub> H <sub>12</sub> O	88.10	733.30	212.38	1.24	1345.37	536.44	604.16	303.66
27	2-Methyl butanol dimer	137-32-6	C <sub>5</sub> H <sub>12</sub> O	88.10	732.30	211.57	1.48	234.51	109.16	132.78	115.12
28	1-Pentanol monomer	71-41-0	C <sub>5</sub> H <sub>12</sub> O	88.10	769.10	240.91	1.25	2664.65	2232.20	2174.30	1471.84
29	1-Pentanol dimer	71-41-0	C <sub>5</sub> H <sub>12</sub> O	88.10	767.70	239.82	1.51	1942.41	1299.55	1044.89	418.53
30	<i>n</i> -Hexanol monomer	111-27-3	C <sub>6</sub> H <sub>14</sub> O	102.20	873.90	351.80	1.33	5152.66	3858.82	2780.85	2074.24
31	<i>n</i> -Hexanol dimer	111-27-3	C <sub>6</sub> H <sub>14</sub> O	102.20	877.80	356.14	1.64	3317.66	1421.44	902.39	396.66
Ketones											
32	Acetone	67-64-1	C <sub>3</sub> H <sub>6</sub> O	58.10	519.30	102.76	1.12	855.15	1631.75	1879.06	699.04
33	2-Butanone monomer	78-93-3	C <sub>4</sub> H <sub>8</sub> O	72.10	578.00	128.41	1.07	583.94	1101.97	820.49	634.48
34	2-Butanone dimer	78-93-3	C <sub>4</sub> H <sub>8</sub> O	72.10	582.30	130.30	1.24	91.71	579.76	244.76	87.60
35	2-Heptanone	110-43-0	C <sub>7</sub> H <sub>14</sub> O	114.20	889.00	368.42	1.26	260.18	747.61	506.66	245.34
Esters											
36	Ethyl acetate monomer	141-78-6	C <sub>4</sub> H <sub>8</sub> O <sub>2</sub>	88.10	597.20	136.78	1.10	696.06	1132.11	1108.32	744.64
37	Ethyl acetate dimer	141-78-6	C <sub>4</sub> H <sub>8</sub> O <sub>2</sub>	88.10	596.60	136.51	1.33	204.00	634.49	583.87	132.23
38	Ethyl hexanoate	123-66-0	C <sub>8</sub> H <sub>16</sub> O <sub>2</sub>	144.20	999.00	561.96	1.34	187.27	136.78	334.07	133.00
Furan											
39	2-Pentylfuran	3777-69-3	C <sub>9</sub> H <sub>14</sub> O	138.20	991.00	547.42	1.25	122.66	294.23	158.84	95.68
Ether											
40	Propylsulfide	111-47-7	C <sub>6</sub> H <sub>14</sub> S	118.20	895.30	377.43	1.15	135.72	206.52	151.46	96.99

RI, the retention index; Rt, the retention time; Dt, the drift time; MW, microwave dried noodles; HA, hot air dried noodles; RF, radio frequency dried noodles.



of GC-MS. Esters are an important component of VOCs and are the main carrier of odor (38). Ester compounds are mainly formed through the esterification of alcohols and fatty acids. HA drying produced ethyl caproate, which added a strong aroma of liquor and pineapple to the noodles (39).

Of the three drying methods, MW retained the most amounts of VOCs present in fresh noodles. The substances in area B were used to represent the characteristic VOCs of MW dried noodles. These substances included three aldehydes (3-methylbutyraldehyde, butyraldehyde, and glutaraldehyde), three ketones (2-butanone, 2-heptanone, and acetone), one ether (propylene sulfide), one heterocyclic compound (2-pentylfuran), and one ester (ethyl acetate). Noodles aroma was informed largely by aldehydes (40). Compared with fresh noodles, MW noodles contained fewer types of alcohol and aldehyde, but, in general, the types of VOCs in MW dried noodles were more abundant than in fresh noodles. Ketones, ethers, and heterocyclic compounds were the characteristic substances of MW dried noodles. The main formation pathways of ketones are the oxidation of fatty acids, the oxidation of alcohols, and the decomposition of esters (41). The ketone compounds detected in MW dried noodles mostly contributed to a fruit flavor. Heterocyclic compounds are a series of products, intermediates, and derivatives of the Maillard reaction, caramelization reaction, and Strecker degradation reaction. Some intermediates of the Maillard reaction further degrade with lipids to form a series of derived compounds, such as 2-*n*-pentyl furan. Heterocyclic compounds create a roasting aroma (42). They were the main compounds that form the wheat aroma of wheat products. Even in small amounts, sulfur compounds often produce very strong aromas; propyl sulfide was one of the main flavor contributors to MW dried noodles, adding an ether flavor.

Radio frequency dried noodles had fewer kinds and lower concentrations of VOCs, suggesting that RF drying VOCs retention was inferior to MW and HA drying. The fruit flavor ketones (acetone, 2-butanone) detected in MW dried noodles were also produced by RF drying, but the threshold of the ketones was high and their flavor contribution was limited. Wang et al. (43) found that RF dried strawberries better retained color and nutrients (e.g., carotenoids, anthocyanins, and total phenols), but poorly retained flavor, a finding which matches our own. Most fresh noodles' characteristic VOCs were decreased or went undetected following RF drying. RF drying also changed short chain lower aldehydes into long chain higher fatty aldehydes [(*E*)-2-nonanal and nonanal], but to a far less than HA drying. During RF drying, when the local temperature of the sample exceeded 80°C, the activities of enzymes such as lipoxygenase decreased significantly (44), a state which is not conducive to aldehyde formation. This may contribute to the poor flavor retention of RF. In addition, in the RF drying process, noodles samples were exposed to high temperatures for an extended period. Exposure time impacted the degree of

thermal damage during food heating and drying. Although the high temperature is conducive to the Maillard reaction, it also promotes the volatilization of substances with a boiling point of 50–80°C (e.g., acetone and 2-pentylfuran). This contributed to the low detection of flavor substances in RF noodles. Dielectric heating results in rapid energy coupling with food moisture and leads to fast heating and drying. Hemis et al. (45) studied the effect of MW drying on wheat drying kinetics. The results showed that product quality increases with the decrease in drying time. Therefore, inferred that the poor retention of flavor substances by RF drying compared with MW drying may be due to the significant increase in drying time. With these factors in mind, MW drying may be the best drying method to optimize noodle flavor.

## Conclusion

The results showed that the drying efficiency of dielectric drying methods (MW and RF) significantly exceeded that of HA drying. The E-nose, HS-SPME-GC-MS, and HS-GC-IMS technologies were used to qualitatively and quantitatively analyze fresh and dried noodles (MW, RF, and HA), and the effects of these drying methods on the flavor of dried noodles were determined and discussed. The results of E-nose showed that the basic flavor differences of noodles mainly came from inorganic sulfides, alcohols, aldehydes, and ketones. HS-SPME-GC-MS and HS-GC-IMS identified 47 and 26 VOCs in various noodle samples, respectively. The results showed that fresh noodles and noodles dried by HA, MW, and RF had different aroma characteristics, and the three types of drying methods had a significant effect on the aroma characteristics of noodles. MW drying best retained these critical flavor substances, while RF drying resulted in lower concentrations of VOCs. Considering flavor retention, drying efficiency, and production capacity, MW drying is the appropriate drying method. There remains a lack of research on the effects of different drying methods on noodle flavor. The results provide a useful basis for the aroma quality analysis of noodles. The effect of MW and RF on the texture and structure of noodles needs to be further investigated.

## Data availability statement

The original contributions presented in this study are included in the article/supplementary material, further inquiries can be directed to the corresponding author.

## Author contributions

HJ developed the idea of the work. HJ and QL designed the study and drafted the original manuscript. AR and RL searched

the literature. XY and HJ critically revised and improved the manuscript. All authors contributed to the article and approved the submitted version.

## Funding

This work was supported by National Natural Science Foundation of China (No. 3207161197), general projects of key industrial chains in Shaanxi Province (2021NY-166), and Chinese Universities Scientific Fund (2452019066).

## Acknowledgments

We are immensely thankful to all the participants and social media admins for their generous support. Besides, we are incredibly grateful to the Hebei Jinshahe Flour and Noodle

Group. We thank Elizabeth Tokarz at Yale University for her assistance with the English language and grammatical editing.

## Conflict of interest

The authors declare that the research was conducted in the absence of any commercial or financial relationships that could be construed as a potential conflict of interest.

## Publisher's note

All claims expressed in this article are solely those of the authors and do not necessarily represent those of their affiliated organizations, or those of the publisher, the editors and the reviewers. Any product that may be evaluated in this article, or claim that may be made by its manufacturer, is not guaranteed or endorsed by the publisher.

## References

- Jiang Z, Liu Q, Zhou X, Li X, Wang F, Liu Y. Identification of characteristic starch properties of wheat varieties used to commercially produce dried noodles. *Int J Food Sci Technol*. (2021) 56:794–803. doi: 10.1111/ijfs.14723
- Liu Y, Guan L, Meng N, Wang L, Liu M, Tan B. Evaluation of quality deterioration of dried whole-wheat noodles with extrusion-stabilized bran and germ during storage. *J Cereal Sci*. (2021) 97:103143. doi: 10.1016/j.jcs.2020.103143
- Zhou X, Wang S. Recent developments in radio frequency drying of food and agricultural products: a review. *Dry Technol*. (2019) 37:271–86. doi: 10.1080/07373937.2018.1452255
- Zhang YQ, Hui Y, Wang Y, Zhang B, Guo BL, Zhang GQ, et al. Effects of drying temperature and relative humidity on quality properties of chinese dried noodles. *J Food Quality*. (2020) 2020:974. doi: 10.1155/2020/8843974
- Feng H, Yin Y, Tang J. Microwave drying of food and agricultural materials: basics and heat and mass transfer modeling. *Food Eng Rev*. (2012) 4:89–106. doi: 10.1007/s12393-012-9048-x
- Carvalho GR, Monteiro RL, Laurindo JB, Augusto PED. Microwave and microwave-vacuum drying as alternatives to convective drying in barley malt processing. *Innov Food Sci Emerg Technol*. (2021) 73:102770. doi: 10.1016/j.ifset.2021.102770
- Jia Y, Khalifa I, Hu L, Zhu W, Li J, Li K, et al. Influence of three different drying techniques on persimmon chips' characteristics: a comparison study among hot-air, combined hot-air-microwave, and vacuum-freeze drying techniques. *Food Bioprod Proc*. (2019) 118:67–76. doi: 10.1016/j.fbp.2019.08.018
- Pongpichaiudom A, Songsermpong S. Characterization of frying, microwave-drying, infrared-drying, and hot-air drying on protein-enriched, instant noodle microstructure, and qualities. *J Food Proc Preservat*. (2018) 42:1–10. doi: 10.1111/jfpp.13560
- Shen L, Zhu Y, Liu C, Wang L, Liu H, Kamruzzaman M, et al. Modelling of moving drying process and analysis of drying characteristics for germinated brown rice under continuous microwave drying. *Biosyst Eng*. (2020) 195:64–88. doi: 10.1016/j.biosystemseng.2020.05.002
- Wang H, Zhang M, Mujumdar AS. Comparison of three new drying methods for drying characteristics and quality of shiitake mushroom (*Lentinus edodes*). *Dry Technol*. (2014) 32:1791–802. doi: 10.1080/07373937.2014.947426
- Jiang H, Shen Y, Zhen L, Li W, Zhang Q. Evaluation of strawberries dried by radio frequency energy. *Dry Technol*. (2019) 37:312–21. doi: 10.1080/07373937.2018.1439503
- Wang Y, Zhang L, Johnson J, Gao M, Tang J, Powers JR, et al. Developing hot air-assisted radio frequency drying for in-shell macadamia nuts. *Food Bioproc Technol*. (2014) 7:278–88. doi: 10.1007/s11947-013-1055-2
- Huang Z, Zhu H, Yan R, Wang S. Simulation and prediction of radio frequency heating in dry soybeans. *Biosyst Eng*. (2015) 129:34–47. doi: 10.1016/j.biosystemseng.2014.09.014
- Zhang L, Lyng JG, Brunton NP. Effect of radio frequency cooking on the texture, colour and sensory properties of a large diameter comminuted meat product. *Meat Sci*. (2004) 68:257–68. doi: 10.1016/j.meatsci.2004.03.011
- Zhang Y, Pandiselvam R, Zhu H, Su D, Wang H, Ai Z, et al. Impact of radio frequency treatment on textural properties of food products: an updated review. *Trends Food Sci Technol*. (2022) 124:154–66. doi: 10.1016/j.tifs.2022.04.014
- Wang S, Chen H, Sun B. Recent progress in food flavor analysis using gas chromatography-ion mobility spectrometry (GC-IMS). *Food Chem*. (2020) 315:126158. doi: 10.1016/j.foodchem.2019.126158
- Zhao G, Ding LL, Hadiatullah H, Li S, Wang X, Yao Y, et al. Characterization of the typical fragrant compounds in traditional Chinese-type soy sauce. *Food Chem*. (2020) 312:126054. doi: 10.1016/j.foodchem.2019.126054
- Mohammadhosseini M, Akbarzadeh A, Flamini G. Profiling of compositions of essential oils and volatiles of salvia limbata using traditional and advanced techniques and evaluation for biological activities of their extracts. *Chem Biodiv*. (2017) 14:361. doi: 10.1002/cbdv.201600361
- Mohammadhosseini M. Chemical composition of the essential oils and volatile fractions from flowers, stems and roots of salvia multicaulis vahl. by using MAHD, SFME and HS-SPME methods. *J Essent Oil Bear Plants*. (2015) 18:1360–71. doi: 10.1080/0972060X.2015.1024447
- Mohammadhosseini M. Chemical composition of the volatile fractions from flowers, leaves and stems of *Salvia mirzayanii* by HS-SPME-GC-MS. *J Essent Oil Bear Plants*. (2015) 18:464–76. doi: 10.1080/0972060X.2014.1001185
- Min C, Biyi M, Jianneng L, Yimin L, Yijun L, Long C. Characterization of the volatile organic compounds produced from green coffee in different years by gas chromatography ion mobility spectrometry. *RSC Adv*. (2022) 12:15534–42. doi: 10.1039/d2ra01843h
- Guo S, Zhao X, Ma Y, Wang Y, Wang D. Fingerprints and changes analysis of volatile compounds in fresh-cut yam during yellowing process by using HS-GC-IMS. *Food Chem*. (2022) 369:130939. doi: 10.1016/j.foodchem.2021.130939

23. Wang Z, Zhang Y, Zhang B, Yang F, Yu X, Zhao B, et al. Analysis on energy consumption of drying process for dried Chinese noodles. *Appl Ther Eng.* (2017) 110:941–8. doi: 10.1016/j.applthermaleng.2016.08.225
24. Zhang X, Wei J, Zhao S, Jia H, Guo C, Wang Z, et al. Flavor differences between commercial and traditional soybean paste. *Lwt.* (2021) 142:111052. doi: 10.1016/j.lwt.2021.111052
25. Zhang K, Zhao D, Song J, Guo D, Xiao Y, Shen R. Effects of green wheat flour on textural properties, digestive and flavor characteristics of the noodles. *J Food Proc Preservat.* (2021) 45:1–12. doi: 10.1111/jfpp.15199
26. Yi C, Zhu H, Tong L, Zhou S, Yang R, Niu M. Volatile profiles of fresh rice noodles fermented with pure and mixed cultures. *Food Res Int.* (2019) 119:152–60. doi: 10.1016/j.foodres.2019.01.044
27. Kubo MTK, dos Reis BHG, Sato LNI, Gut JAW. Microwave and conventional thermal processing of soymilk: inactivation kinetics of lipoxygenase and trypsin inhibitors activity. *Lwt.* (2021) 145:111275. doi: 10.1016/j.lwt.2021.111275
28. Cao Z, Liu Y, Zhu H, Li Y, Xiao Q, Yi C. Effect of soy protein isolate on textural properties, cooking properties and flavor of whole-grain flat rice noodles. *Foods.* (2021) 10:1–11. doi: 10.3390/foods10051085
29. Shen S, Chi C, Zhang Y, Li L, Chen L, Li X. New insights into how starch structure synergistically affects the starch digestibility, texture, and flavor quality of rice noodles. *Int J Biol Macromol.* (2021) 184:731–8. doi: 10.1016/j.ijbiomac.2021.06.151
30. Huang J, Sun Q, Song G, Qi S, Chen J, Zhang P, et al. Antioxidant and anti-isomerization effects of sesamol and resveratrol on high oleic acid peanut oil. *Lwt.* (2020) 123:109077. doi: 10.1016/j.lwt.2020.109077
31. Chen Y, Li P, Liao L, Qin Y, Jiang L, Liu Y. Characteristic fingerprints and volatile flavor compound variations in liuyang douchi during fermentation via HS-GC-IMS and HS-SPME-GC-MS. *Food Chem.* (2021) 361:130055. doi: 10.1016/j.foodchem.2021.130055
32. Chen J, Tao L, Zhang T, Zhang J, Wu T, Luan D, et al. Effect of four types of thermal processing methods on the aroma profiles of acidity regulator-treated tilapia muscles using E-nose, HS-SPME-GC-MS, and HS-GC-IMS. *Lwt.* (2021) 147:111585. doi: 10.1016/j.lwt.2021.111585
33. Shahidi F, Rubin LJ, D'Souza LA. Meat flavor volatiles: a review of the composition, techniques of analysis, and sensory evaluation. *CRC Crit Rev Food Sci Nutr.* (1986) 24:141–243. doi: 10.1080/10408398609527435
34. Li M, Chung SJ. Flavor principle as an implicit frame: its effect on the acceptance of instant noodles in a cross-cultural context. *Food Quality Prefer.* (2021) 93:104293. doi: 10.1016/j.foodqual.2021.104293
35. Wang J, Yu Y, Gao X, Jiang X, Huang M, Ye H, et al. Succession patterns of aroma components during brewing process of broomcorn millet (*Panicum miliaceum* L.) huangjiu. *Food Res Int.* (2022) 154:110982. doi: 10.1016/j.foodres.2022.110982
36. Olsson J, Börjesson T, Lundstedt T, Schnürer J. Detection and quantification of ochratoxin A and deoxynivalenol in barley grains by GC-MS and electronic nose. *Int J Food Microbiol.* (2002) 72:203–14. doi: 10.1016/S0168-1605(01)00685-7
37. Sun Z, Lyu Q, Chen L, Zhuang K, Wang G, Ding W, et al. An HS-GC-IMS analysis of volatile flavor compounds in brown rice flour and brown rice noodles produced using different methods. *Lwt.* (2022) 2022:113358. doi: 10.1016/j.lwt.2022.113358
38. Xia J, Guo Z, Fang S, Gu J, Liang X. Effect of drying methods on volatile compounds of burdock. *Foods.* (2021) 70:1–17. doi: 10.3390/foods10040868
39. Components A. *Evaluation of Perceptual Interactions between Ester.* (2020).
40. Wu Y, Liang S, Zheng Y, Zhang M. Volatile compounds of different fresh wet noodle cultivars evaluated by headspace solid-phase microextraction-gas chromatography-mass spectrometry. *Anais Acad Brasil Cien.* (2020) 92:1–11. doi: 10.1590/0001-3765202020190063
41. Liu H, Xu Y, Wu J, Wen J, Yu Y, An K, et al. GC-IMS and olfactometry analysis on the tea aroma of yingde black teas harvested in different seasons. *Food Res Int.* (2021) 150:110784. doi: 10.1016/j.foodres.2021.110784
42. Cho S, Kays SJ. Aroma-active compounds of wild rice (*Zizania palustris* L.). *Food Res Int.* (2013) 54:1463–70. doi: 10.1016/j.foodres.2013.09.042
43. Wang C, Kou X, Zhou X, Li R, Wang S. Effects of layer arrangement on heating uniformity and product quality after hot air assisted radio frequency drying of carrot. *Innov Food Sci Emerg Technol.* (2021) 69:102667. doi: 10.1016/j.ifset.2021.102667
44. Qu C, Wang H, Liu S, Wang F, Liu C. Effects of microwave heating of wheat on its functional properties and accelerated storage. *J Food Sci Technol.* (2017) 54:3699–706. doi: 10.1007/s13197-017-2834-y
45. Hemis M, Singh CB, Jayas DS. Microwave-assisted thin layer drying of wheat. *Dry Technol.* (2011) 29:1240–7. doi: 10.1080/07373937.2011.584999



## OPEN ACCESS

## EDITED BY

Baoguo Xu,  
Jiangsu University, China

## REVIEWED BY

Xu Duan,  
Henan University of Science  
and Technology, China  
Bin Wang,  
Shaoguan University, China  
Bimal Chitrakar,  
Agricultural University of Hebei, China

## \*CORRESPONDENCE

Zhaoxia Wu  
wuzxsau@163.com

## SPECIALTY SECTION

This article was submitted to  
Nutrition and Food Science  
Technology,  
a section of the journal  
Frontiers in Nutrition

RECEIVED 11 August 2022

ACCEPTED 08 September 2022

PUBLISHED 06 October 2022

## CITATION

Li C, Wang S, Wang J, Wu Z, Xu Y and  
Wu Z (2022) Ozone treatment  
promotes physicochemical properties  
and antioxidant capacity of fresh-cut  
red pitaya based on phenolic  
metabolism.  
*Front. Nutr.* 9:1016607.  
doi: 10.3389/fnut.2022.1016607

## COPYRIGHT

© 2022 Li, Wang, Wang, Wu, Xu and  
Wu. This is an open-access article  
distributed under the terms of the  
[Creative Commons Attribution License  
\(CC BY\)](https://creativecommons.org/licenses/by/4.0/). The use, distribution or  
reproduction in other forums is  
permitted, provided the original  
author(s) and the copyright owner(s)  
are credited and that the original  
publication in this journal is cited, in  
accordance with accepted academic  
practice. No use, distribution or  
reproduction is permitted which does  
not comply with these terms.

# Ozone treatment promotes physicochemical properties and antioxidant capacity of fresh-cut red pitaya based on phenolic metabolism

Chen Li<sup>1</sup>, Shan Wang<sup>2</sup>, Jiayi Wang<sup>3</sup>, Zhaohui Wu<sup>4</sup>, Yaping Xu<sup>5</sup>  
and Zhaoxia Wu<sup>1\*</sup>

<sup>1</sup>College of Food Science, Shenyang Agricultural University, Shenyang, China, <sup>2</sup>College of Light Industry, Liaoning University, Shenyang, China, <sup>3</sup>College of Life Science & Technology, Xinjiang University, Xinjiang, China, <sup>4</sup>Institute of Food and Processing, Liaoning Academy of Agricultural Sciences, Shenyang, China, <sup>5</sup>Chaoyang Engineering Technical School, Chaoyang, China

Pitaya is an important fresh-cut product in the global fruit market. The health benefits of fresh-cut red pitaya fruit are attributed to its unique phenolic content and other antioxidants, but the fruit is highly susceptible to spoilage which causes a decline in nutritional quality. In this study, we monitored changes in quality and phenolic compounds of pitaya fruit treated with gaseous ozone during storage at  $8 \pm 2^\circ\text{C}$  for 4 days. Compared with the control group, ozone treatment was an effective strategy for preserving quality by controlling the growth of microorganisms, preventing weight loss and softening, and improving the content of soluble solids and titratable acids. The results showed that ozone induced the accumulation of phenolic compounds while maintaining the quality. The content of phenolic compounds in fresh-cut pitaya was positively correlated with antioxidant activity. Ultra-performance liquid chromatography-electrospray tandem mass spectrometry was used to fingerprint the phenolic metabolites and metabolomic analysis identified 26 phenolic compounds. The majority of these were phenylpropanoids, and the key metabolic pathways were phenylpropane metabolism and flavonoid synthesis. This study illustrated the mechanism by which of ozone prolongs the shelf life of fresh-cut pitaya fruit and validated ozone as a valuable phenolic inducer and regulator of antioxidant activity, positively influencing the potential health benefits of fresh-cut products.

## KEYWORDS

ozone treatment, fresh-cut pitaya, quality, antioxidant activity, phenolic metabolism

## Introduction

Fruits and vegetables are an important part of the human diet. They are rich in vitamins, polyphenols, minerals, and dietary fiber, and their increased consumption can reduce the risk of heart disease, colon cancer, obesity, and diabetes, and have a health promoting effect on the human body (1). A growing desire for natural products and lifestyle changes by consumers has led to an increase in the consumption rate of fresh agricultural products, thus increasing the demand for fresh-cut fruits and vegetables which are popular with consumers.

Red pitaya is fresh, healthy, nutritious, and excellent in flavor and has become an indispensable element in fresh-cut fruit plates. Recently, the fruit has become increasingly popular with consumers (2). However, compared with unprocessed fruits and vegetables, fresh-cut fruits and vegetables have a shorter shelf life and faster decline in quality because the mechanical damage during processing induces a series of physiological and metabolic changes in their tissues (3). In addition, cutting also affects the flavor and safety of fruits and vegetables because it increases ethylene production and respiration rate, water loss, color changes, tissue softening, loss of nutrients, and susceptibility to microbial contamination (4). Therefore, there is an urgent need to expand the supply of fresh-cut pitaya in the consumer market whilst maintaining nutritional quality, flavor, and safety.

Postharvest treatment plays an important role in improving the storage life of fruits and vegetables. Pulsed electric fields (5), heating (6), cold plasma technology (7), edible coating (8), and pulsed light (9) are some of the emerging technologies for postharvest treatments. Currently, attention is focused on ozone as a powerful antibacterial agent, characterized by rapid decomposition and oxidation, and is approved by the U.S. Food and Drug Administration as an antibacterial additive in direct contact with food. An appropriate concentration of ozone treatment significantly affects the storage quality of fruits and vegetables. For example, studies have reported that ozone can significantly reduce the number of microorganisms on the surface of fresh-cut cantaloupe (10), kiwi fruit (11), strawberry (12), and carrot (13), maintaining physical and chemical quality, and prolonging shelf life.

As an effective postharvest treatment for fresh-cut fruits and vegetables, ozone can activate the antioxidant defense mechanism in plant cells and metabolize reactive oxygen species (ROS), which may become an important regulator of the antioxidant potential of plant cells (14, 15). Recent studies have shown that appropriate ozone treatment can significantly increase peroxidase (POD) activity, inhibit polyphenol oxidase (PPO) activity, maintain high total phenols (TPs) and flavonoids, improve the antioxidant capacity of fruit, and maintain fruit quality (16–18). Red pitaya contains many phenolic compounds (such as anthocyanins, flavonoids, and

phenolic acids), which can be used as free radical scavengers to inhibit lipid oxidation and are important antioxidants (19, 20). Therefore, it can be speculated that the antioxidant capacity of fresh-cut pitaya may be closely related to changes in phenolic compounds. Ozone has attracted extensive attention for activating the postharvest antioxidant system and inducing phenolic metabolism in fruits and vegetables. Therefore, we aimed to evaluate the effects of different ozone concentrations on prolonging the storage life, maintaining quality, and regulating the antioxidant capacity of fresh-cut pitaya based on phenolic metabolism.

## Materials and methods

### Plant material preparation

The study confirmed that 5°C is the critical temperature for postharvest storage of pitaya fruit. If the temperature is lower than 5°C, cold damage will occur (21). Red pitaya [*Hylocereus polyrhizus* (Weber) Britt. & Rose] was ordered online from its place of origin (Hainan, China). Once harvested, the fruit is transported to the laboratory by air from the cold chain (6°C, 85% RH) within 24 h. Pitaya was stored in a refrigerator at  $8 \pm 2^\circ\text{C}$  until processing. As a result, the selected fruits had the same degree of maturity without any pests or mechanical damage. The fruit was manually peeled, cut into quarter slices (1/4 part of a 1 cm thick slice), and randomly divided into  $15\text{ cm} \times 10\text{ cm} \times 4\text{ cm}$  polypropylene containers. Each container weighed approximately 150 g. The samples were stored for 4 days to simulate the actual sales process of fresh-cut fruits in China. Fresh-cut fruits are generally displayed for 1–2 days in Chinese supermarkets. After the pitaya was cut, it was immediately fumigated with ozone, and the experiment was replicated three times and stored at  $8 \pm 2^\circ\text{C}$ .

### Ozone gas fumigation treatment

Ozone was prepared using a corona discharge method (22). Dried oxygen was introduced into the corona discharge pipe to obtain pure gaseous ozone. Ozone gas was released into the treatment chamber connected to the inlet and outlet, and an ozone gas concentration detector was installed in the treatment chamber. The concentration of ozone gas was controlled by adjusting the flow knob of the ozone generator, and the real-time concentration of ozone in the treatment chamber was determined using a gas concentration detector. Samples were placed in the chamber with different concentrations of ozone gas (2, 4, and  $6\text{ mg L}^{-1}$ ) for 20 min. Fresh-cut pitaya fruits without ozone gas treatment were used as the control group. During storage, samples were taken every 24 h, frozen in liquid



TABLE 1 Treatments prepared for the experiments.

#	Treatment	Abbreviation
1	Control	CK
2	2 mg L <sup>-1</sup> ozone 20 min	T1
3	4 mg L <sup>-1</sup> ozone 20 min	T2
4	6 mg L <sup>-1</sup> ozone 20 min	T3
5	Day 0 results for CK group	CKD0
6	Day 2 results for CK group	CKD2
7	Day 0 results for T2 group	TD0
8	Day 2 results for T2 group	TD2

nitrogen, and stored at  $-80^{\circ}\text{C}$  until use. Abbreviations for the different treatments are shown in [Table 1](#).

## Microbial analysis

The total number of microbial colonies formed and the number of molds and yeasts were determined during storage, according to the Chinese Official Analysis Method (Chinese Official Document number: GB 4789.15-2016).

## Physicochemical properties

### Weight loss

Weight loss is expressed as the ratio of weight loss to the initial fresh weight (%):

$$\text{Weight loss} = (\text{initial mass} - \text{observed mass}) / \text{initial mass} \times 100\% \quad (1)$$

### Fruit firmness

The firmness of fresh-cut pitaya fruit was measured using a CT3 10 K texture analyzer (CT3, Brookfield, Middleboro, MA, USA) at six different positions with equal spacing from the equator. A 4 mm diameter stainless steel probe was selected, and the penetration displacement was 5 mm at a speed of  $5 \text{ mm.s}^{-1}$ . The result was expressed as the maximum force (N) recorded during the penetration process.

### Total soluble solids

Total soluble solids (TSS) was expressed as a percentage (%) using a hand-held refractometer (LB 90T, Guangzhou, China). This analysis was repeated three times; five fruits were used for each replicate.

### Titrateable acidity

Total titrateable acidity (TA) was determined according to the method described by Fan et al. (2). The results were expressed as a percentage (%) of citric acid.

## Color measurement

We measured the  $L^*$ ,  $a^*$ , and  $b^*$  values at five points on the fresh-cut pitaya using the Minolta CR-400 colorimeter (Konica Minolta Sensing, Inc., Osaka, Japan). Measurements were performed at the center of both sides of the fruit.

## Ozone treatment on antioxidants and antioxidant capacity of fresh-cut red pitaya fruit

### Determination of total phenol content

Total phenol (TP) content was determined using the method described by Gutiérrez et al. (23). The 4 g of frozen pitaya samples were homogenized with 20 ml of methanol and  $10,000 \times g$  for 20 min. The supernatant of each sample was used as an extract. Results was expressed on a fresh weight (FW) basis. TP content was shown as milligrams (mg) of gallic acid per 100 g.

### Determination of ascorbic acid content

The ascorbic acid (AsA) content was determined by titration with 2, 6-dichlorophenolindophenol as reported by Carbone et al. (24). This analysis was repeated three times. Results were expressed on a fresh weight basis. The ascorbic acid content was expressed as milligrams (mg) per 100 g of fresh weight.

### Determination of antioxidant capacity

Antioxidant activity was evaluated as described by Li et al. (25). The extraction method for the antioxidant activity assay was similar to that used for the total phenolic analysis (section "Determination of total phenol content"). The absorbance values were determined at 515 nm to calculate antioxidant activity using Equation 2:

$$\text{Antioxidant activity (\%)} = [(A_1 - A_2) / A_1] \times 100\% \quad (2)$$

Where  $A_1$  indicates the absorbance of the control and  $A_2$  indicates to the absorbance of the samples.

## Determination of phenolic metabolism enzyme activity

### Enzyme solution extraction

The sample was ground into a fine paste with liquid nitrogen, then 2 g of the sample were added to 10 ml of 100 mM sodium phosphate buffer (pH 6.4, containing 0.2 g of cross-linked polyvinylpyrrolidone), centrifuged for 30 min at  $4^{\circ}\text{C}$  and  $10,000 \times g$ ; further, the crude enzyme extract was the supernatant.

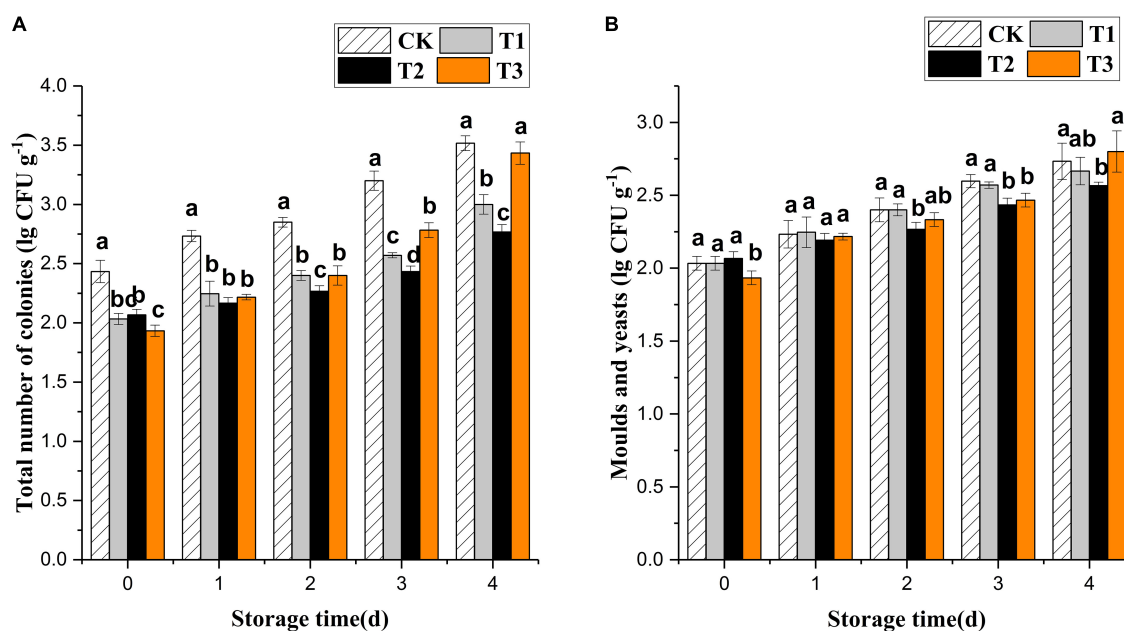


FIGURE 1

Effect of ozone treatments on total number of microbial colonies (A) and molds and yeasts (B) of fresh-cut pitaya during storage. Data were expressed as means  $\pm$  standard deviations (SD) from three replications.

### Superoxide dismutase

Superoxide dismutase (SOD) activity was determined based on the method described by Li et al. (25). One unit of SOD activity was calculated as the quantity of enzyme that caused 50% nitroblue tetrazolium reduction per second. It was expressed as U g<sup>-1</sup> based on protein content.

### Polyphenol oxidase

The activity of PPO was determined according to the method of Yingsanga et al. (26), with a slight modification. A small amount of crude enzyme extract (0.1 ml) was added to 3 ml of 100 mM catechol (prepared with sodium phosphate buffer), and then the increase in absorbance at 410 nm was measured for 3 min. Enzyme activity was expressed as  $\Delta A_{410} \text{ min}^{-1} \text{ g}^{-1} \text{ FW}$ .

### Peroxidase

Peroxidase activity was determined according to the method of Yingsanga et al. (26), with slight modifications. A small amount of crude enzyme extract (0.1 ml) was added to 2 ml of 8 mM guaiacol (prepared in sodium phosphate buffer) and incubated at 30°C for 30 min; subsequently, 1 ml of 24 mM H<sub>2</sub>O<sub>2</sub> was added, and the increase in absorbance was measured at 470 nm for 3 min. Enzyme activity was expressed as  $\Delta A_{470} \text{ min}^{-1} \text{ g}^{-1} \text{ FW}$ .

### Targeted metabolic analysis of phenolic acids and flavonoids

#### Sample preparation and extraction for metabolomic analysis

Pitaya fruits in the control group on day 0 (CKD0), day 2 (CKD2), and 4 mg L<sup>-1</sup> ozone treated groups on day 0 (TD0) and day 2 (TD2) were used as experimental materials. The extraction method was as in Labadie et al. (27). The fresh-cut pitaya fruits were ground into a powder with liquid nitrogen, and the extraction and centrifugation were repeated three times at 4°C. The supernatant (200  $\mu$ l) was filtered using a 0.22  $\mu$ m organic phase pinhole filter, transferred to a brown glass injection vial, and stored at -80°C until liquid chromatography mass spectrometry (LC-MS) analysis.

#### Chromatography and mass spectrometry conditions

According to the method of Labadie et al. (27), the phenolic acid and flavonoid contents were determined using ultra-performance liquid chromatography-electrospray tandem mass spectrometry (UPLC-ESI-MS)/MS analysis to qualitatively and quantitatively detect the target metabolites. Therefore, various phenolic compounds were identified and quantified using reliable standards. Three technical replicates were used.

**TABLE 2** Effect of ozone treatment on weight loss, firmness, total soluble solids, titratable acid content,  $L^*$ ,  $a^*$ , and  $b^*$  of fresh-cut pitaya during storage.

Quality changes	Storage time (d)	Treatments			
		CK	T1	T2	T3
Weight loss (%)	0	0	0	0	0
	1	0.07 ± 0.02a	0.05 ± 0.01a	0.05 ± 0.01a	0.05 ± 0.01a
	2	0.13 ± 0.02a	0.08 ± 0.01b	0.09 ± 0.01b	0.09 ± 0.01b
	3	0.24 ± 0.02a	0.21 ± 0.02b	0.22 ± 0.01ab	0.23 ± 0.01ab
	4	0.31 ± 0.05a	0.26 ± 0.02b	0.26 ± 0.01ab	0.27 ± 0.01ab
Firmness (N)	0	0.36 ± 0.01a	0.38 ± 0.02a	0.36 ± 0.06a	0.34 ± 0.02a
	1	0.32 ± 0.04ab	0.29 ± 0.01b	0.39 ± 0.03a	0.31 ± 0.03b
	2	0.29 ± 0.01b	0.34 ± 0.03a	0.34 ± 0.01a	0.30 ± 0.02b
	3	0.37 ± 0.03a	0.27 ± 0.02b	0.36 ± 0.01a	0.28 ± 0.01b
	4	0.35 ± 0.02a	0.30 ± 0.02bc	0.31 ± 0.01b	0.29 ± 0.01c
TSS (%)	0	10.83 ± 0.24a	10.50 ± 0.41a	10.67 ± 0.47a	10.67 ± 0.47a
	1	10.17 ± 0.24b	10.17 ± 0.24b	10.50 ± 0.01a	10.67 ± 0.24a
	2	9.67 ± 0.24c	9.83 ± 0.24bc	10.00 ± 0.01b	10.67 ± 0.24a
	3	9.17 ± 0.24c	10.17 ± 0.24a	9.58 ± 0.12b	10.33 ± 0.24a
	4	8.33 ± 0.24d	9.67 ± 0.24b	9.17 ± 0.24c	10.17 ± 0.24a
TA (%)	0	0.41 ± 0.01a	0.41 ± 0.01a	0.43 ± 0.01a	0.41 ± 0.01a
	1	0.37 ± 0.01a	0.39 ± 0.01a	0.39 ± 0.01a	0.39 ± 0.01a
	2	0.35 ± 0.01a	0.36 ± 0.01a	0.37 ± 0.01a	0.36 ± 0.01a
	3	0.35 ± 0.01a	0.36 ± 0.01a	0.35 ± 0.01a	0.36 ± 0.01a
	4	0.34 ± 0.01a	0.35 ± 0.01a	0.35 ± 0.01a	0.35 ± 0.01a
$L^*$	0	25.49 ± 1.54b	26.96 ± 2.15a	28.45 ± 1.83a	28.75 ± 1.08a
	1	25.25 ± 1.09b	27.34 ± 1.87a	28.21 ± 1.53a	28.50 ± 1.61a
	2	25.44 ± 1.91a	27.24 ± 2.39a	27.48 ± 1.32a	27.85 ± 1.42a
	3	25.56 ± 0.92a	26.92 ± 2.20a	28.06 ± 1.84a	28.49 ± 2.25a
	4	25.74 ± 0.98b	27.52 ± 2.85ab	27.57 ± 1.99ab	29.09 ± 0.80a
$a^*$	0	36.71 ± 2.60a	33.75 ± 3.81a	38.91 ± 4.85a	37.66 ± 2.99a
	1	35.35 ± 2.74a	34.67 ± 3.87a	38.69 ± 4.20a	35.99 ± 3.14a
	2	35.35 ± 3.19a	34.02 ± 4.30a	36.34 ± 2.35a	34.44 ± 3.14a
	3	37.08 ± 1.21a	34.59 ± 4.42a	36.81 ± 4.28a	36.71 ± 4.20a
	4	37.07 ± 1.19a	35.25 ± 5.38a	36.77 ± 5.57a	39.13 ± 2.24a
$b^*$	0	1.22 ± 1.25a	1.45 ± 2.02a	1.87 ± 0.79a	1.07 ± 0.43a
	1	1.14 ± 0.83a	1.48 ± 2.18a	1.70 ± 0.75a	0.87 ± 0.89a
	2	0.73 ± 1.12a	0.96 ± 1.66a	1.31 ± 1.15a	0.79 ± 0.74a
	3	1.44 ± 0.55a	1.88 ± 1.55a	2.37 ± 1.15a	1.15 ± 0.60a
	4	1.02 ± 1.30a	1.21 ± 1.65a	2.28 ± 0.91a	1.05 ± 0.46a

Data were expressed as means ± standard deviations (SD) from three replications. Means with different letters are significantly different ( $P < 0.05$ ) at each storage period.

## Statistical analysis

All analyses were performed using the SPSS software package (version 20.0; SPSS, Chicago, Illinois, USA). Each treatment was repeated three times and all results are presented as the mean and the standard

deviation for  $n$  replicates. The significant difference among the treatment means were compared using Tukey's multiple range test at the 5% significance level, and the figures were created using Origin (Version 2017).  $P$ -values  $< 0.05$  were considered statistically significant.

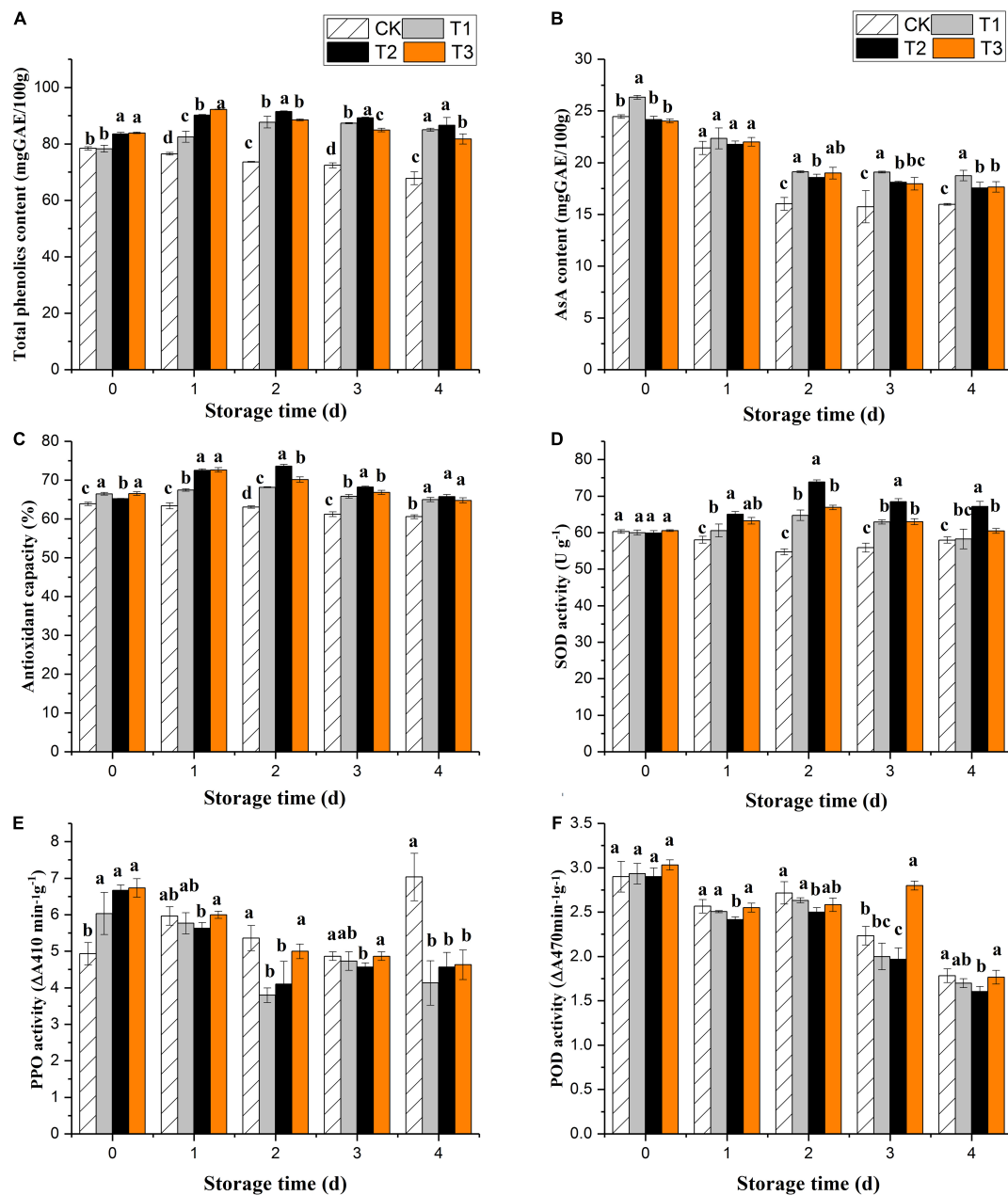


FIGURE 2

Effect of ozone treatment on total phenol (A), ascorbic acid (B), antioxidant capacity (C), SOD activity (D), PPO activity (E), and POD activity (F) of fresh-cut pitaya during storage. Data were expressed as means  $\pm$  standard deviations (SD) from three replications.

## Results

### Ozone treatment on microbial growth of fresh-cut pitaya

Ozone treatment inhibited the growth of total colonies of fresh-cut pitaya but had no significant effect on mold and yeast (Figure 1). The treatment with 4 mg L<sup>-1</sup> of ozone

had the best effect, which was a significantly lower growth of microbial colonies than that of the control group during storage ( $P < 0.05$ ). At the early storage stage, the 6 mg L<sup>-1</sup> treatment group showed the most apparent inhibition of total colony growth. However, the growth rate of microorganisms in the 6 mg L<sup>-1</sup> treatment increased and was higher than in the 2 and 4 mg L<sup>-1</sup> treatment groups on the 4th day, even though it had an edible value.

TABLE 3 Pearson's correlation coefficients between some selected quality factors of fresh-cut pitaya fruit during storage.

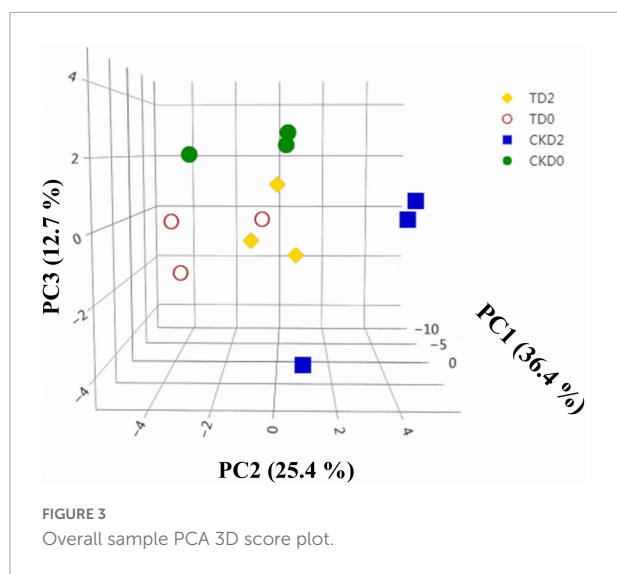
	Weight loss	Firmness	TSS	TA	AsA	TP	Antioxidant capacity	POD activity	SOD activity	PPO activity
Weight loss	1									
Firmness	−0.710	1								
TSS	−0.779	0.574	1							
TA	−0.797	0.718	0.654	1						
AsA	−0.821	0.764	0.789	0.848	1					
TP	−0.203	0.161	0.338	−0.058	0.176	1				
Antioxidant capacity	−0.381	0.297	0.393	0.056	0.239	0.860	1			
POD activity	−0.827	0.454	0.678	0.662	0.627	0.004	0.198	1		
SOD activity	−0.039	0.116	0.078	−0.156	−0.038	0.769	0.767	−0.090	1	
PPO activity	−0.328	0.310	0.145	0.156	0.415	−0.375	−0.215	0.326	−0.401	1

TABLE 4 Effects of ozone treatment on individual phenolic compounds of fresh-cut pitaya fruits during storage.

Component Name	Day 0		Day 2		Category
	CK	T2	CK	T2	
3,4-Dihydroxybenzaldehyde	421.26 ± 99.20ab	458.56 ± 69.23a	303.47 ± 46.60b	381.02 ± 51.12ab	Catechin derivatives
Catechin	68.14 ± 1.54b	102.47 ± 27.21a	76.91 ± 7.66ab	109.89 ± 46.47ab	Catechin derivatives
Epicatechin	32.33 ± 6.54a	42.55 ± 14.21a	18.67 ± 13.20a	74.30 ± 42.08a	Catechin derivatives
Protocatechuic acid	108.96 ± 16.34a	136.93 ± 26.85a	96.30 ± 15.83a	102.16 ± 12.25a	Catechin derivatives
Syringaldehyde	ND	16.78 ± 3.45a	10.09 ± 6.20a	ND	Benzoic acid derivatives
<i>trans</i> -Cinnamic acid	285.37 ± 180.10a	254.68 ± 20.57a	205.20 ± 100.70a	328.53 ± 222.78a	Benzoic acid derivatives
Vanillic acid	113.50 ± 16.31b	206.74 ± 59.50a	116.04 ± 38.41ab	93.39 ± 2.25c	Benzoic acid derivatives
4-Hydroxybenzoic acid	49.59 ± 5.56b	68.51 ± 9.03a	ND	30.91 ± 2.86c	Benzoic acid derivatives
Salicin	17.23 ± 2.37a	12.57 ± 0.42b	9.07 ± 1.16d	10.88 ± 0.09c	Benzoic acid derivatives
Salicylic acid	168.68 ± 7.89a	63.34 ± 15.93c	124.88 ± 5.27b	42.88 ± 0.09cd	Benzoic acid derivatives
4-Hydroxycinnamic acid	100.66 ± 41.53b	156.66 ± 1.67a	71.19 ± 20.29b	75.54 ± 6.98b	Phenylpropanoids
Caffeic acid	87.09 ± 7.60a	91.99 ± 32.71a	71.93 ± 19.29a	75.54 ± 8.17a	Phenylpropanoids
Chlorogenic acid	26203.59 ± 1958.92ab	21189.03 ± 2949.51b	22645.40 ± 2962.79b	28589.03 ± 2039.63a	Phenylpropanoids
Cryptochlorogenic acid	1870.08 ± 104.66a	1613.89 ± 236.85a	1639.37 ± 135.87a	1721.94 ± 197.00a	Phenylpropanoids
Ferulic acid	1566.84 ± 644.49ab	3848.25 ± 1732.91a	1209.96 ± 96.01b	605.83 ± 160.64c	Phenylpropanoids
Sinapic acid	881.50 ± 438.48ab	1192.94 ± 443.81a	524.18 ± 200.74b	364.88 ± 98.49b	Phenylpropanoids
Nicotiflorin	259.11 ± 84.51b	298.80 ± 61.00b	170.64 ± 70.52b	1784.04 ± 629.73a	Flavonols
Rutin	1148.77 ± 367.18bc	1455.22 ± 341.50b	736.61 ± 237.05c	7650.01 ± 164.58a	Flavonols
Narcissin	30.67 ± 10.60bc	56.64 ± 26.10b	16.57 ± 8.04c	165.68 ± 57.68a	Flavonols
Hesperidin	9.30 ± 1.06b	3.85 ± 0.32c	4.87 ± 0.83bc	150.59 ± 9.74a	Flavanones
Naringenin	2.47 ± 0.32a	2.47 ± 0.19a	2.12 ± 0.26a	2.12 ± 0.62a	Flavanones
Naringin	13.35 ± 5.17a	8.61 ± 5.05a	1.89 ± 1.20b	12.17 ± 1.95a	Flavanones
Cyanidin 3-O-rutinoside chloride	222.41 ± 61.80b	325.14 ± 79.69b	171.71 ± 76.17b	1812.35 ± 724.66a	Anthocyanins
Cyanin chloride	42.07 ± 1.80b	41.59 ± 1.40b	26.30 ± 2.82c	60.61 ± 0.90a	Anthocyanins
Aesculin	9.59 ± 0.99a	9.62 ± 1.28a	7.56 ± 1.52a	8.60 ± 1.13a	Coumarins
4-Methylumbelliferone	ND	25.30 ± 4.39	ND	ND	Coumarins

The results are expressed as μg/kg. CK represents the control group and T represents the treatment group. Data were expressed as mean ± standard deviations (SD) from three replications. Means with different letters within the same row are significantly different ( $P < 0.05$ ) at each storage period.





## Ozone treatment on physicochemical properties of fresh-cut pitaya

### Ozone treatment on firmness and weight loss of fresh-cut pitaya

Firmness is directly related to fruit texture and consumer acceptance concerning the texture and storage life of fruits. The treatments with 2 and 6 mg L<sup>-1</sup> of ozone resulted in fruit firmness and edible quality being maintained (Table 2). However, the firmness of untreated fruits increased in the later stages of storage.

During storage, the weight loss of fresh-cut pitaya increased. However, compared with the control group, ozone treatment significantly inhibited weight loss during the entire storage period. The weight loss of untreated pitaya was highest (0.29%), and the inhibition effect of the 4 mg L<sup>-1</sup> ozone treatment was the best (0.22%).

### Ozone treatment on total soluble solids and titratable acidity of fresh-cut pitaya

Compared with the control group, the treatment groups delayed the decrease in soluble solids in fresh-cut pitaya and had no negative effect on titratable acid content. At the end of storage, the soluble solid content of the control group decreased by 23.8%, and that of the 4 mg L<sup>-1</sup> treatment group decreased by 14.06% (Table 2).

Titratable acid represents the content of organic acids in fruits and vegetables, which directly affects the edible quality of fresh-cut pitaya fruit, such as flavor and texture. Both the control and treatment groups showed a continuous decline in TA during the storage period, while the treatment group showed a slow decline in the late storage period. The titratable acid content of fresh-cut pitaya fruit in the 4 mg L<sup>-1</sup> treatment group remained the highest during storage (Table 2). Suitable ozone

gas treatment can delay physiological metabolism, delaying the decline in TA content and improving the storage of fresh-cut pitaya.

### Ozone treatment on the color of fresh-cut pitaya

The color change of fresh-cut fruits and vegetables is an important index that affects the quality of edible products and directly affects consumer acceptability. Ozone postharvest treatment and storage time had no significant effect on the color of fresh-cut pitaya, including brightness and redness (Table 2).

### Ozone treatment on bioactive compounds and antioxidant capacity of fresh-cut pitaya

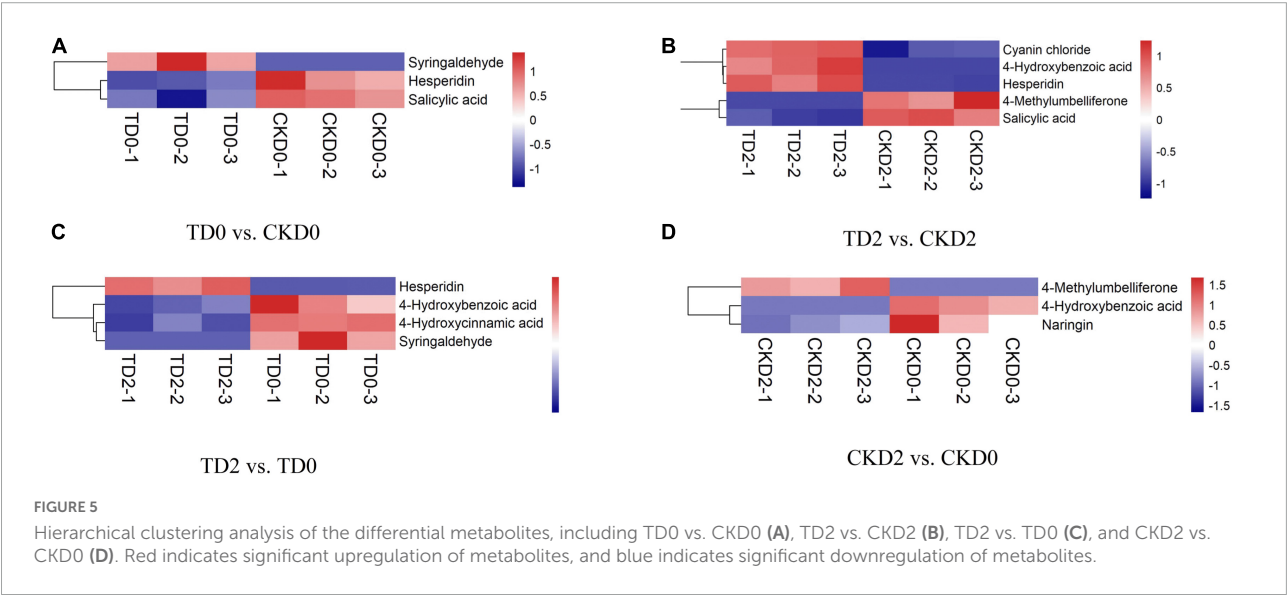
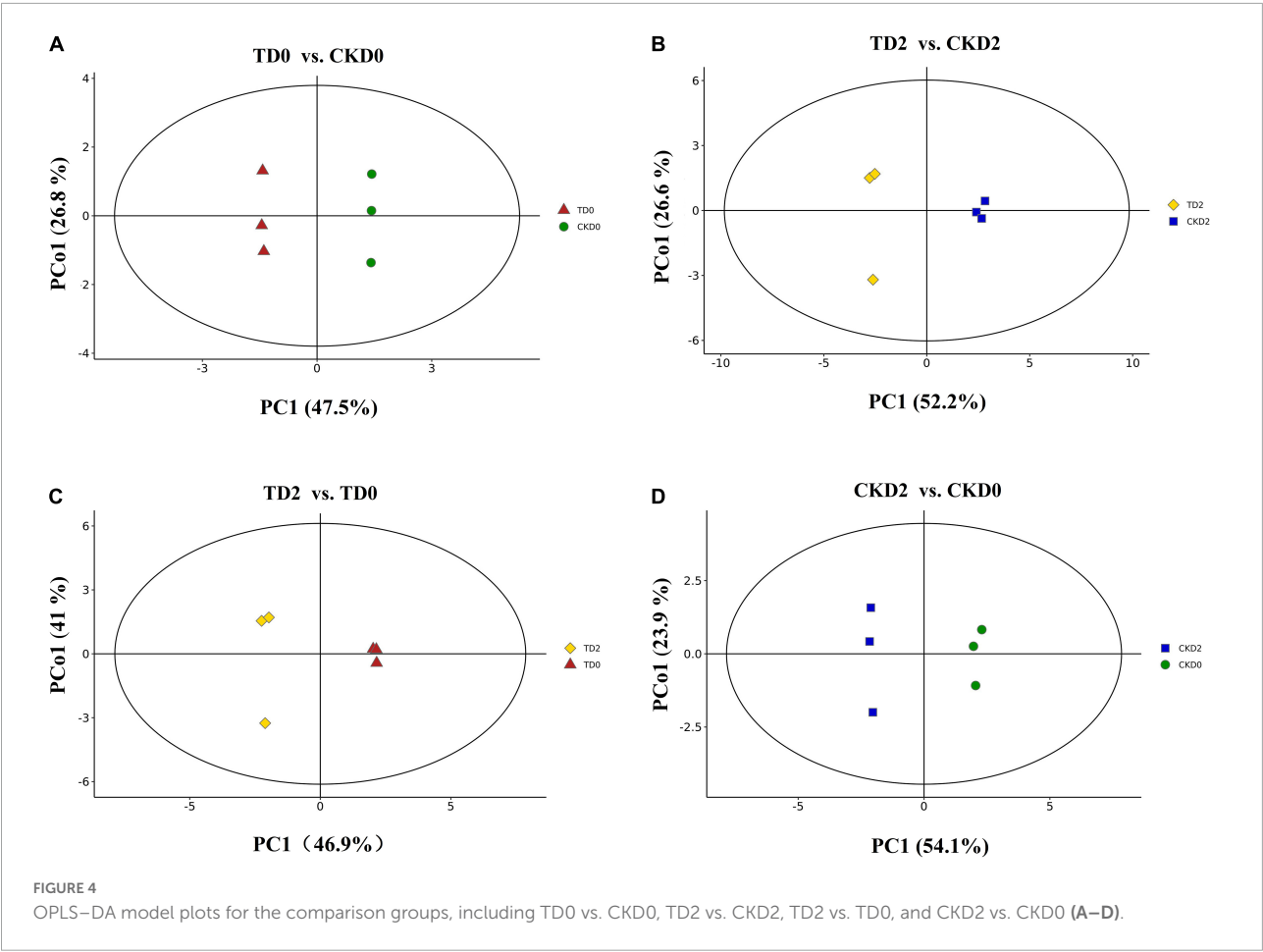
The total phenol content of the untreated fruits decreased significantly during storage. Ozone gas treatment induced phenolic accumulation in fresh-cut pitaya fruit over the first 2 days of storage, and total phenol contents reached their maximum values on the second day, increasing by 3.9, 9.5, and 9.9% for 2, 4, and 6 mg L<sup>-1</sup> treatments, respectively (Figure 2A). After 2 days of storage, the fresh-cut pitaya tissues showed a decline in total phenol content, but it was still higher than the control, and the 4 mg L<sup>-1</sup> treatment maintained the highest total phenol level.

All fresh-cut pitaya fruits showed a decline in the ascorbic acid content with the extension of storage time, while ozone treatment delayed the decline of ascorbic acid. On the fourth day of storage, the content of ascorbic acid in the control group decreased by 40.1%, while that in the 2, 4, and 6 mg L<sup>-1</sup> ozone groups decreased by 30.0, 28.9, and 27.9%, respectively (Figure 2B). Therefore, proper ozone treatment can slow down the oxidation of ascorbic acid and maintain the nutritional quality of fresh-cut pitaya fruit.

The results showed that ozone treatment could enhance the antioxidant capacity of fresh-cut pitaya. From day 0 after ozone treatment, the antioxidant capacity of fresh-cut pitaya fruit increased, and the antioxidant activity reached its maximum value after 2 days of storage (Figure 2C).

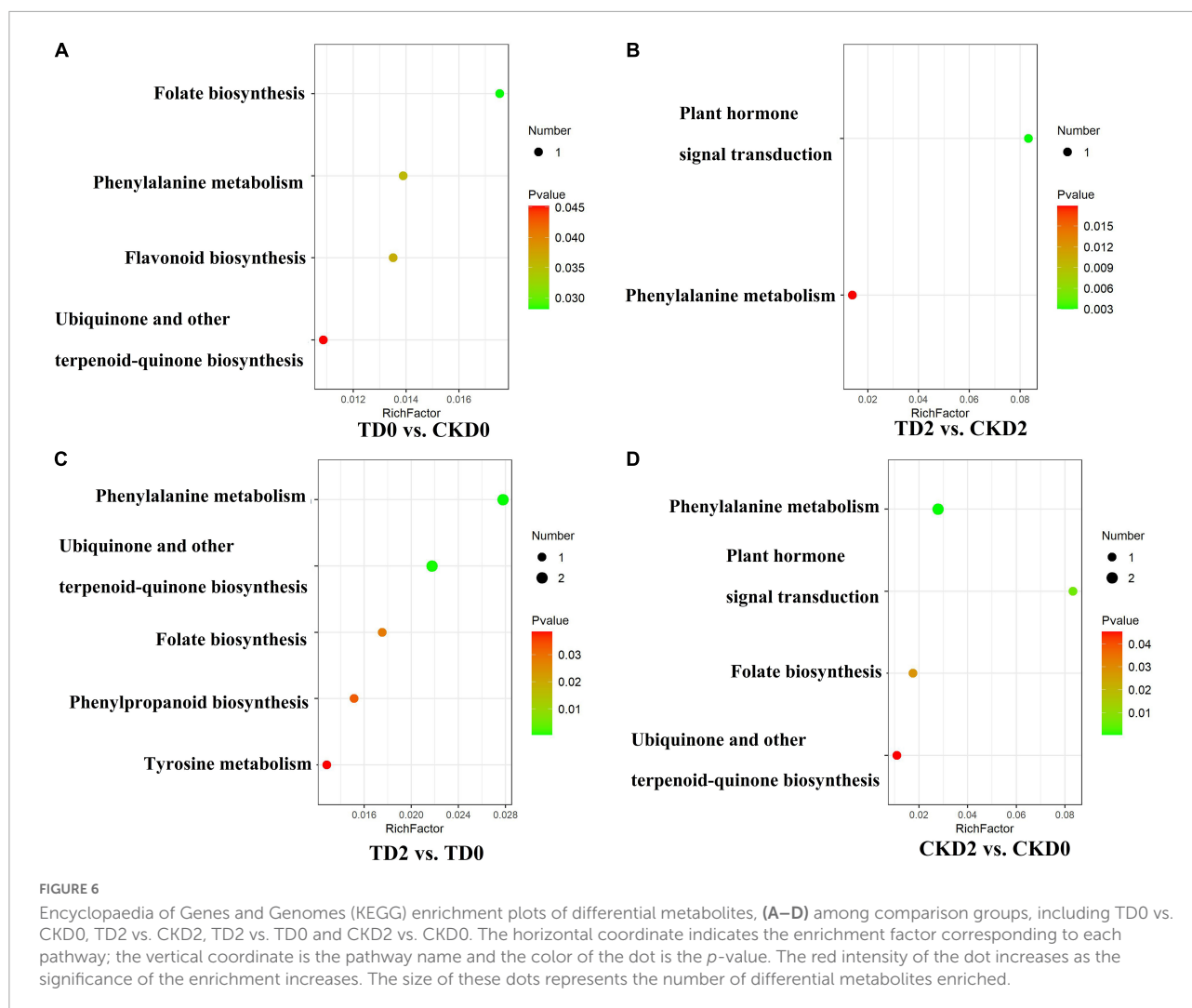
### Ozone treatment on antioxidant enzymes and antioxidant capacity of fresh-cut pitaya

Superoxide dismutase, polyphenol oxidase, and peroxidase are key enzymes involved in the metabolism of fruits and vegetables. They are particularly important in removing reactive oxygen species (ROS), thus prolonging the shelf life of fruits and vegetables. In Figure 2D, ozone treatment induced an increase in SOD activity. Compared with the control fruit, SOD activity was still relatively high until the last day of storage. As shown in Figures 2E,F, compared with untreated fruits, ozone treatment significantly inhibited



the PPO activity, but the inhibitory effect between different treatment groups was not significant. The results showed that the POD activity of the treatment and control groups

decreased during storage, and there was no significant difference between the ozone treatment and control groups ( $P > 0.05$ ).



## Correlation analysis

**Table 3** shows the relationship between different attributes achieved using the Pearson correlation coefficient. Weight loss was negatively correlated with fruit firmness and TSS, and PPO activity was negatively correlated with TP. The antioxidant capacity was positively correlated with TP content and SOD activities. The results further showed that the antioxidant capacity of fresh-cut pitaya fruit was improved after ozone treatment, and phenolic compounds might play the main role.

## Ozone treatment on phenolic metabolism of fresh-cut pitaya

### Individual phenolic compounds

Twenty-six phenolic compounds were identified and quantified, including four catechin derivatives, six benzoic acid derivatives, six phenylpropanoids, three flavanols, three

flavanones, two anthocyanins, and two coumarins. The initial chlorogenic acid content was  $26203.59 \mu\text{g kg}^{-1}$ , the highest content of phenolic compounds in fresh-cut pitaya fruit, followed by cryptochlorogenic acid, with an initial content of  $1870.08 \mu\text{g kg}^{-1}$  (**Table 4**). The ferulic acid content and the vanillic acid content of the treatment group on day 0 was 2.46 times and 1.82 times that of the control group, respectively. Notably, on day 2, the hesperidin content of the treatment group was 30.91 times that of the control group, and the contents of rutin, narcissin, and cyanidin 3-O-rutinoside chloride in the treatment group were 10 times higher than those of the control group.

### Metabolomic analysis

In the present study, three principal components PC1, PC2, and PC3 were extracted (36.4, 25.4, and 12.7%, respectively) (**Figure 3**). In the present study, the orthogonal partial least squares discriminant analysis (OPLS-DA) model was used to perform a pairwise comparison between the samples to assess

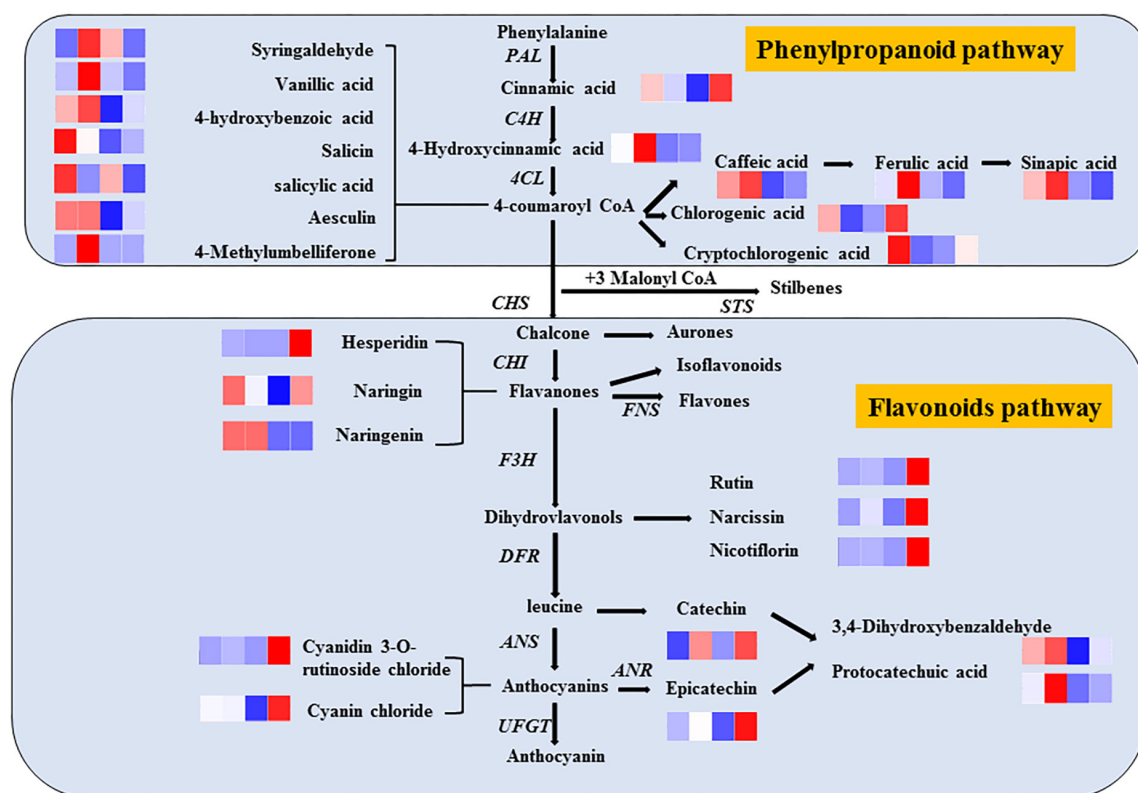


FIGURE 7

Metabolic pathways of ozone-induced phenolic accumulation in fresh-cut red pitaya fruit. The cluster heatmap showed all detected phenolic acids and flavonoid metabolites. The upregulated and downregulated metabolites were expressed by different shades of red and blue, respectively. As the abundance value increases, the color of the bar graph changes from blue to red. If the abundance value is zero, the color of the column is white.

further differences; the  $R^2$  (goodness-of-fit) and  $Q^2$  (goodness-of-prediction) values of all the comparison groups were close to 1 (Figure 4). The results indicate that the data were reproducible and reliable.

In order to more visually display the relationship between samples and the expression differences of metabolites among different samples, we carried out Hierarchical Clustering on the expression levels of all significantly different metabolites and visually analyzed the expression levels of different metabolites. The results are shown in Figure 5. There were three significantly different metabolites between TD0 and CKD0 (two downregulated and one upregulated), five between TD2 and CKD2 (three downregulated and two upregulated), and four between TD2 and TD0 (3 downregulated, 1 upregulated), and 3 between CKD2 and CKD0 (2 downregulated, 1 upregulated). These significantly different metabolites were mainly derivatives of benzoic acid, flavanones, coumarins, anthocyanins, and phenylpropanoids.

The differential metabolites of each comparison group were annotated using the Kyoto Encyclopaedia of Genes and Genomes (KEGG) database. The above-mentioned annotated results were classified and enriched based on the pathway types

in KEGG, and the enrichment results of each comparison group are shown in Figure 6. Based on the enrichment results, we observed that the differential metabolites of the comparison groups were mainly distributed in pathways including the biosynthesis of phenylalanine metabolism, ubiquinone and other terpenoid-quinone biosynthesis, folate biosynthesis, tyrosine metabolism, isoquinoline alkaloid biosynthesis, plant hormone signal transduction, and flavonoid biosynthesis.

## Discussion

Ozone is widely used as a sanitizer for storing and preserving fruits and vegetables, mainly for gaseous or aqueous ozone treatment of food products. The advantage of gaseous ozone is that it can be used as a direct antimicrobial additive to food products after diffusion in the studied system (28). Undoubtedly, fresh-cut fruits are more suitable for gaseous ozone treatment and require lower ozone concentrations compared to whole fruits. For example, room-temperature storage of raspberries at 8–10 ppm ozone oxidation for 30 min every 12 h for 3 days effectively reduced the growth of aerobic

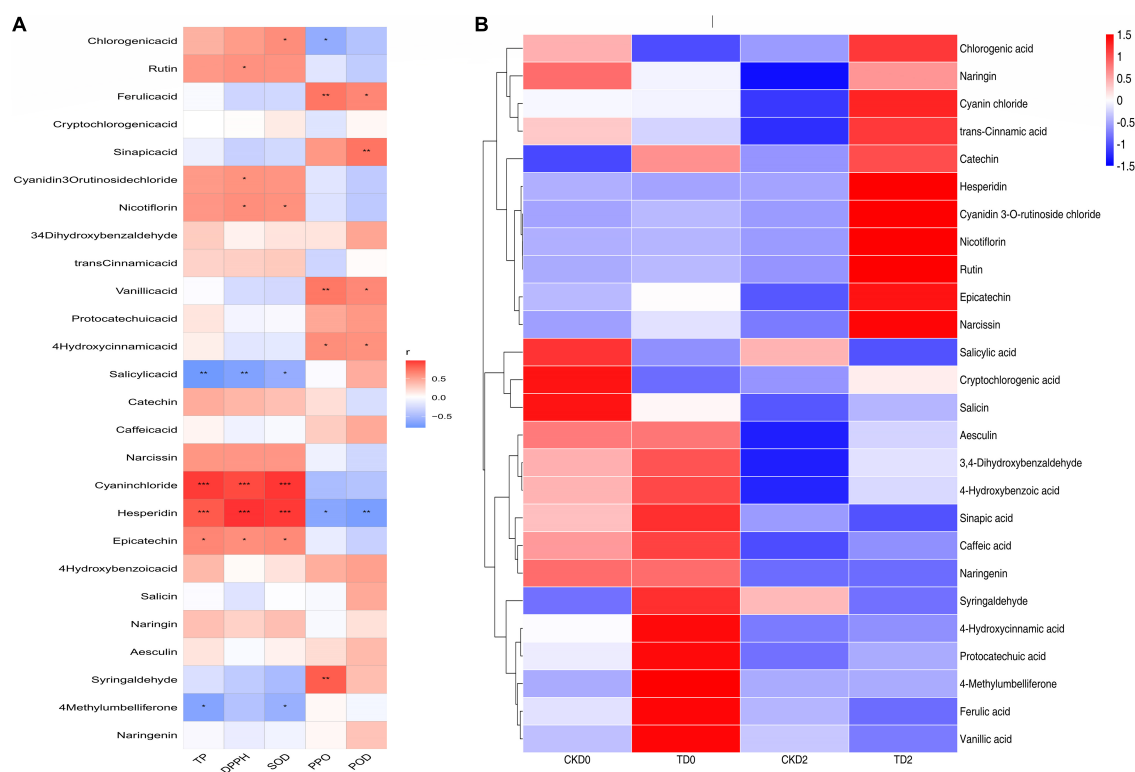


FIGURE 8

Heatmap of Spearman's rank correlations between the individual phenolic compounds and five variables (TP, DPPH, SOD, PPO, and POD) of the fresh-cut pitaya (A). The heat map of the correlation between individual phenolic compound and the storage time in fresh-cut pitaya fruit (B). The significance levels are shown below: \* $p < 0.05$ ; \*\* $p < 0.01$ ; \*\*\* $p < 0.001$ .

mesophilic bacteria and fungi (29). Blueberry fruit can be stored at 4°C for 28 days with ozone oxidation at 15 ppm for 30 min every 12 h, while for fresh-cut apples, it is recommended that disinfecting with 1.4 mg L<sup>-1</sup> for 5 min can extend the shelf life to 10 days (18). Thus, ozone treatment varies according to the type of fruit, actual shelf life, and storage time in marketing. In addition, the ozone treatment dose was found to be a key factor affecting quality. Alwi and Ali (30) found that exposure of bell peppers to low concentrations of ozone (1 and 3 ppm) did not affect fruit respiration, color, titratable acidity, and firmness. However, exposure to ozone at 7 and 9 ppm reduced fruit quality due to excessive oxidative stress. In this study, 2, 4, and 6 mg L<sup>-1</sup> ozone treatments effectively prolonged the shelf life of fresh-cut pitaya fruit compared with the control group. Therefore, it is necessary to choose an optimum ozone treatment concentration to extend the shelf life of fruits.

Ozone treatment activated protective mechanisms against antioxidant stress in fresh-cut pitaya. The levels of phenolic compounds and total antioxidant capacity were higher in fresh-cut pitaya after ozone treatment than in non-ozone-treated fruit. Zhang et al. (15) demonstrated that ozone could activate the antioxidant defense mechanism of plant cells to metabolize ROS, which may be an important regulator of superoxide anion

scavenging by plant cells. In this study, we observed that ozone induced SOD enzyme activity and inhibited PPO and POD activities. Similarly, enzyme activities related to the antioxidant system, especially SOD, were induced by ozone in orange and fresh-cut green pepper (31, 32). Thus, recently, ozone has been receiving extensive attention as a suitable treatment to activate antioxidant enzyme systems in postharvest fruits and vegetables.

Many studies have revealed the potential of ozone treatment for increasing antioxidants in fruits. Fresh vegetables and fruits are often rich in antioxidant substances, such as ascorbic acid, flavonoids, and polyphenols, which are affected by ozone treatment. However, it is difficult to determine which substances play a key role in improving antioxidant activity. Therefore, we used phenolic metabolomics correlation analysis and observed that antioxidant capacity is positively correlated with total phenols, which is different from the treatment effect of green peppers. Glowacz and Rees (33) reported that ascorbic acid plays a major role because the vitamin C content of peppers is the highest among all vegetables. Ali et al. (34) reached a similar conclusion when they treated papaya fruits with 1.5, 2.5, and 3.5 ppm ozone. After 10 days of storage, the antioxidant capacity of papaya was significantly improved, and the trend obtained from DPPH and FRAP analysis was similar to the total



phenol content, and phenolic compounds could be inferred as the main antioxidant in papaya. Therefore, due to the individual differences in fruits and vegetables, more research is needed to evaluate the efficacy of ozone and understand its mode of action as a postharvest treatment.

Phenols are widely considered the most important secondary metabolites that contribute to the antioxidant capacity of fruits (35). With the increase in phenolic compounds, the oxidation resistance of products can be greatly improved, providing us with a method to improve the efficacy of products through processing, as shown in **Figure 7**. Significantly, different metabolites are mainly regulated by key enzymes involved in phenanthrene metabolism and flavonoid synthesis pathways. From the expression of up- and down-regulation of significantly different metabolites, it is speculated that ozone may upregulate the expression of key enzymes in the metabolic pathway, such as anthocyanin synthase, chalcone synthase, and 4-coumaroyl-coenzyme A ligase. The heat map of the correlation between individual phenolic compound and five variables (TP, DPPH, SOD, PPO, and POD) and the storage time in fresh-cut pitaya fruit is shown in **Figure 8**. It can be inferred that hesperidin, 4-hydroxybenzoic acid, and cyanin chloride significantly affect the changes in phenolic substances in fresh-cut pitaya fruit, and hesperidin showed the most significant changes. Therefore, hesperidin may be a potential biomarker for ozone-induced fresh-cut pitaya fruit. Whether such a principle exists in the effect of ozone treatment on other fruits remains to be confirmed.

## Conclusion

Gaseous ozone treatment effectively maintained the sensory and nutritional properties of fresh-cut red pitaya. Postharvest ozone treatment also resulted in higher antioxidant activity, which was significantly related to changes in phenolic compound content. The regulatory effect of ozone on phenolic compounds mainly involved flavonoid biosynthesis and the biosynthesis of phenylalanine metabolism in response to ozone treatment. These findings provided new information on the effects of ozone on phenolic compounds and will help to design foods, drugs, and other products that extract health attributes from pitaya resources. However, to better understand the exact mechanism of ozone action in fresh-cut red pitaya

and whether it can be used at the industrial scale, it is necessary to further study the mechanism of ozone induced phenol accumulation or oxidative stress at the molecular level.

## Data availability statement

The data analyzed in this study is subject to the following licenses/restrictions: the data that support the findings of this study are available from the corresponding author, upon reasonable request. Requests to access these datasets should be directed to ZXW, [wuzxsau@163.com](mailto:wuzxsau@163.com).

## Author contributions

CL and ZXW: conceptualization. SW: methodology and data curation. JW: software. CL, ZHW, and YX: validation and visualization. CL: formal analysis, investigation, and writing—original draft preparation and review and editing. ZXW: resources. All authors contributed to the article and approved the submitted version.

## Funding

This work was supported by the Application and Foundation Research Project of Liaoning Province, China.

## Conflict of interest

The authors declare that the research was conducted in the absence of any commercial or financial relationships that could be construed as a potential conflict of interest.

## Publisher's note

All claims expressed in this article are solely those of the authors and do not necessarily represent those of their affiliated organizations, or those of the publisher, the editors and the reviewers. Any product that may be evaluated in this article, or claim that may be made by its manufacturer, is not guaranteed or endorsed by the publisher.

## References

- More AS, Ranadheera CS, Fang Z, Warner R, Ajlouni S. Biomarkers associated with quality and safety of fresh-cut produce. *Food Biosci.* (2020) 34:100524. doi: 10.1016/j.foodchem.2019.100524
- Fan P, Huber DJ, Su Z, Hu M, Gao Z, Li M, et al. Effect of postharvest spray of apple polyphenols on the quality of fresh-cut red pitaya fruit during shelf life. *Food Chem.* (2018) 243:19–25. doi: 10.1016/j.foodchem.2017.09.103
- Hashemi SMB, Jafarpour D. Bioactive edible film based on *Konjac glucomannan* and probiotic *Lactobacillus plantarum* strains: physicochemical properties and shelf life of fresh-cut kiwis. *J Food Sci.* (2021) 86:513–22. doi: 10.1111/1750-3841.15568
- Toivonen PMA, Brummell DA. Biochemical bases of appearance and texture changes in fresh-cut fruit and vegetables. *Postharvest Biol Technol.* (2008) 48:1–14. doi: 10.1016/j.postharvbio.2007.09.004
- Andreou V, Sigala A, Limnais A, Dimopoulos G, Taoukis P. Effect of pulsed electric field treatment on the kinetics of rehydration, textural properties, and the extraction of intracellular compounds of dried chickpeas. *J Food Sci.* (2021) 86:2539–52. doi: 10.1111/1750-3841.15768
- Tadini CC, Gut JAW. The importance of heating unit operations in the food industry to obtain safe and high-quality products. *Front Nutr.* (2022) 9:853638. doi: 10.3389/fnut.2022.853638
- Jin T, An Q, Qin X, Qin X, Hu Y, Hu J, et al. Applying cold atmospheric plasma to preserve the postharvest qualities of winter jujube (*Zizyphus jujuba* Mill. cv. Dongzao) during cold storage. *Front Nutr.* (2022) 9:934841. doi: 10.3389/fnut.2022.934841
- Won JS, Lee SJ, Park HH, Song KB, Min SC. Edible coating using a chitosan-based colloid incorporating grapefruit seed extract for cherry tomato safety and preservation. *J Food Sci.* (2018) 83:138–46. doi: 10.1111/1750-3841.14002
- Cao X, Huang R, Chen H. Evaluation of food safety and quality parameters for shelf life extension of pulsed light treated strawberries. *J Food Sci.* (2019) 84:1494–500. doi: 10.1111/1750-3841.14613
- Chen C, Zhang H, Zhang X, Dong C, Xue W, Xu W. The effect of different doses of ozone treatments on the postharvest quality and biodiversity of cantaloupes. *Postharvest Biol Technol.* (2020) 163:111124. doi: 10.1016/j.postharvbio.2020.111124
- Beirão-da-costa S, Moura-guedes MC, Ferreira-pinto MM, Empis J, Moldão-martins M. Alternative sanitizing methods to ensure safety and quality of fresh-cut kiwifruit. *J Food Process Preserv.* (2014) 38:1–10. doi: 10.1111/j.1745-4549.2012.00730.x
- Chen C, Zhang H, Dong C, Ji L, Zhang X, Li L, et al. Effect of ozone treatment on the phenylpropanoid biosynthesis of postharvest strawberries. *RSC Adv.* (2019) 9:25429–38. doi: 10.1039/C9RA03988K
- de Souza LP, D'Antonino Faroni LR, Heleno FF, Cecon PR, Carvalho Gonçalves TD, da Silva GJ, et al. Effects of ozone treatment on postharvest carrot quality. *LWT.* (2018) 90:53–60. doi: 10.1016/j.lwt.2017.11.057
- Xue Z, Li J, Yu W, Lu X, Kou X. Effects of nonthermal preservation technologies on antioxidant activity of fruits and vegetables: a review. *Food Sci Technol Int.* (2016) 22:440–58. doi: 10.1177/1082013215606835
- Zhang H, Zhang X, Dong C, Zhang N, Ban Z, Li L, et al. Effects of ozone treatment on SOD activity and genes in postharvest cantaloupe. *RSC Adv.* (2020) 10:17452–60. doi: 10.1039/D0RA00976H
- Lv Y, Tahir I, Olsson ME. Effect of ozone application on bioactive compounds of apple fruit during short-term cold storage. *Sci Hortic.* (2019) 253:49–60. doi: 10.1016/j.scienta.2019.04.021
- Shezi S, Magwaza LS, Mditshwa A, Tesfay SZ. Changes in biochemistry of fresh produce in response to ozone postharvest treatment. *Sci Hortic.* (2020) 269:109397. doi: 10.1016/j.scienta.2020.109397
- Piechowiak T, Skóra B, Balawejder M. Ozone treatment induces changes in antioxidative defense system in blueberry fruit during storage. *Food Bioprocess Technol.* (2020) 13:1240–5. doi: 10.1007/s11947-020-02450-9
- Ignat I, Volf I, Popa VI. A critical review of methods for characterisation of polyphenolic compounds in fruits and vegetables. *Food Chem.* (2011) 126:1821–35. doi: 10.1016/j.foodchem.2010.12.026
- Carocho M, Ferreira IC. A review on antioxidants, prooxidants and related controversy: natural and synthetic compounds, screening and analysis methodologies and future perspectives. *Food Chem Toxicol.* (2013) 51:15–25. doi: 10.1016/j.fct.2012.09.021
- Longhao L. *Study on Optimum Storage Conditions and Chilling Injury Mechanism of Pitaya*. Fuzhou: Fujian Agriculture and Forestry University (2014).
- Wang J, Wang S, Sun Y, Li C, Li Y, Zhang Q, et al. Reduction of *Escherichia coli* O157: H7 and naturally present microbes on fresh-cut lettuce using lactic acid and aqueous ozone. *RSC Adv.* (2019) 9:22636–43. doi: 10.1039/C9RA03544C
- Gutiérrez DR, Chaves AR, Rodríguez SDC. UV-C and ozone treatment influences on the antioxidant capacity and antioxidant system of minimally processed rocket (*Eruca sativa* Mill.). *Postharvest Biol Technol.* (2018) 138:107–13. doi: 10.1016/j.postharvbio.2017.12.014
- Katya C, Valentina M, Greta P, Daniel OC, Laura M. *Humulus lupulus* cone extract efficacy in alginate-based edible coatings on the quality and nutraceutical traits of fresh-cut kiwifruit. *Antioxidants.* (2021) 10:1395. doi: 10.3390/antiox10091395
- Li X, Li M, Wang L, Wang J, Jin P, Zheng Y. *Methyl jasmonate* primes defense responses against wounding stress and enhances phenolic accumulation in fresh-cut pitaya fruit. *Postharvest Biol Technol.* (2018) 145:101–7. doi: 10.1016/j.postharvbio.2018.07.001
- Yingsanga P, Srilaong V, Kanlayanarat S, Noichinda S, McGlasson WB. Relationship between browning and related enzymes (PAL, PPO and POD) in rambutan fruit (*Nephelium lappaceum* Linn.) cvs. Rongrien and See-Chompoo. *Postharvest Biol Technol.* (2008) 50:164–8. doi: 10.1016/j.postharvbio.2008.05.004
- Labadie M, Vallin G, Petit A, Ring L, Hoffmann T, Gaston A, et al. Metabolite quantitative trait loci for flavonoids provide new insights into the genetic architecture of strawberry (*Fragaria × ananassa*) fruit quality. *J Agric Food Chem.* (2020) 68:6927–39. doi: 10.1021/acs.jafc.0c01855
- Patil S, Bourke P, Frias JM, Tiwari BK, Cullen PJ. Inactivation of *Escherichia coli* in orange juice using ozone. *Innovat Food Sci Emerg Technol.* (2009) 10:551–7. doi: 10.1016/j.ifset.2009.05.011
- Piechowiak T, Balawejder M. Impact of ozonation process on the level of selected oxidative stress markers in raspberries stored at room temperature. *Food Chem.* (2019) 298:125093. doi: 10.1016/j.foodchem.2019.125093
- Alwi NA, Ali A. Dose-dependent effect of ozone fumigation on physiological characteristics, ascorbic acid content and disease development on bell pepper (*Capsicum annuum* L.) during storage. *Food Bioprocess Technol.* (2015) 8:558–66. doi: 10.1007/s11947-014-1419-2
- Boonkorn P, Gemma H, Sugaya S, Setha S, Uthaibutra J, Whangchai K. Impact of high-dose, short periods of ozone exposure on green mold and antioxidant enzyme activity of tangerine fruit. *Postharvest Biol Technol.* (2012) 67:25–8. doi: 10.1016/j.postharvbio.2011.12.012
- Chen J, Hu Y, Wang J, Hu H, Cui H. Combined effect of ozone treatment and modified atmosphere packaging on antioxidant defense system of fresh-cut green peppers. *J Food Proc Preserv.* (2016) 40:1145–50. doi: 10.1111/jfpp.12695
- Glowacz M, Colgan R, Rees D. Influence of continuous exposure to gaseous ozone on the quality of red bell peppers, cucumbers and zucchini. *Postharvest Biol Technol.* (2015) 99:1–8. doi: 10.1016/j.postharvbio.2014.06.015
- Ali A, Ong MK, Forney CF. Effect of ozone pre-conditioning on quality and antioxidant capacity of papaya fruit during ambient storage. *Food Chem.* (2014) 142:19–26. doi: 10.1016/j.foodchem.2013.07.039
- Haminiuk CWI, Maciel GM, Plata-Oviedo MSV, Peralta RM. Phenolic compounds in fruits—an overview. *Int J Food Sci Technol.* (2012) 47:2023–44. doi: 10.1111/j.1365-2621.2012.03067.x



## OPEN ACCESS

## EDITED BY

Yuanyuan Shan,  
Northwest A&F University, China

## REVIEWED BY

Qun Huang,  
Guizhou Medical University, China  
Tao Yin,  
Huazhong Agricultural  
University, China

## \*CORRESPONDENCE

Wei Wang  
wangwei812002@hotmail.com  
Shumin Yi  
yishumin@bhu.edu.cn

<sup>†</sup>These authors have contributed  
equally to this work and share first  
authorship

## SPECIALTY SECTION

This article was submitted to  
Nutrition and Food Science  
Technology,  
a section of the journal  
Frontiers in Nutrition

RECEIVED 17 September 2022

ACCEPTED 03 October 2022

PUBLISHED 18 October 2022

## CITATION

Wang Z, Ma R, Jia Z, Lin P, Zhao Z,  
Wang W, Yi S, Li X and Li J (2022)  
Investigating on the influence  
mechanism of sausage of sea bass on  
calcium absorption and transport  
based on Caco-2 cell monolayer  
model. *Front. Nutr.* 9:1046945.  
doi: 10.3389/fnut.2022.1046945

## COPYRIGHT

© 2022 Wang, Ma, Jia, Lin, Zhao,  
Wang, Yi, Li and Li. This is an  
open-access article distributed under  
the terms of the [Creative Commons  
Attribution License \(CC BY\)](#). The use,  
distribution or reproduction in other  
forums is permitted, provided the  
original author(s) and the copyright  
owner(s) are credited and that the  
original publication in this journal is  
cited, in accordance with accepted  
academic practice. No use, distribution  
or reproduction is permitted which  
does not comply with these terms.

# Investigating on the influence mechanism of sausage of sea bass on calcium absorption and transport based on Caco-2 cell monolayer model

Zhongqiang Wang<sup>†</sup>, Ranzhuo Ma<sup>†</sup>, Zhihui Jia, Peng Lin,  
Zhenhua Zhao, Wei Wang\*, Shumin Yi\*, Xuepeng Li and  
Jianrong Li

College of Food Science and Technology, National & Local Joint Engineering Research Center of  
Storage, Processing and Safety Control Technology for Fresh Agricultural and Aquatic Products,  
National R&D Branch Center of Surimi and Surimi Products Processing, National and Local United  
Engineering Lab of Marine Functional Food, College of Mathematical Sciences, College of  
International Education, Bohai University, Jinzhou, China

A monolayer Caco-2 cell model was established to explore the effects of sea bass sausage digestive juice containing phosphate on calcium ion transport. Differential proteins of Caco-2 cells treated with fish sausage juice were detected and analyzed by gene ontology (GO) functional annotation and Kyoto encyclopedia of genes and genomes (KEGG) pathway analyses. Results revealed that after treatment with 0.23 mg/mL digestive juice of perch sausage *in vitro*, Caco-2 cell viability was the highest at 72 h (99.84%). Additionally, 0.23 mg/mL digestive juice of perch sausage *in vitro* significantly increased calcium ion transport. The transfer volume was 1.396  $\mu\text{g}/\text{well}$ . Fish sausages containing phosphate significantly affected the protein expression levels of Caco-2 cells. Two hundred one differential proteins were detected, including 114 up-regulated and 87 down-regulated proteins. The main differential proteins included P02795, Q9P0W0, Q96PU5, Q9GZT9 and Q5EBL8. The adjustment ratios of the fish sausage group were 0.7485, 1.373, 1.2535, 0.6775, and 0.809, respectively. The pathway analysis showed that phosphate affected calcium ion absorption and transport through the P02795 enrichment pathway. The fish sausage group showed that the immune-related functions of cells were affected. This study expounds the effects of water-retaining agents on the nutritional quality of aquatic products and provides theoretical support for the research and application of surimi products.

## KEYWORDS

sea bass sausages, proteomics, Caco-2 cell, calcium ion transport, pathway analysis

## Introduction

Surimi is a concentrate of myogenic fibrous proteins obtained by completely removing fish bones, fins, and viscera, and continuously washing the fish flesh (1, 2). Good quality surimi and surimi products have good gel strength, sensory quality, and economic value. However, the current moisture content of commercially available surimi in China is 73–80% and is susceptible to juice loss during freezing, refrigeration, storage, and transportation (3). The addition of food additives is an effective method for improving the quality of the gel of surimi products, among which, phosphate complex is widely used as it improves the water-holding capacity of these products and prevents protein denaturation (4). Phosphate compounds have been widely used as additives in fish and seafood to improve the functional properties of these products by increasing the water retention capacity of fresh fish and reducing the thawing loss of frozen fish (5). When fish die at a low pH, the addition of phosphate increases the pH and thereby avoids the isoelectric point of proteins. The charges then repel each other, leaving more space between proteins, and moisture is retained in the muscle (6).

Calcium is the most abundant mineral found in the human body, which forms teeth and bones and participates in various physiological activities as a second messenger of cellular activities (7). Calcium homeostasis disorders induce the risk of bone diseases, metabolic diseases, and epithelial tumors (8, 9). Dietary calcium generally exists in bound form, which is decomposed into calcium ions under the action of gastric acid (10). Ionized calcium is found mainly in the duodenum and upper jejunum and is absorbed by the human body through active or passive transport and enters the blood through intestinal epithelial cells (11). Phosphorus and calcium homeostasis play important roles in many physiological systems and disorders in calcium and phosphorus metabolism lead to serious consequences, such as bone-related and cardiovascular diseases, which can be life-threatening (12).

Due to their spontaneous differentiation into small intestinal phenotypes and ability to maintain proton gradients (13), Caco-2 cells have been widely used in medicine and food as a cell model for the study of drug transport, metabolism, and toxicity (14). In a specific culture environment, Caco-2 cells carry out biochemical and morphological differentiation *in vitro* during the early stages of culturing, producing microvilli and enzymes related to the brush margin epithelium in the small intestines (15). The Caco-2 cell monolayer shows brush-like characteristics after close fusion, which forms a good carrier transport system. Differentiated Caco-2 cells have better morphological and functional differentiation than other colon cancer cell lines (16, 17). Therefore, the Caco-2 cell model can partly reveal the transport

mechanism of nutrients or drug molecules in the human intestinal tract.

Proteomics refers to the characterization of the proteome (18), which is an important method for understanding gene functions (19). Changes in gene expression levels can be elucidated by analyzing the transcriptome or proteome (20). As the main regulator of life activities, the expression levels of proteins are closely related to the corresponding mRNA and host translation regulation, thus, proteomics is the most relevant method through which the biological system can be characterized (21). Tandem quality labeling (Tandem Mass Tags, TMT) is a proteomic quantitative method (22). By specifically labeling the amino groups of peptide ends and side chains, and after tandem mass spectrometry (MS/MS) analysis, the relative protein contents in 2, 6, or 10 groups of different samples can be simultaneously compared. It has the advantages of high throughput, high resolution, accurate protein quantification, good repeatability, and rich data (23); thus, it is suitable for a wide range of sample markers, including cells and tissues, and also has a fast reaction speed and high labeling rate. Moreover, TMT is widely used in disease marker screening, disease pathogenesis research, drug target research, and physiological and pathological research of animals and plants (24–31).

In this study, a monolayer Caco-2 cell model was established to explore calcium ion absorption and transport in surimi products. The differential proteins of Caco-2 cells treated with compound phosphate were detected by TMT protein quantitative technology using David software. The identified differential proteins were detected by GO functional annotation and KEGG pathway analyses. This paper preliminarily expounds the effects of water-retaining agents on the nutritional quality of aquatic products, as well as provides nutritional theoretical support for the research, development, and application of surimi products.

## Materials and methods

### Materials

Dulbecco's modified eagle medium (DMEM) (Gibco Co., USA); 0.25% trypsin-ethylene diamine tetraacetic acid (EDTA) solution (Gibco Co., USA); fetal bovine serum (Biological Industries Co., Israel); phosphate buffered saline (PBS) (Beijing Solebao Technology Co., Ltd., Beijing, China); Caco-2 cell line (Cell Resource Center, Institute of Basic Medicine, Chinese Academy of Medical Sciences, China); penicillin-streptomycin (Sigma, USA); Cell Counting Kit-8 (CCK-8) (Biyuntian Biology Co., Ltd.), cell culture plate, cell culture bottle (Wuxi Ness Biotechnology Co., Ltd.); DL-Dithiothreitol (DTT) (Chemical Pure Plomag Biotechnology Co., Ltd., Beijing,

China); iodoacetamide (IAM) (Chemical Pure Promeg Beijing Biotechnology Co., Ltd., Beijing, China).

## Sample pretreatment

Fresh sea bass was used to make surimi by adding salt and 0.5% compound phosphate for vacuum chopping, then exhausting the enema. The simulated *in vitro* digestion of sea bass sausages was carried out by stimulating the digestive system of a bionic dynamic human stomach *in vitro*. An appropriate amount of digestive juice from sea bass sausages *in vitro* was obtained and freeze-dried for 72 h. Dry powder of the digestive juice was added to the DMEM cell culture medium according to the set concentrations; the complete cell culture medium was prepared. The control group consisted of a complete cell culture medium. Positive control group: consisted of cells and complete medium, in which complete medium contained 1 mg/L potassium phosphate. The experimental groups were based on a numerical range of normal human blood phosphorus levels and concentrations of freeze-dried powder of sea bass sausages *in vitro* (referred to as digestive juice of sea bass sausages simulated *in vitro*). Normal blood phosphorus levels in humans range from 0.74 to 1.39 mmol/L (32). The experimental groups were set to 0.11 mg/mL (0.06 mg/L), 0.15 mg/mL (0.09 mg/L) and 0.23 mg/mL (0.13 mg/L) (0.06 mg/L, 0.09 mg/L and 0.13 mg/L represent the concentrations of phosphate obtained from the freeze-dried powder of sea bass sausages).

## Culture of Caco-2 cells

After resuscitation, Caco-2 cells were transferred to a cell culture flask and supplemented with a culture medium. After gentle shaking and mixing, the cells were cultured at a constant temperature in a cell incubator; the culture medium was changed according to the cell growth state. Cell passage was carried out when the cell density reached 80–90%. The mouth of the culture bottle was disinfected with alcohol and transferred to a super-clean worktable. Then, the original medium was disposed and cells were washed with PBS two or three times to remove dead cells and cells in bad condition. Trypsin was added for digestion for 2–3 min. Subsequently, the cells were observed and a medium was added to stop digestion. When cells were digested and retracted, but not completely slipped off, cells that were still attached to the wall of the cell culture bottle were gently blown down and repeated as needed to make the cell suspension. The digested cells were sub-cultured in flasks in appropriate proportions and the complete culture medium was supplemented to the required amount. The Caco-2 cell culture flasks were placed in a cell culture box at 37°C and 5% CO<sub>2</sub> for further experimentation (33).

## Effects of fish sausage digestive juice on Caco-2 cell activity

Cells with a density of 80–90% after inoculation were digested, which were then inoculated on a culture plate by adjusting the cell density. All experimental groups were set up at the same time. After cells adhered to the wall, the cell culture plates were removed and the original medium was discarded. Complete cell culture mediums in the same volume were added to the blank and control groups. The cell culture medium containing the highest phosphate concentration was added to the positive control group. In the experimental groups, the complete culture medium containing digestive juice with different phosphate concentrations was added. Five multiple holes were set up for each group and placed in the incubator to continue culturing. After incubating for a fixed time, the culture plates were removed and a corresponding volume of CCK-8 determination reagent was added according to the volume of the cell culture medium of each well. Then, plates were shaken evenly by the cross method and placed in a CO<sub>2</sub> cell incubator under complete darkness. The optical density (OD) was measured at a wavelength of 450 nm by an enzyme labeling instrument. The cell activity was calculated as follows:

$$\text{Cell activity} = \frac{A_s - A_b}{A_c - A_b} \times 100\%$$

where  $A_s$  is the experimental well, containing cell culture medium, CCK-8 and digestion solution;  $A_c$  is the control well, containing the medium of the cells and CCK-8, but without the digestion solution;  $A_b$  is a blank well, which is medium without cells and digestive juices, but containing CCK-8.

## Establishment of Caco-2 cells absorption model

When the density of Caco-2 cells reached 80%, the original culture medium was discarded and the cells were gently rinsed with PBS two or three times to remove dead cells and cells in bad condition. Then, trypsin was added for digestion, and the digested cells were added to the top of a Transwell cell transport chamber, followed by adding a fresh cell culture medium to the bottom. The liquid was changed every other day during the initial stage of cell inoculation and every day after 1 week. The blank group contained the same amount of buffer. After cells were cultured for 21 d, cell differentiation was observed under an inverted microscope. During the culture period, the transmembrane resistance (TEER) values and transmittance of sodium fluorescein were measured regularly to determine whether the model was successful.



## Evaluation of Caco-2 cells absorption model

### Morphological observation of Caco-2 cells

After culturing for 21 d, the liquid on both sides of the Transwell chamber was discarded and cells were washed with PBS. Pentanediol solution was added to the cells on both sides of the chamber to fix the cells. The polyester film was cut into a  $0.5 \times 0.8$  cm rectangle, rinsed twice with 0.1 mol/L buffer (10 min each time), and fixed with 1% osmic acid for 3 h. The fixed polyester film was washed with buffer and dehydrated for 30 min with alcohol in gradient concentrations until completely dry. The dried sample was fixed on a sample holder, sprayed with gold, and observed and photographed under an emission scanning electron microscope.

### Cell transmembrane resistance detection

The TEER of cells after 3, 6, 9, 12, 15, 18, and 21 d of inoculation were measured using a resistance meter. The TEER was calculated as follows:

$$\text{TEER} = (\text{R assay group} - \text{R blank group}) \times A$$

where A is the cell monolayer membrane area ( $1.12 \text{ cm}^2$ ), the unit is  $\Omega \cdot \text{cm}^2$ .

### Permeability experiment of Caco-2 cell monolayer model

The buffer was used to configure the standard solution of sodium fluorescein in gradient concentrations. The OD of sodium fluorescein was determined at 492 nm and the standard curve was made. The absorption rate of fluorescein sodium was evaluated using the monolayer model. The original culture medium in the Transwell transport chamber was discarded, cells were washed with PBS, and placed in an incubator for balance (buffer was added to each well). Then, 0.5 mL  $10 \mu\text{g/mL}$  sodium fluorescein solution was added to the AP side of the chamber and 1.5 mL PBS (preheated to  $37^\circ\text{C}$ ) was added to the BL side. The Transwell chamber was subsequently placed in an incubator. Every 30 min, a certain volume of buffer was removed from the lower chamber. The OD of sodium fluorescein was measured at 492 nm and the transmittance was calculated as follows:

$$P_{\text{app}} = \frac{dQ}{dt \times A \times C_0}$$

where  $dQ/dt$  is the transmittance of sodium fluorescein per unit time, A is the area of the Transwell chamber floor, and  $C_0$  is the concentration of the experimental group.

## Caco-2 cell transport experiment

The cell transport experiment was carried out using the Caco-2 cell monolayer model with transmembrane resistance and sodium fluorescein transmittance. The original medium was discarded and the cells were gently rinsed with PBS buffer (preheated to  $37^\circ\text{C}$ ) two or three times to remove impurities on the cell surface. Then, the transmittance of sodium fluorescein was measured; the blank experiment was run at the same time. The culture plates were incubated and the liquid on both sides after each 30 min interval was collected in a centrifuge tube and diluted to a suitable concentration. The liquid was filtered with a  $0.22\text{-}\mu\text{m}$  needle filter. The calcium content was detected by a calcium chromogenic detection kit. The calcium transport volume was calculated using the following formula:

$$B_n = 0.5 \times A_n + 0.05 \times \sum_{k=1}^{n-1} A_k$$

where  $B_n$  is the calcium content of 0.5 mL buffer on the BL side at different time points,  $\mu\text{g}$  is the calcium concentration on the BL side at different time points, and n is an independent variable (1, 2, 3, and 4 represent 30, 60, 90, and 120 min, respectively).

## Caco-2 cell pretreatment

Caco-2 cells were inoculated in cell culture plates according to the appropriate density. After the cells were full, they were treated with the cell culture medium containing phosphate at a concentration and divided into the control, positive control, and fish sausage groups with three repeats of each group. After the cells met the requirements of the follow-up experiment, the corresponding proportion of phosphate buffer was added according to the bottom area of the cell culture plate. Caco-2 cells were gently scraped off with a cell scraper on the ice box, transferred to a frozen cell tube, and placed in liquid nitrogen. After quick freezing in liquid nitrogen, Caco-2 cell samples were mailed to the Beijing Huada Protein Research and Development Center Co., Ltd. (China) for proteomic analysis.

## Caco-2 cell protein extraction

An appropriate amount of cell samples was added to the lysate and placed under ultrasonication for 5 min to facilitate cleavage {the lysate buffer included 8 m urea, 30 mM 2-[4-(2-hydroxyethyl) piperazin-1-yl] ethanesulfonic acid (HEPES), 1 mM phenylmethanesulfonyl fluoride (PMSF), 2 mM EDTA, and 10 mM DTT}. The supernatant was obtained after centrifugation at 20,000 g for 30 min. The final concentration of the solution after pyrolysis was adjusted to 10 mmol/L by

adding DTT. After bathing at 56°C for 1 h, IAM was added to adjust the final concentration to 55 mmol/L and placed in a dark room for 1 h. At the end of the static placement, pre-cooled acetone was added and precipitated at −20°C for >3 h. Then, the supernatant was discarded after centrifugation at 4°C and 20,000 g for 30 min. After the addition of resolvable buffer, the final concentration of the solution was adjusted and placed under ultrasonication for 3 min. After centrifugation at 4°C and 20,000 g for 30 min, the supernatant was obtained and the extracted proteins were quantified using the Bradford method.

Caco-2 cell protein digestion

Using an appropriate amount of cell sample, the lysate was added and the sample was placed under ultrasonication for 5 min to facilitate lysis. After centrifugation, the supernatant was obtained. Dithiothreitol and iodoacetamide were added to the supernatant to adjust the final concentration of the solution after pyrolysis. After static placement, acetone was added to the sample to precipitate at a low temperature and the supernatant was discarded after centrifugation. The final concentration was adjusted by adding resolvable buffer and ultrasonication was used to assist with solubilization. The supernatant was obtained after centrifugation and the extracted proteins were quantitatively analyzed using the Bradford method.

Mass spectrometry detection

After balancing the TMT labeling reagent at room temperature, 41 µL acetonitrile was added then mixed for 1 min and centrifuged. A labeling reagent at room temperature was added to the redissolved peptide, mixed, and left at room temperature for 1 h. Then, 8 µL 5% hydroxylamine was added and placed at room temperature for 15 min. The sample was mixed and vacuum dried.

An appropriate amount of protein was added to the ultrafiltration tubes from each group of samples and the waste liquid was discarded after centrifugation. Tetraethyl ammonium bromide buffer was added for centrifugation and the precipitation was subsequently obtained. After repeating the above operations, trypsin was added to digest the extracted proteins and the protein digestion liquid was freeze-dried into a dry powder. Then, tetraethyl ammonium bromide (TEAB) was added to each tube to redissolve the peptides.

After the TMT labeling reagent reached room temperature, 41 µL acetonitrile was added, mixed for 1 min, and centrifuged. The labeling reagent was added to the redissolved peptide,

TABLE 1 The parameter of mass spectrometer.

Parameter name	Parameter	Parameter value
Ion mode	Polarity	Parameter value
Parent ion scanning range	MS scan range	350–2,000 m/z
Secondary resolution	Resolution	17,500
Capillary temperature	Capillary temperature	320°C
Source voltage	Ion source voltage	1,800 V
Fragmentation mode	MS/MS acquisition modes	Higher collision energy dissociation (HCD)
Collision energy normalization	Normalized collision energy (NCE)	28

TABLE 2 The parameter of Dionex ultimate 3,000 nano LC system.

Item	Parameter
Nano LC trap	Acclaim pepmap 100; 150 µm × 2 cm nanoviper C18 5 µm 100A
Nano LC column	C18 5 µm 75 µm × 15 µm 300A
Solvent A	0.1% formic acid 2% ACN 98% water
Solvent B	0.1% formic acid 2% water 98% ACN
Flow rate	0.4 µL/min

mixed well, and placed at room temperature. After adding hydroxylamine, the sample was mixed and vacuum dried after standing at room temperature.

The purified samples were detected using a Q-Exactive mass spectrometer. The original MS data were searched in the database and the results were filtered with a false discovery rate (FDR) <1%. The specific test parameters are shown in [Tables 1–3](#).

Biological and data analyses

Based on the identified differential protein IDs between the control and fish sausage groups, we annotated the related proteins in the GO database. The corresponding proteins were listed according to three components in the GO database and made into a statistical chart (34). Through a KEGG pathway analysis, the differential proteins were annotated and their distributions in the related pathways were directly observed (35). The differential proteins were also searched in the String database (medium confidence, 0.400) and selected to further construct a protein interaction network (36). The data were processed and analyzed using Thermo Fisher Proteome Discoverer v1.3 and Mascot v2.3.01 software.

TABLE 3 The parameter of identification and retrieval.

Parameter name	Parameter	Experimental options
Mascot version number	Mascot version	2.3.0
Fixed modification	Fixed modification	Carbamidomethyl (C), itraq 8 plex (K), itraq 8 plex (N-term)
Variable modification	Variable modification	Oxidation (M), Gln→ Pyro-Glu (N-term Q), Itraq 8 plex (Y)
Primary quality deviation	Peptide tol	15 ppm
Secondary quality deviation	MS/MS tol	20 mmu
Maximum allowable missed cleavage	Max missed cleavages	1
Enzyme typ	Enzyme	Trypsin
Database	Database	2019-uni-human; Time files compressed: 2019.10.22; Number of sequences: 172097

## Results

### Activity of Caco-2 cells

High phosphate levels can damage endothelial cells. The intake of processed foods with high phosphate additives leads to higher levels of phosphorus in the human body, which increases the risk of cardiovascular disease (37). Therefore, a concentration range of normal human blood phosphorus levels was selected to evaluate the response of Caco-2 cells to increased extracellular phosphate levels.

The digestive juice of sea bass sausages under different phosphate concentrations over time greatly affected the proliferation of Caco-2 cells (Figure 1). After Caco-2 cells were treated with 0.23 mg/mL perch sausage digestive juice for 24, 48, and 72 h, the Caco-2 cell activity increased significantly over time and was the highest after 72 h (99.84%). Compared to the control group, the digestive liquid of sea bass sausages with higher or lower phosphate concentrations inhibited the proliferation of Caco-2 cells, but when the concentration of phosphate was 0.13 mg/L, the digestive liquid of 0.23 mg/mL of sea bass sausages promoted the proliferation of Caco-2 cells. Therefore, in the subsequent experiment, 0.23 mg/mL was selected for the experimental group.

### Morphological observation of Caco-2 cells

The Caco-2 cell line was first established by Fogh et al. (38), while screening the cytotoxicity of antineoplastic drugs and

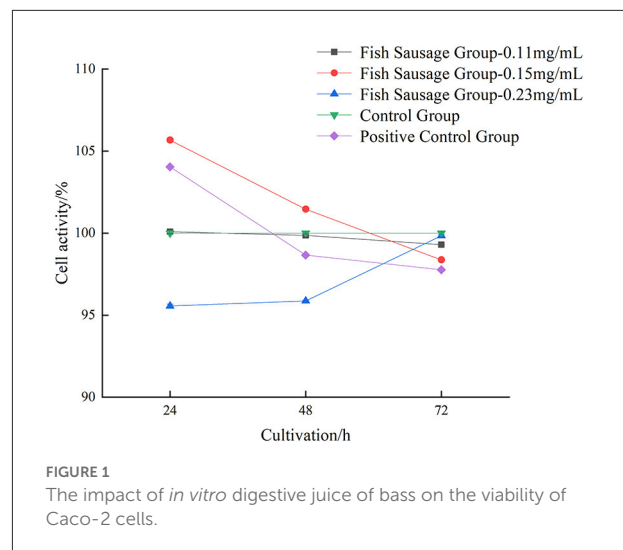


FIGURE 1 The impact of *in vitro* digestive juice of bass on the viability of Caco-2 cells.

studying the mechanism of drug resistance. Over time, Caco-2 cells gradually and spontaneously differentiate into dense cell monolayers. The structure, morphology, and function of cells at this stage are similar to human intestinal epithelial cells. One side of the brush marginal membrane differentiate into microvilli, while the other side of the serosa differentiate into the basal surface (39, 40).

After 21 d, the morphology of Caco-2 cells was observed under an emission site scanning electron microscope. Caco-2 cells were complete and dense, and in a good state at this time (Figure 2A). The next step of the cell transmembrane resistance and sodium fluorescein transmittance test was subsequently carried out. After Caco-2 cells were inoculated on a cell plate for 24 h, the distribution of cells was sparse and some cells were still round (Figure 2B). Caco-2 cells began to fuse slowly 48 h after inoculation (Figure 2C). After 72 h, Caco-2 cells gradually formed into a state of close distribution and grew well (Figure 2D). These results indicated that the cells formed a dense cell monolayer within 21 d of culturing. In a previous study, after continuous culturing for 22 d, Xiang et al. initially established a uniform and dense, tight junction into a seamless single cell layer (41). Our findings were slightly different.

### Determination of electrical resistance of Caco-2 cell monolayer model

Cell transmembrane resistance refers to the ability of the passive diffusion of ionic charges in epithelial cells. Generally, transmembrane resistance should be 200–1,000  $\Omega \text{ cm}^2$  (42). In this study, the transmembrane resistance of Caco-2 cells increased over time (Figure 3). Specifically, after 3, 6, 9, 12, 15, 18, and 21 d, the transmembrane resistance of Caco-2 cells mainly increased. From day 3 to 6, the TEER value increased

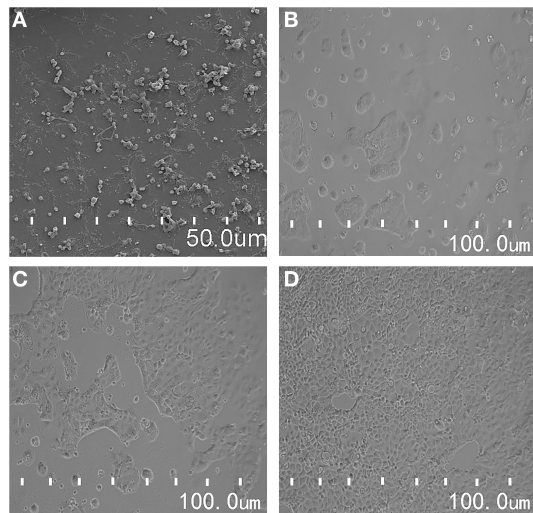


**FIGURE 2**  
(A) The morphological observation of Caco-2 cells by scanning electron microscope; (B–D) is the morphological changes of Caco-2 cells in different culture time.

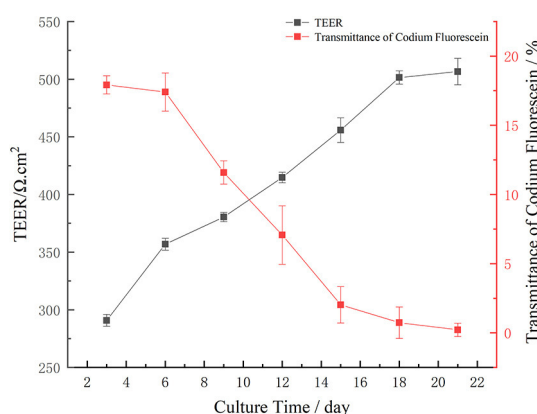


**FIGURE 3**  
Trend of monolayer transmembrane resistance of Caco-2 cell during different culture periods, and transmittance of fluorescein sodium in different culture time: Transmittance of sodium fluorescein from AP side to BL side.

rapidly from 290.83 to 356.91 Ω cm<sup>2</sup>. From day 6 to 18, the TEER value steadily increased from 356.91 to 501.39 Ω cm<sup>2</sup>. On day 12, the TEER value was >400 Ω cm<sup>2</sup>. After 18 d, the TEER value tended to be stable until day 21 when it was ~500 Ω cm<sup>2</sup>. These results are consistent with Li et al. (43). Who found that the transmembrane resistance of cells was >500 Ω cm<sup>2</sup> after 21 d. These findings showed that the compactness of Caco-2 cells was good within 21 d and was thus selected for use in the next experiment.

## Verification of sodium fluorescein permeability in Caco-2 cell monolayer model

Intestinal mucosal permeability is an important characteristic of the intestinal tract that determines the selectivity of intestinal mucosa for nutrients entering the blood and lymphatic circulation and depends on epithelial cell characteristics and a tight junction complex (44). Intestinal permeability refers to the non-mediated intestinal permeation of medium-sized hydrophilic molecules without the assistance of carrier systems (45). Intestinal permeability can be evaluated by measuring the transmembrane resistance or extracellular markers, such as sodium fluorescein, mannitol, and phenol red, among others. The linear regression equation for the absorbance of sodium fluorescein is as follows:

$$y = 0.0285x + 0.0141 \quad (R^2 = 0.9998)$$

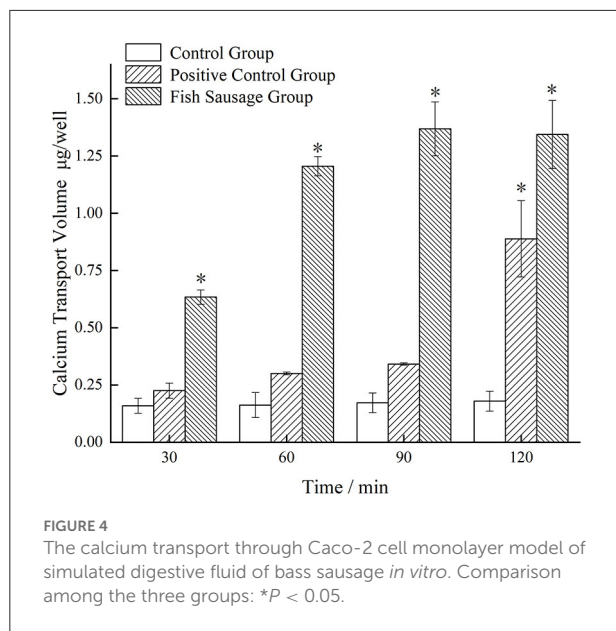
where “y” is the absorbance value and “x” is the concentration of sodium fluorescein (μg/mL).

The transmittance of sodium fluorescein from the AP side to the BL side is shown in Figure 3. The transmittance of sodium fluorescein decreased over time. From day 3 to 6, the transmittance of sodium fluorescein decreased slowly, which was 17.920 and 17.403%, respectively. The transmittance of sodium fluorescein decreased significantly from 17.403% on day 6 to 2.018% on day 15. The transmittance of sodium fluorescein decreased slowly from day 15 to 0.220% on day 21. Over time, the monolayer model of Caco-2 cells found that the sodium fluorescein permeability decreased gradually, then gradually decreased, which indicated that the monolayer Caco-2 cell model had good compactness and could be used for subsequent transport experiments.

## Calcium transport experiment of Caco-2 cells

Figure 4 shows the changes in calcium transport in the monolayer Caco-2 cell model treated with simulated digestive juice of sea bass sausages *in vitro*. Compared to the control group, the amount of calcium transport in the fish sausage group significantly increased after transport through the monolayer Caco-2 cell model ( $P < 0.05$ ). Over time, the calcium transport amount also increased. After incubating for 90 min, the amount of calcium transport in the fish sausage group was significantly higher than the control group ( $P < 0.05$ ). The calcium transport amount in the fish sausage group reached its maximum value of 1.369 μg/well.

The calcium transport volume of the control and positive control groups did not change significantly over time; the



calcium transport amount was relatively small, which may be because the control group only contained a complete cell culture medium. Calcium ions in a complete medium can maintain osmotic pressure balance in the cells, but their content is lower, thus, the amount of calcium transport in the control group was lower. One reason why the amount of calcium transport in the positive control group may have been higher is that the control group may have had high  $K^+$  concentrations that affected the cell membrane potential, thereby affecting the voltage-dependent calcium channel in the membrane. These conditions lead to an influx of extracellular calcium or release of calcium from the intracellular calcium pool, resulting in a rapid increase in the intracellular calcium content (46). However, to maintain a lower intracellular calcium content, calcium ions entering the cytoplasm can be returned to the extracellular environment or calcium pool through the  $Ca^{2+}$ -ATP enzyme (47). To summarize, there is a certain content of calcium present in the digestive juice of sea bass sausages simulated *in vitro* and the amount of promoting calcium transport was higher than the control and positive control groups.

## Identification after protein extraction

Table 4 shows the protein quantification results in Caco-2 cells after treatment. The linear regression equation for protein quantification is as follows:

$$y = 0.1616x + 0.0077 (R^2 = 0.9924)$$

where “y” is the absorbance value and “x” is the protein concentration ( $\mu\text{g}/\mu\text{L}$ ).

According to the quantitative results, the total amount of extracted protein was about 200  $\mu\text{g}$ . it can meet the amount needed for protein enzymatic hydrolysis. Thus, the MS detection of differential proteins could be carried out.

## Protein qualitative analysis

### Display of qualitative results

For the TMT quantitative detection of proteins, there were six groups of samples, the control, positive control, and fish sausage group with two biological repeats of each group. 179,396 spectrums were generated after MS detection. According to the identification results, the number of matching peptides identified by the data was 25,125, the number of matching spectra was 63,046, and the number of protein groups was 4,959 (Table 5).

### Analysis of qualitative results of extracted protein

The number of protein-matching peptides can be used to analyze the specific number of peptides contained in the identified proteins. The greater the number of matching peptides, the lower the number of proteins corresponding to the number of peptides. In the 4,959 groups of identified proteins, 27% of the proteins contained one peptide and the number of proteins composed of two and three peptides accounted for 16 and 12%, respectively (Figure 5A).

Figure 5B shows the statistics of the corresponding coverage of the identified proteins, in which, different colors represent the coverage of different proteins and the number above each color represents the specific number of proteins. Protein coverage refers to the proportion of the number of amino acids identified in a protein to the original number of amino acids in the protein (48). In 4,954 groups of identified proteins, there were 1,256 groups of proteins with a corresponding coverage rate of 0–15%, accounting for 25.3% of the total proteins, and 1,191 groups with a coverage rate of 5–10%, accounting for 24%. There were 733 groups of proteins with a coverage rate of 10–15%, which accounted for 15.6%. The coverage of most proteins was small and mainly concentrated at 0–13%.

## Protein quantitative analysis

The volcano map shows the distribution of the identified differential proteins according to their multiples of change and  $P$ -values. Figures 6A–C show the volcano map of differential proteins among groups, in which, red dots represent the



TABLE 4 The quantitative results of protein samples.

Sample name	Positive control group 1-1	Positive control group 1-2	Fish sausage group 1-1	Fish sausage group 1-2	Control group 1-1	Control group 1-2
Concentration (μg/μL)	1.18	1.00	1.09	0.99	1.69	1.35
Sample volume (μL)	200	200	200	200	200	200
Total protein (μg)	236	200	218	197	338	270

TABLE 5 The information of qualitative result.

Item	Number of tests
Sample information	6
Repeat experiment	1
Matching spectrum	63,046
Matching number of peptides	25,125
Number of proteomes	4,959

expression of significant differential proteins and gray dots represent the expression of non-significant differential proteins.

An ANOVA was conducted, using  $P < 0.05$  and difference multiple  $>1.2$ -times as the screening criteria to determine significant differences between the screened differential proteins (Figure 6D). The number of up-regulated and down-regulated differential proteins in each comparison group was calculated. Red represents the number of up-regulated proteins and green represents the number of downregulated proteins. Compared with the control group, the total number of differential proteins detected in the fish sausage group was 201, including 114 up-regulated proteins and 87 down-regulated proteins. A total of 45 differential proteins were detected in the fish sausage group compared with the positive control group, including 30 up-regulated proteins and 15 down-regulated proteins. Compared with the positive control group, the total number of differential proteins detected in the control group was 266, including 165 up-regulated proteins and 101 down-regulated proteins. Results revealed that both the positive control and fish sausage group significantly affected the protein expression levels in Caco-2 cells.

## GO analysis results

### Go notes

The identified differential proteins were compared to the Uniprot database using David software for classification and annotation. The identified protein GO annotation classifications

are mainly divided into three parts: cellular components (CC), molecular functions (MF), and biological processes (BP) (Figures 7A–C) (49). In BP, the functions with more annotations were mainly concentrated in biochemical processes, cell metabolic processes, metabolic processes, and nitrogen compound metabolic processes, while in CC, the annotated functions mainly included cellular components, intracellular components, and cytoplasm. In MF, the annotated functions mainly focused on catalytic activity, heterocyclic compound binding, and organic ring compound binding. Based on the GO annotation analysis of the top 50 differential proteins, in order of significance, 21 components were concentrated in BP, 18 were concentrated in CC, and the remaining 11 were concentrated in MF.

### GO enrichment analysis

$P$ -value  $< 0.01$  is the selection ranges of differential proteins. The GO enrichment analysis of the differential proteins identified in Caco-2 cells treated with compound phosphate was carried out using David software. Figures 8A,B show the GO analysis bubble diagrams of the differential proteins identified between the control and fish sausage groups, and the control and positive control groups. Z-score represents the overall expression trend of differential proteins enriched to this function, with Z-score  $>0$  indicating up-regulation and Z-score  $<0$  indicating down-regulation. Red represents the CC component, blue represents the MF component, and green represents the BP component. The circle size represents the number of differential proteins enriched in a given function; the larger the circle, the greater the number of differential proteins.

The top 10 differential proteins were mainly enriched in CC and the main enriched GO items included mitochondria, cytoplasm, organelles, and nucleosomes on the inner surface of the cell (Figure 8A). The second was enriched in BP and mainly included histone H3–K27 trimethylation, nucleosome localization, nucleosome assembly, and histone H3–K4 trimethylation. The differential proteins between the control and positive control groups were mainly enriched in CC,

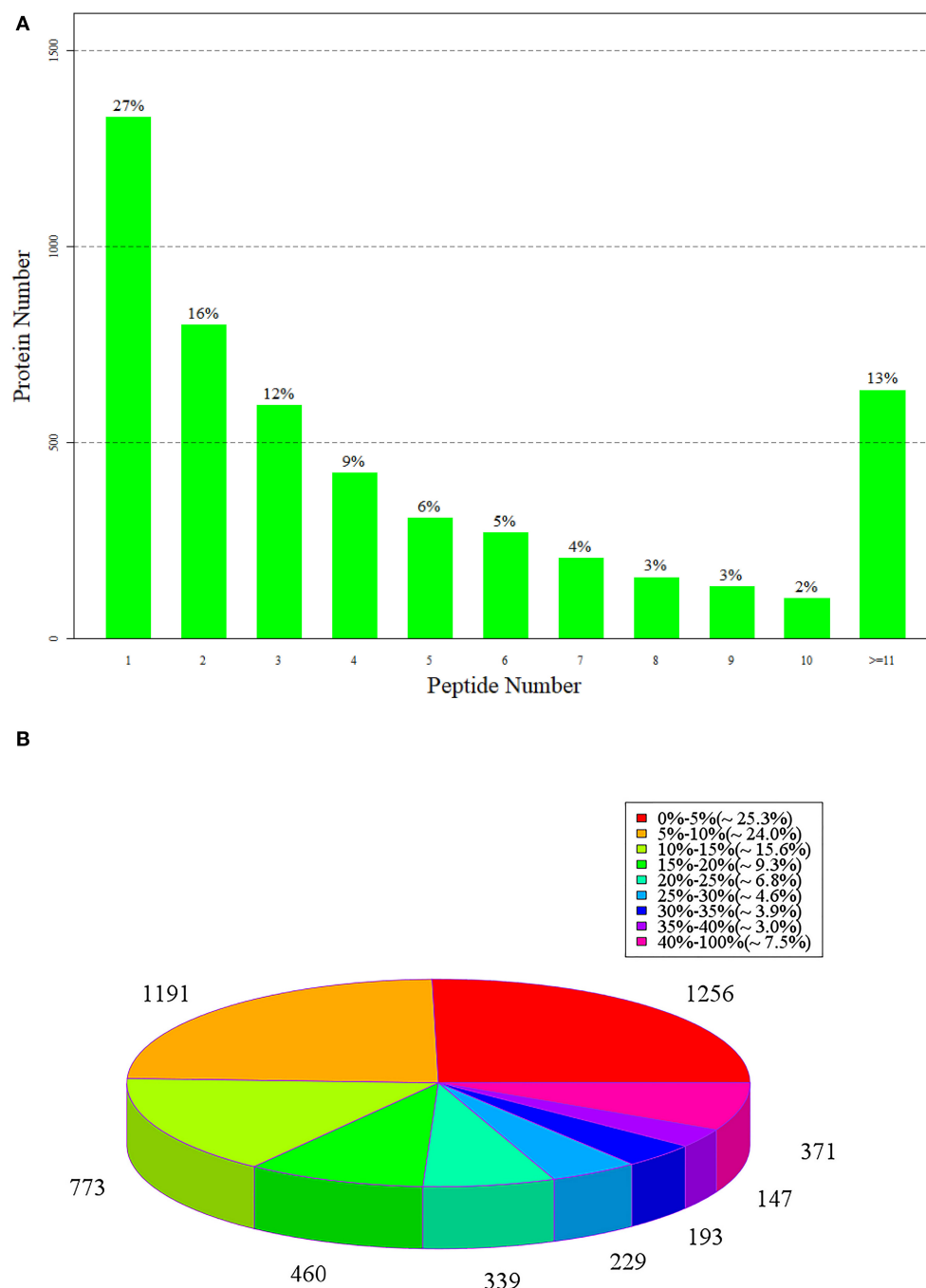
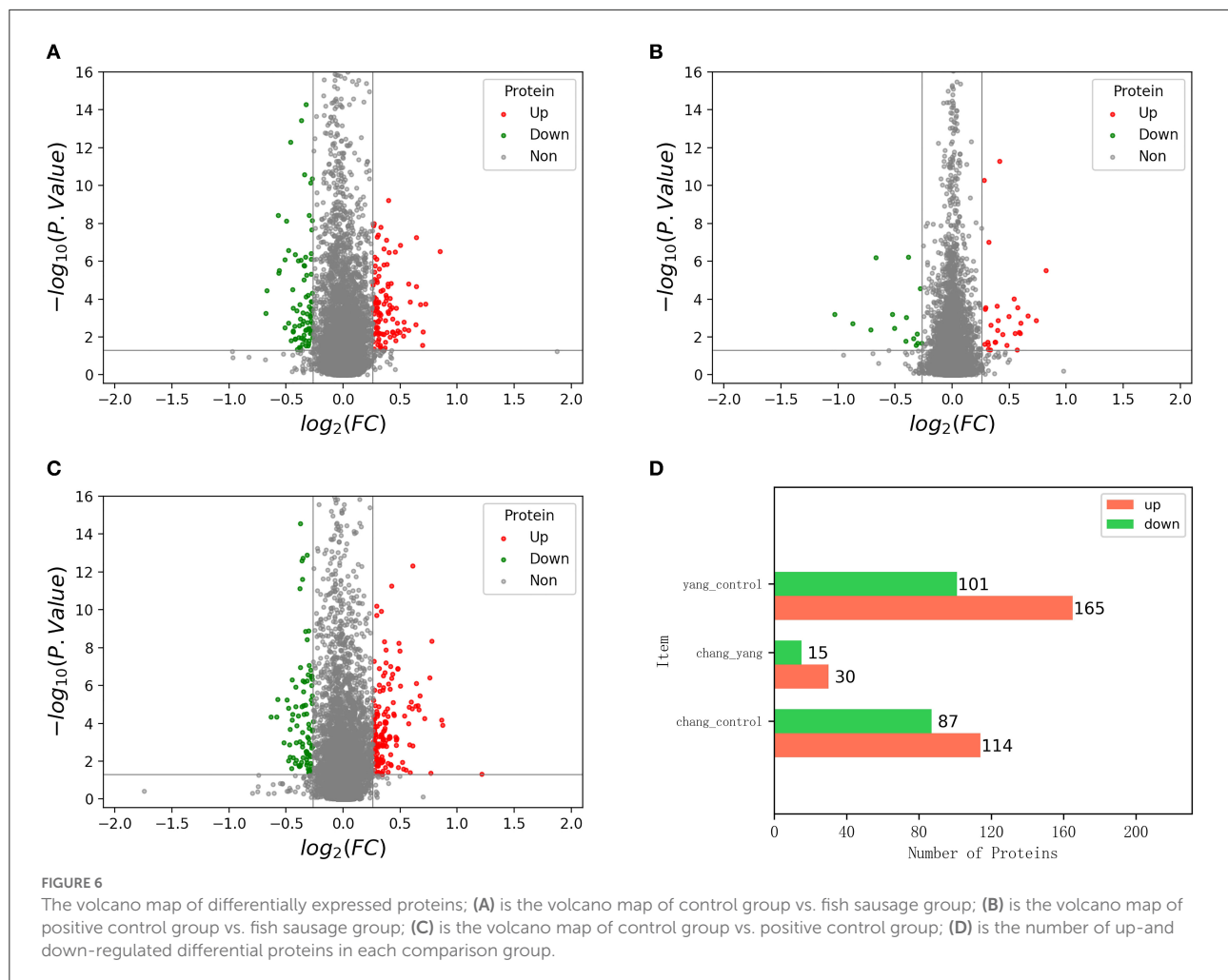


FIGURE 5

(A) The number of peptides matched to proteins; (B) is the statistical diagram of protein identification coverage.

including cytoplasm, mitochondria, cytoplasm, exosomes, and perinuclear regions of the cytoplasm, and in BP, including glycolysis, typical glycolysis, virus reaction, and redox process (Figure 8B). The functions of the differential proteins between the control and fish sausage groups and the control and positive control groups were mostly enriched in areas with a Z-score

>0, indicating that the overall expression of differential proteins was upregulated (Figures 8A,B). Thus, compound phosphate can promote this series of functions, these include: poly (A) RNA binding, cytosol, nucleosome, cytoplasm, histone H3–K27 trimethylation, nucleosome positioning, nucleosome assembly, histone H3–K4 trimethylation, protein binding, perinuclear



region of cytoplasm, mitochondrion, extracellular exosome and oxidation-reduction process.

## KEGG pathway analysis results

The KEGG pathway enrichment analysis of differential proteins was carried out using David software. Figures 9A,B show the pathway chord diagrams of the differential proteins between the control and fish sausage groups, and the control and positive control groups. The differential proteins between the control and fish sausage groups were mainly enriched in the metabolic pathway, followed by fructose and mannose metabolism and pyrimidine metabolism. The differential proteins between the control and positive control groups were mainly enriched in metabolic pathways, antibiotic biosynthesis, and carbon metabolism. The above data suggest that complex phosphate may greatly affect the transport of calcium ions through the metabolic pathway, then the radiation of the

biosynthetic signaling pathway may thereby affect the transport of calcium ions.

Table 6 shows the differential proteins identified in the three groups. Through biological process and pathway analysis, it was found that the key differential proteins included Q5EBL8, P02795, Q9GZT9, Q96PU5, and Q9P0W0, among them, Q5EBL8 and P02795 are closely related to metal ion transport, Q9GZT9, Q96PU5, and Q9P0W0 were enriched, and they were different from the positive group. P02795 (Metallothionein-2, MT-2) is an important member of the metallothionein family. Its main physiological characteristics include metal ion binding and reducibility, and it can reversibly bind to divalent ions, such as zinc, copper, iron, and cadmium, to maintain metal ion balance *in vivo* (50). The concentration of calcium affected the expression of MT-2. In keratinocyte serum-free medium (K-SFM), 4mM  $\text{Ca}^{2+}$  significantly decreased the expression of MT-1/2 proteins in RWPE-1 cells exposed to  $\text{Cd}^{2+}$  (51). The expression of MT-2 in the positive control and fish sausage

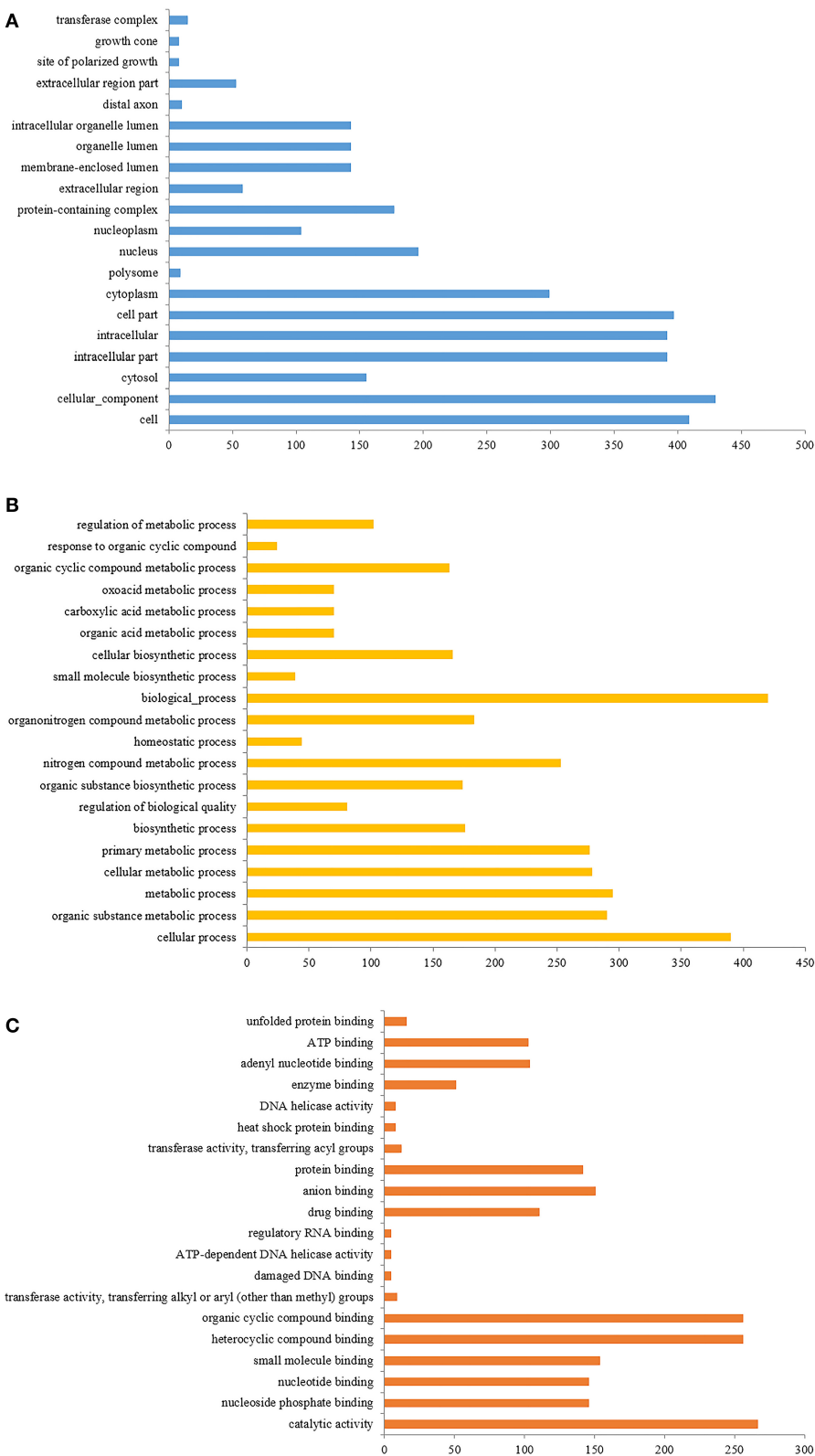


**FIGURE 7**  
(A) The GO enrichment analysis of differentially expressed proteins (cell components); (B) is the GO enrichment analysis of differentially expressed proteins (Biological Process); (C) is the GO enrichment analysis of differentially expressed proteins (Molecular Function).

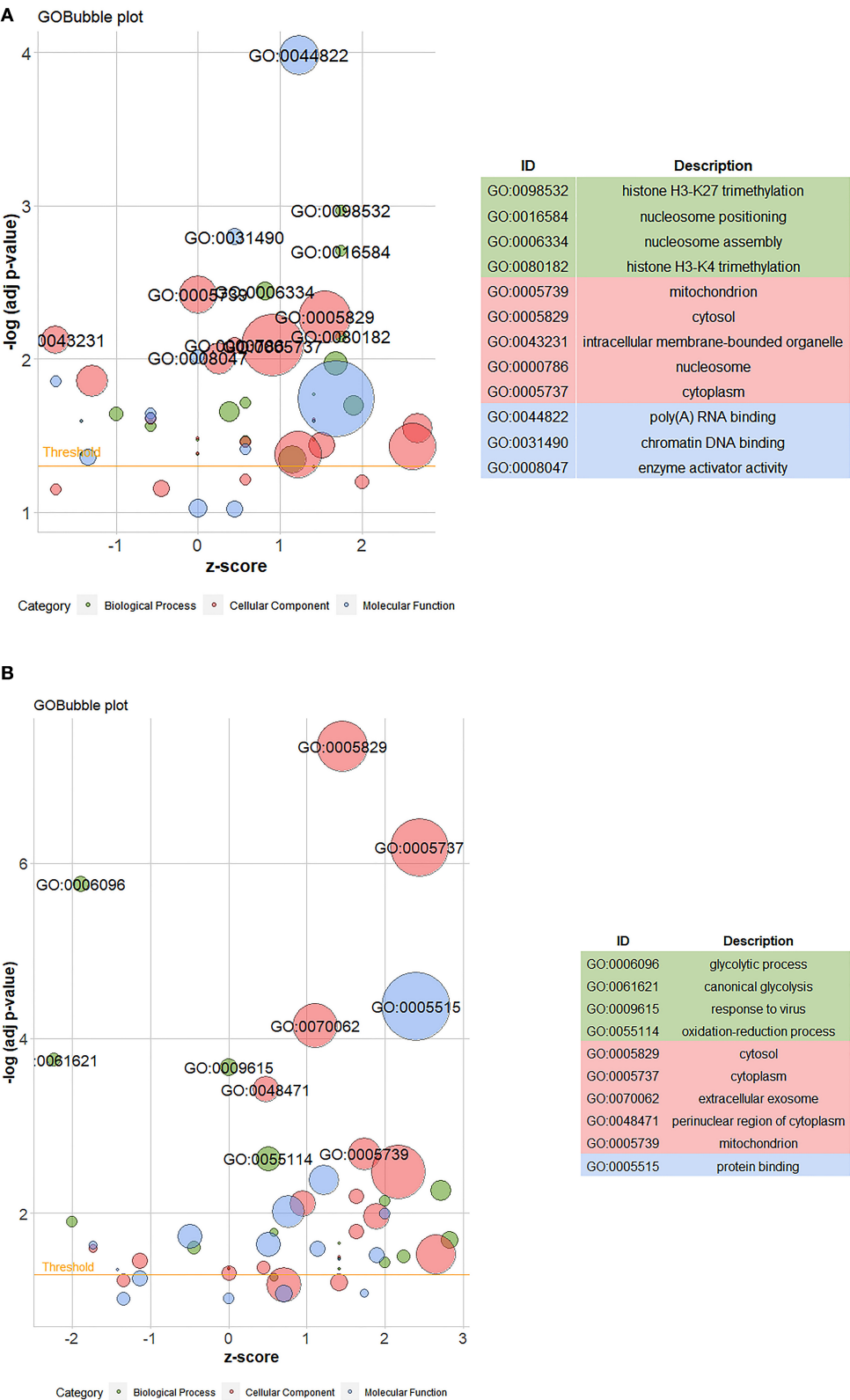


**FIGURE 8**  
(A) The GO bubble map of differential proteins between control (0 mg/mL phosphate residue) and fish sausage group (0.13 mg/L phosphate residue); (B) is the GO bubble map of differential proteins between positive control (1 mg/L phosphate residue) and control group (0 mg/L phosphate residue).



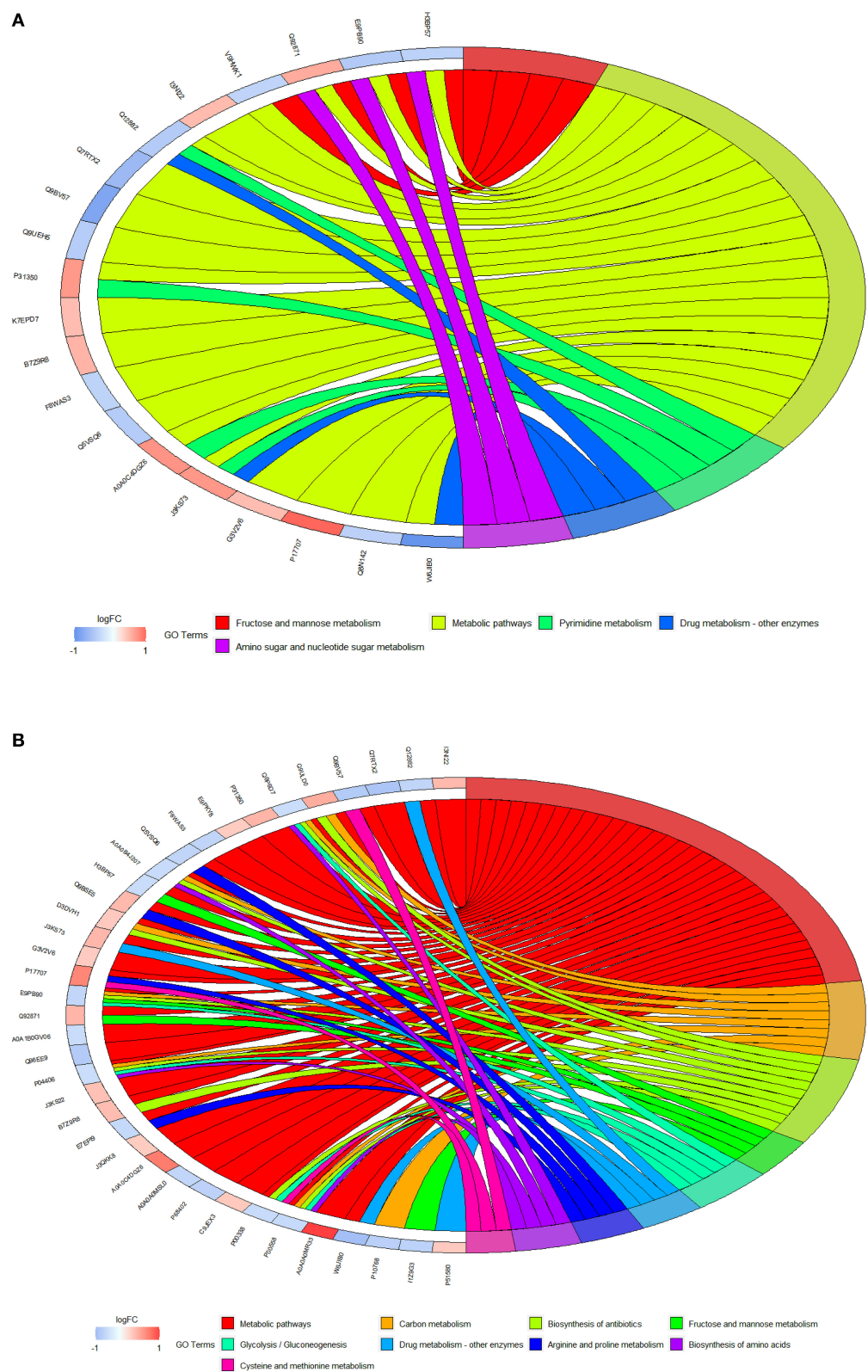


**FIGURE 9**  
(A) The GO chord diagrams of differential proteins between control (0 mg/L phosphate residue) and fish sausage group (0.13 mg/L phosphate residue); (B) is the GO chord diagrams of differential proteins between control (0 mg/L phosphate residue) and positive control group (1 mg/1L phosphate residue).

TABLE 6 The comparison of the main differential proteins among the three groups.

Accession	Description	P-value	Positive vs. control	P-value	Fish sausage vs. control	P-value	Fish sausage vs. positive
Q5EBL8	PDZ domain-containing protein 11	0.00493679	0.8165	0.0000625	0.809	0.36	1.045
Q96PU5	E3 ubiquitin-protein ligase NEDD4-like	0.001600833	1.299	0.027334657	1.2535	0.97	1.0033
Q9P0W0	Interferon kappa	1.49E-08	1.412	0.000000318	1.373	0.54	0.9795
Q9GZT9	Egl nine homolog	0.0000153	0.717	0.00000302	0.6775	0.32	0.956
P02795	Metallothionein-2	3.77E-09	0.802	0.000000427	0.7485	0.01	1.089

groups was down-regulated, which may be due to the decrease in MT-2 expression due to the increased calcium concentration. In the KEGG analysis, P02795 was enriched. The enriched pathway was mineral absorption; phosphate may affect the absorption of calcium through the mineral absorption pathway. Q5EBL8 (PDZ Domain-Containing Protein 11, PDZD11) is a PDZ protein that interacts with plasma membrane calcium ATPase (52). PDZD11 interacts with  $\text{Ca}^{2+}$ -ATPase (PMCA) and affects the biology of PMCA (53). PDZD11 was down-regulated in the positive control and fish sausage groups, indicating that phosphate and fish sausage digestive fluid containing phosphate affected the expression of PDZD11 (Table 6). Q9P0W0 (Interferon-Kappa, IFNK) is a type I interferon with 30% similarity to other type I interferon subclasses (54). In addition to antiviral activity, interferon is involved in a wide range of cellular functions, such as inhibiting the proliferation of normal and tumor cells, stimulating natural killer cells, increasing the expression of major histocompatibility complex antigens, and stimulating tumor antigens (55). The fish sausage and positive control groups promoted IFNK expression, and the positive control group upregulated the expression of IFNK. Therefore, phosphate promoted IFNK expression. Q96PU5 (E3 Ubiquitin-Protein Ligase NEDD4-like, NED4L) is a highly conserved Het E3 ligase (56). NEDD4L mediates the ubiquitination of epithelial Na/K/2Cl cotransporter NKCC1/SLC12A2 and inhibits the cell surface expression of NKCC1/SLC12A2 (57). NEDD4L inhibits tumor growth through the proliferation of ubiquitinated proteins and plays an important role in the occurrence and development of colorectal cancer (58). In this study, phosphate promoted the expression of NED4L, and fish sausages containing phosphate significantly increased NED4L expression. Q9GZT9 (Eglninehomolog1, EGLN1, also known as PHD2) is an oxygen-sensitive factor that regulates the expression of downstream genes by sensing the oxygen content in cells, thereby affecting important physiological processes, such as glucose uptake, metabolic regulation, angiogenesis,

and cell cycle (59). Previous studies have shown that EGLN1 expression is closely related to the occurrence and prognosis of colorectal cancer (60). In the Caco-2 cell model, we found that the fish sausage and positive control groups inhibited EGLN1 expression.

In the KEGG analysis, Q9GZT9, Q96PU5, and Q9P0W0 were differential proteins identified in the positive control and fish sausage groups, which were enriched in the fish sausage group, but not in the positive control group. The enrichment pathways included hypoxia-inducible factor-1 (HIF-1) signaling pathway, ubiquitin-mediated protein hydrolysis, endocytosis, and Janus kinase-signal transducer, an activator of the transcription (JAK-STAT) signaling pathway. The HIF-1 signaling pathway plays an important role in autoimmune diseases (51–63). Endocytosis and ubiquitin-mediated proteolysis belong to the cellular immune pathway (64). The JAK-STAT signaling pathway is related to cell development, cell growth, and survival, thus playing an important role in immune functions. For example, STAT proteins play an important role in the differentiation of T helper lymphocytes (65). Therefore, the fish sausage group may have affected the immune-related function of the cells.

## Conclusions

In this study, a monolayer model of Caco-2 cells cultured *in vitro* was established to explore the transport of calcium in the digestive juice of sea bass. Results revealed that the sausage digestive fluid of sea bass at different phosphate concentrations and culture times greatly affected the proliferation of Caco-2 cells. Cell culture medium containing 0.23 mg/mL sea bass sausage digestive solution effectively increased the proliferation activity of Caco-2 cells. After 21 d of culture, Caco-2 cells formed a dense monolayer structure and the monolayer model had good permeability. According to the

calcium transport data, after Caco-2 cells were treated with perch sausage juice, the amount of calcium transport in the digestive juice increased significantly over time. After 90 min, calcium transport reached its maximum, indicating that compound phosphate effectively promoted intracellular calcium transport.

The TMT protein quantitative technique was used to detect the differential proteins of Caco-2 cells treated with compound phosphate. Results revealed that the number of matching peptides identified by the data was 25,125, the number of matching maps was 63,046, and the number of protein groups was 4,959. Compared to the control group, the total number of differential proteins detected in the fish sausage group was 201, including 114 upregulated and 87 downregulated proteins. The identified differential proteins were analyzed by bioinformatics analysis. Results revealed that the differential proteins between the control and fish sausage groups were mainly enriched in CC and the overall expression of the corresponding functions enriched by the differential proteins between the control and fish sausage groups, the control, and positive control groups tended to be upregulated. Therefore, it can be inferred that compound phosphate may promote this series of functions. The differential proteins between the control and fish sausage groups were enriched in the metabolic pathway, while the differential proteins between the control and positive control groups were enriched in metabolic pathways, antibiotic biosynthesis, and carbon metabolism. Complex phosphate may affect the absorption of calcium through the mineral absorption pathway. The immune-related function of the cells in the fish sausage group may have also been affected.

## Data availability statement

The original contributions presented in the study are included in the article/[Supplementary material](#), further inquiries can be directed to the corresponding author/s.

## References

1. Tang S, Feng G, Gao R, Ren J, Zeng M. Thermal gel degradation (*modori*) in sturgeon (*acipenseridae*) surimi gels. *J Food Sci.* (2019) 84:3601–7. doi: 10.1111/1750-3841.14919
2. Yi S, Huo Y, Qiao C, Wang W, Li X. Synergistic gelation effects in surimi mixtures composed of *nemipterus virgatus* and *hypophthalmichthys molitrix*. *J Food Quality.* (2016) 84:3634–41. doi: 10.1111/1750-3841.14761
3. Filomena-Ambrosio A, Ximena M, Hernando I, Hernández-Carrión M, Sotelo-Díaz I. Changes of the water-holding capacity and microstructure of panga and tilapia surimi gels using different stabilizers and processing methods. *Food Sci Technol Int.* (2016) 22:68–78. doi: 10.1177/1082013214568876
4. Julavittayanukul O, Benjakul S, Visessanguan W. Effect of phosphate compounds on gel-forming ability of surimi from bigeye snapper (*Priacanthus tayenus*). *Food Hydrocoll.* (2006) 20:1153–63. doi: 10.1016/j.foodhyd.2005.12.007
5. Chang CC, Regenstien JM. Water uptake, protein solubility, and protein changes of cod mince stored on ice as affected by polyphosphates. *J Food Sci.* (1997) 62:305–09. doi: 10.1111/j.1365-2621.1997.tb03990.x
6. Liang P, Cheng W, Zhang H, Chen L. Effect of phosphate compounds on water retention capacity of round scad surimi during frozen storage. *Adv J Food Sci Technol.* (2016) 12:265–70. doi: 10.19026/ajfst.12.2909
7. Shoback DM, Bilezikian JP, Turner SA, McCarty LC, Guo M, Munro P. The calcimimetic cinacalcet normalizes serum calcium in subjects with primary hyperparathyroidism. *J Clin Endocrinol Metab.* (2003) 88:5644–9. doi: 10.1210/jc.2002-021597
8. Bartlett PJ, Gaspers LD, Pierobon N, Thomas AP. Calcium-dependent regulation of glucose homeostasis in the liver. *Cell Calcium.* (2014) 55:306–16. doi: 10.1016/j.ceca.2014.02.007

## Author contributions

WW and SY provided experimental design. SY provided project administration and funding acquisition. ZJ and PL performed the initial literature research. ZW and RM carried out experimental research, analyzed the data, and wrote the manuscript. XL, ZZ, and JL reviewed manuscript. All authors contributed to the article and approved the submitted version.

## Funding

We were grateful for the financial support from the National Key R&D Program of China (2018YFD0901004).

## Conflict of interest

The authors declare that the research was conducted in the absence of any commercial or financial relationships that could be construed as a potential conflict of interest.

## Publisher's note

All claims expressed in this article are solely those of the authors and do not necessarily represent those of their affiliated organizations, or those of the publisher, the editors and the reviewers. Any product that may be evaluated in this article, or claim that may be made by its manufacturer, is not guaranteed or endorsed by the publisher.

## Supplementary material

The Supplementary Material for this article can be found online at: <https://www.frontiersin.org/articles/10.3389/fnut.2022.1046945/full#supplementary-material>

9. Teixeira MC, Braghiroli MI, Sabbaga J, Hoff PM. Primary prevention of colorectal cancer: myth or reality? *World J Gastroenterol.* (2014) 20:15060–9. doi: 10.3748/wjg.v20.i41.15060
10. Kopic S, Geibel JP. Gastric acid, calcium absorption, and their impact on bone health. *Physiol Rev.* (2013) 93:189–268. doi: 10.1152/physrev.00015.2012
11. Beggs MR, Alexander RT. Intestinal absorption and renal reabsorption of calcium throughout postnatal development. *Exp Biol Med.* (2017) 242:840–9. doi: 10.1177/1535370217699536
12. Sun M, Wu X, Yu Y, Wang L, Xie D, Zhang Z, et al. Disorders of calcium and phosphorus metabolism and the proteomics/metabolomics-based research. *Front Cell Dev Biol.* (2020) 8:576110. doi: 10.3389/fcell.2020.576110
13. Tse CM, Levine SA, Yun CH, Brant SR, Pouyssegur J, Montrose MH, et al. Functional characteristics of a cloned epithelial Na<sup>+</sup>/H<sup>+</sup> exchanger (NHE3): resistance to amiloride and inhibition by protein kinase C. *Proc Natl Acad Sci USA.* (1993) 90: 9110–4. doi: 10.1073/pnas.90.19.9110
14. Birch D, Diedrichsen RG, Christophersen PC, Mu H, Nielsen HM. Evaluation of drug permeation under fed state conditions using mucus-covered Caco-2 cell epithelium. *Eur J Pharm Sci.* (2018) 118:144–53. doi: 10.1016/j.ejps.2018.02.032
15. Pinto M, Leon SR, Appay MD. Enterocyte-like differentiation and polarization of the human colon carcinoma cell line Caco-2 in culture. *Biol Cell.* (1983) 47:323–30.
16. Matsumoto H, Erickson RH, Gum JR, Yoshioka M, Kim YS. Biosynthesis of alkaline phosphatase during differentiation of the human colon cancer cell line Caco-2. *Gastroenterology.* (1990) 98:1199–207. doi: 10.1016/0016-5085(90)90334-W
17. Chantret I, Barbat A, Dussaux L, Brattain MG, Zweibaum A. Epithelial polarity, villin expression, and enterocytic differentiation of cultured human colon carcinoma cells: a survey of twenty cell lines. *Cancer Res.* (1988) 48:1936–42.
18. Pla-Pagà L, Guirro M, Gual-Grau A, Gibert-Ramos A, Foguet-Romero E, Catalán U, et al. Proteomic analysis of heart and kidney tissues in healthy and metabolic syndrome rats after hesperidin supplementation. *Mol Nutr Food Res.* (2020) 64:e1901063. doi: 10.1002/mnfr.201901063
19. Lander ES, Linton LM, Birren B, Nusbaum C, Zody MC, Baldwin J, et al. Initial sequencing and analysis of the human genome. *Nature.* (2001) 409:860–921. doi: 10.1038/35057062
20. Canales RD, Luo Y, Willey JC, Austermler B, Barbacioru CC, Boysen C, et al. Evaluation of DNA microarray results with quantitative gene expression platforms. *Nat Biotechnol.* (2006) 24:1115–22. doi: 10.1038/nbt1236
21. Cox J, Mann M. Is proteomics the new genomics? *Cell.* (2007) 130:395–8. doi: 10.1016/j.cell.2007.07.032
22. Thompson A, Schäfer J, Kuhn K, Kienle S, Schwarz J, Schmidt G, et al. Tandem mass tags: a novel quantification strategy for comparative analysis of complex protein mixtures by MS/MS. *Anal Chem.* (2003) 75:1895–904. doi: 10.1021/ac0262560
23. Kan L, Cui D, Chai Y, Ma L, Li X, Zhao M. TMT-based quantitative proteomic analysis of antitumor mechanism of *Sporisorium reilianum* polysaccharide WM-NP-60 against HCT116 cells. *Int J Biol Macromol.* (2020) 165:1755–64. doi: 10.1016/j.ijbiomac.2020.10.056
24. Ma S, Wang C, Zhao B, Ren X, Tian S, Wang J, et al. Tandem mass tags labeled quantitative proteomics to study the effect of tobacco smoke exposure on the rat lung. *BBA Proteins Proteom.* (2018) 1866:496–506. doi: 10.1016/j.bbapap.2018.01.002
25. Wu L, Guo X, Hartson SD, Davis MA, He H, Medeiros DM, et al. Lack of  $\beta$ ,  $\beta$ -carotene-9', 10'-oxygenase 2 leads to hepatic mitochondrial dysfunction and cellular oxidative stress in mice. *Mol Nutr Food Res.* (2017) 61:1600576. doi: 10.1002/mnfr.201600576
26. Wang M, An S, Wang D, Ji H, Geng M, Guo X, et al. Quantitative proteomics identify the possible tumor suppressive role of protease-activated receptor-4 in esophageal squamous cell carcinoma cells. *Pathol Oncol Res.* (2019) 25:937–43. doi: 10.1007/s12253-018-0395-7
27. Yang L, Zou QH, Zhang Y, Shi Y, Hu CR, Hui CX, et al. Proteomic analysis of plasma from rheumatoid arthritis patients with mild cognitive impairment. *Clin Rheumatol.* (2018) 37:1773–82. doi: 10.1007/s10067-017-3974-1
28. Stryński R, Mateos J, Pascual S, González Á F, Gallardo JM, Łopieńska-Biernat E, et al. Proteome profiling of L3 and L4 *Anisakis simplex* development stages by TMT-based quantitative proteomics. *J Proteomics.* (2019) 201:1–11. doi: 10.1016/j.jpro.2019.04.006
29. Moreira RJ, Castro É, Oliveira TE, Belchior T, Peixoto AS, Chaves-Filho AB, et al. Lipotrophy-associated insulin resistance and hepatic steatosis are attenuated by intake of diet rich in omega 3 fatty acids. *Mol Nutr Food Res.* (2020) 64:e1900833. doi: 10.1002/mnfr.201900833
30. Li S, Li L, Zeng Q, Liu J, Yang Y, Ren D. Quantitative differences in whey proteins among Murrah, Nili-Ravi and Mediterranean buffaloes using a TMT proteomic approach. *Food Chem.* (2018) 269:228–35. doi: 10.1016/j.foodchem.2018.06.122
31. Zhao Z, Liu J, Jia R, Bao S, Hai X, Chen X. Physiological and TMT-based proteomic analysis of oat early seedlings in response to alkali stress. *J Proteomics.* (2019) 193:10–26. doi: 10.1016/j.jpro.2018.12.018
32. Dhirga R, Sullivan LM, Fox CS, Wang TJ, Vasan RS. Relations of serum phosphorus and calcium levels to the incidence of cardiovascular disease in the community. *Arch Intern Med.* (2007) 167:879–85. doi: 10.1001/archinte.167.9.879
33. Manzano S, Williamson G. Polyphenols and phenolic acids from strawberry and apple decrease glucose uptake and transport by human intestinal Caco-2 cells. *Mol Nutr Food Res.* (2010) 54:1773–80. doi: 10.1002/mnfr.201000019
34. Klopfenstein DV, Zhang L, Pedersen BS, Ramírez F, Warwick VA, Naldi A, et al. Goatoools: a python library for gene ontology analyses. *Sci Rep.* (2010) 8:10872. doi: 10.1038/s41598-018-28948-z
35. Xie C, Mao X, Huang J, Ding Y, Wu J, Dong S, et al. KOBAS 20: a web server for annotation and identification of enriched pathways and diseases. *Nucleic Acids Res.* (2011) 39:316–22. doi: 10.1093/nar/gkr483
36. Szklarczyk D, Franceschini A, Wyder S, Forslund K, Heller D, Huerta-Cepas J, et al. STRING v10: protein-protein interaction networks, integrated over the tree of life. *Nucleic Acids Res.* (2015) 43:447–52. doi: 10.1093/nar/gku1003
37. Takeda E, Yamamoto H, Yamanaka-Okumura H, Taketani Y. Dietary phosphorus in bone health and quality of life. *Nutr Rev.* (2012) 70:311–21. doi: 10.1111/j.1753-4887.2012.00473.x
38. Fogh J, Fogh JM, Orfeo T. One hundred and twenty-seven cultured human tumor cell lines producing tumors in nude mice. *J Natl Cancer Inst.* (1977) 59:221–6. doi: 10.1093/jnci/59.1.221
39. Mullen W, Edwards CA, Crozier A. Absorption, excretion and metabolite profiling of methyl-, glucuronyl-, glucosyl- and sulpho-conjugates of quercetin in human plasma and urine after ingestion of onions. *Br J Nutr.* (2006) 96:107–16. doi: 10.1079/bjn20061809
40. Santos MR, Rodríguez-Gómez MJ, Justino GC, Charro N, Florencio MH. Mira, L. Influence of the metabolic profile on the in vivo antioxidant activity of quercetin under a low dosage oral regimen in rats *Br J Pharmacol.* (2008) 153:1750–61. doi: 10.1038/bjp.2008.46
41. Xiang Q, Zhang W, Li Q, Zhao J, Feng W, Zhao T, et al. Investigation of the uptake and transport of polysaccharide from *Se-enriched Grifola frondosa* in Caco-2 cells model. *Int J Biol Macromol.* (2020) 158:1330–41. doi: 10.1016/j.ijbiomac.2020.04.160
42. Anderson JM. Molecular structure of tight junctions and their role in epithelial transport. *News Physiol Sci.* (2001) 16:126–30. doi: 10.1152/physiologyonline.2001.16.3.126
43. Li F, Wei Y, Zhao J, Yu G, Huang L, Li Q. Transport mechanism and subcellular localization of a polysaccharide from *Cucurbita Moschata* across Caco-2 cells model. *Int J Biol Macromol.* (2021) 182:1003–14. doi: 10.1016/j.ijbiomac.2021.04.107
44. Madara JL. Regulation of the movement of solutes across tight junctions. *Annu Rev Physiol.* (1998) 60:143–59. doi: 10.1146/annurev.physiol.60.1.143
45. France MM, Turner JR. The mucosal barrier at a glance. *J Cell Sci.* (2017) 130:307–14. doi: 10.1242/jcs.193482
46. Gu XY, Jin B, Qi ZD, Yin XF. MicroRNA is a potential target for therapies to improve the physiological function of skeletal muscle after trauma. *Neural Regen Res.* (2022) 17:1617–22. doi: 10.4103/1673-5374.330620
47. Meyer B, Papisotiriou DG, Karas M. 100% protein sequence coverage: a modern form of surrealism in proteomics. *Amino Acids.* (2011) 41:291–310. doi: 10.1007/s00726-010-0680-6
48. Lakk M, Yarishkin O, Baumann JM, Iuso A, Križaj D. Cholesterol regulates polymodal sensory transduction in Müller glia. *Glia.* (2017) 65:2038–50. doi: 10.1002/glia.23213
49. Zhang G, Xue W, Dai J, Xu Q, Wang Y, Yuan H, et al. Quantitative proteomics analysis reveals proteins and pathways associated with anthocyanin accumulation in barley. *Food Chem.* (2019) 298:124973. doi: 10.1016/j.foodchem.2019.124973
50. Sutherland DE, Stillman MJ. The “magic numbers” of metallothionein. *Metallomics.* (2011) 3:444–63. doi: 10.1039/c0mt00102c
51. Singh RK, Albrecht AL, Somji S, Sens MA, Sens DA, Garrett SH. Alterations in metal toxicity and metal-induced metallothionein gene expression elicited by growth medium calcium concentration. *Cell Biol Toxicol.* (2008) 24:273–81. doi: 10.1007/s10565-007-9036-8
52. Stephenson SE, Dubach D, Lim CM, Mercer JF, La FS. A single PDZ domain protein interacts with the Menkes copper ATPase, ATP7A. A new

protein implicated in copper homeostasis. *J Biol Chem.* (2005) 280:33270–9. doi: 10.1074/jbc.M505889200

53. Goellner GM, DeMarco SJ, Strehler EE. Characterization of PISP, a novel single-PDZ protein that binds to all plasma membrane  $\text{Ca}^{2+}$ -ATPase b-splice variants. *Ann N Y Acad Sci.* (2003) 986:461–71. doi: 10.1111/j.1749-6632.2003.tb07230.x

54. Atschekzei F, Dörk T, Schürmann P, Geffers R, Witte T, Schmidt RE. Limited role of interferon-kappa (IFNK) truncating mutations in common variable immunodeficiency. *Cytokine.* (2017) 96:71–4. doi: 10.1016/j.cyto.2017.03.005

55. LaFleur DW, Nardelli B, Tsareva T, Mather D, Feng P, Semenuk M, et al. Interferon-kappa, a novel type I interferon expressed in human keratinocytes. *J Biol Chem.* (2001) 276:39765–71. doi: 10.1074/jbc.M102502200

56. Manning JA, Kumar S. Physiological functions of nedd4-2: lessons from knockout mouse models. *Trends Biochem Sci.* (2018) 43:635–47. doi: 10.1016/j.tibs.2018.06.004

57. Jiang C, Kawabe H, Rotin D. The ubiquitin ligase Nedd4L regulates the Na/K/2Cl co-transporter NKCC1/SLC12A2 in the Colon. *J Biol Chem.* (2017) 292:3137–45. doi: 10.1074/jbc.M116.770065

58. Novellademunt L, Kucharska A, Jamieson C, Prange-Barczynska M, Baulies A, Antas P, et al. NEDD4 and NEDD4L regulate Wnt signalling and intestinal stem cell priming by degrading LGR5 receptor. *EMBO J.* (2020) 39:e102771. doi: 10.15252/embj.2019102771

59. Li A, Zhang Y, Wang Z, Dong H, Fu N, Han X. The roles and signaling pathways of prolyl-4-hydroxylase 2 in the tumor microenvironment. *Chem Biol Interact.* (2019) 303:40–9. doi: 10.1016/j.cbi.2019.02.019

60. Di CG, Trusso CS, Lorocho S, Mennerich D, Deschoemaeker S, Di Matteo M, et al. The mTOR and PP2A pathways regulate PHD2 phosphorylation to fine-tune HIF1 $\alpha$  levels and colorectal cancer cell survival under hypoxia. *Cell Rep.* (2017) 18:1699–712. doi: 10.1016/j.celrep.2017.01.051

61. Li L, Liu H, Xu L, Qiu X, Xiao Y, Ying N, et al. Hypoxia-inducible factor-1  $\alpha$  perpetuates synovial fibroblast interactions with T cells and B cells in rheumatoid arthritis. *Eur J Immunol.* (2016) 46:742–51. doi: 10.1002/eji.201545784

62. Wang JC, Li XX, Sun X, Li GY, Sun JL, Ye YP, et al. Activation of AMPK by simvastatin inhibited breast tumor angiogenesis via impeding HIF-1 $\alpha$ -induced pro-angiogenic factor. *Cancer Sci.* (2018) 109:1627–37. doi: 10.1111/cas.13570

63. Huang Q, Chen SS, Li J, Tao SS, Wang M, Leng RX, et al. MiR-210 expression in PBMCs from patients with systemic lupus erythematosus and rheumatoid arthritis. *Ir J Med Sci.* (2018) 187:243–9. doi: 10.1007/s11845-017-1634-8

64. Zhou Y, Zhu X, Tang H, Zhang Z, Zhang X. Immune related gene expression analysis of *Macrobrachium nipponense* in different hours post-infection by non-O1 *Vibrio cholerae*. *Aquac Res.* (2020) 19:100571. doi: 10.1016/j.aqrep.2020.100571

65. Heneghan AF, Pierre JF, Kudsk KA. JAK-STAT and intestinal mucosal immunology. *Jakstat.* (2013) 2:e25530. doi: 10.4161/jkst.25530





## OPEN ACCESS

## EDITED BY

Baoguo Xu,  
Jiangsu University, China

## REVIEWED BY

Qun Huang,  
Guizhou Medical University, China  
Xu Duan,  
Henan University of Science and  
Technology, China  
Xiang Duan,  
Northwest A&F University, China

## \*CORRESPONDENCE

Jicheng Xu  
xujicheng@ahpu.edu.cn

## SPECIALTY SECTION

This article was submitted to  
Nutrition and Food Science  
Technology,  
a section of the journal  
Frontiers in Nutrition

RECEIVED 24 August 2022

ACCEPTED 04 October 2022

PUBLISHED 19 October 2022

## CITATION

Du T, Xu J, Zhu S, Yao X, Guo J and  
Lv W (2022) Effects of spray drying,  
freeze drying, and vacuum drying on  
physicochemical and nutritional  
properties of protein peptide powder  
from salted duck egg white.  
*Front. Nutr.* 9:1026903.  
doi: 10.3389/fnut.2022.1026903

## COPYRIGHT

© 2022 Du, Xu, Zhu, Yao, Guo and Lv.  
This is an open-access article  
distributed under the terms of the  
[Creative Commons Attribution License  
\(CC BY\)](https://creativecommons.org/licenses/by/4.0/). The use, distribution or  
reproduction in other forums is  
permitted, provided the original  
author(s) and the copyright owner(s)  
are credited and that the original  
publication in this journal is cited, in  
accordance with accepted academic  
practice. No use, distribution or  
reproduction is permitted which does  
not comply with these terms.

# Effects of spray drying, freeze drying, and vacuum drying on physicochemical and nutritional properties of protein peptide powder from salted duck egg white

Tianyin Du<sup>1</sup>, Jicheng Xu<sup>1\*</sup>, Shengnan Zhu<sup>1</sup>, Xinjun Yao<sup>1</sup>,  
Jun Guo<sup>1</sup> and Weiqiao Lv<sup>2</sup>

<sup>1</sup>College of Biological and Food Engineering, Anhui Polytechnic University, Wuhu, China, <sup>2</sup>College of Engineering, China Agricultural University, Beijing, China

Salted duck egg white contains many kinds of high quality protein, but it is often discarded as food factory waste because of high salinity and other reasons. The discarded salted duck egg white not only causes a waste of resources, but also causes environmental pollution. Using salted duck egg white as raw material, this study was completed to investigate the effects of three drying methods including freeze drying, vacuum drying, and spray drying on physicochemical and nutritional properties of protein powder from salted duck egg white. The results showed that the solubility, foaming and foaming stability, emulsification and emulsification stability of the protein peptide of salted duck egg white decreased to different degrees after drying. The scavenging rates of freeze-dried samples for superoxide anion, hydroxyl radical, and 1,1-Diphenyl-2-picrylhydrazyl (DPPH·) reached 48.76, 85.03, and 80.17%, respectively. Freeze drying had higher scavenging rates than vacuum drying and spray drying. The results of electron microscopy showed that freeze-drying had the least effect on the structure of protein peptide powder of salted duck egg white. The purpose of this experiment was to provide theoretical guidance and technical support for industrial drying of salted duck egg white protein solution.

## KEYWORDS

salted duck egg white, protein peptide powder, freeze drying, physicochemical and nutritional properties, spray drying

## Introduction

The vast majority of duck eggs are made into salted duck egg products and are consumed by the public. Among them, salted duck egg yolk is favored by consumers for its unique taste and is used in traditional Chinese delicacies such as moon cakes (1, 2). In the production of salted duck egg yolk, the salted duck egg white has not been properly used because its salt content is as high as 7–12% (3, 4). Discarded salted duck egg white not only causes a waste of resources but also causes environmental pollution

(5, 6). Therefore, the comprehensive utilization of salted duck egg white is an urgent problem to be solved in food factories. The team of researchers previously compared the enzymatic hydrolysis effects of papain, trypsin, acid protease, alkaline protease, neutral protease, and flavor protease on salted duck egg white. The results showed that papain was the most suitable protease for enzymatic hydrolysis of salted duck egg white, and the supernatant of enzymatic hydrolysis of salted duck egg white was finally obtained.

The main physicochemical and nutritional properties of egg white protein peptide powder include solubility, foaming, emulsification, and antioxidant (7, 8). The processing properties of protein include solubility, foaming, and emulsification. These functional properties play an important role in food processing and storage (9, 10). Free radicals are abundant in the human body. Under normal circumstances, free radicals in the body are in a dynamic balance of production and removal (11, 12). However, when free radicals are produced too much or removed too slowly, they will cause damage to the body. Excessive free radicals lead to a series of diseases such as aging and carcinogenesis (13, 14). Free radicals mainly include superoxide anion ( $O_2^{\cdot-}$ ), molecular hydrogen peroxide, hydroxyl radical ( $\cdot OH$ ), and singlet oxygen ( $O_2^1$ ). The free radical scavenging ability test is considered as the most important method to evaluate the antioxidant activity of bioactive peptides (15). Studies have shown that the active peptide in salted duck egg white can effectively remove the excess free radicals in the body, protect the body from free radical attack, and prevent free radical induced disease or aging (16). Therefore, it is of great significance to study the processing characteristics and antioxidant activity of protein peptide powder of salted duck egg white.

In this experiment, the supernatant of enzymatic hydrolysis of salted duck egg white was processed by spray drying, freeze drying, and vacuum drying to prepare protein peptide powder of salted duck egg white. The effects of three drying methods on the main physicochemical and nutritional properties of egg white protein peptide powder were studied. The experimental results can provide theoretical reference and technical support for the preparation of protein peptide powder of salted duck egg white, and have important practical significance for the efficient development and utilization of salted duck egg white.

## Materials and methods

### Raw materials

The salted duck egg white was provided by Anhui Tianhe Food Co., LTD. The salted duck egg white was placed in the refrigerator at  $-20^\circ C$  and thawed at room temperature before use. Papain was purchased from Beijing Hongrun

Baishun Technology Co., LTD. All the other reagents were analytically pure.

### Preparation of protein peptide powder of salted duck egg white

Protein peptide powder was prepared from enzymatic hydrolysate of salted duck egg white by spray drying, freeze drying, and vacuum drying. According to the previous research results of the research team, the optimal conditions for spray drying were the inlet air temperature of  $180^\circ C$  and outlet air temperature of  $80^\circ C$ . The optimal conditions for freeze-drying were  $-60^\circ C$  for 48 h. The best vacuum drying conditions were  $70^\circ C$ , vacuum degree 100 Pa, and vacuum drying for 12 h. The process flow of the three drying methods was shown in Figure 1.

### Determination of solubility of protein peptide powder from salted duck egg white

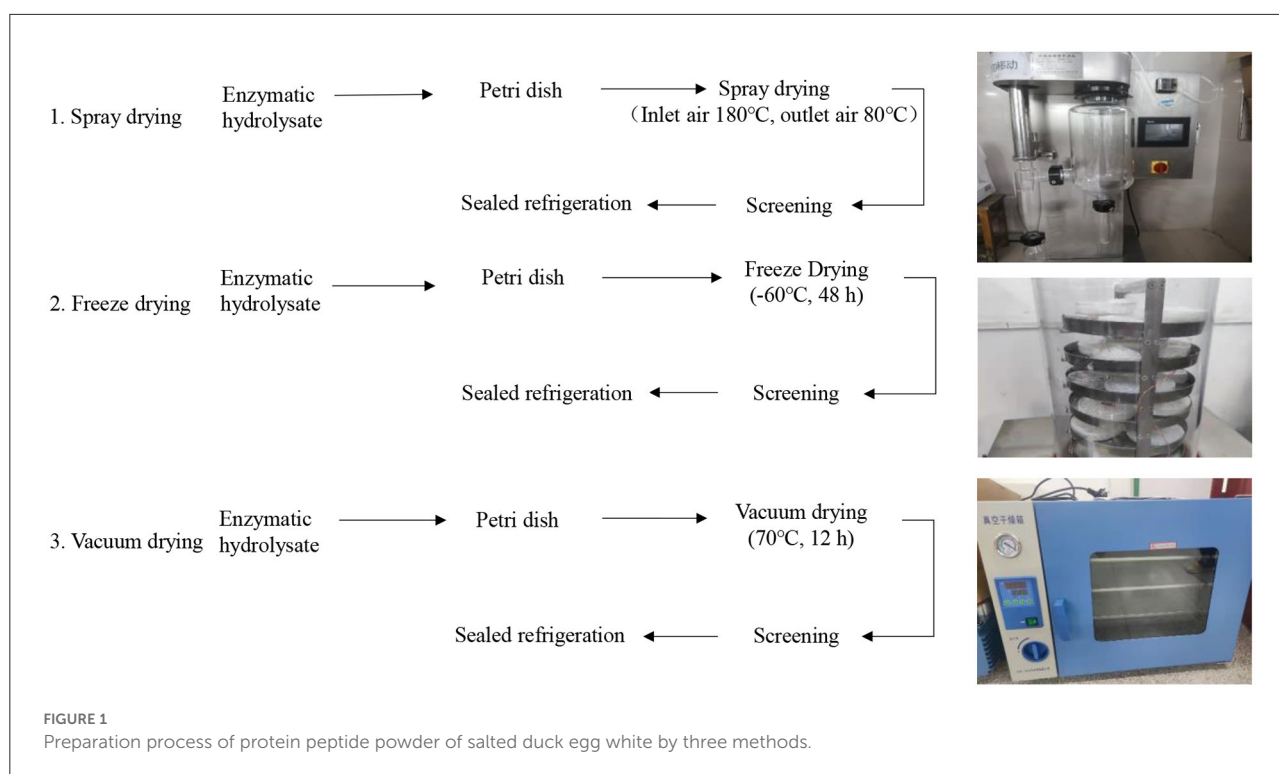
The solubility of protein peptide powder was determined according to the Gao method and adjusted appropriately (17). The protein peptide powder was prepared in a solution with a concentration of 10 mg/mL. The prepared solution was stirred by a magnetic stirrer for 30 min at room temperature and centrifuged at  $6797 \times g$  for 15 min. The nitrogen content in the supernatant and protein peptide solution before centrifugation was determined by the Kjeldahl method. The calculation formula of protein peptide solubility of salted duck egg white is as follows:

$$\text{Solubility (\%)} = A/B \times 100\% \dots \dots \dots$$

Where A is the nitrogen content in supernatant and B is the nitrogen content in protein peptide solution before centrifugation.

### Determination of foaming of protein peptide powder from salted duck egg white

The foaming of protein peptide powder was determined according to the Eljoudi method and adjusted appropriately (18). The protein peptide powder was prepared in a solution with a concentration of 10 mg/mL. Then, 50 mL of peptide solution was taken and bubbled with a high-speed stirrer at the speed of  $8603 \times g$  for 5 min, and immediately pour into the measuring cylinder to read the volume number of foam recorded as  $V_0$ . Then, the protein peptide solution was stationary for 30 min, and the volume number of foam was read again as  $V_{30}$ .



The calculation formula of protein peptide foaming capacity and foaming stability of salted duck egg white were as follows:

$$\text{Foaming capacity (\%)} = \frac{V_0 - 50}{50} \times 100\%$$

$$\text{Foam stability (\%)} = \frac{V_{30} - 50}{V_0 - 50} \times 100\%$$

Where  $V_0$  is the volume number of foam of 0 min and  $V_{30}$  is the volume number of foam of 30 min.

## Determination of emulsification of protein peptide powder from salted duck egg white

The foaming of protein peptide powder was determined according to the Li method and adjusted appropriately (19). The protein peptide powder was prepared to a solution with a concentration of 1 mg/mL. Then, 30 mL of protein peptide sample solution at a concentration of 1 mg/mL was mixed with 10 mL soybean salad oil. The mixed solution was homogenized at 8603 ×g for 15 min. At the end of homogenization, 50 μL of the emulsion was immediately sucked through a straw from the bottom of the solution and added to 5 mL of 0.1% SDS solution. The absorbance ( $A_0$ ) of the solution was measured at 500 nm using a spectrophotometer, which is the emulsification of the solution. Then the solution was allowed to stand for 10 min. Again, 50 μL of emulsion was absorbed from the bottom of the solution and added to 5 mL of 0.1% SDS solution. The absorbance ( $A_{10}$ ) was measured at 500 nm

using a spectrophotometer. The calculation formula of emulsion stability is as follows:

$$\text{Emulsification stability (\%)} = \frac{A_0 \times 10}{A_0 - A_{10}}$$

Where  $A_0$  is the absorbance of the solution of 0 min, which is the emulsification of the solution, and  $A_{10}$  is the absorbance of the solution of 10 min.

## Determination of protein peptide powder from salted duck egg white by scanning electron microscope

A small amount of protein peptide powder was glued to the double-sided tape on the scanning electron microscope sample table. After coating with an ion sputtering apparatus (BAL-TEC, SCD 005), the samples were observed under a scanning electron microscope (FEI-Quanta 200). The powder structure of protein peptide powder of salted duck egg white prepared by three different drying methods was analyzed.

## Determination of superoxide anion ( $O_2^{\cdot-}$ ) scavenging ability of protein peptide powder from salted duck egg white

In this study, based on the study of Misak et al. (20), the pyrogallol autoxidation method was used to determine the

superoxide anion scavenging activity of protein peptide powder from salted duck egg white. Deionized water was added to the protein peptide powder of salted duck egg white and prepared into a 5 mg/mL sample solution. Reagent A: Sample solution (0.2 mL) was added to test tube A. Then, 4.5 mL of Tris-HCl buffer (pH 8.2, 50 mmol/L) and 4 mL of distilled water were added to the tube. After shaking well, the test tube was placed in a 37°C incubator for 20 min. Reagent B: Pyrogallol solution (0.5 mL, 3 mmol/L) was added to test tube B. The tube B was kept warm in a 37°C incubator for 10 min. Reagents A and B were rapidly mixed and the absorbance was measured at 30 s intervals at 325 nm. In total, the absorbance value of 3 min was measured, and the regression line was made to find the slope  $K_1$  of the absorbance change. The blank control was carried out with distilled water instead of sample liquid, and the absorbance change slope  $K_0$  was obtained by the same method. The samples of each group were measured three times and then the average value was taken. The calculation formula of superoxide anion ( $O_2^{\cdot-}$ ) scavenging ability of protein peptide powder is as follows:

$$\text{Scavenging ability (\%)} = \frac{K_0 - K_1}{K_0} \times 100\% \dots\dots\dots$$

Where  $K_0$  is the change slope of absorbance in the blank group within 3 min and  $K_1$  is the change slope of absorbance in the sample group within 3 min.

## Determination of hydroxyl radical scavenging ability of protein peptide powder from salted duck egg white

This test referred to the method of Prasad and Mishra (21), for determining the hydroxyl radical scavenging ability of protein peptide powder from salted duck egg white, and made appropriate modifications. Deionized water was added to the protein peptide powder of salted duck egg white to form a sample solution of 5 mg/mL. Then, 0.4 mL phosphate buffer (pH 7.4, concentration 200 mmol/L), 0.6 mL o-dinitrogen solution (5 mmol/L), and 0.6 mL ferrous sulfate solution (5 mmol/L) were added to the test tube. The test tube was shaken to mix the mixture well. After shaking, 2 mL of sample solution (5 mg/mL) and 0.4 mL of hydrogen peroxide (mass fraction 0.1%) was added to the mixture. The test tube was shaken again to mix the mixture well. The mixture was placed in a constant temperature incubator at 37°C for 60 min. Then the mixture was removed and the absorbance  $A_1$  was measured at 536 nm. Using deionized water instead of sample solution, the absorbance value  $A_0$  was measured by the same method as above. Using deionized water instead of sample solution and hydrogen peroxide solution, the absorbance  $A_2$  was measured by the same method. The samples of each group were measured three times and then the average value was taken. The calculation formula of hydroxyl radical scavenging ability of protein peptide powder is as follows:

TABLE 1 Proportion of reagents in EP tubes.

Reagents (μL)	Blank tube	Test tube	Control tube
Supernatant	–	25	25
Reagents three	–	–	–
Extract solution	25	–	–
Reagents one	–	–	975
Working liquid	975	975	–

$$\text{Hydroxyl radical scavenging ability (\%)} = \frac{A_1 - A_0}{A_2 - A_0} \times 100\% \dots\dots\dots$$

Where  $A_0$  is the absorbance measured by deionized water instead of sample liquid;  $A_1$  is the absorbance measured by sample liquid;  $A_2$  is the absorbance measured by deionized water instead of sample liquid and hydrogen peroxide.

## Determination of 1,1-diphenyl-2-picrylhydrazyl (DPPH·) scavenging ability of active peptide from salted duck egg white

DPPH· free radical scavenging ability was determined by a visible spectrophotometer and detection kit. Deionized water was added to the protein peptide powder of salted duck egg white to form a sample solution of 50 g/L. Then, 100 μL of sample solution and 900 μL of extract solution provided by the kit were added to a test tube for sample processing. The mixture was mixed with a vortex oscillator and centrifuged at  $8603 \times g$  for 15 min. After centrifugation, the supernatant was placed on ice to be tested. The spectrophotometer was preheated for more than 30 min, the wavelength was adjusted to 515 nm, and the wavelength was adjusted to zero with absolute ethanol.

The reagents in Table 1 were added to 1.5 mL EP tubes. The mixture was mixed with a whirlpool oscillator, and the absorbance value was measured at 515 nm after standing at room temperature (25°C) for 30 min in the dark. Each measurement tube shall be provided with a control unit. Blank tube only needs to be measured 1~2 times.

The calculation formula of DPPH· scavenging ability of protein peptide powder is as follows:

$$\text{DPPH· scavenging ability} = \frac{A_0 - (A_1 - A_2)}{A_0} \times 100\% \dots\dots\dots$$

Where  $A_0$  is the absorbance value of the blank tube;  $A_1$  is the absorbance value of the test tube;  $A_2$  is the absorbance value of the control tube.

## Statistical analysis

The SPSS 20.0 software (IBM, Chicago, IL, USA) was used for the ANOVA of the samples in the study. Significant

differences were determined by Duncan's multiple comparison test ( $P < 0.05$ ).

## Results and discussion

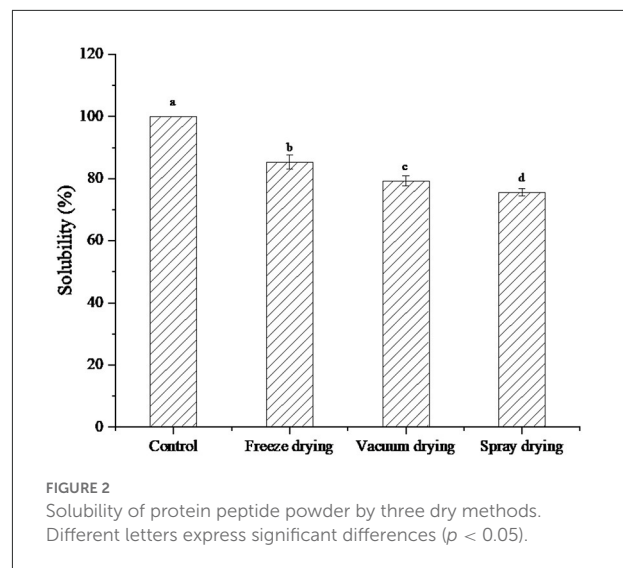
### Solubility analysis under three drying methods

Solubility is an important indicator of protein applicability. Most of the functional properties of proteins are closely related to their solubility (22). The solubility of a protein is affected by conditions such as pH, ionic strength, temperature, and solvent type. The solubility of protein decreases with the extension of heating time (23).

The solubility of protein peptides under the three drying methods was shown in Figure 2. After drying in different ways, the solubility of protein peptides from salted duck egg white decreased to different degrees. The solubility of freeze-dried protein peptide samples was significantly higher than that of vacuum-dried and spray-dried samples. Li et al. (24) found that heating temperature can significantly affect the solubility of sarcoplasmic proteins. With the increase in heating intensity, the protein structure is depolymerized and aggregated. This cross-linking phenomenon increased the hydrophobic groups in sarcoplasmic proteins, resulting in enhanced surface hydrophobicity of protein molecules. The lowest solubility was found in the spray-dried samples. This may be because, in the process of spray drying, high temperature caused the structure of protein peptide molecules to unfold, and the hydrophobic groups originally embedded in the molecules were exposed to the surface of the molecules. The exposure of hydrophobic groups attenuated the interaction with water molecules, resulting in a significant decrease in solubility. However, due to the low temperature of freeze-dried samples, the protein peptides still maintained good solubility.

### Foaming analysis under three drying methods

The foaming ability and foam stability of proteins are closely related to the hydrophobic amino acid residues on the molecular surface (25). Foams are generally two-phase systems in which the gas is distributed in a liquid phase. Since the gas phase is separated from a continuous phase, it has high surface tension and an unstable system, so the bubbles are easy to accumulate and fracture (26). The foaming property and foam stability changes of protein peptides under three drying methods were shown in Figure 3. As can be seen from the figure, the foaming value of the original protein peptide solution was 166.32%, and the foam stability value was 53.68%.

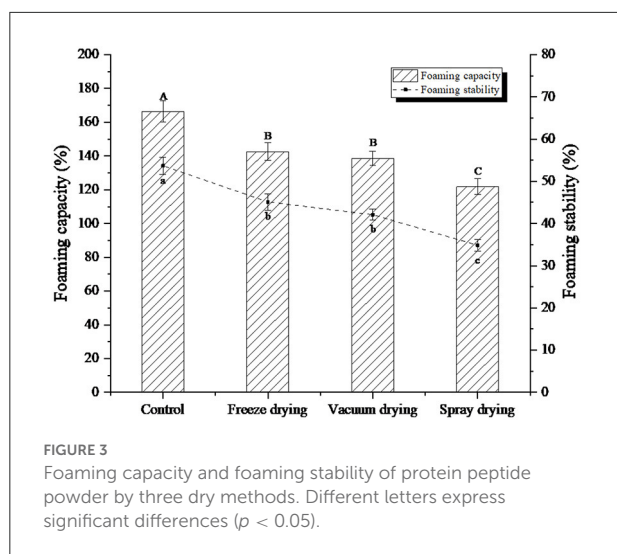


Compared with the liquid phase of the original protein peptide, the foaming property and foam stability of the protein peptide were significantly decreased under the three drying methods. However, the frothiness and foam stability of freeze-dried protein peptide samples were significantly higher than those of vacuum-dried samples and spray-dried samples. When the protein peptide solution of salted duck egg white is stirred by the machine, a lot of gas will be sucked into it, thus creating a water vapor interface. The protein peptide of salted duck egg white is a kind of amphiphilic substance, which can bond between water and atmosphere, thereby reducing surface tension and accelerating the formation of bubbles. The intermolecular binding of egg white protein peptides can enhance the stability of foam (27). The foamability and foam stability of spray-dried samples decreased to 121.79 and 34.83%, respectively. The protein peptide should be soluble for foam formation. The decrease in foaming ability indicated that insoluble molecules were formed by the aggregation of protein peptides during the drying process, which reduced foaming ability and foam stability. Ovalbumin can be modified with glucose molecules to improve its heat-induced aggregation resistance. Aoki et al. (28) used oligo-galacturonic acid to modify ovalbumin through non-enzymatic Browning reaction, and the results showed that the thermal stability of ovalbumin was significantly improved.

### Emulsification analysis under three drying methods

Emulsification of proteins refers to the ability of proteins to participate in the formation of emulsions, while emulsification stability refers to the ability of emulsion droplets to remain



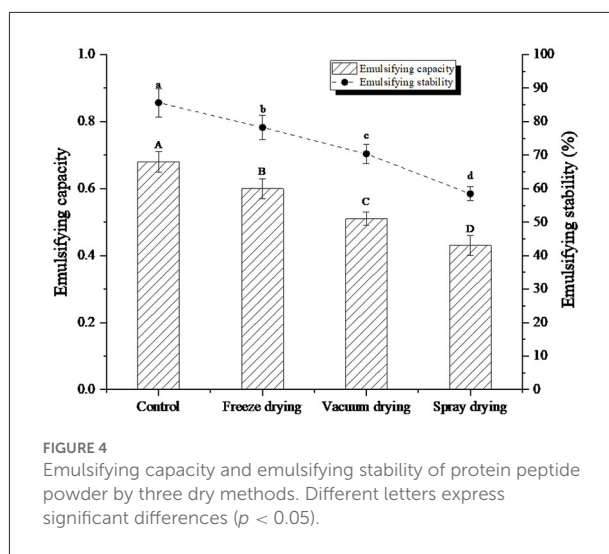


dispersed without fat floating, flocculation, and aggregation within a certain period (29). The emulsification and emulsification stability of the protein peptide of salted duck egg white under three drying methods were shown in Figure 4. After drying, the emulsification and emulsification stability of protein peptides decreased to different degrees. Among them, the emulsification and emulsification stability of freeze-dried samples were the closest to the control samples. However, the emulsification and emulsification stability of spray-dried samples decreased the most, which may be due to the destruction of hydrophilic and hydrophobic groups of protein peptides caused by heating, leading to the degradation of emulsification and emulsification stability of protein peptides.

Salted duck egg white protein is a kind of parental structure, and its molecular structure contains both hydrophilic and hydrophobic structures. In a mixture of oil and water, the egg white protein can form a protective film. The protective film can effectively prevent the accumulation and destruction of oil beads (30). Dickinson (31) found in their study that less molecular aggregation improved the viscosity of the solution system and can maintain the emulsion stability of the solution. In addition, under spray drying and heating, protein molecules re-form aggregated through hydrogen and disulfide bonds and other forces. Aggregation can reduce the flexibility of protein peptide molecules, which was also an important reason for its emulsification and emulsification stability.

## Structural characterization of three drying methods of protein peptide powder

The powder structure of protein peptide powder of salted duck egg white prepared by different drying methods was



analyzed by scanning electron microscope (SEM). As can be seen from Figure 5, at 5,000 times magnification, the protein powder of salted duck egg white under freeze-drying treatment was relatively regular. The protein powder structure was close, with local subtle holes, and the texture was full. The size of protein powder particles was round and the surface was glossy. The surface of salted duck egg white protein powder under spray drying treatment was unfolded. The size of the protein powder was uniform. The texture was loose and no longer spherical.

Heat can cause protein molecules to denature and change the secondary structure of the protein. In scanning electron microscopy, the spray-dried protein structure was the most heterogeneous. This may be because the side chain groups buried deep inside the protein molecules were exposed by spray drying. The molecular flexibility was enhanced, and the unfolding and morphological change of the protein molecules at the interface was easier (32). The surface of salted duck egg white protein powder under vacuum drying treatment was poor, and the protein structure become rough and more irregular. In general, freeze-drying had the least effect on the microstructure of protein and peptide powder from salted duck egg white.

## Analysis of superoxide anion ( $O_2^{\cdot-}$ ) scavenging ability of protein peptides under three drying methods

Superoxide anion ( $O_2^{\cdot-}$ ) belongs to reactive oxygen species and is the precursor of oxygen radical. Superoxide anion has strong oxidation property. Under certain conditions, the superoxide anion can be converted into other free radicals (33). In this experiment, the pyrogallol autoxidation method was used to determine the superoxide anion. Under alkaline conditions, pyrogallol underwent rapid autoxidation to form a

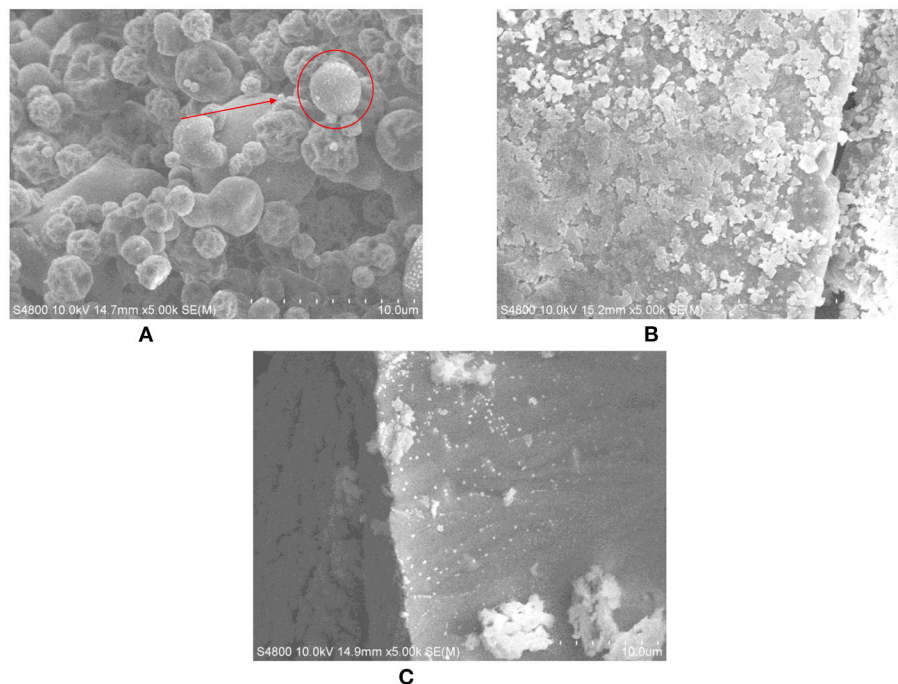


FIGURE 5  
Microstructure of protein peptide powder by three drying methods. (A) Freeze drying. (B) Spray drying. (C) Vacuum drying.

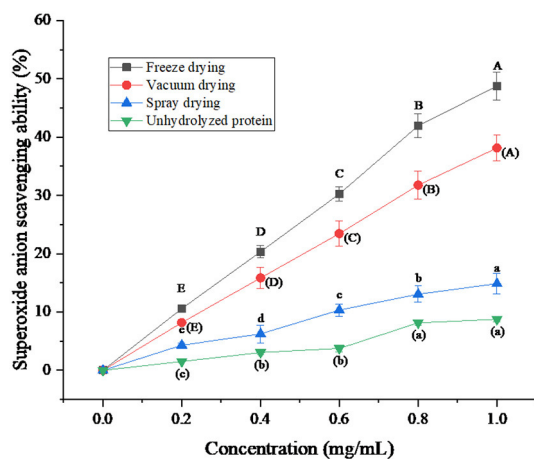


FIGURE 6  
Superoxide anion ( $O_2^{\cdot-}$ ) scavenging ability of protein peptide powder by three dry methods. Different letters express significant differences ( $p < 0.05$ ).

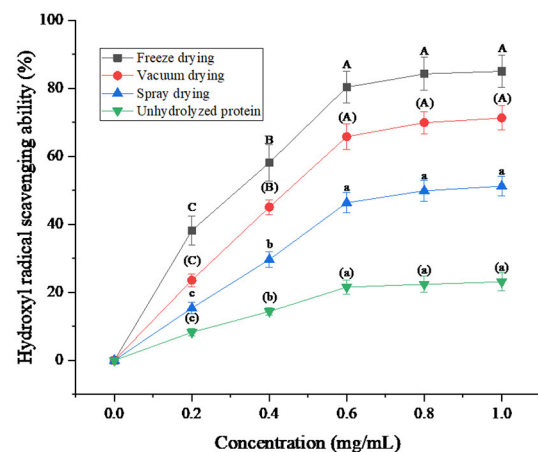
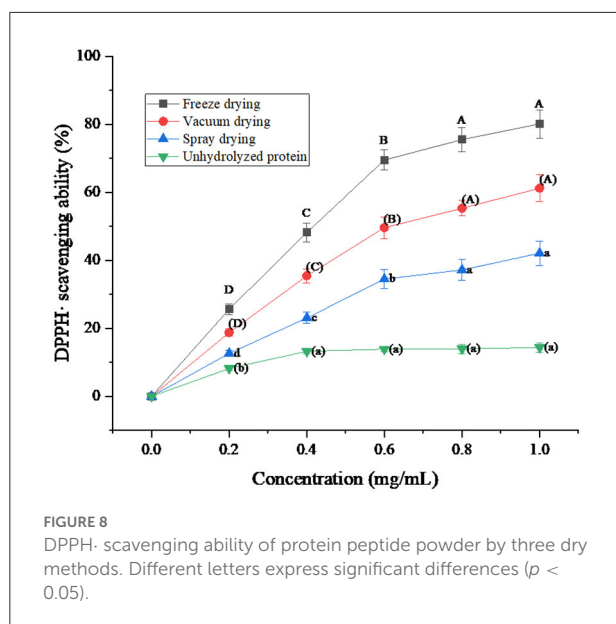


FIGURE 7  
Hydroxyl radical ( $\cdot OH$ ) scavenging ability of protein peptide powder by three dry methods. Different letters express significant differences ( $p < 0.05$ ).

semi-quinone radical and superoxide anion. Subsequently, the semi-quinone radical is further oxidized by superoxide anion to form quinone with strong absorption, so the absorbance increases accordingly. The superoxide anion will be quenched in the presence of antioxidant substances in the solution.

Semi-quinone radicals cannot form strongly absorbed quinones. Therefore, the antioxidant activity of the sample can be determined by measuring its absorbance.

The superoxide anion scavenging ability of protein peptides and unhydrolyzed proteins was compared under three drying



methods. As can be seen from Figure 6, the ability of the protein peptide of salted duck egg white to remove superoxide anion increased with the increase of the protein peptide concentration. The scavenging capacity of unhydrolyzed proteins was much lower than that of enzymatic peptides. Niranjana et al. (34) found that the ability of protein peptides to clear superoxide anion was positively correlated with its concentration. The scavenging ability of freeze-dried protein peptides was better than that of vacuum-dried and spray-dried samples. When the concentration of protein peptide was 1 mg/mL, the clearance rate of superoxide anion by freeze-dried protein peptide could reach 48.76%. This indicates that the freeze-drying method to dry the protein peptide of salted duck egg white can effectively ensure the ability of its active peptide to remove superoxide anion.

### Analysis of hydroxyl radical ( $\cdot\text{OH}$ ) scavenging ability of protein peptides under three drying methods

Hydroxyl radical is a highly reactive free radical with rapid reaction and strong attack power, which is more active in cell reaction (35). Hydroxyl radicals react with various molecules in the body mainly through electron transfer, addition reaction, and dehydrogenation, thereby causing oxidative damage to carbohydrates, proteins, nucleic acids, and other substances, and even leading to aging or carcinogenesis (36).

Hydroxyl radical scavenging rate is an important index to reflect the antioxidant capacity of protein peptides from salted

duck egg white. As can be seen from Figure 7, the hydroxyl radical scavenging rate of protein peptides increased with the increase of protein peptide concentration under the three drying methods and was greater than that of unhydrolyzed protein. The hydroxyl radical scavenging ability of freeze-dried protein peptides was better than that of vacuum-dried and spray-dried samples. Sarabandi and Jafari (37) also found that the shear tension and dehydration during spray-drying resulted in instability of the peptides, and reduced the hydroxyl radical scavenging ability of peptides. When the concentration of protein peptide was 1 mg/mL, the hydroxyl radical scavenging rate of freeze-dried protein peptide was up to 85.03%. The experimental results showed that the freeze-drying method to dry the protein peptide of salted duck egg white could effectively guarantee the hydroxyl radical scavenging ability of its active peptide.

### DPPH· scavenging ability analysis of protein peptides under three drying methods

DPPH· free radical is a very stable free radical with a nitrogen center, which is one of the important indicators of the antioxidant capacity of samples (38). The DPPH· radical has one electron and its alcohol solution is purple with strong absorption at 515 nm. In the presence of antioxidants, DPPH· radicals were scavenged, the solution became lighter in color, and the absorbance at 515 nm decreased. The change of absorbance is proportional to the degree of free radical scavenging in a certain range (39).

It can be seen from Figure 8 that the protein peptide of salted duck egg white has a relatively obvious scavenging effect on DPPH·. When the protein concentration was below 0.6 mg/mL, the clearance rate of DPPH· by the protein peptide increased linearly. When the protein concentration was higher than 0.6 mg/mL, the clearance rate of DPPH· by protein peptides began to increase slowly. In addition, it was obvious that the DPPH· scavenging rate of protein peptides under the three drying methods was higher than that of unhydrolyzed protein. The DPPH· scavenging ability of freeze-dried protein peptides was better than that of vacuum-dried and spray-dried samples. When the protein peptide concentration was 1 mg/mL, the clearance rate of DPPH· by freeze-dried protein peptide could reach 80.17%. Foh et al. (40) hydrolyzed tilapia freeze-dried protein powder to obtain peptides. Then the DPPH· scavenging ability of the peptides was determined. The results showed that the scavenging ability of DPPH· by tilapia peptides was as high as 86.67%. It can be concluded that the protein peptide of salted duck egg white dried by the freeze-drying method has a higher antioxidant capacity than that of unhydrolyzed salted egg white.

## Conclusions

The physicochemical properties and antioxidant capacity of the protein peptide powder of salted duck egg white prepared by different drying methods were studied in this paper. The results showed that under the same conditions, the physicochemical properties and antioxidant activity of protein peptide powder of salted duck egg white could be maintained better by freeze-drying, while the effect of spray drying was the worst. After drying in different ways, the solubility, foaming and foaming stability, emulsification and emulsification stability of the protein peptide of salted duck egg white decreased to different degrees. Among them, the samples dried by freeze-drying had the lowest decrease. While the air inlet temperature of spray drying (180°C) was higher, the solubility, foaming and foaming stability, emulsification and emulsification stability of samples by spray drying decreased the most. This may be due to the low temperature of freeze drying, which is not easy to cause protein denaturation. The spatial structure of protein peptide was changed by drying, and the physicochemical properties and antioxidant activity of protein peptide powder were changed.

The scavenging rates of superoxide anion, hydroxyl radical, and DPPH· in the protein peptide of salted duck egg white were decreased by different drying methods. Freeze-dried samples showed the smallest decrease. When the concentration of protein peptide was 1 mg/mL, the scavenging rates of superoxide anion, hydroxyl radical, and DPPH· of freeze-dried samples were 48.76, 85.03, and 80.17%, respectively. The microstructure analysis of protein peptide of salted duck egg white showed that the protein powder of salted duck egg white under freeze-drying treatment was regular and the protein powder particles were round. The protein particles of salted duck egg white were no longer spherical under spray drying. The results showed that freeze-drying was an ideal drying method for the protease hydrolysate of salted duck egg white.

## References

1. Dai Y, Zhao J, Liang H, Deng Q, Wan C, Li B, et al. Desalination of salted duck egg white assisted by gelatin: foaming and interface properties of the mixed system. *Food Hydrocolloid*. (2022) 124:107260. doi: 10.1016/j.foodhyd.2021.107260
2. Chen X, Pei Y, Li B, Wang Y, Zhou B, Li B, et al. Interfacial decoration of desalted duck egg white nanogels as stabilizer for Pickering emulsion. *Food Hydrocolloid*. (2022) 132:107858. doi: 10.1016/j.foodhyd.2022.107858
3. Yu L, Xue H, Xiong C, Xin X, Wang P, Feng F, et al. Characterization of duck egg white gel under the action of baijiu (Chinese liquor). *LWT Food Sci Technol*. (2021) 147:111487. doi: 10.1016/j.lwt.2021.111487
4. Du M, Sun Z, Liu Z, Yang Y, Liu Z, Wang Y, et al. High efficiency desalination of wasted salted duck egg white and processing into food-grade pickering emulsion stabilizer. *LWT Food Sci Technol*. (2022) 161:113337. doi: 10.1016/j.lwt.2022.113337
5. Zhao J, Guo X, Chen Z, Dai Y, Liang H, Deng Q, et al. Desalted duck egg white nanogels as Pickering stabilizers for food-grade oil-in-water emulsion. *Food Sci Hum Well*. (2022) 11:1306–14. doi: 10.1016/j.fshw.2022.04.012
6. Ding Z, Li S, Cao X. Separation of lysozyme from salted duck egg white by affinity precipitation using pH-responsive polymer with an l-thyroxine ligand. *Sep Purif Technol*. (2014) 138:153–60. doi: 10.1016/j.seppur.2014.10.021
7. Toldra F, Reig M, Mora L. Management of meat by- and co-products for an improved meat processing sustainability. *Meat Sci*. (2021) 181:108608. doi: 10.1016/j.meatsci.2021.108608
8. Ismail BP, Senaratne-Lenagala L, Stube A, Brackenridge A. Protein demand: review of plant and animal proteins used in alternative protein product development and production. *Anim Front*. (2020) 10:53–63. doi: 10.1093/af/vfaa040

## Data availability statement

The raw data supporting the conclusions of this article will be made available by the authors, without undue reservation.

## Author contributions

TD, SZ, and XY: writing—original draft. JX, JG, and WL: writing—review and editing. All authors contributed to the article and approved the submitted version.

## Funding

The authors acknowledged the support of the Anhui Provincial Science and Technology Major Special Project (202003b06020004), the Anhui Provincial Natural Science Foundation (No. 1908085MC79), and the Overseas Visiting and Study Program for Outstanding Young Backbone Talents of Anhui Universities (No. gxxwfx2020056).

## Conflict of interest

The authors declare that the research was conducted in the absence of any commercial or financial relationships that could be construed as a potential conflict of interest.

## Publisher's note

All claims expressed in this article are solely those of the authors and do not necessarily represent those of their affiliated organizations, or those of the publisher, the editors and the reviewers. Any product that may be evaluated in this article, or claim that may be made by its manufacturer, is not guaranteed or endorsed by the publisher.



9. Kim IS, Yang WS, Kim CH. Beneficial effects of soybean-derived bioactive peptides. *Int J Mol Sci.* (2021) 22:8570. doi: 10.3390/ijms22168570
10. Yue J, Yao X, Gou Q, Li D, Liu N, Yang D, et al. Recent advances of interfacial and rheological property based techno-functionality of food protein amyloid fibrils. *Food Hydrocolloid.* (2022) 132:107827. doi: 10.1016/j.foodhyd.2022.107827
11. Kocic G, Veljkovic A, Sokolovic D, Ulrih NP. Exposomic fingerprint in the development of diseases: the role of free radicals and multiomics. *Oxid Med Cell Longev.* (2022) 2022:9851253. doi: 10.1155/2022/9851253
12. Clavijo NA, Pinto JC, Melo PA. Continuous diabatic free-radical solution polymerization reactors: search engines for non-linear dynamical solutions. *Chem Eng Sci.* (2022) 248:117221. doi: 10.1016/j.ces.2021.117221
13. Chen X, Li X, Xu X, Li L, Liang N, Zhang L, et al. Ferroptosis and cardiovascular disease: role of free radical-induced lipid peroxidation. *Free Radic Res.* (2021) 55:405–15. doi: 10.1080/10715762.2021.1876856
14. Balakrishna Pillai A, JeanPierre AR, Mariappan V, Ranganadin P, S RR. Neutralizing the free radicals could alleviate the disease severity following an infection by positive strand RNA viruses. *Cell Stress Chaperones.* (2022) 27:189–95. doi: 10.1007/s12192-022-01269-x
15. Yin R, Wang M, Huang YY, Landi G, Vecchio D, Chiang LY, et al. Antimicrobial photodynamic inactivation with decacationic functionalized fullerenes: oxygen-independent photokilling in presence of azide and new mechanistic insights. *Free Radic Biol Med.* (2015) 79:14–27. doi: 10.1016/j.freeradbiomed.2014.10.514
16. Silina EV, Stupin VA, Abramov IS, Bolevich SB, Deshpande G, Achar RR, et al. Oxidative stress and free radical processes in tumor and non-tumor obstructive jaundice: influence of disease duration, severity and surgical treatment on outcomes. *Pathophysiology.* (2022) 29:32–51. doi: 10.3390/pathophysiology29010005
17. Gao K, Zha F, Yang Z, Rao J, Chen B. Structure characteristics and functionality of water-soluble fraction from high-intensity ultrasound treated pea protein isolate. *Food Hydrocolloid.* (2022) 125:107409. doi: 10.1016/j.foodhyd.2021.107409
18. Eljoudi S, Feki A, Bkhaireia I, Barkia A, Ben Amara I, Nasri M, et al. New polysaccharides extracted from *Malcolmia triloba*: structure characterization, biological properties and application to beef meat preservation. *J Food Compos Anal.* (2022) 107:104380. doi: 10.1016/j.jfca.2021.104380
19. Li J, Fu J, Ma Y, He Y, Fu R, Qayum A, et al. Low temperature extrusion promotes transglutaminase cross-linking of whey protein isolate and enhances its emulsifying properties and water holding capacity. *Food Hydrocolloid.* (2022) 125:107410. doi: 10.1016/j.foodhyd.2021.107410
20. Misak A, Grman M, Bacova Z, Rezuchova I, Hudecova S, Ondriasova E, et al. Polysulfides and products of H<sub>2</sub>S/S-nitrosoglutathione in comparison to H<sub>2</sub>S, glutathione and antioxidant Trolox are potent scavengers of superoxide anion radical and produce hydroxyl radical by decomposition of H<sub>2</sub>O<sub>2</sub>. *Nitric Oxide.* (2018) 76:136–51. doi: 10.1016/j.niox.2017.09.006
21. Prasad AK, Mishra PC. Scavenging of superoxide radical anion and hydroxyl radical by urea, thiourea, selenourea and their derivatives without any catalyst: a theoretical study. *Chem Phys Lett.* (2017) 684:197–204. doi: 10.1016/j.cplett.2017.06.040
22. Ren J, Hwang S, Shen J, Kim H, Kim H, Kim J, et al. Enhancement of the solubility of recombinant proteins by fusion with a short-disordered peptide. *J Microbiol.* (2022) 1:2122. doi: 10.1007/s12275-022-2122-z
23. Kosugi T, Ohue M. Solubility-aware protein binding peptide design using alphafold. *Biomedicines.* (2022) 10:1626. doi: 10.3390/biomedicines10071626
24. Li Y, Xu Y, Xu X. Continuous cyclic wet heating glycation to prepare myofibrillar protein-glucose conjugates: a study on the structures, solubility and emulsifying properties. *Food Chem.* (2022) 388:133035. doi: 10.1016/j.foodchem.2022.133035
25. Zhang T, Gong P, Wang Y, Jiang H, Zhang M, Yang M, et al. Lipid oxidation induced egg white protein foaming properties enhancement: the mechanism study revealed by high resolution mass spectrometry. *Food Res Int.* (2022) 152:110713. doi: 10.1016/j.foodres.2021.110713
26. Wu Y, Zhang Y, Duan W, Wang Q, An F, Luo P, et al. Ball-milling is an effective pretreatment of glycosylation modified the foaming and gel properties of egg white protein. *J Food Eng.* (2022) 319:110908. doi: 10.1016/j.jfoodeng.2021.110908
27. Li X, Wang Y, Lv J, Yang Y. Investigations of foaming, interfacial and structural properties of dispersions, batters and cakes formed by industrial yolk-contaminated egg white protein. *LWT Food Sci Technol.* (2022) 154:112776. doi: 10.1016/j.lwt.2021.112776
28. Aokia T, Hiidome Y, Sugimoto Y, Ibrahim H, Kato Y. Modification of ovalbumin with oligogalacturonic acids through the Maillard reaction. *Food Res Int.* (2001) 34:127–32. doi: 10.1016/S0963-9969(00)00140-X
29. Farjami T, Babaei J, Nau F, Dupont D, Madadlou A. Effects of thermal, non-thermal and emulsification processes on the gastrointestinal digestibility of egg white proteins. *Trends Food Sci Tech.* (2021) 107:45–56. doi: 10.1016/j.tifs.2020.11.029
30. Liu B, Jin F, Li Y, Wang H, Chi Y, Tian B, et al. Pasteurization of egg white by integrating ultrasound and microwave: effect on structure and functional properties. *Innov Food Sci Emerg.* (2022) 79:103063. doi: 10.1016/j.ifset.2022.103063
31. Dickinson E. Hydrocolloids as emulsifiers and emulsion stabilizers. *Food Hydrocolloid.* (2009) 23:1473–82. doi: 10.1016/j.foodhyd.2008.08.005
32. Ulrichs T, Drotleff AM, Ternes W. Determination of heat-induced changes in the protein secondary structure of reconstituted livetins (water-soluble proteins from hen's egg yolk) by FTIR. *Food Chem.* (2015) 172:909–20. doi: 10.1016/j.foodchem.2014.09.128
33. Liu B, Gao Q, Liu B, Song C, Sun C, Liu M, et al. Application of transcriptome analysis to understand the adverse effects of hypotonic stress on different development stages in the giant freshwater prawn *Macrobrachium rosenbergii* post-larvae. *Antioxidants.* (2022) 11:440. doi: 10.3390/antiox11030440
34. Niranjana R, Eresha M, Won-Kyo J, Jae-Young Je, Se-Kwon K. Purification of a radical scavenging peptide from fermented mussel sauce and its antioxidant properties. *Food Res Int.* (2005) 38:175–82. doi: 10.1016/j.foodres.2004.10.002
35. Nishimura K, Suzuki M, Saeki H. Glucose-conjugated chicken myofibrillar proteins derived from random-centroid optimization present potent hydroxyl radical scavenging activity. *Biosci Biotechnol Biochem.* (2019) 83:2307–17. doi: 10.1080/09168451.2019.1662276
36. Ghatasheh MK, Malik A, Ola MS, Alhomida AS. Photo-activated proflavine degrades protein and impairs enzyme activity: involvement of hydroxyl radicals. *Toxicol Rep.* (2022) 9:78–86. doi: 10.1016/j.toxrep.2021.12.009
37. Sarabandi K, Jafari SM. Improving the antioxidant stability of flaxseed peptide fractions during spray drying encapsulation by surfactants: physicochemical and morphological features. *J Food Eng.* (2020) 286:110131. doi: 10.1016/j.jfoodeng.2020.110131
38. Anitha S, Krishnan S, Senthilkumar K, Sasirekha V. A comparative investigation on the scavenging of 2,2-diphenyl-1-picrylhydrazyl radical by the natural antioxidants (+) catechin and (-) epicatechin. *J Mol Struct.* (2021) 1242:130805. doi: 10.1016/j.molstruc.2021.130805
39. Zhu J, Zhong L, Kong S, Zhang Y, Huang P. Comprehensive evaluation of the antioxidant capacity of *Sceptridium ternatum* using multiple colorimetric methods and 1,1-diphenyl-2-picrylhydrazyl-high-performance liquid chromatography analysis. *J Sep Sci.* (2020) 43:3615–24. doi: 10.1002/jssc.202000550
40. Foh MBK, Amadou I, Foh BM, Kamara MT, Xia WS. Functionality and antioxidant properties of Tilapia (*Oreochromis niloticus*) as influenced by the degree of hydrolysis. *Int J Mol Sci.* (2010) 11:1851–69. doi: 10.3390/ijms11041851





## OPEN ACCESS

## EDITED BY

Yuanyuan Shan,  
Northwest A&F University, China

## REVIEWED BY

Ying Liu,  
Huazhong Agricultural University,  
China  
Zhi Xiang Ng,  
University of Nottingham Malaysia,  
Malaysia

## \*CORRESPONDENCE

Mingchang Chang  
sxndcmc@163.com  
Lijing Xu  
xulijingsx@hotmail.com

## SPECIALTY SECTION

This article was submitted to  
Nutrition and Food Science  
Technology,  
a section of the journal  
Frontiers in Nutrition

RECEIVED 11 August 2022

ACCEPTED 22 September 2022

PUBLISHED 21 October 2022

## CITATION

Yuan H, Xu L, Chang M, Meng J,  
Feng C, Geng X, Cheng Y and Liu Z  
(2022) Effects of different cooking  
methods on volatile flavor  
compounds, nutritional constituents,  
and antioxidant activities of *Clitocybe  
squamosa*.  
*Front. Nutr.* 9:1017014.  
doi: 10.3389/fnut.2022.1017014

## COPYRIGHT

© 2022 Yuan, Xu, Chang, Meng, Feng,  
Geng, Cheng and Liu. This is an  
open-access article distributed under  
the terms of the [Creative Commons  
Attribution License \(CC BY\)](https://creativecommons.org/licenses/by/4.0/). The use,  
distribution or reproduction in other  
forums is permitted, provided the  
original author(s) and the copyright  
owner(s) are credited and that the  
original publication in this journal is  
cited, in accordance with accepted  
academic practice. No use, distribution  
or reproduction is permitted which  
does not comply with these terms.

# Effects of different cooking methods on volatile flavor compounds, nutritional constituents, and antioxidant activities of *Clitocybe squamosa*

Hui Yuan<sup>1</sup>, Lijing Xu<sup>1,2\*</sup>, Mingchang Chang<sup>1,3\*</sup>,  
Junlong Meng<sup>1,3</sup>, Cuiping Feng<sup>1,2</sup>, Xueran Geng<sup>1,2</sup>,  
Yanfen Cheng<sup>1,2</sup> and Zongqi Liu<sup>1</sup>

<sup>1</sup>College of Food Science and Engineering, Shanxi Agricultural University, Taigu, China, <sup>2</sup>Shanxi Key Laboratory of Edible Fungi for Loess Plateau, Taigu, China, <sup>3</sup>Shanxi Engineering Research Center of Edible Fungi, Taigu, China

To explore a scientific and reasonable cooking method for *Clitocybe squamosa*, four cooking methods (boiling, steaming, microwaving, and frying) were applied to *C. squamosa*, and the effects of different cooking methods on volatile flavor compounds, nutritional constituents, and antioxidant activities in *C. squamosa* were systematically investigated. The results showed that 54, 53, 61, 63, and 49 volatile flavor compounds were detected in raw, boiled, steamed, microwaved, and fried samples, respectively. Large differences in volatile flavor compounds between the four cooking and raw samples were determined by using relative odor activity values (ROAV) and principal component analysis (PCA). In addition, steaming and microwaving could protect the nutrients of *C. squamosa*, reduce losses during the cooking process and improve the color of cooked products compared to boiling and frying cooking methods. Meanwhile, cooking treatment exerted different effects on the antioxidant activity of *C. squamosa*, and the antioxidant activity of *C. squamosa* was the highest after microwave cooking treatment. This research can provide a theoretical basis for the cooking, processing and utilization of *C. squamosa* and other wild edible fungi.

## KEYWORDS

*Clitocybe squamosa*, cooking methods, volatile compounds, quality, antioxidant

## Introduction

*Clitocybe squamulosa*, as a kind of “Yinpan” in “Taimo,” belongs to the family Tricholomataceae and genus *Clitocyb*. It is widely eaten as a wild edible fungus with medicinal and edible homology. It is one of the famous specialties of Shanxi Province, China, mainly growing on the ground in the mix of pine, spruce, and birch in Wutai Mountain, Xinzhou (1). Its fruiting bodies are rich in protein, amino acids, carbohydrates, minerals, and a variety of bioactive compounds, including polysaccharides, polyphenols, and flavonoids (2). Bioactive compounds have antioxidant (3, 4), antitumor (5), anti-inflammatory (6), hypoglycemic and hypolipidemic (7, 8) functions have been extensively reported. In addition, the sensory characteristics of edible fungi have also attracted attention. *C. squamulosa* has a unique flavor and is deeply loved by local residents. In recent years, with the promotion of the concept of “one meat, one vegetable, and one mushroom,” the market demand for edible fungi has increased rapidly (9). *C. squamulosa*, as a delicacy, has important cultural and commercial values. It is noteworthy that eating wild edible fungi without heating may result in serious safety hazards to human beings, and edible fungi must undergo different cooking treatments before people can eat them safely (10, 11), making it important to study the effect of cooking treatment on the quality of *C. squamulosa*.

China has a long cooking history and culture, including various cooking methods such as boiling, steaming, frying, grilling, smoking, etc. In recent years, with the fusion of Chinese and Western food cultures, new cooking methods have gradually emerged in the domestic market, such as microwave, vacuum low-temperature, and high-pressure cooking (12). Cooking plays an essential role in dietary quality attributes by not only disinfecting and sterilizing and improving the nutritional value but also improving the flavor, color and texture of food (13). However, the heat-transfer medium, cooking time, and cooking temperature of the cooking method in the ripening process are different, which will lead to different degrees of changes in the color, texture, flavor, and nutrients of food materials (14). These are closely related to the edible value of edible fungi. For instance, Liu et al. (15) evaluated the effects of four domestic cooking methods on the bioavailability of nutrients and antioxidant activity of *Oudemansiella radicata*. The results showed that when *O. radicata* was used as food material, steaming and microwaving which can improve the edible value of *O. radicata* to a greater extent were recommended. Mena García et al. (16) discovered that the phenolic compound concentrations of wild *Boletus edulis* mushroom were significantly decreased in all cooking treatments (confit, grill, roast, and marinade), and the antioxidant activities of DPPH and FRAP were reduced. In addition, the flavor, nutritional characteristics, and antioxidant activity of mushrooms may vary with the

varieties and thermostability. For example, Selli et al. (17) found that the volatiles and key odorants of two edible fungi (*Agaricus bisporus* and *Pleurotus ostreatus*) differed significantly depending upon cooking method (boiling and oven cooking). Ng and Tan (18) studied the changes of *in vitro* antioxidant activity of five edible fungi (*A. bisporus*, *Flammulina velutipes*, *Lentinula edodes*, *P. ostreatus*, and *Pleurotus eryngii*) after being treated with different cooking methods (boiling, microwave, steam, and pressure). Among them, the antioxidant activity of pressure-cooked *P. eryngii* was the highest. In the meanwhile, the researchers further explored whether the antioxidant activity was significantly different due to the different types of mushrooms and cooking methods. The results showed that microwaving *A. bisporus* and *F. velutipes*, boiling *Auricularia polytricha*, and pressure-cooking *L. edodes* and *Pleurotus sajor-caju* yielded the best antioxidant activities (19). However, there remains a lack of systematic research into the effects of different cooking methods on the volatile flavor, nutritional content, and antioxidant activity of *C. squamulosa*.

Therefore, to find the scientific and reasonable processing and cooking methods of mushrooms, by taking *C. squamulosa* as the research object, the effects of boiling, steaming, microwaving, and frying on the flavor, color, nutrients, and antioxidant activity of *C. squamulosa* were compared. The purpose of this study was to select the most suitable cooking method for *C. squamulosa* and to provide a theoretical basis for the cooking, processing, and utilization of wild edible fungi.

## Materials and methods

### Materials

*Clitocybe squamulosa* was selected from Wutai Mountain in Shanxi Province, China, and provided by the Shanxi Edible Fungi Engineering Technology Research Center. *C. squamulosa* was identified by Hu and Wang (1, 2, 20, 21), and the complete fruiting body was selected as the experimental sample. *C. squamulosa* was washed with paper towels and freeze-dried for further processing in this study, before being randomly divided into five groups: raw and four cooking samples.

### Cooking methods

Four different cooking methods were tested: boiling, steaming, microwaving, and frying (15).

Boiling: 50 g *C. squamulosa* could be boiled in 500 mL of boiling water on a hot plate at 100°C for 6 min.

Steaming: *C. squamulosa* (50 g) was placed into a steamer and steamed for 6 min at 100°C.

Microwaving: 50 g *C. squamulosa* was placed into a porcelain bowl filled with 100 mL of water and microwaved at 800 W for 2 min.

Frying: first, *C. squamulosa* could be placed in water at 37°C for 1 min, removed, and filter paper was used to absorb the excess water. Then, 50 mL of soybean oil was heated to 180°C in a temperature-controlled frying pan. Finally, 50 g *C. squamulosa* was added and fried for 2 min.

All cooking experiments were performed in triplicate. All samples were drained of water or oil on the surface with filter paper. At the same time, vacuum freeze drying was conducted before the determination of nutrient components and activity to prevent water interference in the determination.

## Volatile flavor compound analysis

### Headspace solid-phase microextraction-gas chromatography-mass spectrometry analysis

The volatile flavor compounds of the raw and cooked samples of *C. squamulosa* were determined by headspace solid-phase microextraction (HS-SPME) (Stable Flex, Supelco, Bellefonte, PA, USA) combined with gas chromatography-mass spectrometry (GC-MS) (Trace ISQ, Thermo Fisher Scientific, Waltham, MA, USA) (22). The specific steps in these operations are described as follows:

Method: all samples were weighed, placed into 10 mL headspace bottles and heated at 80°C for 30 min. Then, the extraction head was pulled back and quickly inserted into the GC-MS injection port. The volatiles in *C. squamulosa* were desorbed at 250°C for 5 min and GC-MS determination and analysis.

Gas chromatography-mass spectrometry analysis: the column used was a TG-5MS capillary column (30 m × 0.25 mm × 0.25 μm), with high purity helium (99.999%) as the carrier. The flow rate was 1.0 mL/min and the sample was injected without partial flow. The initial column temperature was maintained at 35°C for 3 min and then increased to 180°C at 5°C/min with a 3 min hold time. Finally, it was raised to 250°C at 10°C/min with a 5 min hold time. The MS electronic energy was 70 eV, the transmission line temperature was 250°C, the quadrupole temperature was 150°C, and the mass scanning range was  $35 \leq m/z \leq 500$ .

The chemical components were determined by searching the NIST W8N08L standard spectral library, the retention index (RI) was determined using the C<sub>5</sub>-C<sub>30</sub> n-alkanes (Sigma-Aldrich, Louis, MO, USA) as the standard, and the relative content of each aroma component was obtained according to the peak area normalization method.

### Determination of relative odor activity values

The relative odor activity value (ROAV) method determines the key volatile flavor compounds in

*C. squamulosa* (23). The ROAV<sub>max</sub> of the compound that contributes the most to the overall flavor of the sample is defined as 100, and the ROAV of other compounds are calculated according to the following formula:

$$ROAV_i \approx \frac{C_i}{C_{max}} \times \frac{T_{max}}{T_i} \times 100$$

where  $C_i$  and  $T_i$  are the relative percentage and odor threshold of each flavor compound, respectively;  $C_{max}$  and  $T_{max}$  denote the relative percentage and odor threshold of the flavor compound that contributes the most to the overall flavor, respectively. All components satisfy  $0 < ROAV \leq 100$ , and the larger the ROAV, the greater the component contribution to the overall flavor of the *C. squamulosa* samples. In the case of the  $ROAV \geq 1$ , the compounds significantly affect the overall flavor of *C. squamulosa* and are considered as key volatile flavor compounds; when  $0.1 \leq ROAV < 1$ , the compounds exert a modifying effect on the overall flavor of *C. squamulosa*.

## Color measurement

The changes in color between raw and cooked samples were evaluated by an automatic colorimeter (ColorQuest XE, HunterLab, Shanghai, China) (24). Standard whiteboards and blackboards were used for calibration, and nine sites on the pileus surface were randomly selected to measure and record the values of  $L^*$ ,  $a^*$ , and  $b^*$ , representing lightness, greenness/redness, and blueness/yellowness, respectively. Then the hue angle ( $H$ ),  $a/b$  values ( $h$ ), chroma ( $C^*$ ), and total color difference ( $\Delta E$ ) were calculated according to the following formula:

$$\Delta E = (\Delta L^* + \Delta a^* + \Delta b^*)^{\frac{1}{2}} \quad C^* = (a^{*2} + b^{*2})^{\frac{1}{2}}$$

$$H = \frac{\arctan b^*}{a^*} \quad h = \frac{a}{b}$$

## Conventional nutrient analysis

The composition of ash, water, protein, and fat was analyzed according to standard official analysis methods (AOAC) (25). Then, the total carbohydrates and total energy were calculated based on the following formula (15):

$$\text{Total carbohydrates (g)} = 100 - (\text{g ash} + \text{g water} + \text{g crude protein} + \text{g crude fat})$$

$$\text{Total energy (kJ)} = 17 \times (\text{g crude protein} + \text{g total carbohydrates}) + 37 \times (\text{g crude fat})$$

## Amino acid analysis

Amino acids (AAS) in all samples were extracted following the method described in the Association of Official Analytical Chemists procedures (AOAC). The hydrolyzed amino acid (HAAS) contents of raw and cooked samples were determined using an amino acid auto-analyzer (Biochrom, Cambridge, UK) (26).

## Bioactive compounds analysis

### Polysaccharide content determination

The polysaccharide was extracted according to the method described by Guo et al. (2). The polysaccharide content was determined by the phenol-sulfuric acid method and using glucose (0–0.15 mg/mL) as a standard. The polysaccharide content was expressed as milligrams of glucose equivalent per gram mass of dry sample.

### Total phenolic content determination

The total phenolic was extracted according to the method described by Deng et al. (27). The total phenolic content was determined by the Folin–Ciocalteu method and using gallic acid (0–600 µg/mL) as a standard. The total phenolic content was expressed as milligrams of gallic acid equivalent per gram mass of dry samples.

### Flavonoid content determination

The flavonoid was extracted according to the method described by Liu et al. (28). The flavonoid content was determined by the sodium nitrite-aluminum nitrate colorimetric method and using rutin (0–2.5 µg/mL) as a standard (29). The flavonoid content was expressed as milligrams of rutin equivalent per gram mass of dry sample.

## Antioxidant activities

### Preparation of aqueous extract

The aqueous extract was prepared following the procedure described by Guo et al. (21) and Sharpe et al. (30) with some modifications. Briefly, all samples were pulverized and mixed with ultrapure water at a ratio of 1:30 (*w/v*). The mixture was extracted after 3.6 h in a water bath at 80°C and centrifuged at 5,000 rpm for 10 min, and the supernatant was collected. The obtained filtrate was concentrated on a rotary evaporator (IKA, China). Finally, vacuum freeze drying was performed. The dry samples were stored at 4°C for further analysis.

### Determination of antioxidant activities

The DPPH, ABTS, and OH radical scavenging abilities of all samples were determined according to the methods of Pan et al. (31). The extracts were prepared into different

mass concentration gradients (0.25, 0.5, 1, 2, and 4 mg/mL). The DPPH radical scavenging abilities of raw and cooked samples were determined according to the method of the DPPH Kit (Solarbio Science, Beijing, China). In short, the sample solution (0.25, 0.5, 1, 2, and 4 mg/ml) and reaction reagent were added to the 96-well plate in sequence, vortexed, and incubated at room temperature in the dark for 30 min, and the absorbance was measured at 515 nm. The ABTS radical scavenging abilities of raw and cooked samples were determined according to the method of the ABTS kit (Solarbio Science, Beijing, China). Briefly, 50 µL of sample solutions (0.25, 0.5, 1, 2, and 4 mg/mL) were added and then reaction reagent was added to the 96-well plate. After full mixing, the mixture was incubated at room temperature in the dark for 6 min, and the absorbance was measured at 405 nm. The OH radical scavenging abilities of raw and cooked samples were determined according to the method of the OH Kit (Solarbio Science, Beijing, China). Briefly, the reaction reagents were added to the 96-well plate in turn, vortexed, and placed in a constant temperature incubator at 37°C for 60 min, centrifuged at 10,000 rpm for 10 min, and the absorbance was measured at 536 nm. Notably, ascorbic acid (Vc) was used as a positive control for the DPPH, ABTS, and OH radical scavenging methods and the half inhibitory concentration (IC<sub>50</sub>) values for scavenging DPPH, ABTS, and OH radicals were calculated by linear regression analysis. A higher IC<sub>50</sub> value corresponds to a lower antioxidant activity.

## Statistical analysis

Statistical analysis was conducted using the SPSS 20.0 software (IBM Inc., Chicago, IL, USA). All data are expressed as the mean ± standard deviation (SD) and were analyzed by one-way analysis of variance (ANOVA). Differences were considered significant at *p* < 0.05. Principal component analysis (PCA) was performed using JMP Pro 16.

## Results and discussion

### Effects of cooking methods on volatile flavor compounds of *Clitocybe squamulosa*

#### Headspace solid-phase microextraction-gas chromatography-mass spectrometry analysis of *Clitocybe squamulosa* with different cooking methods

Table 1 lists the volatile flavor compounds identified using HS-SPME-GC-MS to study the effects of different cooking methods on volatile components of *C. squamulosa*. A total of 128 volatile components were identified in all samples, including alcohols, aldehydes, ketones, esters, acids, alkanes, heterocyclic,

TABLE 1 Relative contents of volatile compounds in *C. squamulosa* with different cooking methods.

	English names	RI	Molecular formula	Relative percentage (%)				
				CS	BCS	SCS	MCS	FCS
Alcohol	Ethanol	–	C <sub>2</sub> H <sub>6</sub> O	–	–	–	–	23.9
	2,3-Butanediol	–	C <sub>4</sub> H <sub>10</sub> O <sub>2</sub>	–	–	–	–	0.2
	3-Methyl-1-butanol	708	C <sub>5</sub> H <sub>12</sub> O	0.36	–	–	–	–
	1-Pentanol	750	C <sub>5</sub> H <sub>12</sub> O	–	–	0.2	0.15	–
	Hexyl alcohol	799	C <sub>6</sub> H <sub>14</sub> O	0.21	–	–	–	–
	1,2,6-hexanetriol	834	C <sub>6</sub> H <sub>14</sub> O <sub>3</sub>	–	–	0.14	–	0.6
	2-Methylcyclohexanol	902	C <sub>7</sub> H <sub>14</sub> O	–	–	–	0.2	–
	1-Octen-3-ol	982	C <sub>8</sub> H <sub>16</sub> O	1.15	25.35	2.15	2.54	32.99
	Phenethyl alcohol	989	C <sub>8</sub> H <sub>10</sub> O	4.68	0.53	0.65	0.67	0.26
	3-Heptanol, 6-methyl-	997	C <sub>8</sub> H <sub>18</sub> O	–	–	–	–	0.16
	2-Heptanol, 6-methyl-	1024	C <sub>8</sub> H <sub>18</sub> O	–	–	1.6	–	–
	2-Octyn-1-ol	1032	C <sub>8</sub> H <sub>14</sub> O	–	0.69	0.51	0.38	–
	(Z)-5-Octen-1-ol	1036	C <sub>8</sub> H <sub>16</sub> O	–	–	0.2	–	–
	5-Octyn-4-ol, 2-methyl-	1097	C <sub>9</sub> H <sub>16</sub> O	–	–	–	0.51	–
	Trans-2-Octen-1-ol	1100	C <sub>8</sub> H <sub>16</sub> O	–	2.6	–	–	3.9
	Alpha-Terpineol	1187	C <sub>10</sub> H <sub>18</sub> O	–	–	0.68	–	–
	Rac-Isopinocampheol	1196	C <sub>10</sub> H <sub>18</sub> O	–	–	0.81	–	–
	2-propyl-1-Heptanol	1197	C <sub>10</sub> H <sub>22</sub> O	–	–	–	0.2	–
	2,4-Decadien-1-ol	1230	C <sub>10</sub> H <sub>18</sub> O	–	–	–	–	0.38
	2-Undecen-1-ol, (2E)-	1298	C <sub>11</sub> H <sub>22</sub> O	–	–	–	–	0.7
	1-Octanol, 2-butyl-	1460	C <sub>12</sub> H <sub>26</sub> O	0.8	0.11	0.27	0.13	–
	1-Tridecanol	1523	C <sub>13</sub> H <sub>28</sub> O	–	–	0.15	–	0.6
	Nonadecanol	1698	C <sub>19</sub> H <sub>40</sub> O	–	0.11	0.17	–	–
	Isophytol	1826	C <sub>20</sub> H <sub>40</sub> O	–	–	0.3	0.19	–
	11-Hexadecyn-1-ol	1853	C <sub>16</sub> H <sub>30</sub> O	–	–	0.22	–	–
	Hexadecanol	1860	C <sub>16</sub> H <sub>34</sub> O <sub>4</sub>	–	0.29	–	–	–
Aldehyde	Butanedial	–	C <sub>4</sub> H <sub>6</sub> O <sub>2</sub>	–	–	–	–	0.5
	Isovaleraldehyde	735	C <sub>5</sub> H <sub>10</sub> O	–	0.15	–	–	0.21
	Valeraldehyde	802	C <sub>5</sub> H <sub>10</sub> O	0.15	0.28	0.42	0.19	0.2
	Hexanal	867	C <sub>6</sub> H <sub>12</sub> O	0.81	2.76	3.31	1.92	1.57
	Hexanal, 2-ethyl-	898	C <sub>8</sub> H <sub>16</sub> O	–	–	–	0.15	–
	Methyl valeraldehyde	902	C <sub>6</sub> H <sub>12</sub> O	–	0.12	–	0.13	–
	Decanal	902	C <sub>10</sub> H <sub>20</sub> O	–	0.97	0.72	0.46	0.14
	Heptaldehyde	953	C <sub>7</sub> H <sub>14</sub> O	–	0.47	0.29	0.21	0.9
	(E)-2-Octenal	979	C <sub>8</sub> H <sub>14</sub> O	0.24	0.39	0.27	0.23	0.22
	octanal	995	C <sub>8</sub> H <sub>16</sub> O	–	0.93	–	0.43	0.55
	Benzaldehyde	1004	C <sub>7</sub> H <sub>6</sub> O	–	0.44	–	0.37	0.39
	(E)-2-Nonen-1-al	1068	C <sub>9</sub> H <sub>16</sub> O	–	0.17	0.15	–	2.5
	1-Nonanal	1112	C <sub>9</sub> H <sub>18</sub> O	–	2.86	1.53	1.44	–
	Undecan-4-olide	1306	C <sub>11</sub> H <sub>20</sub> O <sub>2</sub>	0.2	–	–	–	–
Ketones	2-Pyrrolidinone	–	C <sub>4</sub> H <sub>7</sub> NO	1.15	–	1.84	1.13	–
	2H-Pyran-2-one, 5,6-dihydro-	734	C <sub>5</sub> H <sub>6</sub> O <sub>2</sub>	1.66	2.48	2.4	1.66	0.82
	2-Heptanone	948	C <sub>7</sub> H <sub>14</sub> O	0.61	2.25	4.3	3.25	–
	3-Octanone	981	C <sub>8</sub> H <sub>16</sub> O	6.91	0.87	1.41	1.82	0.44
	3-Octen-2-one	991	C <sub>8</sub> H <sub>14</sub> O	0.46	0.68	1.9	0.69	–
	1-Octen-3-one	998	C <sub>8</sub> H <sub>14</sub> O	2.25	2.47	4.74	3.8	0.9
	6-Undecanone	1321	C <sub>11</sub> H <sub>22</sub> O	0.21	–	–	–	–
	2-Undecanone	1328	C <sub>11</sub> H <sub>22</sub> O	2.86	1.26	1.64	–	–
	2-Dodecanone	1432	C <sub>12</sub> H <sub>24</sub> O	0.32	0.17	0.24	0.2	–
	Methanone, dicyclohexyl-	1513	C <sub>13</sub> H <sub>22</sub> O	–	–	0.75	0.26	0.5
Ester	Geranylacetone	1524	C <sub>13</sub> H <sub>22</sub> O	–	0.39	0.31	1.42	0.12
	Butanoic acid, 4-hydroxy-	–	C <sub>4</sub> H <sub>8</sub> O <sub>3</sub>	–	0.17	0.35	–	0.54
	γ-Butyrolactone	–	C <sub>4</sub> H <sub>6</sub> O <sub>2</sub>	–	–	–	0.2	–

(Continued)



TABLE 1 (Continued)

	English names	RI	Molecular formula	Relative percentage (%)				
				CS	BCS	SCS	MCS	FCS
Acids	δ-Valerolactone	689	C <sub>5</sub> H <sub>8</sub> O <sub>2</sub>	0.83	–	–	0.11	–
	γ-Valerolactone	694	C <sub>5</sub> H <sub>8</sub> O <sub>2</sub>	0.16	–	–	–	0.8
	Isoamyl nitrite	715	C <sub>5</sub> H <sub>11</sub> NO <sub>2</sub>	–	–	–	0.15	0.17
	γ-Valerolactone	752	C <sub>5</sub> H <sub>8</sub> O <sub>2</sub>	0.86	–	–	–	–
	4-Hexanolide	792	C <sub>6</sub> H <sub>10</sub> O <sub>2</sub>	1.23	–	–	–	–
	DL-sec-Butyl acetate	814	C <sub>6</sub> H <sub>12</sub> O <sub>2</sub>	0.17	–	–	–	–
	Dihydro-3-methyl-2(3H)-Furanone	840	C <sub>5</sub> H <sub>8</sub> O <sub>2</sub>	0.19	–	–	–	–
	Isobutyl acetate	845	C <sub>6</sub> H <sub>12</sub> O <sub>2</sub>	0.31	–	–	–	–
	Pentanoic acid, 2- methyl-, methyl ester	933	C <sub>7</sub> H <sub>14</sub> O <sub>2</sub>	0.35	–	0.15	–	0.5
	Banana oil	941	C <sub>7</sub> H <sub>14</sub> O <sub>2</sub>	1.59	–	–	0.2	–
	Isoamyl acetate	963	C <sub>7</sub> H <sub>14</sub> O <sub>2</sub>	2.31	–	–	0.39	–
	Hexyl acetate	1018	C <sub>8</sub> H <sub>16</sub> O <sub>2</sub>	2.46	–	–	0.18	–
	γ-Nonanolactone	1087	C <sub>9</sub> H <sub>16</sub> O <sub>2</sub>	3.53	1.5	1.43	1.25	–
	Phenethyl acetate	1164	C <sub>10</sub> H <sub>12</sub> O <sub>2</sub>	2.13	–	–	–	–
	Ethyl caprylate	1179	C <sub>10</sub> H <sub>20</sub> O <sub>2</sub>	0.64	0.33	–	–	0.1
	3-octyl acetate	1182	C <sub>10</sub> H <sub>20</sub> O <sub>2</sub>	1.3	–	–	–	–
	Isobutyl hexanoate	1186	C <sub>10</sub> H <sub>20</sub> O <sub>2</sub>	0.2	–	–	0.14	–
	Hexanoic acid, pentyl ester	1276	C <sub>11</sub> H <sub>22</sub> O <sub>2</sub>	–	–	–	0.13	–
	Isopentyl hexanoate	1286	C <sub>11</sub> H <sub>22</sub> O <sub>2</sub>	0.66	0.24	0.46	0.56	–
	Hexanoic acid, 2-methylbutyl ester	1329	C <sub>11</sub> H <sub>22</sub> O <sub>2</sub>	0.22	–	–	0.19	–
	Isovaleric acid, phenethyl ester	1498	C <sub>13</sub> H <sub>18</sub> O <sub>2</sub>	–	0.21	–	–	–
	Butanoic acid, 2-ethylhexyl ester	1560	C <sub>12</sub> H <sub>24</sub> O <sub>2</sub>	–	–	–	–	0.8
	Geranyl 3-methylbutanoate	1725	C <sub>15</sub> H <sub>26</sub> O <sub>2</sub>	0.16	–	–	–	–
	2,2,4-trimethyl-1,3-pentanediol diisobutyrate	1867	C <sub>16</sub> H <sub>30</sub> O <sub>4</sub>	–	0.27	0.8	0.14	–
	Glycine, L-alanyl-	–	C <sub>2</sub> H <sub>7</sub> NO <sub>2</sub>	–	0.25	0.4	0.27	0.34
	DL-Homocysteine	–	C <sub>4</sub> H <sub>9</sub> NO <sub>2</sub> S	–	–	3.7	–	–
	Isobutyric acid	–	C <sub>4</sub> H <sub>8</sub> O <sub>2</sub>	–	–	–	–	0.1
	Isovaleric acid	734	C <sub>5</sub> H <sub>10</sub> O <sub>2</sub>	0.46	0.31	0.46	0.23	0.21
	DL-2-Methylbutyric acid	736	C <sub>5</sub> H <sub>10</sub> O <sub>2</sub>	–	–	0.17	–	–
	Acetic acid glacia	835	C <sub>2</sub> H <sub>4</sub> O <sub>2</sub>	3.32	–	4.57	2.38	4.71
	2-Methylhexanoic acid	964	C <sub>7</sub> H <sub>14</sub> O <sub>2</sub>	–	–	–	0.14	–
	4-Methyloctanoic acid	1126	C <sub>9</sub> H <sub>18</sub> O <sub>2</sub>	–	–	0.19	–	–
Alkanes	Hexane	600	C <sub>6</sub> H <sub>14</sub>	–	–	3.2	1.46	–
	1,3- dimethyl-, cis-Cyclopentane	700	C <sub>7</sub> H <sub>14</sub>	1.13	–	–	–	–
	1-Chlorohexane	845	C <sub>6</sub> H <sub>13</sub> Cl	–	–	–	0.24	–
	Octane, 3,5-dimethyl-	1000	C <sub>10</sub> H <sub>22</sub>	0.13	–	–	0.45	–
	Undecane	1100	C <sub>11</sub> H <sub>24</sub>	0.65	0.29	0.42	1.41	0.48
	Dodecane	1200	C <sub>12</sub> H <sub>26</sub>	2.39	1.32	1.23	1.6	0.97
	Decane, 2-methyl-	1200	C <sub>12</sub> H <sub>26</sub>	–	–	0.15	0.21	–
	Tetradecane	1400	C <sub>14</sub> H <sub>30</sub>	4.3	1.67	3.8	1.29	0.65
	Tridecane, 3-methylene-	1400	C <sub>14</sub> H <sub>28</sub>	–	0.21	–	–	–
	Undecane, 3-methyl-	1458	C <sub>12</sub> H <sub>24</sub> O	–	0.35	0.28	–	0.25
	Pentadecane	1500	C <sub>15</sub> H <sub>32</sub>	1.29	–	–	–	–
	Hexadecane	1600	C <sub>16</sub> H <sub>34</sub>	–	1.13	0.93	0.99	0.3
	Heptadecane	1700	C <sub>17</sub> H <sub>36</sub>	–	0.43	–	–	–
	Oxirane, 2-tetradecyl-	1861	C <sub>16</sub> H <sub>32</sub> O	–	0.27	–	–	0.6
	Heneicosane	2100	C <sub>21</sub> H <sub>44</sub>	0.4	–	–	–	–
Pyrazines	Heptacosane	2700	C <sub>27</sub> H <sub>56</sub>	–	–	0.28	–	–
	2,6-Dimethylpyrazine	843	C <sub>6</sub> H <sub>8</sub> N <sub>2</sub>	4.16	–	0.33	0.38	–
	2,5-Dimethyl pyrazine	843	C <sub>6</sub> H <sub>8</sub> N <sub>2</sub>	–	0.25	–	–	–
	2-Ethyl-5-methylpyrazine	954	C <sub>7</sub> H <sub>10</sub> N <sub>2</sub>	0.68	–	–	–	–
	2,3,5-Trimethylpyrazine	954	C <sub>7</sub> H <sub>10</sub> N <sub>2</sub>	–	–	–	0.76	–

(Continued)

TABLE 1 (Continued)

	English names	RI	Molecular formula	Relative percentage (%)				
				CS	BCS	SCS	MCS	FCS
Aromatic	Pyrazine,2-ethyl-3,5-dimethyl-	1031	C <sub>8</sub> H <sub>12</sub> N <sub>2</sub>	0.49	–	–	–	–
	Pyrazine,2-butyl-3-methyl-	1098	C <sub>9</sub> H <sub>14</sub> N <sub>2</sub>	0.44	–	–	0.11	–
	Ethylbenzene	890	C <sub>8</sub> H <sub>10</sub>	–	0.22	0.25	–	–
	1,4-Xylene	921	C <sub>8</sub> H <sub>10</sub>	–	0.22	–	0.15	0.44
	1,3-Xylene	925	C <sub>8</sub> H <sub>10</sub>	–	–	0.49	–	–
	Ethylbenzene	926	C <sub>8</sub> H <sub>10</sub>	–	–	–	0.13	0.34
	1,3,5,7-cyclooctatetraene	964	C <sub>8</sub> H <sub>8</sub>	–	–	–	–	1.15
	Naphthalene	1196	C <sub>10</sub> H <sub>8</sub>	0.16	0.33	0.42	0.32	0.11
Ethers	1-isopropyl-2-methylbenzene	1209	C <sub>10</sub> H <sub>14</sub>	–	–	0.17	–	0.7
	7H-Benzocycloheptene	1280	C <sub>11</sub> H <sub>10</sub>	–	–	0.17	0.11	–
	7-Tetradecene	1598	C <sub>14</sub> H <sub>28</sub>	–	–	0.23	–	–
	Ethene, (2-methoxyethoxy)-	636	C <sub>5</sub> H <sub>10</sub> O <sub>2</sub>	–	4.49	–	–	–
	N-Hexyl n-octyl ether	1631	C <sub>14</sub> H <sub>30</sub> O	–	–	–	–	0.6
	1,1'-oxybis-Decane	1793	C <sub>20</sub> H <sub>42</sub> O	0.87	–	–	–	–
	Octane, 1,1'-oxybis-	1877	C <sub>16</sub> H <sub>34</sub> O	–	–	0.15	–	–
	Lenthionine	–	C <sub>2</sub> H <sub>4</sub> S <sub>5</sub>	–	0.27	–	–	0.15
Other	Trimethylamine	–	C <sub>3</sub> H <sub>9</sub> N	–	–	2.54	2.4	–
	Ammonium acetate	–	C <sub>2</sub> H <sub>7</sub> NO <sub>2</sub>	–	3.33	–	–	–
	Hexanenitrile	831	C <sub>6</sub> H <sub>11</sub> N	–	0.11	0.27	–	–
	1H-Pyrrole,1,2,5-trimethyl-	934	C <sub>7</sub> H <sub>11</sub> N	0.5	–	–	0.12	–
	2-Pentylfuran	1102	C <sub>9</sub> H <sub>14</sub> O	3.6	5.2	9.37	3.93	1.26
	2-Dodecanone	1496	C <sub>12</sub> H <sub>24</sub> O	–	0.17	–	0.2	–
	2a,3a-Epoxy-5a-androstan-17b-ol	1706	C <sub>19</sub> H <sub>30</sub> O <sub>2</sub>	–	0.12	–	–	0.7

CS, *C. squamulosa*; BCS, boiling-cooked *C. squamulosa*; SCS, steaming-cooked *C. squamulosa*; MCS, microwaving-cooked *C. squamulosa*; FCS, frying-cooked *C. squamulosa*.

aromatic hydrocarbons, ethers, and others. Moreover, a total of 54, 53, 61, 63, and 49 volatile components were detected in raw, boiled, steamed, microwaved, and fried cooking samples, respectively, of which alcohols, aldehydes, esters, and ketones were the major chemical classes.

Cooking methods altered the volatile flavor profiles of *C. squamulosa*. Briefly, esters were abundant in the saw sample, but large losses occurred during the cooking process. This may be attributed to the conversion of ester compounds into other substances as the result of thermal decomposition or the action of enzymes in the cooking process, such as degrading esters and producing alcohols and acids compounds (32). In addition, different cooking methods had different effects on alcohols, aldehydes and ketones in *C. squamulosa*. During high-temperature ripening, these compounds will be lost, but many new compounds will also be produced. This series of changes can be caused by the Maillard reaction, the interaction of amino acids or proteins with oxidized lipids, and the degradation of long-chain compounds during heating (22). Therefore, the flavors of *C. squamulosa* processed by different cooking methods are different, due to the comprehensive effect of a variety of volatile flavor compounds with different characteristics.

Alcohols, with a mild characteristic odor, are important volatile compounds in mushrooms (22). Among alcohols, 1-octene-3-ol is the key volatile component of edible fungi, also

known as “mushroom alcohol,” which is mainly derived from the reaction of lipooxygenases in polyunsaturated fatty acids, and its stability is poor (33). In contrast, boiling and frying cooking have the greatest effect on alcohols, and the relative contents of 1-octene-3-ol in boiled and fried samples were 22.02 times and 28.69 times that of the raw sample, respectively. In addition, a large amount of ethanol is produced in the fried cooking sample, which has a mellow aroma and flavor.

Aldehydes and ketones are mainly derived from polyunsaturated fatty acid oxidation, amino acid degradation, and the Maillard reaction (2, 34). Due to the low odor threshold, they are more critical volatile compounds than alcohols, which will strongly affect the aroma of mushroom products. It is worth noting that all cooked samples show an increase in the content of aldehydes. The contents of hexanal, 1-nonanal and decanal are high. Among them, hexanal has the flavor of grass, 1-nonanal shows the flavor of rose and citrus and decanal has the aroma of fat (16), which increases the complexity of mushroom aroma. The relative contents of 1-nonanal and decanal in boiling samples are higher, and the content of hexanal in cooked samples is greater. The threshold of ketone is higher than that of aldehyde. Among the four cooking methods, microwaved samples retain ketones better and are more conducive to the formation of ketones. The contents of 1-octene-3-one, 2-heptanone, 2h-pyran-2-one, 5,6-dihydrogen, 3-octene-2-one, and 2-pyrrolidone are higher.

## Key aroma component analysis of *Clitocybe squamulosa* after different cooking methods

The contribution of volatile flavor compounds to the overall aroma of the sample depends on the concentration and threshold (23). Through searching, a total of 33 volatile flavor components of aroma thresholds were found. ROAV values were calculated through the concentrations and thresholds of volatile flavor compounds (Table 2). In the raw samples, 10 compounds were screened out as the key volatile flavor components of *C. squamulosa*. After cooking, the boiled, steamed, microwaved, and fried samples contained 8, 17,

14, and 3 key flavor compounds, respectively. It is the differences between these flavor compounds that form their own unique volatile flavors under different cooking methods. Notably, in raw samples, 2,6-dimethylpyrazine was defined as the component that contributed the most to the overall flavor. However, among all the cooked samples, 1-octen-3-ol was defined as the component that contributed the most to the overall flavor. 1-octen-3-ol mainly has a mushroom flavor, so the mushroom flavor of *C. squamulosa* is better released after cooking. In addition, key flavor compounds were significantly increased after steaming and microwave cooking,

TABLE 2 Key volatile compounds in *C. squamulosa* with different cooking methods.

English names	Odor threshold ( $\mu$ g/kg)	ROAV				
		CS	BCS	SCS	MCS	FCS
1-Octen-3-ol	1.00	47.55	100.00	100.00	100.00	100.00
Hexyl alcohol	5.60	1.55	–	–	–	–
Phenethyl alcohol	1000.00	0.19	0.00	0.03	0.03	0.00
1-Pentanol	5.00	–	–	1.86	1.18	–
Ethanol	100,000.00	–	–	–	–	0.00
Valeraldehyde	12	0.52	0.09	1.63	0.62	0.05
Hexanal	4.50	7.44	2.42	34.21	16.80	1.06
(E)-2-Octenal	3.00	3.31	0.51	4.19	3.02	0.22
Isovaleraldehyde	9	–	0.07	–	–	0.07
Benzaldehyde	3.00	–	0.58	–	4.86	0.39
octanal	3.40	–	1.08	–	4.98	0.49
1-Nonanal	1.10	–	10.26	64.69	51.54	–
(E)-2-Nonen-1-al	0.19	–	3.53	36.72	–	39.88
Decanal	3	–	1.28	11.16	6.04	0.14
Heptaldehyde	3.00	–	–	4.50	–	0.52
Butanedial	7.00	–	–	–	–	0.22
2-Heptanone	140	0.18	0.06	1.43	0.91	–
1-Octen-3-one	5.00	18.61	1.95	44.09	29.92	0.55
3-Octanone	28.00	10.20	0.12	2.34	2.56	0.05
2-Undecanone	7.00	16.89	0.71	10.90	–	–
Geranylacetone	10	–	0.15	1.44	5.59	0.04
Isobutyl acetate	66.00	0.19	–	–	–	–
Acetic acid glacia	22000.00	0.01	–	0.01	0.00	0.00
Isovaleric acid	400.00	0.05	0.00	0.05	0.02	0.00
Isobutyric acid	4100.00	–	–	–	–	0.00
Hexane	580.00	–	–	0.26	0.10	–
2-Methylpyrazine	60.00	0.21	–	–	–	–
2,6-Dimethylpyrazine	1.72	100.00	–	8.92	8.70	–
2-Ethyl-5-methylpyrazine	16.00	1.76	–	–	–	–
2,5-Dimethyl pyrazine	1.82	–	0.54	–	–	–
2,3,5-Trimethylpyrazine	400	–	–	–	0.07	–
2-Pentylfuran	6.00	24.81	3.42	72.64	25.79	0.64
Trimethylamine	2.40	–	–	49.22	39.37	–

CS, *C. squamulosa*; BCS, boiling-cooked *C. squamulosa*; SCS, steaming-cooked *C. squamulosa*; MCS, microwaving-cooked *C. squamulosa*; FCS, frying-cooked *C. squamulosa*. The odor thresholds were referenced from a book named odor threshold compilations of odor threshold values in air, water and other media (second enlarged and revised edition) or taken from references (23, 50).

especially aldehydes, including valeraldehyde, hexanal, (E)-2-octenal, benzaldehyde, octanal, 1-nonanal, (E)-2-nonen-1-al, decanal, and heptaldehyde, which mainly have fruit, almond, fat, and grass flavors (16).

## Principal component analysis of volatile components

Principal component analysis was performed to visualize the underlying relationships between raw and four cooked samples. As shown in Figure 1, PC1 and PC2 accounted for 78.7% of the total variance. The score plot clearly compares the differences between raw and cooked samples. In addition, load plots were also performed to estimate the differences between samples. Samples could be divided into two groups: one represents the raw samples, steamed samples, and microwaved samples, and the other represents the boiled samples and fried samples. These results showed that the volatile components of *C. squamulosa* changed after cooking, and the choice of cooking technique exerted varying degrees of influence on thereon. Compared with the other two cooking methods, steaming and microwaving cooked can retain the original flavor and give unique flavor.

## Effects of cooking methods on the color of *Clitocybe squamulosa*

Color is the visual indicator used when judging the quality change of a foodstuff in the cooking process (35). It is the most intuitive indicator for evaluating the quality change in *C. squamulosa*. As shown in Table 3, the different heating principles, heating temperatures, and times of different cooking methods led to varying degrees of changes in the color characteristics of *C. squamulosa*. Specifically, boiled samples showed the highest brightness ( $L^*$  value), and fried samples showed the lowest  $L^*$  value, which may be attributed to the strong Maillard reaction that occurs during frying (36). The  $a^*$  values of raw and cooked samples are all positive, indicating that mushrooms belong to the red variety. There is no significant difference between the boiled, steamed, and raw samples, and the microwave and fried samples were significantly lower (in terms of  $a^*$  value) than the raw samples. The  $b^*$  value observed in boiled and steamed samples is higher, and the  $b^*$  value observed in microwave samples is closest to that of raw samples. The hue angle ( $H$ ) is used to describe the changes in mushroom color, and values between 0 and 90 indicate that the color of *C. squamulosa* is between yellow, and the larger the value is, the more yellow the color (37). During the different cooking methods, the difference between the hue angle of the microwave and raw samples is minimized. Chroma ( $C^*$ ) is an index that describes the color intensity and visual characteristics related to color (22). The higher the saturation value, the brighter the color intensity. In contrast, boiling and steaming cooked samples have the highest  $C^*$  values. The larger the  $a/b$  values ( $h$ ) are, the darker the color is. Among them, the  $h$  values of fried

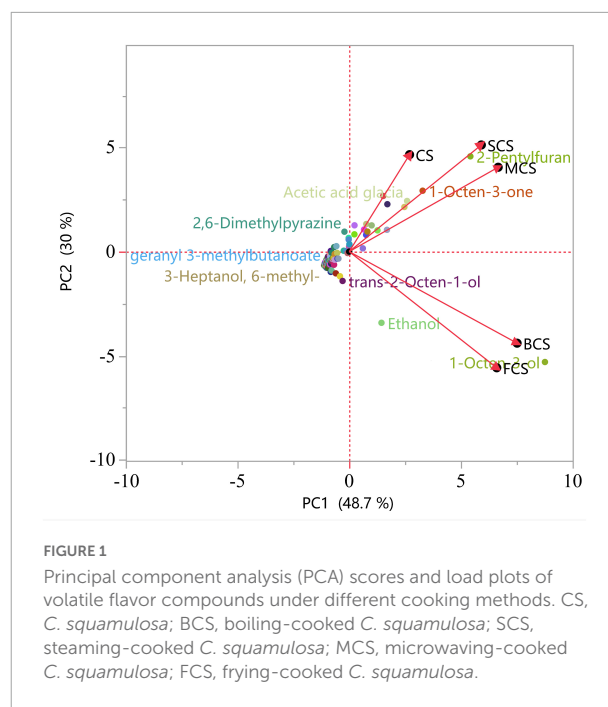


FIGURE 1

Principal component analysis (PCA) scores and load plots of volatile flavor compounds under different cooking methods. CS, *C. squamulosa*; BCS, boiling-cooked *C. squamulosa*; SCS, steaming-cooked *C. squamulosa*; MCS, microwaving-cooked *C. squamulosa*; FCS, frying-cooked *C. squamulosa*.

samples are the highest, and there is no significant difference between steamed cooked and raw samples. The total color ( $\Delta E$ ) difference of the microwaved samples is the smallest.

To summarize, the raw samples are yellowish-brown. The color of steamed and fried samples is darker, and the color of boiled samples is shown to be brighter. Microwave cooking can better maintain the primary color of *C. squamulosa*.

## Effects of cooking methods on conventional nutrients of *Clitocybe squamulosa*

Table 4 lists the effects of conventional nutrients of raw samples and cooking treatment on their nutritional value. The conventional nutrient contents of *C. squamulosa* are different after use of different cooking methods. The carbohydrate contents of the boiled and microwaved samples were higher than that of the steamed, microwave, and raw samples. Moreover, the loss of protein, ash, and moisture content of microwaved samples are the lowest, followed by the steamed samples. This may be because the steaming temperature is relatively low, and the microwave cooking is faster, so various chemical reaction rates and reaction times are reduced (38). The steamed and microwaved samples are not in direct contact with water or oil, which also reduces the loss of protein, ash, and water. Boiled and fried samples have suffered significant loss of nutrients, which may be related to water or oil absorption during boiling or frying, which has a dilutive effect on other nutrients (39). It is worth noting that the temperature can be as high as 180°C during frying, leading to severe oxidation of protein and fat

TABLE 3 Effects of different cooking methods on color in *C. squamulosa*.

Cooking methods	<i>L</i> *	<i>a</i> *	<i>b</i> *	<i>C</i> *	<i>H</i>	<i>h</i>	$\Delta E^*$
CS	28.6 ± 0.76 <sup>d</sup>	9.74 ± 1.19 <sup>a</sup>	11.54 ± 1.53 <sup>b</sup>	15.13 ± 1.69 <sup>b</sup>	49.79 ± 3.54 <sup>d</sup>	0.85 ± 0.10 <sup>a</sup>	
BCS	36.86 ± 1.20 <sup>a</sup>	9.17 ± 0.54 <sup>ab</sup>	16.32 ± 1.65 <sup>a</sup>	18.73 ± 1.51 <sup>a</sup>	60.57 ± 2.65 <sup>a</sup>	0.57 ± 0.06 <sup>d</sup>	9.74 ± 1.76 <sup>a</sup>
SCS	33.64 ± 1.02 <sup>b</sup>	9.96 ± 1.06 <sup>a</sup>	15.31 ± 1.17 <sup>a</sup>	18.28 ± 1.41 <sup>a</sup>	57.01 ± 2.20 <sup>b</sup>	0.65 ± 0.06 <sup>c</sup>	6.74 ± 1.48 <sup>b</sup>
MFS	29.47 ± 0.60 <sup>c</sup>	8.68 ± 0.99 <sup>b</sup>	11.08 ± 1.44 <sup>b</sup>	14.08 ± 1.68 <sup>c</sup>	51.9 ± 1.89 <sup>c</sup>	0.79 ± 0.05 <sup>b</sup>	3.19 ± 1.42 <sup>c</sup>
FCS	27.43 ± 1.09 <sup>c</sup>	6.53 ± 0.73 <sup>c</sup>	6.88 ± 0.76 <sup>c</sup>	9.50 ± 0.95 <sup>d</sup>	46.5 ± 2.64 <sup>c</sup>	0.95 ± 0.09 <sup>a</sup>	6.03 ± 2.35 <sup>b</sup>

CS, *C. squamulosa*; BCS, boiling-cooked *C. squamulosa*; SCS, steaming-cooked *C. squamulosa*; MCS, microwaving-cooked *C. squamulosa*; FCS, frying-cooked *C. squamulosa*. Values represent the mean ± standard deviation, and different superscript lowercase letters denote significance ( $p < 0.05$ ) in each column.

TABLE 4 Effects of different cooking methods on conventional nutrient components in *C. squamulosa*.

Nutrient component	CS	BCS	SCS	MCS	FCS
Energy (kJ/100 g)	1536.28 ± 3.82 <sup>c</sup>	1467.26 ± 4.99 <sup>c</sup>	1518.65 ± 1.25 <sup>d</sup>	1553.34 ± 4.55 <sup>b</sup>	1890.03 ± 4.82 <sup>a</sup>
Protein (g/100 g)	39.56 ± 0.16 <sup>a</sup>	34.68 ± 0.44 <sup>c</sup>	37.1 ± 0.16 <sup>b</sup>	37.69 ± 0.75 <sup>b</sup>	30.35 ± 0.99 <sup>d</sup>
Fat (g/100 g)	9.70 ± 0.24 <sup>b</sup>	7.74 ± 0.35 <sup>d</sup>	8.89 ± 0.07 <sup>c</sup>	9.08 ± 0.09 <sup>c</sup>	22.93 ± 0.32 <sup>a</sup>
Carbohydrate (g/100 g)	29.34 ± 0.45 <sup>d</sup>	34.78 ± 0.12 <sup>a</sup>	32.87 ± 0.17 <sup>b</sup>	33.92 ± 0.98 <sup>ab</sup>	30.63 ± 0.92 <sup>c</sup>
Ash (g/100 g)	10.69 ± 0.20 <sup>a</sup>	9.09 ± 0.12 <sup>b</sup>	10.44 ± 0.13 <sup>a</sup>	9.37 ± 0.19 <sup>b</sup>	6.97 ± 0.25 <sup>c</sup>
Moisture (g/100 g)	10.40 ± 0.27 <sup>b</sup>	13.81 ± 0.29 <sup>a</sup>	10.67 ± 0.06 <sup>b</sup>	9.90 ± 0.27 <sup>c</sup>	9.06 ± 0.25 <sup>d</sup>

CS, *C. squamulosa*; BCS, boiling-cooked *C. squamulosa*; SCS, steaming-cooked *C. squamulosa*; MCS, microwaving-cooked *C. squamulosa*; FCS, frying-cooked *C. squamulosa*. Values represent the mean ± standard deviation, and different superscript lowercase letters denote significance ( $p < 0.05$ ) in each row.

and deterioration of mushroom quality (40). As the heating temperature of the water boiling, steaming, and microwave cooking methods is low, excessive oxidation can be avoided.

## Effects of cooking methods on the hydrolytic amino acids in *Clitocybe squamulosa*

The nutritional value and flavor of edible fungi are closely related to the type and content of amino acids, especially essential amino acids and flavoring amino acids (41). The differences in hydrolytic amino acid content in *C. squamulosa* with different cooking methods are listed in Table 5; in raw samples and cooked samples, the Arg content was significantly higher, followed by Glu and Asp, which together represent 32.64, 33.37, 32.42, 31.80, and 32.58% of the total amino acids in raw samples, boiled, steamed, microwaved, and fried samples. Among them, Arg is a functional essential amino acid that plays a vital role in hormone release, neurotransmission and maintenance of blood pressure, cell division and wound healing (42). In addition, Glu, Asp, Phe, Ala, Gly, and Tyr are all aromatic amino acids, which together represent 36.26, 37.40, 36.48, 36.02, and 37.11% of the total amino acids in raw samples, boiling, steaming, microwaved and frying cooked samples. These amino acids affect the flavor of *C. squamulosa*.

Cooking temperature and time affect the rate of protein degradation, resulting in changes in the amino acid content (43). Compared with the raw samples, all cooking treatments resulted from decreased amino acid contents, and the degree of

loss caused by different cooking methods was different. In terms of the total amount of amino acids, the order of their content is: raw > steamed > boiled > microwave > fried. Fried samples lost the most, which was possibly due to increasing degree of oxidation caused by the high temperature and oil, followed by microwaved and boiled samples. Microwave cooking is prone to thermal degradation, deformation, polymerization, and other reactions, leading to the loss of amino acids from the food (44). Boiled cooking readily causes a loss of amino acids in the soup. Thus, steamed cooking preserves the content of amino acid better than the other three cooking methods.

## Effects of cooking methods on bioactive compounds of *Clitocybe squamulosa*

The effects of cooking methods on the bioactive compounds of *C. squamulosa* are listed in Table 6. The polysaccharide content is shown to be higher, and the total phenol and flavonoid contents are lower. However, the four cooking treatments all decrease the amounts of bioactive compounds therein, but the extent of this loss is different. The difference in cooking conditions of all samples is undoubtedly the main reason for the difference in bioactive compound content. Among the four cooking methods, fried cooking lost the most, followed by boiled cooking. Steam cooking demonstrated a minimal loss of polysaccharides and microwave cooking showed minimal losses of total phenolics and flavonoids. The reason may be that different degrees of damage to the cell wall are caused by



TABLE 5 Effects of different cooking methods on the hydrolytic amino acids in *C. squamulosa*.

Amino acid (g/100 g)	CS	BCS	SCS	MCS	FCS
Thr	1.69 ± 0.08 <sup>a</sup>	1.51 ± 0.00 <sup>b</sup>	1.60 ± 0.05 <sup>ab</sup>	1.36 ± 0.05 <sup>c</sup>	1.30 ± 0.06 <sup>c</sup>
Val	1.84 ± 0.19 <sup>a</sup>	1.54 ± 0.03 <sup>cd</sup>	1.78 ± 0.13 <sup>ab</sup>	1.59 ± 0.14 <sup>bc</sup>	1.34 ± 0.02 <sup>d</sup>
Met	0.67 ± 0.01 <sup>a</sup>	0.58 ± 0.01 <sup>c</sup>	0.62 ± 0.02 <sup>b</sup>	0.57 ± 0.03 <sup>c</sup>	0.53 ± 0.01 <sup>d</sup>
Ile	1.58 ± 0.17 <sup>a</sup>	1.39 ± 0.06 <sup>ab</sup>	1.48 ± 0.12 <sup>a</sup>	1.35 ± 0.16 <sup>ab</sup>	1.17 ± 0.04 <sup>b</sup>
Leu	2.44 ± 0.24 <sup>a</sup>	2.09 ± 0.06 <sup>ab</sup>	2.29 ± 0.20 <sup>ab</sup>	2.02 ± 0.24 <sup>b</sup>	1.56 ± 0.21 <sup>c</sup>
Phe	1.22 ± 0.04 <sup>a</sup>	1.25 ± 0.04 <sup>a</sup>	1.25 ± 0.09 <sup>a</sup>	1.10 ± 0.09 <sup>b</sup>	1.13 ± 0.01 <sup>ab</sup>
Lys	2.02 ± 0.08 <sup>a</sup>	1.99 ± 0.02 <sup>a</sup>	1.99 ± 0.09 <sup>a</sup>	1.81 ± 0.26 <sup>ab</sup>	1.69 ± 0.06 <sup>b</sup>
Asp	2.85 ± 0.06 <sup>a</sup>	2.61 ± 0.02 <sup>c</sup>	2.74 ± 0.03 <sup>b</sup>	2.27 ± 0.05 <sup>d</sup>	2.17 ± 0.04 <sup>f</sup>
Ser	1.55 ± 0.05 <sup>a</sup>	1.36 ± 0.02 <sup>b</sup>	1.47 ± 0.05 <sup>a</sup>	1.30 ± 0.02 <sup>bc</sup>	1.23 ± 0.07 <sup>c</sup>
Glu	2.99 ± 0.02 <sup>a</sup>	3.05 ± 0.09 <sup>a</sup>	2.91 ± 0.09 <sup>a</sup>	2.64 ± 0.30 <sup>b</sup>	2.43 ± 0.07 <sup>b</sup>
Gly	1.93 ± 0.11 <sup>a</sup>	1.73 ± 0.04 <sup>b</sup>	1.87 ± 0.02 <sup>a</sup>	1.62 ± 0.01 <sup>c</sup>	1.46 ± 0.04 <sup>d</sup>
Ala	1.72 ± 0.05 <sup>a</sup>	1.58 ± 0.02 <sup>c</sup>	1.65 ± 0.02 <sup>ab</sup>	1.46 ± 0.06 <sup>d</sup>	1.33 ± 0.07 <sup>e</sup>
Cys	0.88 ± 0.05 <sup>a</sup>	0.86 ± 0.00 <sup>ab</sup>	0.89 ± 0.02 <sup>a</sup>	0.87 ± 0.01 <sup>ab</sup>	0.83 ± 0.00 <sup>b</sup>
Tyr	1.21 ± 0.05 <sup>a</sup>	1.00 ± 0.01 <sup>bc</sup>	1.17 ± 0.06 <sup>a</sup>	1.07 ± 0.07 <sup>b</sup>	0.96 ± 0.01 <sup>c</sup>
His	1.13 ± 0.04 <sup>a</sup>	1.04 ± 0.02 <sup>b</sup>	1.10 ± 0.01 <sup>a</sup>	0.99 ± 0.02 <sup>c</sup>	0.90 ± 0.01 <sup>d</sup>
Arg	4.89 ± 0.20 <sup>a</sup>	4.23 ± 0.10 <sup>b</sup>	4.65 ± 0.02 <sup>a</sup>	4.06 ± 0.04 <sup>b</sup>	3.73 ± 0.21 <sup>c</sup>
Pro	2.27 ± 0.01 <sup>a</sup>	2.18 ± 0.03 <sup>b</sup>	2.30 ± 0.03 <sup>a</sup>	2.11 ± 0.03 <sup>c</sup>	1.79 ± 0.02 <sup>d</sup>
Essential amino acids (EAA)	11.45	10.34	11.02	9.81	8.72
Non-essential amino acids (NEAA)	21.41	19.63	20.76	18.40	16.84
Umami amino acids (UAA)	11.92	11.21	11.59	10.16	9.49
Total amino acids (TAA)	32.87	29.97	31.77	28.21	25.57

CS, *C. squamulosa*; BCS, boiling-cooked *C. squamulosa*; SCS, steaming-cooked *C. squamulosa*; MCS, microwaving-cooked *C. squamulosa*; FCS, frying-cooked *C. squamulosa*. Values represent the mean ± standard deviation, and different superscript lowercase letters denote significance ( $p < 0.05$ ) in each row.

TABLE 6 Effects of different cooking methods on bioactive compounds contents in *C. squamulosa*.

Bioactive compounds	CS	BCS	SCS	MCS	FCS
Polysaccharide (mg/g)	129.76 ± 0.67 <sup>a</sup>	91.46 ± 0.88 <sup>d</sup>	106.78 ± 0.88 <sup>b</sup>	101.45 ± 0.67 <sup>c</sup>	62.93 ± 0.58 <sup>e</sup>
Total phenolic (mg/g)	4.29 ± 0.28 <sup>a</sup>	3.56 ± 0.01 <sup>d</sup>	4.11 ± 0.01 <sup>c</sup>	4.17 ± 0.02 <sup>b</sup>	3.47 ± 0.03 <sup>e</sup>
Flavonoids (mg/g)	15.00 ± 0.28 <sup>a</sup>	13.78 ± 0.01 <sup>b</sup>	14.55 ± 0.01 <sup>b</sup>	14.94 ± 0.02 <sup>b</sup>	12.69 ± 0.03 <sup>c</sup>

CS, *C. squamulosa*; BCS, boiling-cooked *C. squamulosa*; SCS, steaming-cooked *C. squamulosa*; MCS, microwaving-cooked *C. squamulosa*; FCS, frying-cooked *C. squamulosa*. Values represent the mean ± standard deviation, and different superscript lowercase letters denote significance ( $p < 0.05$ ) in each row.

different heat-transfer media and cooking temperatures (45). For example, during the boiling process, the water content increases, the tissue was softened to make it easy for water-soluble compounds to dissolve in the soup (46). During the frying process, the oil covers the cell surface, hindering the extraction of bioactive compounds (46).

## Effects of cooking methods on the antioxidant activity in *Clitocybe squamulosa*

The effects of cooking methods on the antioxidant activity of *C. squamulosa* were evaluated by DPPH, ABTS, and OH radical scavenging capacity (Figures 2A–F). The antioxidant activities for all measured concentrations of *C. squamulosa* extracts were dose-dependent, however, with a different extent. The DPPH,

ABTS, and OH radical scavenging activities of the microwaved sample extract were greater than those of the raw sample and the other three cooked samples, but lower than that of the positive control (Vc). The IC<sub>50</sub> values of the DPPH, ABTS, and OH radical scavenging activities of the microwaved sample were 0.20, 0.22, and 0.32 mg/mL, respectively. Compared with other cooking methods, microwave-cooked samples exhibited superior antioxidant activity, which may be attributed to the high contents of total phenols, polysaccharides, and flavonoids in microwaved samples. Of course, these were related not only to the content of bioactive components in mushrooms, but also to other components related to antioxidant activity therein (47). The IC<sub>50</sub> values of ABTS radical scavenging activities between the steamed samples and raw samples were not statistically significant ( $p < 0.05$ ). The IC<sub>50</sub> values of the OH radical scavenging activities of the fried samples were significantly lower than that of the raw samples. Previous studies have

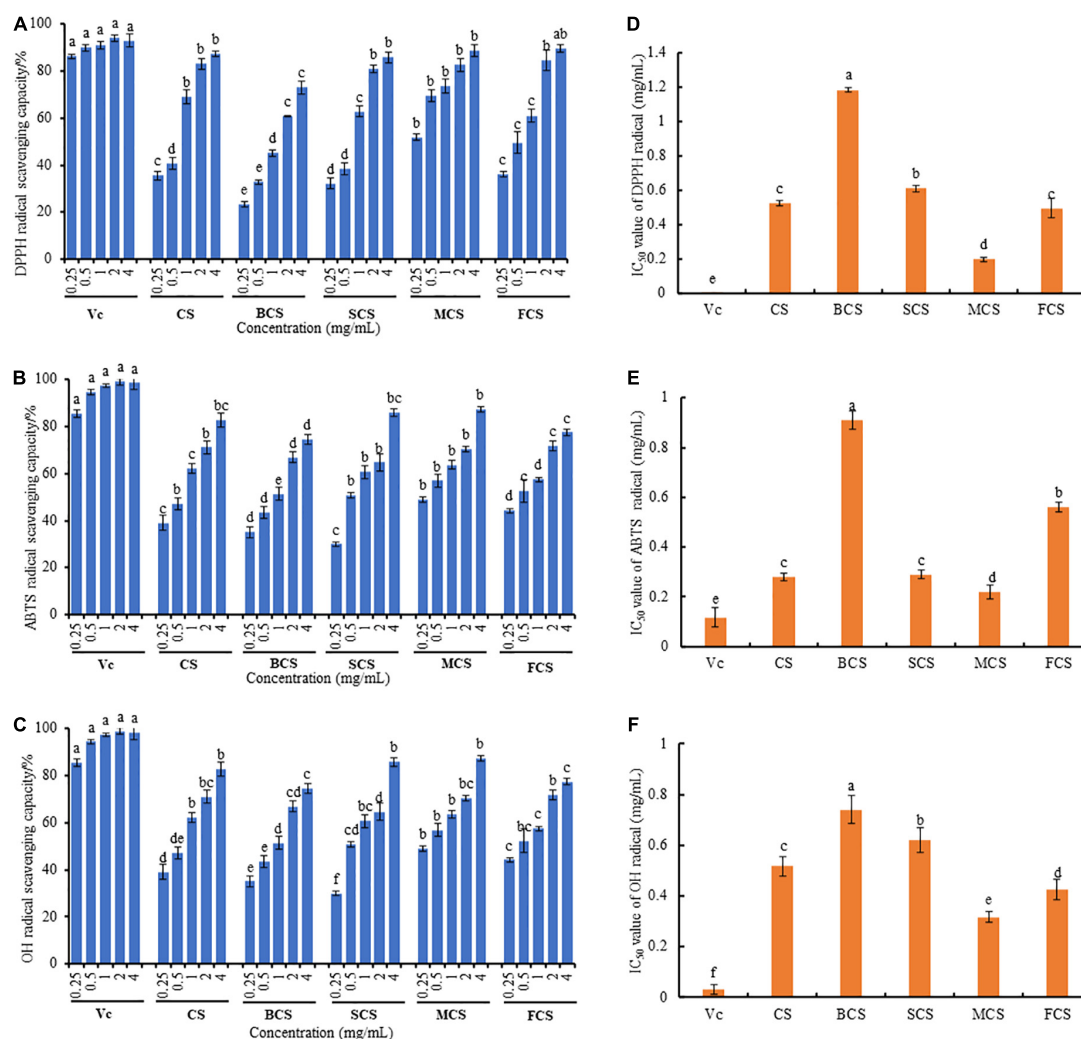


FIGURE 2

Effects of cooking methods on antioxidant activity of extracts from *C. squamulosa*. (A) DPPH radical scavenging activity. (B) ABTS radical scavenging activity. (C) OH radical scavenging activity. (D) IC<sub>50</sub> value of DPPH radical. (E) IC<sub>50</sub> value of ABTS radical. (F) IC<sub>50</sub> value of OH radical. CS, *C. squamulosa*; BCS, boiling-cooked *C. squamulosa*; SCS, steaming-cooked *C. squamulosa*; MCS, microwaving-cooked *C. squamulosa*; FCS, frying-cooked *C. squamulosa*. Each value represents the mean  $\pm$  SD ( $n = 3$ ) and different lowercase letters denote statistical significance ( $p < 0.05$ ).

found a positive correlation between bioactive compounds and antioxidant activity (48), therefore, after cooking, the enhanced antioxidant activity of *C. squamulosa* may be ascribed to the destruction of covalent bonds during heating, allowing cells to release more active ingredients (49).

## Conclusion

The effects of different cooking methods on the volatile flavor compounds and nutritional constituents, and antioxidant activities of *C. squamulosa* were investigated by boiling, steaming, microwaving, and frying. From the perspective of volatile compounds, after cooking treatment, the lipids of

*C. squamulosa* were lost to a significant extent, but new alcohol and acid compounds were produced, and the quantity and content of alcohols, aldehydes and ketones increased. Based on ROAV values and PCA, steaming and microwave cooking can improve the flavor of *C. squamulosa*. From a color difference and nutritional content perspective, each cooking treatment resulted in positive color changes, with microwave cooking closest to the color of raw samples. Among all samples, steamed and microwaved *C. squamulosa* had a higher nutrient content. An antioxidant capacity analysis found that microwave-cooked samples showed the highest antioxidant activity. Comprehensive analysis found that steaming and microwave cooking were more suitable for cooking *C. squamulosa*.

In the diet, the nutritional value of food is not only related to how it is cooked, but also related to the digestion and absorption of nutrients by the body. During digestion, the nutritional value contained in the food is transmitted to the parts needed by the body, providing energy for the human body and maintaining health. Exploring the effects of different cooking methods on the nutritional value and volatile flavor of food is crucial to basic research in the early stage. In the later stage, attention should also be paid to the degree of digestion and absorption of food nutrients in the human body after use of different cooking methods. Therefore, the further to explore the digestion and absorption of *C. squamulosa* by the human body during the digestion after use of different cooking methods, the samples should also be subjected to *in vitro* simulated digestion tests. Then, the effects of different cooking methods on the quality of *C. squamulosa* were comprehensively evaluated. This provides a theoretical basis for people to choose appropriate cooking methods and provides a reference for the cooking and processing of other edible fungi.

## Data availability statement

The original contributions presented in this study are included in the article/supplementary material, further inquiries can be directed to the corresponding authors.

## Author contributions

HY: conceptualization, methodology, formal analysis, data curation, and writing-original draft. ZL: data curation and software. LX: resources, methodology, investigation, and writing-review. MC: resources and funding acquisition. JM, CF, XG, and YC: resources, conceptualization, formal analysis, and

supervision. All authors contributed to the article and approved the submitted version.

## Funding

This study was financially supported by the Shanxi Provincial Basic Research and Development Project (202103021224127) and the Youth Project of Basic Research Program in Shanxi (20210302124071). This study was also funded by the Research Project Supported by Shanxi Scholarship Council of China (2022-096).

## Acknowledgments

The authors thank all the members of the research group for their cooperation in the laboratory.

## Conflict of interest

The authors declare that the research was conducted in the absence of any commercial or financial relationships that could be construed as a potential conflict of interest.

## Publisher's note

All claims expressed in this article are solely those of the authors and do not necessarily represent those of their affiliated organizations, or those of the publisher, the editors and the reviewers. Any product that may be evaluated in this article, or claim that may be made by its manufacturer, is not guaranteed or endorsed by the publisher.

## References

- Hu HZ. *Investigation on Edible and Medicinal Fungi and "Taimo" in Wutai Mountain*. Jilin: Jilin Agricultural Universal (2020). 2020.000309 doi: 10.27163/d.cnki.gjlnu
- Guo DD, Lei JY, He C, Peng ZJ, Liu RZ, Pan X, et al. In vitro digestion and fermentation by human fecal microbiota of polysaccharides from *Clitocybe squamulose*. *Int J Biol Macromol*. (2022) 208:343–55. doi: 10.1016/j.ijbiomac.2022.03.126
- Si J, Meng G, Wu Y, Ma HF, Cui BK, Dai YC. Medium composition optimization, structural characterization, and antioxidant activity of exopolysaccharides from the medicinal mushroom *Ganoderma lingzhi*. *Int J Biol Macromol*. (2019) 124:1186–96. doi: 10.1016/j.ijbiomac.2018.11.274
- Bach F, Zielinski AAF, Helm CV, Maciel GM, Pedro AC, Stafussa AP, et al. Bio Compounds of edible mushrooms: *in vitro* antioxidant and antimicrobial activities. *LWT*. (2019) 107:214–20. doi: 10.1016/j.lwt.2019.03.017
- Pathak MP, Pathak K, Saikia R, Gogoi U, Ahmad MZ, Patowary P, et al. Immunomodulatory effect of mushrooms and their bioactive compounds in cancer: a comprehensive review. *Biomed Pharmacother*. (2022) 149:112901. doi: 10.1016/j.biopha.2022.112901
- Sillapachaiyaporn C, Chuchawankul S, Nilkhet S, Mounkote N, Sarachana T, Ung AT, et al. Ergosterol isolated from cloud ear mushroom (*Auricularia polytricha*) attenuates bisphenol a-induced Bv2 microglial cell inflammation. *Food Res Int*. (2022) 157:111433. doi: 10.1016/j.foodres.2022.111433
- Yang Y, Lin L, Zhao M, Yang X. The hypoglycemic and hypolipemic potentials of *Moringa oleifera* leaf polysaccharide and polysaccharide-flavonoid complex. *Int J Biol Macromol*. (2022) 210:518–29. doi: 10.1016/j.ijbiomac.2022.04.206
- Reis FS, Martins A, Vasconcelos MH, Morales P, Ferreira ICFR. Functional foods based on extracts or compounds derived from mushrooms. *Trends Food Sci Technol*. (2017) 66:48–62. doi: 10.1016/j.tifs.2017.05.010
- CEFA. *Analysis of 2019 National Edible Fungi Statistical Survey*. Lianyungang: CEFA (2021). p. 104–10.
- Tan Y, Zeng NK, Xu B. Chemical profiles and health-promoting effects of porcini mushroom (*Boletus edulis*): a narrative review. *Food Chem*. (2022) 390:133199. doi: 10.1016/j.foodchem.2022.133199
- Jaworska G, Pogon K, Skrzypczak A, Bernas E. Composition and antioxidant properties of wild mushrooms *Boletus edulis* and *Xerocomus badius* prepared for

- consumption. *J Food Sci Technol.* (2015) 52:7944–53. doi: 10.1007/s13197-015-1933-x
12. Lozano-Castellon J, Rocchetti G, Vallverdu-Queralt A, Illan M, Torrado-Prat X, Lamuela-Raventos RM, et al. New vacuum cooking techniques with extra-virgin olive oil show a better phytochemical profile than traditional cooking methods: a foodomics study. *Food Chem.* (2021) 362:130194. doi: 10.1016/j.foodchem.2021.130194
13. da Silva FLF, de Lima JPS, Melo LS, da Silva YSM, Gouveia ST, Lopes GS, et al. Comparison between boiling and vacuum cooking (Sous-Vide) in the bioaccessibility of minerals in bovine liver samples. *Food Res Int.* (2017) 100:566–71. doi: 10.1016/j.foodres.2017.07.054
14. Cilla A, Bosch L, Barberá R, Alegria A. Effect of processing on the bioaccessibility of bioactive compounds – a review focusing on carotenoids, minerals, ascorbic acid, tocopherols and polyphenols. *J Food Compos Anal.* (2018) 68:3–15. doi: 10.1016/j.jfca.2017.01.009
15. Liu Y, Li Y, Ke Y, Li C, Zhang Z, Liu A, et al. Processing of four different cooking methods of *Oudemansiella radicata*: effects on *in vitro* bioaccessibility of nutrients and antioxidant activity. *Food Chem.* (2021) 337:128007. doi: 10.1016/j.foodchem.2020.128007
16. Mena García M, Paula VB, Olloqui ND, García DF, Combarros-Fuertes P, Estevinho LM, et al. Effect of different cooking methods on the total phenolic content, antioxidant activity and sensory properties of wild *Boletus edulis* mushroom. *Int J Gastron Food Sci.* (2021) 26:100416.
17. Selli S, Guclu G, Sevindik O, Kelebek H. Variations in the key aroma and phenolic compounds of champignon (*Agaricus bisporus*) and oyster (*Pleurotus ostreatus*) mushrooms after two cooking treatments as elucidated by GC–MS–O and LC–Dad–ESI–MS/MS. *Food Chem.* (2021) 354:129576. doi: 10.1016/j.foodchem.2021.129576
18. Ng ZX, Tan WC. Impact of optimised cooking on the antioxidant activity in edible mushrooms. *J Food Sci Technol.* (2017) 54:4100–11. doi: 10.1007/s13197-017-2885-0
19. Ng ZX, Rosman NF. *In vitro* digestion and domestic cooking improved the total antioxidant activity and carbohydrate-digestive enzymes inhibitory potential of selected edible mushrooms. *J Food Sci Technol.* (2019) 56:865–77. doi: 10.1007/s13197-018-3547-6
20. Wang SR, Chang MC, Li G, Meng JL, Feng CF, Xu LJ, et al. *The Key Technology of Shanxi Taimo Mushroom Resources Development*. Jinzhong: Shanxi Agricultural University (2021).
21. Guo DD, Lei JY, Xu LJ, Cheng YF, Feng CP, Meng JM, et al. Two novel polysaccharides from *Clitocybe squamulosa*: their isolation, structures, and bioactivities. *Front Nutr.* (2022) 9:934769. doi: 10.3389/fnut.2022.934769
22. Xun W, Wang GY, Zhang YJ, Liao GZ, Ge CR. Analysis of flavor-related compounds in four edible wild mushroom soups. *Microchem J.* (2020) 159:105548. doi: 10.1016/j.microc.2020.105548
23. Zhang H, Huang D, Pu D, Zhang Y, Chen H, Sun B, et al. Multivariate relationships among sensory attributes and volatile components in commercial dry porcini mushrooms (*Boletus edulis*). *Food Res Int.* (2020) 133:109112. doi: 10.1016/j.foodres.2020.109112
24. Kulapichitr F, Borompichaichartkul C, Fang M, Suppavorasatit I, Cadwallader KR. Effect of post-harvest drying process on chlorogenic acids, antioxidant activities and Cie-Lab Color of Thai Arabica green coffee beans. *Food Chem.* (2022) 366:130504. doi: 10.1016/j.foodchem.2021.130504
25. AOAC. *Association of Official Analytical Chemists: Official Methods of Analysis*. (Vol. 1). Washington DC: AOAC (1990). p. 69–90.
26. Motta C, Castanheira I, Gonzales GB, Delgado I, Torres D, Santos M, et al. Impact of cooking methods and malting on amino acids content in amaranth, buckwheat and Quinoa. *J Food Compos Anal.* (2019) 76:58–65. doi: 10.1016/j.jfca.2018.10.001
27. Deng LZ, Xiong CH, Pei YP, Zhu ZQ, Zheng X, Zhang Y, et al. Effects of various storage conditions on total phenolic, carotenoids, antioxidant capacity, and color of dried apricots. *Food Control.* (2022) 136:108846. doi: 10.1016/j.foodcont.2022.108846
28. Liu XM, Liu Y, Shan CH, Yang XQ, Zhang Q, Xu N, et al. Effects of five extraction methods on total content, composition, and stability of flavonoids in Jujube. *Food Chem X.* (2022) 14:100287. doi: 10.1016/j.fochx.2022.100287
29. Shraim AM, Ahmed TA, Rahman MM, Hijji YM. Determination of total flavonoid content by aluminum chloride assay: a critical evaluation. *LWT.* (2021) 150:111932. doi: 10.1016/j.lwt.2021.111932
30. Sharpe E, Farragher-Gnadt AP, Igbunugo M, Huber T, Michelotti JC, Milenkovic A, et al. Comparison of antioxidant activity and extraction techniques for commercially and laboratory prepared extracts from six mushroom species. *J Agr Food Res.* (2021) 4:100130. doi: 10.1016/j.jafr.2021.100130
31. Pan X, Xu L, Meng J, Chang M, Cheng Y, Geng X, et al. Ultrasound-assisted deep eutectic solvents extraction of polysaccharides from *Morchella importuna*: optimization, physicochemical properties, and bioactivities. *Front Nutr.* (2022) 9:912014. doi: 10.3389/fnut.2022.912014
32. Wei CK, Ni ZJ, Thakur K, Liao AM, Huang JH, Wei ZJ. Aromatic effects of immobilized enzymatic oxidation of chicken fat on flaxseed (*Linum usitatissimum* L.) derived maillard reaction products. *Food Chem.* (2020) 306:125560. doi: 10.1016/j.foodchem.2019.125560
33. Zhuang J, Xiao Q, Feng T, Huang Q, Ho CT, Song S. Comparative flavor profile analysis of four different varieties of boletus mushrooms by instrumental and sensory techniques. *Food Res Int.* (2020) 136:109485. doi: 10.1016/j.foodres.2020.109485
34. Dermiki M, Phanphensophon N, Mottram DS, Methven L. Contributions of non-volatile and volatile compounds to the umami taste and overall flavour of shiitake mushroom extracts and their application as flavour enhancers in cooked minced meat. *Food Chem.* (2013) 141:77–83. doi: 10.1016/j.foodchem.2013.03.018
35. Argyropoulos D, Khan MT, Müller J. Effect of air temperature and pre-treatment on color changes and texture of dried *Boletus edulis* mushroom. *Dry Technol.* (2011) 29:1890–900. doi: 10.1080/07373937.2011.594194
36. Shams R, Singh J, Dash KK, Dar AH. Comparative study of freeze drying and cabinet drying of button mushroom. *Appl Food Res.* (2022) 2:100084. doi: 10.1016/j.afres.2022.100084
37. Chatham LA, Howard JE, Juvik JA. A natural colorant system from corn: flavone-anthocyanin copigmentation for altered hues and improved shelf life. *Food Chem.* (2020) 310:125734. doi: 10.1016/j.foodchem.2019.125734
38. Chin L, Therdthai N, Ratphitagsanti W. Effect of conventional and microwave cooking conditions on quality and antioxidant activity of Chinese Kale (*Brassica Alboglabra*). *Appl Food Res.* (2022) 2:100079. doi: 10.1016/j.afres.2022.100079
39. Tang D, Wang R, He X, Chen X, Huo X, Lu X, et al. Comparison of the Edible quality of liquid egg with different cooking methods and their antioxidant activity after *in vitro* digestion. *Food Res Int.* (2021) 140:110013. doi: 10.1016/j.foodres.2020.110013
40. Banerjee S, Sahu CK. A short review on vacuum frying-a promising technology for healthier and better fried foods. *Int J Nutrit Health Sci.* (2017) 1:68–71.
41. Sa AGA, Pacheco MTB, Moreno YMF, Carciofi BAM. Cold-pressed sesame seed meal as a protein source: effect of processing on the protein digestibility, amino acid profile, and functional properties. *J Food Compos Anal.* (2022) 111:104634. doi: 10.1016/j.jfca.2022.104634
42. Mohanty B, Mahanty A, Ganguly S, Sankar TV, Chakraborty K, Rangasamy A, et al. Amino acid compositions of 27 food fishes and their importance in clinical nutrition. *J Amino Acids.* (2014) 2014:269797. doi: 10.1155/2014/269797
43. Sissons J, Davila M, Du X. Sautéing and roasting effect on free amino acid profiles in portobello and shiitake mushrooms, and the effect of mushroom-and cooking-related volatile aroma compounds on meaty flavor enhancement. *Int J Gastron Food Sci.* (2022) 28:100550. doi: 10.1016/j.ijgfs.2022.100550
44. Khatib RY, Arntfield SD, Nyachoti CM. Nutritional quality of legume seeds as affected by some physical treatments, part 1: protein quality evaluation. *LWT.* (2009) 42:1107–12. doi: 10.1016/j.lwt.2009.02.008
45. Lemos MA, Aliyu MM, Hungerford G. Influence of cooking on the levels of bioactive compounds in purple majesty potato observed via chemical and spectroscopic means. *Food Chem.* (2015) 173:462–7. doi: 10.1016/j.foodchem.2014.10.064
46. Mehmood A, Zeb A. Effects of different cooking techniques on bioactive contents of leafy vegetables. *Int J Gastron Food Sci.* (2020) 22:100246. doi: 10.1016/j.ijgfs.2020.100246
47. Wan FC, Feng CF, Luo KY, Cui WY, Xia ZH, Cheng AW. Effect of steam explosion on phenolics and antioxidant activity in plants: a review. *Trends Food Sci Tech.* (2022) 124:13–24. doi: 10.1016/j.tifs.2022.04.003
48. Skrovankova S, Sumczynski D, Mlcek J, Jurikova T, Sochor J. Bioactive compounds and antioxidant activity in different types of berries. *Int J Mol Sci.* (2015) 16:24673–706. doi: 10.3390/ijms161024673
49. Yao L, Fan L, Duan Z. Effect of different pretreatments followed by hot-air and far-infrared drying on the bioactive compounds, physicochemical property and microstructure of mango slices. *Food Chem.* (2020) 305:125477. doi: 10.1016/j.foodchem.2019.125477
50. Qiu D, Duan R, Wang Y, He Y, Li C, Shen X, et al. Effects of different drying temperatures on the profile and sources of flavor in semi-dried golden pompano (*Trachinotus ovatus*). *Food Chem.* (2023) 401:134112. doi: 10.1016/j.foodchem.2022.134112



## OPEN ACCESS

EDITED BY  
Baoguo Xu,  
Jiangsu University, China

REVIEWED BY  
Fang Liu,  
Northwest A&F University Apple  
Research Center, China  
Yue Zhang,  
China Agricultural University, China  
Liuping Fan,  
Jiangnan University, China  
Yuting Tian,  
Fujian Agriculture and Forestry  
University, China

\*CORRESPONDENCE  
Xu Duan  
duanxu\_dx@163.com  
Xiangyong Meng  
nelmeng@163.com

SPECIALTY SECTION  
This article was submitted to  
Nutrition and Food Science  
Technology,  
a section of the journal  
Frontiers in Nutrition

RECEIVED 06 September 2022  
ACCEPTED 24 October 2022  
PUBLISHED 09 November 2022

CITATION  
Ren A, Cao Z, Tang X, Duan Z, Duan X  
and Meng X (2022) Reduction of oil  
uptake in vacuum fried *Pleurotus  
eryngii* chips via ultrasound assisted  
pretreatment.  
*Front. Nutr.* 9:1037652.  
doi: 10.3389/fnut.2022.1037652

COPYRIGHT  
© 2022 Ren, Cao, Tang, Duan, Duan  
and Meng. This is an open-access  
article distributed under the terms of  
the [Creative Commons Attribution  
License \(CC BY\)](#). The use, distribution  
or reproduction in other forums is  
permitted, provided the original  
author(s) and the copyright owner(s)  
are credited and that the original  
publication in this journal is cited, in  
accordance with accepted academic  
practice. No use, distribution or  
reproduction is permitted which does  
not comply with these terms.

# Reduction of oil uptake in vacuum fried *Pleurotus eryngii* chips via ultrasound assisted pretreatment

Aiqing Ren<sup>1</sup>, Zhenzhen Cao<sup>1</sup>, Xiaoxian Tang<sup>1</sup>,  
Zhenhua Duan<sup>1</sup>, Xu Duan<sup>2\*</sup> and Xiangyong Meng<sup>3\*</sup>

<sup>1</sup>College of Food and Bioengineering, Hezhou University, Hezhou, China, <sup>2</sup>College of Food and Bioengineering, Henan University of Science and Technology, Luoyang, China, <sup>3</sup>College of Life Sciences, Anhui Normal University, Wuhu, China

The reduction of oil uptake in vacuum-fried *Pleurotus eryngii* chips by ultrasound assisted pretreatment was investigated regarding the pore structure changes. Pore structure of *P. eryngii* chips with four pretreatments, such as blanching, blanching + osmosis, blanching + ultrasound and blanching + ultrasound assisted osmosis was determined by mercury intrusion porosimetry (MIP) and scanning electron microscopy (SEM). In addition, the quality parameters of vacuum-fried *P. eryngii* chips such as hardness, rehydration ratio, reducing sugar, protein and oil content were also measured. The results showed that the oil absorption of vacuum fried *P. eryngii* chips was affected by the porous structure. The oil content of vacuum fried *P. eryngii* chips was significantly and positively correlated with the pores with diameters above 50, 5–50, and 0.5–5  $\mu\text{m}$  in the samples both before and after vacuum frying, while negatively correlated with the pores with diameters below 0.5  $\mu\text{m}$ . Ultrasound pretreatment changed the microporous structure of *P. eryngii* chips, effectively hindering the oil absorption of samples. In particular, ultrasound assisted osmosis pretreatment induced the formation of more micropores. It was concluded that blanching + ultrasound assisted osmosis pretreatment is a promising method to reduce oil absorption and improve the quality of vacuum fried foods.

## KEYWORDS

*Pleurotus eryngii*, ultrasound, vacuum frying, pore structure, oil uptake

## Introduction

*Pleurotus eryngii* is considered as a delicious and healthy food material, which is rich in protein, polysaccharides, essential amino acids, vitamins and other nutrients (1). Many studies have shown that it has a variety of biological activities such as anti-oxidation, anti-tumor, immune boosting, regulation of intestinal microorganisms and other health care functions (2, 3). However, *P. eryngii* has a moisture content of 89.8%,



and a high respiration rate and is rich in nutrients. Therefore, it is susceptible to spoilage due to the microbial reproduction. The short shelf-life of *P. eryngii* mushrooms hinders its exploitation. It is necessary to find a processing technology that can extend the shelf-life of mushroom and produce a snack food with a rich flavor and nutritional value.

Atmospheric frying involves the immersion of foods in edible oil at a temperature above the boiling point of water to make the surface temperature of food rapidly rise (4). Subsequently, a dry layer is quickly formed on the surface of the material, then the water vaporization layer gradually moved inward and finally the food is completely dried and cooked (5). As a consequence, water and other soluble materials are transferred from the food being fried as the oil penetrates the product, resulting in high levels of oil in the food. Furthermore, some adverse reaction products, such as acrylamide may be generated.

Finding a frying technology that could reduce energy consumption and oil uptake and decrease the formation of harmful substances in fried products has become a research hotspot. Some of the innovative frying technologies have emerged, such as pressure frying, microwave frying, or vacuum frying. Vacuum frying is a process carried out under atmospheric pressures (below 100 kPa) leading to decrease the boiling point of water, which makes it possible to considerably decrease the frying temperature (6). Due to the lower frying temperature, vacuum frying preserves the nutritional value and color of the fried product better and keeps the lower oil uptake compared to atmospheric frying. Another approach to reduce oil uptake is the use of different pretreatments prior to frying, such as coating (7), osmotic dehydration and preliminary drying. The reason for the reduction in oil absorption is thought to be related to the increased solids content of the raw material and changes in the microstructure of the material, which favors a reduction in the surface area of the sample in contact with the oil (8). However, it takes a long time for osmosis pretreatment, while ultrasound assisted osmosis pretreatment can effectively shorten the osmosis time and the subsequent drying time, and reduce the energy consumption.

In recent years, ultrasound has attracted widespread attention due to its numerous advantages over traditional methods. It has been widely used in the food processing, such as extraction (9), freezing (10), drying (11, 12), thawing (13), fermentation (14), enzymolysis of protein (15), modification of starch (16), inactivation of enzymes (17), as well as cleaning (18). As a non-thermal processing method, ultrasound pretreatment before frying can improve the crispness of fried food, reduce the loss of nutrients. Piyalungka et al. (19) reported that ultrasound-assisted osmosis pretreatment could improve the osmotic dehydration efficiency of maltodextrin-immersed pumpkin, it also improved the color, texture and carotenoid content of vacuum-fried pumpkin crisps, and reduced the oil content of the products. Although ultrasound pretreatment can reduce

the oil content of vacuum-fried crisps, the mechanism of the effect of ultrasound and ultrasound assisted osmosis on the oil absorption of vacuum-fried crisps was not clear (20, 21). Zhang et al. (22, 23) found that ultrasound pretreatment altered the pore structure of potato, which was thought to be related to the oil absorption of fried potato chips. The mechanism of the effect of ultrasound pretreatment on the oil absorption during vacuum frying might be revealed from the differences of the pore structure and distribution of the raw materials.

At present, there is little literature about the effect of ultrasound and ultrasound assisted osmosis on the absorption of oil in vacuum fried fruit and vegetable chips. The purpose of this study was to investigate the effect of the pore characteristics on the oil absorption of vacuum fried *P. eryngii* chips by analyzing the pore characteristics of ultrasound pretreatment and ultrasound assisted osmosis, which is expected to provide a valuable basic theory for controlling the oil content of vacuum fried fruit and vegetable chips.

## Materials and methods

### Pretreatments

Fresh *P. eryngii* without mildew and mechanical damage was selected, washed and cut into 40 mm × 12 mm × 6 mm slices. The chemical composition of fresh *P. eryngii* was determined as shown in Table 1, the indexes were indicated as dry basis. Before frying, the slices were processed using four pretreatments (19, 24, 25): (1) Blanching: the *P. eryngii* slices were blanched in the boiling water at 100°C for 3 min; (2) Blanching + osmosis: the *P. eryngii* slices were blanched in the boiling water at 100°C for 3 min, and then immersed in 40% maltodextrin solution at 30°C for 30 min (the ratio of material to liquid was 1:10); (3) Blanching + ultrasound: the *P. eryngii* slices were blanched in the boiling water at 100°C for 3 min, and then subjected to ultrasound pretreatment (JY92-IIN, Ningbo Xinzhi Biotechnology Co., Ltd., Ningbo, China. 25 kHz, 300 W, pulse time 10 s, interval 2 s) at 30°C for 30 min with samples immersing in distilled water (the ratio of material to liquid was 1:10); (4) Blanching + ultrasound assisted osmosis: after blanching in the boiling water at 100°C for 3 min, the *P. eryngii* slices were immersed in 40% maltodextrin solution (the ratio of material to liquid was 1:10) and subjected to the ultrasound pretreatment at 30°C (25 kHz, 300 W, pulse time 10 s, interval 2 s) for 30 min.

### Frying process

The frying process was performed in a vacuum fryer (VF-40C, Zhongshan Weijia Vacuum Machinery Factory, Zhongshan, China). About 40 L of soybean oil (Yihai Kerry,

TABLE 1 Quality analysis of *Pleurotus eryngii* chips.

	Hardness (g)	Rehydration ratio (g/g)	Reducing sugar (g/100 g)	Protein (g/100 g)	Moisture content (g/100 g)	Oil content (g/100 g)
Fresh	–	–	2.86 ± 0.22 <sup>a</sup>	19.35 ± 0.25 <sup>a</sup>	880.39 ± 17.65 <sup>a</sup>	2.53 ± 0.53 <sup>e</sup>
Blanching	–	–	2.05 ± 0.21 <sup>b</sup>	18.35 ± 0.18 <sup>b</sup>	857.19 ± 12.78 <sup>b</sup>	2.05 ± 0.62 <sup>e</sup>
Blanching + Osmosis	–	–	1.94 ± 0.19 <sup>b</sup>	17.85 ± 0.15 <sup>b</sup>	805.15 ± 15.21 <sup>c</sup>	2.35 ± 0.54 <sup>e</sup>
Blanching + Ultrasound	–	–	1.95 ± 0.25 <sup>b</sup>	17.92 ± 0.19 <sup>b</sup>	832.46 ± 21.47 <sup>b</sup>	2.13 ± 0.55 <sup>e</sup>
Blanching + Ultrasound + Osmosis	–	–	1.94 ± 0.18 <sup>b</sup>	18.05 ± 0.22 <sup>b</sup>	795.36 ± 19.45 <sup>c</sup>	2.16 ± 0.53 <sup>e</sup>
Blanching (Fried)	842.21 ± 8.51 <sup>a</sup>	2.99 ± 0.12 <sup>d</sup>	1.95 ± 0.18 <sup>b</sup>	18.19 ± 0.12 <sup>b</sup>	4.93 ± 0.48 <sup>d</sup>	20.54 ± 0.85 <sup>a</sup>
Blanching + Osmosis (Fried)	597.18 ± 3.44 <sup>b</sup>	3.08 ± 0.14 <sup>c</sup>	1.83 ± 0.25 <sup>b</sup>	17.83 ± 0.25 <sup>b</sup>	4.99 ± 0.45 <sup>d</sup>	12.15 ± 0.55 <sup>b</sup>
Blanching + Ultrasound (Fried)	484.68 ± 4.24 <sup>c</sup>	3.54 ± 0.09 <sup>b</sup>	1.88 ± 0.23 <sup>b</sup>	17.95 ± 0.24 <sup>b</sup>	4.55 ± 0.45 <sup>d</sup>	10.53 ± 0.61 <sup>c</sup>
Blanching + Ultrasound + Osmosis (Fried)	469.78 ± 1.53 <sup>d</sup>	3.63 ± 0.17 <sup>a</sup>	1.84 ± 0.27 <sup>b</sup>	17.85 ± 0.22 <sup>b</sup>	4.85 ± 0.49 <sup>d</sup>	8.32 ± 0.65 <sup>d</sup>

Values are displayed as mean ± standard deviation. Different letters in the same column indicate significant differences ( $P < 0.05$ ).

Shanghai, China) was preheated to  $90 \pm 1^\circ\text{C}$ , and then 300 g of *P. eryngii* slices were fried at 10 kPa for 14 min. After frying, deoiling was performed under vacuum conditions at the speed of 300 r/min for 3 min (25).

## Examination of pore properties

The fried samples were immersed in petroleum ether for 10 min to remove the oil, and then dehydrated by a vacuum freeze dryer (Labconco, Kansas City, MO, USA). The conditions of vacuum freeze drying were that the cold trap temperature of  $-80^\circ\text{C}$  and a pressure of 5 Pa. Pores with an equivalent diameters of 0.005–350  $\mu\text{m}$  were determined by mercury intrusion porosimetry (MIP) (Poremaster GT-60, Quantachrome Instruments, Boynton Beach, FL, USA) according to the method of Zhang et al. (23).

## Microstructure evaluation

The dehydrated *P. eryngii* chips were cut into slices with thickness of 2 mm and coated with a thin gold layer. The morphology was observed with a scanning electron microscopy (SEM, S4800, Japan, Hitachi High-Tech Group, Tokyo, Japan) under the condition of 5 kV acceleration voltage and vacuum (26).

## Examination of oil distribution

The oil distribution of fried *P. eryngii* chips was determined by LF-NMR (NMI20, Niumag Electronic Technology Co., Ltd., Shanghai, China) as described by Zhang et al. (23) with some modifications. One piece of *P. eryngii* chips was placed in a nuclear magnetic coil (diameter of 12 mm), and the temperature was maintained at  $32^\circ\text{C}$ . The signal of proton decay was measured using Carr-Purcell-Meiboom-Gill sequence with the

following parameters: the number of slices was 3, slice width was 5.0 mm, repetition time was 500 ms; time echo was 20 ms and number of averages was 4.

## Examination of moisture, protein and oil content

According to the methods described by AOAC with minor modifications (27), the content of moisture, protein and oil was measured and weight as g/g dry basis (db) of *P. eryngii* chips.

## Texture analysis

A texture analyzer (TAXT2i, Stable Micro System Co., Ltd., Surrey, UK) equipped with a cylindrical probe with a diameter of 2.5 mm was used to measure the texture of fried *P. eryngii* chips. The operating conditions were target distance of 5 mm, pre-test speed of 1 mm/s, test speed of 1 mm/s, post-test speed of 10 mm/s. The puncture test was repeated three times (28).

## Determination of rehydration rate

According to the methods described by Yang, Li and Hu (1) with modifications, about 5 g of the sample was accurately weighed and its weight ( $W_0$ ) was recorded. Then the sample was immersed in distilled water for 30 min at  $25^\circ\text{C}$  and weighed again ( $W_1$ ). The rehydration ratio  $RR = (W_1 - W_0)/W_0$ .

## Determination of reducing sugar content

According to the methods described by Li et al. (29), reducing sugar content was determined by colorimetric method of 3, 5-dinitrosalicylic acid.

## Determination of color

A chromaticity instrument (CR-400, Konica Minolta Sensing, Inc., Osaka, Japan) was used to determine the color of vacuum fried *P. eryngii* chips. The  $L^*$  represents brightness (0 = black, 100 = white),  $a^*$  represents red index ( $-a^*$  is green,  $+a^*$  is red),  $b^*$  represents yellow index ( $-b^*$  is blue,  $+b^*$  is yellow),  $\Delta E = [(L^* - L_o)^2 + (a^* - a_o)^2 + (b^* - b_o)^2]^{1/2}$ , where  $L_o$ ,  $a_o$ , and  $b_o$  referred to the color reading of fresh samples, which was used as control. Each sample was determined three times.

## Statistical analysis

All experiments and determinations were repeated three times. Then the results were analyzed by SPSS (SPSS

v19.0, IBM, Armonk, NY, USA) and Origin (Origin Lab Corporation, Northampton, MA, USA), and expressed as means  $\pm$  standard deviations. The significant difference among samples was performed statistically by one-way analysis of variance (ANOVA) with Duncan's  $t$ -test at a significance level of  $P < 0.05$ .

## Results and discussion

### Pore structure

The porosity of *P. eryngii* chips after different pretreatments and vacuum frying measured by MIP were shown in **Figure 1**. The results showed that the porosity of *P. eryngii* slices pretreated with blanching + ultrasound and

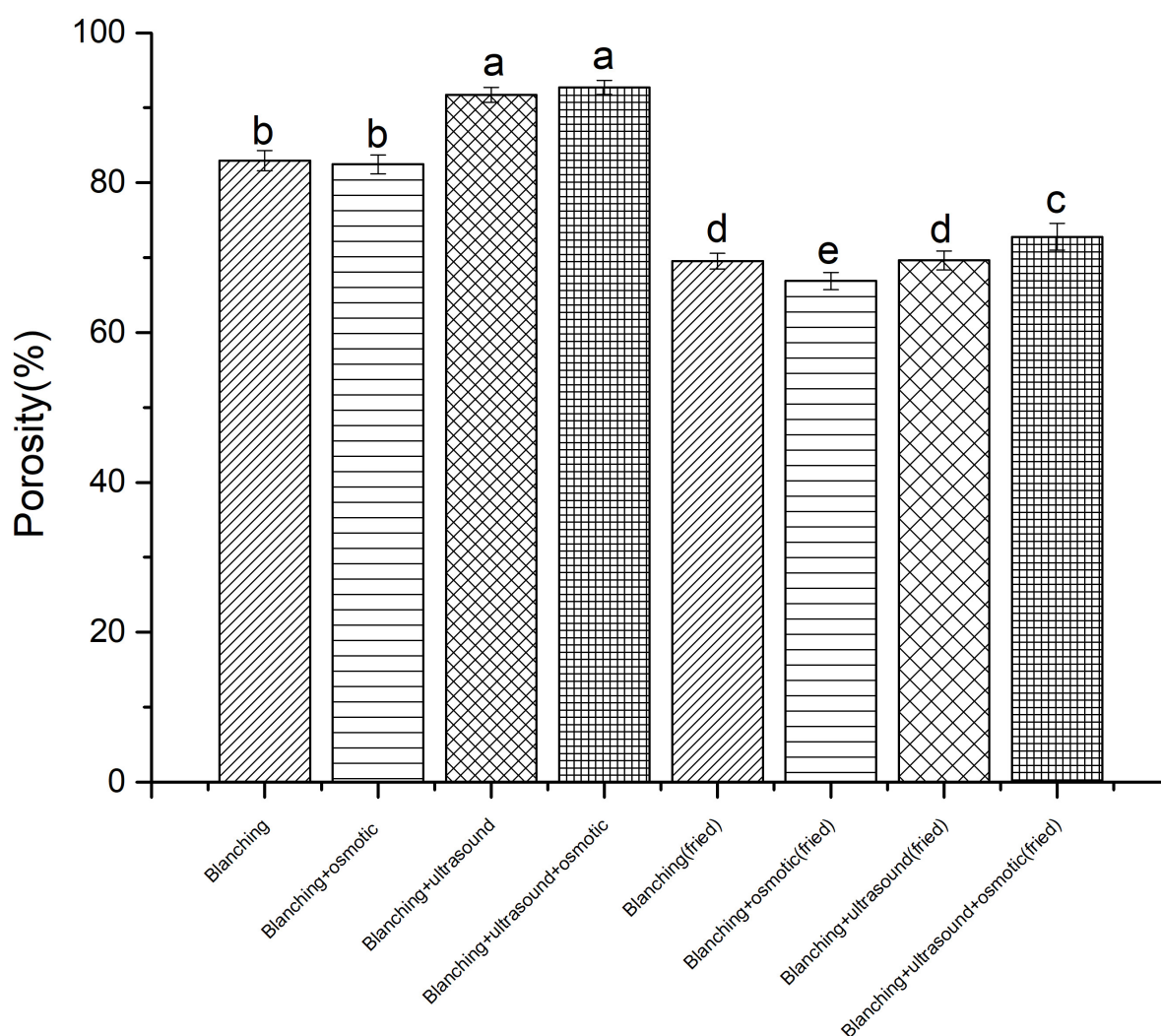


**FIGURE 1**  
Porosity of *Pleurotus eryngii* chips. Different superscript letters in the graph indicate significant differences between means ( $P < 0.05$ ).

blanching + ultrasound assisted osmosis were 91.7 and 92.7%, respectively, which were higher than that of samples treated with blanching (82.94%) and blanching + osmosis (82.44%). The porosity of *P. eryngii* slices with ultrasound pretreatment were greater than that of without ultrasound treated samples. This was consistent with the result reported by Zhang et al. (22), it may be due to the rapid alternating contraction and expansion of ultrasound waves resulting in the formation microchannels.

After vacuum frying, the porosity of *P. eryngii* chips decreased. The order of porosity for fried *P. eryngii* chips treated with different pretreatments was as follows: blanching + ultrasound + osmosis (72.67%) > blanching + ultrasound (69.63%) > blanching (69.52%) > blanching + osmosis (66.88%). There were many studies on the change in porosity of foods during frying. It was reported that the porosity of potato increased after frying (30). The increase in porosity was probably attributed to the disruption of pore structure and the expansion of vapors (31). The different findings in porosity were probably due to that soxhlet extraction and vacuum freeze-drying methods were carried out to remove the oil and water of *P. eryngii* chips before the determination of porosity by mercury intrusion method, resulting in larger porosity because of high moisture content of *P. eryngii* chips before frying. Moreover, Kassama et al. reported the cumulative pore volume and the porosity of chicken meat decreased in 360 s of frying (32, 33). Apart from that, the pore microstructure of vacuum fried and atmospheric fried products was different (34).

The pore structure of the *P. eryngii* chips treated by different pretreatments was determined by MIP as shown in Figure 2. According to the pore size distribution characteristics, the pore size of *P. slices* could be divided into four regions: above 50, 5–50, 0.5–5  $\mu\text{m}$  and below 0.5  $\mu\text{m}$ . The pore size distribution of *P. eryngii* slices and vacuum-fried *P. eryngii* chips showed a single peak at 5–50  $\mu\text{m}$ , indicating that the pore size distribution of the samples was relatively uniform. The most probable pore diameter of *P. eryngii* slices was 10  $\mu\text{m}$  before frying, but it increased to 20–30  $\mu\text{m}$  after vacuum frying. Zhang et al. also found that the most probable pore diameter of potato chips was 10  $\mu\text{m}$ , and it increased to 50  $\mu\text{m}$  after atmospheric frying (23). The main distribution area of the pore diameter of vacuum fried samples in this study was different from that of atmospheric fried potato chips. Liu et al. (35) found that more than 90% of potato chips had pore size distributions in the range of 10–250  $\mu\text{m}$ . However, Yang et al. (36) reported that the pore size distribution of three types of potato chips, i.e., flat potato chips, batch cooked potato chips, and ridged potato chips, was mainly in 300–800  $\mu\text{m}$ , which differed from the experimental results of Liu et al. (35). Furthermore, the pores volume and pore distribution of the three potato chips was also different. Different frying methods, frying time and material structure of fried samples resulted in various pore distribution (23). The difference in pore size distribution between *P. eryngii*

chips in this experiment and the fried potato chips reported in references might be caused by different raw materials or differences between vacuum frying process and atmospheric pressure frying.

Figure 3 showed the total pore number (volume) distribution of *P. eryngii* slices. Before vacuum frying, the total pore volume and pore volumes with a diameter of 5–50, 0.5–5  $\mu\text{m}$  and above 50  $\mu\text{m}$  of *P. eryngii* slices pretreated with different methods showed the same trend and followed the following order: blanching > blanching + osmosis > blanching + ultrasound > blanching + ultrasound assisted osmosis. However, the pore volume with a diameter below 0.5  $\mu\text{m}$  showed an opposite trend. It was speculated that the immersion pretreatment led to volume shrinkage due to sample dehydration, and the penetration of maltodextrin penetrated into the material to occupy part of the space volume. Due to the cavitation effect of ultrasound pretreatment, the macropores of the sample shrunk and the number of small pores increased. Zhang et al. found that the microstructure of potato chips changed after ultrasound pretreatment, the pores with a diameter of 0.4–3  $\mu\text{m}$  increased slightly, while the pores with diameters of 11–300  $\mu\text{m}$  decreased (22). For samples subjected to different pretreatments followed by vacuum frying, the total pore volume, pore volumes with a diameter of 5–50  $\mu\text{m}$  and 0.5–5  $\mu\text{m}$  decreased, while the pore volume with a diameter above 50  $\mu\text{m}$  did not change significantly, but the pore volume for diameters below 0.5  $\mu\text{m}$  increased. The results are not the same as those of atmospheric fried potato chips (22).

Figures 2, 3 showed that the pore diameter of *P. eryngii* was mainly distributed in the range of 5–50  $\mu\text{m}$ , it was more appropriate to observe using SEM with a magnification of 5,000 times. As shown in Figure 4, the pore structure of *P. eryngii* chips with different pretreatments was in the following order from loose to tight: blanching, blanching + osmosis, blanching + ultrasound, blanching + ultrasound assisted osmosis, which was consistent with the results shown in Figures 2, 3. After vacuum frying (A2–D2), the number of pores in the four different pretreated *P. eryngii* chips was further significantly reduced compared to that before frying (A1–D1). Changes in pores with a diameter less than 0.5  $\mu\text{m}$  were difficult to observe by SEM. Because osmosis causes pore shrinkage through osmotic dehydration and solute diffusion, Wang et al. (37) reported that osmotic dehydration could shrink the cell structure of yam slices, thereby reducing their porosity. Ultrasound could cause cell fragmentation under the effect of shearing effect, cavitation effect and collision effect, which may lead to the contraction of macropores and a reduction in the number of pores. Compared with ultrasound pretreatment, the structure of *P. eryngii* slices treated by ultrasound assisted osmosis were more compact with fewer pores. Piyalungka et al. (19) observed that both osmosis and ultrasound assisted osmosis reduced the oil content of vacuum fried pumpkin slices. SEM

showed that the blanching pretreatment samples had largest and most pores, while the osmosis group had fewer pores; in addition, the ultrasound assisted osmosis pretreatment samples had the least amount of large pores but most small pores. These findings were consistent with the effect of pretreatment on the pore structure of *P. eryngii* chips in this experiment. The quantitative data of pore characteristics measured by MIP were further qualitatively verified to a certain extent by SEM analysis of *P. eryngii* chips.

The reduction in pore number of *P. eryngii* chips after vacuum frying was inconsistent with the results of studies on potato slices subjected to atmospheric pressure frying (23, 26). Llorca et al. (38) investigated the effect of frying on the microstructure of frozen squid rings. The results revealed that the fibers of squid muscle tissue became closer after frying. During the frying process, water vaporized at high temperature, and migrated from the center of the sample to the outer layer, resulting in the changes of microstructure and formation of microchannels during the frying process. Pore characteristics are closely related to raw material composition, processing

methods and other factors. It may also be due to the different structures of raw materials. For example, the structure of *P. eryngii* is spongy, while the structure of potato chips is relatively close.

## Quality analysis of vacuum fried *Pleurotus eryngii* chips

To compare the effects of different pretreatments on the quality of vacuum-fried *P. eryngii* chips, the physicochemical properties such as hardness, rehydration ratio, contents of reducing sugar and protein were investigated. As shown in Table 1, the contents of reducing sugar, protein, moisture and fat for fresh *P. eryngii* were consistent with previous study (1, 39). Vacuum frying led to a decrease in the contents of reducing sugar, protein and moisture and an increase in fat content, which was attributed to the loss of water – soluble during blanching process and fat-soluble nutrients during the vacuum frying process. This result was confirmed by Lu et al., who found that there existed many nutrients,

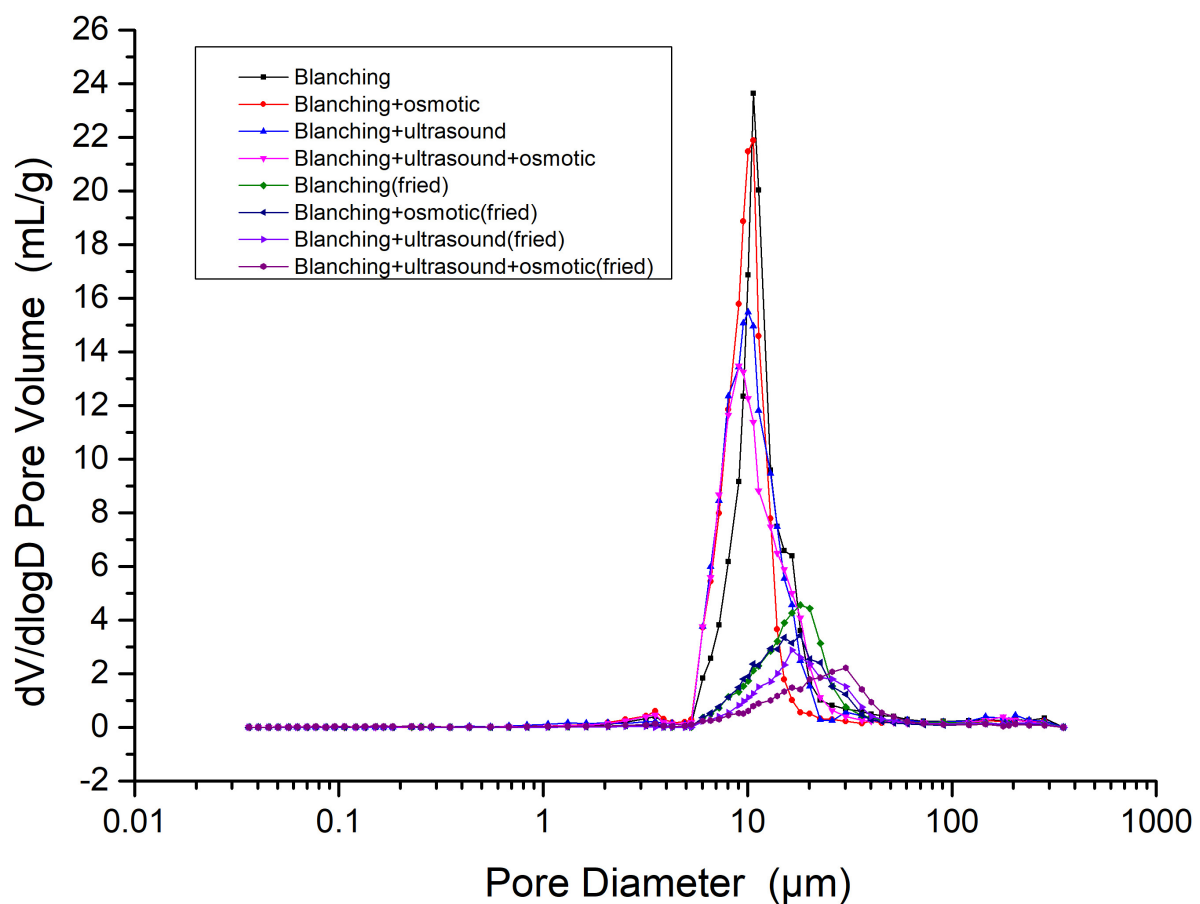


FIGURE 2  
Pore size distribution of *Pleurotus eryngii* chips.



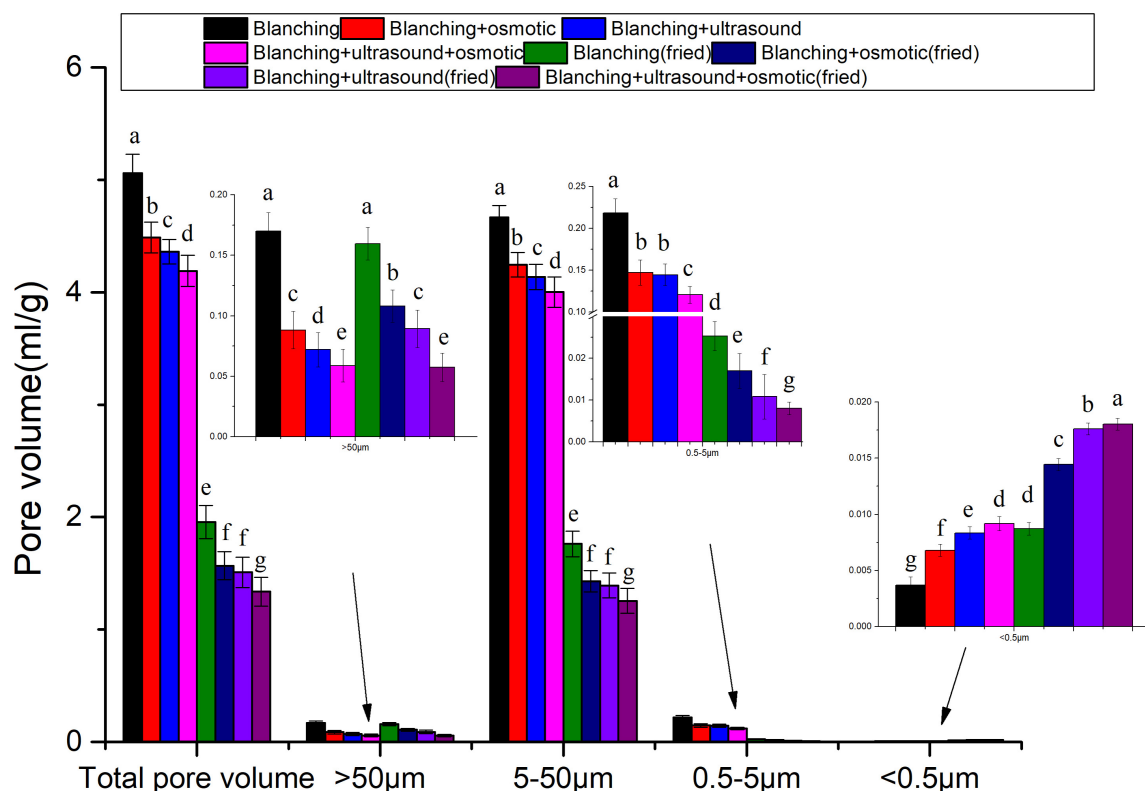


FIGURE 3

Pore volume distribution of *Pleurotus eryngii* chips. Different superscript letters in the graph indicate significant differences between means ( $P < 0.05$ ).

such as polysaccharides, soluble proteins, and soluble solids in the blanching water of *P. eryngii* (40). Furthermore, vacuum frying process resulted in increased oil content and loss of fat-soluble nutrients in samples (41). There were no significant differences in reducing sugar, protein and moisture contents of vacuum fried *P. eryngii* chips with different pretreatments. Hardness could be used to measure the crispness of *P. eryngii* chips, the lower hardness indicated the higher crispness (42), therefore, the crispness of different pretreatments from high to low was blanching + ultrasound assisted osmosis > blanching + ultrasound > blanching + osmosis > blanching, this may be due to immersion of maltodextrin increase the crispness of the *P. eryngii* chips, and the change of structure caused of samples by ultrasonic pretreatment also increased the crispness of the *P. eryngii* chips. The results of rehydration rate were consistent with the crispness, while opposite with oil content. This may be due to ultrasound changed the intercellular space of *P. eryngii* chips, and microporous pores was formed (20), which caused the increased rehydration rate of *P. eryngii* chips. The reduction of oil content was in agreement with what was obtained by obvious research (24). The mechanism of ultrasonic assisted osmosis reduction in oil absorption was due to ultrasound pretreatment enhanced the

movement of moisture within the structure of samples during vacuum frying. This created high vapour pressure within the structure of samples which then lowered the absorption of oil during frying (24). Moreover, when the chips were deoiled, changes in organizational structure facilitate the discharge of oil, thereby reducing the oil content of the chips (20).

The color values of fresh and vacuum fried *P. eryngii* chips with different pretreatments were shown in Table 2. Except blanching + ultrasound assisted osmosis, all vacuum fried samples exhibited lower lightness ( $L^*$  value) compared with fresh *P. eryngii*, while there were no significant difference about redness ( $a^*$  value) and yellowness ( $b^*$  value). Generally, the smaller the total color difference ( $\Delta E$ ), the closer the color to the fresh sample. As expected, the  $L^*$  values closer to the fresh sample and lower  $\Delta E$  values were found in blanching + ultrasound assisted osmosis and blanching + ultrasound samples (Table 2), indicating that the color parameters of these pretreatments were closer to those of fresh sample. This may be due to the fact that ultrasonic pretreatment destroyed the cell structure, which led to the outflow of polyphenols, preventing non-enzymatic browning reactions (including Maillard reaction, caramelization and chemical oxidation), thereby reducing color deterioration (20).

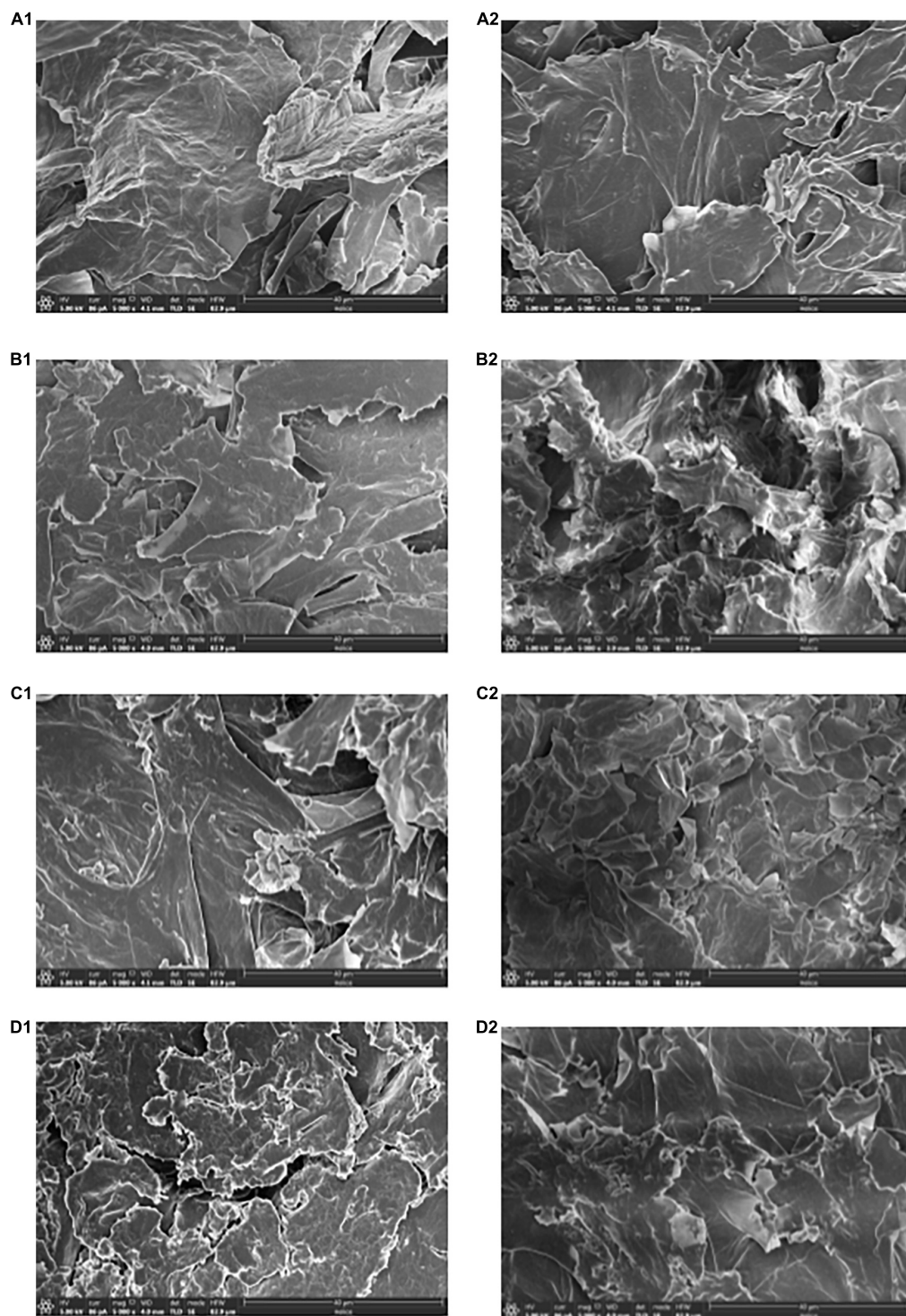


FIGURE 4

SEM images of *Pleurotus eryngii* chips before frying (A1–D1) and after frying (A2–D2): (A) Blanching; (B) Blanching + osmosis; (C) Blanching + ultrasound; (D) Blanching + ultrasound + osmosis.

Overall, the *P. eryngii* chips treated by blanching + ultrasound assisted osmosis showed the best quality in terms of crispness, rehydration rate, oil content and

color. Ultrasound assisted osmosis could be used to produce high-quality vacuum fried *P. eryngii* chips with outstanding advantages in terms of controlling oil content.

TABLE 2 The color analysis of *Pleurotus eryngii* chips.

	$L^*$	$a^*$	$b^*$	$\Delta E$
Fresh	$76.27 \pm 1.25^b$	$2.03 \pm 0.25^a$	$21.11 \pm 1.02^a$	
Blanching (Fried)	$70.23 \pm 1.38^d$	$2.28 \pm 0.22^a$	$20.85 \pm 0.95^a$	$6.05 \pm 0.85^a$
Blanching + Osmosis (Fried)	$72.25 \pm 1.72^d$	$2.15 \pm 0.25^a$	$19.25 \pm 1.14^a$	$4.43 \pm 0.55^b$
Blanching + Ultrasound (Fried)	$75.55 \pm 1.45^c$	$2.06 \pm 0.23^a$	$19.62 \pm 1.26^a$	$1.66 \pm 0.53^c$
Blanching + Ultrasound + Osmosis (Fried)	$78.17 \pm 1.32^a$	$2.15 \pm 0.21^a$	$20.5 \pm 0.95^a$	$1.99 \pm 0.42^c$

Values are displayed as mean  $\pm$  standard deviation. Different letters in the same column indicate significant differences ( $P < 0.05$ ).

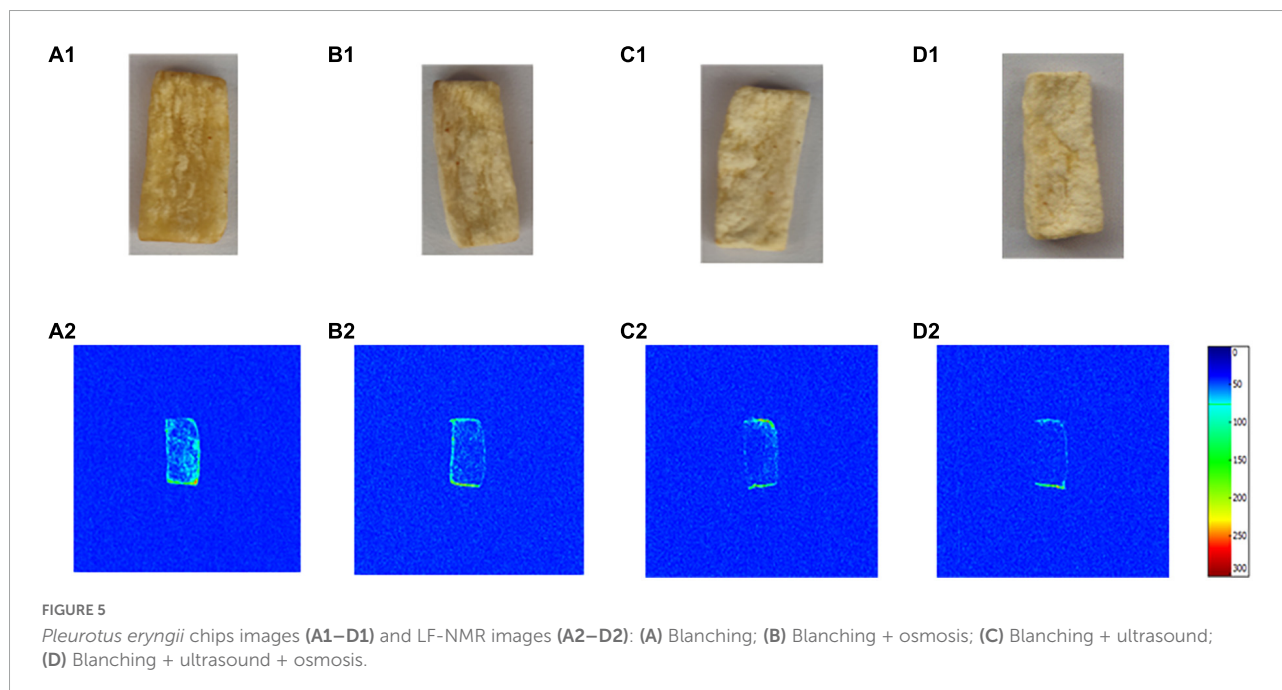


Figure 5 A1–D1 showed the product picture of vacuum fried *P. eryngii* chips with different pretreatments obtained by a digital camera, and A2–D2 showed the pseudocolor images of *P. eryngii* chips with different pretreatments obtained by LF-NMR imaging. LF-NMR images can present visual information on the distribution of the oil. The color difference indicated the intensity of the signal in the LF-NMR image, which was proportional to the hydrogen proton density (43). The color bars in Figure 5 from blue to red represented the increase of signal density. It could be observed that there was a significant difference in signal intensity among samples with different pretreatments. The oil content in the samples gradually decreased from A to D (Figure 5). The results were consistent with the oil content of samples in Table 1. Meanwhile, A2–D2 in Figure 5 show that the signal at the edge of *P. eryngii* chips was stronger than that of other areas, indicating the oil content in the edge area of the vacuum fried sample was higher than in the other areas. It was similar to the findings reported by Isik et al. and Wang et al. (44, 45). It was speculated that the explanation for the variation in oil distribution was that, during the vacuum frying process, the oil was directly in contact with the edge

areas, where it first adsorbed before gradually penetrating into the central of the sample. In addition, a large number of pores and cracks were formed on the surface of the samples due to the evaporation of water. They were not only the channels for water evaporation, but also for the penetration of oil into the interior of the sample. Furthermore, surface roughness played a crucial role in the permeability of oil (23).

## Relationship between pore structure and oil content

The difference in oil content of vacuum fried *P. eryngii* chips with four pretreatment as presented in Table 1 and Figure 5 may be caused by the different pore characteristic. Pearson correlation between oil content and pore size distribution of vacuum fried *P. eryngii* chips was investigated and results were shown in Table 3. The oil content of vacuum fried *P. eryngii* chips was significantly and positively correlated with the pores with diameters in the range  $>50$ ,  $5\text{--}50$ , and  $0.5\text{--}5\text{ }\mu\text{m}$  of the samples both before and after vacuum frying, while the

**TABLE 3** Numerical values of Pearson's correlation coefficients between oil contents and pore structure.

Pore structure		Pearson correlation coefficient	Significance difference
		<i>R</i>	<i>p</i>
Before frying	Pore diameter >50	0.9977	0.0023
	( $\mu\text{m}$ ) 5–50	0.9984	0.0016
	0.5–5	0.9952	0.0048
	<0.5	−0.9885	0.0116
After frying	Pore diameter >50	0.9777	0.0223
	( $\mu\text{m}$ ) 5–50	0.9957	0.0043
	0.5–5	0.9718	0.0282
	<0.5	−0.9823	0.0177

oil content showed a negative correlation with the pores with diameters below 0.5  $\mu\text{m}$ . Vauvre et al. (46) considered that the more pores with pore size of 10–200  $\mu\text{m}$  resulted in the higher oil permeability. Zhang et al. (23) believed that oil content was significantly positively correlated with pores with diameters of 100–200 and 10–100  $\mu\text{m}$ , and negatively correlated with pores with diameters of 0.3–10  $\mu\text{m}$ . Dueik et al. also believed that oil may not penetrate into micropores (<1.25 nm) (34). These conclusions were consistent with this experiment.

In the process of vacuum frying, water escapes from the surface of the samples and vaporizes violently to water vapor, thus pores are formed. The heated oil then penetrates into the samples through the pores. Heated oil is adsorbed on the surface of the samples and then penetrates inward through the pores, so oil absorption was related to pore structure (34). The oil content of the product was significantly negatively correlated with the pores with diameters below 0.5  $\mu\text{m}$ . It was attributed that some of the pores were not connected to the surface or a possible force prevented oil to migrate deeper into products (22). Besides, the effects of pore on oil absorption differ from pore size, more amount of the pores with diameters above 0.5  $\mu\text{m}$  led to more oil penetration. The increase in the number of pores with bigger diameters created less tortuous channels for oil penetration (47). In summary, ultrasound assisted osmosis pretreatment induced the formation of less macropores and more micropores than the other pretreatments, which prevented oil penetrates into the samples.

## Conclusion

The oil absorption of vacuum fried *P. eryngii* chips was affected by the porous structure. The oil content of vacuum fried *P. eryngii* chips was significantly and positively correlated with the pores with diameters above 50, 5–50, and 0.5–5  $\mu\text{m}$

in the samples both before and after vacuum frying, while negatively correlated with the pores with diameters below 0.5  $\mu\text{m}$ . Ultrasound pretreatment changed the microporous structure of *P. eryngii* chips, effectively hindering the oil absorption of samples. In particular, ultrasound assisted osmosis pretreatment induced the formation of more micropores. In summary, this manuscript revealed that the improvement of quality and the reduction of oil absorption of fried *P. eryngii* chips could be achieved by ultrasound assisted osmosis pretreatment before frying.

## Data availability statement

The raw data supporting the conclusions of this article will be made available by the authors, without undue reservation.

## Author contributions

XD and XM: conceptualization. AR, ZC, and XT: methodology. ZD: investigation. AR and XT: software. XD, XM, and AR: data curation. AR: writing – original draft preparation. AR and ZC: writing – review and editing. ZD, XM, and XD: supervision. XD, AR, and XT: funding acquisition. All authors contributed to the article and approved the submitted manuscript.

## Funding

This research was financially supported by the National Natural Science Foundation of China Regional Fund Project (Nos. 32160573 and 32160575).

## Conflict of interest

The authors declare that the research was conducted in the absence of any commercial or financial relationships that could be construed as a potential conflict of interest.

## Publisher's note

All claims expressed in this article are solely those of the authors and do not necessarily represent those of their affiliated organizations, or those of the publisher, the editors and the reviewers. Any product that may be evaluated in this article, or claim that may be made by its manufacturer, is not guaranteed or endorsed by the publisher.



## References

- Yang R, Li Q, Hu Q. Physicochemical properties, microstructures, nutritional components, and free amino acids of *Pleurotus eryngii* as affected by different drying methods. *Sci Rep.* (2020). 10:121. doi: 10.1038/s41598-019-56901-1
- Zhou F, Peng Q, Wang M, Liu N, Dinh QT, Zhai H, et al. Influence of processing methods and exogenous selenium species on the content and in vitro bioaccessibility of selenium in *Pleurotus eryngii*. *Food Chem.* (2020) 338:127661. doi: 10.1016/j.foodchem.2020.127661
- Nakahara D, Nan C, Mori K, Hanayama M, Kikuchi H, Hirai S, et al. Effect of mushroom polysaccharides from *Pleurotus eryngii* on obesity and gut microbiota in mice fed a high-fat diet. *Eur J Nutr.* (2020) 59:3231–44. doi: 10.1007/s00394-019-02162-7
- Asokapandian S, Swamy GJ, Hajjil H. Deep fat frying of foods: a critical review on process and product parameters. *Crit Rev Food Sci Nutr.* (2020) 60:3400–13. doi: 10.1080/10408398.2019.1688761
- Xu ZH, Leong SY, Farid M, Silcock P, Bremer P, Oey I. Understanding the frying process of plant-based foods pretreated with pulsed electric fields using frying models. *Foods.* (2020) 9:949. doi: 10.3390/foods9070949
- Moreira RG. Vacuum frying versus conventional frying – an overview. *Eur J Lipid Sci Technol.* (2014) 116:723–34. doi: 10.1002/ejlt.201300272
- Trujillo-Agudelo S, Osorio A, Gomez F, Contreras-Calderon J, Mesias-Garcia M, Delgado-Andrade C, et al. Evaluation of the application of an edible coating and different frying temperatures on acrylamide and fat content in potato chips. *J Food Process Eng.* (2020) 43:e13198. doi: 10.1111/jfpe.13198
- Rastogi NK, Raghavarao K, Niranjana K, Knorr D. Recent developments in osmotic dehydration: methods to enhance mass transfer. *Trends Food Sci Technol.* (2002) 13:48–59. doi: 10.1016/s0924-2244(02)00032-8
- Xu B, Feng M, Tiliwa ES, Yan W, Wei B, Zhou C, et al. Multi-frequency power ultrasound green extraction of polyphenols from Pingyin rose: optimization using the response surface methodology and exploration of the underlying mechanism. *LWT.* (2022) 156:113037.
- Xu B, Azam RSM, Wang B, Zhang M, Bhandari B. Effect of infused CO<sub>2</sub> in a model solid food on the ice nucleation during ultrasound-assisted immersion freezing. *Int J Refrig.* (2019) 108:53–9. doi: 10.1016/j.ijrefrig.2019.09.005
- Xu B, Chen J, Sylvain Tiliwa E, Yan W, Roknul Azam SM, Yuan J, et al. Effect of multi-mode dual-frequency ultrasound pretreatment on the vacuum freeze-drying process and quality attributes of the strawberry slices. *Ultrason Sonochem.* (2021) 78:105714.
- Xu B, Sylvain Tiliwa E, Yan W, Roknul Azam SM, Wei B, Zhou C, et al. Recent development in high quality drying of fruits and vegetables assisted by ultrasound: a review. *Food Res Int.* (2022) 152:110744.
- Xu, B, Chen J, Yuan J, Azam SM, Zhang M. Effect of different thawing methods on the efficiency and quality attributes of frozen red radish. *J Sci Food Agric.* (2020) 101:3237–45. doi: 10.1002/jsfa.10953
- Gao X, Liu E, Zhang J, Yang M, Chen S, Liu Z, et al. Effects of sonication during moromi fermentation on antioxidant activities of compounds in raw soy sauce. *LWT.* (2019) 116:108605. doi: 10.1016/j.lwt.2019.108605
- Xu B, Azam SMR, Feng M, Wu B, Yan W, Zhou C, et al. Application of multi-frequency power ultrasound in selected food processing using large-scale reactors: a review. *Ultrason Sonochem.* (2021) 81:105855.
- Xu B, Ren A, Chen J, Li H, Wei B, Wang J, et al. Effect of multi-mode dual-frequency ultrasound irradiation on the degradation of waxy corn starch in a gelatinized state. *Food Hydrocolloids.* (2021) 113:106440. doi: 10.1016/j.foodhyd.2020.106440
- Xu B, Chen J, Chitrakar B, Li H, Wang J, Wei B, et al. Effects of flat sweep frequency and pulsed ultrasound on the activity, conformation and microstructure of mushroom polyphenol oxidase. *Ultrason Sonochem.* (2022) 82:105908.
- Roknul Azam SM, Ma H, Xu B, Devi S, Stanley SL, Bakar Siddique MA, et al. Multi-frequency multi-mode ultrasound treatment for removing pesticides from lettuce (*Lactuca sativa* L.) and effects on product quality. *LWT.* (2021) 143:111147. doi: 10.1016/j.lwt.2021.111147
- Piyalungka P, Sadiq MB, Assavarachan R, Nguyen LT. Effects of osmotic pretreatment and frying conditions on quality and storage stability of vacuum-fried pumpkin chips. *Int J Food Sci Technol.* (2019) 54:2963–72. doi: 10.1111/ijfs.14209
- Shen X, Zhang M, Bhandari B, Guo ZM. Effect of ultrasound dielectric pretreatment on the oxidation resistance of vacuum-fried apple chips. *J Sci Food Agric.* (2018) 98:4436–44. doi: 10.1002/jsfa.8966
- Qiu LQ, Zhang M, Wang YC, Bhandari B. Effects of ultrasound pretreatments on the quality of fried sweet potato (*Ipomea batatas*) chips during microwave-assisted vacuum frying. *J Food Process Eng.* (2018) 41:e12879. doi: 10.1111/jfpe.12879
- Zhang J, Yu PB, Fan LP, Sun Y. Effects of ultrasound treatment on the starch properties and oil absorption of potato chips. *Ultrason Sonochem.* (2021) 70:105347. doi: 10.1016/j.ultsonch.2020.105347
- Zhang J, Liu Y, Fan LP. Effect of pore characteristics on oil absorption behavior during frying of potato chips. *Innov Food Sci Emerg Technol.* (2020) 66:102508. doi: 10.1016/j.ifset.2020.102508
- Oladejo AO, Ma H, Qu W, Zhou C, Wu B, Yang X, et al. Effects of ultrasound pretreatments on the kinetics of moisture loss and oil uptake during deep fat frying of sweet potato (*Ipomea batatas*). *Innov Food Sci Emerg Technol.* (2017) 43:7–17. doi: 10.1016/j.ifset.2017.07.019
- Ren AQ, Pan SY, Li WR, Chen GB, Duan X. Effect of various pretreatments on quality attributes of Vacuum-Fried shiitake mushroom chips. *J Food Qual.* (2018) 2018:4510126. doi: 10.1155/2018/4510126
- Yang D, Wu GC, Li PY, Zhang H, Qi XG. Comparative analysis of the oil absorption behavior and microstructural changes of fresh and pre-frozen potato strips during frying via MRI, SEM, and XRD. *Food Res Int.* (2019) 122:295–302. doi: 10.1016/j.foodres.2019.04.024
- The Association of Official Analytical Chemists [AOAC]. *Official Methods of Analysis of AOAC International*. Washington, DC: Association of Official Analysis Chemists International (2000). doi: 10.3109/15563657608988149
- Maity T, Bawa AS, Raju PS. Effect of vacuum frying on changes in quality attributes of jackfruit (*Artocarpus heterophyllus*) bulb slices. *Int J Food Sci.* (2014) 2014:752047. doi: 10.1155/2014/752047
- Li WQ, Hu QP, Xu JG. Changes in physicochemical characteristics and free amino acids of hawthorn (*Crataegus pinnatifida*) fruits during maturation. *Food Chem.* (2015) 175:50–6. doi: 10.1016/j.foodchem.2014.11.125
- Ziaifar AM, Courtois F, Trystram G. Porosity development and its effect on oil uptake during frying process. *J Food Process Eng.* (2010) 33:191–212. doi: 10.1111/j.1745-4530.2008.00267.x
- Adedede AA, Ngadi M. Characterisation of pore properties of deep-fat-fried chicken nuggets breeding coating using mercury intrusion porosimetry technique. *Int J Food Sci Technol.* (2010) 11:2219–26. doi: 10.1111/j.1365-2621.2010.02324.x
- Kassama LS, Ngadi MO. Pore development in chicken meat during deep-fat frying. *LWT.* (2004) 37:841–7. doi: 10.1016/j.lwt.2004.03.010
- Kassama LS, Ngadi MO. Pore structure characterization of deep-fat-fried chicken meat. *J Food Eng.* (2005) 66:369–75. doi: 10.1016/j.jfoodeng.2004.04.003
- Dueik V, Moreno MC, Bouchon P. Microstructural approach to understand oil absorption during vacuum and atmospheric frying. *J Food Eng.* (2012) 111:528–36. doi: 10.1016/j.jfoodeng.2012.02.027
- Liu Y, Tian JJ, Zhang TT, Fan LP. Effects of frying temperature and pore profile on the oil absorption behavior of fried potato chips. *Food Chem.* (2021) 345:128832. doi: 10.1016/j.foodchem.2020.128832
- Yang J, Martin A, Richardson S, Wu CH. Microstructure investigation and its effects on moisture sorption in fried potato chips. *J Food Eng.* (2017) 214:117–28. doi: 10.1016/j.jfoodeng.2017.06.034
- Wang H, Duan X, Zhao LJ, Duan LL, Ren GY. Effects of different pretreatments on the pore structure of Chinese yam during microwave freeze drying. *Int J Agric Biol Eng.* (2020) 13:232–7. doi: 10.25165/IJABE.V13I4.5605
- Llorca E, Hernando I, Perez-Munuera I, Fiszman SM, Lluch MA. Effect of frying on the microstructure of frozen battered squid rings. *Eur Food Res Technol.* (2001) 213:448–55. doi: 10.1007/s002170100382
- Cui FJ, Li YH, Yang Y, Sun WJ, Wu D, Ping LF. Changes in chemical components and cytotoxicity at different maturity stages of *Pleurotus eryngii* fruiting body. *J Agric Food Chem.* (2014) 62:12631–40. doi: 10.1021/jf5048354
- Lu F, Li Y, Zhang Y, Xu Y, Li B. Effect of blanching frequency on physicochemical properties of blanch water of *Pleurotus eryngii*. *Adv J Food Sci Technol.* (2015) 8:636–41. doi: 10.19026/ajfst.8.1578
- Sosa-Morales ME, Solares-Alvarado AP, Aguilera-Bocanegra SP, Muñoz-Roa JF, Cardoso-Ugarte GA. Reviewing the effects of vacuum frying on frying medium and fried foods properties. *Int J Food Sci Technol.* (2022) 57:3278–91. doi: 10.1111/ijfs.15572



42. Fan L, Zhang M, Mujumdar AS. Effect of various pretreatments on the quality of vacuum-fried carrot chips. *Drying Technol.* (2006) 24:1481–6. doi: 10.1080/07373930600952826
43. Xu BG, Zhang M, Bhandari B, Cheng XF, Sun J. Effect of ultrasound immersion freezing on the quality attributes and water distributions of wrapped red radish. *Food Bioprocess Technol.* (2015) 8:1366–76. doi: 10.1007/s11947-015-1496-x
44. Isik B, Sahin S, Sumnu G. Pore development, oil and moisture distribution in crust and core regions of potatoes during frying. *Food Bioprocess Technol.* (2016) 9:1653–60. doi: 10.1007/s11947-016-1748-4
45. Wang C, Su G, Wang X, Nie S. Rapid assessment of deep frying oil quality as well as water and fat contents in French fries by low-field nuclear magnetic resonance. *J Agric Food Chem.* (2019) 67:2361–8. doi: 10.1021/acs.jafc.8b05639
46. Vauvre JM, Kesteloot R, Patsioura A, Vitrac O. Microscopic oil uptake mechanisms in fried products. *Eur J Lipid Sci Technol.* (2014) 116:741–55. doi: 10.1002/ejlt.201300278
47. Alam T, Takhar PS. Microstructural characterization of fried potato disks using X-Ray micro computed tomography. *J Food Sci.* (2016) 81:651–64. doi: 10.1111/1750-3841.13219



## OPEN ACCESS

## EDITED BY

Yuanyuan Shan,  
Northwest A&F University, China

## REVIEWED BY

Winy Routray,  
National Institute of Technology  
Rourkela, India  
Ying Yang,  
Central South University of Forestry  
and Technology, China  
Junzhou Ding,  
Shenzhen University, China  
Li Jiangtao,  
Central South University of Forestry  
and Technology, China

## \*CORRESPONDENCE

Siming Zhao  
zsmjx@mail.hzau.edu.cn

## SPECIALTY SECTION

This article was submitted to  
Nutrition and Food Science  
Technology,  
a section of the journal  
Frontiers in Nutrition

RECEIVED 07 September 2022

ACCEPTED 18 October 2022

PUBLISHED 15 November 2022

## CITATION

Kong J, Tao J, Fu S, Wen Y, Zhao S and  
Zhang B (2022) Corner coil heating  
mode improves the matrix uniformity  
of cooked rice in an induction heating  
cooker.  
*Front. Nutr.* 9:1038708.  
doi: 10.3389/fnut.2022.1038708

## COPYRIGHT

© 2022 Kong, Tao, Fu, Wen, Zhao and  
Zhang. This is an open-access article  
distributed under the terms of the  
[Creative Commons Attribution License](#)  
(CC BY). The use, distribution or  
reproduction in other forums is  
permitted, provided the original  
author(s) and the copyright owner(s)  
are credited and that the original  
publication in this journal is cited, in  
accordance with accepted academic  
practice. No use, distribution or  
reproduction is permitted which does  
not comply with these terms.

# Corner coil heating mode improves the matrix uniformity of cooked rice in an induction heating cooker

Jinxi Kong<sup>1,2</sup>, Jinxuan Tao<sup>2</sup>, Shanlin Fu<sup>2</sup>, Ya Wen<sup>2</sup>,  
Siming Zhao<sup>1\*</sup> and Binjia Zhang<sup>3</sup>

<sup>1</sup>Key Laboratory of Environment Correlative Dietology (Ministry of Education), College of Food Science and Technology, Huazhong Agricultural University, Wuhan, China, <sup>2</sup>Department of Home Appliance Technology Research, Zhuhai Gree Electric Appliances Co., Ltd., Zhuhai, China,

<sup>3</sup>Chongqing Key Laboratory of Speciality Food Co-Built by Sichuan and Chongqing, College of Food Science, Southwest University, Chongqing, China

Nowadays, an increasing number of people worldwide use induction heating cookers to cook rice for consumption. This work reveals the influence of induction heating cooker heating modes on the quality attributes of cooked rice. Three heating modes, including bottom coil heating mode (mode 1), corner coil heating mode (mode 2), and side coil heating (mode 3), were used. Among the three modes, mode 2 allowed for an intermediate heating rate during rice cooking. For mode 2, the minimized temperature difference between the upper layer (including the central upper layer and peripheral upper layer) and the lower layer (including the central lower layer and peripheral lower layer) can reduce the effect of water absorption time difference on rice quality. Consequently, the rice cooked using mode 2 exhibited improved matrix uniformity, as indicated by the similar moisture content (59.92–61.89%), hardness (15.87–18.24 N), and water mobility (the relaxation time and peak area of the third relaxation peak) of rice samples at four different positions in the pot. The rice cooked by mode 2 showed better texture appearance and a more uniform porous microstructure. Consistently, the cooked rice samples by mode 2 at different positions did not show substantial differences in their starch digestion features.

## KEYWORDS

rice, induction heating cooker, heating mode, texture uniformity, digestion

## Introduction

Rice is one of the most important staple foods for humans, feeding more than half of the world's population. During cooking, rice kernels undergo many changes, such as hydration, swelling (1), cracking (2, 3), starch gelatinization, and leaching of solids (4–6), all of which may contribute to the final texture of cooked rice.

In recent years, researches have studied various cooking methods to maximize the taste and edible value of cooked rice. Many studies have shown that both

cooking temperature and cooking time have significant impacts on the physicochemical properties (7–10). Additionally, high hydrostatic pressure soaking could increase the hydration degree of rice, leading to a smaller network of channels (11). It has also been indicated that changing the cooking mode can slow the digestion of starch in brown rice (12). Researchers have attempted to correlate the physicochemical properties of cooked rice with different cooking processing parameters. A recent study demonstrated heating rates influenced the final texture of rice by affecting the water distribution and starch gelatinization of rice during cooking (13). Furthermore, with a gradual decrease in the heating power of cooked rice during cooking, the appearance, taste, comprehensive score, and sensory score of cooked rice are enhanced (14).

Due to convenience, induction heating cookers have become the main cooking appliances in family cooking and its primary mechanism involves electromagnetism and heat transfer domains (15). However, most studies investigated the characteristics of a small amount of rice, or only some of the rice from a larger pot used to feed a whole family (16–19). When the amount of rice cooked in the rice cooker increases, differences in the water absorption and temperature at different positions in the pot can be observed, and these differences lead to variability in its texture (13, 20). Research on the eating quality differences in rice prepared in a rice cooker is scarce. Moreover, the electromagnetic coil, as the heating source, is an important factor in the formation of a temperature field in the pot. Studies on the influence of heat source position on rice quality have not yet been reported.

Therefore, in this study, rice quality using three typical heat sources in induction heating cookers by changing the positions of the electromagnetic coil were firstly investigated. The temperature distribution characteristics, the differences in appearance, moisture, texture, and digestion characteristics of cooked rice were examined, which is helpful to guide the design of the electromagnetic coil of induction heating cookers.

## Materials and methods

### Experiment materials

The indica rice used in this study was purchased from local supermarkets in Zhuhai City, with a rice moisture content of 12.2% and dry base starch level of 68.3% (dry basis). Two enzymes  $\alpha$ -amylase (activity: 50 U/mg) and amyloglucosidase (activity: 100 U/mg) were purchased from Shanghai Yuanye Biological Co., Ltd. (Shanghai, China). A glucose oxidase/peroxidase kit (GOPOD reagent) was provided by Shanghai Rongsheng Bio-pharmaceutical Co., Ltd. (Shanghai, China). All chemical reagents were of analytical grade.

### Rice cooking temperature acquisition

Six hundred grams of rice was quickly washed with water three times, combined with pure water at a rice:water mass ratio of 1:1.4, and cooked in an electromagnetic heating rice cooker (Gree Electric Appliances Co., Ltd., Zhuhai, China) to prepare a rice sample. During the cooking process, the heating power and heating time were the same in the three heating modes, and the electromagnetic coils at three typical positions in the rice cooker were used separately for heating. The bottom coil was used in mode 1 (Figure 1A); the corner coil was used in mode 2 (Figure 1B); and the side coil was used in mode 3 (Figure 1C). The cooking temperature was acquired according to a previously reported method, with slight modification (21). Prior to cooking, T-type thermocouples were placed at four different positions in the central upper layer (CU), peripheral upper layer (PU), central lower layer (CL), and peripheral lower layer (PL) in the inner pot (Figure 1) due to its symmetrical structure, and a temperature acquisition instrument (34970A, Keysight Technologies Co., Ltd., Guangzhou, China) was used for real-time recording of the temperature field data in the pot under different heating modes.

### Observation of rice appearance

In order to investigate the difference in rice morphology under different modes, the appearance of cooked rice was observed using a high-resolution stereomicroscope (VHX-7000, KEYENCE, Osaka, Japan) with a magnification of 20 $\times$  (22).

### Rice low-field NMR test

The moisture characteristics of rice under different heating modes and with different heat sources were measured on a LF-NMR spectrometer (Niumai Instruments, NMI20-015V-I, Suzhou, China), as previously described (23, 24). In order to ensure the parallelism of the experiment and the reliability of the results, each measurement was conducted at the same fixed time period. The preparation and measurement of the rice samples were completed within 40 min of cooking, so as to prevent the samples from being exposed to the air for too long and losing water, which would affect the experimental results. The measurement parameters were as follows: P1 = 13.52  $\mu$ s, TW = 4000 ms, and P2 = 26.00  $\mu$ s. For each sample, six parallel tests were conducted. After the measurement, the data were saved, and the inversion software (NMR relaxation time inversion fitting software Ver4.09 provided by Shanghai Niumai Electronic Technology Co., Ltd. Shanghai, China) was used to obtain the distribution of T<sub>2</sub>.

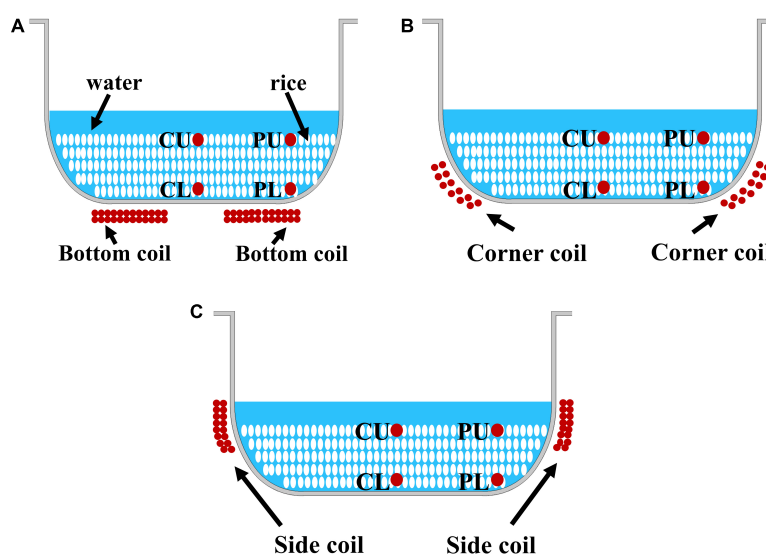


FIGURE 1

Schematics of different heating modes and sampling points. (A) Mode 1. (B) Mode 2. (C) Mode 3. CU, central upper layer; PU, peripheral upper layer; CL, central lower layer; and PL, peripheral lower layer.

## Scanning electron microscope observation of rice cross-section

The cooked rice samples were immediately dried by a vacuum freeze dryer (ALPHA1-4, Marin Christ Inc., Osterode, Germany), following a previously reported method (25). After drying, the rice sample was broken with tweezers to observe its cross-section. The samples were adhered with double-sided tape with the cross-section facing upward and gold-plated under vacuum. The cross-section structure of the sample was observed using a scanning electron microscope at  $2000\times$  magnification (TESCAN CLAR LMH, TESCAN Trading Co., Ltd., Brno, Czechia).

## Determination of physicochemical properties of rice

After cooking was finished, the rice was quickly sampled from the different positions, as shown in Figure 1, to measure the moisture content, expansion ratio (ER), and texture properties of the rice. The moisture content of the rice sample was determined using the standard association of official analytical chemists (AOAC) method (26). The expansion rate was determined *via* the drainage method with minor modification, as reported by Pan et al. and Wang et al. (27, 28). Briefly, 50 ml of water was transferred to a 100 ml measuring cylinder. Twenty-five grams of rice was added to the water and immediately stirred with a glass rod to evenly disperse

the rice grains in the water. The difference in volume was taken as the volume of rice. The expansion rate of rice from different positions was calculated using the ratio of the volume of rice from different positions to the volume of raw rice. For each rice sample, three parallel experiments were performed.

The texture properties of the rice samples were determined in a two-cycle compression mode (TPA mode) using a texture profile analyzer (TMS-TOUCH, Food Technology Corporation, Virginia, USA), as previously described (25). Three whole grains of rice were placed in parallel on an aluminum plate. During the measurement process, a cylindrical probe with a diameter of 38.1 mm was used for compression, with a deformation amount of 70%. The detection speed was 120 mm/min, and the initial force was 0.5 N. Based on the force-time curves obtained in the test, the firmness and stickiness of the rice were determined. Six parallel experiments were carried out for each rice sample.

## Determination of *in vitro* digestion characteristics of rice starch

As shown in Figure 1, 50 g of rice was taken from each sampling point, combined with 150 ml of anhydrous ethanol, quickly stirred and dispersed with a glass rod, and dehydrated. After suction filtration, the samples were dried at  $40^{\circ}\text{C}$  to constant weight, pulverized with a pulverizer, passed through a 100-mesh sieve, and placed in a desiccator.

Referring to the method reported by Liu et al. (29) with slight modification, the rice powder containing about 90 mg of

starch was placed in a 50 ml conical flask. Then, 6 ml of distilled water and 10 ml of sodium acetate buffer solution (pH 6.0) were added, and the mixture was heated for 10 min at 37 °C. Next, 5.0 ml of mixed enzyme buffer solution containing 42 U/ml  $\alpha$ -amylase and 42 U/ml amyloglucosidase was added, and the sample solution was hydrolyzed in a water bath at 37 °C for 0, 10, 20, 30, 60, 90, 120, and 180 min, respectively. At 180 min, 0.2 ml of the hydrolysis solution was removed, and 0.8 ml of absolute ethanol was added to inactivate the enzyme. The mixture was centrifuged at 4,000 r/min for 10 min. The absorbance value of the samples was measured using a glucose oxidase/peroxidase kit (GOPOD reagent) with 5.55 mmol/L glucose reagent as the standard. The starch hydrolysis rate of the sample at a certain time was calculated according to the following formula:

$$\text{starch hydrolysis rate (\%)} = \frac{\frac{A_{\text{sample}}}{A_{\text{standard}}} \cdot C_{\text{standard}} \cdot V_{\text{total}} \cdot 0.9 \cdot f}{m_{\text{starch}}} \times 100 \quad (1)$$

where  $A_{\text{sample}}$  is the absorbance of the sample;  $A_{\text{standard}}$  is the absorbance of the glucose standard solution;  $C_{\text{standard}}$  is the glucose standard solution concentration (5.55 mmol/L);  $V_{\text{total}}$  is the total volume of the digestion solution;  $f$  is the dilution folds; 0.9 is the conversion coefficient from glucose into starch; and  $m_{\text{starch}}$  is the product of the mass of the sample and the percentage of contained starch. The contents of rapidly digestible starch (RDS), slowly digestible starch (SDS), and resistant starch (RS) were calculated according to a previously reported method (30). The *in vitro* starch digestion process was consistent with first-order kinetics, and the formula was as follows:

$$C_t = C_{\infty} (1 - e^{-kt}) \quad (2)$$

where  $C_t$  is the percentage of hydrolyzed starch when the digestion time is  $t$ ;  $C_{\infty}$  is the percentage of hydrolyzed starch in the case of the hydrolysis equilibrium during the digestion process;  $k$  is the first-order kinetic constant; and  $t$  is the digestion time. The transfer function of the logarithm of slope (LOS) plot was obtained by taking the logarithm of the first derivative of the first order equation using the following formula:

$$\ln \frac{dc}{dt} = -kt + \ln(C_{\infty}k) \quad (3)$$

where  $\ln (dc/dt)$  is the logarithm of the slope. The parameters  $C_{\infty}$  and  $k$  were calculated by linear fitting of LOS and starch hydrolysis time  $t$ , and the starch digestion behavior of different rice powder samples was further evaluated.

## Statistical analysis

The data are expressed as mean values  $\pm$  standard deviations. Origin (version 2021 for windows, Origin-Lab, Northampton, MA, USA) was used to draw plots. The

comparison of means was conducted by SPSS software (version 17.0 for windows, SPSS Inc., Chicago, IL, USA).

## Results and discussion

### Temperature distribution during cooking

The temperature distribution curves under three specific heating modes are shown in **Figure 2**, and significant differences were found between the three cooking modes. The cooking process could be divided into the rice soaking stage (0–10 min), the rapid heating stage (10–20 min), and the high-temperature maintenance stage (20–32 min). Temperature differences were found at the initial rice soaking stage of mode 1, in which the temperature of the central lower layer (CL) was the highest and that of the central upper layer (CU) was the lowest. At the end of the soaking stage, the temperature of the entire pot maintained approximately 30–35°C. During the rapid heating stage, the temperature at the four sampling points increased sharply and reached boiling (100°C) with different heating rates. The heating rate at the CL and the CU was faster than that at the PU and the PL. During the high-temperature maintenance stage, the rice temperature at four different positions (CU, PU, CL, and PL) in the pot was maintained at 100°C until the end of cooking. Under mode 2, the temperature of PU was higher than that of the other three sampling points during the rice soaking and rapid heating stages. Furthermore, the rate of increasing temperature at different sampling points was slower and more consistent under mode 2 than under mode 1. However, the temperature at CU and PU gradually decreased and maintained at 95°C during the high-temperature maintenance stage. For rice heated by mode 3, the temperature of the rice in different layers of the rice cooker was not maintained at 100°C. In particular, the temperature at CU decreased fastest, due to the distance from the heat source and the heat dissipation of the rice cooker. These results indicate differences in temperature distribution between the three cooking modes. Among them, the heating rate of mode 1 was the fastest. The heating rate of the mode 2 was moderate, and the heating temperature of mode 3 was the slowest. Moreover, the temperature difference at various sampling points was the largest for mode 3.

### Morphologic properties of cooked rice

The morphology of rice samples under different heating modes is shown in **Figure 3**. The rice surface cooked by modes 2 and 3 was relatively smooth and intact, for a lower degree of starch gelatinization resulted in higher density of the tissue (31). A slower heating rate during the heating



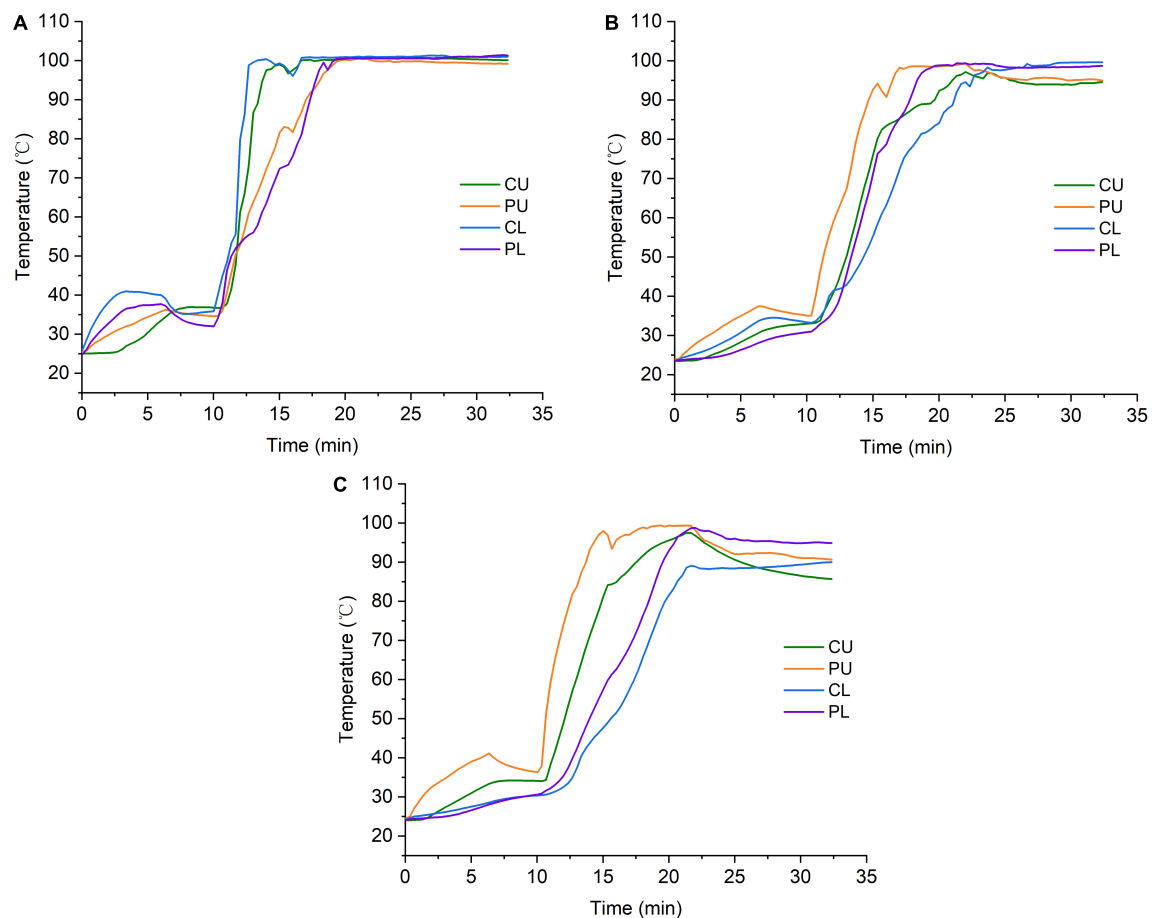


FIGURE 2

Temperature distribution under different heating modes. (A) Mode 1. (B) Mode 2. (C) Mode 3. CU, central upper layer; PU, peripheral upper layer; CL, central lower layer; and PL, peripheral lower layer.

stage and lower maintained temperature (85–95°C) during the high-temperature maintenance stage resulted in insufficient gelatinization of rice sample of mode 3. The cooked rice of mode1-CU and mode1-CL were prone to disruption and deformation (Figure 3), compared with other samples. This is probably due to the higher heating rate and longer maintenance time at a high temperature (above 98°C) of mode1-CU and mode1-CL (27, 32). Furthermore, these changes led to the disruption of the rice surface, due to contact between boiling water and the rice surface (33). Tamura et al. (18) found starch gelatinization between 85 and 100°C damaged the cell wall along the rice surface and changed the rice shape.

## Microstructure of cooked rice

In order to clarify the morphological and textural properties of cooked rice, Scanning electron microscope (SEM) was employed to observe the microstructure of cooked rice at the center (Figure 4). Significant differences

in microstructure between the different heating modes were observed. For mode 2, the cooked rice at different sampling positions showed porous structures with similar pore size. Compared with other samples, rice cooked at CU and CL positions of mode 1 had large cavities. This may be due to the fact that kernels located at CU and CL (mode 1) absorbed more water during cooking. For CU, CL, and PL (mode 3), most of the starch granules were tightly packed because of lower moisture content in the inner areas (31, 34), which was consistent with the results observed by stereomicroscope.

## Moisture characteristics of rice

To gain further insight into water state differences of cooked rice at a molecular lever, the cooked rice was analyzed using proton relaxation measurements. Similar populations were observed for the cooked rice at different cooking modes (Table 1). The range of  $T_2$  values of the cooked rice was  $T_{21}$

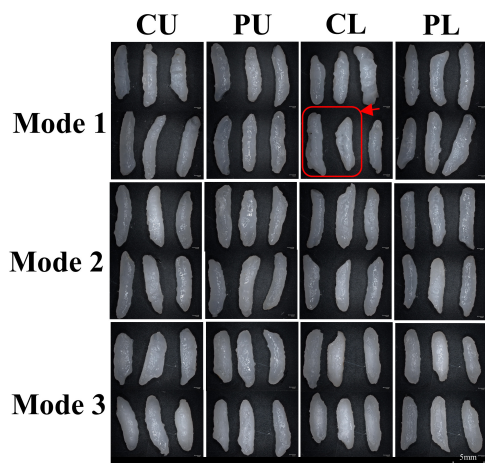


**FIGURE 3**  
Morphological changes in rice under different heating modes. The red line marked damaged rice. CU, central upper layer; PU, peripheral upper layer; CL, central lower layer; and PL, peripheral lower layer.

time of  $T_{23}$  and peak area of  $T_{23}$  between different positions in the pot. In contrast, significant differences between modes 1 and 3 were observed, which were consistent with the moisture content distribution. In mode 1, the rice samples at CU and CL had larger holes than those at PU and PL (Figure 3). This is because more bulk water was found at PU and PL, leading to a higher relaxation time of  $T_{23}$  (35, 37). In mode 3, the upper layer had a larger  $T_{23}$  peak area than the lower layer, indicating higher mobility of water in the upper layer. With regard to the microstructure of the cooked rice, the insufficient gelatinization of rice resulted in a tightly packed tissue structure with fewer and smaller holes. Thus, fewer water molecules were intercepted (35).

Compared with the rice cooked using mode 1, the cooked rice of mode 3 had a low relaxation time and a small  $T_{23}$  peak area, indicating the rice cooked by mode 3 had a more restrictive microenvironment, which agreed with the microstructure of cooked rice.

## Rice texture

To further investigate whether the cooked rice using the three heating modes had different textures, the moisture content, expansion rate, and texture characteristics of rice were analyzed. In general, the expansion rate of cooked rice was positively correlated with moisture content (28), while the hardness of rice was negatively correlated with moisture content (38, 39). As shown in Table 2, modes 1 and 3 displayed varied moisture content, expansion rates, and hardness at different positions in the pot, but rice adhesiveness was similar. In

(0.1–1 ms),  $T_{22}$  (1–10 ms), and  $T_{23}$  (10–100 ms), which were named according to the order they appeared in the time scale.

As shown in Table 2, the peak area of  $T_{23}$  varied from 77–86% for the three cooking modes, presenting typical  $T_{23}$  predominant peak characteristics of the cooked rice (35, 36). The time scale and peak area of the relaxation singles were different, indicating varied mobilities of the polymers and water state in cooked rice under different cooking modes (25). In mode 2, there was no significant difference in the relaxation

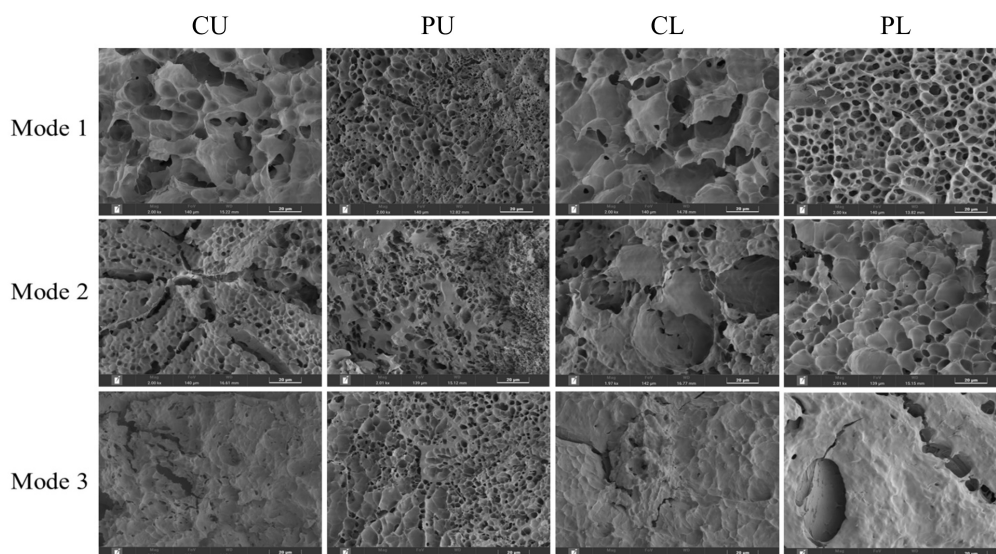


**FIGURE 4**  
Morphological structure of the center of cooked rice cross-sections under different heating modes.

TABLE 1 Moisture characteristics of rice under different heating modes ( $n = 6$ , mean  $\pm$  STDEV).

Mode	Position	T21 (ms)	A21 (%)	T22 (ms)	A22 (%)	T23 (ms)	A23 (%)
Mode 1	CU	0.46 $\pm$ 0.09 <sup>a</sup>	3.25 $\pm$ 1.48 <sup>c</sup>	3.11 $\pm$ 0.56 <sup>abc</sup>	9.75 $\pm$ 1.79 <sup>a</sup>	50.41 $\pm$ 6.14 <sup>a</sup>	86.75 $\pm$ 1.48 <sup>a</sup>
	PU	0.51 $\pm$ 0.33 <sup>a</sup>	6.33 $\pm$ 4.11 <sup>bc</sup>	2.24 $\pm$ 0.29 <sup>bc</sup>	8.68 $\pm$ 6.17 <sup>a</sup>	36.25 $\pm$ 1.56 <sup>c</sup>	84.00 $\pm$ 2.16 <sup>ab</sup>
	CL	0.56 $\pm$ 0.17 <sup>a</sup>	9.00 $\pm$ 2.94 <sup>abc</sup>	3.71 $\pm$ 0.36 <sup>a</sup>	8.00 $\pm$ 0.82 <sup>a</sup>	42.28 $\pm$ 3.99 <sup>b</sup>	83.00 $\pm$ 3.56 <sup>abc</sup>
	PL	0.40 $\pm$ 0.20 <sup>a</sup>	7.50 $\pm$ 2.69 <sup>abc</sup>	2.39 $\pm$ 0.95 <sup>abc</sup>	10.00 $\pm$ 3.08 <sup>a</sup>	32.74 $\pm$ 0.48 <sup>cd</sup>	82.75 $\pm$ 1.09 <sup>abc</sup>
Mode 2	CU	0.38 $\pm$ 0.10 <sup>a</sup>	8.50 $\pm$ 0.50 <sup>abc</sup>	2.19 $\pm$ 0.45 <sup>bc</sup>	10.50 $\pm$ 1.50 <sup>a</sup>	35.41 $\pm$ 1.23 <sup>c</sup>	81.00 $\pm$ 1.00 <sup>abc</sup>
	PU	0.40 $\pm$ 0.10 <sup>a</sup>	14.00 $\pm$ 4.36 <sup>ab</sup>	2.78 $\pm$ 0.60 <sup>abc</sup>	7.50 $\pm$ 3.50 <sup>a</sup>	31.10 $\pm$ 1.19 <sup>cd</sup>	78.75 $\pm$ 2.28 <sup>bc</sup>
	CL	0.29 $\pm$ 0.09 <sup>a</sup>	5.50 $\pm$ 3.50 <sup>bc</sup>	2.36 $\pm$ 0.79 <sup>abc</sup>	12.50 $\pm$ 2.50 <sup>a</sup>	33.85 $\pm$ 4.09 <sup>cd</sup>	82.00 $\pm$ 1.00 <sup>abc</sup>
	PL	0.21 $\pm$ 0.03 <sup>a</sup>	6.50 $\pm$ 3.50 <sup>bc</sup>	2.15 $\pm$ 0.58 <sup>c</sup>	12.50 $\pm$ 1.50 <sup>a</sup>	34.21 $\pm$ 1.19 <sup>cd</sup>	81.50 $\pm$ 1.50 <sup>abc</sup>
Mode 3	CU	0.39 $\pm$ 0.24 <sup>a</sup>	7.33 $\pm$ 4.99 <sup>abc</sup>	3.61 $\pm$ 0.20 <sup>ab</sup>	9.33 $\pm$ 2.05 <sup>a</sup>	44.14 $\pm$ 2.55 <sup>b</sup>	83.00 $\pm$ 4.32 <sup>abc</sup>
	PU	0.46 $\pm$ 0.28 <sup>a</sup>	7.25 $\pm$ 3.56 <sup>abc</sup>	2.64 $\pm$ 0.82 <sup>abc</sup>	9.75 $\pm$ 4.44 <sup>a</sup>	35.15 $\pm$ 2.15 <sup>c</sup>	82.75 $\pm$ 1.92 <sup>abc</sup>
	CL	0.48 $\pm$ 0.28 <sup>a</sup>	15.50 $\pm$ 0.50 <sup>a</sup>	2.12 $\pm$ 0.44 <sup>c</sup>	7.50 $\pm$ 4.50 <sup>a</sup>	27.79 $\pm$ 0.96 <sup>d</sup>	77.00 $\pm$ 4.00 <sup>c</sup>
	PL	0.34 $\pm$ 0.12 <sup>a</sup>	9.25 $\pm$ 4.82 <sup>abc</sup>	2.30 $\pm$ 0.37 <sup>abc</sup>	11.50 $\pm$ 1.80 <sup>a</sup>	30.85 $\pm$ 1.51 <sup>cd</sup>	79.50 $\pm$ 3.57 <sup>bc</sup>

The values in the table are the mean  $\pm$  standard deviation and the different lower-case letters in the same column represent significant differences ( $p < 0.05$ ).

TABLE 2 Moisture content, expansion ratio and texture properties of rice under different heating modes.

Mode	Position	Moisture content (%wb)	ER (%)	Hardness (N)	Adhesiveness (mJ)
Mode 1	CU	68.03 $\pm$ 0.26 <sup>b</sup>	245.5 $\pm$ 5.63 <sup>b</sup>	11.04 $\pm$ 1.02 <sup>bc</sup>	0.35 $\pm$ 0.19 <sup>a</sup>
	PU	59.21 $\pm$ 1.52 <sup>ef</sup>	166.5 $\pm$ 1.96 <sup>efg</sup>	18.20 $\pm$ 0.92 <sup>ab</sup>	0.60 $\pm$ 0.39 <sup>a</sup>
	CL	73.00 $\pm$ 0.83 <sup>a</sup>	321.2 $\pm$ 5.71 <sup>a</sup>	9.81 $\pm$ 1.66 <sup>c</sup>	0.42 $\pm$ 0.13 <sup>a</sup>
	PL	62.04 $\pm$ 0.62 <sup>cd</sup>	195.9 $\pm$ 5.19 <sup>d</sup>	17.91 $\pm$ 1.48 <sup>ab</sup>	0.68 $\pm$ 0.18 <sup>a</sup>
Mode 2	CU	59.96 $\pm$ 1.3 <sup>def</sup>	167 $\pm$ 2.03 <sup>efg</sup>	16.93 $\pm$ 0.70 <sup>ab</sup>	0.43 $\pm$ 0.08 <sup>a</sup>
	PU	59.92 $\pm$ 0.16 <sup>def</sup>	178.2 $\pm$ 0.16 <sup>c</sup>	15.87 $\pm$ 1.83 <sup>abc</sup>	0.61 $\pm$ 0.28 <sup>a</sup>
	CL	60.67 $\pm$ 0.59 <sup>def</sup>	174.9 $\pm$ 1.54 <sup>ef</sup>	17.60 $\pm$ 1.68 <sup>ab</sup>	0.55 $\pm$ 0.14 <sup>a</sup>
	PL	61.89 $\pm$ 0.27 <sup>cde</sup>	195.5 $\pm$ 1.47 <sup>d</sup>	18.24 $\pm$ 3.39 <sup>ab</sup>	0.56 $\pm$ 0.12 <sup>a</sup>
Mode 3	CU	63.62 $\pm$ 0.38 <sup>c</sup>	200.7 $\pm$ 1.98 <sup>d</sup>	14.40 $\pm$ 0.50 <sup>abc</sup>	0.51 $\pm$ 0.14 <sup>a</sup>
	PU	64.48 $\pm$ 0.59 <sup>c</sup>	226.7 $\pm$ 5.10 <sup>c</sup>	15.07 $\pm$ 2.44 <sup>abc</sup>	0.64 $\pm$ 0.10 <sup>a</sup>
	CL	58.44 $\pm$ 0.56 <sup>f</sup>	158.5 $\pm$ 2.19 <sup>g</sup>	19.68 $\pm$ 3.24 <sup>a</sup>	0.35 $\pm$ 0.08 <sup>a</sup>
	PL	58.45 $\pm$ 0.79 <sup>f</sup>	164.1 $\pm$ 0.69 <sup>fg</sup>	19.71 $\pm$ 2.64 <sup>a</sup>	0.43 $\pm$ 0.08 <sup>a</sup>

The values in the table are the mean  $\pm$  standard deviations. The different lower-case letters in the same column represent significant differences ( $p < 0.05$ ). CU, central upper layer; PU, peripheral upper layer; CL, central lower layer; and PL, peripheral lower layer.

contrast, these characteristics of rice from mode 2 showed no significant differences.

During the cooking process, the moisture content of rice at different positions in the pot was mainly affected by cooking temperature and water absorption time (13, 40). The water absorption rate was positively correlated with the two factors, especially when the cooking temperature was above 60°C (25). Thus, the temperature differences in the rapid heating stage caused differences in the moisture content. In addition, the water absorption time depended on its location in the pot, which indicates the rice closer to the bottom of the pot had longer water absorption time. In mode 1, the higher cooking temperature and longer water absorption time (mode1-CL, Figure 1), resulted in higher moisture content (mode1-CL, 73.00%). Combined with the microstructure of cooked rice, the higher moisture content led to a large cavity structure, which might be the cause of large expansion rate and low hardness. In contrast, lower cooking temperature (mode 1-PU, Figure1) and shorter

water absorption time, led to lower moisture content (mode1-PU, 59.21%) and expansion rate and higher hardness, which was consistent with the moisture distribution characteristics and microstructure. Thus, the rice cooked using mode 1 exhibits poor texture uniformity. In mode 3, the moisture content at PU and CU was higher than that at PL and CL because of the higher cooking temperature curve. This indicates cooking temperature differences in the rapid heating stage contributed more than water absorption time to the water absorption differences of rice. In mode 2, the cooking temperature differences compensated for the water absorption time differences between the upper layer (CU and PU) and the lower layer (CL and PL), presenting similar moisture content of rice at the four sampling positions in the pot. Compared to modes 1 and 3, rice cooked at mode 2 presented the best texture uniformity. Above all, an appropriate cooking temperature distribution during the rapid heating stage in the pot should lead to the best texture uniformity.

## Digestion properties of rice

The starch digestion curves and first-order kinetic fittings of rice and raw rice under different heating modes of the rice cooker are shown in **Figure 5**. Raw rice and rice starch

under different heating modes were rapidly digested in the first 30 min of *in vitro* digestion, and then the hydrolysis rate gradually decreased with the extension of digestion time. The starch digestion rate parameters were obtained based on the linear fitting of the LOS diagram (**Table 3**). Compared with the

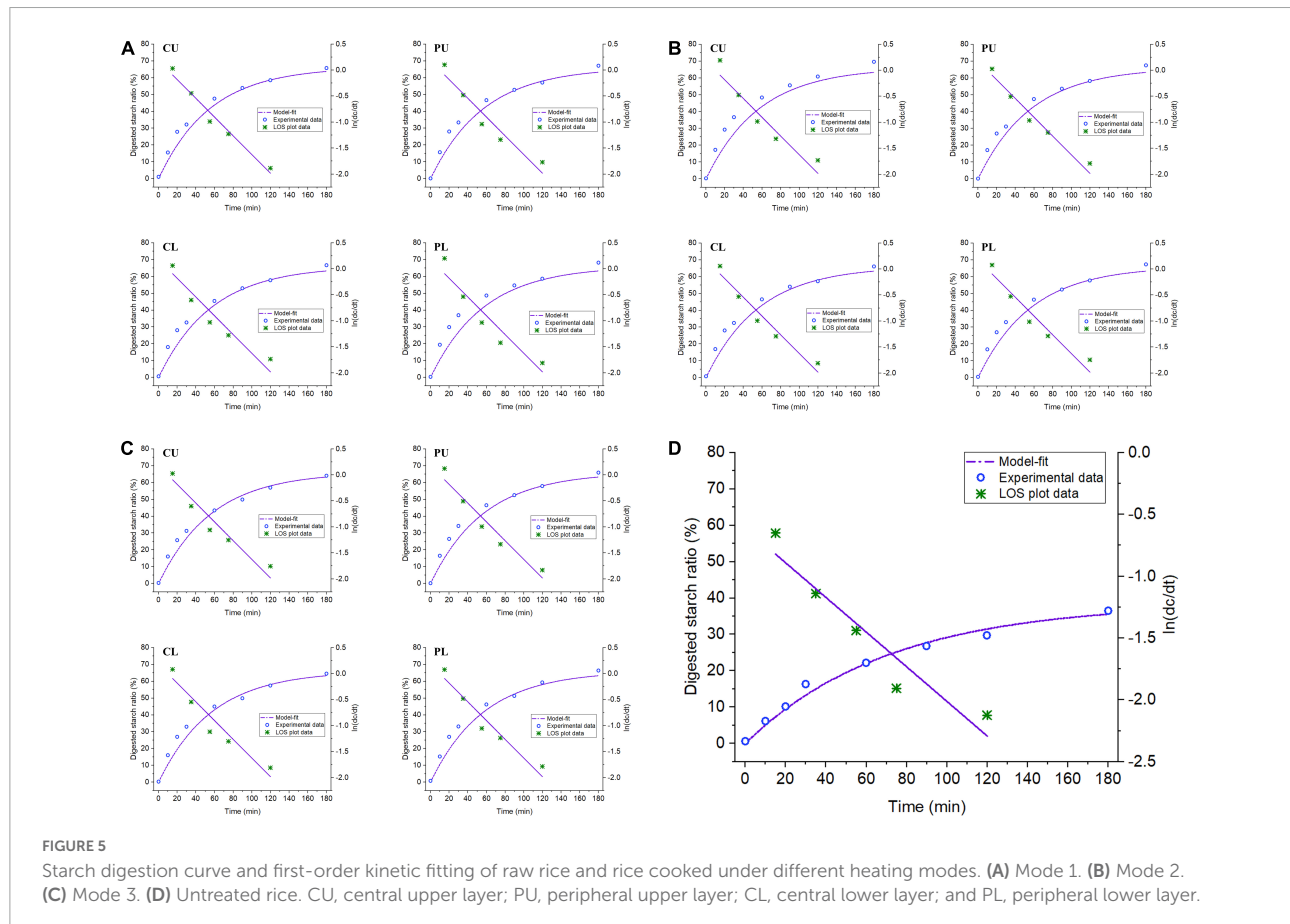


**TABLE 3** Starch digestion characteristic parameters of raw rice and rice cooked under different heating modes.

Mode	Position	$C_{\infty}$ (%)	$k \times 10^{-2}$ ( $\text{min}^{-1}$ )	RDS content (%)	SDS content (%)	RS content (%)
Mode 1	CU	$66.36 \pm 1.22^a$	$1.80 \pm 0.14^a$	$38.93 \pm 2.27^a$	$44.67 \pm 4.09^a$	$16.40 \pm 3.28^a$
	PU	$66.16 \pm 1.92^a$	$1.75 \pm 0.04^a$	$40.59 \pm 1.49^a$	$42.39 \pm 2.84^a$	$17.02 \pm 3.81^a$
	CL	$65.32 \pm 3.95^a$	$1.64 \pm 0.07^{ab}$	$39.81 \pm 1.62^a$	$43.48 \pm 1.85^a$	$16.72 \pm 2.66^a$
	PL	$65.17 \pm 3.33^a$	$1.86 \pm 0.03^a$	$43.06 \pm 3.70^a$	$42.02 \pm 2.63^a$	$14.92 \pm 4.16^a$
Mode 2	CU	$68.90 \pm 4.57^a$	$1.78 \pm 0.05^a$	$42.33 \pm 2.92^a$	$45.95 \pm 3.85^a$	$11.72 \pm 6.13^a$
	PU	$67.19 \pm 3.16^a$	$1.67 \pm 0.12^{ab}$	$38.99 \pm 4.61^a$	$45.52 \pm 3.33^a$	$15.48 \pm 5.39^a$
	CL	$65.38 \pm 3.15^a$	$1.73 \pm 0.08^a$	$39.83 \pm 3.21^a$	$42.53 \pm 2.91^a$	$17.63 \pm 5.19^a$
	PL	$66.37 \pm 2.55^a$	$1.68 \pm 0.12^{ab}$	$38.71 \pm 2.87^a$	$44.93 \pm 1.44^a$	$16.36 \pm 3.70^a$
Mode 3	CU	$64.52 \pm 3.27^a$	$1.62 \pm 0.00^{ab}$	$36.99 \pm 4.34^a$	$45.66 \pm 1.20^a$	$17.34 \pm 5.07^a$
	PU	$66.17 \pm 3.16^a$	$1.81 \pm 0.04^a$	$38.48 \pm 5.48^a$	$45.78 \pm 0.47^a$	$15.73 \pm 5.86^a$
	CL	$63.70 \pm 2.98^a$	$1.74 \pm 0.09^a$	$38.82 \pm 4.15^a$	$44.29 \pm 1.87^a$	$16.89 \pm 4.68^a$
	PL	$66.92 \pm 2.96^a$	$1.72 \pm 0.19^a$	$38.21 \pm 5.13^a$	$47.11 \pm 1.87^a$	$14.68 \pm 5.88^a$
Untreated rice	/	$38.66 \pm 1.37^b$	$1.41 \pm 0.03^b$	$13.81 \pm 2.53^b$	$28.54 \pm 0.66^b$	$57.65 \pm 3.01^b$

The values in the table are the mean  $\pm$  standard deviation and different lower-case letters in the same column represent significant differences ( $p < 0.05$ ).  $C_{\infty}$ , the equilibrium hydrolysis rate of starch;  $k$ , the kinetic constant; RDS, rapidly digestible starch; SDS, slowly digestible starch; and RS, resistant starch.

raw rice, the cooked rice had a significantly reduced resistant starch (RS) content, while the rapidly digestible starch (RDS) and slowly digestible starch (SDS) starch content significantly increased (41). However, there were no significant differences in the content of RS, RDS, and SDS among the rice at different sampling positions under different heating modes. This is consistent with the improved digestibility of rice after cooking. Additionally, no significant difference in equilibrium hydrolysis rate of rice cooked under different heating methods was detected. Schematic diagrams and the SEM data of rice showed rice cooked under different heating modes underwent water absorption and gelatinization, despite slight differences in gelatinization degree, thus forming a loose porous structure. This might explain why the starch hydrolysis rate of the cooked rice samples was significantly improved. The porous structure of rice can enhance the diffusion and accessibility of enzymes in the matrix, contributing to the increase in the digestion rate of rice (42). This may be because the powder samples used in this study further reduced the influence of the internal and external structure of cooked rice on the digestion rate of rice. A similar observation was reported in a previous study (43).

## Conclusion

In this study, the effects of three typical heating sources of rice cookers on the water absorption characteristics, texture, morphological structure, and digestion characteristics of rice at different sampling positions in the pot were investigated. The different cooking modes affected the texture and tissue structure of the entire pot of rice, but there was no significant difference in the digestibility of rice. For mode 2, the temperature consistency in the pot was high, resulting in greater texture, appearance uniformity and similar moisture binding state of rice in the entire pot. For mode 1, the heating rate of the rice at the center position was the fastest across the entire pot, leading to the poorest moisture content, expansion ratio and hardness uniformity of rice samples from different position in the pot. The cooked rice of mode1-CU and mode1-CL were prone to disruption and deformation. Moreover, the microstructure was looser and more porous. For mode 3, the bottom center is the farthest from the heat source, and the temperature was relatively low during the high-temperature maintenance stage. Therefore, the lower layer of rice had a lower moisture content

and expansion rate, which resulted in a tighter microstructure, and greater hardness. Compared to modes 1 and 3, rice cooked at mode 2 presented the best texture uniformity. Therefore, this study provides theoretical guidance to improve the texture uniformity of cooked rice in induction heating cooker.

## Data availability statement

The original contributions presented in this study are included in the article/supplementary material, further inquiries can be directed to the corresponding author.

## Author contributions

JK: data curation, investigation, and writing—original draft preparation. JT: project administration, investigation, and methodology. SF: data curation and methodology. YW: formal analysis and validation. SZ: conceptualization, supervision, and writing—review and editing. BZ: conceptualization, supervision, and writing—review and editing. All authors contributed to the article and approved the submitted version.

## Conflict of interest

Authors JK, JT, SF, and YW were employed by Zhuhai Gree Electric Appliances Co., Ltd.

The remaining authors declare that the research was conducted in the absence of any commercial or financial relationships that could be construed as a potential conflict of interest.

## Publisher's note

All claims expressed in this article are solely those of the authors and do not necessarily represent those of their affiliated organizations, or those of the publisher, the editors and the reviewers. Any product that may be evaluated in this article, or claim that may be made by its manufacturer, is not guaranteed or endorsed by the publisher.

## References

1. Perez JH, Tanaka F, Uchino T. Comparative 3D simulation on water absorption and hygroscopic swelling in japonica rice grains under various isothermal soaking conditions. *Food Res Int.* (2011) 44:2615–23. doi: 10.1016/j.foodres.2011.05.003
2. Murata S, Koide S, Kawano T. Study on the cracking of polished rice soaked in water. *J Soc Agr Mach.* (1992) 54:67–72. doi: 10.11357/jsam1937.54.67
3. Koide S, Takko T, Nishiyama Y. Open crack formation in rice with cracked endosperm and cracked surface during soaking. *J Jpn Soc Mech Eng.* (2001) 48:69–72. doi: 10.3136/nskkk.48.69
4. Patindol J, Gu X, Wang Y-J. Chemometric analysis of cooked rice texture in relation to starch fine structure and leaching



characteristics. *Starch*. (2010) 62:188–97. doi: 10.1002/star.20090181

5. Li H, Yu L, Yu W, Li H, Gilbert R. Autoclaved rice: the textural property and its relation to starch leaching and the molecular structure of leached starch. *Food Chem.* (2019) 283:199–205. doi: 10.1016/j.foodchem.2019.01.030

6. Tao K, Yu W, Prakash S, Gilbert R. High-amylose rice: starch molecular structural features controlling cooked rice texture and preference. *Carbohydr Polym.* (2019) 219:251–60. doi: 10.1016/j.carbpol.2019.05.031

7. He M, Qiu C, Liao Z, Sui Z, Corke H. Impact of cooking conditions on the properties of rice: combined temperature and cooking time. *Int J Biol Macromol.* (2018) 117:87–94. doi: 10.1016/j.ijbiomac.2018.05.139

8. Vidal V, Pons B, Brunnschweiler J, Handschin S, Mestres C. Cooking behavior of rice in relation to kernel physicochemical and structural properties. *J Agric Food Chem.* (2007) 55:336–46. doi: 10.1021/jf061945o

9. Syafutri MI, Pratama F, Syaiful F, Faizal A. Effects of varieties and cooking methods on physical and chemical characteristics of cooked rice. *Rice Sci.* (2016) 23:282–6. doi: 10.1016/j.rsci.2016.08.006

10. Batista S, Santos P, Dittgen L, Colussi R, Bassinello Z, Elias C, et al. Impact of cooking temperature on the quality of quick cooking brown rice. *Food Chem.* (2019) 286:98–105. doi: 10.1016/j.foodchem.2019.01.187

11. Tian Y, Zhao J, Xie Z, Wang J, Xu X, Jin Z. Effect of different pressure-soaking treatments on color, texture, morphology and retrogradation properties of cooked rice. *LWT Food Sci Technol.* (2014) 55:368–73. doi: 10.1016/j.lwt.2013.09.020

12. Wang L, Zhao S, Kong J, Li N, Qiao D, Zhang B, et al. Changing cooking mode can slow the starch digestion of colored brown rice: a view of starch structural changes during cooking. *Int J Biol Macromol.* (2020) 155:226–32. doi: 10.1016/j.ijbiomac.2020.03.203

13. Zhu L, Bi S, Wu G, Zhang H, Wang L, Qian H, et al. Comparative Analysis of the texture and physicochemical properties of cooked rice based on adjustable rice cooker. *LWT Food Sci Technol.* (2020) 130:109650. doi: 10.1016/j.lwt.2020.109650

14. Wang G. *Variable Parameter Rice Cooking Process and Quality Measurement and Evaluation*. [Master's Thesis]. Changchun: Jilin University (2020).

15. Patil, M, Choubey K, Jain K. Influence of coil shapes on temperature distribution in induction heating process. *Mater Today Proc.* (2022) doi: 10.1016/j.matpr.2022.08.376.

16. Ghasemi E, Mosavian MTH, Khodaparast MHH. Effect of stewing in cooking step on textural and morphological properties of cooked rice. *Rice Sci.* (2009) 16:243–6. doi: 10.1016/S1672-6308(08)60086-4

17. Zhu L, Zhang H, Wu G, Qi X, Wang L, Qian H. Effect of structure evolution of starch in rice on the textural formation of cooked rice. *Food Chem.* (2021) 342:128205. doi: 10.1016/j.foodchem.2020.128205

18. Tamura M, Nagai T, Hidaka Y, Noda T, Yokoe M, Ogawa Y. Changes in histological tissue structure and textural characteristics of rice grain during cooking process. *Food Str.* (2014) 1:164–70. doi: 10.1016/j.foostr.2013.10.003

19. Li H, Lei N, Yan S, Gao M, Yang J, Wang J, et al. Molecular causes for the effect of cooking methods on rice stickiness: a mechanism explanation from the view of starch leaching. *Int J Biol Macromol.* (2019) 128:49–53. doi: 10.1016/j.ijbiomac.2019.01.113

20. Das T, Subramanian R, Chakkaravarthi A, Singh V, Ali SZ, Bordoloi PK. Energy conservation in domestic rice cooking. *J Food Eng.* (2006) 75:156–66. doi: 10.1016/j.jfoodeng.2005.04.005

21. Lakshmi S, Chakkaravarthi A, Subramanian R, Singh V. Energy consumption in microwave cooking of rice and its comparison with other domestic appliances. *J Food Eng.* (2007) 78:715–22. doi: 10.1016/j.jfoodeng.2005.11.011

22. Tamura M, Singh J, Kaur L, Ogawa Y. Impact of structural characteristics on starch digestibility of cooked rice. *Food Chem.* (2015) 191:91–7. doi: 10.1016/j.foodchem.2015.04.019

23. Zhang Q, Xia S, Li J, Zhang X, Yu J. Effect of moisture transfer on texture uniformity of cooked rice after heat preservation with electric rice cooker. *J Cereal Sci.* (2020) 91:102862. doi: 10.1016/j.jcs.2019.102862

24. Hemdane S, Jacobs PJ, Bosmans GM, Verspreet J, Delcour JA, Courtin CM. Study of biopolymer mobility and water dynamics in wheat bran using

time-domain  $^1\text{H}$  NMR relaxometry. *Food Chem.* (2017) 236:68–75. doi: 10.1016/j.foodchem.2017.01.020

25. Zhu L, Cheng L, Zhang H, Wang L, Qian H, Qi X, et al. Research on Migration path and structuring role of water in rice grain during soaking. *Food Hydrocoll.* (2019) 92:41–50. doi: 10.1016/j.foodhyd.2019.01.051

26. Association of Official Analytical Chemists [AOAC]. *Official Methods of Analysis*. 15th ed. Washington DC: AOAC (1990).

27. Pan T, Lin L, Zhang L, Zhang C, Liu Q, Wei C. Changes in kernel properties, in situ gelatinization, and physicochemical properties of waxy rice with inhibition of starch branching enzyme during cooking. *Int J Food Sci Tech.* (2019) 54:2780–91. doi: 10.1111/ijfs.14193

28. Wang L, Wang M, Guo M, Ye X, Ding T, Liu D. Numerical simulation of water absorption and swelling in dehulled barley grains during canned porridge cooking. *Processes* (2018) 6:230–42. doi: 10.3390/pr6110230

29. Liu T, Zhang B, Wang L, Zhao S, Qiao D, Zhang L, et al. Microwave reheating increases the resistant starch content in cooked rice with high water contents. *Int J Biol Macromol.* (2021) 184:804–11. doi: 10.1016/j.ijbiomac.2021.06.136

30. Englyst HN, Kingman SM, Cummings JH. Classification and measurement of nutritionally important starch fractions. *Eur J Clin Nutr.* (1992) 46:S33. doi: 10.1128/IAI.01649-06

31. Ogawa Y, Glenn GM, Orts WJ, Wood DF. Histological structures of cooked rice grain. *J Agric Food Chem.* (2003) 51:7019–23. doi: 10.1021/jf034758o

32. Bi S. *Research and Analyses on Influence of Heating Rate and Soaking Temperature on Qualities of Rice*. [Master's Thesis]. Wuxi: Jiangnan University (2020).

33. Tamura M, Kumagai C, Kaur L, Ogawa Y, Singh J. Cooking of short, medium and long-grain rice in limited and excess water: effects on microstructural characteristics and gastro-small intestinal starch digestion in vitro. *LWT.* (2021) 146:111379. doi: 10.1016/j.lwt.2021.111379

34. Wang L, Wang M, Lv R, Guo M, Ye X, Ding T, et al. Modelling the physical properties change of canned glutinous rice porridge during cooking. *RSC Adv.* (2019) 9:5521–9. doi: 10.1039/C8RA07790H

35. Li T, Tu C, Rui X, Gao Y, Li W, Wang K, et al. Study of water dynamics in the soaking, steaming, and solid-state fermentation of glutinous rice by  $^1\text{H}$ -Nmr: a novel monitoring approach. *J Agric Food Chem.* (2015) 63:3261–70. doi: 10.1021/acs.jafc.5b00769

36. Xu D, Hong Y, Gu Z, Cheng L, Li Z, Li C. Effect of high pressure steam on the eating quality of cooked rice. *LWT Food Sci Technol.* (2019) 104:100–8. doi: 10.1016/j.lwt.2019.01.043

37. Utrilla-Coello RG, Bello-Pérez LA, Vernon-Carter EJ, Rodriguez E, Alvarez-Ramirez J. Microstructure of retrograded starch: quantification from lacunarity analysis of Sem micrographs. *J Food Eng.* (2013) 116:775–81. doi: 10.1016/j.jfoodeng.2013.01.026

38. Sowbhagya CM, Ramesh BS, Bhattacharya KR. The relationship between cooked-rice texture and the physicochemical characteristics of rice. *J Cereal Sci.* (1987) 5:287–97. doi: 10.1016/S0733-5210(87)80029-2

39. Saleh M, Meullenet J-F. Broken rice kernels and the kinetics of rice hydration and texture during cooking. *J Sci Food Agric.* (2013) 93:1673–9. doi: 10.1002/jsfa.5948

40. Bello M, Tolaba MP, Aguerre RJ, Suarez C. Modeling water uptake in a cereal grain during soaking. *J Food Eng.* (2010) 97:95–100. doi: 10.1016/j.jfoodeng.2009.09.020

41. Li F, Guan X, Li C. Effects of degree of milling on the starch digestibility of cooked rice during (in Vitro) small intestine digestion. *Int J Biol Macromol.* (2021) 188:774–82. doi: 10.1016/j.ijbiomac.2021.08.079

42. Syahariza ZA, Sar S, Hasjim J, Tizzotti MJ, Gilbert RG. The importance of amylose and amylopectin fine structures for starch digestibility in cooked rice grains. *Food Chem.* (2013) 136:742–9. doi: 10.1016/j.foodchem.2012.08.053

43. Tamura M, Singh J, Kaur L, Ogawa Y. Impact of the degree of cooking on starch digestibility of rice – an in vitro study. *Food Chem.* (2016) 191:98–104. doi: 10.1016/j.foodchem.2015.03.127



## OPEN ACCESS

## EDITED BY

Hao Jiang,  
Northwest A&F University, China

## REVIEWED BY

Yiting Guo,  
Jiangsu University, China  
Di Zhao,  
Nanjing Agricultural University, China

## \*CORRESPONDENCE

Qingquan Fu  
fuqingquan@126.com  
Renlei Wang  
wrl@jssnu.edu.cn

## SPECIALTY SECTION

This article was submitted to  
Nutrition and Food Science  
Technology,  
a section of the journal  
Frontiers in Nutrition

RECEIVED 26 August 2022

ACCEPTED 31 October 2022

PUBLISHED 16 November 2022

## CITATION

Zhu X, Shi X, Liu S, Gu Y, Liu J, Fu Q  
and Wang R (2022) Physicochemical  
properties and gel-forming ability  
changes of duck myofibrillar protein  
induced by hydroxyl radical oxidizing  
systems. *Front. Nutr.* 9:1029116.  
doi: 10.3389/fnut.2022.1029116

## COPYRIGHT

© 2022 Zhu, Shi, Liu, Gu, Liu, Fu and  
Wang. This is an open-access article  
distributed under the terms of the  
Creative Commons Attribution License  
(CC BY). The use, distribution or  
reproduction in other forums is  
permitted, provided the original  
author(s) and the copyright owner(s)  
are credited and that the original  
publication in this journal is cited, in  
accordance with accepted academic  
practice. No use, distribution or  
reproduction is permitted which does  
not comply with these terms.

# Physicochemical properties and gel-forming ability changes of duck myofibrillar protein induced by hydroxyl radical oxidizing systems

Xueshen Zhu<sup>1</sup>, Xiandong Shi<sup>1,2</sup>, Shaohua Liu<sup>1</sup>, Ying Gu<sup>1</sup>,  
Junya Liu<sup>1</sup>, Qingquan Fu<sup>3\*</sup> and Renlei Wang<sup>1\*</sup>

<sup>1</sup>Key Laboratory of Biological Functional Molecules of Jiangsu Province, College of Life Science and Chemistry, Jiangsu Second Normal University, Nanjing, China, <sup>2</sup>School of Life Science, Nanjing Normal University, Nanjing, China, <sup>3</sup>School of Food Science, Nanjing Xiaozhuang University, Nanjing, China

This paper focuses on the changes of physicochemical properties and gel-forming ability of duck myofibrillar proteins (DMPs) induced using hydroxyl radical oxidizing systems. DMPs were firstly extracted and then oxidized at various H<sub>2</sub>O<sub>2</sub> concentrations (0, 4, 8, and 12 mmol/L) using Fenton reagent (Fe<sup>3+</sup>-Vc-H<sub>2</sub>O<sub>2</sub>) to generate hydroxyl radicals, and the effects of hydroxyl radical oxidation on the physicochemical changes and heat-induced gel-forming capacity of DMPs were analyzed. We observed obvious increases in the carbonyl content ( $p < 0.05$ ) and surface hydrophobicity of DMPs with increasing of H<sub>2</sub>O<sub>2</sub> concentrations (0–12 mmol/L). In contrast, the free thiol content ( $p < 0.05$ ) and water retention ability of DMPs decreased with increasing H<sub>2</sub>O<sub>2</sub> concentrations (0–12 mmol/L). These physicochemical changes suggested that high concentrations of hydroxyl radicals significantly altered the biochemical structure of DMPs, which was not conducive to the formation of a gel mesh structure. Furthermore, the gel properties were reduced based on the significant decrease in the water holding capacity ( $p < 0.05$ ) and increased transformation of immobilized water of the heat-induced gel to free water ( $p < 0.05$ ). With the increase of H<sub>2</sub>O<sub>2</sub> concentrations, secondary structure of proteins analysis results indicated  $\alpha$ -helix content decreased significantly ( $p < 0.05$ ), however, random coil content increased ( $p < 0.05$ ). And more cross-linked myosin heavy chains were detected at higher H<sub>2</sub>O<sub>2</sub> concentrations groups through immunoblot analysis ( $p < 0.05$ ). Therefore, as H<sub>2</sub>O<sub>2</sub> concentrations increased, the gel mesh structure became loose and porous, and the storage modulus and loss modulus values also decreased during heating. These results demonstrated that excessive oxidation led to explicit cross-linking of DMPs, which negatively affected the gel-forming ability of DMPs. Hence, when processing duck meat products, the oxidation level of meat gel products should be controlled, or suitable antioxidants should be added.

## KEYWORDS

duck myofibrillar proteins, hydroxyl radical, protein oxidation, gel-forming capacity, physicochemical changes

## Introduction

Myofibrillar proteins are the most abundant and important proteins in duck breast tissue, accounting for 50–60% of the total protein. A key functional property of these proteins is their ability to form heat-induced gels, which provide good texture and mouthfeel to meat products (1). Therefore, factors affecting these physicochemical properties, such as protein oxidation, must be identified. Reactive oxygen species, the main initiators of protein oxidation, can be generated during the manufacture of meat products (2). Protein oxidation includes all reactions that result in the removal of electrons from protein-binding sites, including free individual amino acids and peptides are oxidized (3). Protein oxidation may lead to modification of protein side chain groups, cross-linking and aggregation of protein macromolecules, altering the physicochemical properties of proteins to affect the color, texture, and taste of meat and meat products. In the past two decades, the biochemical and functional properties of myofibrillar proteins have been widely examined *in vitro* (4, 5). At increasing hydroxyl radical concentrations, the carbonyl value and surface hydrophobicity of myofibrillar proteins typically exhibit increasing trends, and the free thiol content in myofibrillar proteins shows a decreasing trend, indicating an increased degree of protein oxidation. Gel hardness, chewiness, and elastic modulus are significantly negatively correlated with the concentration of hydroxyl radicals (6). Recently, Bao et al. (7) reported that oxidation of porcine myofibrils leads to the loss of free sulfhydryl groups and histidine residues and the formation of myofibrillar protein carbonyl groups, eventually leading to the formation of large cross-linked fractions. However, other studies reported contrasting results, particularly regarding the effect of oxidation on gel properties. Previous studies indicated that within a certain range, disulfide cross-linking promoted stiffness to some extent because aggregation and denaturation of myofibrillar components may affect the properties of myofibrillar protein gels (8). Shen et al. (9) investigated the effect of oxidation on myofibrillar protein gel properties and their ability to bind specific species. Their results demonstrated that with increasing  $H_2O_2$  concentrations, DMPs tended to expose their internal hydrophobic amino acids, leading to enhanced aggregation and increased surface hydrophobicity. Li et al. (10) found that changes in the microstructure of myofibrillar protein gels caused by hydroxyl radical-induced oxidation altered the ability to form gels. Furthermore, Wang et al. (11) reported that hydrophobic interactions between protein molecules were significantly enhanced by oxidation, which was not conducive to formation of a gel network structure. Thus, protein oxidation does not always lead to a decrease in protein gel-forming properties and corresponding functional properties, and moderate protein oxidation may improve or enhance the functional properties of muscle proteins.

Duck meat and its products are widely consumed in southern China because of their high nutritional value, good taste, and low price. Numerous world-famous duck meat products have emerged, including roasts and salted ducks. However, the gelation properties of duck breast muscle remain unclear. Gelling properties depend on several intrinsic factors, including the meat species, muscle type, and fiber type (12). Researchers have used a hydroxyl radical system to simulate systematic muscle oxidation *in vitro* to better understand the mechanism underlying the effect of protein oxidation on meat gelation. The effects of hydroxyl radicals on the physicochemical susceptibility and gel properties of DMPs have not been evaluated in detail, in which further investigation is still needed. In this study, hydroxyl radicals were used to oxidize DMPs *in vitro*, the physicochemical properties and gel properties changes would be investigated aiming to provide new information for understanding the mechanism of protein oxidation in complex DMPs gel system.

## Materials and methods

### Sample and duck myofibrillar proteins preparation

Five duck carcasses were purchased from a local market in Lishui district, Nanjing, China. All chemicals were analytical grade. DMPs were extracted as described by Park et al. (13), with appropriate modifications. The pre-prepared duck breast was removed, thawed on ice for 30 min, and transferred to a 500 mL centrifuge bottle. The breast was homogenized in  $5 \times$  phosphate buffer I (pH 7.0, 100 mmol/L NaCl, 2 mmol/L  $MgCl_2$ , 1 mmol/L EGTA, 10 mmol/L  $K_2HPO_4$ ) for 3 min using a high-speed homogenizer (Ultra Turrax, IKA, Germany) and centrifuged at  $4^\circ C$ ,  $5,000 \times g$  for 10 min; Supernatant was then discarded. The above steps were repeated three times. During this process, the sample was filtered through a double layer of gauze to remove excess connective tissue. Subsequently, homogenization was performed in  $5 \times$  phosphate buffer II (125 mmol/L NaCl, 2.5 mmol/L  $MgCl_2$ , 1.25 mmol/L EGTA, 12.5 mmol/L  $K_2HPO_4$  containing 1% Triton X-100), the mixture was centrifuged at  $4^\circ C$ ,  $5,000 \times g$  for 10 min, and the resulting supernatant was discarded to remove membrane proteins. This process was repeated three times. Finally, washing was performed with  $4 \times 0.1$  mol/L NaCl, followed by centrifugation at  $4^\circ C$ ,  $5,000 \times g$  for 10 min, This process was repeated three times to obtain pure DMPs precipitates. The proteins were placed in a small beaker, sealed, and stored at  $4^\circ C$  until analysis.

## Hydroxyl radical-generation system and physicochemical properties of proteins

### Oxidation of duck myofibrillar proteins

The protein precipitate was dissolved in phosphate buffer (0.6 mol/L NaCl, 10 mmol/L K<sub>2</sub>HPO<sub>4</sub>, pH 7.0). The protein concentration was determined using the Biuret method and was adjusted to 33 mg/mL. Protein solutions were then treated with Fenton's reagent [containing of 0.01 mmol/L ferric trichloride (FeCl<sub>3</sub>), 0.1 mmol/L ascorbic acid (V<sub>C</sub>), and different concentrations of hydrogen peroxide (H<sub>2</sub>O<sub>2</sub>; 0, 4, 8, and 12 mmol/L)]. After oxidation for 24 h at 4°C, 40 µL 500 mmol/L EDTA was added to terminate the reaction. Phosphate buffer (30 mL; 0.1 mol/L NaCl containing 10 mmol/L K<sub>2</sub>HPO<sub>4</sub>, pH 7.0) was added to wash precipitated proteins, followed by centrifugation at 4°C, 10,000 × *g* for 10 min. This process was repeated twice to obtain the final oxidized protein precipitate.

### Determination of carbonyl and free thiol contents

The carbonyl content was determined as described by Soglia et al. (14), with appropriate modifications. Briefly, the protein precipitate obtained *via* oxidation termination was dissolved in phosphate buffer (0.6 mol/L NaCl containing 10 mmol/L K<sub>2</sub>HPO<sub>4</sub>, pH 7.0). The absorbance of the group treated with 2,4-dinitrophenylhydrazine was measured at 280 and 370 nm. The carbonyl content was calculated using 22,000 L/(mol·cm) as the molar extinction coefficient for conversion and expressed in units of nmol/mg protein, as shown in Equation (1). The average value was obtained by repeating three times for each treated samples.

$$\text{Carbonyl content} = \frac{[A_{370} - A_{370(\text{blank})}]}{22000 \times [A_{280} - [A_{370} - A_{370(\text{blank})}] \times 0.43]} \times 10^6 [\text{nmol/mg protein}] \quad (1)$$

The free thiol group content was determined using Ellman's 5,5'-dithiobis-(2-nitrobenzoic acid) colorimetric method according to the method described by Bao et al. (15). Briefly, the protein precipitate was dissolved by adding 0.6 mol/L NaCl containing 10 mmol/L K<sub>2</sub>HPO<sub>4</sub> (pH 7.0), and the protein concentration was adjusted to 5 mg/mL. 5,5'-Dithiobis-(2-nitrobenzoic acid) reacted with the thiol group and was used for subsequent absorbance detection at 412 nm. The thiol content was calculated using 14,150 L/(mol·cm) as the molar extinction coefficient for conversion and expressed in units of nmol/mg protein, as shown in Equation (2) with 3 repetitions for each

treated group.

$$\text{Free thiol group content} = \frac{[A_{412} - A_{412(\text{blank})}]}{14150 \times A_{280}} \times 10^6 [\text{nmol/mg protein}] \quad (2)$$

### Surface hydrophobicity measurement

Surface hydrophobicity was determined as described by Chelh et al. (16), with some modifications. The oxidized protein precipitate was dissolved in phosphate buffer (0.6 mol/L NaCl containing 10 mmol/L K<sub>2</sub>HPO<sub>4</sub>, pH 7.0), and the protein concentration was adjusted to 5 mg/mL. Briefly, 200 µL of bromophenol blue was added to 1 mL of protein solution, and absorbance was measured at 595 nm. The surface hydrophobicity was calculated using Equation (3) with 3 repetitions for each treated group.

$$\text{Surface hydrophobicity} = \frac{[A_{595(\text{blank})} - A_{595}]}{A_{595(\text{blank})}} \times 200 [\mu\text{g}](3)$$

### Water retention ability of DMPs

The oxidized protein precipitate was weighed (recorded as *m*<sub>1</sub>) and transferred to an empty centrifuge tube (recorded as *m*<sub>2</sub>). Samples were heated at 80°C for 2 h, then cooled to atmospheric temperature, and weighed again (recorded as *m*<sub>3</sub>). The water retention ability of the oxidized protein precipitate sample was calculated according to Equation (4). The average value was obtained by repeating three times for each treated samples.

$$\text{Water retention ability} = \frac{m_3 - m_2}{m_1} \times 100\% \quad (4)$$

### SDS-PAGE and myosin heavy chain immunoblot

Sample preparation and electrophoresis were conducted as described by Laemmli (17), with appropriate modifications. The oxidized protein precipitate obtained above was dissolved in phosphate buffer (0.6 mol/L NaCl containing 10 mmol/L K<sub>2</sub>HPO<sub>4</sub>, pH 7.0), and the concentration of the sample was adjusted to 2 mg/mL. The protein solution was mixed with sample buffer (NuPAGE™, Invitrogen, Carlsbad, CA, USA) as well as dithiothreitol (DTT) or without DTT and heated at 100°C for 2 min. After electrophoresis, the gel was stained with Coomassie brilliant blue G-250.

After electrophoresis, immunoblotting was performed using a Mini Cell SureLock equipped with an XCell II Blot Module (Invitrogen). The peptides were transferred to a cellulose acetate membrane, and the membrane was incubated with myosin heavy chain (MHC) rabbit polyclonal antibody (Beyotime,



Shanghai, China). The membrane was washed and incubated with conjugated secondary antibody, alkaline phosphatase-labeled goat anti-rabbit IgG (H+L) (Beyotime), at 20°C for 1 h. Finally, a BCIP/NBT alkaline phosphatase color development kit (Beyotime) was used to develop the blots. Images were then photoed for analysis.

## Gelation and gel-forming ability parameter measurements

### Preparation of duck myofibrillar proteins gel

A heat-induced gel formed from oxidized DMPs was prepared as follows. The oxidized protein precipitate was dissolved in phosphate buffer (0.6 mol/L NaCl containing 10 mmol/L  $K_2HPO_4$ , pH 7.0), adjusted to 30 mg/mL, heated at 85°C for 45 min, cooled in ice water, and then placed at 4°C overnight until use.

### Gel strength measurements

The strength of the DMPs gel was determined based on the method reported by Zhu et al. (18) using a texture analyzer (TA-XT plus Plaser, Stable Micro Systems, Godalming, UK) with a p/5 probe. The samples were subjected to a double compression cycle at a probe depth of 5 mm, pre-test rate of 0.5 mm/s, test rate of 0.5 mm/s, and post-test rate of 0.5 mm/s. Three parallel tests were performed for each treatment.

### Dynamic rheological analysis

Dynamic rheological tests of the oxidized DMPs solution were performed using a rheometer (MCR-301, Anton Paar, Graz, Austria) in oscillatory mode. The oxidized protein precipitate was dissolved in 0.6 mol/L NaCl containing 10 mmol/L  $K_2HPO_4$  (pH 7.0) and adjusted to 30 mg/mL. The instrument was initialized prior to use. The rheological parameters were as follows: selected fixture: 50 mm plate, gap: 1 mm, scan range: 25–80°C, temperature increase rate: 2°C/min, hold at 80°C for 5 min, cool at 5°C/min, oscillation frequency: 0.1 Hz, strain: 2%. Changes in the storage modulus ( $G'$ ) and loss modulus ( $G''$ ) during temperature scanning were recorded.

### Water holding capacity and low-field nuclear magnetic resonance measurements

The water-holding capacity (WHC) of the DMPs gels was determined using the centrifugation method described by Salvador et al. (19). The nuclear magnetic resonance (NMR) spin relaxation time ( $T_2$ ) was determined as reported by Gravelle et al. (20) using an NMR analyzer (NMI20-040H-I, Niumag Electric Co., Shanghai, China) with appropriate modifications. The conditions were set as follows: resonance frequency, 40

MHz; sampling number, 8; wait time, 2,000 ms; number of echoes, 9,000; scan range, 0–10,000 ms; each treatment group was measured three times in parallel. The data were inverted in batches using the data query option.

### Protein secondary structure content analysis

The secondary structure of the DMPs gels was determined as described by Chen et al. (21) using a Labram HR800 spectrometer (Horiba Jobi Yvon S.A.S., Longjumeau, France) with a 532 nm argon ion laser and 600 mm grating. The conditions were as follows: scan range of the raman spectra: 400–3,600  $cm^{-1}$  with a resolution of 1  $cm^{-1}$ , an acquisition time of 30 s, and a cumulative number of acquisitions: 2. The spectra were standardized with the phenylalanine band at 1,003  $cm^{-1}$  using LabSpec version 5 (Horiba Jobi Yvon, Longjumeau, France). Secondary structure content was calculated as described by Alix et al. (22) according to changes in the amide I band with 3 repetitions for each treated group.

### Microstructure analysis

The microstructure of the oxidized DMPs gels was determined using a Hitachi S-3000N scanning electron microscope (Tokyo, Japan) at an accelerating voltage of 20 kV. Briefly, the gels were cut to  $0.5 \times 0.5 \times 0.2$  cm in size, fixed in glutaraldehyde at a concentration of 4% for 24 h at 4°C, and washed three times with phosphate buffer for 10 min each time. The samples were dehydrated in a gradient of 50, 70, 80, and 90% ethanol for 15 min at each concentration and in 100% ethanol for 30 min. The samples were taped to the sample table, plated with a 10 nm gold film on the observation surface by ion sputtering, evaluated using scanning electron microscopy to determine the microstructure of the DMPs gels, and photographed.

### Statistical analysis

Data were processed using SPSS software (version 20.0, SPSS, Inc., Chicago, IL, USA) and subjected to one-way analysis of variance with Duncan's multiple range test for statistical analysis.

## Results and discussion

### Effects of oxidation on physicochemical changes

The carbonyl content can be used as an indicator of protein oxidation (23). As shown in Figure 1A, following treatment with  $H_2O_2$ , the carbonyl content in DMPs varied from 5.45 to 9.21 nmol/mg protein. Furthermore, with increases



in the hydroxyl radical strength, the DMPs carbonyl content increased significantly, indicating that hydroxyl radicals had dose-dependent effects on the carbonyl content from 0 to 12 mmol/L  $\text{H}_2\text{O}_2$ . The amino groups of DMPs with  $-\text{NH}-$  or  $-\text{NH}_2$  on the side chain are very sensitive to  $\cdot\text{OH}$  and were easily converted into carbonyl groups through oxidative deamination reactions (24, 25).

As shown in Figure 1B, the content of free thiol groups decreased significantly ( $p < 0.05$ ) with increasing  $\text{H}_2\text{O}_2$  concentrations and decreased to the minimum value of 63.24 nmol/mg protein when  $\text{H}_2\text{O}_2$  reached 12 mmol/L compared to the blank group, indicating that protein oxidation had occurred. The SH content of the blank group was 87.16 nmol/mg protein, which was similar to that of porcine myofibrillar proteins (1). The reason for the significant decrease in the content of the free thiol group might be related to the fact that thiol residues in sulfhydryl-containing amino acids are extremely easily oxidized, and hydroxyl radicals react with free thiol groups and eventually generate disulfide bonds. Alternatively, protein sulfhydryl groups undergo complex changes following the oxidation of hydroxyl radicals to generate reversible or irreversible oxidation products (26). Myosin is rich in SH groups that can be readily converted to disulfide linkages upon oxidative stress (27). Therefore, myosin may form disulfide bonds following oxidation by hydroxyl radicals as a significant decrease in the content of free thiol groups was observed in our study (28).

As shown in Figure 1C, the surface hydrophobicity index was 48.19  $\mu\text{g}$  in the absence of hydroxyl radicals. As  $\text{H}_2\text{O}_2$  concentrations increased from 0 to 12 mmol/L, the surface hydrophobicity of the DMPs increased significantly ( $p < 0.05$ ) and reached a maximum value of 87.13  $\mu\text{g}$  when the  $\text{H}_2\text{O}_2$  concentrations was 12 mmol/L. This result was significantly different from that in the blank group ( $p < 0.05$ ), suggesting that oxidation at high concentrations induced further protein unfolding. These results agree with those reported previously, protein unfolding and loss of MHC of porcine myofibrillar proteins occurred continuously with increasing  $\text{H}_2\text{O}_2$  concentrations (13). In summary, a higher content of oxidation radicals results in more denaturation of partial myofibrillar proteins, leading to more unfolded spatial conformational changes and exposure of a larger number of hydrophobic side chain amino acid residues to the polar water environment during oxidation (29). Oxidative damage may have induced partial unfolding of DMPs, thereby exposing hydrophobic amino acids that are normally buried inside protein molecules (30). This speculation agrees with the finding of Li et al. (31), who also observed that oxidation enhanced the surface hydrophobicity of porcine myofibrillar proteins.

Figure 1D showed that the water retention ability of the DMPs decreased with increasing  $\text{H}_2\text{O}_2$  concentrations ( $p < 0.05$ ). In the absence of hydroxyl radicals, the water retention

ability of the DMPs was 67.33%, which decreased markedly to 52.33% following treatment with 12 mmol/L  $\text{H}_2\text{O}_2$  ( $p < 0.05$ ). Water loss was related to the influence of the intact myofibril structure. A possible explanation for the significant decrease in the water retention ability is that under attack by a high concentration of hydroxyl radicals, some protein aggregates with larger molecular weight among DMPs through disulfide bonds, leading to structural damage and a reduced ability to retain water molecules. This speculation is consistent with the electrophoretic results as described in section Myofibril protein profiles below. Protein oxidation in meat alters has been suggested to alter its electronic arrangement, thereby affecting the chemical interaction between myofibrillar proteins and water molecules (30). Generally, the effect of protein oxidation on cross-linking and aggregation is among the most important factors influencing the water retention ability (32).

## Myofibril protein profiles

SDS-PAGE was performed to detect oxidation-induced covalent aggregation of the DMPs. The samples were prepared with or without DTT to determine the involvement of disulfide bonds in aggregation. As shown in Figure 2A, protein bands were observed at approximately 220, 45, and 22 kDa, corresponding to MHC, actin, and myosin light chain, respectively (13). The SDS-PAGE patterns did not reveal major differences in the protein composition between samples. However, the intensity of MHC at 220 kDa appeared to be much weaker in the 12 mmol/L-treated group than in the blank group, which might reflect a decrease in the solubility of myosin over time as a result of protein cross-linking, as previously suggested (33, 34).

In the absence of DTT, DMPs were oxidized, and the intensity of the myosin and actin bands decreased slightly, whereas more cross-linked polymers appeared in the upper layer of the sampling well. These results revealed that oxidation by high concentrations of hydroxyl radicals causes amino acid side-chain groups within the protein or those on different peptide chains to aggregate. The formation of protein aggregates increased the molecular weight of proteins, causing the protein to remain in the loading gel (15). The large reduction in protein aggregates at the top of the gel in the presence of DTT indicated that the aggregates were formed through disulfide bonds oxidized by SH with MHC, which is consistent with the western blotting results (Figure 2B) and agrees with those of a previous study showing that MHC is cross-linked through disulfide bonds during oxidation (35). Shen et al. (9) also reported that porcine MHC,  $\alpha$ -actinin, and actin participate in aggregate formation after oxidation. However, myosin fragmentation was not observed under the present oxidative conditions (36), possibly because lower concentrations of  $\text{H}_2\text{O}_2$  were used in the present study (0–12 mmol/L). Figures 2A,B clearly showed

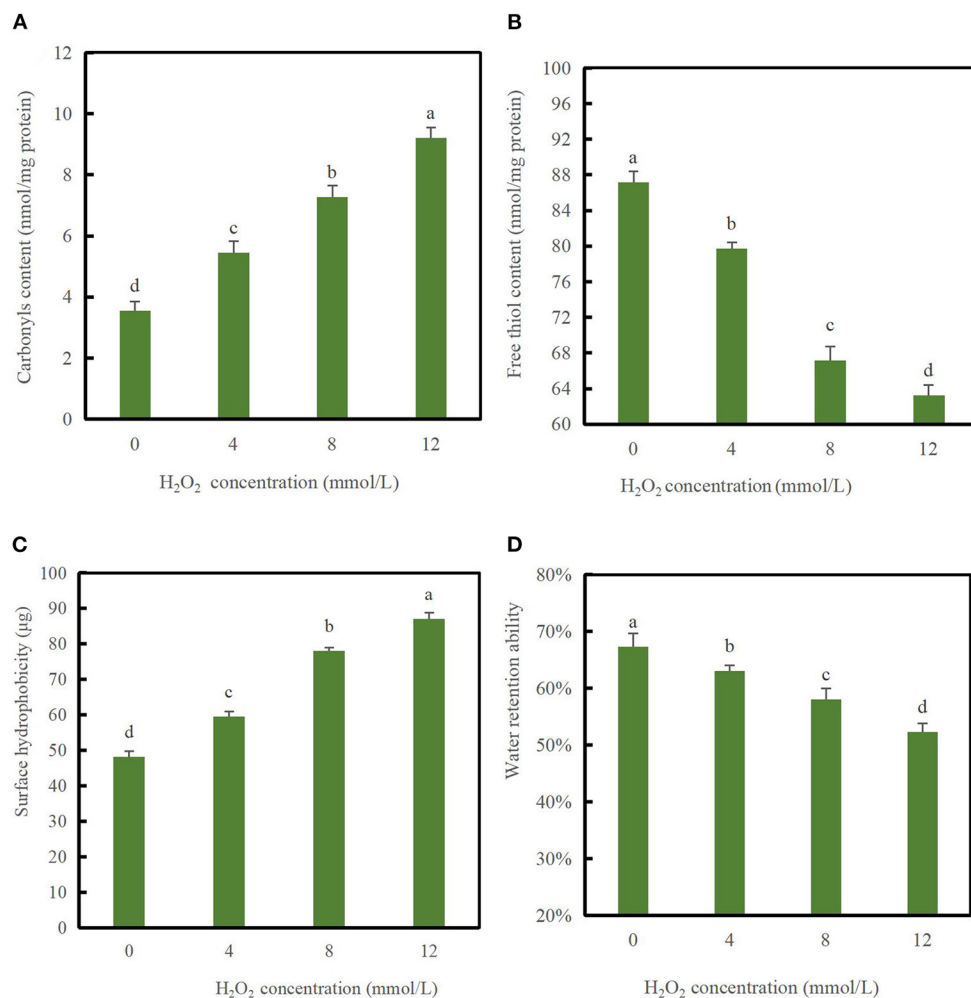


FIGURE 1

Changes in carbonyl values (A), free thiol content (B), surface hydrophobicity (C), and water retention ability (D) of duck myofibrillar proteins (DMPs) treated with various hydroxyl radical levels ( $\text{H}_2\text{O}_2$  concentrations: 0, 4, 8, 12 mmol/L). Different lowercase letters (a–d) indicate significant differences between the treated and control groups ( $p < 0.05$ ).

that after the addition of DTT, protein aggregates remained at the top of the gel, indicating that protein-protein cross-linking also occurred *via* other non-disulfide covalent bonds, such as Tyr-Tyr and carbonyl- $\text{NH}_2$  interactions (37).

## Gel properties analysis

Gel strength is a good indicator of the structural integrity of proteins and their ability to form a gel mesh. The process of forming a gel mesh by thermal induction of DMPs involves denaturation of proteins by increased temperature, mutual agglutination between proteins, and mutual cross-linking, each of which affects the properties of the gel (12). As shown in Figure 3A, the gel strength decreased significantly ( $p <$

0.05) with increasing concentrations of  $\text{H}_2\text{O}_2$ . For example, when the hydroxyl radical concentration reached 12 mmol/L, the gel strength decreased to a minimum value of 14.19 g, which was 33.9% lower than that of the blank group ( $p < 0.05$ ). This result indicates that the textural properties of DMPs gels decreased after oxidation with hydroxyl radicals, and the significant decrease in gel strength was likely due to cross-linking of proteins caused by oxidation, which disrupted the conformation and was not conducive to the formation of an ordered gel mesh. This was further supported by the continuous loss of MHC in the aforementioned SDS-PAGE profile results, which is consistent with the gel microstructure results discussed below. Notably, a previous study demonstrated that the texture parameters of chicken DMPs gel from myofibrillar protein treated with 0–10 mmol/L  $\text{H}_2\text{O}_2$  could

not be measured; however, those of duck meat gel could be measured. This result may be related to differences in the animal species. Generally, excessive disulfide cross-links in oxidized

myofibrillar proteins may hinder the ordered interactions of reactive functional groups and cause the reduction of hydrogen bonds in the protein matrix, which can eventually decrease the degree of association between proteins and proteins or water molecules, thus inhibiting the formation of a stable three-dimensional network structure (38). Notably, oxidation modification by hydroxyl radicals is also not favorable for gel whiteness. Compared with the blank group, the whiteness of the 12 mmol/L group decreased by 19.7% (data not shown), indicating the occurrence of structural changes that eventually led to decreased light scattering and thus a decreased gel whiteness value.

The WHC is a quantitative indicator of water retained within the structure of the protein gel network and can reflect the spatial structure of protein gels (39). As shown in Figure 3B, the gel WHC significantly decreased with increasing  $H_2O_2$  concentrations ( $p < 0.05$ ). At hydroxyl radical concentrations of 0, 4, 8, and 12 mmol/L, the gel WHC values were 67.33, 63.02, 58.04, and 52.33%, respectively. When the  $H_2O_2$  concentration reached 12 mmol/L, the WHC of the gels decreased by 22.28% compared to that of the blank group. Oxidation modification caused by hydroxyl radicals induced DMPs cross-linking and made the proteins less likely to form a gel mesh structure, decreasing the capillary effect and making it difficult to retain water (1). Xiong et al. (40) reported that the WHC of myofibrillar protein gels was not affected by oxidation at relatively low  $H_2O_2$  concentrations ( $\leq 0.5$  mmol/L), whereas the WHC markedly decreased upon oxidation at high  $H_2O_2$  concentrations. In addition, Li et al. (38) confirmed that the WHC of common carp myofibrillar protein gels was reduced after  $H_2O_2$ -mediated oxidation, which was consistent with the gel status and microstructure changes.

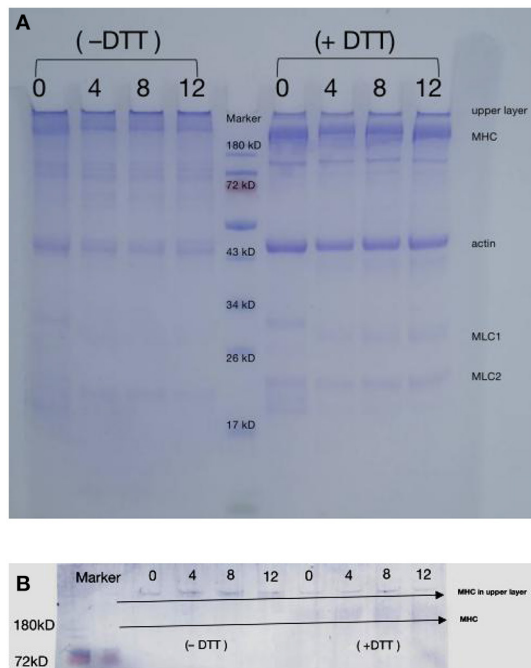


**FIGURE 2**  
Changes in SDS-PAGE patterns (A) and myosin heavy chain immunoblot (B) of duck myofibrillar proteins treated with various hydroxyl radical levels ( $H_2O_2$  concentrations: 0, 4, 8, 12 mmol/L). DTT means treated sample without dithiothreitol (DTT); + DTT means treated sample with dithiothreitol (DTT).

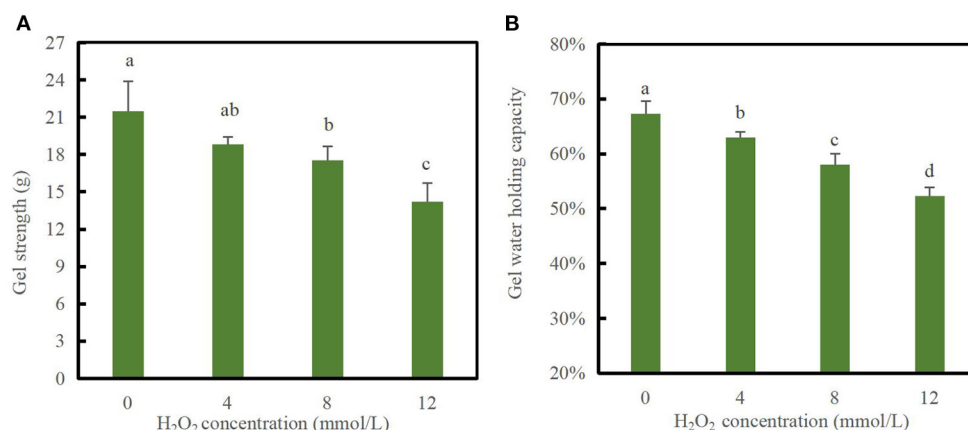


**FIGURE 3**  
Changes in gel strength (A) and water-holding capacity (B) of duck myofibrillar protein (DMPs) gels pretreated with various hydroxyl radical levels ( $H_2O_2$  concentrations: 0, 4, 8, 12 mmol/L). Different lowercase letters (a–d) indicate significant differences between the treatment and control groups ( $p < 0.05$ ).

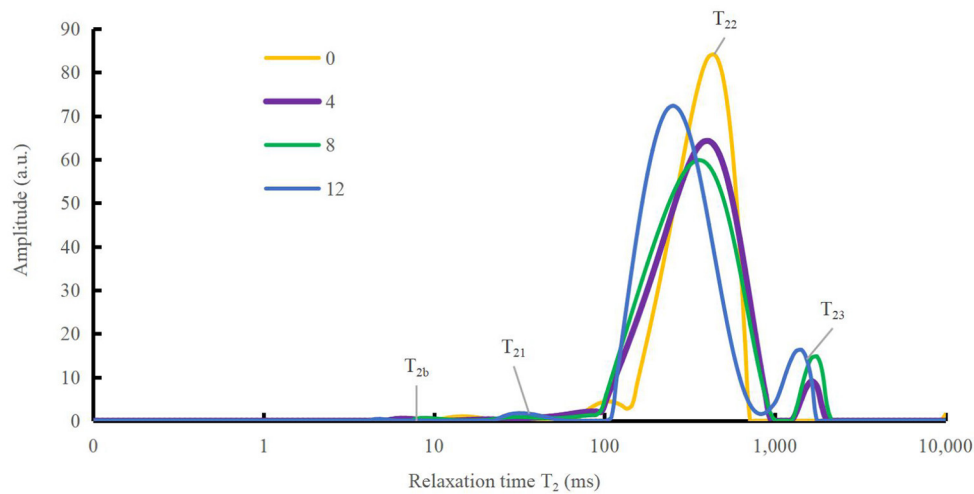


FIGURE 4

Variation in spin relaxation time ( $T_2$ ) of water molecules in duck myofibrillar proteins (DMPs) gels pretreated with various hydroxyl radical levels ( $H_2O_2$  concentrations: 0, 4, 8, 12 mmol/L).  $T_{2b}$ ,  $T_{21}$ ,  $T_{22}$ , and  $T_{23}$  denote bound, immobilized, moderately immobilized, and free water, respectively.

**TABLE 1** Changes in peak relaxation times and the ratio of peak areas of water molecules in duck myofibrillar proteins (DMPs) gels pretreated with various hydroxyl radicals levels ( $H_2O_2$  concentrations: 0, 4, 8, 12 mmol/L).

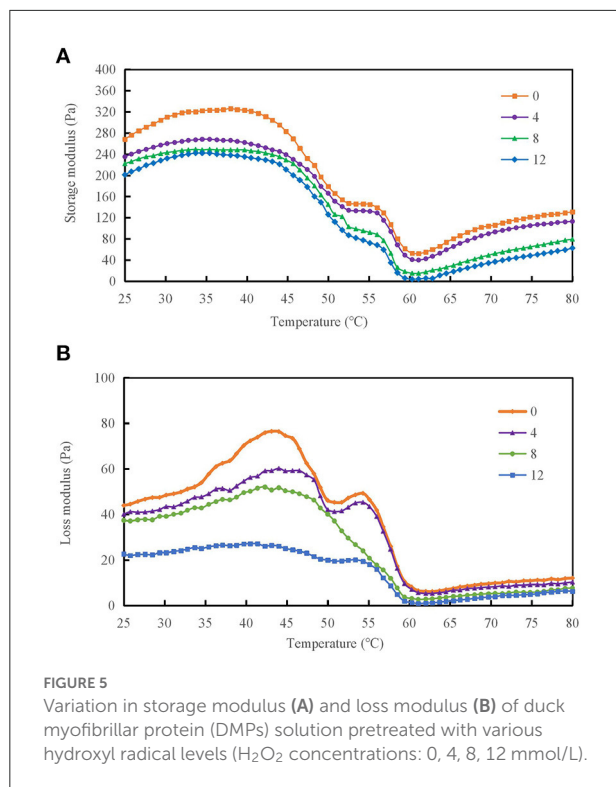
$H_2O_2$ concentration/mmol/L	0	4	8	12
$T_{2b}$ /ms	$15.33^a \pm 1.00$	$6.39^b \pm 0.03$	$8.74^b \pm 0.39$	$6.35^b \pm 2.16$
$T_{21}$ /ms	$99.31^a \pm 4.29$	$16.41^b \pm 3.05$	$27.44^b \pm 2.83$	$20.33^b \pm 7.86$
$T_{22}$ /ms	$423.65^a \pm 22.78$	$380.00^a \pm 42.80$	$391.25^a \pm 48.32$	$263.08^b \pm 15.17$
$T_{23}$ /ms	$9841.33^a \pm 224.40$	$1611.50^{bc} \pm 46.92$	$1813.81^b \pm 71.98$	$1331.45^c \pm 141.44$
$P_{2b}$ /%	$0.47^a \pm 0.22$	$0.31^a \pm 0.16$	$0.44^a \pm 0.18$	$0.38^a \pm 0.37$
$P_{21}$ /%	$2.04^a \pm 1.11$	$1.07^a \pm 1.26$	$1.37^a \pm 0.91$	$1.34^a \pm 0.29$
$P_{22}$ /%	$97.31^a \pm 1.25$	$95.70^{ab} \pm 1.62$	$92.74^{bc} \pm 1.46$	$90.51^c \pm 0.87$
$P_{23}$ /%	$0.18^d \pm 0.08$	$2.92^c \pm 0.21$	$5.43^b \pm 0.37$	$7.78^a \pm 0.20$

Different lowercase letters (a–d) between the treatment and control groups indicate significant differences ( $p < 0.05$ );  $T_{2b}$ ,  $T_{21}$ ,  $T_{22}$ , and  $T_{23}$  indicate the capping relaxation times of water molecules in different states of the gel.  $P_{2b}$ ,  $P_{21}$ ,  $P_{22}$ , and  $P_{23}$  indicate the proportions of peak areas of water molecules in different gels.

## Low-field nuclear magnetic resonance analysis

To better understand the mechanism of how oxidation affects water-holding properties, the water status of the DMPs was determined, as shown in Figure 4. The distribution and movement of water in the DMPs gel system can be expressed using the NMR proton spin relaxation time ( $T_2$ ). Han et al. (41) detected four peaks in the fitted NMR relaxation spectrum of myofibrillar protein gels, which correspond to four states of water (bound water, immobilized water, moderately immobilized water, and free water), and the second and third peaks are commonly treated as immobilized water (42). The peak relaxation times of the DMPs gels after adding hydroxyl radicals are listed in Table 1. A shorter peak relaxation time

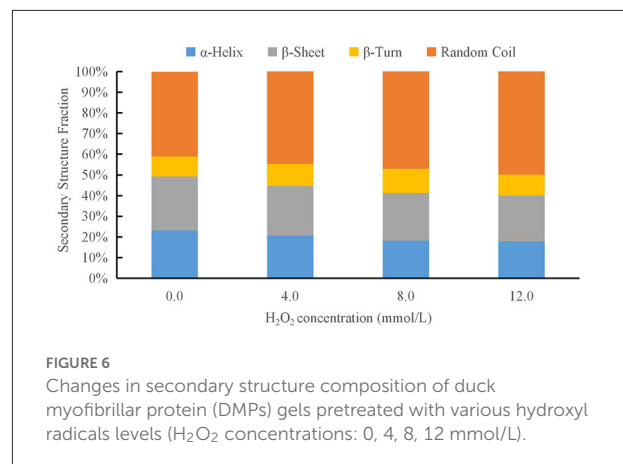
indicates that water is bound more tightly.  $T_{22}$  indicates immobilized water with a peak relaxation time between 100 and 500 ms.  $T_{23}$  indicates free water with a peak relaxation time after 500 ms. The effect of increasing the hydroxyl radical concentration did not significantly affect the peak relaxation times of  $T_{2b}$ ,  $T_{21}$ , and  $T_{22}$ . However, the effect on the peak relaxation time of  $T_{23}$  was significant ( $p < 0.05$ ). As shown in Table 1, with increasing concentrations of hydroxyl radicals, the effect on the ratio of the peak areas of  $T_{22}$  and  $T_{23}$  was more obvious and significant ( $p < 0.05$ ). The peak area ratio of  $T_{22}$  decreased to 90.51% and that of  $T_{23}$  increased to 7.78% when the concentration of hydroxyl radicals reached 12 mmol/L compared to those in the blank group. This result indicates that the amount of immobilized water in the gel decreased, and the amount of free water in the gel increased with increasing  $H_2O_2$



concentrations. This result may have been obtained because the oxidation of DMPs by hydroxyl radicals is not conducive to the formation of a gel mesh structure (8), as the structure cannot lock the distribution of water during thermal induction, causing some immobilized water to dissociate from the substrate to free water (10). These results correspond to recent findings by Zhang et al. (43), who observed that as the degree of oxidation increased, more protein hydrophobic groups unfolded. This condition possibly avianized the binding ability of the proteins to water, in turn causing some of the immobilized water to transform into free water.

## Rheological property analysis

Rheological properties were measured for protein-protein interactions and the formation of gel mesh during the formation of gels from protein solutions (12). The storage modulus ( $G'$ ) and loss modulus ( $G''$ ) of the DMPs solution are important parameters of the rheological properties. Figure 5A shows that as the temperature increased, the  $G'$  of the DMPs solution increased when different concentrations of H<sub>2</sub>O<sub>2</sub> were added. When the temperature was increased to 38°C, the  $\alpha$ -helix of the myosin head coalesced and initially formed a gel mesh structure, and  $G'$  reached a maximum value. When the temperature was increased to 62°C, because of the breakage of myosin tail coalescence, the mobility of DMPs increased, and  $G'$  decreased



to the minimum value. When the temperature was further increased to 80°C, most of the myosin structures were stretched and coalescence occurred, leading to the formation of an ordered gel mesh structure, and  $G'$  continued to slowly increase. The final  $G'$  value decreased by 25.7% in the 12 mmol/L-treated group compared to the blank group. Therefore, oxidation is detrimental to gel formation in the reticular structure (37). Generally,  $G''$  reflects viscous characteristics of DMPs. As the temperature was increased, the  $G''$  of the DMPs solution also increased when different concentrations of hydroxyl radicals were added. When the temperature was increased to 43°C,  $G''$  reached a maximum value because of the coalescence of the  $\alpha$ -helix of the myosin head and the initial formation of the gel mesh structure. When the temperature was increased to 63°C,  $G''$  decreased to the minimum value because of aggregation of the myosin tail. When the temperature was further increased to 80°C,  $G''$  continued to increase slowly because of the stretching of most myosin structures and coalescence, leading to the formation of an orderly gel mesh structure (44). As shown in Figure 5B, the final  $G''$  of the warming process significantly decreased by 65.7% when the hydroxyl radical concentration was 12 mmol/L compared to the value in the blank group ( $p < 0.05$ ). As the concentration of hydroxyl radicals increased, myosin and actin in DMPs became severely cross-linked, which was not conducive to gel meshwork formation; therefore,  $G''$  was also reduced.

## Analysis of the secondary structure

The raman spectra of proteins include discrete bands that represent the vibrational modes of the peptide backbone and its side chains. The spectral position, intensity, and polarization of the raman bands are sensitive to protein secondary, tertiary, and quaternary structures, as well as side-chain orientation and the local environment (45). The secondary structure of the



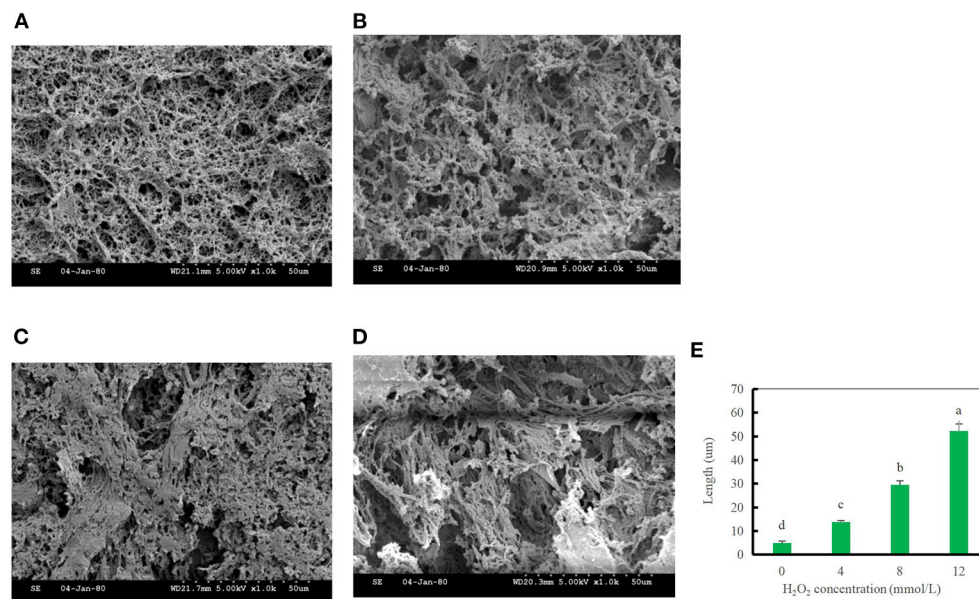


**FIGURE 7**  
Changes in the gel microstructure of duck myofibrillar protein (DMPs) gels pretreated with 0 mmol/L (A), 4 mmol/L (B), 8 mmol/L (C), 12 mmol/L  $H_2O_2$  (D), and changes in the pore diameter of DMPs gels (E) pretreated with various hydroxyl radicals levels.

proteins was evaluated *via* Raman spectroscopy using the amide I ( $1,600\text{--}1,700\text{ cm}^{-1}$ ) band. Four different protein secondary structures were present in the control amide region, including  $\alpha$ -helices, random coils,  $\beta$ -sheets, and  $\beta$ -turns, corresponding to the ranges  $1,640\text{--}1,659$ ,  $1,660\text{--}1,669$ ,  $1,670\text{--}1,679$ , and  $1,680\text{--}1,689\text{ cm}^{-1}$ , respectively (44). The effect of different hydroxyl radical concentrations on the DMPs gel conformation was analyzed using Raman spectroscopy, as shown in Figure 6. There were significant differences in the composition of the DMPs secondary structures treated with different concentrations of hydroxyl radicals. As the  $H_2O_2$  concentration was increased, the percentage of  $\alpha$ -helix area decreased, whereas the percentage of random coil area increased, and the  $\beta$ -sheet and  $\beta$ -turn remained relatively stable. The  $\alpha$ -helix structure is mainly maintained by hydrogen bonds within the protein, and the hydroxyl radical attacks the amino group in the protein, which disrupts hydrogen bonds within the protein and eventually leads to a reduction in the  $\alpha$ -helix structure, unfolding of the protein, and a gradual shift in protein structure from ordered to disordered (46). A previous study showed similar results, with an increase in myofibrillar protein aggregation. However, although the  $\alpha$ -helix content decreased, the  $\beta$ -sheet content increased after oxidation (10). The decrease in  $\alpha$ -helix content may, in turn, catalyze random coil transformation (21). Conversion of the secondary structure of DMPs caused by oxidation can lead to the unfolding of the myofibrillar protein structure, further enhancing the protein-protein interaction and thus affecting the gel properties (47).

## Microstructure analysis

The gel microstructure reflects the relationship between the gel properties and structure. In the blank group, myosin and actin rapidly stretched and coalesced to form a more uniform gel mesh structure. With increasing hydroxyl radical concentrations, the number of cavities in the gel decreased, and the mesh structure gradually changed from a uniform and tightly ordered to randomly distributed, loose, and porous. This result indicates that after oxidation modification by hydroxyl radicals, DMPs are not conducive to the formation of the gel mesh structure, as shown in Figure 7, which also explains the decrease in the WHC after oxidation at high concentrations of hydroxyl radicals (46). The diameter of the gel pores was significantly lower in the blank group than in the treated group, particularly when the hydroxyl radical concentration reached 12 mmol/L (Figure 7E). Oxidation of hydroxyl radicals alters the gel microstructure, possibly because hydroxyl radicals induce myosin and actin to cross-link in advance, as most of the myosin and actin are involved in forming the gel meshwork during thermally induced gel formation. It is also possible that the oxidation of high concentrations of hydroxyl radicals induced severe denaturation of the proteins, which disrupted the spatial conformation of the proteins and thus was not conducive to the formation of a gel meshwork, resulting in a disorganized, loose, and porous gel structure (13). This result was consistent with our previous finding of the gel strength.

## Conclusion

Oxidation by high concentrations of hydroxyl radicals causes changes in the physicochemical structure of DMPs. In addition, a greater degree of oxidation leads to more obvious changes in structural indices, combined with more cross-linking of proteins and the production of protein aggregation with higher molecular weights. Importantly, protein oxidation caused by hydroxyl radicals may not improve the gel properties, WHC, water status and distribution, or gel-forming capacity of DMPs. Therefore, the oxidation level of meat gel products should be carefully controlled during the handling, processing, and transportation of duck gel products. Further studies are needed to explore whether the stability of the gel properties of duck meat products can be improved using appropriate antioxidants. Our results provide a foundation for further studies of protein oxidation behavior in the processing of duck and duck meat products and its effects on meat products and industrial use.

## Data availability statement

The raw data supporting the conclusions of this article will be made available by the authors, without undue reservation.

## Author contributions

XZ: conceptualization, project administration, writing-review and editing, and methodology. XS: sample collection, investigation, data curation, and writing-original draft. SL: funding acquisition and visualization. YG and JL: funding acquisition and validation. QF and RW: supervision. All authors have read and agreed to the published version of the

manuscript. All authors contributed to the article and approved the submitted version.

## Funding

This research was supported by the National Natural Science Foundation of China (31301507) and the Natural Science Fund for Colleges and Universities in Jiangsu Province (13KJB550006, 19KJB550005, and 21KJA550002).

## Acknowledgments

The authors thank Ms. Yun Bai (Nanjing Agricultural University) for technical support and Editage for English language editing.

## Conflict of interest

The authors declare that the research was conducted in the absence of any commercial or financial relationships that could be construed as a potential conflict of interest.

## Publisher's note

All claims expressed in this article are solely those of the authors and do not necessarily represent those of their affiliated organizations, or those of the publisher, the editors and the reviewers. Any product that may be evaluated in this article, or claim that may be made by its manufacturer, is not guaranteed or endorsed by the publisher.

## References

- Li Y, Li X, Wang JZ, Zhang CH, Sun HM, Wang CQ, et al. Effects of oxidation on water distribution and physicochemical properties of porcine myofibrillar protein gel. *Food Biophys.* (2014) 9:169–78. doi: 10.1007/s11483-013-9329-9
- Wang H, Luo Y, Ertbjerg P. Myofibrillar protein gel properties are influenced by oxygen concentration in modified atmosphere packaged minced beef. *Food Chem.* (2017) 230:475–81. doi: 10.1016/j.foodchem.2017.03.073
- Hellwig M. The chemistry of protein oxidation in food. *Angew Chem Int Ed.* (2019) 58:16742–63. doi: 10.1002/anie.201814144
- Fu QQ, Liu R, Wang HO, Hua C, Song SX, Zhou GH, et al. Effects of oxidation *in vitro* on structures and functions of myofibrillar protein from beef muscles. *J Agric Food Chem.* (2019) 67:5866–73. doi: 10.1021/acs.jafc.9b01239
- Deng X, Lei Y, Liu J, Zhang J, Qin J. Biochemical changes of Coregonus peled myofibrillar proteins isolates as affected by HRGS oxidation system. *J Food Biochem.* (2018) 43:e12710. doi: 10.1111/jfbc.12710
- Liu C, Li W, Zhou M, Yi S, Ye B, Mi H, et al. Effect of oxidation modification induced by peroxy radicals on the physicochemical and gel characteristics of grass carp myofibrillar protein. *J Food Meas Charact.* (2021) 15:5572–83. doi: 10.1007/s11694-021-01123-1
- Bao Y, Puolanne E, Ertbjerg P. Effect of oxygen concentration in modified atmosphere packaging on color and texture of beef patties cooked to different temperatures. *Meat Sci.* (2016) 121:189–95. doi: 10.1016/j.meatsci.2016.06.014
- Nyaisaba BM, Liu X, Zhu S, Fan X, Sun L, Hatab S, et al. Effect of hydroxyl-radical on the biochemical properties and structure of myofibrillar protein from Alaska pollock (*Theragra chalcogramma*). *LWT.* (2019) 106:15–21. doi: 10.1016/j.lwt.2019.02.045
- Shen H, Elmore JS, Zhao M, Sun W. Effect of oxidation on the gel properties of porcine myofibrillar proteins and their binding abilities with selected flavour compounds. *Food Chem.* (2020) 329:127032. doi: 10.1016/j.foodchem.2020.127032
- Li DY, Tan ZF, Liu ZQ, Wu C, Liu HL, Guo C, et al. Effect of hydroxyl radical induced oxidation on the physicochemical and gelling properties of shrimp myofibrillar protein and its mechanism. *Food Chem.* (2021) 351:129344. doi: 10.1016/j.foodchem.2021.129344
- Wang J, Yang Y, Tang X, Ni W, Zhou L. Effects of pulsed ultrasound on rheological and structural properties of chicken myofibrillar protein. *Ultrason Sonochem.* (2017) 38:225–33. doi: 10.1016/j.ultrasonch.2017.03.018

12. Han Y, Shen H, Zhao M, Sun W. Changes in structural and gel properties of myofibrillar proteins induced by sodium chloride and hydroxyl radical. *Food Sci Technol Res.* (2019) 25:97–106. doi: 10.3136/fstr.25.97
13. Park D, Xiong YLL, Alderton AL. Concentration effects of hydroxyl radical oxidizing systems on biochemical properties of porcine muscle myofibrillar protein. *Food Chem.* (2007) 101:1239–46. doi: 10.1016/j.foodchem.2006.03.028
14. Soglia F, Petracci M, Ertbjerg P. Novel DNPH-based method for determination of protein carbonylation in muscle and meat. *Food Chem.* (2016) 197:670–5. doi: 10.1016/j.foodchem.2015.11.038
15. Bao Y, Boeren S, Ertbjerg P. Myofibrillar protein oxidation affects filament charges, aggregation and water-holding. *Meat Sci.* (2018) 135:102–8. doi: 10.1016/j.meatsci.2017.09.011
16. Chelch I, Gatellier P, Santé-Lhoutellier V. Technical note: a simplified procedure for myofibril hydrophobicity determination. *Meat Sci.* (2006) 74:681–3. doi: 10.1016/j.meatsci.2006.05.019
17. Laemmli UK. Cleavage of structural proteins during the assembly of the head of bacteriophage T4. *Nature.* (1970) 227:680–5. doi: 10.1038/227680a0
18. Zhu X, Tan B, Li K, Liu S, Gu Y, Xia T, et al. The impacts of different pea protein isolate levels on functional, instrumental and textural quality parameters of duck meat batters. *Foods.* (2022) 11:1620. doi: 10.3390/foods11111620
19. Salvador P, Toldra M, Sauer E, Carretero C, Pares D. Microstructure-function relationships of heat-induced gels of porcine haemoglobin. *Food Hydrocoll.* (2009) 23:1654–9. doi: 10.1016/j.foodhyd.2008.12.003
20. Gravelle AJ, Marangoni AG, Barbut S. Insight into the mechanism of myofibrillar protein gel stability: influencing texture and microstructure using a model hydrophilic filler. *Food Hydrocoll.* (2016) 60:415–24. doi: 10.1016/j.foodhyd.2016.04.014
21. Chen J, Deng T, Wang C, Mi H, Yi S, Li X, et al. Effect of hydrocolloids on gel properties and protein secondary structure of silver carp surimi. *J Sci Food Agric.* (2020) 100:2252–60. doi: 10.1002/jsfa.10254
22. Alix AJP, Pedanou G, Berjot M. Fast determination of the quantitative secondary structure of proteins by using some parameters of the Raman Amide I band. *J Mol Struct.* (1988) 174:159–64. doi: 10.1016/0022-2860(88)80151-0
23. Estevez M, Ventanas S, Cava R. Protein oxidation in frankfurters with increasing levels of added rosemary essential oil: effect on color and texture deterioration. *J Food Sci.* (2005) 70:C427–32. doi: 10.1111/j.1365-2621.2005.tb11464.x
24. Stadtman ER, Levine RL. Free radical-mediated oxidation of free amino acids and amino acid residues in proteins. *Amino Acids.* (2003) 25:207–18. doi: 10.1007/s00726-003-0011-2
25. Eymard S, Jacobsen C, Baron CP. Assessment of washing with antioxidant on the oxidative stability of fatty fish mince during processing and storage. *J Agric Food Chem.* (2010) 58:6182–9. doi: 10.1021/jf904013k
26. Sante-Lhoutellier V, Astrijs T, Marinova P, Greve E, Gatellier P. Effect of meat cooking on physicochemical state and *in vitro* digestibility of myofibrillar proteins. *J Agric Food Chem.* (2008) 56:1488–94. doi: 10.1021/jf072999g
27. Cao Y, True AD, Chen J, Xiong YL. Dual role (anti- and pro-oxidant) of gallic acid in mediating myofibrillar protein gelation and gel *in vitro* digestion. *J Agric Food Chem.* (2016) 64:3054–61. doi: 10.1021/acs.jafc.6b00314
28. Liu G, Xiong YLL. Electrophoretic pattern, thermal denaturation, and *in vitro* digestibility of oxidized myosin. *J Agric Food Chem.* (2000) 48:624–30. doi: 10.1021/jf990520h
29. Riebroys S, Benjakul S, Visessanguan W, Erikson U, Rustad T. Acid-induced gelation of natural actomyosin from Atlantic cod (*Gadus morhua*) and burbot (*Lota lota*). *Food Hydrocoll.* (2009) 23:26–39. doi: 10.1016/j.foodhyd.2007.11.010
30. Estevez M. Protein carbonyls in meat systems: a review. *Meat Sci.* (2011) 89:259–79. doi: 10.1016/j.meatsci.2011.04.025
31. Li C, Xiong YL, Chen J. Oxidation-induced unfolding facilitates myosin cross-linking in myofibrillar protein by microbial transglutaminase. *J Agric Food Chem.* (2012) 60:8020–7. doi: 10.1021/jf302150h
32. Bao Y, Ertbjerg P. Relationship between oxygen concentration, shear force and protein oxidation in modified atmosphere packaged pork. *Meat Sci.* (2015) 110:174–9. doi: 10.1016/j.meatsci.2015.07.022
33. Eymard S, Baron CP, Jacobsen C. Oxidation of lipid and protein in horse mackerel (*Trachurus trachurus*) mince and washed minces during processing and storage. *Food Chem.* (2009) 114:57–65. doi: 10.1016/j.foodchem.2008.09.030
34. Baron CP, Kjaersgard IVH, Jessen F, Jacobsen C. Protein and lipid oxidation during frozen storage of rainbow trout (*Oncorhynchus mykiss*). *J Agric Food Chem.* (2007) 55:8118–25. doi: 10.1021/jf070686f
35. Wang BW, Xiong YLL. Functional stability of antioxidant-washed, cryoprotectant-treated beef heart surimi during frozen storage. *J Food Sci.* (1998) 63:293–8. doi: 10.1111/j.1365-2621.1998.tb15729.x
36. Oozumi T, Xiong YL. Biochemical susceptibility of myosin in chicken myofibrils subjected to hydroxyl radical oxidizing systems. *J Agric Food Chem.* (2004) 52:4303–7. doi: 10.1021/jf03521v
37. Cao Y, Ma W, Wang J, Zhang S, Wang Z, Zhao J, et al. Influence of sodium pyrophosphate on the physicochemical and gelling properties of myofibrillar proteins under hydroxyl radical-induced oxidative stress. *Food Funct.* (2020) 11:1996–2004. doi: 10.1039/C9FO02412C
38. Li Y, Kong B, Xia X, Liu Q, Diao X. Structural changes of the myofibrillar proteins in common carp (*Cyprinus carpio*) muscle exposed to a hydroxyl radical-generating system. *Process Biochem.* (2013) 48:863–70. doi: 10.1016/j.procbio.2013.03.015
39. Lu H, Zhang L, Li Q, Luo Y. Comparison of gel properties and biochemical characteristics of myofibrillar protein from bighead carp (*Aristichthys nobilis*) affected by frozen storage and a hydroxyl radical-generation oxidizing system. *Food Chem.* (2017) 223:96–103. doi: 10.1016/j.foodchem.2016.11.143
40. Xiong YL, Blanchard SP, Oozumi T, Ma Y. Hydroxyl radical and ferryl-generating systems promote gel network formation of myofibrillar protein. *J Food Sci.* (2010) 75:C215–21. doi: 10.1111/j.1750-3841.2009.01511.x
41. Han M, Wang P, Xu X, Zhou G. Low-field NMR study of heat-induced gelation of pork myofibrillar proteins and its relationship with microstructural characteristics. *Int Food Res J.* (2014) 62:1175–82. doi: 10.1016/j.foodres.2014.05.062
42. Qin H, Xu P, Zhou C, Wang Y. Effects of l-Arginine on water holding capacity and texture of heat-induced gel of salt-soluble proteins from breast muscle. *LWT.* (2015) 63:912–8. doi: 10.1016/j.lwt.2015.04.048
43. Zhang D, Li H, Emara AM, Hu Y, Wang Z, Wang M, et al. Effect of *in vitro* oxidation on the water retention mechanism of myofibrillar proteins gel from pork muscles. *Food Chem.* (2020) 315. doi: 10.1016/j.foodchem.2020.126226
44. Zhu X, Zhang J, S, Gu Y, Yu X, Gao F, et al. Relationship between molecular structure and heat-induced gel properties of duck myofibrillar proteins affected by the addition of pea protein isolate. *Foods.* (2022) 11:1040. doi: 10.3390/foods11071040
45. Benevides JM, Overman SA, Thomas GJ Jr. Raman spectroscopy of proteins. *Curr Protoc Protein Sci.* (2003) 33:17.8.1–35. doi: 10.1002/0471140864.ps1708s33
46. Ullah N, Wang X, Chen L, Xu X, Li Z, Feng X. Influence of biofilm surface layer protein A (BslA) on the gel structure of myofibril protein from chicken breast. *J Sci Food Agric.* (2017) 97:4712–20. doi: 10.1002/jsfa.8339
47. Wang L, Zhang M, Fang Z, Bhandari B. Gelation properties of myofibrillar protein under malondialdehyde-induced oxidative stress. *J Sci Food Agric.* (2017) 97:50–57. doi: 10.1002/jsfa.7680



## OPEN ACCESS

EDITED BY  
Baoguo Xu,  
Jiangsu University, China

REVIEWED BY  
Enbo Xu,  
Zhejiang University, China  
Bipan Tudu,  
Jadavpur University, India

\*CORRESPONDENCE  
Jianmei Zheng  
✉ Zhengjm75@126.com

†These authors have contributed  
equally to this work and share first  
authorship

SPECIALTY SECTION  
This article was submitted to  
Nutrition and Food Science  
Technology,  
a section of the journal  
Frontiers in Nutrition

RECEIVED 20 October 2022  
ACCEPTED 19 December 2022  
PUBLISHED 09 January 2023

CITATION  
Ma R, Shen H, Cheng H, Zhang G and  
Zheng J (2023) Combining e-nose  
and e-tongue for improved  
recognition of instant starch noodles  
seasonings.  
*Front. Nutr.* 9:1074958.  
doi: 10.3389/fnut.2022.1074958

COPYRIGHT  
© 2023 Ma, Shen, Cheng, Zhang and  
Zheng. This is an open-access article  
distributed under the terms of the  
[Creative Commons Attribution License](#)  
(CC BY). The use, distribution or  
reproduction in other forums is  
permitted, provided the original  
author(s) and the copyright owner(s)  
are credited and that the original  
publication in this journal is cited, in  
accordance with accepted academic  
practice. No use, distribution or  
reproduction is permitted which does  
not comply with these terms.

# Combining e-nose and e-tongue for improved recognition of instant starch noodles seasonings

Rong Ma<sup>†</sup>, Huishan Shen<sup>†</sup>, Hao Cheng, Guoquan Zhang and  
Jianmei Zheng\*

Engineering Research Center of Grain and Oil Functionalized Processing in Universities of Shaanxi,  
College of Food Science and Engineering, Northwest A&F University, Xianyang, Shaanxi, China

Seasonings play a key role in determining sensory attributes of instant starch noodles. Controlling and improving the quality of seasoning is becoming important. In this study, five different brands along with fifteen instant starch noodles seasonings (seasoning powder, seasoning mixture sauce and the mixture of powder and sauce) were characterized by electronic nose (e-nose) and electronic tongue (e-tongue). Feature-level fusion for the integration of the signals was introduced to integrate the e-nose and e-tongue signals, aiming at improving the performances of identification and prediction models. Principal component analysis (PCA) explained over 85.00% of the total variance in e-nose data and e-tongue data, discriminated all samples. Multilayer perceptron neural networks analysis (MLPN) modeling demonstrated that the identification rate of the combined data was basically 100%. PCA, cluster analysis (CA), and MLPN proved that the classification results acquired from the combined e-nose and e-tongue data were better than individual e-nose and e-tongue result. This work demonstrated that in combination e-nose and e-tongue provided more comprehensive information about the seasonings compared to each individual e-nose and e-tongue. E-nose and e-tongue technologies hold great potential in the production, quality control, and flavor detection of instant starch noodles seasonings.

## KEYWORDS

instant starch noodles seasonings, e-nose, e-tongue, combined data, multilayer perceptron neural networks analysis

## 1. Introduction

Instant starch noodles are made from various starch (potato, bean, or cereal starch), water and other ingredients, and processed into dry, no-cooking, convenience food (1). It usually with the seasonings sprinkled over the starch noodles and are ready to eat after soaked in boiling water for 3–4 min. Along with the national health consciousness



enhancement, fortification has become an accepted practice in order to improve the nutritional properties of instant starch noodles. Instant starch noodles can be fortified with seasonings or additives to improve their nutritional properties (2). For example, many additives such as chitosan and polysaccharide gum are used to improve the properties of starch noodles (3). Secondly, changing the processing method can improve its taste and quality characteristics. Compared with the traditional hot air drying and open sun drying, the heat-moisture treatment improved the hardness, springiness, and chewiness textural properties of starch noodles (4). Greenhouse drying improved the quality and sustainability of starch noodles (5). Research is still underway to produce instant starch noodles that are more nutritious and meet taste requirements.

Seasonings play a key role in determining sensory attributes of instant starch noodles. Seasonings are mainly used for improving aroma and taste. Aroma is an important sensory attribute of flavor in food and volatile compounds plays an important role in it (6). Nowadays, only few studies have examined the volatile compounds in instant noodle seasonings (7). Therefore, further studies on aroma of instant noodle seasoning are required to elucidate the characteristic volatile compounds. Instant starch noodles seasonings usually come as either seasoning powder or seasoning mixture sauce. The seasoning powder contains various spices, such as salt, yeast extract, sodium glutamate, disodium 5'-ribonucleotide, paprika powder, and pepper. The seasoning mixture sauce is made with refined vegetable oil, various spices, yeast extract, soybean paste, and bone broth. Instant starch noodles seasonings contain various amino acids, nucleotides, vitamins, and minerals.

Consumers are mainly concerned about the flavor of instant starch noodles and the major difference of flavors is the variety of instant starch noodles seasonings. Different brands of instant starch noodles seasonings with the same taste vary greatly in flavor. To a certain extent, brand is an indicator of the product's quality and flavor. Different brands of instant starch noodles seasonings possessed variant chemical ingredients, aroma, taste, and price (8). Basically, the flavor of seasoning is evaluated by the experts through senses, however, the experts are expensive, time-consuming, and susceptible to the external environment and the interior factors of man himself, which leads to biased conclusions (9). Therefore, it is essential to establish a rapid and accurate technology to perceive the quality differences among different brands of instant starch noodles seasonings, which could also be used to detect the phenomenon of selling disqualified products at best quality prices.

Electronic nose (e-nose) and electronic tongue (e-tongue) are sensor-based apparatus which imitate the olfactory and gustatory perception of human. They provide fast detection and comprehensive information about the sample, and they can monitor and differentiate samples that are otherwise difficult for human sensory panels to discriminate (10). The e-nose and e-tongue are used to characterize small differences in taste and odor of food. They are powerful tools for distinguishing flavor

characteristics and are widely used in food quality evaluation (11). Xu et al. (10) applied e-nose, e-tongue, and e-eye combined with three chemometrics methods to identify and predict the tea quality, results indicated that fusion signals outperformed the independent signals, could perfectly predict the contents of the main chemical components. Qiu et al. (12) employed e-nose and e-tongue to discriminate two types of Satsuma mandarins from different developmental stages and trace the change in internal quality. Yu et al. (13) and Yin et al. (14) used HS-SPME-GC/MS combined with e-nose and e-tongue to analyze the volatile profiles and taste properties of soybean paste and Harbin red sausages. However, to the best of our knowledge, there are few studies on the combination of e-nose and e-tongue to detect and analyze the comprehensive flavor profile of instant starch noodles seasonings.

The main objectives of this study was to establish an easy, rapid and objective identification method for instant starch noodles seasonings based on different flavor profiles. Therefore, we used e-nose and e-tongue independently and in combination to discriminate different brands of instant starch noodles seasonings. Then, recognition of the seasonings was performed by principal components analysis (PCA), cluster analysis (CA), and multilayer perceptron neural networks analysis (MLPN), with the intention of testing whether e-nose and e-tongue can provide a rapid and accurate approach for flavor recognition and quality assurance of instant starch noodles seasonings.

## 2. Materials and methods

### 2.1. Sample selection and preparation

Five different brands of instant starch noodles with braised beef were obtained at the commercial market in China. The five brands were marked as C, D, G, L, and Z, respectively. Each brand contained three categories: seasoning powder (P), seasoning mixture sauce (S), and the mixture of powder and sauce (M). **Table 1** summarizes detailed information about the tested seasoning samples.

### 2.2. E-nose analysis

The PEN3 portable e-nose (Airsense Analytics GmbH, Schwerin, Germany) was applied to classify and characterize the instant starch noodles seasonings. The apparatus is composed of a sampling unit and a gas detection system consisting of 10 metal oxide semiconductor (MOS) sensors with varying sensitivity to each volatile compound (15). Prior to analysis, the e-nose was preheated and calibrated with pure air.

Based on the preliminary experimental results, 7 g of seasoning powder, 4 g of seasoning mixture sauce, and 11 g of the mixture of powder and sauce were put into three 150 mL



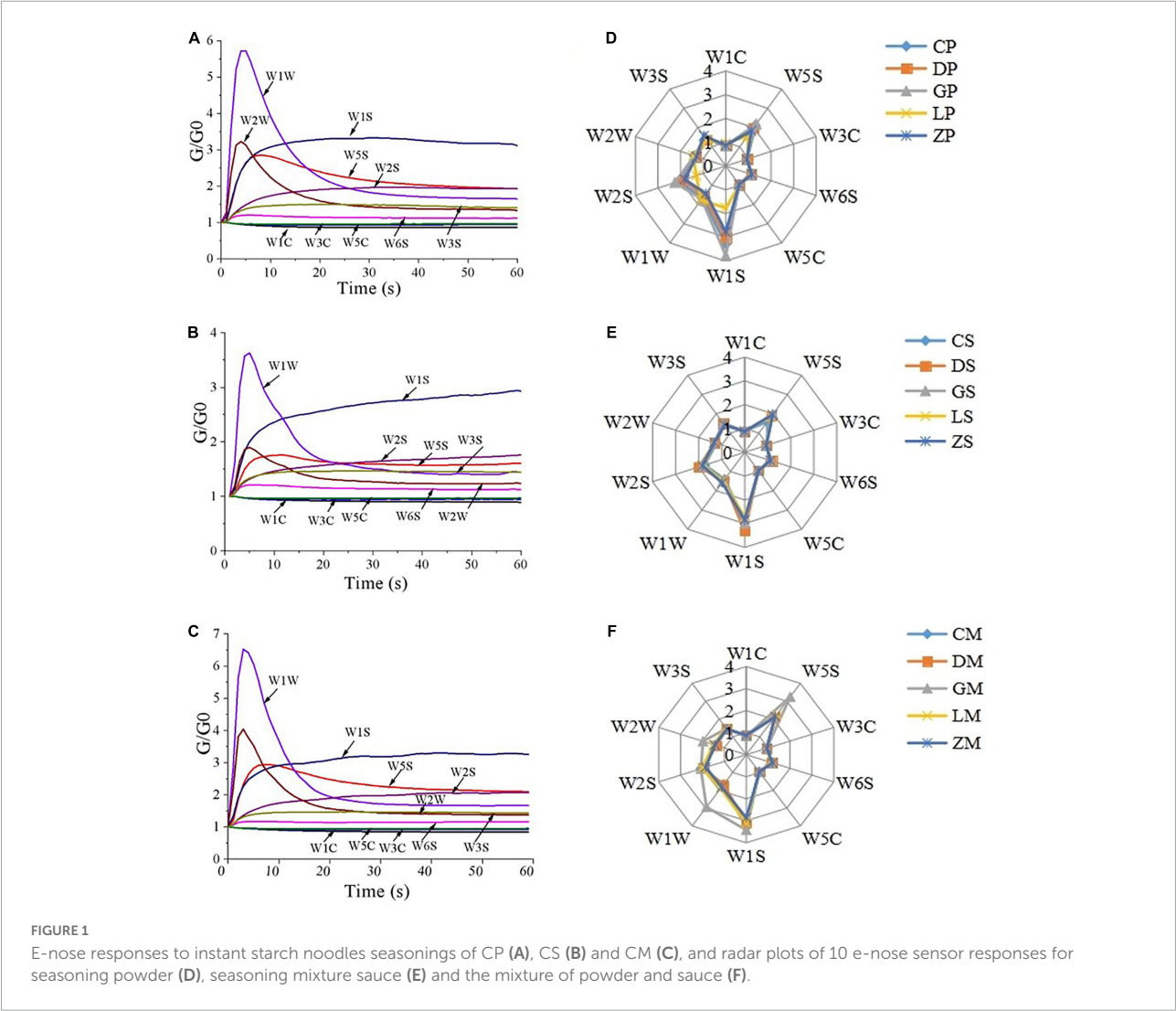
beakers, respectively. The seasoning solution was prepared after pouring 100 mL boiling water into the beaker and stirring for 2 min. A volume of 10 mL sample solution was put into a 30 mL sealed glass vial and incubated for 30 min at 40°C. The chamber and injection flow rate was 400 mL/min. The measurement time, sample interval time, flush time, and automatic zero adjustment time were 60, 1, 300, and 5 s. Each sample was measured 10 times.

2.3. E-tongue analysis

Instant starch noodles seasonings were analyzed using ASTREE e-tongue (Alpha M. O. S. Co., Toulouse, France). The instrument consists of an automatic sampler, chemical sensor array, and chemometric software package (16). The sensor array includes seven different chemical sensors and a reference electrode (Ag/AgCl) (17).

TABLE 1 Five brands of instant starch noodles seasonings samples.

	Seasoning powder (P)	Seasoning mixture sauce (S)	The mixture of powder and sauce (M)	Producing area
Samples	CP	CS	CM	Guangdong
	DP	DS	DM	Zhejiang
	GP	GS	GM	Sichuan
	LP	LS	LM	Jiangsu
	ZP	ZS	ZM	Anhui



According to preliminary experiments, 6 g of seasoning powder, 8 g of seasoning mixture sauce, and 14 g of the mixture of powder and sauce were put into three 500 mL beakers, respectively. The seasoning solution was prepared after pouring 400 mL boiling water into the beaker and stirring for 2 min. The seasoning solution was first filtered using a piece of gauze and the filtrate was then filtered through a 0.45  $\mu\text{m}$  nylon syringe filters. Then, 80 mL of filtrate of each sample was analyzed using the e-tongue. Before the test begins, 0.01 mol/L HCl, NaCl, and sodium glutamate were applied to activate, calibrate, and diagnose the chemical sensors (18). The e-tongue parameters were as follows: acquisition time of 120 s, clean time of 10 s,

acquisition period of 1 s, stirring rate of 3 r/s. Each sample was measured in three times.

## 2.4. Combining the e-nose and e-tongue datasets

Data fusion involves different levels of data abstraction (19), with low-level fusion being the most common method and giving good results. In low-level fusion, the e-nose and e-tongue signals were simply concatenated before model construction. In the resulting data matrix, the number of rows is equivalent to the number of samples, and the number of columns is equivalent to

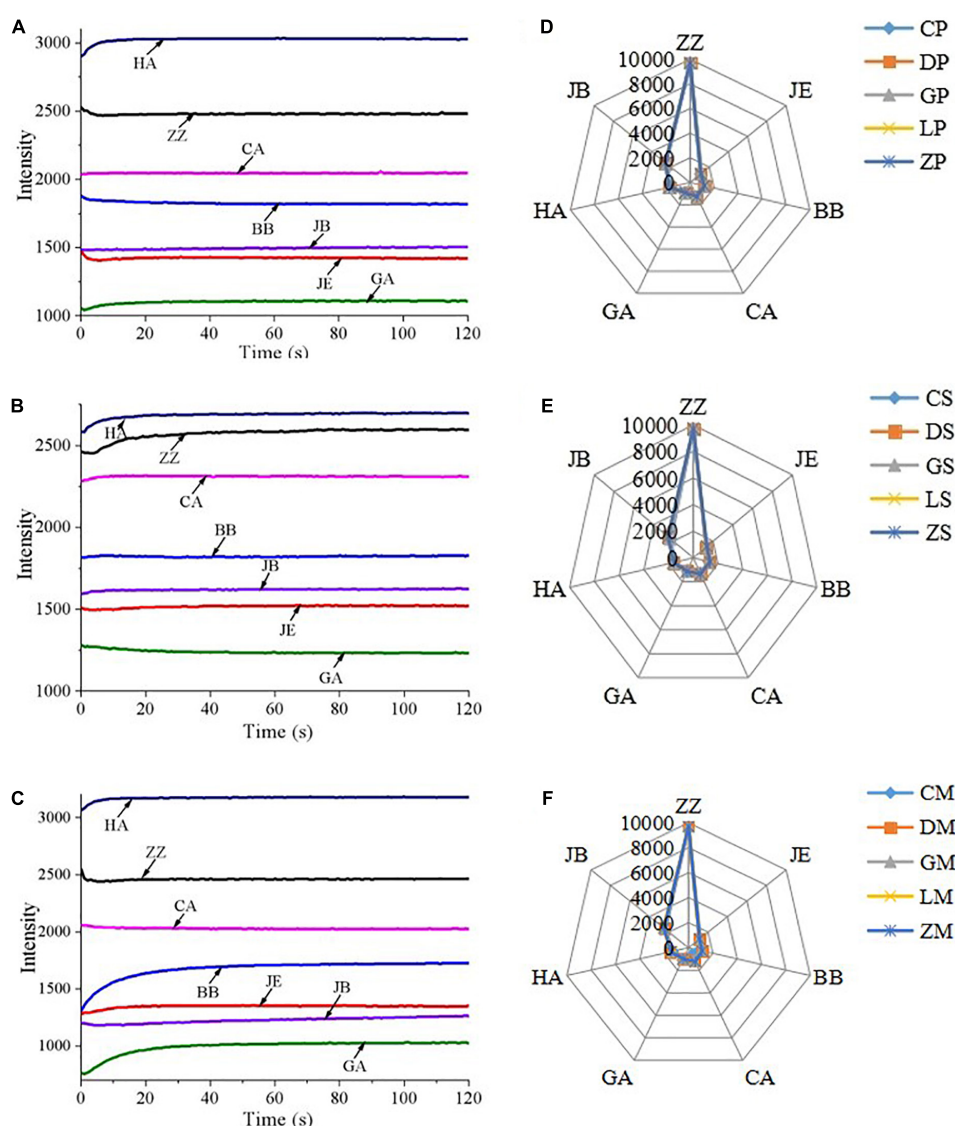


FIGURE 2

E-tongue responses to instant starch noodles seasonings of CP (A), CS (B) and CM (C), and radar plots of 10 e-tongue sensor responses for seasoning powder (D), seasoning mixture sauce (E) and the mixture of powder and sauce (F). ZZ, JE, BB, CA, GA, HA, and JB are seven different liquid cross-selection sensors for the electronic tongue.

the number of signals obtained from e-nose and e-tongue (20). We used this low-level fusion to combine e-nose and e-tongue data for the combined analyses discussed below.

## 2.5. Data analysis

The individual e-nose and e-tongue data and their fusion were applied to PCA, CA, and MLPN. PCA is the most popular feature extraction method in pattern recognition. It is used to differentiate samples and extract the most important information from data. PCA reduces the dimensionality of datasets while retaining most of the information of the original data (21). PCA interprets the data in two or three dimensions by

the first two or three PCs, which explain the largest amount of variance in the data (22).

Cluster analysis is an unsupervised classification technology which can cluster samples according to their similarity in multidimensional space (23). It identifies degrees of homogeneity of samples that are similar, while samples placed in different clusters reflect dissimilarity (24). A hierarchical CA method was applied to classify 60 samples based on the response signals of 17 sensors (7 e-tongue sensors and 10 e-nose sensors), with the squared Euclidean distance taken as a measure of similarity and the Ward's method taken as the amalgamation rule.

Multilayer perceptron neural networks analysis is a feed-forward supervised classification method consisting of an input layer, several hidden layers, and an output layer (22). It can be described as a non-linear projection vector from input to output. The sensors and different brands of instant starch noodles seasonings were used as the input layer and output layer, respectively. Training dataset used 10 sensors as inputs, eight neurons in the first hidden layer and six neurons in the second hidden layer. The four groups of different drop heights were used as the outputs, so there were four neurons in the output layer. The activation function of the hidden layer is a hyperbolic tangent function, and the activation function of the output layer is a Softmax function (25). Besides, to achieve a good generalization capability, the dataset used for adjusting the neural networks was again divided into a training set and a testing set. Again the 60 samples (12 samples for each group) were divided into two groups: 9 samples (75 percent of samples) for the training, and 3 samples (25 percent of samples) for the testing.

Principal component analysis and MLPN were performed using Statistical Product and Service Solutions (SPSS) 20.0. CA was conducted using Minitab 16.2.

## 3. Results and discussion

### 3.1. Response signals of e-nose

The typical e-nose response curves of CB, CS, and CM are shown in Figures 1A–C. The response signal was denoted by relative resistivity ( $G/G_0$ ), where  $G$  and  $G_0$  are the conductivities of the sensors when exposed to sample gas and pure air, respectively (26, 27). The e-nose response curves in the three figures exhibited similar temporal changes. The response values of sensors W1W, W2W, and W5S reached peak value at the 5th second and reduced quickly anaphase, finally, it reached a stable value. The response values of W1S rose rapidly from 0 to 10 s, then increased more slowly slightly, and finally remained high for the rest of the measurement. The response values of W3S, W2S, and W6S was appearing to increase slightly. In contrast, W1C, W3C, and W5C reduced

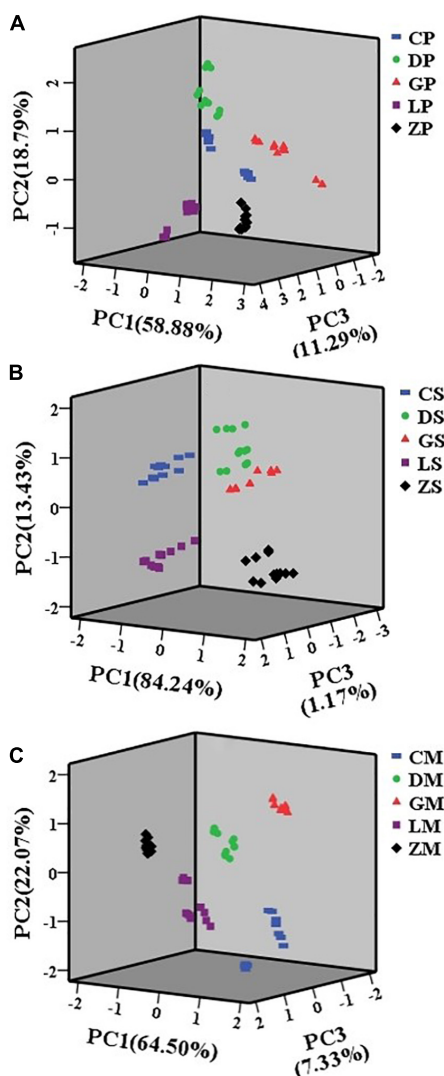


FIGURE 3  
Principal component analysis (PCA) plots of seasoning powder (A), seasoning mixture sauce (B), and the mixture of powder and sauce (C) using e-nose.

slightly, where  $G/G_0$  values were generally less than one since they are negative metal-oxide sensors (28). Overall, the response signals of W1S, W2S, W5S, and W1W remained at a high level (Figures 1A–C). The results suggested that aromatic compounds, nitrogen oxides, terpenes, and sulfur-containing compounds were the main constituents in the aroma of instant starch noodles seasonings (29).

The radar plots of e-nose sensor responses are presented in Figures 1D–F. There were no significant differences among the 10 sensors in seasoning powder, seasoning mixture sauce, and the mixture of powder and sauce (except GM), indicating that all seasonings had similar aromas. The W1S, W2S, W5S, and W1W sensors had stronger responses than other sensors. These results were in accordance with the typical e-nose response curves

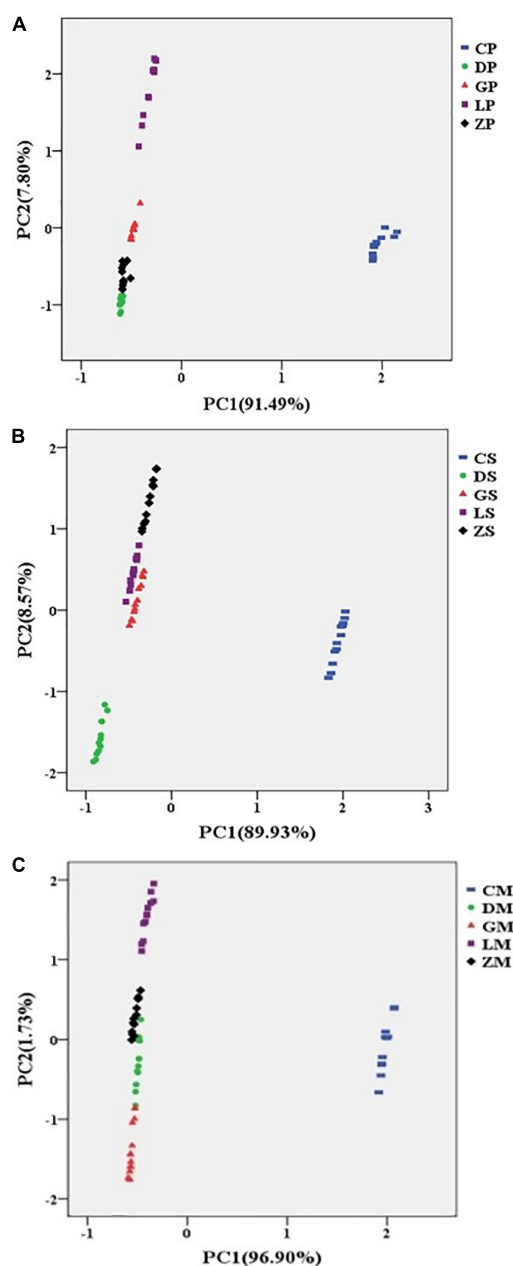


FIGURE 4  
Principal component analysis (PCA) plots of seasoning powder (A), seasoning mixture sauce (B), and the mixture of powder and sauce (C) using e-tongue.

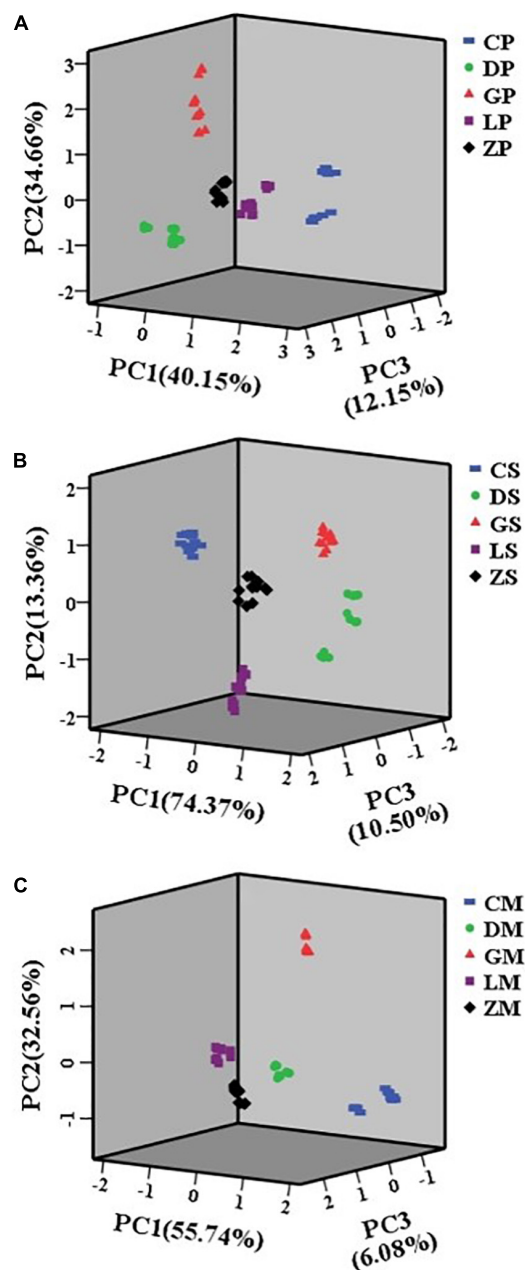


FIGURE 5  
Principal component analysis (PCA) plots of seasoning powder (A), seasoning mixture sauce (B), and the mixture of powder and sauce (C) using combined data.

(Figures 1A–C). The GP sample had higher values of W1S, W2S, and W5S than other samples, while LP had lower values of W1S, W2S, and W5S than other samples (Figure 1D). The DS sample had higher values of W1S and W2S than other samples (Figure 1E). Similarly, GM exhibited the highest response values in the sensors of W1S, W2S, W5S, W1W, and W2W (Figure 1F). The results suggested that different brands of instant starch noodles seasonings had significant difference in aromas.

### 3.2. Response signals of e-tongue

The e-tongue sensor responses of CP, CS, and CM are shown in Figures 2A–C. For the seasoning powder, the signals of HA

and GA increased from 0 to 10 s, while the signals of ZZ, BB, and JE decreased during this time period. These signals started to stabilize after approximately 30 s, and fully stabilized at 120 s. For the seasoning mixture sauce, the signals of HA, ZZ, and CA increased from 0 to 30 s, and other response sensors had no significant changes. These results suggested that HA, ZZ, BB, and GA are the main contributors to taste profiles of instant starch noodles seasonings.

The radar plots of e-tongue sensor responses are presented in Figures 2D–F, which show similar overall trends. Instant starch noodles seasonings of different brands cannot be distinguished by simply observing the response curves and radar charts of the samples. It is necessary to use multivariate statistical analysis to process the e-tongue data. Therefore, we used the stable signals at 120 s for PCA analysis.

### 3.3. Analysis of e-nose data

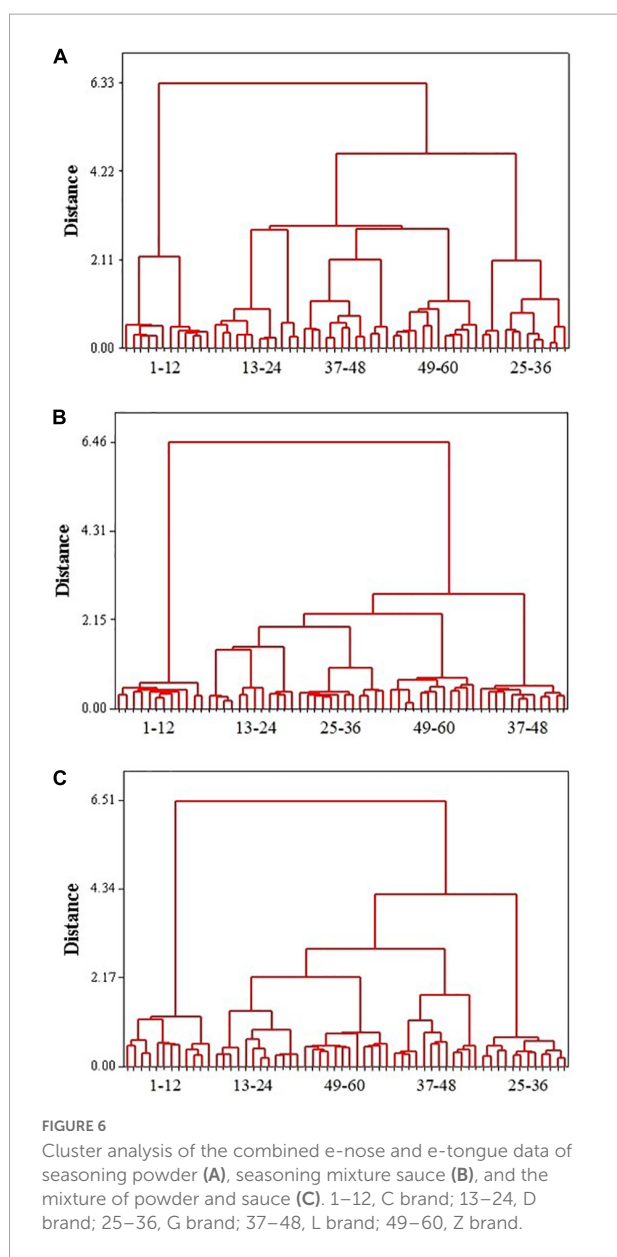
The e-nose PCA plots are presented in Figure 3. The seasoning powder samples of the same brand were located together. PC1, PC2, and PC3 explained a combined 88.96% of the total variation. For the seasoning mixture sauce, the first three PCs explained 98.84% of the total variance. PC1 explained 84.24% of the total variance, and PC2 explained 13.43% of the total variance, PC3 explained 1.17% of the total variance. For the mixture of powder and sauce, PC1 accounted for 64.50% of the total variance, PC2 accounted for 22.07% of the total variance and PC3 accounted for 7.33% of the total variance. In total, the first three PCs explained over 85.00% of the total variance in e-nose data.

In multidimensional space, the samples were clustered into five non-overlapping groups. Samples with more similar flavor would appear closer to each other. The CP and DP samples were located very close to each other, suggesting that CP and DP had similar aromas. The characteristic aroma attributes of CS, DS, and GS were also similar. The results showed that principal components analysis of e-nose data can be used to classify different brands of instant starch noodles seasonings.

### 3.4. Analysis of e-tongue data

The e-tongue PCA plots are presented in Figure 4. For seasoning powder, 91.49% of the total variance was explained by PC1 and 7.80% of the total variance was explained by PC2. Similarly, for seasoning mixture sauce, the first two PCs explained 98.50% of the total variance among samples. For the mixture of powder and sauce, the first two PCs explained 98.63% of the total variation. Thus, for all three types of samples, PC1 and PC2 explained almost all the total variance.

As shown in Figures 4A–C, the CP, CS, and CM samples were distributed mainly on the positive side of PC1, while





the rest of samples were mainly located in the negative side for PC1. The results indicated that the taste profiles of CP, CS, and CM were strikingly different from other samples. The possible reasons were that different manufacturers used different materials and production processes, which may cause the chemical ingredients and tastes of instant starch noodles seasonings to differ among brands. In general, the PCA results suggested that e-tongue can properly characterize different brands of instant starch noodles seasonings (30).

### 3.5. Analysis of combined e-nose and e-tongue datasets

Combination of e-nose and e-tongue data has been applied in various foods analysis and quality control (31). PCA and CA were applied on the combined e-nose and e-tongue dataset to discriminate between different brands of instant starch noodles seasoning (Figures 5, 6). For the seasoning powder, seasoning mixture sauce, and the mixture of powder and sauce, the first three PCs explained 86.96, 98.09, and 94.38% of the total variance, respectively. As shown in Figure 5, all instant starch noodles seasonings were grouped into five different clusters, with no overlap among groups. Combining e-nose and e-tongue

data resulted in much better clustering than occurred when analyzing either e-nose or e-tongue data alone.

Relationships between samples were visualized with a dendrogram based on a nearest neighbor method that used Euclidean distances. The combined e-nose and e-tongue data were analyzed using CA, for comparison to PCA. As shown in Figure 6, all seasoning powder samples of the same brand clustered together, with five distinct groups representing the five brands of samples. The seasoning mixture sauce and the mixture of powder and sauce similarly clustered by brand. CA gave us a preliminary classification even though the group divisions were different at different distances. The results of CA were in agreement with those from PCA, providing enough information to discriminate different brands of instant starch noodles seasonings.

### 3.6. MLPN predicted modeling

Table 2 shows the identification results of MLPN models. For the seasoning powder and seasoning mixture sauce, the identification rate of the combined data was 100% in both the training and test groups. For the mixture of powder and sauce,

TABLE 2 Results of multilayer perceptron neural networks analysis (MLPN) models.

Samples			Accuracy (%)					Total accuracy (%)
			C	D	G	L	Z	
Seasoning powder	E-nose	Train group	100.0	100.0	100.0	100.0	100.0	100.0
		Test group	100.0	100.0	100.0	100.0	100.0	100.0
	E-tongue	Train group	100.0	100.0	100.0	100.0	90.9	97.6
		Test group	100.0	100.0	100.0	100.0	100.0	100.0
	Fusion data	Train group	100.0	100.0	100.0	100.0	100.0	100.0
		Test group	100.0	100.0	100.0	100.0	100.0	100.0
Seasoning mixture sauce	E-nose	Train group	100.0	100.0	100.0	100.0	100.0	100.0
		Test group	100.0	100.0	100.0	100.0	100.0	100.0
	E-tongue	Train group	100.0	100.0	100.0	33.3	100.0	95.2
		Test group	100.0	100.0	100.0	66.7	100.0	83.3
	Fusion data	Train group	100.0	100.0	100.0	100.0	100.0	100.0
		Test group	100.0	100.0	100.0	100.0	100.0	100.0
The mixture of powder and sauce	E-nose	Train group	100.0	100.0	100.0	100.0	100.0	100.0
		Test group	100.0	100.0	100.0	100.0	100.0	100.0
	E-tongue	Train group	100.0	100.0	100.0	100.0	90.9	97.6
		Test group	100.0	100.0	100.0	100.0	100.0	100.0
	Fusion data	Train group	100.0	100.0	100.0	100.0	100.0	100.0
		Test group	100.0	100.0	100.0	66.7	100.0	83.3

the identification rate of combined data was 100% in the training group. MLPN modeling demonstrated that the combination of e-nose and e-tongue data enabled better discrimination than individual e-nose and e-tongue data alone. These indicated excellent performance of classification of samples into their correct treatment groups by using the MLPN. This improvement resulted from the complementarity of e-nose and e-tongue data. The e-nose and e-tongue were sensitive to aroma and taste of instant starch noodles seasonings. This complementary behavior of cross-sensitivity plays an important role in multisensor systems (22).

## 4. Conclusion

In this paper, e-nose, e-tongue, and the combination of their data were used to discriminate instant starch noodles seasonings from five different brands. PCA explained over 85.00% of the total variance in e-nose and e-tongue data, suggested that both individual e-nose and e-tongue could discriminate different brands of instant starch noodles seasonings. For the combination data of seasoning powder, seasoning mixture sauce, and mixture of powder and sauce, the first three PCs explained 86.96, 98.09, and 94.38% of the total variance and the results of CA were in agreement with those from PCA. PCA and CA results suggested that the combination of e-nose and e-tongue showed much better classification ability than either alone. MLPN modeling demonstrated that the identification rate of the combined data was basically 100%, further indicated that the combination of e-nose and e-tongue produced more optimal discrimination and analysis of samples.

In summary, e-nose and e-tongue can provide integrated information of flavors to distinguish among samples. The combination of e-nose and e-tongue an effective method for rapid, easy, and accurate food odor analysis that is objective, highly automated and lower cost. This work may be helpful in providing some valuable information on evaluating and discriminating the quality of instant starch noodles seasoning to consumers.

## References

1. Shen H, Wei T, Zhang Z, Zheng Q, Guo R, Jiang H, et al. Discrimination of five brands of instant vermicelli seasonings by HS-SPME/GC-MS and electronic nose. *J Food Sci Technol*. (2020). 57:4160–70. doi: 10.1007/s13197-020-04454-x
2. Gulia N, Dhaka V, Khatkar B. Instant noodles: processing, quality, and nutritional aspects. *Crit Rev Food Sci Nutr*. (2014) 54:1386–99. doi: 10.1080/10408398.2011.638227
3. Chen P, Xie Q, Wang R, Wang S, Cheng J, Zhang B. Effects of pullulanase enzymatic hydrolysis on the textural of acorn vermicelli and its influencing mechanism on the quality. *Food Res Int*. (2022) 156:111294. doi: 10.1016/j.foodres.2022.111294
4. Liao L, Liu H, Gan Z, Wu W. Structural properties of sweet potato starch and its vermicelli quality as affected by heat-moisture treatment. *Int J Food Prop*. (2019) 22:1122–33. doi: 10.1080/10942912.2019.1626418
5. Kumar M, Sahdev R, Tiwari S, Manchanda H, Chhabra D, Panchal H, et al. Thermal performance and kinetic analysis of vermicelli drying inside a greenhouse for sustainable development. *Sustain Energy Technol Assessments*. (2021) 44:101082. doi: 10.1016/j.seta.2021.101082
6. Liu Y, Li W, Wang Y, Zhong K, Zhao L, Gao H. Characterization of volatile compounds in ten different instant noodle seasonings by gas chromatography-mass spectrometry and odor activity values. *Chinese J Anal Chem*. (2021) 49:e21104–11. doi: 10.1016/S1872-2040(21)60105-6

## Data availability statement

The raw data supporting the conclusions of this article will be made available by the authors, without undue reservation.

## Author contributions

RM: conceptualization, investigation, writing – original draft, and data curation. HS: methodology and writing – review and editing. HC: software and formal analysis. GZ: project administration and supervision. JZ: supervision and resources. All authors contributed to the article and approved the submitted version.

## Acknowledgments

We would like to thank Professor Jiang Tao of Centre Européen des Sciences du Goût for writing and experimental design guidance and Dr. Adam Roddy at Yale University for his assistance with English language and grammatical editing.

## Conflict of interest

The authors declare that the research was conducted in the absence of any commercial or financial relationships that could be construed as a potential conflict of interest.

## Publisher's note

All claims expressed in this article are solely those of the authors and do not necessarily represent those of their affiliated organizations, or those of the publisher, the editors and the reviewers. Any product that may be evaluated in this article, or claim that may be made by its manufacturer, is not guaranteed or endorsed by the publisher.

7. Lee H, Lee K. Analysis of furan in various instant noodles by solid-phase microextraction-gas chromatography/mass spectrometry. *Food Control*. (2021) 126:108047. doi: 10.1016/j.foodcont.2021.108047
8. Liu F, He Y. Classification of brands of instant noodles using Vis/NIR spectroscopy and chemometrics. *Food Res Int*. (2008) 41:562–7. doi: 10.1016/j.foodres.2008.03.011
9. Jiang S, Ni C, Chen G, Liu Y. A novel data fusion strategy based on multiple intelligent sensory technologies and its application in the quality evaluation of Jinhua dry-cured hams. *Sensors Actuators B Chem*. (2021) 344:130324. doi: 10.1016/j.snb.2021.130324
10. Xu M, Wang J, Zhu L. The qualitative and quantitative assessment of tea quality based on E-nose, E-tongue and E-eye combined with chemometrics. *Food Chem*. (2019) 289:482–9. doi: 10.1016/j.foodchem.2019.03.080
11. Du H, Chen Q, Liu Q, Wang Y, Kong B. Evaluation of flavor characteristics of bacon smoked with different woodchips by HS-SPME-GC-MS combined with an electronic tongue and electronic nose. *Meat Sci*. (2021) 182:108626. doi: 10.1016/j.meatsci.2021.108626
12. Qiu S, Wang J, Tang C, Du D. Comparison of ELM, RF, and SVM on E-nose and E-tongue to trace the quality status of mandarin (*Citrus unshiu* Marc.). *J Food Eng*. (2015) 166:193–203. doi: 10.1016/j.jfoodeng.2015.06.007
13. Yu S, Huang X, Wang L, Ren Y, Zhang X, Wang Y. Characterization of selected Chinese soybean paste based on flavor profiles using HS-SPME-GC/MS, E-nose and E-tongue combined with chemometrics. *Food Chem*. (2022) 375:131840. doi: 10.1016/j.foodchem.2021.131840
14. Yin X, Lv Y, Wen R, Wang Y, Chen Q, Kong B. Characterization of selected Harbin red sausages on the basis of their flavour profiles using HS-SPME-GC/MS combined with electronic nose and electronic tongue. *Meat Sci*. (2021) 172:108345. doi: 10.1016/j.meatsci.2020.108345
15. Zhang X, Wei J, Zhao S, Jia H, Guo C, Wang Z, et al. Flavor differences between commercial and traditional soybean paste. *LWT*. (2021) 142:111052. doi: 10.1016/j.lwt.2021.111052
16. Shen X, Wang Y, Ran L, Liu R, Sun X, Hu L, et al. Flavor deterioration of liquid endosperm in postharvest tender coconut revealed by LC-MS-based metabolomics, GC-IMS and E-tongue. *Postharvest Biol Technol*. (2022) 187:111866. doi: 10.1016/j.postharvbio.2022.111866
17. Dong W, Zhao J, Hu R, Dong Y, Tan L. Differentiation of Chinese robusta coffees according to species, using a combined electronic nose and tongue, with the aid of chemometrics. *Food Chem*. (2017) 229:743–51. doi: 10.1016/j.foodchem.2017.02.149
18. Dong W, Hu R, Long Y, Li H, Zhang Y, Zhu K, et al. Comparative evaluation of the volatile profiles and taste properties of roasted coffee beans as affected by drying method and detected by electronic nose, electronic tongue, and HS-SPME-GC-MS. *Food Chem*. (2019) 272:723–31. doi: 10.1016/j.foodchem.2018.08.068
19. Haddi Z, Alami H, Bari N, Tounsi M, Barhoumi H, Maaref A, et al. Electronic nose and tongue combination for improved classification of Moroccan virgin olive oil profiles. *Food Res Int*. (2013) 54:1488–98. doi: 10.1016/j.foodres.2013.09.036
20. Haddi Z, Mabrouk S, Bougrini M, Tahri K, Sghaier K, Barhoumi H, et al. E-nose and e-tongue combination for improved recognition of fruit juice samples. *Food Chem*. (2014) 150:246–53. doi: 10.1016/j.foodchem.2013.10.105
21. Kaya Z, Yildiz S, Ünlütürk S. Effect of UV-C irradiation and heat treatment on the shelf life stability of a lemon-melon juice blend: multivariate statistical approach. *Innov Food Sci Emerg Technol*. (2015) 29:230–9. doi: 10.1016/j.ifset.2015.03.005
22. Wang Q, Li L, Ding W, Zhang D, Wang J, Reed K, et al. Adulterant identification in mutton by electronic nose and gas chromatography-mass spectrometer. *Food Control*. (2019) 98:431–8. doi: 10.1016/j.foodcont.2018.11.038
23. Yang Y, Zhang M, Yin H, Deng Y, Jiang Y, Yuan H, et al. Rapid profiling of volatile compounds in green teas using micro-chamber/thermal extractor combined with thermal desorption coupled to gas chromatography-mass spectrometry followed by multivariate statistical analysis. *LWT*. (2018) 96:42–50. doi: 10.1016/j.lwt.2018.04.091
24. Chen Q, Song J, Bi J, Meng X, Wu X. Characterization of volatile profile from ten different varieties of Chinese jujubes by HS-SPME/GC-MS coupled with E-nose. *Food Res Int*. (2018) 105:605–15. doi: 10.1016/j.foodres.2017.11.054
25. Ren Y, Ramaswamy H, Li Y, Yuan C, Ren X. Classification of impact injury of apples using electronic nose coupled with multivariate statistical analyses. *J Food Process Eng*. (2018) 41:e12698. doi: 10.1111/jfpe.12698
26. Hong X, Wang J, Hai Z. Discrimination and prediction of multiple beef freshness indexes based on electronic nose. *Sensors Actuators B Chem*. (2012) 161:381–9. doi: 10.1016/j.snb.2011.10.048
27. Hong X, Wang J, Qiu S. Authenticating cherry tomato juices-discussion of different data standardization and fusion approaches based on electronic nose and tongue. *Food Res Int*. (2014) 60:173–9. doi: 10.1016/j.foodres.2013.10.039
28. Li Q, Yu X, Xu L, Gao J. Novel method for the producing area identification of Zhongning goji berries by electronic nose. *Food Chem*. (2017) 221:1113–9. doi: 10.1016/j.foodchem.2016.11.049
29. Feng T, Zhuang H, Ye R, Jin Z, Xu X, Xie Z. Analysis of volatile compounds of *Mesona blumes* gum/rice extrudates via GC-MS and electronic nose. *Sensors Actuators B Chem*. (2011) 160:964–73. doi: 10.1016/j.snb.2011.09.013
30. Liu M, Wang J, Li D, Wang M. Electronic tongue coupled with physicochemical analysis for the recognition of orange beverages. *J Food Qual*. (2012) 35:429–41. doi: 10.1111/jfq.12004
31. Callao M, Ruisánchez I. An overview of multivariate qualitative methods for food fraud detection. *Food Control*. (2018) 86:283–93. doi: 10.1016/j.foodcont.2017.11.034



## OPEN ACCESS

## EDITED BY

Hao Jiang,  
Northwest A&F University, China

## REVIEWED BY

Zhenbin Liu,  
Shaanxi University of Science  
and Technology, China  
Hongjie Lei,  
Northwest A&F University, China

## \*CORRESPONDENCE

Yufang Liu  
✉ yufang.liu@snnu.edu.cn

## SPECIALTY SECTION

This article was submitted to  
Nutrition and Food Science  
Technology,  
a section of the journal  
Frontiers in Nutrition

RECEIVED 09 November 2022

ACCEPTED 16 December 2022

PUBLISHED 09 January 2023

## CITATION

Yang Y, Zhang R, Zhang F, Wang B and  
Liu Y (2023) Storage stability  
of texture, organoleptic,  
and biological properties of goat milk  
yogurt fermented with probiotic  
bacteria.  
*Front. Nutr.* 9:1093654.  
doi: 10.3389/fnut.2022.1093654

## COPYRIGHT

© 2023 Yang, Zhang, Zhang, Wang and  
Liu. This is an open-access article  
distributed under the terms of the  
[Creative Commons Attribution License](#)  
(CC BY). The use, distribution or  
reproduction in other forums is  
permitted, provided the original  
author(s) and the copyright owner(s)  
are credited and that the original  
publication in this journal is cited, in  
accordance with accepted academic  
practice. No use, distribution or  
reproduction is permitted which does  
not comply with these terms.

# Storage stability of texture, organoleptic, and biological properties of goat milk yogurt fermented with probiotic bacteria

Yaling Yang, Ruyue Zhang, Fuxin Zhang, Bini Wang and  
Yufang Liu\*

College of Food Engineering and Nutritional Science, Shaanxi Normal University, Xi'an, China

**Introduction:** Goat milk is an attractive food due to its high nutritional values, easy digestibility and hypoallergenicity, but has an undesirable “goaty” flavor.

**Methods:** In this study, goat yogurt was fermented with four probiotics, respectively, including *Lactobacillus acidophilus* (GYA), *Bifidobacterium animalis* (GYB), *Lactobacillus casei* (GYC) and *Lactobacillus plantarum* (GYP), and tested for texture, organoleptic, and biological properties during a 4-week storage period at the refrigerated temperature.

**Results:** All goat yogurt with probiotics showed an increase on titratable acidity and a corresponding downward trend on pH value. Viable counts of *L. acidophilus* and *L. casei* were above 6 log cfu/mL at the end of the storage, which met the minimum standards for viable probiotic bacteria in yogurt specified by the Food and Agriculture Organization of United Nation (FAO). The texture and organoleptic characteristics of fermented goat milk depended on the strain and the storage period. DPPH free radical scavenging rate and ferric reducing antioxidant power activity gradually increased in all goat yogurts during the storage and yogurt with probiotic bacteria showed higher values than those of GY0.

**Discussion:** Among all probiotic containing goat yogurts, GYC exhibited the desirable characteristics of hardness, adhesiveness, water holding capacity, antioxidant activity during the whole storage. Furthermore, the addition of *L. casei* effectively weakened the goaty flavor and enhanced the overall acceptability. Thus, fermented goat milk with *L. casei* is optional for the development of goat milk product with satisfactory texture properties, pleasant sensory quality and high bioactivity.

## KEYWORDS

goat yogurt, probiotics, texture, organoleptic characteristics, antioxidant activity (AA)

## 1. Introduction

According to statistical data from Food and Agriculture Organization of United Nation (FAO), goat milk is the third milk variety in the world, output of which is only lower than cow milk and buffalo milk. Goat milk is rich in proteins, calcium, antioxidants, antibacterial factors, which meet the requirement for the nutrition and health of human (1). In comparison to bovine milk, goat milk has better digestibility and lower allergenicity (2). In addition, goat milk contains a high level of lysozyme that improves infant immunity, and has been considered as extremely important replacement of human breast milk (3). Nevertheless, goat milk has an undesirable “goaty” flavor, which is generally attributed to volatile components such as branched chain fatty acids (4).

Probiotics are described as live microorganisms that, when ingested in appropriate amounts, confer health advantages to the host (5). Probiotic bacteria confer to goat milk higher antioxidant activity, hypotensive effect and regulatory ability of intestinal flora (6). Ejtahed et al. (7) suggested that ingestion of yogurt with probiotic bacteria might contribute to reduce the cardiovascular disease risk in type 2 diabetes patients (7). Probiotics have powerful antioxidant enzyme system, such as SOD, CAT, GSH-Px, etc. Meanwhile, during the metabolic process, probiotics can also produce organic substances with antioxidant effects such as VE, VC, coenzyme Q, cysteine and so on, which could improve the removal rate of free radicals in the body [V. (8)]. Probiotics prevent hypertension mainly by inhibiting ACE activity, regulating intestinal flora, and enhancing antioxidant capacity. Several bioactive peptides that exert ACE-inhibiting activity have been found in fermented yogurt with probiotics (9). Furthermore, probiotics can also improve the dysbiosis of intestinal flora, leading to the intervene in hypertension. In addition to the health benefits for consumers, probiotic bacteria may develop different patterns of texture and organoleptic properties; each bacterial cultures may lead to a specific product. Probiotic bacteria can create various pleasant volatile flavor compounds during fermentation process (10), and the addition of probiotics contributes to improve rheological properties and organoleptic characteristics of goat milk yogurt. In some cases, yogurt with *L. delbrueckii* ssp. *bulgaricus* was assessed to be too acidic by consumers. Thus, probiotic bacteria were chosen to develop preferred flavors, such as *L. acidophilus*, *Bifidobacterium* and *L. casei* (11).

Yogurt is traditionally fermented by the combination of *L. delbrueckii* ssp. *bulgaricus* and *S. thermophilus*. In this study, four probiotics were used for the fermentation of goat milk yogurt, including *Lactobacillus plantarum*, *Lactobacillus casei*, *Lactobacillus acidophilus*, and *Bifidobacterium animalis* spp. *lactis* to improve their texture, flavor and bioactive activities. Previous studies have shown that these four probiotic bacteria can survive and maintain a certain vitality in human

gastrointestinal tract (12). *L. plantarum* is a kind of facultative heterofermentative lactic acid bacteria. Consumption of fermented milk containing *L. plantarum* brings *in vivo* several benefits to the host (13, 14). *Lactobacillus casei*, *Lactobacillus acidophilus* and *Bifidobacterium animalis* are also widely used for starter cultures to overcome the issue of post-acidification in yogurt during the storage (15). This study aimed to comprehensively evaluate the effect of probiotics supplementation on goat milk yogurt, including biological activity, texture, and sensory characteristics, during the storage at refrigerated temperature using principal component analysis (PCA). The developed novel goat milk yogurt not only weakens the goaty flavor and improves the sensory acceptance, but also has the health benefits of probiotic combined with goat milk. Hence, it would be much favored by consumers and has a good market prospect.

## 2. Materials and methods

### 2.1. Materials

Raw goat milk was purchased from local farmers was used to ferment yogurt. The starter culture YO-MIX 187 was from Danisco DuPont (Dangé-Saint-Romain, France), which consisted of *Streptococcus thermophilus* and *Lactobacillus bulgaricus*. Four different probiotic fermentation starter, *Lactobacillus plantarum*, *Lactobacillus casei*, *Lactobacillus acidophilus*, and *Bifidobacterium animalis* subsp. *Lactis*, were acquired from Beina Culture Collection (Jiangsu province, China). 2,2-Diphenyl-1-picryl-hydrazyl (DPPH), N-hippuryl-His-Leu tetrahydrate (HHL) and 2,4,6-tripyrindyl-s-tria-zine (TPTZ) were purchased from Sigma-Aldrich (Steinheim, Germany). All other chemicals were analytically pure and obtained from Xi'an Chemical Co. (Xi'an, China).

### 2.2. Yogurt preparation

Raw goat milk was pasteurized immediately after the purchase, then cooled to 42°C. Prior to the inoculation, the optical density of four probiotic suspensions at 600 nm was adjusted to 1.0 using sterile saline to ensure that the concentration of each strain of bacteria was about  $1.0 \times 10^8$  CFU/mL. All treated goat milk were randomly divided into five groups: blank control group (GY0) was only inoculated with 3% YO-MIX187 starter culture; GYA group was inoculated with 3% YO-MIX187 starter culture and *Lactobacillus acidophilus*; GYB group was inoculated with 3% YO-MIX187 starter culture and *Bifidobacterium animalis* ssp. *lactis*; GYC group was inoculated with 3% YO-MIX187 starter culture and *Lactobacillus casei*; GYP group was inoculated with 3% YO-MIX187 starter culture



and *Lactobacillus plantarum*. The inoculated goat milk was placed at 42°C for 6 h until they were coagulated, and then all samples were refrigerated at 4°C for 28 days. During the storage, goat milk yogurt was analyzed for texture, organoleptic properties and bioactivity at 1, 7, 14, 21, and 28 days. All the experiments were performed in triplicate.

## 2.3. Determination of the titratable acidity and the pH value

Potentiometric titration was used to determinate the titratable acidity of goat yogurt. The concrete operation referred to the Gharibzadeh's method (16), and results were expressed as the Thorner degree (°T). The pH value was measured by inserting a previously calibrated pH meter by the electrode into 10.0 g goat yogurt samples. All analysis were conducted for three times.

## 2.4. Viable counts of lactic acid bacteria and probiotics

The viable counts of lactic acid bacteria and probiotics in fermented goat yogurt were determined by plate counting on selective medium. Serial dilutions were made for each goat yogurt sample from  $10^{-1}$  to  $10^{-7}$ . *L. bulgaricus* was enumerated on Man, Rogosa, and Sharp (MRS) agar after the anaerobic incubation at 37°C for 72 h; *S. thermophiles* was counted on the modified Chalmers (MC) agar after the aerobic incubation at 37°C for 48 h; the selective medium for *L. acidophilus* was MRS agar medium with clindamycin (17); *Bifidobacteria* colonies were enumerated on the MRS medium with aluminum chloride and sodium propionate on top of MRS agar (MRS-LP) after the anaerobic incubation at 37°C for 72 h (18); The selective medium for *Lactobacillus casei* was LC agar, which consisted of bacteriological peptone, yeast extract, Lab Lemco, sodium acetate, casein hydrolysate, tween 80,  $\text{KH}_2\text{PO}_4$ ,  $\text{MgSO}_4$ , and  $\text{MnSO}_4$  (19); the selective medium of *Lactobacillus plantarum* was configured according to the method of Carmen Bujalance [Bujalance et al. (20)]. The final result was expressed by logarithm of colony forming units per milliliter of yogurt.

## 2.5. Texture measurement

Texture characteristics of goat yogurt were measured by a texture analyzer (Stable Micro System, version 3.0, UK) using A/BE-d835 as the probe, and detailed parameters were set according to Feng's methods (21). The texture properties, including hardness, adhesiveness, springiness, and cohesiveness, were determined by continuous three compression of each sample.

## 2.6. Water holding capacity determination

The water holding capacity of yogurt reflects the water retention ability of its protein gel network. Briefly, the solidified yogurt was put into a centrifuge tube, which weight was defined as M, and centrifuged at 4,000 g for 10 min. The supernatant was discarded, and the sediment was weighted as  $M_0$ . The water holding capacity (%) could be calculated using the following formula:

$$\text{Water holding capacity (\%)} = \frac{M_0}{M} \times 100\%$$

## 2.7. Evaluation of biological activity

### 2.7.1. Antioxidant activity

Ten grams goat yogurt samples were mixed with 30 mL 80% methanol (v/v). The mixture was incubated in an ultrasonic instrument for 20 min at 100 W and then centrifuged at 4,000 g for 10 min. Finally, the supernatant was stored at -20°C prior to the evaluation of DPPH free radical scavenging activity and ferric reducing antioxidant power.

#### 2.7.1.1. DPPH free radical scavenging activity

Half milliliter goat yogurt supernatant was mixed with 4.0 mL DPPH in methanol solution (50.0 mg of DPPH in 1 L of methanol). After the vortex oscillation, the mixture was incubated in dark place for 30 min at room temperature. Ultrapure water was used as blank control and the absorbance at 517 nm was measured by spectrophotometer.

#### 2.7.1.2. Ferric reducing antioxidant power activity

The FRAP analysis was performed according to Benzie and Strain (22) with minor modification (22). Half milliliter supernatant of goat yogurt was mixed with 3.0 mL FRAP reagent. Subsequently, the mixture was water-bathed at 37°C for 10 min and then absorbance at 593 nm was measured with ultrapure water as blank by spectrophotometer. Experimental results were calculated as mmol  $\text{FeSO}_4/\text{g}$  yogurt.

### 2.7.2. Antihypertensive activity

The ACE inhibitory activity was evaluated by Xie's method (23) with slight modification. The pH of goat yogurt was adjusted to 3.4–3.6 with 1 M acetic acid and yogurt samples were centrifuged at 8,000 g for 15 min. Subsequently, the pH of supernatant was altered to 8.3 with 1 M NaOH, and samples were centrifuged at the equal rotational speed for 20 min. One hundred microliter supernatant was mixed with 200  $\mu\text{L}$  HHL solution (6.5 mmol/L, 0.1 mol/L boric acid solution as solvent) and incubated at 37°C for 5 min. ACE (20  $\mu\text{L}$ , 0.1 U/mL) was added to the mixture and incubated for 30 min at 37°C. A total of 0.25 mL HCl (0.1 mol/L) was added to

terminate the reaction. One milliliter ethyl acetate was added to the mixture and incubated at 90°C in the oven. After drying for 1 h, the sample was dissolved in 4 mL ultrapure water and the absorbance value at 228 nm was recorded by ultraviolet spectrophotometer. Before the reaction, ACE was inactivated and added to the sample, which was used as blank control. The ACE activity was calculated using the following formula:

$$\text{ACE inhibitory rate (\%)} = (A_b - A_a) / (A_b - A_c)$$

Where  $A_a$  represents the absorbance value of yogurt;  $A_b$  represents the absorbance value of ultrapure water instead of goat yogurt;  $A_c$  means the absorbance value of blank control.

## 2.8. Sensory evaluation and flavor compound determination

### 2.8.1. Sensory evaluation

Sensory analysis was carried out on probiotic goat yogurt that had been refrigerated for 14 days. The panelists (5 males and 5 females, aged between 20 and 35) for the sensory evaluation had undergone initial training and were selected because of their habit of consuming yogurt. Criteria for sensory assessment included pure white, syneresis, acidity, aroma, taste fineness, oral viscosity, goaty flavor, sweetness, bitter, and overall acceptability among goat yogurt samples. The detailed evaluation process was essentially the same as the method described previously (24).

### 2.8.2. Flavor compound determination

Flavor is strongly dependent on the volatile components of the fermented dairy products (25). Acetaldehyde and diacetyl were two important aroma compounds in yogurt, which differed from milk and other fermented dairy products. In this study, acetaldehyde and diacetyl contents were determined to verify the acceptability and preference of yogurt (26).

#### 2.8.1.1. Acetaldehyde content

Determination of acetaldehyde content in fermented goat yogurt by iodine titration. Twenty milliliter goat yogurt and 16% (v/v) trichloroacetic acid solution with the same volume were fully mixed in a centrifuge tube and centrifuged at 4,500 g for 10 min. At the same time, sterile fresh milk was used as a blank control. Two milliliter 1% NaHSO<sub>3</sub> solution and 10 mL supernatant of goat yogurt were mixed evenly and incubated at room temperature for 1 h. One milliliter 1% starch solution was added and titrated with 0.10 M iodine standard solution until the solution changed to pale blue. Twenty milliliter NaHCO<sub>3</sub> (1 M) was further mixed to the above solution under the oscillation until the pale blue disappear. The solution was titrated with 0.01 M iodine standard solution and the volume of

standard iodine consumed was recorded. Experiments were repeated for three times.

$$\text{Acetaldehyde content (mg/L)} = (V_1 - V_2) \times C \times 0.022 \times 10^5$$

Where  $V_1$  represents the volume of iodine standard solution consumed by the titration for goat yogurt (mL);  $V_2$  represents the volume of iodine standard solution consumed by the titration in blank control (mL);  $C$  represents the concentration of iodine standard solution (M).

#### 2.8.1.2. Diacetyl content determination

O-phenylenediamine colorimetry method was used to determine the content of diacetyl. Five milliliter yogurt sample was mixed with 5 mL 16% trichloroacetic acid (v/v) and 0.5 mL 1% o-phenylenediamine solution (v/v). The mixture was incubated at room temperature for 30 min and 2 mL 4 M hydrochloric acid was added to terminate the reaction. Finally, the optical density was measured by ultraviolet spectrophotometer (EasyPlus, Mettler Toledo) at 335 nm using quartz cuvette. Fresh goat milk was used as blank control.

## 2.9. Statistical analysis

All tests were measured for three times independently. One-way analysis of variances (ANOVA) and Duncan's multiple-range test were carried out in the statistical analysis by using SPSS Statistics 22.0 to analyze the difference. Only  $p$ -value of  $< 0.05$  was considered as statistical significance between samples.

## 3. Results and discussion

### 3.1. Changes in titratable acidity and pH of probiotic goat yogurt during the storage

The acidity of yogurt is one of the most significant physicochemical indicators of yogurt quality. It is only when the acidity rises to a certain degree that the proteins in goat milk form a gel network and begin to coagulate (27). In addition, acidity plays a key role on the organoleptic characteristics and shelf life of yogurt, thus it is important to monitor the acidity of goat yogurt with probiotic bacteria. Figure 1A visualized the effect of probiotics on the acidity and pH of goat yogurt during the storage at refrigerated temperature. All goat yogurts have an acidity level above 90°T. The titratable acidity of goat yogurt increased with the extension of the storage and pH values presented a corresponding downward trend. Goat yogurt with *Lactobacillus acidophilus* (GYA), *Bifidobacterium animalis* subsp. *Lactis* (GYB) and *Lactobacillus plantarum* (GYP) had more titratable acidity than the sample control ( $p < 0.05$ ). As

shown in **Figure 1B**, there is no significant difference in pH among the experimental groups on the first day of storage. At the end of the storage, the pH values of all goat yogurt with probiotic bacteria were significantly lower than that of the GY0 group ( $p < 0.05$ ). Therefore, the acidification process of goat yogurt is significantly influenced by monoculture of probiotic bacteria used in the manufacturing process. A similar trend was observed by Mituniewicz-Malek et al. (28), who reported a different increase in the titratable acidity of testing milk samples fermented with different probiotic bacteria between day 1 and 21 of storage (28). Bezerra et al. reported the glycolytic effect of added *L. acidophilus*, *L. casei*, *Lactococcus lactis* subsp. *lactis* and *L. paracasei* separately to goat “coalho” cheese and among the bacteria used for supplementation, *L. acidophilus* and *L. paracasei* showed a higher lactose hydrolysis potential with increasing storage time, indicating a consequent increase in acid production that caused a final product with a more abundant flavor and aroma (29).

### 3.2. Changes in the viable counts of lactic acid bacteria and probiotics of goat yogurt during storage

Differences in the acidity and pH of fermented milk could be correlated with the different production of lactic acid from the growth of lactic acid bacteria. Thus, viable counts of lactic acid bacteria in all goat yogurt were monitored in this study. It could be observed in **Figure 2** that the amount of living lactic acid bacteria and probiotic bacteria gradually reduced during the storage of goat yogurt, and GYA and GYC presented more viable counts of probiotic bacteria than the other goat yogurts. It is noteworthy that *L. acidophilus* and *L. casei* in the GYA and GYC group exhibited higher viable counts than 6.0 Log cfu/mL at the end of storage, which met the requirement of the recommended minimum counts of 6.0 Log cfu/mL, showing that goat yogurt could provide a suitable environment for *L. acidophilus* and *L. casei*. *Bifidobacterium animalis* survived at a low level with the prolongation of storage, mainly because the high titratable acidity and production of hydrogen peroxide by *Lactobacillus bulgaricus* (30). Hydrogen peroxide has a certain inhibitory effect on *Bifidobacterium animalis* and reduces its survival rate. Microencapsulation is a process in which the cells are retained within an encapsulating membrane to reduce cell loss or cell injury. Proteins, polysaccharides and prebiotics are frequently used as wall materials for microcapsules to protect and control the release of probiotics (31). Depending on the method used to form the beads, the encapsulation techniques applied to probiotics in fermented dairy products or biomass production can be classified into two groups: emulsion and extrusion. Both emulsion and extrusion techniques can increase the survival of probiotics by 80–95% (32). According to Heidebach et al. (33), casein-based microencapsulation could improve the survival

rate of freeze-dried *Bifidobacterium* strains during the storage for up to 90 days. Thus, microencapsulation was a promising way to protect the *Bifidobacterium* strains against the unsuitable environment in goat yogurt.

### 3.3. Effects of added probiotics on textural characteristics of goat yogurt during storage

Texture parameters are considered as an important quality assessment of fermented products that determine whether these products are attractive components in human diet. In the texture test, four indicators directly related to yogurt performance are evaluated: hardness is a parameter that measures the strength of yogurt gel network, and yogurt with higher hardness has better coagulation and more resistance to deformation; adhesiveness reveals its adhesion to the probe, and the thicker yogurt has greater adhesiveness; higher springiness of yogurt leads to a more welcoming taste; cohesiveness reveals the smoothness of goat yogurt, and the smaller cohesiveness, the better smoothness (34). As could be seen from **Table 1**, the hardness, adhesiveness and cohesion of goat milk yogurt gradually increased during the first 2 weeks, and subsequently decreased with the extension of the storage period, while the springiness showed an opposite tendency. The addition of probiotics had a significant influence on the texture characteristics of goat milk yogurt during the storage period. Several texture characteristics, including hardness and adhesiveness, of goat yogurt were significantly lower than these of cow milk yogurt, which explained that the coagulation of goat milk was worse than cow milk (21).

PCA is one of the significant statistical techniques for chemometrics and applied to the food quality evaluation. PCA was frequently used to reduce the dimension of the original data by the orthogonal transformation of vector space, which can effectively extract relevant information from complex datasets (35). In this study, the influence of probiotic bacteria on the texture of goat yogurt during the whole storage at the refrigerated temperature was summarized using PCA (**Figure 3**). During the entire storage of goat yogurt, the cumulative variance contributions of principal component 1 (PC1) and principal component 2 (PC2) are 76.578, 79.978, 85.462, 89.515, and 88.325%, which demonstrates that PC1 and PC2 are representative and well expressed for all indicators of mass structure analysis. **Table 2** showed the correlation coefficients between the four qualitative indicators and the PC. When this value is  $> \pm 0.7$ , the PC indicates a strong correlation with each attribute. As shown in **Table 2**, the indicators correlated with PC1 were hardness, adhesiveness and cohesion, and the indicator correlated with PC2 was springiness. In **Figure 3(I)**, PC1 and PC2 showed a consistent change throughout the whole storage and GYB samples had more

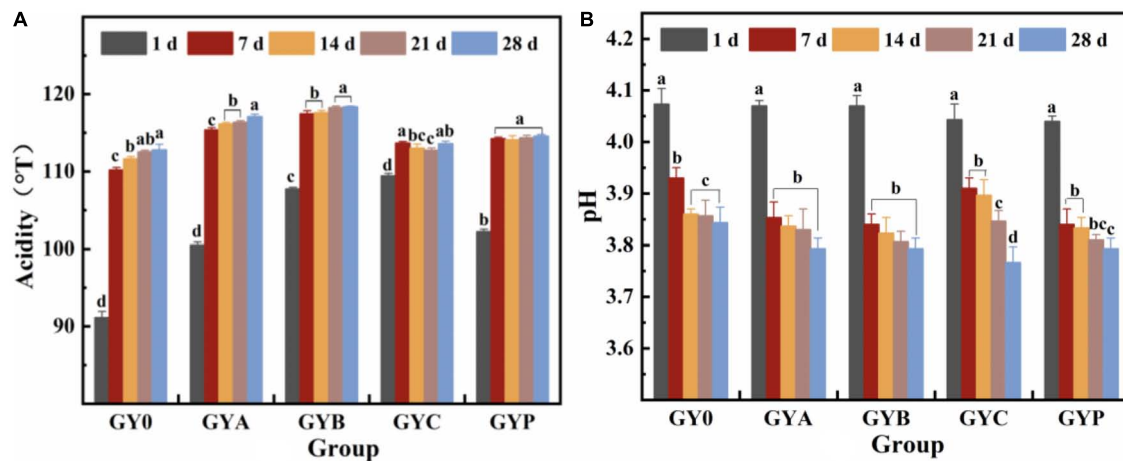


FIGURE 1

Changes in titratable acidity (A) and pH value (B) of probiotic goat yogurt stored at 4°C for 1, 7, 14, 21, and 28 days. GY0: goat yogurt fermented with 3% of YO-MIX187 commercial starter culture; GYA: goat yogurt fermented with 3% of YO-MIX187 commercial starter culture and *Lactobacillus acidophilus*; GYB: goat yogurt fermented with 3% of YO-MIX187 commercial starter culture and *Bifidobacterium animalis* ssp. *lactis*; GYC: goat yogurt fermented with 3% of YO-MIX187 commercial starter culture and *Lactobacillus casei* and GYP: goat yogurt fermented with 3% of YO-MIX187 commercial starter culture and *Lactobacillus plantarum*. The meaning of “a–d” refers to the significant differences in acidity and pH of the same experimental group during different storage periods ( $p < 0.05$ ).

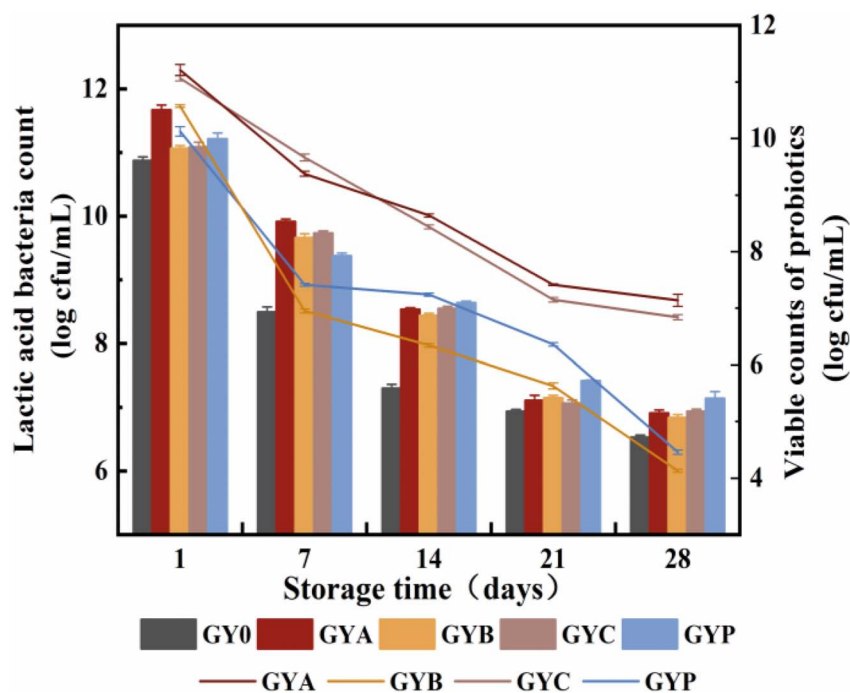


FIGURE 2

Changes in the viable counts of lactic acid bacteria and probiotics of goat yogurt during the storage.

distance with GY0 in the PC1 direction than the other probiotic bacteria at the end of the storage, indicating that the addition of *B. animalis* caused the different texture properties of goat yogurt. In Figure 3(II), GY0 obtained the highest scores in both PC1 and PC2 at the end of storage, showing that probiotic

bacteria had a negative effect on the texture characteristics of goat yogurt. Numerous reports suggest that the addition of probiotics to dairy products can result in the improvement of textural properties such as hardness, adhesiveness and so on (36). These differences could be attributed to the type of bacterial

strains used. The textural characteristics of GYB group were the lowest in all goat yogurt samples in the PC1 direction (Figure 3), probably because the lower pH environment affected the growth and reproduction of *Bifidobacterium animalis* (37).

### 3.4. Effects of added probiotics on water holding ability of goat yogurt during the storage

Yogurt water holding capacity refers to the ability of yogurt to retain all or part of its own water, and yogurt with low water holding capacity could lead to whey precipitation, thus, resulting in worse quality of fermented milk. As shown in Figure 4, water holding capacity of goat yogurt significantly decreased with the prolongation of storage, and the addition of probiotic bacteria greatly increased the water holding capacities of goat yogurt after 28 days of storage. At the end of storage, the water holding capacity of goat yogurt with probiotic bacteria fluctuated around 53%, indicating that the gel network of probiotic yogurt was relatively dense and compact. This phenomenon could be associated with the secretion of exo-polysaccharide (EPS) by probiotic bacteria, which could interact with proteins in goat

milk to enhance the hydration and water holding capacity of yogurt (38). It is worth noting that goat yogurt with *L. acidophilus* and *L. casei* had higher water holding capacity than those for tested yogurt with *B. animalis* and *L. plantarum*. It could be speculated that *Lactobacillus acidophilus* and *Lactobacillus casei* might produce more EPS during goat milk fermentation. These results were in concordance with earlier studies reported by Tong Dan et al. (39).

### 3.5. Effects of added probiotics on biological activities of goat yogurt during storage

Figures 5A, B showed the influence of probiotics on the DPPH free radical scavenging capabilities and FRAP values, respectively. DPPH free radical scavenging rate and FRAP value gradually increased in all goat yogurt formulation during the storage and yogurt with probiotic bacteria showed higher values than those of GY0. On the 28th day, the free radical scavenging rate of the four probiotics goat yogurt groups basically reached approximately 70%.

TABLE 1 Changes of texture properties of goat yogurt during the storage.

Texture properties	Group	Storage time (days)				
		1	7	14	21	28
Hardness (g)	GY0	51.418 ± 0.423 <sup>a</sup>	53.448 ± 1.309 <sup>a</sup>	72.385 ± 1.041 <sup>a</sup>	61.073 ± 0.106 <sup>a</sup>	57.879 ± 0.533 <sup>a</sup>
	GYA	48.533 ± 0.552 <sup>b</sup>	52.834 ± 0.300 <sup>a</sup>	68.026 ± 1.628 <sup>b</sup>	58.445 ± 1.075 <sup>b</sup>	53.547 ± 0.375 <sup>b</sup>
	GYB	46.352 ± 1.255 <sup>c</sup>	52.632 ± 1.509 <sup>ab</sup>	61.404 ± 1.039 <sup>d</sup>	52.183 ± 0.515 <sup>d</sup>	48.935 ± 0.903 <sup>c</sup>
	GYC	44.877 ± 0.337 <sup>d</sup>	50.827 ± 0.618 <sup>b</sup>	69.625 ± 1.352 <sup>b</sup>	59.563 ± 0.584 <sup>b</sup>	51.894 ± 2.397 <sup>b</sup>
	GYP	51.655 ± 0.474 <sup>a</sup>	54.169 ± 0.738 <sup>a</sup>	63.894 ± 1.052 <sup>c</sup>	55.954 ± 1.230 <sup>c</sup>	53.410 ± 0.741 <sup>b</sup>
Adhesiveness (g·s)	GY0	40.010 ± 0.242 <sup>b</sup>	61.819 ± 0.452 <sup>b</sup>	52.470 ± 1.171 <sup>c</sup>	48.599 ± 1.171 <sup>b</sup>	42.736 ± 0.886 <sup>b</sup>
	GYA	39.409 ± 0.073 <sup>b</sup>	49.933 ± 0.797 <sup>d</sup>	47.714 ± 0.435 <sup>d</sup>	37.457 ± 0.335 <sup>c</sup>	35.151 ± 0.287 <sup>c</sup>
	GYB	37.277 ± 0.778 <sup>c</sup>	44.598 ± 0.477 <sup>c</sup>	47.755 ± 0.210 <sup>d</sup>	32.396 ± 0.436 <sup>d</sup>	26.834 ± 0.303 <sup>d</sup>
	GYC	39.678 ± 0.244 <sup>b</sup>	63.994 ± 0.675 <sup>a</sup>	55.532 ± 0.379 <sup>b</sup>	47.572 ± 0.361 <sup>b</sup>	42.253 ± 0.344 <sup>b</sup>
	GYP	43.253 ± 0.953 <sup>a</sup>	56.621 ± 0.505 <sup>c</sup>	60.193 ± 0.629 <sup>a</sup>	50.501 ± 0.805 <sup>a</sup>	44.654 ± 0.409 <sup>a</sup>
Springiness	GY0	0.953 ± 0.002 <sup>a</sup>	0.947 ± 0.002 <sup>bc</sup>	0.929 ± 0.008 <sup>b</sup>	0.951 ± 0.003 <sup>a</sup>	0.957 ± 0.006 <sup>a</sup>
	GYA	0.902 ± 0.009 <sup>b</sup>	0.974 ± 0.007 <sup>a</sup>	0.948 ± 0.002 <sup>a</sup>	0.952 ± 0.001 <sup>a</sup>	0.943 ± 0.004 <sup>b</sup>
	GYB	0.956 ± 0.005 <sup>a</sup>	0.944 ± 0.003 <sup>c</sup>	0.935 ± 0.001 <sup>b</sup>	0.947 ± 0.001 <sup>ab</sup>	0.951 ± 0.004 <sup>a</sup>
	GYC	0.953 ± 0.002 <sup>a</sup>	0.953 ± 0.004 <sup>b</sup>	0.948 ± 0.001 <sup>a</sup>	0.945 ± 0.004 <sup>b</sup>	0.951 ± 0.002 <sup>a</sup>
	GYP	0.947 ± 0.002 <sup>a</sup>	0.941 ± 0.002 <sup>c</sup>	0.950 ± 0.002 <sup>a</sup>	0.945 ± 0.001 <sup>b</sup>	0.944 ± 0.003 <sup>b</sup>
Cohesion	GY0	26.757 ± 0.203 <sup>c</sup>	30.036 ± 0.212 <sup>b</sup>	32.591 ± 1.071 <sup>b</sup>	28.726 ± 0.403 <sup>b</sup>	24.084 ± 0.255 <sup>b</sup>
	GYA	27.257 ± 0.122 <sup>b</sup>	30.477 ± 0.286 <sup>c</sup>	32.790 ± 0.609 <sup>b</sup>	26.531 ± 0.438 <sup>c</sup>	24.498 ± 0.347 <sup>b</sup>
	GYB	17.527 ± 0.392 <sup>c</sup>	21.299 ± 0.251 <sup>c</sup>	24.739 ± 0.301 <sup>c</sup>	24.569 ± 0.528 <sup>d</sup>	17.289 ± 0.054 <sup>c</sup>
	GYC	28.453 ± 0.183 <sup>a</sup>	34.313 ± 0.141 <sup>a</sup>	36.180 ± 0.088 <sup>a</sup>	30.954 ± 0.271 <sup>a</sup>	25.693 ± 0.483 <sup>a</sup>
	GYP	24.609 ± 0.095 <sup>d</sup>	27.715 ± 0.020 <sup>d</sup>	33.532 ± 0.202 <sup>b</sup>	26.819 ± 0.142 <sup>c</sup>	25.545 ± 0.122 <sup>a</sup>

Lowercase letters (a–d) for each indicator in this table indicate significant differences between experimental groups ( $p < 0.05$ ).



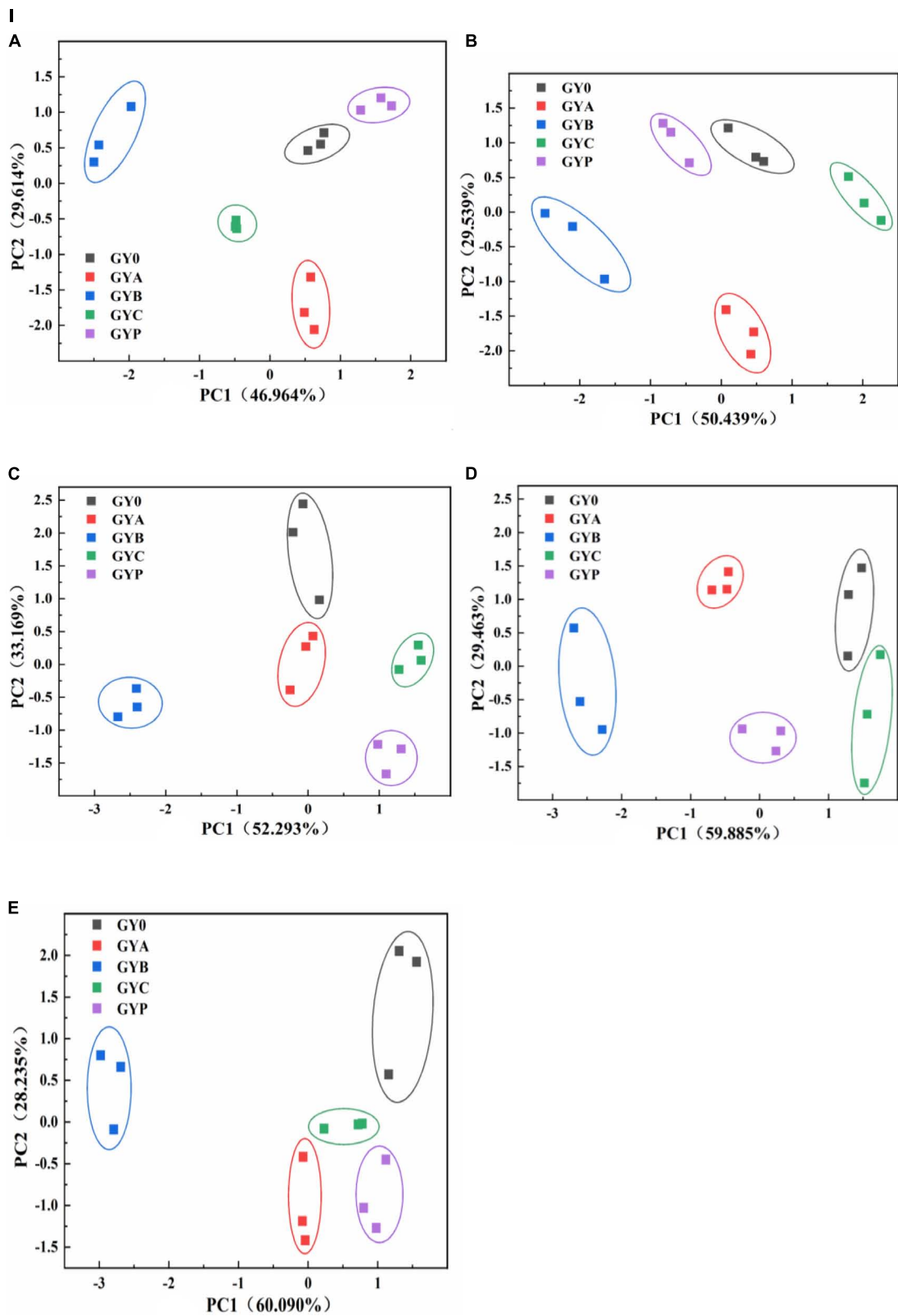


FIGURE 3  
(continued)

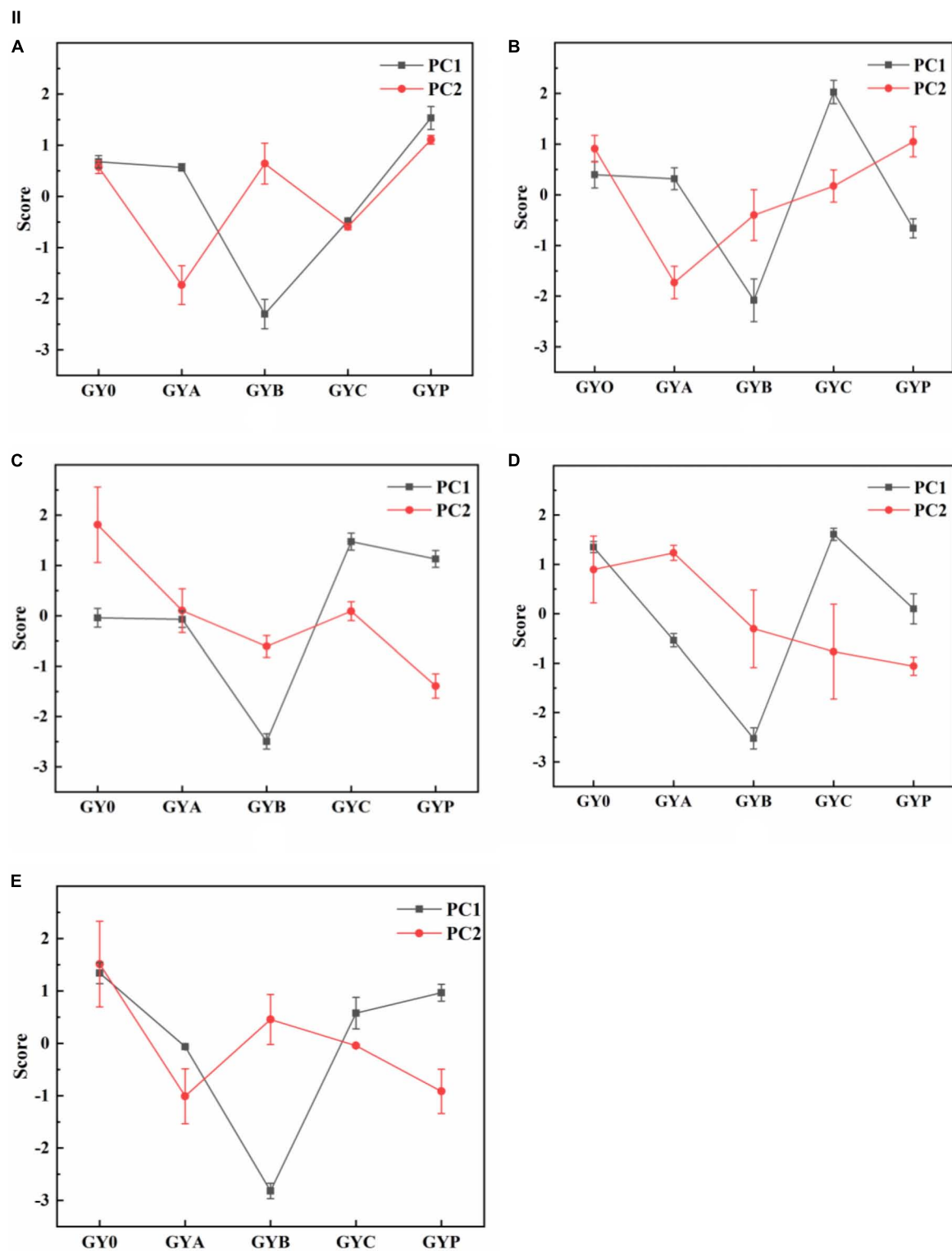


FIGURE 3

Effect of probiotic supplementation on textural characteristics of goat yogurt during the storage. (I) The principal component analysis scatter plot showed textural properties of goat yogurt at various storage times. (II) The principal component analysis score plot. (A–E) Represented the textural principal component analysis of goat yogurt stored for 1, 7, 14, 21, and 28 days, respectively.

TABLE 2 Factor loading of two principal components during the storage at refrigerated temperature.

Storage (d)	Component	Hardness (g)	Adhesiveness (g.s)	Springiness	Cohensiveness
1	1	0.752	0.868	−0.330	0.671
	2	0.431	0.319	0.805	−0.500
7	1	−0.539	0.799	0.383	0.970
	2	0.359	0.591	−0.838	0.043
14	1	0.507	0.765	0.573	0.960
	2	0.846	−0.311	−0.686	0.211
21	1	0.894	0.857	−0.013	0.929
	2	0.364	−0.257	0.985	−0.100
28	1	0.807	0.953	0.070	0.916
	2	0.306	−0.036	0.971	−0.305

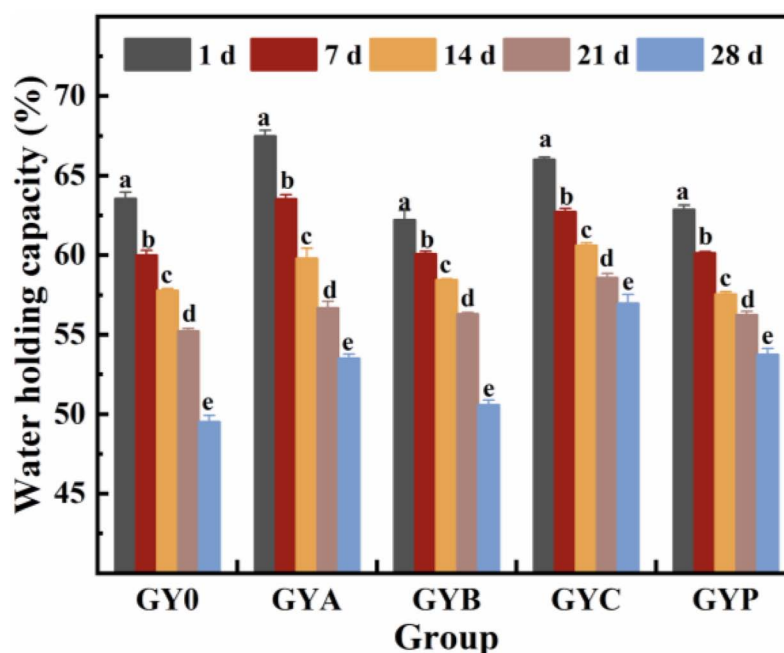


FIGURE 4

Effect of probiotic supplementation on water holding capacity of goat yogurt during the storage. The meaning of “a–e” refers to the significant differences in water holding capacity of the same experimental group during different storage periods ( $p < 0.05$ ).

Reactive oxygen species are by-products of natural aerobic metabolisms or host defense mechanism. Reactive oxygen species-mediated oxidative stress plays a key role in the incidence and development of several chronic diseases, including cancer, diabetes, aging, heart diseases and Alzheimer's disease. During the last decades, antioxidant substances derived from natural sources have received more and more attention due to their abilities to eliminate reactive oxygen species and radicals. Yogurt has a certain antioxidant effect due to the large amount of amino acids and polypeptides with antioxidant activity produced during the fermentation. Except for the peptides and amino acids, bacterial EPS also have the ability

to upregulate the enzymatic and non-enzymatic antioxidant activities by degrading of superoxide anion and hydrogen peroxide. In a previous study from Rahmawati and Suntornsuk (40), compared to yogurt made from ordinary cow's milk, goat yogurt has considerably better antioxidant activity due to the high protein content of goat milk (40). Probiotic bacteria, as dietary additives, have long history been used to improve the antioxidant activity of foods. In both *vivo* and *vitro* experiments, probiotics had antioxidant potential to reduce the oxidative damage to cells. As described by Ejtahed et al. (41), the consumption of probiotic yogurt with *L. acidophilus* and *B. lactis* could improve fasting blood glucose and antioxidant status in

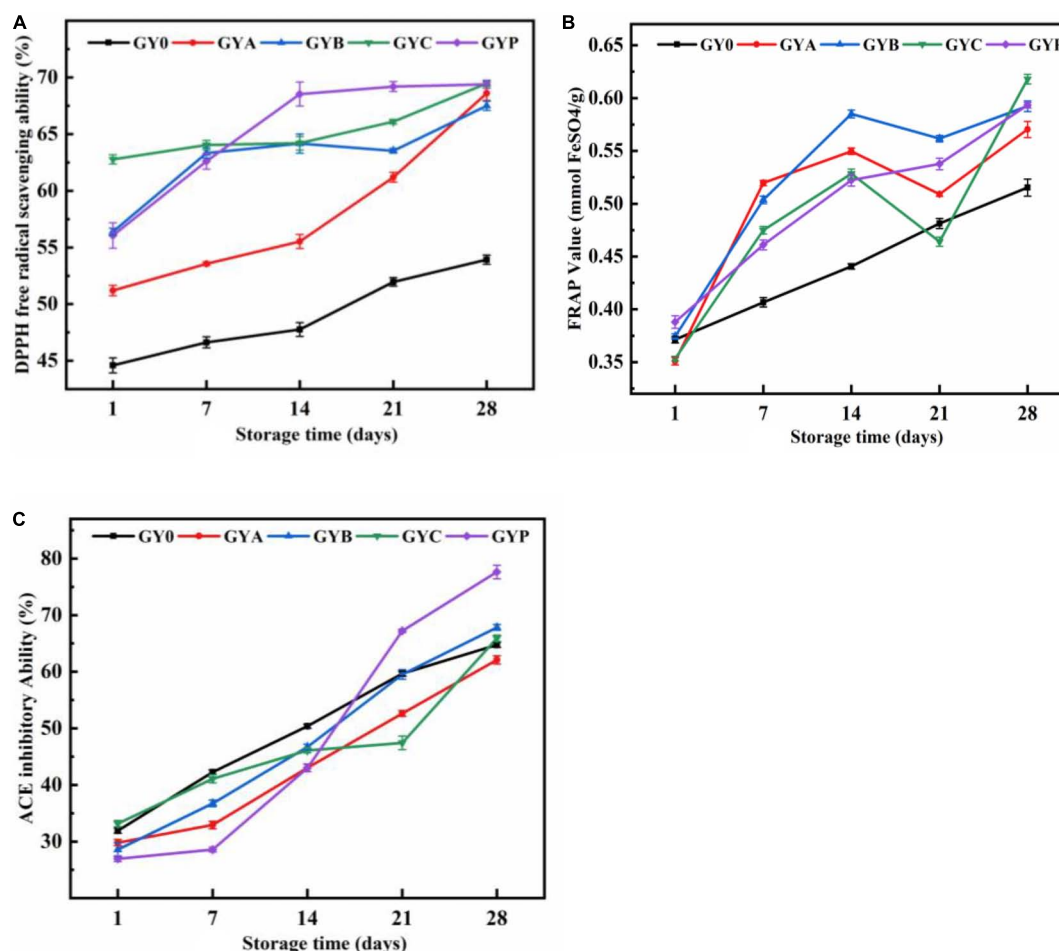


FIGURE 5

Effect of added probiotics on DPPH free radical scavenging ability (A), ferric reducing antioxidant activity (B) and ACE inhibitory activity (C) of goat yogurt during the storage.

type two diabetic patients, thus, resulting in the prevention of diabetes progression (41).

The effect of probiotic bacteria on the antihypertensive activity of goat yogurt was shown in Figure 5C. ACE inhibitory activity of goat yogurt gradually increased with the extension of the storage. Antihypertensive ability of GYP group was higher than those in the other yogurt groups, demonstrating a synergistic effect of *Lactobacillus plantarum* and commercial starter cultures. Antihypertensive function of probiotic yogurt is derived from antihypertensive peptides that inhibit ACE activity during the fermentation, not from the probiotics themselves. Thus, increases in the ACE inhibitory activity during the storage could be explained by the constant hydrolysis of the protein, resulting in the modification of small molecular peptides with ACE inhibition potential (42). The concentration of ACE inhibitory peptides depends on a balance between their formation and degradation into inactive peptide and amino acid (43).

### 3.6. Effect of probiotics on organoleptic evaluation of the yogurt stored for 14 days

The organoleptic evaluation of goat yogurt with probiotics was shown in the Figure 6A. It could be seen that the overall acceptability and various indicators of the yogurt containing probiotics were significantly higher than those of the control GY0 group. It showed that the addition of probiotics improved the organoleptic properties of yogurt, especially in terms of flavor and aroma. Moreover, GYC obtained the lowest scores in goaty taste, which indicated that the proper addition of *L. casei* could effectively cover the undesirable goaty aroma in goat milk, thus, improving the flavor of goat yogurt. The butter-like aroma from the fermentation of *Lactobacillus casei* resulted in the highest flavor and aroma scores in GYC group. Several studies pointed out that *Lactobacillus casei* is highly capable of utilizing the proteins in the whey and produces abundant

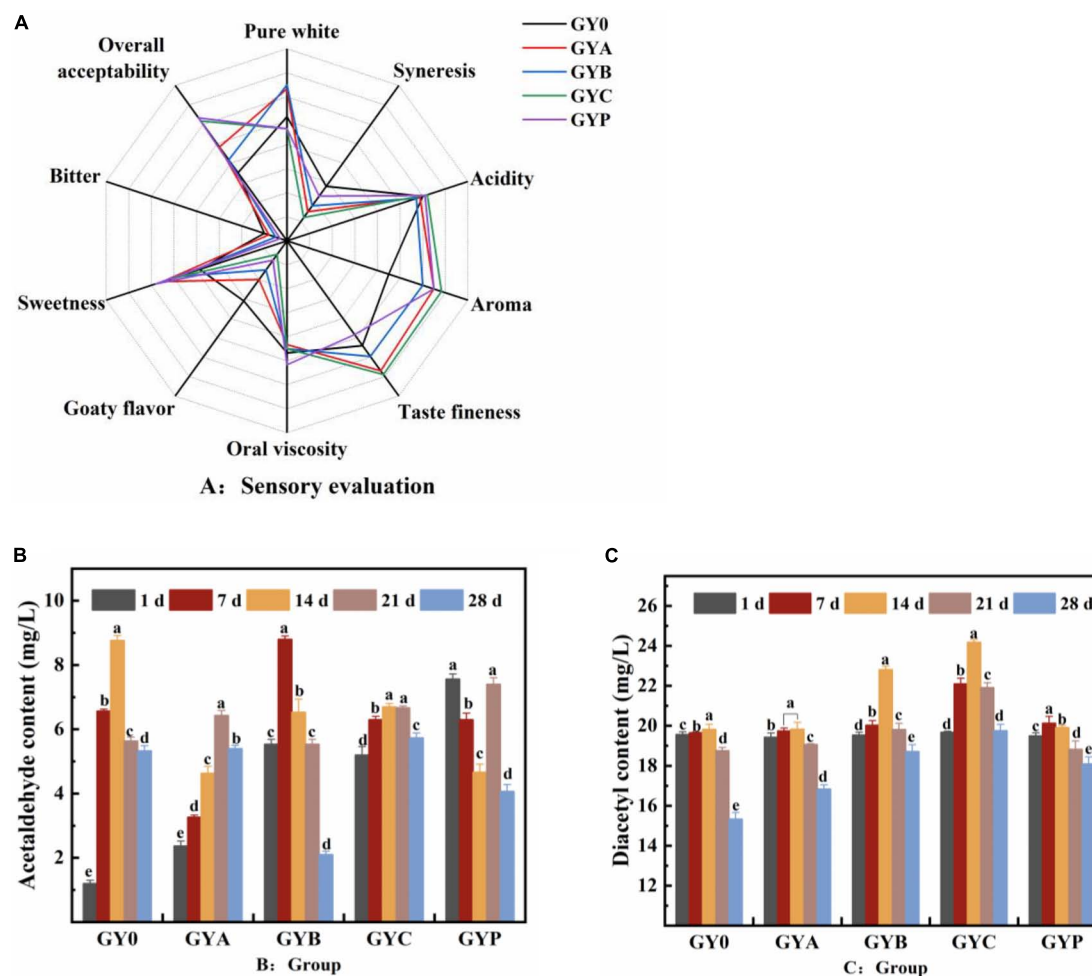


FIGURE 6

(A) The sensory evaluation of probiotic goat yogurt after the storage at the refrigerated temperature for 28 days. (B) Changes in acetaldehyde content of probiotic goat yogurt during the storage at 4°C. (C) Changes in diacetyl content of goat yogurt fermented with probiotic bacteria during the storage at 4°C. The meaning of "a–e" refers to the significant differences in acetaldehyde content and diacetyl content of the same experimental group during different storage periods ( $p < 0.05$ ).

peptides, which was associated with the higher acceptance of GYC group.

The flavor components of goat yogurt are mainly composed of two parts, one is the original volatile compounds in milk, and the other is flavor compounds produced by the fermentation of lactic acid bacteria (26). Acetaldehyde and diacetyl were two important aroma compounds in yogurt, which differ from milk and other fermented dairy products (44, 45). Acetaldehyde is demonstrated to have a green apple or nutty aroma and is considered as the most significant contributor to the typical yogurt flavor. Diacetyl confers a sweet and butter-like aroma and is frequently applied to improve the buttery aroma (46). As is shown in Figure 6B, GY0, GYA, GYB, and GYC groups displayed a significant increase in the acetaldehyde content followed by a decrease at the end of the storage. The acetaldehyde content of both GYB and GYP groups was similar

to that of GY0 group. The acetaldehyde content of the GY0 group was always at a high-level during storage, presumably due to the high content of *Streptococcus thermophilus* and *Lactobacillus bulgaricus*. The enzymes secreted by these two bacteria could generate acetaldehyde, and co-cultivation can increase the production of acetaldehyde in goat yogurt (47, 48).

The addition of probiotics had a more significant effect on the diacetyl content in goat yogurt (Figure 6C). The diacetyl concentration of yogurt in the four goat yogurts containing probiotics was greater than that in the GY0 group with the extension of the storage. Especially, the diacetyl concentration in GYC group is above 20 mg/L and significantly higher than those in other groups. These results suggested that the addition of probiotics during the fermentation of goat milk led to the increase of diacetyl, bringing preferred aromatic properties to goat yogurt.



## 4. Conclusion

During the storage, the types of probiotics had a considerable influence on the texture characteristics, microbial viable count and organoleptic of goat yogurt. Moreover, the addition of probiotics could significantly improve the biological activity of goat yogurt, including antioxidant activity and ACE inhibitory activity. GYC presented the best properties of hardness, adhesiveness, water holding capacity, antioxidant activity and overall acceptability. The viable counts in GYC and GYA remained adequate to promote the health benefits to the consumer during the storage at the refrigerated temperature. Based on our results, *L. casei* are recommended for the production of fermented goat milk with satisfactory texture properties, pleasant sensory quality and high bioactivity.

## Data availability statement

The raw data supporting the conclusions of this article will be made available by the authors, without undue reservation.

## Author contributions

YY: investigation and methodology. RZ: writing—original draft. FZ: reviewing and software. BW: conceptualization. YL:

supervision and funding acquisition. All authors contributed to the article and approved the submitted version.

## Funding

This work was supported by the Shaanxi Key Research and Development Plan (2021ZDLNY02-08), the National Natural Science Foundation of China (31801566), and the Xi'an Science and Technology Project (22GXFW0022).

## Conflict of interest

The authors declare that the research was conducted in the absence of any commercial or financial relationships that could be construed as a potential conflict of interest.

## Publisher's note

All claims expressed in this article are solely those of the authors and do not necessarily represent those of their affiliated organizations, or those of the publisher, the editors and the reviewers. Any product that may be evaluated in this article, or claim that may be made by its manufacturer, is not guaranteed or endorsed by the publisher.

## References

1. Prajapati DB, Kapadiya DB, Jain AK, Mehta BM, Darji VB, Aparnathi KD. Comparison of Surti goat milk with cow and buffalo milk for physicochemical characteristics, selected processing-related parameters and activity of selected enzymes. *Vet World*. (2017) 10:477–84. doi: 10.14202/vetworld.2017.477-484
2. Sousa YRF, Medeiros LB, Manuela M, Pintado E, Queiroga RCRE. Trends in food science & technology goat milk oligosaccharides: composition, analytical methods and bioactive and nutritional properties. *Trends Food Sci Technol*. (2019) 92:152–61. doi: 10.1016/j.tifs.2019.07.052
3. Niyazbekova Z, Yao XT, Liu MJ, Bold N, Tong JZ, Chang JJ, et al. Compositional and functional comparisons of the microbiota in the colostrum and mature milk of dairy goats. *Animals*. (2020) 10:1955. doi: 10.3390/ani10111955
4. Watkins PJ, Jaborek JR, Teng F, Day L, Castada HZ, Baringer S, et al. Branched chain fatty acids in the flavour of sheep and goat milk and meat: a review. *Small Rumin Res*. (2021) 200:106398. doi: 10.1016/j.smallrumres.2021.106398
5. Hill C, Guarner F, Reid G, Gibson GR, Merenstein DJ, Pot B, et al. Expert consensus document: the international scientific association for probiotics and prebiotics consensus statement on the scope and appropriate use of the term probiotic. *Nat Rev Gastroenterol Hepatol*. (2014) 11:506–14. doi: 10.1038/nrgastro.2014.66
6. Ranadheera CS, Evans CA, Baines SK, Balthazar CF, Cruz AG, Esmerino EA, et al. Probiotics in goat milk products: delivery capacity and ability to improve sensory attributes. *Compr Rev Food Sci Food Saf*. (2019) 18:867–82. doi: 10.1111/1541-4337.12447
7. Ejtahed HS, Mohtadi-Nia J, Homayouni-Rad A, Niafar M, Asghari-Jafarabadi M, Mofid V, et al. Effect of probiotic yogurt containing *Lactobacillus acidophilus* and *Bifidobacterium lactis* on lipid profile in individuals with type 2 diabetes mellitus. *J Dairy Sci*. (2011) 94:3288–94. doi: 10.3168/jds.2010-4128
8. Mishra V, Shah C, Mokashe N, Chavan R, Yadav H, Prajapati J. Probiotics as potential antioxidants: a systematic review. *J Agric Food Chem*. (2015) 63:3615–26. doi: 10.1021/jf506326t
9. Moreno-Montoro M, Olalla-Herrera M, Rufián-Henares J, Martínez RG, Miralles B, Bergillos T, et al. Antioxidant, ACE-inhibitory and antimicrobial activity of fermented goat milk: activity and physicochemical property relationship of the peptide components. *Food Funct*. (2017) 8:2783–91. doi: 10.1039/c7fo00666g
10. Balthazar CF, Silva HLA, Esmerino EA, Rocha RS, Moraes J, Carmo MAV, et al. The addition of inulin and *Lactobacillus casei* 01 in sheep milk ice cream. *Food Chem*. (2018) 246:464–72. doi: 10.1016/j.foodchem.2017.12.002
11. Verruck S, Dantas A, Schwinden E. Functionality of the components from goat's milk, recent advances for functional dairy products development and its implications on human health. *J Funct Foods*. (2019) 52:243–57. doi: 10.1016/j.jff.2018.11.017
12. Park YW, Oglesby J, Hayek SA, Aljaloud SO, Gyawali N, Ibrahim SA. Impact of different gums on textural and microbial properties of goat milk yogurts during refrigerated storage. *Foods*. (2019) 8:169. doi: 10.3390/foods8050169
13. Moreno-Montoro M, Navarro-Alarcón M, Bergillos-Meca T, Giménez-Martínez R, Sánchez-Hernández S, Olalla-Herrera M. Physicochemical, nutritional, and organoleptic characterization of a skimmed goat milk fermented with the probiotic strain *Lactobacillus plantarum* C4. *Nutrients*. (2018) 10:633. doi: 10.3390/nu10050633
14. Zhang SS, Xu ZS, Qin LH, Kong J. Low-sugar yogurt making by the co-cultivation of *Lactobacillus plantarum* WCFS1 with yogurt starter cultures. *J Dairy Sci*. (2020) 103:3045–54. doi: 10.3168/jds.2019-17347

15. Kailasapathy K, Harmstorff I, Phillips M. Survival of *Lactobacillus acidophilus* and *Bifidobacterium animalis* ssp. *lactis* in stirred fruit yogurts. *LWT*. (2008) 41:1317–22. doi: 10.1016/j.lwt.2007.08.009
16. Gharibzadeh SMT, Chronakis IS. Crosslinking of milk proteins by microbial transglutaminase: utilization in functional yogurt products. *Food Chem.* (2018) 245:620–32. doi: 10.1016/j.foodchem.2017.1.0.138
17. Mishra S, Mishra HN. Effect of synbiotic interaction of fructooligosaccharide and probiotics on the acidification profile, textural and rheological characteristics of fermented soy milk. *Food Bioproc Tech.* (2012) 6:3166–76. doi: 10.1007/s11947-012-1021-4
18. Lapiere L, Undeland P, Cox LJ. Lithium chloride-sodium propionate agar for the enumeration of bifidobacteria in fermented dairy products. *J Dairy Sci.* (1992) 75:1192–6. doi: 10.3168/jds.S0022-0302(92)77866-7
19. Ravula RR, Shah NP. Selective enumeration of *Lactobacillus* casei from yogurts and fermented milk drinks. *Biotechnol Tech.* (2008) 12:819–22.
20. Bujalance C, Jiménez-valera M, Moreno E, Ruiz-bravo A. A selective differential medium for *Lactobacillus plantarum*. *J Microbiol Methods.* (2006) 66:572–5. doi: 10.1016/j.mimet.2006.02.005
21. Feng C, Wang B, Zhao A, Wei L, Shao Y, Wang Y, et al. Quality characteristics and antioxidant activities of goat milk yogurt with added jujube pulp. *Food Chem.* (2019) 277:238–45. doi: 10.1016/j.foodchem.2018.10.104
22. Benzie IFF, Strain JJ. The ferric reducing ability of plasma (FRAP) as a measure of “antioxidant power”: the FRAP assay. *Anal Biochem.* (1996) 76:70–6.
23. Xie J, Du M, Shen M, Wu T, Lin L. Physico-chemical properties, antioxidant activities and angiotensin-I converting enzyme inhibitory of protein hydrolysates from Mung bean (*Vigna radiate*). *Food Chem.* (2019) 270:243–50. doi: 10.1016/j.foodchem.2018.07.103
24. Machado TADG, de Oliveira MEG, Campos MIF, de Assis POA, de Souza EL, Madruga MS, et al. Impact of honey on quality characteristics of goat yogurt containing probiotic *Lactobacillus acidophilus*. *LWT Food Sci Technol.* (2017) 80:221–9. doi: 10.1016/j.lwt.2017.02.013
25. Ka N. The relative importance of texture, taste and aroma on a yogurt-type snack food preference in the young and the elderly. *Food Qual Prefer.* (2003) 14:177–86.
26. Taylor P, Cheng H. Volatile flavor compounds in yogurt: a review volatile flavor compounds in yogurt. *Crit Rev Food Sci Nutr.* (2010) 50:938–50. doi: 10.1080/10408390903044081
27. Vasbinder AJ, Alting AC, Visschers RW, De Kruif CG. Texture of acid milk gels: formation of disulfide cross-links during acidification. *Int Dairy J.* (2003) 13:29–38. doi: 10.1016/S0958-6946(02)00141-3
28. Mituniewicz-Malek A, Ziarno M, Dmytrów I, Balejko J. Short communication: effect of the addition of *Bifidobacterium* monocultures on the physical, chemical, and sensory characteristics of fermented goat milk. *J Dairy Sci.* (2017) 100:6972–9. doi: 10.3168/jds.2017-12818
29. Bezerra TKA, de Oliveira Arcanjo NM, Garcia EF, Gomes AMP, de Cássia Ramos do Egypto Queiroga R, de Souza EL, et al. Effect of supplementation with probiotic lactic acid bacteria, separately or combined, on acid and sugar production in goat ‘coalho’ cheese. *LWT.* (2017) 75:710–8. doi: 10.1016/j.lwt.2016.1.0.023
30. Dave RI, Shah NP. Effect of cysteine on the viability of yoghurt and probiotic bacteria in yoghurts made with commercial starter cultures. *Int Dairy J.* (1997) 7:537–45. doi: 10.1016/S0958-6946(97)00053-8
31. Krasaekoopt W, Bhandari B, Deeth H. Evaluation of encapsulation techniques of probiotics for yoghurt. *Int Dairy J.* (2003) 13:3–13.
32. Gruskiene R, Bockuviene A, Sereikaite J. Microencapsulation of bioactive ingredients for their delivery into fermented milk products: a review. *Molecules.* (2021) 26:4601. doi: 10.3390/molecules26154601
33. Heidebach T, Forst P, Kulozik U. Microencapsulation of probiotic cells for food applications. *Crit Rev Food Sci Nutr.* (2012) 52:291–311. doi: 10.1080/10408398.2010.499801
34. Gauche C, Tomazi T, Barreto PLM, Ogliari PJ, Bordinon-Luiz MT. Physical properties of yoghurt manufactured with milk whey and transglutaminase. *LWT.* (2009) 42:239–43. doi: 10.1016/j.lwt.2008.05.023
35. Wu J, Ouyang Q, Park B, Kang R, Wang Z, Wang L, et al. Physicochemical indicators coupled with multivariate analysis for comprehensive evaluation of matcha sensory quality. *Food Chem.* (2022) 371:131100. doi: 10.1016/j.foodchem.2021.131100
36. Gramile Q, Meira S, Magnani M, Cesino F, Júnior DM, Cássia R, et al. Effects of added *Lactobacillus acidophilus* and *Bifidobacterium lactis* probiotics on the quality characteristics of goat ricotta and their survival under simulated gastrointestinal conditions. *Food Res Int.* (2015) 76:828–38. doi: 10.1016/j.foodres.2015.08.002
37. Jayamanne VS, Adams MR. Original article Modelling the effects of pH, storage temperature and redox potential (E h) on the survival of bifidobacteria in fermented milk. *Int J Food Sci Technol.* (2009) 44:1131–8. doi: 10.1111/j.1365-2621.2009.01931.x
38. Pan L, Wang Q, Qu L, Liang L, Han Y, Wang X, et al. Pilot-scale production of exopolysaccharide from *Leuconostoc pseudomesenteroides* XG5 and its application in set yogurt. *J Dairy Sci.* (2022) 105:1072–83. doi: 10.3168/jds.2021-20997
39. Dan T, Jin R, Ren W, Li T, Chen H, Sun T. Characteristics of milk fermented by *Streptococcus thermophilus* MGA45-4 and the profiles of associated volatile compounds during fermentation and storage. *Molecules.* (2018) 23:878. doi: 10.3390/molecules23040878
40. Rahmawati IS, Suntornasuk W. Effects of fermentation and storage on bioactive activities in milks and yoghurts. *Proc Chem.* (2016) 18:53–62. doi: 10.1016/j.proche.2016.01.010
41. Ejtahed HS, Mohtadi-Nia J, Homayouni-Rad A, Niafar M, Asghari-Jafarabadi M, Mofid V. Probiotic yogurt improves antioxidant status in type 2 diabetic patients. *Nutrition.* (2012) 28:539–43. doi: 10.1016/j.nut.2011.08.013
42. Ramchandran L, Shah NP. LWT - Food science and technology characterization of functional, biochemical and textural properties of synbiotic low-fat yogurts during refrigerated storage. *LWT Food Sci Technol.* (2010) 43:819–27. doi: 10.1016/j.lwt.2010.01.012
43. López-Fandiño R, Otte J, van Camp J. Physiological, chemical and technological aspects of milk-protein-derived peptides with antihypertensive and ACE-inhibitory activity. *Int Dairy J.* (2006) 16:1277–93. doi: 10.1016/j.idairyj.2006.06.004
44. Hernandez-Valdes JA, Solopova A, Kuipers OP. Development of *Lactococcus lactis* biosensors for detection of diacetyl. *Front Microbiol.* (2020) 11:1032. doi: 10.3389/fmicb.2020.01032
45. Yekta M, Ansari S. Jujube mucilage as a potential stabilizer in stirred yogurt: improvements in the physicochemical, rheological, and sensorial properties. *Food Sci Nutr.* (2019) 7:3709–21. doi: 10.1002/fsn3.1230
46. Tian H, Shi Y, Zhang Y, Yu H, Mu H, Chen C. Screening of aroma - producing lactic acid bacteria and their application in improving the aromatic profile of yogurt. *J Food Biochem.* (2019) 43:e12837. doi: 10.1111/jfbc.12837
47. Beshkova D, Simova E, Frengova G, Simov Z. Production of flavour compounds by yogurt starter cultures. *J Ind Microbiol Biotechnol.* (1998) 20:180–6.
48. Chaves ACS, Fernandez M, Lerayer ALS, Mierau I, Kleerebezem M, Hugenoltz J. Metabolic engineering of acetaldehyde production by *Streptococcus thermophilus*. *Appl Environ Microbiol.* (2002) 68:5656–62. doi: 10.1128/AEM.68.11.5656



## OPEN ACCESS

## EDITED BY

Hao Jiang,  
Northwest A&F University, China

## REVIEWED BY

Zhenbin Liu,  
Shaanxi University of Science and  
Technology, China  
Wenchao Cai,  
Shihezi University, China  
Gongnian Xiao,  
Zhejiang University of Science and  
Technology, China

## \*CORRESPONDENCE

Junbo Liu  
✉ junbliu@126.com  
Ligen Zou  
✉ jgszlg@163.com

## SPECIALTY SECTION

This article was submitted to  
Nutrition and Food Science Technology,  
a section of the journal  
Frontiers in Nutrition

RECEIVED 08 November 2022

ACCEPTED 31 December 2022

PUBLISHED 19 January 2023

## CITATION

Liu J, Wang Q, Weng L, Zou L, Jiang H, Qiu J  
and Fu J (2023) Analysis of sucrose addition on  
the physicochemical properties of blueberry  
wine in the main fermentation.  
*Front. Nutr.* 9:1092696.  
doi: 10.3389/fnut.2022.1092696

## COPYRIGHT

© 2023 Liu, Wang, Weng, Zou, Jiang, Qiu and  
Fu. This is an open-access article distributed  
under the terms of the [Creative Commons  
Attribution License \(CC BY\)](#). The use,  
distribution or reproduction in other forums is  
permitted, provided the original author(s) and  
the copyright owner(s) are credited and that  
the original publication in this journal is cited,  
in accordance with accepted academic practice.  
No use, distribution or reproduction is  
permitted which does not comply with these  
terms.

# Analysis of sucrose addition on the physicochemical properties of blueberry wine in the main fermentation

Junbo Liu<sup>1\*</sup>, Qian Wang<sup>1</sup>, Liping Weng<sup>1</sup>, Ligen Zou<sup>1\*</sup>, Huiyan Jiang<sup>1</sup>,  
Jing Qiu<sup>1</sup> and Jiafei Fu<sup>2</sup>

<sup>1</sup>Institute of Agricultural Products Processing, Hangzhou Academy of Agricultural Sciences, Hangzhou, China, <sup>2</sup>Department of Environmental Health and Food Science and Technology, Hangzhou Wanxiang Polytechnic, Hangzhou, China

**Introduction:** Harvested blueberries can be processed into wine to extend their shelf life and increase their commercial value. In order to produce fruit wine, external sugar is often added prior to fermentation to increase the final alcohol content to a target of 8–12% (v/v) to meet consumer expectations.

**Method:** we explore the effect of 8–14% (w/w) sucrose on the physicochemical properties of blueberry wine throughout the main fermentation process. We monitor changes of alcohol content, sugar, color, phenol, acidity, anthocyanin, and odor.

**Results and discussion:** We notice that sucrose affects the fermentation process and physicochemical composition of the final blueberry wine by fermentation rate, fermentation color and protection of functional substances protection. Additional sucrose extends the total time of fermentation, and increases wine acidity. The color of the wine is also affected, with added sugar darkening and yellowing the final product. Interestingly, the sucrose has a protective effect on anthocyanin levels, although total anthocyanin levels are still substantially reduced following fermentation. Finally, the additional sugar increases accumulation of volatile odor components, particularly alcohols and esters, as measured by an electronic nose. We conclude that an addition of 12% sucrose produces wine with superior physicochemical properties of alcohol, anthocyanin loss and odor relative to other conditions tested and recommend this approach to commercial manufacturers.

## KEYWORDS

physicochemical properties, blueberry, wine, main fermentation, sucrose

## Introduction

Blueberries are colloquially referred to as the king of fruits and universally loved by consumers (1, 2). Blueberries are rich in carbohydrates, organic acids, anthocyanins, phenols, flavonoids and other beneficial nutrients with antioxidative (3) and immunostimulatory effects (4), which can improve hypoglycemia (5), and protect eyesight (6). However, blueberries have a limited shelf life of 3–7 days at room temperature, resulting in rapid deterioration and short retail distance (7, 8). Furthermore, blueberries with thin skin and higher flesh content are at increased risk of microbial infection (9). For these reasons, commercial harvest enterprises can incur serious losses from spoilage following a typical summer harvest. To avoid this, fresh blueberries can be fermented into wine (10), dried (11), or juiced to extend their shelf life and increase the profitability of a harvest (12).

Blueberry wine is a high-value processed product from the highly perishable blueberry fruit, which is widely consumed (13). In recent years, the production of blueberries in China has gradually increased. Blueberries have berry characteristics similar to grapes and are used for fermentation and wine production. In the Chinese market, blueberry wine is mainly

dry red. Blueberry wine is produced from fresh or frozen blueberry fruit through crushing, fermentation, aging, filtration, filling and packing (14). The fermentation process produces alcohol and carbon dioxide from metabolism of sugar by wine yeast (*Saccharomyces cerevisiae*). The sugar content of blueberry is generally 80–100 g·L<sup>-1</sup>, and lower than grapes of 214–228 g·L<sup>-1</sup> (15), the most widely-used fruit to produce wine. While 17 g·L<sup>-1</sup> sugar present in blueberries should theoretically produce 1% (v/v) alcohol after fermentation, consumers generally expect an alcohol content of 8–12% (v/v). To produce the proper alcohol content, commercial producers typically supplement the crushed fruit with sucrose, an economical sugar source. However, it is unclear how this additional sucrose affects the odor and physicochemical properties during fermentation.

The fermentation process of blueberry wine can be divided into a main and secondary fermentation stage (16). During main fermentation, yeast propagate and produce ethanol (2). This dynamic stage also results in the degradation, transformation, generation of new substances and chemical byproducts. Conversely, the post fermentation process is predominantly a odor improvement stage during which lactic acid bacteria (LAB) degrade malic acid to produce lactic acid and catalyze additional chemical reactions which influence the aroma of the wine (17).

In this study, we investigate the impact of sucrose addition during the main fermentation process on the physicochemical properties of the finished blueberry wine, including the alcohol content, nutrient abundance, and odor profile. We expect these results can be used to improve commercial-scale production of blueberry wine.

## Materials and methods

### Materials

Blueberries, the variety of rabbit eye, purchased from Hangzhou Gaofeng Blueberry Planting Co., Ltd (Hangzhou, China). Yeast (*S. cerevisiae*, RW) was provided by Angel Yeast Co., Ltd (Yichang, China). Malvidin, delphinidin, cyanidin, peonidin and petunidin were purchased from Beijing Tanmo Quality Inspection Technology Co., Ltd (Beijing, China).

### Preparation of blueberry wine

Fresh or frozen blueberries were washed and crushed at a temperature no >35°C before transfer to a sterilized fermenter and heated to 35°C. Potassium metabisulfite was added to produce a final sulfur dioxide concentration of 30 mg·kg<sup>-1</sup>. Pectinase [ $\geq 5,000$  U/mg, Novozymes (China) Biotechnology Co., Ltd] was added to a final concentration of 30 mg/kg (w/v) and allowed to react for 1.0 h. Additional sucrose, if present, was added at concentrations of 8, 10, 12, and 14% (w/w) prior to fermentation. Yeast was dissolved in 10 times of water at 30°C and activated for 10 min according to manufacturer's instructions and added at a final concentration of 200 mg·L<sup>-1</sup> at 30°C. Samples were taken at 2, 4, 6, 8, and 10 days for further physicochemical analysis. All experimental groups were fermented 3 batches.

TABLE 1 Detection of flavor component corresponding to sensors.

Sensor No.	Sensitive gas
S1	Ammonia, amines
S2	Hydrogen sulfide and sulfide
S3	Hydrogen
S4	Alcohol, organic solvent
S5	Toluene, acetone, ethanol, formaldehyde, hydrogen and other organic vapors
S6	Methane, biogas and natural gas
S7	Methane, propane, isobutane, natural gas, liquefied gas
S8	Smoke, cooking smell, VOC, ammonia, hydrogen sulfide and alcohol of cigarettes
S9	Butane, propane, methane, liquefied gas, natural gas, coal gas
S10	LPG, combustible gas, propane, butane
S11	Propane, smoke and combustible gas
S12	Carbon monoxide, ethanol, organic solvents, other volatile gas
S13	Smoke, cooking odor, hydrogen, carbon monoxide, air pollutants
S14	Methane, natural gas

### Alcohol quantitation

A volume of 100 mL blueberry wine was removed from the fermenter and transferred into a 500 mL distillation flask. The distillate was collected in a water bath held at 20.0 ± 0.1°C for 30 min, and the alcohol content was measured using a density flask.

### Acid quantitation

The Acid content of the wine was assayed according to Chinese national standard (18). A volume of 1 mL blueberry wine was transferred to a conical flask and mixed with 100 mL water and two drops of phenolphthalein indicator solution. Then the solution was titrated to the end point with 50 mM sodium hydroxide until the color remained unchanged for 30 s. A control experiment without blueberry wine was performed in parallel.

Tartaric acid was quantified using the following formula:

$$X = C \times \frac{V_1 - V_0}{V_2} \times 75 \quad (1)$$

where  $X$  is [Tartaric acid] (g·L<sup>-1</sup>),  $C$  is [NaOH], mol/L,  $V_1 - V_0$  is the difference in volume of NaOH added in the sample and control titrations, respectively (mL), and  $V_2$  is the volume of blueberry wine present in the sample titration (mL).

### Sugar quantitation

The total sugar content of the wine was assayed by volumetric analysis according to Chinese national standard (18). First, a volume of blueberry wine was diluted tenfold with pure water and heated to boiling. Then, a solution of freshly prepared Fehling's Reagents were added at a rate of 0.5 drop/s until the end point, indicated by



the disappearance of color. The total consumed volume of sample solution was recorded and repeated three times in parallel.

Sugar content was quantified according to the following formula:

$$X = \frac{F \times V_2}{V_1 \times V_3} \times 1000 \quad (2)$$

where  $X$  is the total sugar content of blueberry wine (g/L),  $F$  represents the total oxidative potential of Fehling's reagents (g of glucose),  $V_1$  is the volume of blueberry wine sample absorbed (mL),  $V_2$  is the volume of blueberry wine sample diluted, mL, and  $V_3$  is the volume of blueberry wine sample consumed (mL).

## Colorimetric analysis

Colorimetric analysis of clarified blueberry wine was performed using a colorimeter in transmittance mode (Hunter Lab, USA). The color of each sample was quantified according to the Hunter  $L$ ,  $a$ ,  $b$  color scale which uses the following parameters:  $L^*$  represents brightness (where 0 is dark, 100 is light),  $a^*$  represents the degree of red and green ( $-a^*$  is green,  $+a^*$  is red), and  $b^*$  represents the degree of yellow and blue ( $-b^*$  is blue,  $+b^*$  is yellow).

## Phenol quantitation

Phenol content determination were assayed according to Martín-Gomez et al. (19)'s analytical method. A volume of 1 mL blueberry wine was diluted fivefold, and 1 mL of this diluted sample was mixed with 1 mL Folin's Phenol Reagent and 5 mL of water. After 3 min, 3 mL 75 g/L sodium bicarbonate was added and the mixture was heated to 50°C for 10 min. The  $A_{647}$  was measured using a spectrophotometer, and used to calculate total phenol content using a standard curve generated with a gallic acid standard.

## Anthocyanin characterization

Anthocyanins were characterized using Liquid chromatography tandem mass spectrometry (LC-MS/MS) (waters, Massachusetts, USA) following ultrasonic extraction at 100 w for 10 min. First, 5 g crushed blueberry mash was transferred into a 25 mL colorimetric tube, combined with two volumes of absolute ethanol, one volume of hydrochloric acid, and one volume of water, and then heated in a boiling water bath for 1 h. The sample was then sonicated for 30 min, and centrifuged at 4,000 r/min. The supernatant was collected, filtered through 0.22  $\mu$ m filter, and analyzed using LC-MS under the following conditions.

Chromatographic column: Waters ACQUITY BEH C18 column (1.7  $\mu$ m, 2.1  $\times$  100 mm); Column temperature: 40°C; Injection volume: 2  $\mu$ L; Flow rate: 0.5 mL/min. Mobile phase: 0.1% formic acid (A) and 100% acetonitrile (B); Gradient elution procedure: 0–1.1 min, 5–10% B; 1.1–5.5 min, 10–50% B; 5.5–6.9 min, 50–5% B; 6.9–7.5 min, 5% B, balance for 1 min.

Ion source: electric spray (ESI+); Detection mode: MRM; Capillary voltage: 1.0 kV; Ion source temperature: 150°C; Cone gas flow rate: 50 L/h; Solvent gas temperature: 500°C; Solvent gas flow rate: 1,000 L/h; Collision gas (argon): 0.15 mL/min; Dwell time: 0.02 s.

Malvidin, delphinidin, cyanidin, peonidin, and petunidin were directly injected as references.

## Electronic nose analysis

A solution of 15 mL blueberry wine was collected into centrifuge tube. A 2 mL injection tube was used absorb volatile gases from the wine and inject into the electronic nose system (Zhejiang Gongshang University, China). The system is composed of an air pump, air chamber, sensor array, signal acquisition system and pattern recognition algorithm. The sensor array is composed of fourteen gas sensitive metal oxide sensors, as shown in Table 1, where each sensor is sensitive to one or more types of gases. When the volatile gases contact the sensor, the conductivity ( $G$ ) of the sensor changes relative to the initial conductivity ( $G_0$ ), and the ratio  $G/G_0$  represents the total response. Each sample is tested six times.

## Statistical analysis

All data were shown as mean  $\pm$  standard deviation. Each test was repeated three times. Statistical analysis was performed using EXCEL (Microsoft, USA) and SPSS version 24 (IBM, USA). Graph Pad Prism 8.3.0 (GraphPad Software, USA) was used to graph. One-way ANOVA was used to analyze the anthocyanins content data with Duncan's test, and means were considered significantly different if  $p < 0.05$ .

## Results and discussion

### Alcohol content

During fermentation, sugars present in the blueberry mash are gradually converted into ethanol, and alcohol content is the key indicator for evaluating the quality of blueberry wine. Fermentation begins with the growth stage  $\sim$ 1–2 days following addition of yeast, during which temperature and sugar content have the greatest influence on the fermentation rate (20). Then, the fermentation enters the stable stage where the total concentration of sugar reaches 5 g·L<sup>-1</sup>, indicating that main fermentation is complete. The main fermentation phase is usually completed in a week (21).

Due to the complexity of the fermentation process, the natural sugar present in the mash is usually not entirely converted into alcohol. For example, although the sugar content of blueberry fruit is 86 g·L<sup>-1</sup>, blueberry wine fermented without supplemental sugar only produces a final alcohol concentration of 4.5% (Figure 1). Alcohol concentration is gradually increased as external sugar is added, with a sugar content of 12% producing a final alcohol concentration of 11.7%. However, increasing sugar content from 12 to 14% does not lead to a significant increase in alcohol concentration, because yeast vitality is inhibited at high alcohol concentrations. Considering demand of consumers and fermentation capacity, 12% sugar content is recommended to obtain more acceptable alcohol.



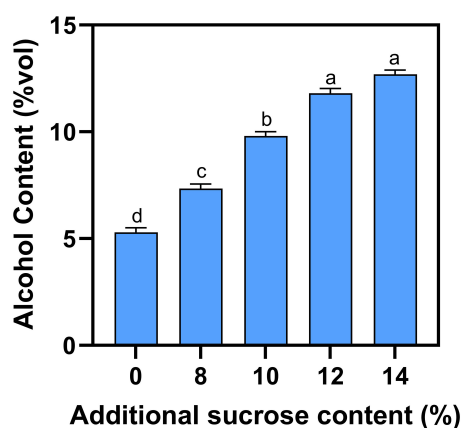


FIGURE 1  
Effect of additional sucrose on alcohol content. Different superscript letters in the graph are significantly different ( $P < 0.05$ ).

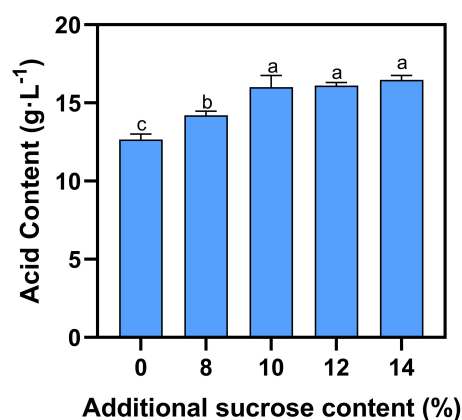


FIGURE 2  
Effect of additional sucrose on acid content. Different superscript letters in the graph are significantly different ( $P < 0.05$ ).

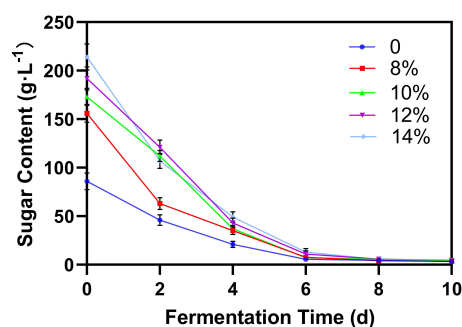


FIGURE 3  
Effect of additional sucrose on sugar content during main fermentation.

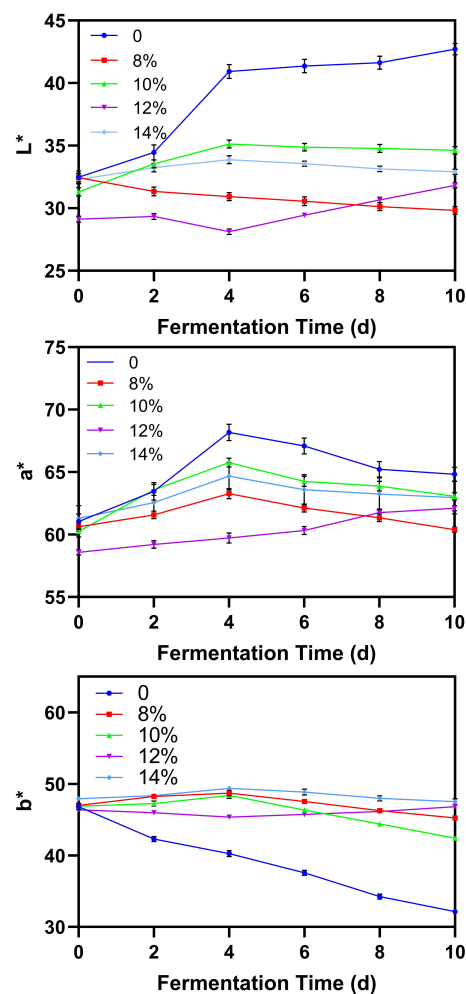


FIGURE 4  
Effect of additional sucrose on  $L^*$ ,  $a^*$ , and  $b^*$  during main fermentation.

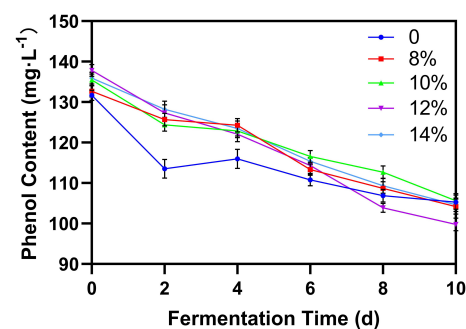
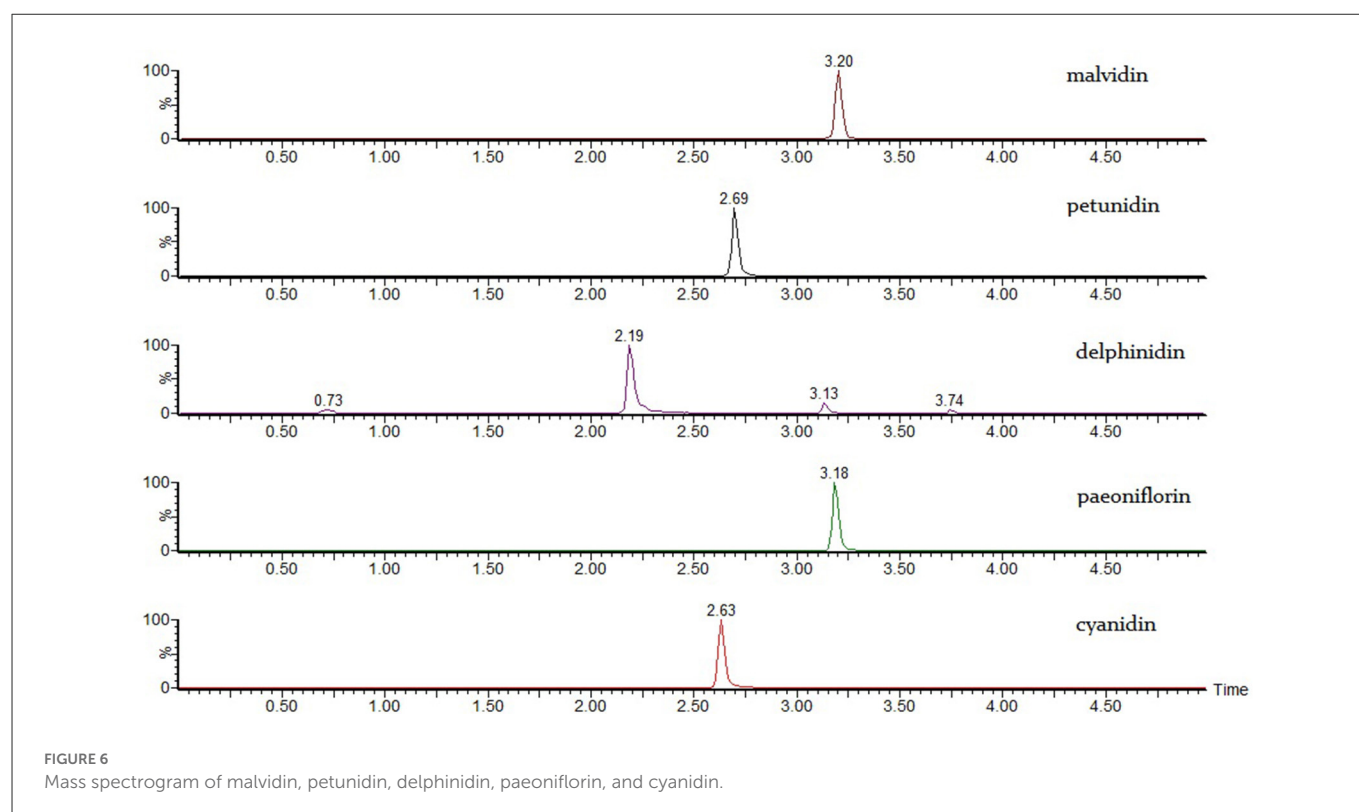


FIGURE 5  
Effect of additional sucrose on phenol content during main fermentation.

## Acid content

Pyruvic acid, acetic acid, lactic acid and other metabolites are produced by yeast during the fermentation process (22). Generally,

potassium bicarbonate is added to reduce the acidity of blueberry wine, as high acidity is undesirable (14). Fermentation of natural blueberry wine without supplemental sugar yields  $12.6 \text{ g·L}^{-1}$  total acid (Figure 2). As external sugar is added during fermentation, the total acid content rises slightly to  $14.2\text{--}16.5 \text{ g·L}^{-1}$  at 8–10% sucrose,



respectively. However, addition of sucrose beyond 10% does not significantly raise acidity.

## Sugar content

Fermentation is mainly the process of decomposing sugar and producing alcohol. Therefore, monitoring the sugar content can indicate the fermentation process. For blueberry wine with external sugar concentration <12% (w/w), the sugar content rapidly decreased to 10 g/L after 6 days and to 5 g/L after 8 days (Figure 3). For blueberry wine with 12 and 14% sugar, this trend was delayed by 2 days. However, in all cases, the fermentation process finishes within 10 days. Total sugar content serves as a proxy for the dynamic blueberry fermentation process (23), and once the post fermentation stage begins, operations such as blueberry residue filtration could be implemented to save time and avoid negative impact of residual microorganisms in wine puree on odor and quality. It is necessary to dynamically monitor the change of sugar content during wine fermentation (24).

## Color

The chromaticity parameters  $L^*$ ,  $a^*$  and  $b^*$  can be used to infer the quality of blueberry wine throughout fermentation (13). In blueberry wine with added sucrose, the  $L^*$  value, representing brightness, is lower than in wine without additional sugar, whereas the  $b^*$  value representing yellow color is higher (Figure 4). This may be a result the added sucrose producing a cumulative increase in fermentation products which darken the wine and alter its color. Interestingly, the  $a^*$  values which represent red color first rose and

then slowly decreased during the fermentation process. The initial increase may be a result of red-colored pigments in residual blueberry peel dissolving into solution, whereas the subsequent decrease may result from yeast metabolizing these compounds as fermentation continues. This result is consistent with current literature, with Li et al. also showing that the  $a^*$  of blueberry wine increased first during fermentation and then decreased.

## Phenol content

Phenols are the key substances determining the biological activity of blueberries (19, 25). The composition of phenolic substances is relatively complex. Figure 5 shows the change in phenol concentration during the blueberry fermentation process. In all cases, phenol concentration declined slowly as fermentation progressed, likely due to the metabolism of phenolic substances by the yeast or the reaction with other byproducts of fermentation (26). Although phenol concentration decreased for all groups, blueberry wines with added sucrose showed higher phenol levels early in the fermentation process, suggesting that additional sugar can prevent the degradation of phenols. However, by the end of fermentation, after the external sucrose was fully converted into ethanol, there was no significant difference in the phenol content between samples.

## Anthocyanin characterization

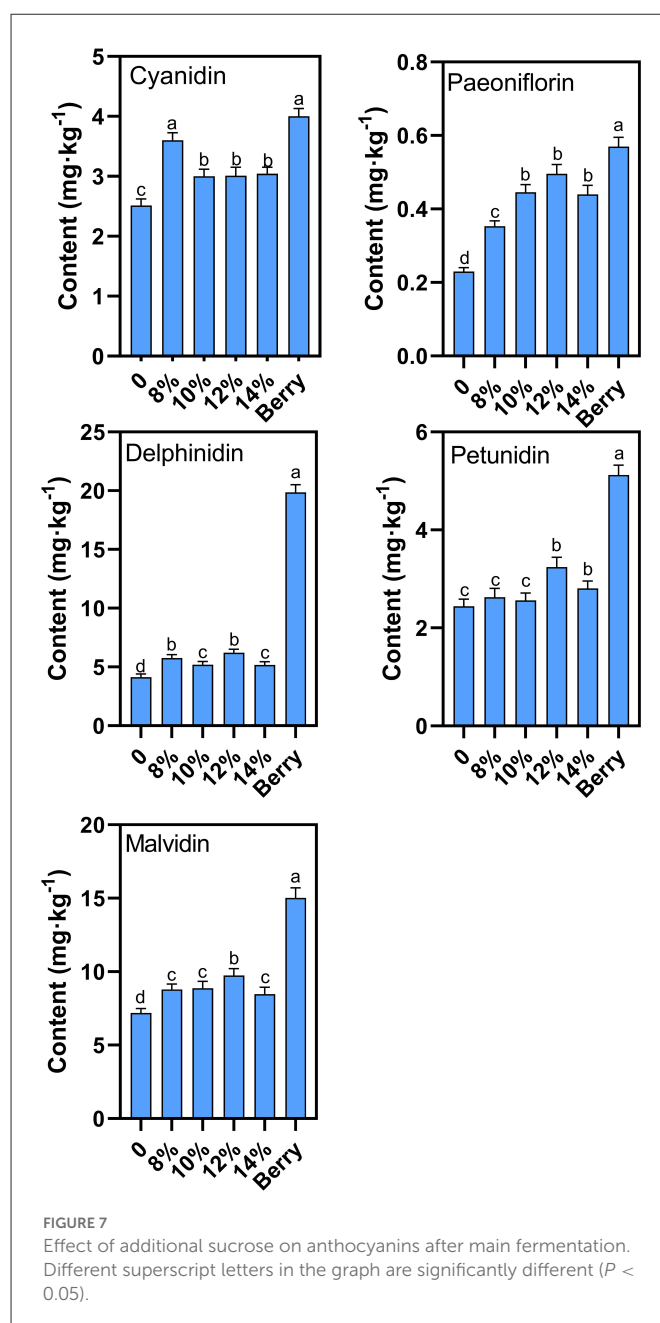
Anthocyanins are the most concerned components in blueberry processing because of antioxidant activity and health benefits (27). Anthocyanins are susceptible to several processing and storage conditions, such as pH condition, temperature and light

exposure, etc. (28) and the degradation and loss of anthocyanin are inevitable during the fermentation solution environment (28). Anthocyanins are composed of cyanidin, delphinidin, malvidin, petunidin and peonidin and glycosidic groups (29), and can be deglycosylated into their corresponding aglycone structure by heating in acidic environment. The resulting cyanidin, delphinidin, malvidin, petunidin, and peonidin correspond to their native anthocyanin forms and can be quantitatively analyzed using LC-MS/MS (30). Because blueberries contain a wide variety of anthocyanins, it can be difficult to find appropriate reference samples to accurately quantify them (31). Furthermore, the retention time of aglycones are similar on HPLC, resulting in poor resolution and inaccurate quantification. However, liquid chromatography coupled with tandem mass spectrometry (LC-MS/MS) can avoid the disadvantages of HPLC by accurately determining and quantifying both the parent ions and the daughter ions of the substance resulting from a specific collision energy. Importantly, the cyanidin, delphinidin, malvidin, petunidin, and peonidin references were well resolved using this technique (Figure 6).

Delphinidin and malvidin are the two most abundant anthocyanins in blueberries, which were both lost to varying degrees after the main fermentation (Figure 7), consistent with previous literature reports (23). Groups with added sucrose show significantly higher anthocyanin levels suggesting that additional sucrose can improve anthocyanin stability during fermentation. A similar protective function resulting from mannoproteins has also been demonstrated in the literature (17). The groups with 12% external sucrose showed the smallest loss in overall anthocyanin concentration during fermentation, with an anthocyanin content of 51.9% relative to levels prior to fermentation. Within the analyzed anthocyanin classes, the degree of degradation varied between classes. Delphinidin and malvidin levels showed the greatest loss during fermentation, with delphinidin levels 31.3% of their original concentration and malvidin levels 64.8% of their original concentration. Therefore, 12% sugar addition concentration was recommended because the favored anthocyanin loss was minimal.

## Electronic nose analysis

It is possible to characterize the odor profile of wine using an electronic nose, which represent fourteen kinds of aromatic substances produced during blueberry wine fermentation (32, 33). For all samples, sensors S8, S1, S2, and S4 have the highest response (Figure 8A), and represent volatile alcohols, aromatic esters, sulfides and amines, respectively, which together constitute the characteristic odor components of blueberry wine. Alcohols, esters and amines are metabolites naturally produced by yeast during fermentation, while sulfides originate from the addition of potassium metabisulfite to inhibit bacteria growth. Additional sucrose does not change the basic odor composition of blueberry wine, reflected by the similar shape of the electronic nose odor profile between all samples. Compared with the experimental group without added sucrose, the added sucrose groups had similar odor composition, which indicates that the added sucrose produces specific odor components. However, additional sucrose enhances the response of each odor substance compared with the control group, especially the group of 12%. Although sucrose is metabolized to produce alcohol in the fermentation process, its



metabolism also promotes the accumulation of odorful substances like esters, indicated by the increased response of sensor S8.

Although the odor composition is similar, different groups of blueberry wine can be distinguished by principal component analysis (PCA) of electronic nose data (Figure 8B). Principal factor 1 (PC1) explained 99.81% of the variance in the data and principal factor 2 (PC2) explained 0.17% of the variance. The DI value was 84.39%, above the required 80% cutoff (34), indicating PCA can effectively discriminate electronic nose profiles with good repeatability.

## Conclusion

The physicochemical properties blueberry wine and the effect of external sucrose during main fermentation process of were analyzed

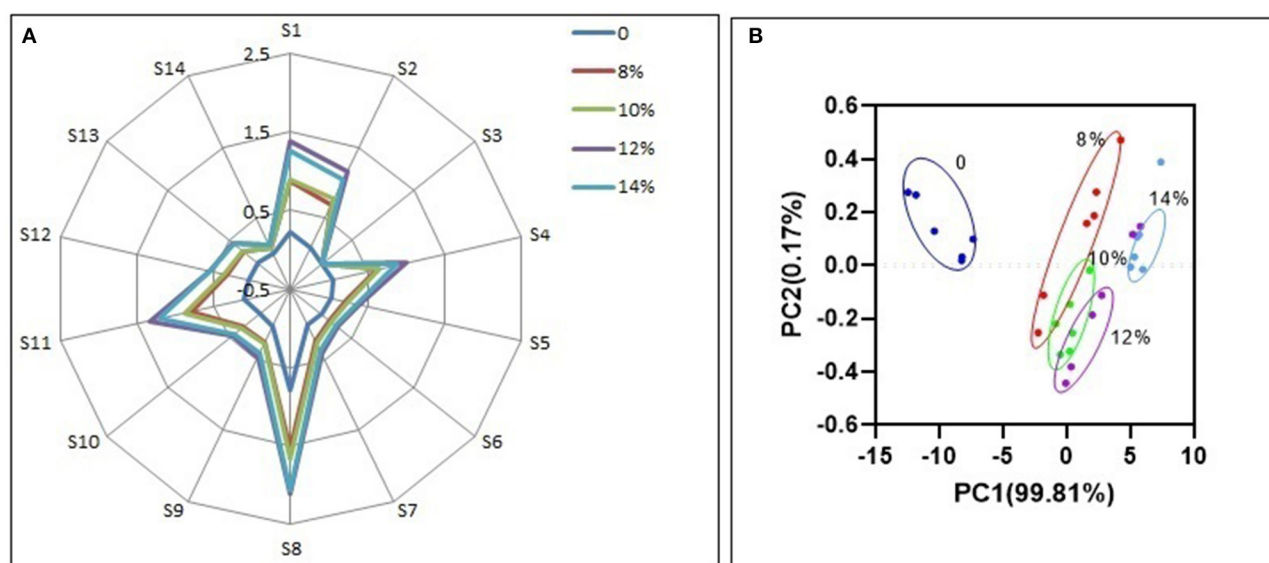


FIGURE 8  
Odor response value of electronic nose (A) and PCA (B).

by measuring alcohol content, sugar, color, phenol, anthocyanins, acid, and odor. Although yeast strain and sulfur dioxide were not investigated as part of this study, these also impact the physicochemical properties of blueberry wine and warrant further investigation. Additional sucrose extends the fermentation time and increases the acid content relative to natural blueberry wine. The extra sugar also alters the color profile of the wine, by lowering  $L^*$  and raising  $b^*$  relative to natural blueberry wine. Although total anthocyanin levels are reduced throughout the fermentation process, addition of sugar produced a protective effect on delphinidin, cyanidin, paeoniflorin, and petunidin, and especially malvidin. Finally, additional sugar enhanced volatile odor components in blueberry wine, particularly of alcohols and esters, as measured by an electronic nose. Taken together, these data recommend addition of 12% sucrose in commercial preparation of blueberry wine especially for physicochemical properties of alcohol, anthocyanin loss and odor.

## Data availability statement

The original contributions presented in the study are included in the article/supplementary material, further inquiries can be directed to the corresponding authors.

## Author contributions

JL and JF designed and conceived the study. LW, JQ, and HJ performed the experiments. QW analyzed the data and drafted the manuscript. JL, QW, LZ, and LW contributed to the writing of the manuscript. LZ provided the funding and resources. All authors revised and approved the submitted version of the manuscript.

## Funding

This research was supported by Zhejiang Provincial Natural Science Foundation of China under Grant No. LGN18C200011, Hangzhou Agricultural Research Initiative Design Foundation No. 20190101A06, Hangzhou Academy of Agricultural Sciences Innovation Foundation No. 2022HNCT-22 and Hangzhou High-level Special Talents Support Plan.

## Acknowledgments

We sincerely thank all participants for their support. Besides, we are incredibly grateful to Joseph Elliot at the University of Kansas for his assistance with English language and grammatical editing of the manuscript.

## Conflict of interest

The authors declare that the research was conducted in the absence of any commercial or financial relationships that could be construed as a potential conflict of interest.

## Publisher's note

All claims expressed in this article are solely those of the authors and do not necessarily represent those of their affiliated organizations, or those of the publisher, the editors and the reviewers. Any product that may be evaluated in this article, or claim that may be made by its manufacturer, is not guaranteed or endorsed by the publisher.

## References

- Li S, Yang T, Dan L, Guang W, Jian Z, Sivakumar M, et al. Fermentation of blueberry juices using autochthonous lactic acid bacteria isolated from fruit environment: Fermentation characteristics and evolution of phenolic profiles. *Chemosphere*. (2021) 276:130090. doi: 10.1016/j.chemosphere.2021.130090
- Liu F, Li S, Gao J, Cheng K, Uan F. Changes of terpenoids and other volatiles during alcoholic fermentation of blueberry wines made from two southern highbush cultivars. *LWT*. (2019) 109:233–40. doi: 10.1016/j.lwt.2019.03.100
- Li D, Li B, Ma Y, Sun X, Lin Y, Meng X. Polyphenols, anthocyanins, and flavonoids contents and the antioxidant capacity of various cultivars of highbush and half-high blueberries. *J Food Compos Anal*. (2017) 62:84–93. doi: 10.1016/j.jfca.2017.03.006
- Byung-Taek O, Jeong S, Velmurugan P, Park J, Jeong D. Probiotic-mediated blueberry (*Vaccinium corymbosum* L.) fruit fermentation to yield functionalized products for augmented antibacterial and antioxidant activity. *J Biosci Bioeng*. (2017) 124:542–50. doi: 10.1016/j.jbiosc.2017.05.011
- Ongekowijoyo P, Luna-vital DA, Elvira GDM. Extraction techniques and analysis of anthocyanins from food sources by mass spectrometry: an update. *Food Chem*. (2018) 250:113–26. doi: 10.1016/j.foodchem.2018.01.055
- Sun X, Zhou T, Wei C, Lan W, Zhao Y, Pan Y, et al. Antibacterial effect and mechanism of anthocyanin rich Chinese wild blueberry extract on various foodborne pathogens. *Food Control*. (2018) 94:155–61. doi: 10.1016/j.foodcont.2018.07.012
- Wang C, Tao Y, Han Y, Zhang R, Li L, Gao Y. Influences of subcellular Ca redistribution induced by  $\gamma$  irradiation on the fruit firmness of refrigerated blueberries. *Postharvest Biol Tec*. (2023) 195:112146. doi: 10.1016/j.postharvbio.2022.112146
- Guo J, Yin M, Han X, You Y, Huang W, Zhan J. The influence of oxygen on the metabolites of phenolic blueberry extract and the mouse microflora during *in vitro* fermentation. *Food Res Int*. (2020) 136:109610. doi: 10.1016/j.foodres.2020.109610
- Jiang B, Liu R, Fang X, Wu W, Han Y, Chen H, et al. *Botrytis cinerea* infection affects wax composition, content and gene expression in blueberry fruit. *Postharvest Biol Technol*. (2022) 192:112020. doi: 10.1016/j.postharvbio.2022.112020
- Ana M, Eduardo C, Catarina B, José M, O'Arlete M. Production of blueberry wine and volatile characterization of young and bottle-aging beverages. *Food Sci Nutr*. (2019) 7:617–27. doi: 10.1002/fsn3.895
- Guisella T, Nidia C, Patricio O, Guillermo P. Blueberry juice: bioactive compounds, health impact, and concentration technologies—a review. *J Food Sci*. (2021) 86:5062–77. doi: 10.1111/1750-3841.15944
- Karolina C, Monika M, Dorota K, Tomasz K. The influence of ultrasound and cultivar selection on the biocompounds and physicochemical characteristics of dried blueberry (*Vaccinium corymbosum* L.). *snacks J Food Sci*. (2018) 83:2305–16. doi: 10.1111/1750-3841.14292
- Li X, Zhang L, Peng Z, Zhao Y, Wu K, Zhou N, et al. The impact of ultrasonic treatment on blueberry wine anthocyanin color and its *in-vitro* anti-oxidant capacity. *Food Chem*. (2020) 333:127455. doi: 10.1016/j.foodchem.2020.127455
- Varo MA, Martín-Gómez J, Serratos MP, Merida J. Effect of potassium metabisulphite and potassium bicarbonate on color, phenolic compounds, vitamin C and antioxidant activity of blueberry wine. *LWT*. (2022) 163:113585. doi: 10.1016/j.lwt.2022.113585
- Van Leeuwen C, Roby J, Alonso-Villaverde V, Gindro K. Impact of clonal variability in vitis vinifera cabernet franc on grape composition, wine quality, leaf blade stilbene content, and downy mildew resistance. *J Agri Food Chem*. (2012) 61:19–24. doi: 10.1021/jf304687c
- Su M, Chien P. Antioxidant activity, anthocyanins, and phenolics of rabbiteye blueberry (*Vaccinium ashei*) fluid products as affected by fermentation. *Food Chem*. (2007) 104:182–7. doi: 10.1016/j.foodchem.2006.11.021
- Sun X, Yan Z, Zhu T, Zhu J, Wang Y, Li B, et al. Effects on the color, taste, and anthocyanins stability of blueberry wine by different contents of mannoprotein. *Food Chem*. (2019) 279:63–9. doi: 10.1016/j.foodchem.2018.11.139
- GB/T 15308. *Analytical Methods of Wine and Fruit Wine*. Beijing: China Standard Press (2006).
- Martín-Gómez J, García-Martínez T, Angeles Varo M, Merida J, Serratos MP. Phenolic compounds, antioxidant activity and color in the fermentation of mixed blueberry and grape juice with different yeasts. *LWT*. (2021) 146:111661. doi: 10.1016/j.lwt.2021.111661
- Zhang N, Gao Y, Fan G, Zhong W, Chen X, Guo X, et al. Combined high-throughput and fractionation approaches reveal changes of polysaccharides in blueberry skin cell walls during fermentation for wine production. *Food Res Int*. (2022) 162:112027. doi: 10.1016/j.foodres.2022.112027
- Liu S, Laaksonen O, Kortensniemi M, Kalpio M, Yang B. Chemical composition of bilberry wine fermented with non-Saccharomyces yeasts (*Torulaspora delbrueckii* and *Schizosaccharomyces pombe*) and *Saccharomyces cerevisiae* in pure, sequential and mixed fermentations. *Food Chem*. (2018) 266:262–74. doi: 10.1016/j.foodchem.2018.06.003
- Chena C, Xiong Y, Xie Y, Zhang H, Jiang K, Pang X, et al. Metabolic characteristics of lactic acid bacteria and interaction with yeast isolated from light-flavor Baijiu fermentation. *Food Biosci*. (2022) 50:102102. doi: 10.1016/j.fbio.2022.102102
- Sun X, Shokri S, Gao B, Xu Z, Li B, Zhu T, et al. Improving effects of three selected co-pigments on fermentation, color stability, and anthocyanins content of blueberry wine. *LWT*. (2022) 156:113070. doi: 10.1016/j.lwt.2022.113070
- Zhao C, Su W, Mu Y, Jiang L, Mu Y. Correlations between microbiota with physicochemical properties and volatile flavor components in black glutinous rice wine fermentation. *Food Res Int*. (2020) 138:109800. doi: 10.1016/j.foodres.2020.109800
- Alexandre-Tudo JL, Buica A, Nieuwoudt H, Alexandre JL, du Toit W. Spectrophotometric analysis of phenolic compounds in grapes and wines. *J Agr Food Chem*. (2017) 20:4009–26. doi: 10.1021/acs.jafc.7b01724
- Morata A, Loira I, MaríaHeras J, JesúsCallejo M, Tesfaye W, González C, et al. Yeast influence on the formation of stable pigments in red winemaking. *Food Chem*. (2016) 197:686–91. doi: 10.1016/j.foodchem.2015.11.026
- Kalt W, Cassidy A, Howard LR, Krikorian R, Stull AJ, Tremblay F, et al. Recent research on the health benefits of blueberries and their anthocyanins. *Adv Nutr*. (2020) 11:224–36. doi: 10.1093/advances/nmz065
- Kalt W, McDonald JE, Donner H. Anthocyanins, phenolics, and antioxidant capacity of processed lowbush blueberry products. *J Food Sci*. (2000) 65:390–3. doi: 10.1111/j.1365-2621.2000.tb16013.x
- Chai Z, Herrera-Balandrano DD, Yu H, Beta T, Zeng Q, Zhang X, et al. A comparative analysis on the anthocyanin composition of 74 blueberry cultivars from China. *J Food Compos Anal*. (2021) 102:104051. doi: 10.1016/j.jfca.2021.104051
- Lang Y, Li E, Meng X, Tian J, Ran X, Zhang Y, et al. Protective effects of bovine serum albumin on blueberry anthocyanins under illumination conditions and their mechanism analysis. *Food Res Int*. (2019) 122:487–95. doi: 10.1016/j.foodres.2019.05.021
- Norberto S, Silva S, Meireles M, Faria A, Pintado M, Calhau C. Blueberry anthocyanins in health promotion: a metabolic overview. *J Funct Foods*. (2013) 5:1518–28. doi: 10.1016/j.jff.2013.08.015
- Sanaeifar A, Dizaji H, Jafari A, de LaGuardia M. Early detection of contamination and defect in foodstuffs by electronic nose: a review. *TrAC Trends Anal Chem*. (2017) 97:257–71. doi: 10.1016/j.trac.2017.09.014
- Zhang L, Hua Y, Wang Y, Kong B, Chen Q. Evaluation of the flavour properties of cooked chicken drumsticks as affected by sugar smoking times using an electronic nose, electronic tongue, and HS-SPME/GC-MS. *LWT*. (2021) 140:110764. doi: 10.1016/j.lwt.2020.110764
- Xu J, Liu K, Zhang C. Electronic nose for volatile organic compounds analysis in rice aging Author links open overlay panel. *Trends Food Sci Tech*. (2021) 109:83–93. doi: 10.1016/j.tifs.2021.01.027





## OPEN ACCESS

## EDITED BY

Hao Jiang,  
Northwest A&F University, China

## REVIEWED BY

Zhenbin Liu,  
Shaanxi University of Science and Technology,  
China

Yingbin Shen,  
Guangzhou University,  
China

Qun Huang,  
Guizhou Medical University,  
China

Hao Dong,  
Zhongkai University of Agriculture and  
Engineering, China  
Thuan Chew Tan,  
University of Science Malaysia,  
Malaysia

## \*CORRESPONDENCE

Jicheng Xu  
✉ xujicheng@ahpu.edu.cn  
Jun Guo  
✉ guojun81\_2001@163.com

## SPECIALTY SECTION

This article was submitted to  
Nutrition and Food Science Technology,  
a section of the journal  
Frontiers in Nutrition

RECEIVED 29 November 2022

ACCEPTED 18 January 2023

PUBLISHED 03 February 2023

## CITATION

Yao X, Xu J, Xun Y, Du T, Huang M and  
Guo J (2023) High gelatinous salted duck egg  
white protein powder gel: Physicochemical,  
microstructure and techno-functional  
properties.  
*Front. Nutr.* 10:1110786.  
doi: 10.3389/fnut.2023.1110786

## COPYRIGHT

© 2023 Yao, Xu, Xun, Du, Huang and Guo. This  
is an open-access article distributed under the  
terms of the [Creative Commons Attribution  
License \(CC BY\)](#). The use, distribution or  
reproduction in other forums is permitted,  
provided the original author(s) and the  
copyright owner(s) are credited and that the  
original publication in this journal is cited, in  
accordance with accepted academic practice.  
No use, distribution or reproduction is  
permitted which does not comply with these  
terms.

# High gelatinous salted duck egg white protein powder gel: Physicochemical, microstructure and techno-functional properties

Xinjun Yao<sup>1</sup>, Jicheng Xu<sup>1\*</sup>, Yu Xun<sup>1</sup>, Tianyin Du<sup>1</sup>, Mengqi Huang<sup>1</sup> and Jun Guo<sup>2\*</sup>

<sup>1</sup>College of Biological and Food Engineering, Anhui Polytechnic University, Wuhu, China, <sup>2</sup>College of Biology and Food Science, Suzhou University, Suzhou, China

Salted duck egg is one of the most popular products, and China is one of the major countries consuming salted duck egg products. However, due to the high salt content of salted egg white and low physical and chemical properties such as gel, many factories generally only use salted egg yolk and discard salted duck egg white (SDEW) as a waste liquid when processing. This is not only a waste of resources, but also a pollution to the environment. In this paper, protein powder was prepared from salted egg white. Then xanthan gum (XG) was added to make it co-gel with ovalbumin to achieve the purpose of preparing high gelatinous salted egg white protein powder. The results showed that the optimum conditions of SDEW-XG composite gel were as follows: the xanthan gum content was 0.08% (w/w), the reaction pH was 6.5, and the heating temperature was 100°C. Under these conditions, the gel strength reaches the maximum value. Meanwhile, compared with the protein powder without xanthan gum, the addition of xanthan gum significantly affected the secondary structure of the protein powder of SDEW and improved the water holding capacity of the gel. In conclusion, the addition of xanthan gum can significantly improve the gel quality of SDEW protein powder, which provides a theoretical basis for the quality improvement of salted egg white.

## KEYWORDS

salted duck egg white, protein peptide powder, high gelatinous, physicochemical properties, xanthan gum

## Introduction

Salted duck eggs are a traditional food in China and South Asia. The salted duck egg white (SDEW) makes up 50 to 60% of the whole salted duck egg (1–3). Salted duck egg in the production process, involves the step of pickling. Pickling does not change the composition of the protein, but it does add a lot of salt. High concentration of NaCl changed the gel performance of SDEW, which would greatly reduce the utilization rate of SDEW (4–6). Currently, only a small portion of SDEW is used in animal feed, and most of it is discarded. So far, many scholars have studied the reuse of SDEW (7–9). Peng et al. (10) prepared a novel composite protein membrane by cross-linking egg white protein with the Transglutaminase enzyme. The study showed that the protein membrane containing the Transglutaminase enzyme was more uniform, smooth, and had better water resistance and thermal stability. Tang et al. (11) investigated the effect of carrageenan on the protein structure and gel properties of SDEW. The results showed that the addition of carrageenan can significantly increase the content of the free sulfhydryl group and surface hydrophobicity of SDEW protein. At

the same time, with the increase of carrageenan content, the hardness, viscosity, chewability, and elasticity of the gel prepared from SDEW were improved.

The production of high gelatinous egg white protein powder in China is very low now, mainly the general protein powder. Therefore, a large number of scholars have studied the preparation of high gelatinous egg white protein powder (12–14). However, most of these studies take egg white as the research object, and it is still rare to use SDEW as raw material to prepare high-quality protein powder. This is mainly because the high concentration of NaCl in SDEW seriously affects its functional properties such as gelation and water holding capacity (15). So, a large amount of salted egg white is discarded, resulting in a waste of high-quality protein resources. At the same time, it also causes pressure to the environment to a certain extent.

When egg white is used as gelling agent in food processing, the addition amount is relatively high and the production cost is high. Although ordinary egg white powder is more hygienic and convenient than fresh egg white, its gel properties are often inferior to fresh egg white. So further systematic research on the gel properties of egg white and the modification of egg white powder has high practical value. The scheme of this research just provided a feasible way to solve this problem. In this research, SDEW was used as raw material, and after desalting, it was mixed with a certain amount of xanthan gum to make the two co-gels to obtain high gelatinous SDEW protein powder. Then, the water holding capacity and gel microstructure of high gelatinous SDEW protein powder were studied. This study provided a new idea for the comprehensive utilization of SDEW. In a sense, it can effectively reduce the waste of resources and environmental pollution.

## Materials and methods

### Raw materials

SDEW was provided by Anhui Tianhe Food Co., LTD. SDEW was placed in the refrigerator at  $-20^{\circ}\text{C}$  and thawed at room temperature before use. Xanthan gum was purchased from Hefei Pomeranian Biotechnology Co., LTD.

### Preparation method of protein powder

SDEW liquid was filtered with four layers of gauze to remove impurities (eggshell and small stones). Then it was diluted five times and the salt content was 9.3% by salinometer. Then, in order to remove salt, the SDEW was ultrafiltered to obtain the final desalted egg white with a salt content of 0.63%. The desalted SDEW liquid was adjusted with 40% citric acid to pH 5.5. Then 0.2% dry yeast was heated in a water bath at  $30^{\circ}\text{C}$  for 4 h. The SDEW liquid was spray dried (feed temperature  $180 \pm 3^{\circ}\text{C}$ , discharge temperature  $70 \pm 3^{\circ}\text{C}$ ) with a spray dryer (B-290, BÜCHI Labortechnik AG, Flawil, Switzerland) to obtain protein powder.

### Preparation method of gel

The protein powder was prepared into a 10% protein powder solution. Xanthan gum was added to the protein powder solution and the pH of the solution was adjusted to 6.5 (40% citric acid, 2 mol/L NaOH). The solution was stirred with a magnetic stirrer (MS123D,

Showrange Ltd., Shanghai, China) at a speed of 120 r/min for 5 min. The beaker was sealed with plastic wrap. After heating in a water bath for 1 h ( $100^{\circ}\text{C}$ ), the beaker was immediately cooled in an ice-cold water bath for 20 min. Then, the beaker was placed in the refrigerator (BCD-485WSPZM, Meidi Ltd., Guangzhou, China) at  $4^{\circ}\text{C}$  for 24 h to make the gel.

## Optimization of experimental conditions using the single-factor test

### Single factor test of xanthan gum addition

Under the conditions of pH 6.5, heating temperature  $100^{\circ}\text{C}$ , and heating time 1 h, six groups of xanthan gum contents (0, 0.04, 0.08, 0.12, 0.16, and 0.20%) were selected as the research objects. The objective of this experiment was to investigate the effect of xanthan gum on the gel formation and properties of SDEW protein powder.

### Single factor test of pH

Under the conditions of adding 0.08% xanthan gum, heating temperature  $100^{\circ}\text{C}$ , and heating time 1 h, six groups of different pH (5.0, 5.5, 6.0, 6.5, 7.0, and 7.5) were selected as the research objects. The objective of this experiment was to investigate the effect of pH on the gel formation and properties of SDEW protein powder.

### Single factor test of heating time

Six groups of different heating times (20, 40, 60, 80, 100, and 120 min) were selected as the research objects under the conditions of xanthan gum dosage of 0.08%, pH 6.5, and heating temperature  $100^{\circ}\text{C}$ . The objective of this experiment was to investigate the effect of heating time on the gel formation and properties of SDEW protein powder.

### Single factor test of heating temperature

Six groups of different heating temperatures (90, 95, 100, 105, 110, and  $115^{\circ}\text{C}$ ) were selected as the research objects under the conditions of xanthan gum dosage of 0.08%, pH 6.5, and 1 h of heating time. The objective of this experiment was to investigate the effect of heating temperature on the gel formation and properties of SDEW protein powder.

## Measurement of gel strength

A cube ( $10\text{ mm} \times 10\text{ mm} \times 10\text{ mm}$ ) was cut in the center of SEDW-XG gel (11). The gel strength of the gel was measured by TA.XT2i texture analyzer (TAXT2 of table Micro Systems, Ltd., Surrey, United Kingdom). The measurement parameters were as follows: the speed before the test was 2.0 mm/s, the speed during the test was 1 mm/s, and the speed after the test was 2 mm/s. The compression ratio of the texture analyzer was set to 50%, and the triggering force was set to 5.0 g. The hardness was recorded as gel strength in  $\text{g/cm}^2$ .

## Measurement of color parameters

Color parameters of protein powder were determined by a chromatic aberration meter (CR-400, Konica Minolta Inc., Tokyo, Japan). Protein powders with different xanthan gum additions were

placed in petri dishes and pressed vigorously. The flattened protein powder was placed under a chromatic meter to measure its  $L^*$ ,  $A^*$ , and  $b^*$ . The total color difference ( $\Delta E$ ) of protein powder samples was calculated using Equation 1 (16):

$$\Delta E = \sqrt{(L_0^* - L^*)^2 + (a_0^* - a^*)^2 + (b_0^* - b^*)^2} \quad (1)$$

where the  $L_0^*$ ,  $a_0^*$ , and  $b_0^*$  indicate color parameter of protein powder sample.

## Measurement of water holding capacity

The determination of water holding capacity was based on the method of Jiang et al. (17). The gel sample (10g) was weighed and denoted as  $M_1$ . Then, the gel sample was put into the centrifuge tube for centrifugation ( $2,655 \times g$ , 30 min). The water on the surface of the centrifuged gel sample was sucked up with filter paper, and the mass of the gel sample was measured, denoted as  $M_2$ . The water holding capacity was calculated using Equation 2:

$$WHC (\%) = (M_2 / M_1) \times 100 \quad (2)$$

## Observation of surface morphology of gel

The microstructure of the gel samples was observed and analyzed by referring to the method of Xu et al. (18). The gel samples were cut into a cube. The cut cubes were soaked in 2.5% glutaraldehyde solution for 12 h ( $4^\circ\text{C}$ ). The soaked gel samples were rinsed with phosphate buffer (0.02 mol/L, pH 7.4) at room temperature for 4 min. After rinsing, the gel samples were immersed in 50, 60, 70, 80, 90, and 100% ethanol solution successively (10 min each time). Then, the gel samples were soaked with isoamyl acetate for 15 min. The soaked samples were freeze-dried in a freeze-dryer. The freeze-dried samples were mounted on the scanning electron microscope screw root using a double-sided conductive adhesive. Then, the samples were coated with a thin layer of gold using a sputtering device. A scanning electron microscope (Quanta-200, FEI, Netherlands) was used to observe the microscopic morphology.

## Determination of Fourier transform infrared spectroscopy of gel

According to the method of Xu et al. (19), the gel samples were analyzed by Fourier transform infrared spectroscopy (IS10, Thermo Nicolet Corp., Madison, WI, United States). The gel samples were lyophilized. The freeze-dried sample (1 mg) was mixed with 100 mg of potassium bromide. The mixture was then ground into a uniform powder. The ground powder was pressed into thin wafers. The protein secondary structure of the gel was determined by an infrared spectrometer (FTIR, IS10, Thermo Nicolet Instruments, United States). The wave number range was  $4,000\text{ cm}^{-1} \sim 400\text{ cm}^{-1}$ , the resolution was  $4\text{ cm}^{-1}$ , the scanning times were 64, and the ambient temperature was

$25^\circ\text{C}$ . OMNICV8.0 software (Nicolet, United States) was used to analyze the spectral data. The relative percentages of secondary structures of different proteins were calculated according to the integrated peak area.

## Statistical analysis

The SPSS 20.0 software (IBM, Chicago, IL, United States) was used for the ANOVA of the samples in the study. Significant differences were determined by Duncan's multiple comparison test ( $p < 0.05$ ).

## Results and discussion

### Test results of xanthan gum content

The effects of different xanthan gum content on gel strength were shown in Figure 1. As can be seen from the figure, when the amount of xanthan gum was less than 0.08%, the gel strength kept increasing. When the amount of xanthan gum was 0.08%, the gel strength of the protein powder was larger. Subsequently, the gel strength of protein powder decreased gradually when the xanthan gum dosage was greater than 0.08%.

Gel strength is one of the important indexes of protein powder gel (20). The three-dimensional network structure formed by proteins is an important factor in maintaining gel properties. Adding material is one of the important means to improve the gel strength of SDEW protein powder (21). Xanthan gum is a kind of hydrophilic colloid, which belongs to polysaccharide. Xanthan gum is composed of D-glucose, D-mannose, and D-glucuronic acid. Appropriate amounts of xanthan gum can co-gel with protein and significantly improve the gel strength of protein powder. This may be since the lower amount of Xanthan gum can co-gel with proteins through electrostatic interaction and promote the formation of a three-dimensional network structure. However, a high amount of xanthan gum will generate electrostatic repulsion with protein, which is not conducive to the formation of gel (22).

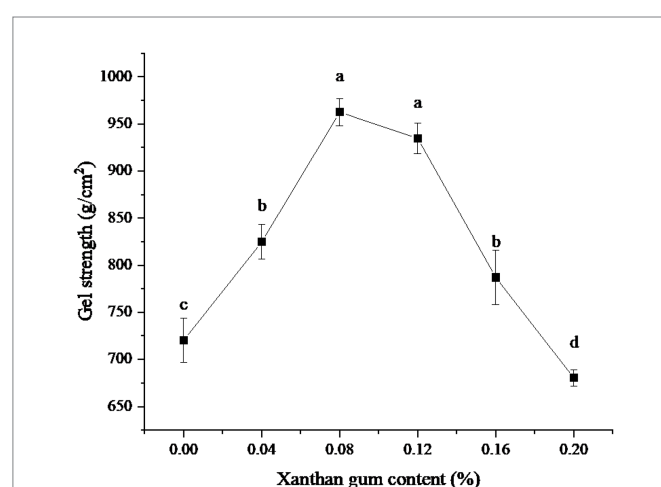
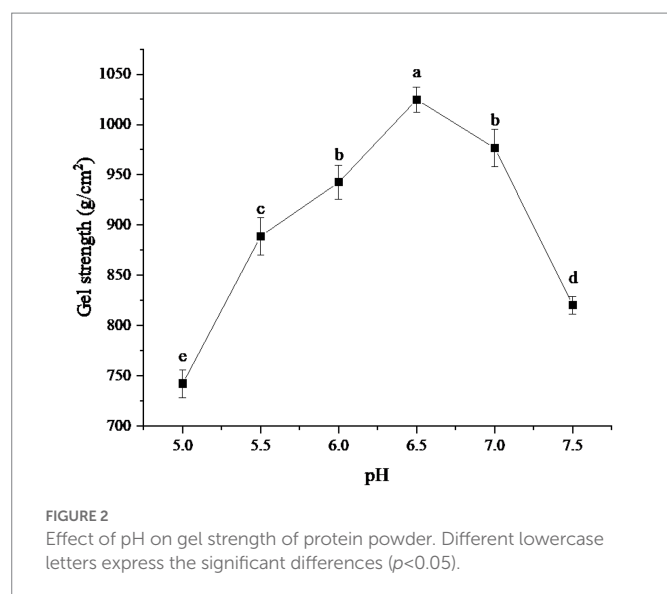


FIGURE 1  
Effect of xanthan gum content on gel strength of protein powder.  
Different lowercase letters express the significant differences ( $p < 0.05$ ).



## Test results of different pH

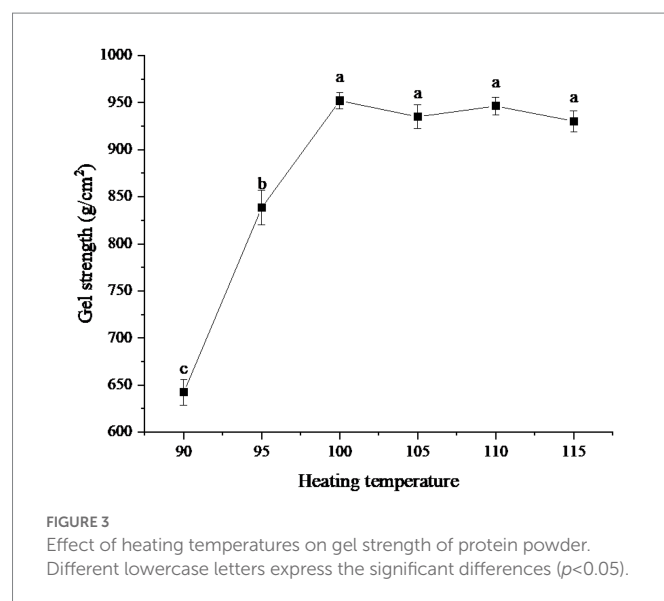
The effects of different pH on the gel strength of protein powder were shown in Figure 2. As can be seen from the figure, the gel strength of the protein powder increased with the increase in pH. When pH was 6.5, the gel strength of protein powder reached the maximum, about 1024.78 g/cm². With the further increase of pH, the gel strength of protein powder gradually decreased. When pH was 7.5, the gel strength showed a sharp decline.

The change of gel strength of protein powder may be due to the break of hydrogen bonds in xanthan gum in an acidic or alkaline medium, which leads to the failure of co-gel interaction with egg albumin in SDEW, thus affecting the formation of three-dimensional network structure (23). The change in the gel strength of protein powder may also be related to the isoelectric point of ovalbumin. When the pH of the protein powder gel is far away from its isoelectric point, the electrostatic repulsion will be larger, and it is easier to form linear aggregation. However, when the pH of the protein powder gel is close to its isoelectric point, the charge on the protein surface is small or even shielded, which is more likely to form a disordered cluster structure (24).

## Test results of different heating temperature

The effects of different heating temperatures on the gel strength of protein powder were shown in Figure 3. As can be seen from the figure, when the heating temperature was 90°C, the gel strength of protein was the lowest, about 642.36 g/cm². Then, with the gradual increase in temperature, the gel strength of the protein powder increased rapidly. When the temperature reached 100°C, the gel strength was about 952.06 g/cm². When the temperature exceeded 100°C, the gel strength was close to 950 g/cm², but fluctuates slightly, and there was no significant difference.

The change in gel strength of protein powder with heating temperature may be because the protein molecular structure becomes more extended with increasing temperature, exposing more hydrophobic groups, which is conducive to the formation of gel (25). In the range below 100°C, the increase in temperature can promote the binding between protein molecules, form a larger network structure,



and increase the gel strength. When the temperature rises above 100°C, protein molecules begin to degrade and destroy the intermolecular network structure, thus reducing the gel strength (26).

## Test results of different heating time

The influence of different heating times on the gel strength of protein powder was shown in Figure 4. It can be seen from the figure that the gel strength of the protein powder reached its maximum when the heating time was 80 min. However, within the range of 60–120 min of heating time, there was no significant difference in gel strength among samples. When the heating time was less than 60 min, the gel strength of the protein powder was low. When the heating time was 20 min, the gel strength of the protein powder was the lowest.

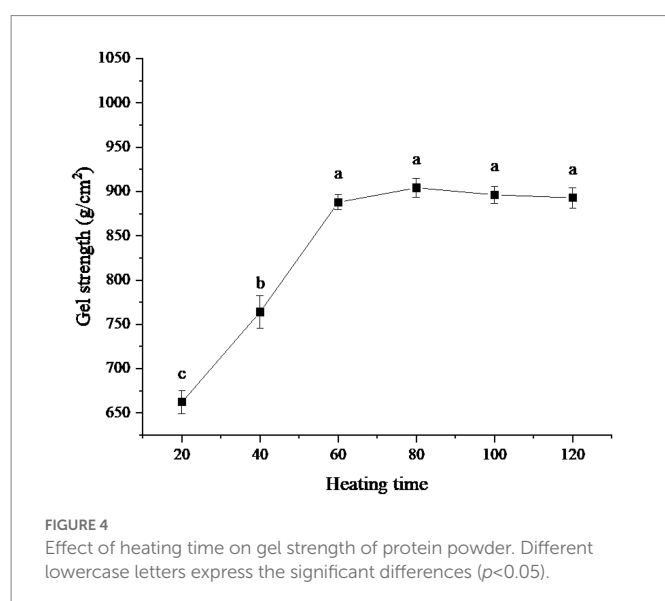
When the heating time was less than 60 min, the gel strength of protein powder was low because xanthan gum cannot fully combine with protein to form SEDW-XG composite gel in a short time (27). However, when the heating time exceeded 60 min, the combination of xanthan gum and protein reached a saturation state due to the limited amount of xanthan gum and protein, so the gel strength of protein powder no longer changes (28).

## Optimization of experimental conditions using the single-factor test

Based on the discussion of xanthan gum addition amount, reaction pH, heating temperature, and heating time four single factors, the quadratic regression rotation design was carried out. Then, the single-factor test was carried out with the additional amount of xanthan gum, reaction pH, and heating temperature as independent variables, which had a great influence on the experimental results. Table 1 showed the results of the single-factor test with gel strength as the response value. Quadratic multivariate regression fitting was performed on the experimental data, and the analysis results showed that the regression equation of gel strength of SDEW protein powder was as follows:  $Y = 1037.00 + 21.88 A - 3.12 B + 69.50 C + 1.00 AB + 10.75 AC + 2.75 BC - 80.25 A^2 - 63.25 B^2 - 122.50 C^2$  (A: Xanthan gum content (%); B: pH; C:

Temperature; D: Time). Variance analysis was performed on the fitted quadratic polynomial, and the results were shown in Table 2.

It can be seen from the Table 2 that A, B, C, A<sup>2</sup>, B<sup>2</sup>, and C<sup>2</sup> have a significant influence on the gel strength of protein powder. The high *F* value was 52.29, and the *p* value is <0.0001. The results showed that the fitting model could well explain the gel strength of SDEW protein powder. The *F* value and *p* value of the lack of fit were 0.81 and 0.0552 respectively, indicating that the predicted value of the model has high accuracy. Single-factor test showed that the optimum conditions of gel strength of SDEW protein powder were as follows: the content of xanthan gum was 0.08%, the reaction pH was 6.50, and the heating temperature was 100°C.



## Effect of xanthan gum content on the color of protein powder gel

As one of the important sensory indexes of food, color directly affects the quality of the high gelatinous salted duck egg protein powder (29). The results of gel color difference determination of SDEW protein powder with different xanthan gum contents were shown in Table 3. It can be intuitively seen from the table that the brightness of SDW was larger when the content of xanthan gum was 0.08 and 0.12. The redness and yellowness of SDW did not change significantly with the increase of xanthan gum content. The total color difference ( $\Delta E$ ) between the groups was significant. It can be seen from the experimental results that the addition of xanthan gum causes changes in the gel brightness and total color difference of protein powder. However, the addition of xanthan gum had little effect on the redness and yellow color of the protein powder gel.

## Effect of xanthan gum content on water holding capacity of protein powder gel

Water holding capacity is one of the important functional properties of heat-induced protein gels. The water holding capacity is related to the pore size of the gel network and the properties of the biopolymer used (30). Figure 5 showed the water holding capacity of SEDW gel with different xanthan gum contents. As can be seen from the figure, SEDW gel containing 0.20% xanthan gum showed the best water holding capacity. However, the water holding capacity of SEDW gel did not increase significantly after the content of xanthan gum reached 0.08%. The possible reason was that the addition of xanthan gum can form a network structure with the macromolecules in SEDW gel and improve the water holding capacity of the gel. However, when the binding reached saturation, the water holding capacity of SEDW gel no longer increased (31).

TABLE 1 Results of single-factor experiment.

Groups	A: Xanthan gum content (%)	B: pH	C: Temperature (°C)	Gel strength (g/cm <sup>2</sup> )
1	0.08	6.5	105	864
2	0.08	6	100	868
3	0.08	6.5	95	763
4	0.08	7	100	873
5	0.1	6	95	786
6	0.1	6.5	100	1,032
7	0.1	7	95	761
8	0.1	7	105	922
9	0.1	6.5	100	1,042
10	0.1	6	105	936
11	0.1	6.5	100	1,020
12	0.1	6.5	100	1,023
13	0.1	6.5	100	1,086
14	0.12	6.5	105	927
15	0.12	7	100	921
16	0.12	6.5	95	783
17	0.12	6	100	912



TABLE 2 Analysis of variance on the results obtained using single-factor experiment.

Source	Square sum	Degrees of freedom	Mean square	F-value	p-Value	Significance
Model	1.615E+005	9	17942.30	52.29	<0.0001	**
A	3828.13	1	3828.13	11.16	0.0124	*
B	78.13	1	78.13	0.23	0.0467	*
C	38642.00	1	38642.00	112.62	<0.0001	**
AB	4.00	1	4.00	0.012	0.9170	
AC	462.25	1	462.25	1.35	0.2838	
BC	30.25	1	30.25	0.088	0.7751	
A <sup>2</sup>	27116.05	1	27116.05	79.03	<0.0001	**
B <sup>2</sup>	16844.47	1	16844.47	49.09	0.0002	**
C <sup>2</sup>	63184.21	1	63184.21	184.15	<0.0001	**
Error	2401.75	7	343.11			
Lack of fit	905.75	3	301.92	0.81	0.5520	
Net error	1496.00	4	374.00			
Total error	1.639E+005	16				

\*Represents a significant difference ( $p < 0.05$ ); \*\*Represents a significant difference ( $p < 0.01$ ).

TABLE 3 Color parameters of protein powder gel with different xanthan gum contents.

Xanthan gum content (%)	L*	a*	b*	$\Delta E$
0.00	31.23 $\pm$ 2.49 <sup>ab</sup>	0.23 $\pm$ 0.12 <sup>a</sup>	3.53 $\pm$ 0.15 <sup>a</sup>	–
0.04	30.67 $\pm$ 1.10 <sup>ab</sup>	0.20 $\pm$ 0.08 <sup>a</sup>	3.57 $\pm$ 0.19 <sup>a</sup>	0.56 $\pm$ 0.05 <sup>c</sup>
0.08	32.90 $\pm$ 1.28 <sup>a</sup>	0.27 $\pm$ 0.09 <sup>a</sup>	3.43 $\pm$ 0.21 <sup>a</sup>	1.67 $\pm$ 0.11 <sup>c</sup>
0.12	32.20 $\pm$ 1.15 <sup>a</sup>	0.23 $\pm$ 0.12 <sup>a</sup>	3.87 $\pm$ 0.42 <sup>a</sup>	1.03 $\pm$ 0.09 <sup>d</sup>
0.16	27.43 $\pm$ 3.29 <sup>b</sup>	0.27 $\pm$ 0.05 <sup>a</sup>	3.50 $\pm$ 0.25 <sup>a</sup>	3.80 $\pm$ 0.17 <sup>a</sup>
0.20	28.50 $\pm$ 0.94 <sup>b</sup>	0.33 $\pm$ 0.05 <sup>a</sup>	3.67 $\pm$ 0.15 <sup>a</sup>	2.74 $\pm$ 0.17 <sup>b</sup>

Results are mean  $\pm$  standard deviation. Different lowercase letters in the same column express the significant differences ( $p < 0.05$ ).

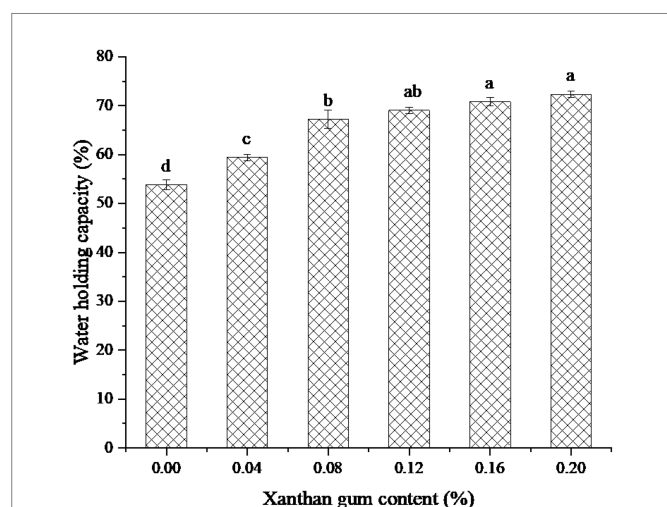


FIGURE 5 The water holding capacity of protein powder gel for xanthan gum addition. Different lowercase letters express the significant differences ( $p < 0.05$ ).

## Effect of xanthan gum content on microstructure of protein powder gel

The microstructure of the thermally induced SDEW-XG gel was observed by scanning electron microscope. The following figures were from sample group (A1, A2): SDEW gel prepared without xanthan gum; Experimental group (A3, A4): SDEW-XG gel prepared under optimal conditions obtained by response surface analysis (Figure 6). As can be seen from the figure, the addition of xanthan gum can significantly improve the microstructure of the gel formed by protein powder. From the enlarged figure of 5.0 k, it can be seen that the surface microstructure of SDEW protein powder without xanthan gum was uneven, and the number of holes was very large. After xanthan gum was added, the gel microstructure particle size was more uniform, the surface was smoother and tighter, and the number of pores was significantly reduced. From the enlarged figure of 10.0 k, it can be more intuitively observed that the pores in the microstructure of SDEW protein powder without xanthan gum were of different sizes and generally had larger pore sizes. However, after the addition of xanthan gum, although there were holes in the gel microstructure, the size was uniform and the pore size was generally small. According to the experimental data, the gel strength of the experimental group was significantly higher than that of the control group. Therefore, the microstructure of the gel network can also be considered an important factor affecting the gel strength of protein powder. Protein powder gel with a more compact structure has higher strength (32).

## Effect of xanthan gum content on the secondary structure of protein powder gel

Proteins can form specific secondary structures, including  $\alpha$ -helix,  $\beta$ -folding, and random curling (33). The amide I region band (1,600–1,700  $\text{cm}^{-1}$ ) in the infrared spectrum is related to C=O tensile vibration, and can be used to evaluate the changes in secondary structure in proteins (34). As can be seen from Figure 7

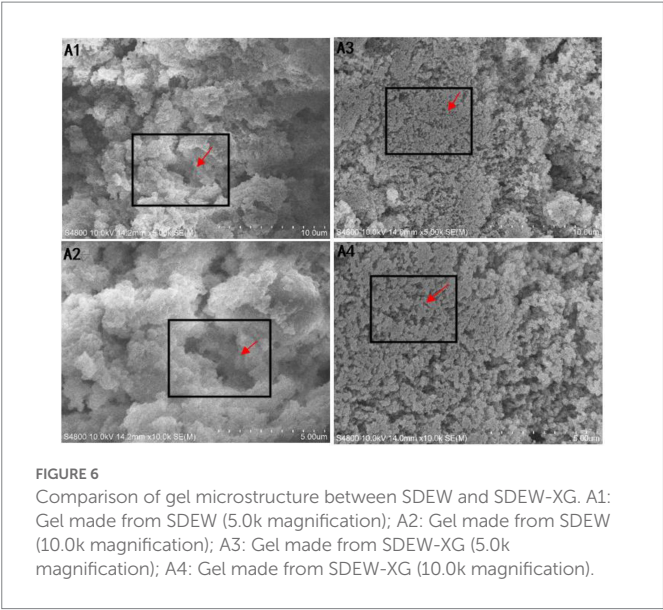


**FIGURE 6**  
Comparison of gel microstructure between SDEW and SDEW-XG. A1: Gel made from SDEW (5.0k magnification); A2: Gel made from SDEW (10.0k magnification); A3: Gel made from SDEW-XG (5.0k magnification); A4: Gel made from SDEW-XG (10.0k magnification).

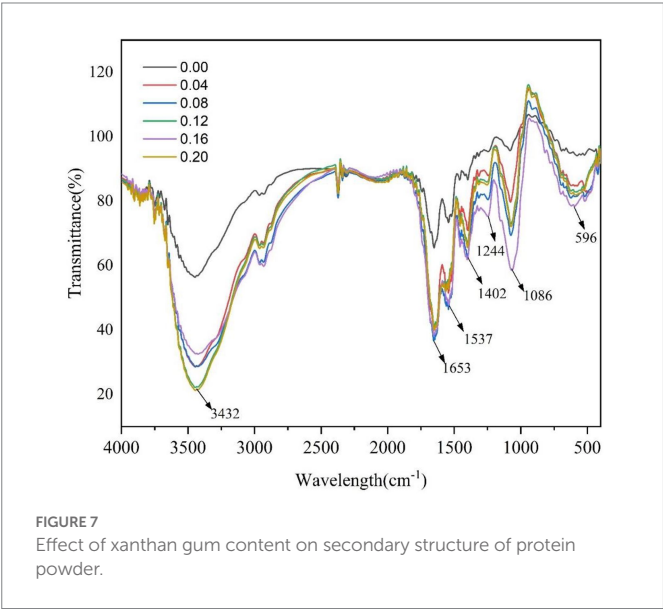


**FIGURE 7**  
Effect of xanthan gum content on secondary structure of protein powder.

and Table 4, the addition of xanthan gum significantly affected the secondary structure of SDEW protein powder. With the increase of xanthan gum content,  $\beta$ -fold content increased and  $\alpha$ -helix content decreased. In the secondary structure of proteins,  $\alpha$ -helix and  $\beta$ -folding are ordered,  $\beta$ -turning is a relatively loose partial order, and random curling is loose and disordered. According to the analysis of the peak value in the figure and the data in the table, the addition of xanthan gum changed the original rigid structure of the gel formed by egg white protein powder, leading to an increase in flexibility (35).

Conclusion

In this work, xanthan gum was added to study the high gelation of salted duck egg protein powder. The results showed that the addition

**TABLE 4** Estimated secondary structure using the amide I region of SDEW protein powder.

Xanthan gum content (%)	$\alpha$ -helix%	$\beta$ -sheet%	$\beta$ -turn%	Random coil%
0.00	29.07 $\pm$ 0.35 <sup>a</sup>	43.67 $\pm$ 1.68 <sup>b</sup>	15.57 $\pm$ 0.41 <sup>b</sup>	11.25 $\pm$ 0.38 <sup>b</sup>
0.04	28.61 $\pm$ 0.52 <sup>a</sup>	44.35 $\pm$ 1.57 <sup>b</sup>	15.67 $\pm$ 0.38 <sup>b</sup>	11.08 $\pm$ 0.47 <sup>b</sup>
0.08	24.35 $\pm$ 0.92 <sup>b</sup>	46.85 $\pm$ 2.37 <sup>ab</sup>	16.09 $\pm$ 0.56 <sup>b</sup>	12.53 $\pm$ 0.53 <sup>a</sup>
0.12	22.48 $\pm$ 1.08 <sup>b</sup>	47.21 $\pm$ 1.95 <sup>ab</sup>	18.36 $\pm$ 1.23 <sup>a</sup>	11.86 $\pm$ 0.96 <sup>ab</sup>
0.16	20.95 $\pm$ 0.69 <sup>bc</sup>	48.64 $\pm$ 2.08 <sup>a</sup>	18.94 $\pm$ 1.68 <sup>a</sup>	11.29 $\pm$ 0.82 <sup>ab</sup>
0.20	18.36 $\pm$ 0.84 <sup>c</sup>	49.63 $\pm$ 3.16 <sup>a</sup>	19.07 $\pm$ 1.38 <sup>a</sup>	12.60 $\pm$ 0.51 <sup>a</sup>

Results are mean  $\pm$  standard deviation. Different lowercase letters in the same column express the significant differences ( $p < 0.05$ ).

of xanthan gum significantly improved the gel properties of salted duck egg protein powder. Compared with the ordinary protein powder, the gel property of the protein powder was greatly improved, and its water holding capacity was also on the rise. Secondly, the gel microstructure of high-gelatinous SDEW protein powder was smoother and tighter. The number of holes in the 3D network structure of the gel was also small, and the pore size was relatively uniform. The research of xanthan gum on the gelation enhancement mechanism of salted duck egg protein powder was not deep enough. In addition, the high gel egg white protein powder is mainly used in industry, and there is still a lot of work to be done in its development and industrial large-scale production.

Data availability statement

The original contributions presented in the study are included in the article/supplementary material, further inquiries can be directed to the corresponding authors.

Author contributions

XY, TD, YX, and MH: experiments and writing – original draft. JX, and JG: writing – review and editing. All authors have read and agreed to the published version of the manuscript.

Funding

The authors acknowledged the support of the Anhui Provincial Science and Technology Major Special Project (202003b06020004), the Anhui Provincial Natural Science Foundation (No. 1908085MC79), and the Overseas Visiting and Study Program for Outstanding Young Backbone Talents of Anhui Universities (No. gxgwfx2020056).

Conflict of interest

The authors declare that the research was conducted in the absence of any commercial or financial relationships that could be construed as a potential conflict of interest.

## Publisher's note

All claims expressed in this article are solely those of the authors and do not necessarily represent those of their affiliated

organizations, or those of the publisher, the editors and the reviewers. Any product that may be evaluated in this article, or claim that may be made by its manufacturer, is not guaranteed or endorsed by the publisher.

## References

- Chen, X, Pei, Y, Li, B, Wang, Y, Zhou, B, Li, B, et al. Interfacial decoration of desalted duck egg white nanogels as stabilizer for Pickering emulsion. *Food Hydrocoll.* (2022) 132:107858. doi: 10.1016/j.foodhyd.2022.107858
- Du, T, Xu, J, Zhu, S, Yao, X, Guo, J, Lv, W, et al. Effects of spray drying, freeze drying, and vacuum drying on physicochemical and nutritional properties of protein peptide powder from salted duck egg white. *Front Nutr.* (2022) 9:1026903. doi: 10.3389/fnut.2022.1026903
- Wang, ZF, Dai, C, and Wang, TY. A simple method to evaluate oil in salted egg. *Int J Food Prop.* (2017) 20:1816–22. doi: 10.1080/10942912.2017.1311345
- Yu, L, Xue, H, Xiong, C, Xin, X, Wang, P, Feng, F, et al. Characterization of duck egg white gel under the action of baijiu (Chinese liquor). *Lebensm Wiss Technol.* (2021) 147:111487. doi: 10.1016/j.lwt.2021.111487
- Zhao, J, Guo, X, Chen, Z, Dai, Y, Liang, H, Deng, Q, et al. Desalted duck egg white nanogels as Pickering stabilizers for food-grade oil-in-water emulsion. *Food Sci Human Wellness.* (2022) 11:1306–14. doi: 10.1016/j.fshw.2022.04.012
- Du, M, Sun, Z, Liu, Z, Yang, Y, Liu, Z, Wang, Y, et al. High efficiency desalination of wasted salted duck egg white and processing into food-grade pickering emulsion stabilizer. *Lebensm Wiss Technol.* (2022) 161:113337. doi: 10.1016/j.lwt.2022.113337
- Dai, Y, Zhao, J, Liang, H, Deng, Q, Wan, C, Li, B, et al. Desalination of salted duck egg white assisted by gelatin: foaming and interface properties of the mixed system. *Food Hydrocoll.* (2022) 124:107260. doi: 10.1016/j.foodhyd.2021.107260
- Du, T, Xu, J, Zhu, S, Yao, X, Guo, J, and Lv, W. Effects of spray drying, freeze drying, and vacuum drying on physicochemical and nutritional properties of protein peptide powder from salted duck egg white. *Front Nutr.* (2022) 9:1026903. doi: 10.3389/fnut.2022.1026903
- Yao, X, Du, T, Guo, J, Lv, W, Adhikari, B, and Xu, J. Extraction and characterization of lysozyme from salted duck egg white. *Foods.* (2022) 11:3567. doi: 10.3390/foods11223567
- Peng, N, Gu, L, Li, J, Chang, C, Li, X, Su, Y, et al. Films based on egg white protein and Succinylated casein cross-linked with transglutaminase. *Food Bioprocess Technol.* (2017) 10:1422–30. doi: 10.1007/s11947-017-1901-8
- Tang, H, Tan, L, Chen, Y, Zhang, J, Li, H, and Chen, L. Effect of kappa-carrageenan addition on protein structure and gel properties of salted duck egg white. *J Sci Food Agric.* (2021) 101:1389–95. doi: 10.1002/jsfa.10751
- Kar, A, Guha, S, Subbiah, J, and Majumder, K. Effect of radiofrequency processing on the structural and bio-functional properties of egg white proteins. *Food Chem.* (2023) 404:134533. doi: 10.1016/j.foodchem.2022.134533
- Zhang, T, Yang, Y, Zhang, M, Jiang, H, Yan, Z, Liu, J, et al. Effect of soy lecithin concentration on physicochemical properties and rehydration behavior of egg white protein powder: role of dry and wet mixing. *J Food Eng.* (2022) 328:111062. doi: 10.1016/j.jfoodeng.2022.111062
- Xia, M, Zhao, Q, Isobe, K, Handa, A, Cai, Z, and Huang, X. Lysozyme impacts gel properties of egg white protein via electrostatic interactions, polarity differences, local pH regulation, or as a filler. *Int J Biol Macromol.* (2022) 223:1727–36. doi: 10.1016/j.ijbiomac.2022.10.101
- Ding, Z, Li, S, and Cao, X. Separation of lysozyme from salted duck egg white by affinity precipitation using pH-responsive polymer with an L-thyroxine ligand. *Sep Purif Technol.* (2014) 138:153–60. doi: 10.1016/j.seppur.2014.10.021
- Xu, J, Zhu, S, Zhang, M, Cao, P, and Adhikari, B. Combined radio frequency and hot water pasteurization of Nostoc sphaeroides: effect on temperature uniformity, nutrients content, and phycocyanin stability. *Lebensm Wiss Technol.* (2021) 141:110880. doi: 10.1016/j.lwt.2021.110880
- Jiang, Y, Li, D, Tu, J, Zhong, Y, Zhang, D, Wang, Z, et al. Mechanisms of change in gel water-holding capacity of myofibrillar proteins affected by lipid oxidation: the role of protein unfolding and cross-linking. *Food Chem.* (2021) 344:128587. doi: 10.1016/j.foodchem.2020.128587
- Xu, J, Zhang, M, Cao, P, and Adhikari, B. Effect of ZnO nanoparticles combined radio frequency pasteurization on the protein structure and water state of chicken thigh meat. *LWT-food. Sci Technol.* (2020) 134:110168. doi: 10.1016/j.lwt.2020.110168
- Xu, J, Zhang, M, Cao, P, Adhikari, B, and Yang, C. Microorganisms control and quality improvement of stewed pork with carrots using ZnO nanoparticles combined with radio frequency pasteurization. *Food Biosci.* (2019) 32:100487. doi: 10.1016/j.fbio.2019.100487
- Gulzar, M, Lechevalier, V, Bouhallab, S, and Croguennec, T. The physicochemical parameters during dry heating strongly influence the gelling properties of whey proteins. *J Food Eng.* (2012) 112:296–303. doi: 10.1016/j.jfoodeng.2012.05.006
- Nicoletti, JF, and Telis, VRN. Viscoelastic and thermal properties of collagen-xanthan gum and collagen-maltodextrin suspensions during heating and cooling. *Food Biophysics.* (2009) 4:135–46. doi: 10.1007/s11483-009-9110-2
- Wang, Y, Li, D, Wang, L-J, Li, S-J, and Adhikari, B. Effects of drying methods on the functional properties of flaxseed gum powders. *Carbohydr Polym.* (2010) 81:128–33. doi: 10.1016/j.carbpol.2010.02.005
- Zhang, S, Huang, W, Roopesh, MS, and Chen, L. Pre-treatment by combining atmospheric cold plasma and pH-shifting to prepare pea protein concentrate powders with improved gelling properties. *Food Res Int.* (2022) 154:111028. doi: 10.1016/j.foodres.2022.111028
- Chen, L, Li, Y, Han, J, Yuan, D, Lu, Z, and Zhang, L. Influence of transglutaminase-induced modification of milk protein concentrate (MPC) on yoghurt texture. *Int Dairy J.* (2018) 78:65–72. doi: 10.1016/j.idairyj.2017.10.001
- Konieczny, P, Andrzejewski, W, Yang, T, Urbanska, M, Stangierski, J, Tomczyk, L, et al. Selected quality attributes of freshwater mussel powder as a promising ingredient for pet food. *Animals.* (2022) 12:90. doi: 10.3390/ani12010090
- Chen, J, Yang, X, Xia, X, Wang, L, Wu, S, and Pang, J. Low temperature and freezing pretreatment for konjac glucomannan powder to improve gel strength. *Int J Biol Macromol.* (2022) 222:1578–88. doi: 10.1016/j.ijbiomac.2022.09.288
- Zisu, B, Lee, J, Chandrapala, J, Bhaskaracharya, R, Palmer, M, Kentish, S, et al. Effect of ultrasound on the physical and functional properties of reconstituted whey protein powders. *J Dairy Res.* (2011) 78:226–32. doi: 10.1017/S0022029911000070
- El-Garawany, GA, and Salam, MHA. Preparation and rheological properties of a dairy dessert based on whey protein/potato starch. *Food Chem.* (2005) 91:261–7. doi: 10.1016/j.foodchem.2004.01.073
- Quan, TH, and Benjakul, S. Impact of salted duck egg albumen powder on proteolysis and gelling properties of sardine surimi. *J Texture Stud.* (2019) 50:434–42. doi: 10.1111/jtxs.12445
- Liu, C, Li, W, Lin, B, Yi, S, Ye, B, Mi, H, et al. Comprehensive analysis of ozone water rinsing on the water-holding capacity of grass carp surimi gel. *LWT Food Sci Technol.* (2021) 150:111919. doi: 10.1016/j.lwt.2021.111919
- Li, YP, Kang, ZL, Sukmanov, V, and Ma, HJ. Effects of soy protein isolate on gel properties and water holding capacity of low-salt pork myofibrillar protein under high pressure processing. *Meat Sci.* (2021) 176:108471. doi: 10.1016/j.meatsci.2021.108471
- Cenini, VL, Gallagher, L, McKerr, G, McCarthy, NA, McSweeney, DJ, Auty, MAE, et al. A novel approach for dynamic in-situ surface characterisation of milk protein concentrate hydration and reconstitution using an environmental scanning electron microscope. *Food Hydrocoll.* (2020) 108:105881. doi: 10.1016/j.foodhyd.2020.105881
- Zhang, L, Sun, X, Lu, X, Wei, S, Sun, Q, Jin, L, et al. Characterization of peanut protein hydrolysate and structural identification of umami-enhancing peptides. *Molecules.* (2022) 27:2853. doi: 10.3390/molecules27092853
- Antony, JV, Koya, R, Pournami, PN, Nair, GG, and Balakrishnan, JP. Protein secondary structure assignment using residual networks. *J Mol Model.* (2022) 28:269. doi: 10.1007/s00894-022-05271-z
- Ye, MP, Zhou, R, Shi, YR, Chen, HC, and Du, Y. Effects of heating on the secondary structure of proteins in milk powders using mid-infrared spectroscopy. *J Dairy Sci.* (2017) 100:89–95. doi: 10.3168/jds.2016-11443



## OPEN ACCESS

## EDITED BY

Hao Jiang,  
Northwest A&F University, China

## REVIEWED BY

Yue Zhang,  
China Agricultural University, China  
Rentang Zhang,  
Shandong Agricultural University, China

## \*CORRESPONDENCE

Xuhai Yang  
✉ yxh\_513@shzu.edu.cn

†These authors have contributed equally to this work

## SPECIALTY SECTION

This article was submitted to  
Nutrition and Food Science Technology,  
a section of the journal  
Frontiers in Nutrition

RECEIVED 23 November 2022

ACCEPTED 04 January 2023

PUBLISHED 08 February 2023

## CITATION

Geng Z, Zhu L, Wang J, Yu X, Li M, Yang W,  
Hu B, Zhang Q and Yang X (2023) Drying sea  
buckthorn berries (*Hippophae rhamnoides* L.):  
Effects of different drying methods on drying  
kinetics, physicochemical properties,  
and microstructure.  
*Front. Nutr.* 10:1106009.  
doi: 10.3389/fnut.2023.1106009

## COPYRIGHT

© 2023 Geng, Zhu, Wang, Yu, Li, Yang, Hu,  
Zhang and Yang. This is an open-access article  
distributed under the terms of the [Creative  
Commons Attribution License \(CC BY\)](#). The use,  
distribution or reproduction in other forums is  
permitted, provided the original author(s) and  
the copyright owner(s) are credited and that the  
original publication in this journal is cited, in  
accordance with accepted academic practice.  
No use, distribution or reproduction is  
permitted which does not comply with  
these terms.

# Drying sea buckthorn berries (*Hippophae rhamnoides* L.): Effects of different drying methods on drying kinetics, physicochemical properties, and microstructure

Zhihua Geng<sup>1†</sup>, Lichun Zhu<sup>1†</sup>, Jun Wang<sup>2</sup>, Xianlong Yu<sup>3</sup>,  
Mengqing Li<sup>1</sup>, Wenxin Yang<sup>1</sup>, Bin Hu<sup>1,4</sup>, Qian Zhang<sup>1</sup> and  
Xuhai Yang<sup>1,5\*</sup>

<sup>1</sup>College of Mechanical and Electrical Engineering, Shihezi University, Shihezi, China, <sup>2</sup>College of Food Science and Engineering, Northwest A&F University, Yangling, China, <sup>3</sup>Shandong Academy of Agricultural Machinery Sciences, Jinan, China, <sup>4</sup>Xinjiang Production and Construction Corps, Key Laboratory of Modern Agricultural Machinery, Shihezi, China, <sup>5</sup>Engineering Research Center for Production Mechanization of Oasis Special Economic Crop, Ministry of Education, Shihezi, China

Sea buckthorn berries are important ingredients in Chinese medicine and food processing; however, their high moisture content can reduce their shelf life. Effective drying is crucial for extending their shelf life. In the present study, we investigated the effects of hot-air drying (HAD), infrared drying (IRD), infrared-assisted hot-air drying (IR-HAD), pulsed-vacuum drying (PVD), and vacuum freeze-drying (VFD) on the drying kinetics, microstructure, physicochemical properties (color, non-enzyme browning index, and rehydration ratio), and total phenol, total flavonoid, and ascorbic acid contents of sea buckthorn berries. The results showed that the IR-HAD time was the shortest, followed by the HAD, IRD, and PVD times, whereas the VFD time was the longest. The value of the color parameter  $L^*$  decreased from 53.44 in fresh sea buckthorn berries to 44.18 (VFD), 42.60 (PVD), 37.58 (IRD), 36.39 (HAD), and 36.00 (IR-HAD) in dried berries. The browning index also showed the same trend as the color change. Vacuum freeze-dried berries had the lowest browning index (0.24 Abs/g d.m.) followed by that of pulsed-vacuum–(0.28 Abs/g d.m.), infrared– (0.35 Abs/g d.m.), hot-air–(0.42 Abs/g d.m.), and infrared-assisted hot-air–dried berries (0.59 Abs/g d.m.). The ascorbic acid content of sea buckthorn berries decreased by 45.39, 53.81, 74.23, 77.09, and 79.93% after VFD, PVD, IRD, IR-HAD, and HAD, respectively. The vacuum freeze-dried and pulsed-vacuum–dried sea buckthorn berries had better physicochemical properties than those dried by HAD, IRD, and IR-HAD. Overall, VFD and PVD had the highest ascorbic acid and total phenolic contents, good rehydration ability, and bright color. Nonetheless, considering the high cost of VFD, we suggest that PVD is an optimal drying technology for sea buckthorn berries, with the potential for industrial application.

## KEYWORDS

drying kinetics, physicochemical properties, pulsed vacuum drying, vacuum freeze-drying, sea buckthorn berries



## 1. Introduction

Sea buckthorn (*Hippophae rhamnoides* L.), of the family Hoiaceae (1) is a perennial deciduous shrub and a berry fruit-bearing tree. This species is light-loving, cold- and heat-tolerant, and can survive in sandy and arid climates in saline soils. Consequently, it is widely used for soil and water conservation and desert greening. Sea buckthorn is a collective name for the plant and its fruits, which are used as food and have medicinal properties (2). Sea buckthorn is widely distributed and is found in temperate zones of Europe and Asia. It is mainly distributed in Eurasia, particularly in China, which is home to the most species. The area of sea buckthorn cultivation worldwide is 918,700 hm<sup>2</sup> with annual production of 400,000 tons, and that in China is 780,900 hm<sup>2</sup> with a production of annual production 250,000 tons (3).

Sea buckthorn berries are used as raw ingredients in Chinese medicine, food processing, and other industries. The berries are rich in flavonoids, vitamins, polyphenols, and other nutrients, and can promote blood circulation and disperse blood stasis, dissolve phlegm and broaden the chest, generate body fluid and quench thirst, and cure diarrhea (4). Sea buckthorn berries contain flavonoid compounds, mainly quercetin, kaempferol, and isorhamnetin, which possess anti-inflammatory activity, regulate the intestinal flora, and exert various physiological effects, including antioxidant release, blood glucose regulation, anti-inflammatory action, and hypolipidemia, and thus help prevent and aid in the treatment of heart diseases, hypertension, hyperlipidemia, hyperglycemia, and cancer (5). Flavonoid compounds in sea buckthorn berries (as nutritional supplements) help regulate intestinal microecology and a significant negative correlation exists between the intake of sea buckthorn berries and the incidence of metabolic diseases (6). Moreover, sea buckthorn berries are rich in vitamin C, have high stability, and find considerable application in the cosmetic industry (7). The vitamins in the berries also play an important role in scavenging free radicals, improving blood circulation, and anti-cellular differentiation. Nowak et al. (8) showed that ascorbic acid and polyphenols have a synergistic effect in determining the antioxidant properties of sea buckthorn juice and play an important role in disease prevention. Polyphenols in sea buckthorn berries are mainly phenolic acids such as protocatechuic acid, gallic acid, caffeic acid, p-coumaric acid, ferulic acid, and other major phenolic acids, and possess hypolipidemic, anticancer, and intestinal flora-improving effects (9). Their ability to inhibit or stimulate specific bacterial species to alleviate intestinal flora imbalance and reduce reactive oxygen species, inflammatory markers, harmful bacterial effects, and colonic tissue damage is important for maintaining intestinal health (10).

Fresh sea buckthorn berries contain up to 80% water and are rich in vitamins and polyphenols with unstable active ingredients that are easily oxidized, making them highly perishable commodities (11). Harvested berries are not suitable for long-term storage as they ferment and deteriorate in a short time at room temperature, thus losing their medicinal value. Therefore, extending the shelf life of sea buckthorn berries and reducing postharvest losses are important issues facing the sea buckthorn industry. In addition to methods such as pre-cooling and preservation, drying preserves the berries by reducing the water content in fruits and vegetables. Sea buckthorn berries are commonly dried by hot-air drying (HAD) through air convection and heat conduction for heat exchange (12). Although

HAD is inexpensive and does not require specialized equipment, heat conduction is necessary for heat transfer. Vacuum freeze-drying (VFD) is an emerging technology that has been used to dry sea buckthorn berries in recent years (13). The color and shape of the berries remain largely unchanged after VFD, which minimizes quality deterioration, including enzymatic and non-enzymatic browning and protein denaturation, preserves nutrition, and maintains color (14). However, VFD equipment is expensive—approximately five times more expensive than that used in traditional drying methods—and the productivity is low, which limits the potential for wide application of this technology (15).

This study aimed to investigate the effects of different drying methods, namely HAD, infrared drying (IRD), infrared-assisted hot air-drying (IR-HAD), pulsed vacuum drying (PVD), and VFD, on the drying kinetics, physicochemical properties, and microstructure of sea buckthorn berries. The results could provide a basis for the selection of an optimal drying method.

## 2. Materials and methods

### 2.1. Materials

Fresh sea buckthorn berries were picked from No. 170 State Farm in E-ming (Tacheng, Xinjiang, China). The hand-selected sea buckthorn berries were of uniform size and color, with no bruises or rotting, and were stored at  $-20^{\circ}\text{C}$  in a refrigerator. The average mass of the selected samples was  $2.5 \pm 0.1$  g, with a long axis length of  $50 \pm 5$  mm and a short axis length of  $30 \pm 5$  mm. The surface dust was removed with water, and the remaining water was blotted off the surface using absorbent paper before the experiment. The average initial moisture content of sea buckthorn berries was measured by drying in a vacuum chamber at  $70^{\circ}\text{C}$  for 24 h (16).

### 2.2. Drying methods

In all tests, the dryer was first switched on and run for 30 min to obtain a steady state. The material (100 g) was first placed in a stainless-steel metal grid tray with a loading density of  $0.2 \text{ kg/m}^2$  and then placed in a drying chamber. The drying was stopped when the moisture content decreased below 10%. All drying experiments were conducted in triplicate. The results were averaged for analysis, and the material was sealed and packed after cooling.

Hot-air drying was performed as described by Zhang et al. (17). The HAD equipment was obtained from Shanghai Yihuan Scientific Instruments Co., Ltd. (Shanghai, China). The drying medium temperature was set at  $60^{\circ}\text{C}$ , the air speed was kept at 2.2 m/s, and the airflow direction was parallel to the drying material tray. IRD was performed as described by Li (18); the IRD equipment was custom-made from Shihezi University (Shihezi, China), with a power of 300 W and drying medium temperature of  $60^{\circ}\text{C}$ . IR-HAD was performed as described by Chang et al. (19). The IR-HAD equipment was obtained from Jiangsu Sentec Co., Ltd. (Shihezi, China), and drying medium temperature of  $60^{\circ}\text{C}$ , IR power of 675 W, and air speed of 2.5 m/s were used. Notably, IR radiation is the heat source in IR-HAD, and the IR radiation tube stops heating when the temperature reaches a set value, subsequently using HAD. When the temperature decreases again, the IR radiation



tube starts heating once more. PVD was performed as described by Deng et al. (16). The PVD equipment was custom-made from Shihezi University (Shihezi, China). The thermal sensors were used to measure and control the far-infrared radiation heating panel temperature. The test was conducted at the far-infrared radiation heating panel temperature of 60°C, and the dryer was set with an atmospheric pressure holding time of 15 min and a vacuum holding time of 4 min. VFD was performed as described by Schössler et al. (20). HAD, IRD, and IR-HAD thermal sensors were used to measure and control the air temperature above the material tray. In the IR-HAD dryer, the distance between the infrared radiation tubes and the material tray was 120 mm. Three quartz glass medium-wave (2–4 μm) infrared tubes were placed parallel to the material tray, and their radiation power was 450, 225, and 225 W, respectively. During the drying experiment, two medium-wave infrared tubes, with a total radiation power of 625 W, were selected. The VFD equipment was obtained from CHRIST Freeze Dryer GmbH (Osterode, Germany), with a cold-trap temperature of −40°C, heating plate temperature of 30°C, and a drying chamber pressure of 12 Pa. Figure 1 shows the schematics of the five dryers, and Figure 2 shows the experimental setup process.

## 2.3. Drying characteristics

During drying, the variation of moisture content—moisture ratio (*MR*) and drying rate (*DR*)—sea buckthorn berries weight loss was

measured every 30 min, and the *MR*-*t* and *DR*-*MR* curves were calculated (21).

The drying moisture ratio *MR* of sea buckthorn berries at drying time *t*, was obtained from Eq. 1:

$$MR = \frac{M_t - M_e}{M_0 - M_e} \quad (1)$$

where *M*<sub>0</sub> is the initial dry-basis moisture content in g/g; *M*<sub>*e*</sub> is the dry-basis moisture content at the time of drying to equilibrium in g/g; *M*<sub>*t*</sub> is the dry-basis moisture content at any drying *t* moment in g/g.

Because the equilibrium dry-basis moisture content *M*<sub>*e*</sub> is much smaller than *M*<sub>0</sub> and *M*<sub>*t*</sub>, Eq. 1 can be simplified to Eq. 2:

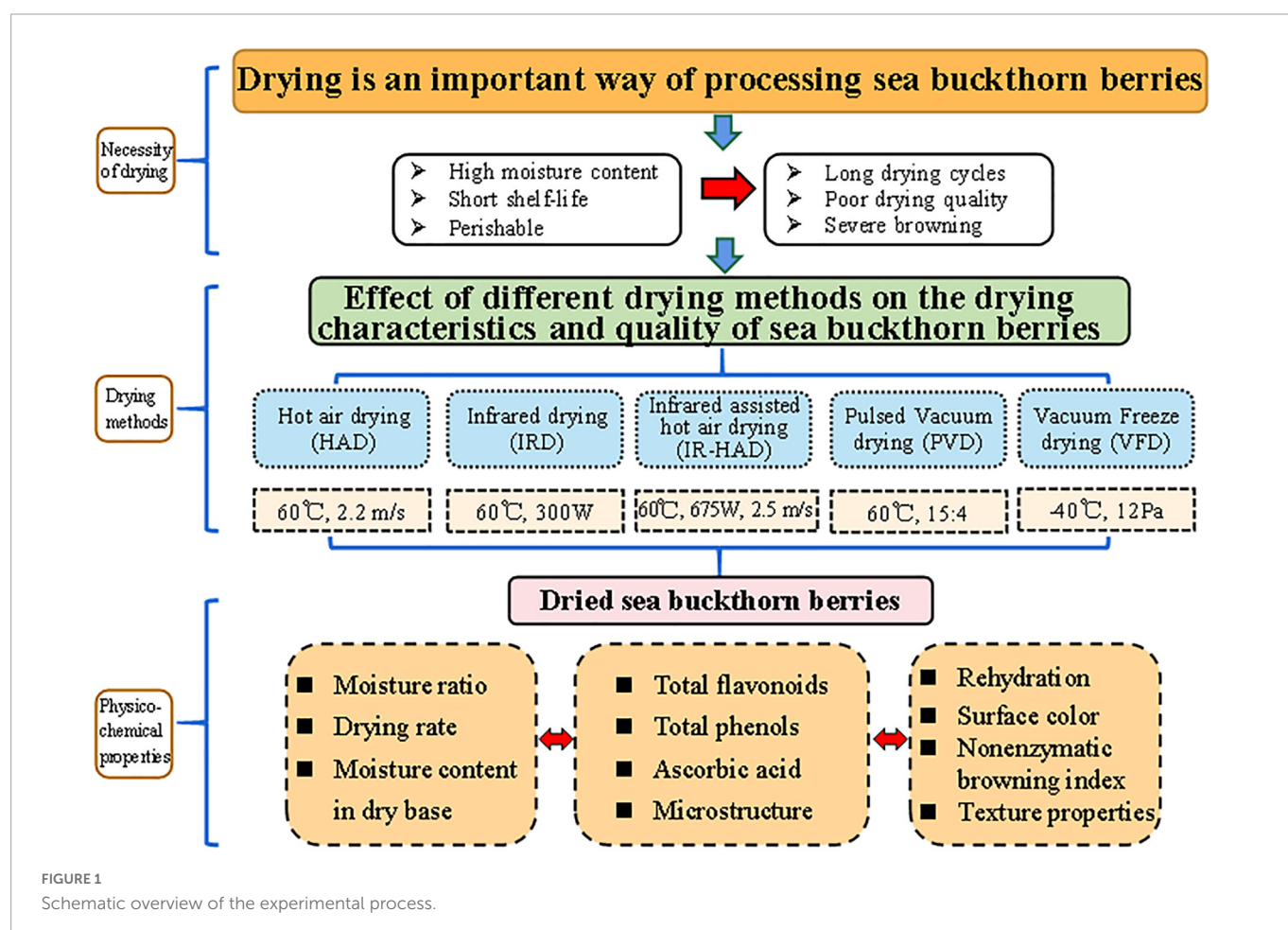
$$MR = \frac{M_t}{M_0} \quad (2)$$

The *DR* of sea buckthorn berries during the drying process can be derived from Eq. 3:

$$DR = \frac{M_{t1} - M_{t2}}{t_1 - t_2} \quad (3)$$

## 2.4. Rehydration ratio

Based on the method of Zhang et al. (22), a glass with deionized water was placed in a water bath at 40°C. When the temperature of deionized water was constant, 5 g of dried sea buckthorn berries was added to the 50 mL deionized water. After 30 min, the berries were removed and drained, and the surface of the material was wiped dry



with absorbent paper and weighed using an analytical balance after rehydration. The rehydration ratio was calculated according to Eq. 4:

$$R_r = \frac{m_2}{m_1} \quad (4)$$

where  $R_r$  is the material rehydration ratio, g/g;  $m_2$  is the rehydrated material mass, g;  $m_1$  is the rehydrated material before the material mass, g.

## 2.5. Color attributes

Fresh and dried sea buckthorn berries were selected. The fresh sea buckthorn berries were homogenized under ice bath conditions and then measured, and the dried sea buckthorn berries were ground into powder and passed through a 40-mesh sieve. The colorimetric  $L^*$ ,  $a^*$ , and  $b^*$  values were measured using SMY-2000SF colorimeter (Beijing Mingyang Technology Development Co., Ltd., Beijing, China). The total color difference value  $\Delta E$  between the treated group and the fresh sample was also calculated according to Eq. 5 (23):

$$\Delta E = \sqrt{(L - L^*)^2 + (a - a^*)^2 + (b - b^*)^2} \quad (5)$$

Where  $L^*$ ,  $a$ , and  $b$  are the brightness, red-green, and blue-yellow values of the sample before drying, respectively; and  $L^*$ ,  $a^*$ , and  $b^*$  are the brightness, red-green, and blue-yellow values of the sample after drying, respectively.

## 2.6. Non-enzymatic browning index

Non-enzymatic browning index analysis was performed according to a method of Deng et al. (16). The 2.0 g of sea buckthorn

was first ground homogeneously with 20 mL of distilled water. The intermixture was centrifuged at 10,000 r/min for 30 min at 4°C. The browning degree represents the absorbance of the supernatant at the 420 nm (spectrophotometer Beijing Purkinje General Instrument Co., Ltd., Beijing, China), with the values calculated as a dry basis.

## 2.7. Texture analysis

The textural characteristics of sea buckthorn berries were determined using a TA.XT2 texture analyzer (Stable Micro System, UK) at 25°C (24). The test was performed using a cylindrical indenter of  $\Phi 36$  mm with a pre-test speed of 1.0 mm/s, test speed of 0.5 mm/s, post-test speed of 1.0 mm/s, sample deformation of 50%, and a trigger induction force of 0.049 N. The hardness value is equal to the peak of the force in the curve, which is the maximum force (N) required to rupture the sample. The crispness result is expressed by the number of peaks generated during the test; the higher the number of peaks, the better the crispness of the product. The test was repeated 10 times, and the results were averaged.

## 2.8. Total flavonoids

Total flavonoid content (TFC) was determined according to the method of Zhang et al. (25). The absorbance was used as the vertical coordinate, and the mass concentration of the standard solution as the horizontal coordinate to draw the standard curve. The absorbance was used to calculate the mass concentration to obtain the regression equation.

Extraction of total flavonoids: 1.00 g of sea buckthorn berries was weighed accurately, and 20 mL of 95% ethanol solution was added

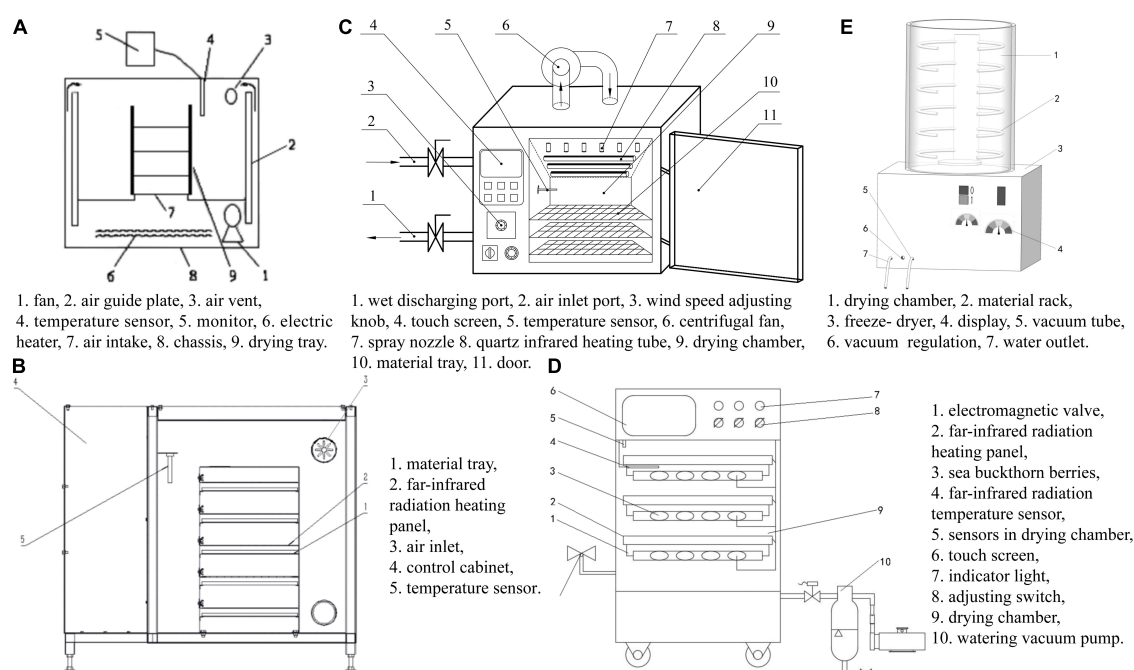


FIGURE 2

The schematics diagram of the five dryers. (A) Hot-air drying (HAD) [adapted from Zhang et al. (17)], (B) infrared drying (IRD) [adapted from Li (18)], (C) infrared-assisted hot-air drying (IR-HAD) [adapted from Chang et al. (19)], (D) pulsed-vacuum drying (PVD) [adapted from Deng et al. (16)], (E) vacuum freeze-drying (VFD) [adapted from Schössler et al. (20)].

in a material-liquid ratio of 1:20. The extract was sonicated at 50°C and 150 W for 40 min. The extract was obtained *via* extraction with a 0.45-μm organic filter membrane, and 1 mL of the extract was used for the determination. Absorbance was measured at 510 nm using a UV spectrophotometer. The total flavonoid content of the sample was expressed as mg rutin equivalent per gram (mg RE/g DW). Total flavonoid content was calculated according to Eq. 6:

$$\text{Total flavanoid content} = \frac{x \cdot V \cdot n}{m} \quad (6)$$

where  $x$  is the experimentally measured total flavonoid mass concentration/(mg/mL);  $V$  is the volume of the extraction solution/mL;  $n$  is the dilution multiple; and  $m$  is the dry basis mass of the sample (g).

## 2.9. Total phenols

Total phenol content (TPC) was determined according to the method of Ai et al. (26). Ten milligrams of gallic acid standard was weighed, dissolved in distilled water, and fixed to 100 mL to obtain a solution with a concentration of 100 mg/L. The solution was stored at 4°C in a refrigerator in the dark. The regression equation was obtained by plotting the standard curve. The extraction method for total phenols was the same as that for total flavonoids, and 1 mL of the extract was taken after extraction for determination (absorbance at 765 nm). The results were expressed as milligrams of equivalent gallic acid per gram of sample (mg GAE/g DW), and the total phenol content was calculated according to Eq. 7:

$$\text{Total phenol content} = \frac{x \cdot V \cdot n}{m} \quad (7)$$

where  $x$  is the experimentally measured mass concentration of total phenols/(mg/mL);  $V$  is the volume of the extract/mL;  $n$  is the dilution multiple; and  $m$  is the dry basis mass of the sample (g).

## 2.10. Ascorbic acid

The ascorbic acid content in large-fruited sea buckthorn berries was determined using the titration method described by Deng et al. (16), with slight modifications. In total, 1.0 g of sea buckthorn powder was weighed and added to a mortar, followed by the addition of 20 mL of 20 g/L oxalic acid solution; thereafter, the mortar containing this mixture was placed in an ice bath and its contents were ground into a slurry. The slurry was then transferred to a 20-mL volumetric flask, fixed with 20 g/L oxalic acid solution, shaken well, and centrifuged at 8,000 g for 10 min. To avoid the color effect of the sample solution, the ascorbic acid content in the sample was calculated using the 2,6-dichlorophenol indophenol reverse titration method expressed as the dry basis (mg/100 g DW), which was calculated according to Eq. 8:

$$A = \frac{c \cdot V_1 \cdot V_2}{V_3 \cdot W} \quad (8)$$

where  $A$  is the vitamin C content, mg/100 g DW;  $c$  is the concentration of L(+)-ascorbic acid standard solution, mg/mL;  $V_1$  is the volume of the ascorbic acid standard solution consumed for the titration of 5 mL of 2,6-dichloroindophenol sodium salt, mL;  $V_2$  is the total volume of the sample solution;  $V_3$  is the volume

of the sample solution consumed for the titration of 5 mL of 2,6-dichloroindophenol sodium salt; and  $W$  is the dry weight of the sample taken (g).

## 2.11. Microstructure

Changes in the surface microstructure of sea buckthorn berries during drying were examined using scanning electron microscopy (JEOL, SU3500, Tokyo, Japan) (16). The dried sea buckthorn berries were cut into 5 mm × 5 mm slices with a razor blade, and the samples were fixed on a sample stage with double-sided tape and observed at a magnification of 500, an accelerating voltage of 5 kV.

## 2.12. Statistical analysis

Data on drying and quality tests were expressed as the mean ± standard deviation (SD) of three measurements and were analyzed using ANOVA and Duncan's multiple range test using SPSS statistical software (version 21.0, Inc., USA). Statistical significance was set at  $P < 0.05$ .

# 3. Results and discussion

## 3.1. Drying characteristics

The average initial moisture content of sea buckthorn berries was found to be  $83.32 \pm 0.50\%$ . Figures 3A, B shows the effect of different drying methods on the drying kinetics of sea buckthorn berries, and the different methods show significant differences in the drying kinetics. The drying times of HAD, IRD, IR-HAD, PVD, and VFD were 19.83, 21.33, 17.83, 23.00, and 24.00 h, respectively. IR-HAD took the shortest time, VFD took the longest time, and the drying time of PVD was 15.99, 7.83, and 29.00% longer than HAD, IRD, and IR-HAD, respectively; the drying time of VFD was 21.03, 12.52, and 34.60% longer than HAD, IRD, and IR-HAD, respectively.

In the drying process, PVD dries the material through pressure change, HAD dries the material by eliminating surface moisture (16), IRD dries the material by radiation penetration (12), and IR-HAD dries the material by the combined action of both (16). Thus, IR-HAD can transfer more moisture and has a shorter drying time, making it the most efficient method.

Based on the drying rate variation curve, the drying rates of the different drying methods varied, and there was a large difference from the beginning of drying; however, the variation curves of HAD, IRD, and IR-HAD were essentially similar, unlike those of VFD and PVD. There are three drying phases in PVD, namely preheating, constant rate, and decreasing periods, which is consistent with the results of Liu et al. (21), and Deng et al. (16). The drying rates of HAD, IRD, IR-HAD, and VFD decreased with decreasing moisture content, and the entire stage of drying occurred in the decreasing drying period, indicating that moisture diffusion affects the drying process.

Compared with IR-HAD and HAD, IRD dried the samples faster in the early stages, but the total drying time was longer, which may be related to the stronger penetration of IR radiation, which generates heat quickly and increases the rate of moisture removal (17). In HAD, the gas flow rate is rapid, and the boundary layer between material

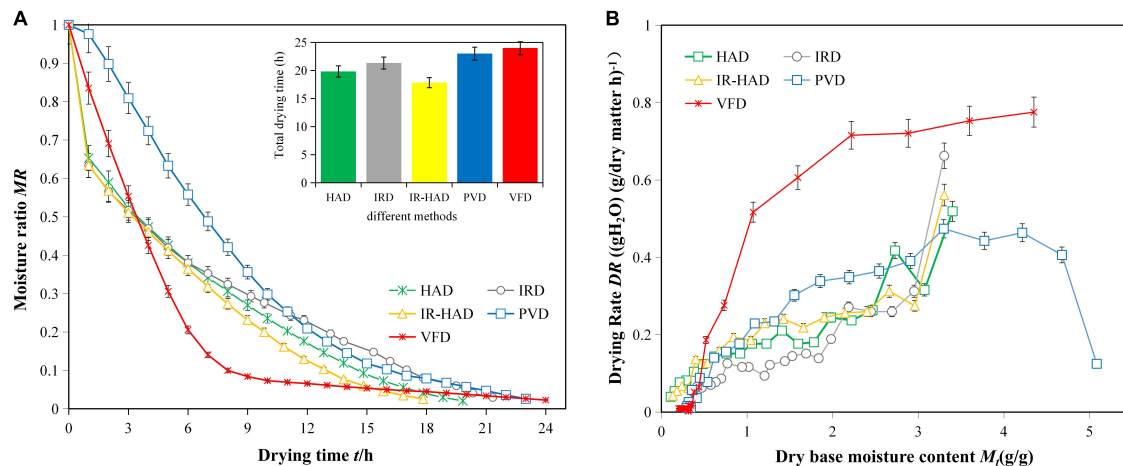


FIGURE 3

(A,B) The drying curves of sea buckthorn under different drying methods.

surface and air is thin; therefore, HAD has a high convective heat transfer coefficient. However, the high air flow and convective heat transfer coefficient can lead to rapid dehydration on the surface of sea buckthorn, causing rapid shrinkage at the early stage of drying and rendering it difficult to diffuse moisture outward inside the berry. In IR-HAD, infrared radiation is absorbed and converted to heat on the material surface. Consequently, the moisture transfer effect of IR-HAD is enhanced; however, at the same time, the high air flow rate during IR-HAD dissipates the heat from the material surface. In the late stage of drying, the combined water present in sea buckthorn is difficult to remove by heat conduction; however, the heat generated by IR radiation during the heating process can penetrate the material and combine with the moisture, which is beneficial for the internal water vapor pressure and moisture removal. Moreover, the drying rate of PVD was higher than that of HAD, IRD, and IR-HAD in the early stages, but the overall drying time was longer. This may be due to the room-temperature cold air entering the drying chamber in the atmospheric pressure state of PVD, which requires re-heating, and a large amount of heat is withdrawn during the operation of the vacuum pump, prolonging the drying time (16). VFD and PVD had significantly lower rates in the later stages of drying, which may be because the intracellular bound water was more difficult to remove by alternating cycles of freezing and vacuum atmospheric pressure, thus prolonging the drying time.

### 3.2. Rehydration ratio

The rehydration ratio is an important indicator in evaluating the dried product and can characterize the degree of destruction of the material structure due to drying (22). A higher rehydration ratio corresponds to better product quality, indicating minimal damage to the product structure (16). Figure 4 shows the effect of the different drying methods on the complex water ratio of dried sea buckthorn berries, which is closely related to changes in the microstructure, thus determining the macroscopic properties (21).

In this study, changes in the microstructure of sea buckthorn berries had a significant effect on the rehydration capacity, with significant differences between most of the groups. No significant

differences were observed for HAD, IRD, and IR-HAD. VFD-dried berries had the best rehydration rate. The vacuum and freezing environment prevented the possibility of structural destruction of sea buckthorn berries, forming a stable solid skeleton that ensured the original structure of the berries; thus, the porous structure caused by VFD gave it a high rehydration rate. It was found that PVD increased the formation of “tunnels” during the drying process and enhanced the water transfer. The experimental results confirmed those reported by Liu et al. (21) and Wang et al. (27), who found that PVD produced a tunneling effect that enlarged and interconnected the material micropores. For HAD, IRD, and IR-HAD, the drying time was approximately the same. With these three methods, the hot air and IR radiation may have caused the structural collapse of the internal matrix of sea buckthorn berries, which could have prevented the water absorption and lowered the rehydration capacity.

### 3.3. Color

Color is an important attribute in evaluating the merit of food products, affecting the consumer's choice and value of the product (28). Table 1 shows the effects of the different drying methods on the color of sea buckthorn berries ( $L^*$ ,  $a^*$ ,  $b^*$ , and  $\Delta E$ ). The brightness values of fresh sea buckthorn berries decreased from  $53.44 \pm 0.30$  to  $36.00 \pm 0.12$ , which may be attributed to the reduction in brightness due to the Maillard reaction owing to drying and oxidation. The brightness values of VFD-dried berries were the highest among the different drying methods at  $44.18 \pm 0.19$ . This was due to the vacuum environment inhibiting enzymatic browning and the occurrence of the Maillard reaction, thus ensuring the original color of sea buckthorn berries; consistent with the study of Liu et al. (21). The second highest brightness value was observed for PVD-dried berries ( $42.60 \pm 0.29$ ), which was significantly higher than that of HAD-, IRD-, and IR-HAD-dried berries. This may be because the vacuum environment prevents the occurrence of enzymatic browning and oxidation reactions, consistent with the findings of Deng et al. (16). The higher  $L^*$  of infrared-dried berries than that of hot-air-and infrared-assisted hot-air-dried berries may be attributed to uneven temperature distribution on the surface of the sea buckthorn berries



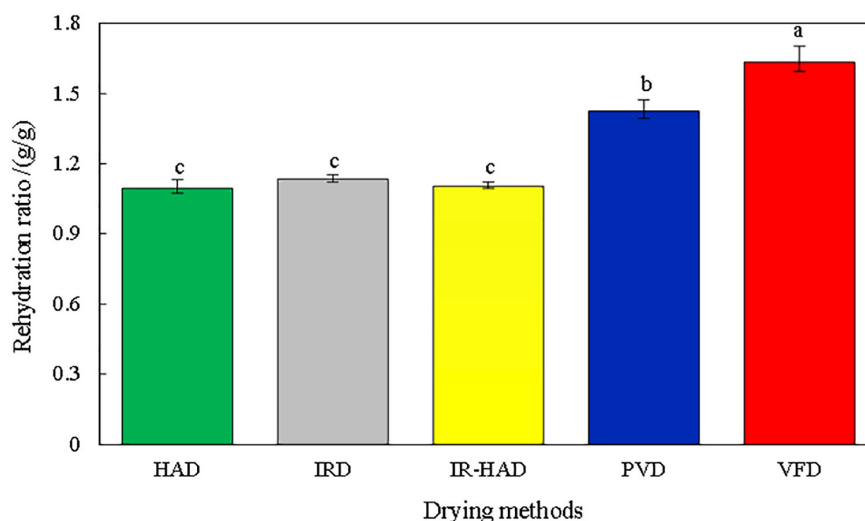








FIGURE 4

Effect of different drying methods on rehydration ratio of sea buckthorn berries. Different letters in the figure reveal significant differences ( $P < 0.05$ ) according to the Duncan test.

TABLE 1 The color parameters of sea buckthorn under different drying methods.

Parameter	Fresh	Drying methods				
		HAD	IRD	IR-HAD	PVD	VFD
						
$L^*$	$53.44 \pm 0.30^a$	$36.39 \pm 0.45^e$	$37.58 \pm 0.19^d$	$36.00 \pm 0.12^f$	$42.60 \pm 0.29^c$	$44.18 \pm 0.19^b$
$a^*$	$25.35 \pm 0.13^c$	$22.05 \pm 0.89^e$	$24.31 \pm 0.21^d$	$22.11 \pm 0.59^e$	$29.73 \pm 0.41^b$	$33.25 \pm 0.20^a$
$b^*$	$47.42 \pm 0.29^a$	$30.96 \pm 1.84^e$	$35.51 \pm 0.25^d$	$32.52 \pm 1.05^e$	$42.34 \pm 0.83^c$	$44.33 \pm 0.43^b$
$\Delta E$	*	$23.95 \pm 1.50^a$	$19.86 \pm 0.28^b$	$22.43 \pm 0.88^a$	$12.76 \pm 0.42^c$	$12.56 \pm 0.13^c$
Browning index /(Abs/g d.m.)	$0.09 \pm 0.00^f$	$0.42 \pm 0.01^b$	$0.35 \pm 0.01^c$	$0.59 \pm 0.01^a$	$0.28 \pm 0.00^d$	$0.24 \pm 0.00^e$

Different letters in the figure reveal significant differences ( $P < 0.05$ ) according to the Duncan test.

during heating. Localized overheating accelerating the browning of the surface of sea buckthorn berries also led to an uneven distribution of internal moisture, which affected the drying rate. It may also lead to the surface crusting phenomenon in the late stage of drying, where the internal structure does not reach a safe moisture content, thus promoting non-enzymatic browning and related biochemical reactions and resulting in color deterioration.

Table 1 shows that the  $b^*$  values of all dried sea buckthorn berry samples were significantly ( $P < 0.05$ ) lower than those of fresh samples, which can be explained by the degradation of flavonoids in sea buckthorn berries (4). VFD- and PVD-dried berries retained the product yellowness to a greater extent than those dried using HAD, IRD, and IR-HAD. This may be because VFD and PVD can minimize the possibility of oxidation of flavonoids in an anoxic environment (16, 21), as oxidation reaction is the main cause of flavonoid loss (12). While the  $a^*$  of VFD- and PVD-dried berries was significantly higher than that of fresh sea buckthorn berries, which may be because drying promotes carotenoid production, the low-oxygen environment promotes the formation of some compounds, resulting in the red coloration of sea buckthorn berries. This is

consistent with the results of Jiang et al. (29) in their study on the drying of *Panax ginseng* roots.

Bondaruk et al. (30) found that color changes could be observed by the naked eye with  $\Delta E$  values greater than five. The  $\Delta E$  was greater than 12 for sea buckthorn berries with different drying methods compared to fresh sea buckthorn berries, indicating that drying significantly changed the color of sea buckthorn berries. The color changes were mainly due to changes in  $L^*$  and  $b^*$ . VFD- and PVD-dried berries had the smallest  $\Delta E$  values of  $12.56 \pm 0.13$  and  $12.76 \pm 0.42$ , respectively. The dried fruits were brightly colored and showed bright yellow color, which was significantly lower than those dried using the other three drying methods ( $P < 0.05$ ), indicating that VFD and PVD were able better to maintain the color of sea buckthorn berries.

### 3.4. Browning index

The browning index is usually used to evaluate the degree of enzymatic browning (26). Table 1 shows the browning index



variations for the different drying methods. VFD-dried berries had the lowest browning index (0.24 Abs/g d.m.), followed by PVD- (0.28 Abs/g d.m.), IRD- (0.35 Abs/g d.m.), HAD- (0.42 Abs/g d.m.), and IR-HAD-dried berries (0.59 Abs/g d.m.). This may be due to the vacuum environment of VFD and PVD preventing the occurrence of the Maillard reaction (31). The contact with oxygen during the drying by HAD, IRD, and IR-HAD may have led to enzymatic browning, probably due to the synthesis of polyphenol oxidase during drying (16). The data showed a negative correlation between the browning index and  $L^*$ , which is consistent with the results of Deng et al. (16).

### 3.5. Texture properties

The final moisture content of sea buckthorn berries varied among the different drying methods and affected the texture of the dried material: the lower the moisture content, the higher the hardness and brittleness of sea buckthorn berries (24). The results are presented in Table 2. The HAD group exhibited the highest hardness, potentially because the hot air quickly took away the moisture from the surface of the material. This caused the crusting phenomenon, making it difficult to transfer moisture to the surface during the later stages of drying, ultimately forming a hard dry film (32). Meanwhile, HAD, IRD, and IR-HAD were more destructive to the cellular tissue structure of sea buckthorn berries, with a more compact overall structure, thus presenting higher hardness values. VFD maintains the original structure of the material's tissue cells and causes less shrinking, so the texture of the dried sea buckthorn berries was softer and more flimsy. This, however, makes it difficult to recover the pre-deformation degree after being compressed, therefore yielding the lowest reversibility. PVD elicits a hollow and porous structure with low overall shrinkage of the material; the hardness and brittleness, therefore, were the lowest.

Chewiness is a reflection of the energy required to move the food from a chewable state to a swallowable state, which integrates the sustained resistance of the sample to chewing. Its value is the product of hardness, cohesiveness, and elasticity, thus having a positive correlation with hardness variation (33). HAD-dried berries had the highest chewiness, which may be due to the surface heating of the drying process, which led to a significant increase in the chewiness of the sea buckthorn berries. The adhesiveness also showed significant differences between the different drying methods, which may be due to the different levels of reducing and total sugars in differently dried sea buckthorn berries (34). Thus, PVD and VFD could better retain reducing sugar substances in sea buckthorn berries, while IRD-dried berries exhibited lower adhesion due to the penetration of thermal radiation that destroyed reducing sugars and other substances.

### 3.6. TFC and TPC

Different drying methods showed significant differences in the total flavonoid content of sea buckthorn berries. The results are presented in Figure 5. It was found that the flavonoid content increased after drying, but after VFD, the flavonoid content of the berries did not differ significantly from that of fresh sea buckthorn berries, which may be due to the high temperature stress during the drying process, which activates the entire system to resist the external environmental changes (35). It is also possible that the high temperatures disrupted the cell wall structure of sea buckthorn berries and reduced the polyphenol oxidase and peroxidase activities, allowing more flavonoid compounds to be released (36), or that the free flavonoids in fresh sea buckthorn berries were converted to flavonoids by condensation reactions during drying, thus leading to an increase in flavonoid content (37). We also found that sea buckthorn berries had the highest flavonoid content after PVD, which could be due to the alternating cycles of pressure that led to the rupture of the cell structure and the release of more flavonoids. IRD penetration also had high flavonoid content, possibly due to a similar mechanism.

Unlike total flavonoids, fresh sea buckthorn berries had the highest total phenolic content, which was significantly higher than that of dried sea buckthorn berries. VFD and PVD helped to retain the phenolics in the sea buckthorn berries after drying. VFD reduces the water content through sublimation, while the vacuum environment avoided contact with oxygen, which reduced the oxidative degradation of phenolics. The vacuum environment in PVD also helped avoid the oxidation reaction. HAD not only had a longer drying time but also had a long time in contact with oxygen in the air; thus, the loss of phenolic substances was the most severe.

### 3.7. Ascorbic acid

The content of ascorbic acid in fresh sea buckthorn berries was 570 mg/100 g. Figure 6 shows that the ascorbic acid content of sea buckthorn berries decreased by 45.39, 53.81, 74.23, 77.09, and 79.93% after VFD, PVD, IRD, IR-HAD, and HAD, respectively, compared to the fresh samples. The retention of ascorbic acid was higher in the VFD samples at 311.27 mg/100 g, mainly because VFD avoids heat and oxidation in sea buckthorn berries, thus reducing the degradation of ascorbic acid, which is consistent with a study on VFD on cornelian cherries by Silva-Espinoza et al. (15). While the vacuum environment of PVD also limited oxidation and reduced the possibility of ascorbic acid degradation, the higher drying temperature of HAD, IRD, and IR-HAD resulted in more heat-related loss of ascorbic acid content in the material.

TABLE 2 Effects of different drying methods on the texture of sea buckthorn.

Drying methods	Hardness /N	Fracturability /N	Adhesiveness /g·s <sup>-1</sup>	Springiness	Cohesiveness	Gumminess	Chewiness	Resilience
HAD	71.88 ± 5.15 <sup>a</sup>	37.14 ± 5.59 <sup>a</sup>	-0.68 ± 0.58 <sup>a</sup>	0.48 ± 0.02 <sup>a</sup>	0.30 ± 0.05 <sup>a</sup>	21.38 ± 3.53 <sup>a</sup>	10.20 ± 1.69 <sup>a</sup>	0.13 ± 0.03 <sup>a</sup>
IRD	51.94 ± 2.86 <sup>b</sup>	29.52 ± 4.39 <sup>a,b</sup>	-0.48 ± 0.08 <sup>a</sup>	0.53 ± 0.01 <sup>a</sup>	0.28 ± 0.03 <sup>a</sup>	14.68 ± 1.03 <sup>b</sup>	7.84 ± 0.72 <sup>b</sup>	0.10 ± 0.01 <sup>b</sup>
IR-HAD	26.43 ± 0.84 <sup>c</sup>	25.13 ± 3.17 <sup>b</sup>	-0.78 ± 0.19 <sup>a</sup>	0.47 ± 0.05 <sup>a</sup>	0.17 ± 0.01 <sup>b</sup>	4.39 ± 0.39 <sup>c</sup>	2.02 ± 0.03 <sup>c</sup>	0.07 ± 0.00 <sup>b</sup>
PVD	3.55 ± 0.18 <sup>c</sup>	3.76 ± 0.04 <sup>c</sup>	-1.08 ± 0.46 <sup>a</sup>	0.51 ± 0.22 <sup>a</sup>	0.08 ± 0.01 <sup>c</sup>	0.30 ± 0.04 <sup>d</sup>	0.16 ± 0.08 <sup>d</sup>	0.02 ± 0.00 <sup>c</sup>
VFD	9.12 ± 0.29 <sup>d</sup>	*	-1.93 ± 1.19 <sup>a</sup>	0.51 ± 0.02 <sup>a</sup>	0.34 ± 0.05 <sup>a</sup>	3.12 ± 0.21 <sup>c,d</sup>	1.58 ± 0.20 <sup>c,d</sup>	0.04 ± 0.00 <sup>c</sup>

Different letters in the figure reveal significant differences ( $P < 0.05$ ) according to the Duncan test.

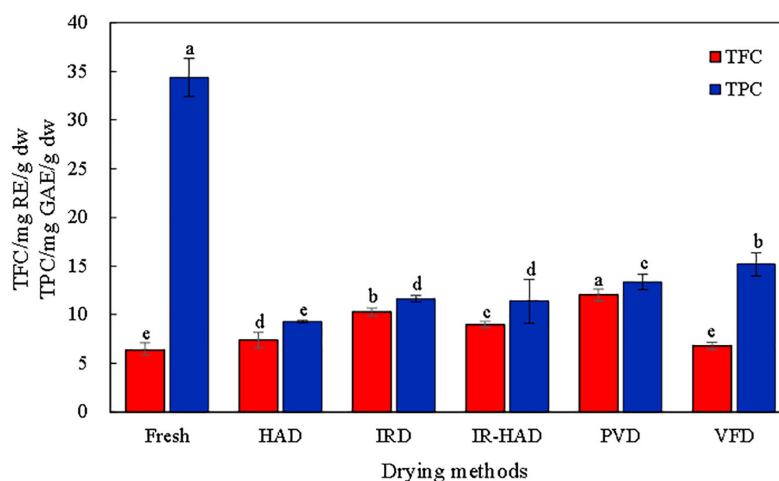


FIGURE 5

Effects of different drying methods on total flavonoid content (TFC) and total phenolic content (TPC) of sea buckthorn berries. Different letters in the figure reveal significant differences ( $P < 0.05$ ) according to the Duncan test.

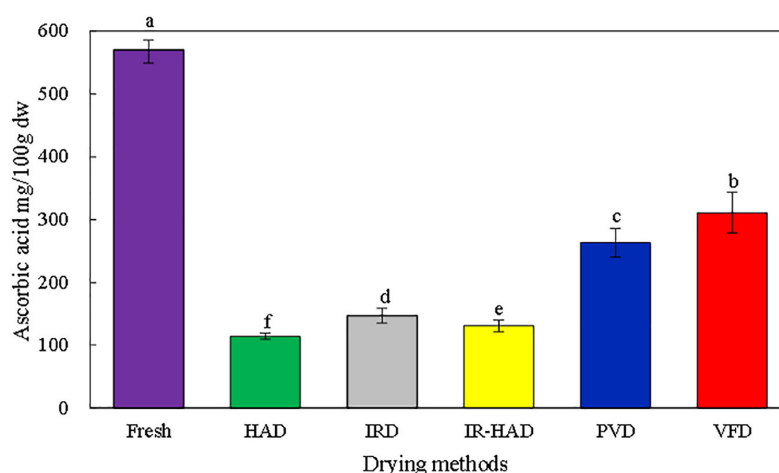


FIGURE 6

Effects of different drying methods on ascorbic acid content of sea buckthorn berries. Different letters in the figure reveal significant differences ( $P < 0.05$ ) according to the Duncan test.

### 3.8. Microstructure

Studies have shown that microstructure affects the performance and quality of dried products; therefore, understanding microstructure can help to resolve the mechanism of material quality changes at the cellular level and improve drying performance (38, 39). To investigate the effect of the different drying methods on the microstructure of sea buckthorn berries, scanning electron microscopy images of the dried berries were selected, as shown in Figure 7. The surface of HAD berries (Figure 7A) was partially folded, which may be due to the folding of the epidermis because of the rapid evaporation of surface water due to hot air. The IRD surface was smoother and had some holes, which might be due to the stronger penetration of IR radiation that destroyed the cellular structure on the surface of sea buckthorn berries, while the shadows around the holes might have been generated by the diffusion of internal oil-like substances to the outside of the cells. In contrast to HAD- and IRD-dried berries, the surface of IR-HAD-dried berries

not only had pores but also microcracks, which might be caused by the combined effect of air speed and IR radiation, promoting the diffusion of water from the interior of the cell to the outside. Many pores were observed on the surface of sea buckthorn berries in the PVD samples, which was also observed by Liu et al. (21). This phenomenon can be explained by the large pressure difference between the inside and outside of the material due to the vacuum illusion that lowered the boiling point of water in sea buckthorn berries. The alternating cycles of vacuum and atmospheric pressure lead to the continuous expansion of the pores, which also explains why the same pore shape is produced, but there is no shadow around the PVD pores like the one produced by the diffusion of greasy substances after IRD treatment. The higher rehydration capacity of sea buckthorn berries after PVD treatment also supports this conjecture. The VFD samples had a smooth surface and no extravasation of grease, which may be due to the direct sublimation of water from a solid to a gaseous state, effectively ensuring the original structural properties of the material.

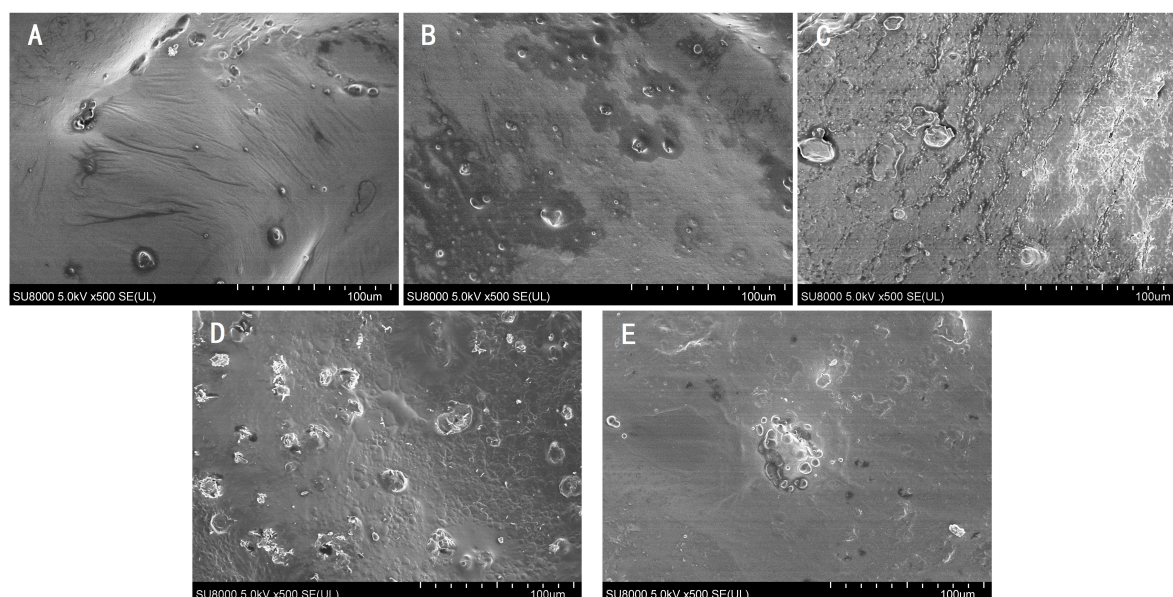


FIGURE 7

Microstructure observation (500 × magnifications) of sea buckthorn berries under different drying methods. (A) Hot air drying (HAD); (B) infrared drying (IRD); (C) infrared-assisted hot air-drying (IR-HAD); (D) pulsed vacuum drying (PVD); (E) vacuum freeze drying (VFD).

## 4. Conclusion

This study investigated the effects of five different drying methods, namely HAD, IRD, IR-HAD, PVD, and VFD, on the drying kinetics, physicochemical properties, and microstructure of sea buckthorn berries. The results showed that the different drying methods had considerable different effects on the drying characteristics, color, total phenols, total flavonoids, rehydration ratio, and texture of sea buckthorn berries. IR-HAD had the shortest drying time, and VFD had the longest time. PVD reduced the occurrence of non-enzymatic browning and better preserved the surface of sea buckthorn berries. VFD and PVD elicited the brightest color and lowest browning in dried sea buckthorn berries, as well as the highest retention of total phenols and ascorbic acid. Sea buckthorn berries obtained by VFD had the best quality, but the long drying time and high cost of VFD hinder its potential for industrial application. PVD, on the other hand, has a low cost and large batch size and could, therefore, be employed industrially to ensure the maximum drying quality while reducing the drying time and energy consumption.

## Data availability statement

The original contributions presented in this study are included in the article/supplementary material, further inquiries can be directed to the corresponding author.

## Author contributions

ZG: conceptualization, methodology, and writing—original draft preparation. LZ: formal analysis investigation and resources. JW and XLY: methodology and software. ML and WY: formal

analysis investigation. BH and QZ: investigation. XHY: resources, validation, funding acquisition, supervision, and writing—reviewing and editing. All authors contributed to the article and approved the submitted version.

## Funding

This work was supported by the High-level Talents Research Start Project of Shihezi University (RCZK201918), the Xinjiang Production and Construction Corps Financial Technology Plan Project (Grant No. 2021CB042), the Xinjiang Production and Construction Corps Key Laboratory of Modern Agricultural Machinery (BTN2021004), and the Engineering Research Center for Production Mechanization of Oasis Special Economic Crop, Ministry of Education (Grant No. PMOC2021A06).

## Conflict of interest

The authors declare that the research was conducted in the absence of any commercial or financial relationships that could be construed as a potential conflict of interest.

## Publisher's note

All claims expressed in this article are solely those of the authors and do not necessarily represent those of their affiliated organizations, or those of the publisher, the editors and the reviewers. Any product that may be evaluated in this article, or claim that may be made by its manufacturer, is not guaranteed or endorsed by the publisher.

## References

- Zhang Z, Peng Y, Meng W, Pei L, Zhang X. Browning inhibition of seabuckthorn leaf extract on fresh-cut potato sticks during cold storage. *Food Chem.* (2022) 389:133076. doi: 10.1016/j.foodchem.2022.133076
- Lan Y, Sun Q, Ma Z, Peng J, Zhang M, Wang C, et al. Seabuckthorn polysaccharide ameliorates high-fat diet-induced obesity by gut microbiota-SCFAs-liver axis. *Food Funct.* (2022) 13:2925–37. doi: 10.1039/d1fo03147c
- Xia B, Liang Y, Hu J, Yan X, Yin L, Chen Y, et al. First report of sea buckthorn stem wilt caused by fusarium sporotrichioides in Gansu, China. *Plant Dis.* (2021) 105:1456. doi: 10.1094/PDIS-03-21-0627-PDN
- Karolina T, Aneta W, Anna M, Igor P, Krzysztof L, Paulina N. Influence carrier agents, drying methods, storage time on physico-chemical properties and bioactive potential of encapsulated sea buckthorn juice powders. *Molecules.* (2020) 25:3801. doi: 10.3390/molecules25173801
- Osborn L, Claesen J, Brown J. Microbial flavonoid metabolism: a cardiometabolic disease perspective. *Annu Rev Nutr.* (2021) 41:433–54. doi: 10.1146/annurev-nutr-120420-030424
- Ren Q, Li X, Li Q, Yang H, Wang H, Zhang H, et al. Total flavonoids from sea buckthorn ameliorates lipopolysaccharide/cigarette smoke - induced airway inflammation. *Phytother Res.* (2019) 33:2102–17. doi: 10.1002/ptr.6404
- Sytarova I, Orsavova J, Snopek L, Mlecek J, Byczynski L, Misurcova L. Impact of phenolic compounds and vitamins C and E on antioxidant activity of sea buckthorn (*Hippophae rhamnoides* L.) berries and leaves of diverse ripening times. *Food Chem.* (2020) 310:125784.
- Nowak D, Goslinski M, Wojtowicz E, Przygonski K. Antioxidant properties and phenolic compounds of vitamin C-rich juices. *J Food Sci.* (2018) 83:2237–46. doi: 10.1111/1750-3841.14284
- Guo R, Chang X, Guo X, Brennan C, Li T, Fu X, et al. Phenolic compounds, antioxidant activity, antiproliferative activity and bioaccessibility of Sea buckthorn (*Hippophae rhamnoides* L.) berries as affected by in vitro digestion. *Food Funct.* (2017) 8:4299–4240. doi: 10.1039/c7fo00917h
- Attri S, Goel G. Influence of polyphenol rich seabuckthorn berries juice on release of polyphenols and colonic microbiota on exposure to simulated human digestion model. *Food Res Int.* (2018) 111:314–23. doi: 10.1016/j.foodres.2018.05.045
- Sytaová I, Orsavová J, Snopek L, Mlček J, Byczyński L, Mišurcová L. Impact of phenolic compounds and vitamins C and E on antioxidant activity of sea buckthorn (*Hippophae rhamnoides* L.) berries and leaves of diverse ripening times. *Food Chem.* (2019) 310:125784. doi: 10.1016/j.foodchem.2019.125784
- Araya-Farias M, Macaigne O, Ratti C. On the development of osmotically dehydrated seabuckthorn fruits: pretreatments, osmotic dehydration, postdrying techniques, and nutritional quality. *Dry Technol.* (2014) 32:813–9. doi: 10.1080/07373937.2013.866143
- Hnin K, Zhang M, Ju R, Wang B. A novel infrared pulse-spouted freeze drying on the drying kinetics, energy consumption and quality of edible rose flowers. *LWT-Food Sci Technol.* (2021) 136:110318. doi: 10.1016/j.lwt.2020.110318
- Tkacz K, Wojdylo A, Michalska-Ciechanowska A, Turkiewicz I, Lech K, Nowicka P. Influence carrier agents, drying methods, storage time on physico-chemical properties and bioactive potential of encapsulated sea buckthorn juice powders. *Molecules.* (2020) 25:25173810.
- Silva-Espinoza M, Camacho M, Martínez-Navarrete N. Effect of storage temperature on the crispness, colour and bioactive compounds of an orange snack obtained by freeze-drying. *Brit Food J.* (2021) 123:2095–106. doi: 10.1108/BFJ-11-2020-1061
- Deng L, Yang X, Mujumdar A, Zhao J, Wang D, Zhang Q, et al. Red pepper (*Capsicum annuum* L.) drying: effects of different drying methods on drying kinetics, physicochemical properties, antioxidant capacity, and microstructure. *Dry Technol.* (2018) 36:893–907. doi: 10.1080/07373937.2017.1361439
- Zhang J, Ma Y, Wang H, Zheng Y. Optimization test of hot air drying process of pepper. *Trans CSAM.* (2007) 38:223–4.
- Li J. *Design and experimental study of seabuckthorn infrared hot air drying oven.* Ph.D. thesis. Shandong: Shandong Agricultural University (2022).
- Chang A, Zheng X, Xiao H, Yao X, Liu D, Li X, et al. Shortand medium-wave infrared drying of cantaloupe (*Cucumis melon* L.) slices: drying kinetics and process parameter optimization. *Processes.* (2022) 10:114. doi: 10.3390/pr10010114
- Schössler K, Jäger H, Knorr D. Novel contact ultrasound system for the accelerated freeze-drying of vegetables. *Innov Food Sci Emerg.* (2012) 16:113–20. doi: 10.1016/j.ifset.2012.05.010
- Liu Z, Xie L, Zielinska M, Pan Z, Deng L, Zhang J, et al. Improvement of drying efficiency and quality attributes of blueberries using innovative far-infrared radiation heating assisted pulsed vacuum drying (FIR-PVD). *Innov Food Sci Emerg.* (2022) 77:102948. doi: 10.1016/j.ifset.2022.102948
- Zhang Y, Zhu G, Li X, Zhao Y, Lei D, Ding G, et al. Combined medium- and short-wave infrared and hot air impingement drying of sponge gourd (*Luffa cylindrical*) slices. *J Food Eng.* (2020) 284:110043. doi: 10.1016/j.jfoodeng.2020.110043
- Geng Z, Huang X, Wang J, Xiao H, Yang X, Zhu LC, et al. Pulsed vacuum drying of pepper (*Capsicum annuum* L.): effect of high-humidity hot air impingement blanching pretreatment on drying kinetics and quality attributes. *Foods.* (2022) 11:318. doi: 10.3390/foods11030318
- Gong C, Zhang H, Yue J, Miao Y, Jiao S. Investigation of hot air-assisted radio frequency heating as a simultaneous dry-blanching and pre-drying method for carrot cubes. *Innov Food Sci Emerg.* (2019) 56:102181. doi: 10.1016/j.ifset.2019.102181
- Zhang Z, Fan X, Zou L, Xing B, Zhu M, Yang X, et al. Phytochemical properties and health benefits of pregelatinized Tartary buckwheat flour under different extrusion conditions. *Front Nutr.* (2022) 9:1052730. doi: 10.3389/fnut.2022.1052730
- Ai Z, Xiao H, Zhang Y, Lei D, Peng Z, Li M, et al. Effect of hot air impingement drying on drying behavior, volatile components profile, shell burst ratio, flavonoid contents, microstructure of Amomum villosum fruits. *Dry Technol.* (2022):41:2087184. doi: 10.1080/07373937.2022.2087184
- Wang J, Bai T, Wang D, Fang X, Xue L, Zheng Z, et al. Pulsed vacuum drying of Chinese ginger (*Zingiber officinale* Roscoe) slices: effects on drying characteristics, rehydration ratio, water holding capacity, and microstructure. *Dry Technol.* (2018) 37:301–11. doi: 10.1080/07373937.2017.1423325
- Ai Z, Lin Y, Xie Y, Mowafy S, Zhang Y, Li M, et al. Effect of high-humidity hot air impingement steaming (HHAIS) on Cistanche deserticola slices: drying characteristics, weight loss, microstructure, color, and active components. *Front Nutr.* (2022) 9:824822. doi: 10.3389/fnut.2022.824822
- Jiang D, Xiao H, Zielinska M, Zhu G, Bai T, Zheng Z. Effect of pulsed vacuum drying on drying kinetics and quality of roots of Panax notoginseng (Burk.) F. H. Chen (Araliaceae). *Dry Technol.* (2021) 39:2234–51. doi: 10.1080/07373937.2020.1761827
- Bondaruk J, Markowski M, Aszczak W. Effect of drying conditions on the quality of vacuum-microwave dried potato cubes. *J Food Eng.* (2007) 81:306–12. doi: 10.1016/j.jfoodeng.2006.10.028
- Siti-Nuramira J, Farhana R, Nabil S, Jafari S, Raseetha S. Impact of drying methods on the quality of grey (*Pleurotus sajor caju*) and pink (*Pleurotus djamor*) oyster mushrooms. *J Food Meas Charact.* (2022) 16:3331–43. doi: 10.1007/s11694-022-01435-w
- Kamal T, Song Y, Tan Z, Zhu B, Tan M. Effect of hot-air oven dehydration process on water dynamics and microstructure of apple (fuji) cultivar slices assessed by LF-NMR and MRI. *Dry Technol.* (2019) 37:1974–87. doi: 10.1080/07373937.2018.1547312
- Zhu Y, Chen X, Pan N, Liu SJ, Su YC, Xiao M, et al. The effects of five different drying methods on the quality of semi-dried Takifugu obscurus fillets. *LWT-Food Sci Technol.* (2022) 161:113340. doi: 10.1016/j.lwt.2022.113340
- Chen X, Kitts D. Characterization of antioxidant and anti-inflammatory activities of bioactive fractions recovered from a glucose-lysine Maillard reaction model system. *Mol Cell Biochem.* (2012) 364:147–57. doi: 10.1007/s11010-011-1213-7
- Li W, Wen L, Chen Z, Zhang Z, Pang X, Deng Z, et al. Study on metabolic variation in whole grains of four proso millet varieties reveals metabolites important for antioxidant properties and quality traits. *Food Chem.* (2021) 357:129791. doi: 10.1016/j.foodchem.2021.129791
- Ibtissem H, Fatma Z, Iness B, Soumaya B, Ferid L, Brahim M. Total phenolics, flavonoids, and antioxidant activity of sage (*Salvia officinalis* L.) plants as affected by different drying methods. *Food Bioprocess Tech.* (2013) 6:806–17. doi: 10.1007/s11947-012-0877-7
- Wohl J, Petersen M. Functional expression and characterization of cinnamic acid 4-hydroxylase from the hornwort anthoceros agrestis in physcomitrella patens. *Plant Cell Rep.* (2020) 39:597–607. doi: 10.1007/s00299-020-02517-z
- Li X, Zhang Y, Zhang Y, Liu Y, Gao Z, Zhu G, et al. Relative humidity control during shiitake mushroom (*Lentinus edodes*) hot air drying based on appearance quality. *J Food Eng.* (2022) 315:110814. doi: 10.1016/j.jfoodeng.2021.110814
- Lee, S, Ferdinand V, Siow L. Effect of drying methods on yield, physicochemical properties, and total polyphenol content of chamomile extract powder. *Front Pharmacol.* (2022) 13:1003209. doi: 10.3389/fphar.2022.1003209





## OPEN ACCESS

EDITED BY  
Baoguo Xu,  
Jiangsu University, China

REVIEWED BY  
Tao Feng,  
Shanghai Institute of Technology, China  
Thuan Chew Tan,  
University of Science Malaysia (USM), Malaysia  
Zhenbin Liu,  
Shaanxi University of Science and Technology,  
China

\*CORRESPONDENCE  
Lizhong Lin  
✉ llz30@csuft.edu.cn

SPECIALTY SECTION  
This article was submitted to  
Nutrition and Food Science Technology,  
a section of the journal  
Frontiers in Nutrition

RECEIVED 16 November 2022  
ACCEPTED 30 January 2023  
PUBLISHED 16 February 2023

CITATION  
Xiao W, Ding Y, Cheng Y, Xu S and Lin L (2023)  
Effect of sodium bicarbonate on  
the physicochemical properties of fermented  
rice flour and quality characteristics  
of fermented semi-dried rice noodles.  
*Front. Nutr.* 10:1100422.  
doi: 10.3389/fnut.2023.1100422

COPYRIGHT  
© 2023 Xiao, Ding, Cheng, Xu and Lin. This is an  
open-access article distributed under the terms  
of the [Creative Commons Attribution License](#)  
(CC BY). The use, distribution or reproduction in  
other forums is permitted, provided the original  
author(s) and the copyright owner(s) are  
credited and that the original publication in this  
journal is cited, in accordance with accepted  
academic practice. No use, distribution or  
reproduction is permitted which does not  
comply with these terms.

# Effect of sodium bicarbonate on the physicochemical properties of fermented rice flour and quality characteristics of fermented semi-dried rice noodles

Wen Xiao<sup>1,2</sup>, Yuqin Ding<sup>1,2</sup>, Ying Cheng<sup>1,2</sup>, Sili Xu<sup>1,2</sup> and  
Lizhong Lin<sup>1,2\*</sup>

<sup>1</sup>National Engineering Research Center of Rice and Byproduct Deep Processing, Changsha, China, <sup>2</sup>College of Food Science and Engineering, Central South University of Forestry and Technology, Changsha, China

Considering the effect that fermentation can improve the quality of rice noodles, and given that fermented rice noodles usually have a significantly acidic taste that is not generally acceptable to consumers, this study aimed to neutralize or eliminate the acidic taste of fermented rice noodles by adding sodium bicarbonate, and improve the quality of fermented rice noodles. The physicochemical properties of fermented rice flour and quality characteristics of fermented semi-dried rice noodles were investigated in this study in relation to the addition of sodium bicarbonate (0~0.5%, w/w). With the increase of sodium bicarbonate addition, the pH value was increased, and lipid and protein content were decreased in rice flour. Meanwhile, thermal properties and farinograph properties showed that the pasting temperature, dough water absorption, dough development time and dough stability time of rice flour increased with the addition of sodium bicarbonate. Pasting properties and rheological properties results showed that a small amount of sodium bicarbonate (0~0.1%) could increase the pasting viscosity, storage modulus ( $G'$ ), and loss modulus ( $G''$ ) of rice flour. Additionally, the hardness and chewiness of semi-dried rice noodles increased with the addition of sodium bicarbonate from 0 to 0.1%. With the addition of a small amount of sodium bicarbonate (0~0.1%), x-ray diffraction showed that it could increase the crystallinity of semi-dried rice noodles. Low-field nuclear magnetic resonance showed that  $A_{21}$  increased, and  $A_{22}$  and  $A_{23}$  decreased in semi-dried rice noodles. Scanning electron microscope showed that it could enhance the starch-protein interaction and starch-protein formed an ordered and stable network structure. Finally, the principal component analysis showed that the chewiness, texture and eating quality of semi-dried rice noodles were the best with the addition of sodium bicarbonate at 0.1%. This study provides practical value for the application of alkali treatment in rice products and provides a reference for the improvement of related rice noodles products.

## KEYWORDS

sodium bicarbonate, semi-dried rice noodles, pasting properties, rheological properties, cooking properties, textural properties



## 1. Introduction

Rice noodles are very popular as a traditional staple food in Southeast Asian countries such as China, Vietnam, and Thailand (1). Based on the moisture content, rice noodles can be divided into fresh (> 60%), dry (< 14%), and semi-dried rice noodles (14~60%) (1). Fresh rice noodles have high moisture content and tend to bind into lumps and break, and have a short shelf life. Dry rice noodles have low moisture content, longer steaming time and cooking loss, and a longer shelf life. Whereas the moisture content of semi-dried rice noodles is in the middle of fresh and dry rice noodles, it has the advantages of a longer shelf life than fresh rice noodles and better taste than dry rice noodles, which is a good choice for consumers' convenience of consumption (2). Nowadays, the production methods of rice noodles are divided into fermented and unfermented. Studies have shown that the texture and eating quality of fermented rice noodles are better than unfermented rice noodles (3). Through fermentation, the tensile strength (4), elasticity (5), and texture (6) of rice noodles can be improved. However, fermented rice noodles usually have a significantly acidic taste, which is not generally acceptable to consumers.

Numerous starch-based foods, like sticky rice cake (7) and yellow alkali noodles (8), have traditionally undergone an alkali treatment. Alkali treatment has several advantages, such as making it simpler to grind grains and enhancing the appearance, flavor, and texture of starch-foods (8, 9). The most frequent alkalis used in rice goods are sodium hydroxide and calcium hydroxide, which are applied by soaking rice in an alkali solution to change the characteristics of rice flour. According to Lai et al. (10), it was reported that soaking glutinous rice in NaOH alkali solution could increase the peak viscosity and pasting temperature of glutinous rice flour. Pedcharat et al. (11) reported that soaking rice in  $\text{Ca}(\text{OH})_2$  and NaOH alkali solutions, respectively, could be increased the swelling power and solubility of rice flour. Reepholkul et al. (7) reported that soaking glutinous rice in  $\text{Na}_2\text{CO}_3$  alkali solution improved the softness and viscosity of glutinous rice flour. The process of adding the necessary quantity of alkali to change alkali noodle characteristics is known as alkali treatment, and the most popular alkalis used in this process are sodium carbonate, potassium carbonate, and sodium bicarbonate. Kruger et al. (12) and Shiauet et al. (13) reported that the cutting force and tensile strength of extruded noodles increased after adding "Kansui" or a mixture of sodium carbonate and potassium carbonate. Suwannaporn et al. (14) reported that the addition of appropriate amounts of potassium carbonate improved the viscosity, toughness and sensory qualities of noodles. Tao et al. (15) reported that the addition of appropriate amounts of sodium carbonate improved the gluten network and had a significant impact on dough structure, and these changes made the cooking loss and rehydration greater of alkaline noodles. According to Fan et al. (16), the addition of an alkaline solution made from sodium and potassium carbonate increased the cooking time, cooking losses, and hardness and chewiness of noodles. However, most of the studies on alkali treatment in rice products have been done by soaking rice in an alkali solution and then investigating the effect on rice flour. There are few studies on the addition of alkali into rice flour, and there is a need to study the effect of adding sodium bicarbonate on rice flour and rice noodles.

This paper neutralizes or eliminates the acidic taste of fermented rice noodles by adding sodium bicarbonate and also improves the

quality of fermented rice noodles. We investigated the effects of different additions of sodium bicarbonate (0~0.5%, w/w) on the farinograph properties, pasting properties, thermal properties, and rheological properties of fermented rice flour and the cooking properties, textural properties, crystallinity, moisture distribution, and microscopic morphological structure of fermented semi-dried rice noodles. This investigation also provides an opportunity to assess the practical value of rice product applications and to provide a reference for product improvement in related industries.

## 2. Materials and methods

### 2.1. Materials

Indica rice and a strain fermentation solution are both available from Jinjian Rice Industry Co., Ltd., (Hunan, China). The latter is a microbial fermentation system composed of yeast and lactic acid bacteria, with a yeast concentration of  $1.0 \times 10^4$  to  $1.0 \times 10^5$  CFU/mL and lactic acid bacteria concentrations of  $1.0 \times 10^8$  to  $1.0 \times 10^9$  CFU/mL, respectively. The only food-grade substance employed in the tests was sodium bicarbonate, and all other chemicals, solvents, and reagents were of the analytical grade.

### 2.2. Fermented rice flour

The method of making fermented rice flour as described by Xiao et al. (17). Indica rice was added to the fermenter along with distilled water in the proportion of 1:1.2 (w:v), 4% of the strain fermentation solution, and the fermenter was then placed in a constant temperature incubator (35°C) for 18 h. Following fermentation, indica rice was washed, drained, and crushed. Rice flour was then dried for 12 h at 50°C, after which it was put through 120 mesh sieves and stored at 4°C.

### 2.3. Rice flour sample preparation

Rice flour samples with different additions (0.02, 0.06, 0.1, 0.2, 0.3, 0.4, and 0.5%, w/w) of sodium bicarbonate per 500 g of rice flour were prepared. Rice flour samples were packed in plastic self-sealing bags and stored at 4°C for preparation.

### 2.4. Basic physicochemical composition

According to the AACC methods (18), we calculated lipid (AOAC Method 922.06) and protein content of rice flour samples (AOAC Method 220). From Beijing Solaibao Technology Co., Ltd., the kits for measuring amylose content of rice flour samples were purchased (Beijing, China). We used a pH meter (FE28-Standard, Lichen Instrument Technology Co., Ltd., Shanghai, China) to determine the pH of rice flour samples. We weighed 5.0 g of the sample, added 20 mL of hot distilled water for mixing and shaking, and stood for 5 min to measure the pH value, following the procedure of Yeoh et al. (19).

## 2.5. Farinograph properties

According to AACC method 54-21 (20), the farinograph meter (Micro-dough LAB, Perten Instrument Co., Stockholm, Sweden) was used to ascertain the farinograph properties of rice flour samples. We calculated the dough's water absorption (WA), dough development time (DDT), and dough stability time were all recorded (DST).

## 2.6. Pasting properties

The pasting properties of rice flour samples were evaluated using a rapid viscosity analyzer (RVA-Super4, Perten Riva Scientific Instruments Ltd., Stockholm, Sweden) by AACC Method 61-02 (20). We created a suspension of 14% rice flour using the sample and distilled water, followed by heating and cooling cycles. The unit of viscosity is CP. RVA characteristic values include peak, trough, final, breakdown, and setback viscosities.

## 2.7. Thermal properties

With a minor modification from the procedures described by Rombouts et al. (21), we used differential scanning calorimetry (DSC 2000, TA Instruments, USA) to determine the thermal properties of rice flour samples. The powder samples were measured into an aluminum crucible, distilled water was added at a ratio of 1:3 (w/w), sealing the container with a tablet press, and the suspension was allowed to equilibrate at 4°C for 12 h. The temperature was raised between 30 and 120 degrees at a pace of 10 degrees per minute. We calculated the onset temperature ( $T_o$ ), peak temperature ( $T_p$ ), conclusion temperature ( $T_c$ ), and gelatinization enthalpy ( $\Delta H$ ).

## 2.8. Rheological properties

Utilizing a rheometer (DHR-2 instrument, TA Instruments, USA), the rheological properties of rice flour samples were evaluated using a modified form of the procedures described by Dorglamud et al. (13). Weighed 5.0 g of rice flour, prepared into a 10% concentration solution by added distilled water, stirred in water bath (95°C) until rice flour paste state, then cooled and measured.

### 2.8.1. Static rheological

Rice flour paste was laid flat on test bench with the temperature of 25°C and scanning range of 0.1~200 s<sup>-1</sup> to determine the trends of shear stress and apparent viscosity of rice flour samples with shear rate.

### 2.8.2. Dynamic rheological

Rice flour paste was laid flat on test bench with the temperature of 25°C, scanning strain of 2% and frequency range of 0.1~20 HZ to determine the trends of storage modulus ( $G'$ ) and loss modulus ( $G''$ ) of rice flour samples with frequency.

## 2.9. Fermented semi-dried rice noodles

The method of making fermented semi-dried rice noodles as described by Xiao et al. (17). Fermented rice flour (50.0 g), distilled

water (62 mL), and different sodium bicarbonate additions were used to make semi-dried rice noodles. Before being extruded into strips by a noodle machine (MS-200, Hualian Shengtong Trading Co., Taiyuan, Shanxi, China), the rice flour was first heated in a water bath (95°C) for 8 min to paste into the dough. This was done to achieve a complete paste. Next, the rice noodles were re-steamed for 3 min and 30 s. Finally, they were aged for 8 h in a room with a constant temperature (90% RH, 25°C). After aging, semi-dried rice noodles were packaged, sterilized for 30 min in hot water (95°C), and then promptly chilled in cold water to stop the growth of bacteria.

## 2.10. Cooking properties

### 2.10.1. Cooked broken rate

The cooked broken rate of semi-dried rice noodles was calculated using a modified form of the Xu et al. (22) methods. We selected 20 semi-dried rice noodles more than 15 cm in length into a beaker, added boiling water, heated them on an electric stove, and placed them in a test sieve for 5 min after the optimal cooking time (2 min and 30 s, completely softened and no white core of cooked rice noodles). Following the Eq. (1), the cooked break rate was determined for a sample of rice noodles with lengths longer than or equal to 7.5 cm and shorter than 7.5 cm.

$$\text{Cooked broken rate} = \frac{m_1}{m_1 + m_2} \times 100\% \quad (1)$$

Where  $m_1$ : after cooking, the weight of semi-dried rice noodles that are shorter than 7.5 cm;  $m_2$ : after cooking, the weight of semi-dried rice noodles that are longer than or equal to 7.5 cm.

### 2.10.2. Cooking loss rate and rehydration ratio

The method of Cham et al. (23) was modified to assess the cooking loss and rehydration ratio of semi-dried rice noodles. We selected 10 semi-dried rice noodles of about 20 cm in length and weighed  $m_0$ . Rice noodles were put in a beaker, filled with boiling water, boiled for the recommended amount of time (2 min and 30 s), then drained and weighed  $m_1$ . Cooked rice noodles were put on a dry dish and dried at 105°C to a constant weight  $m_2$ , and calculated the cooking loss and rehydration ratio according to the Eqs. (2, 3).

$$\text{Cooking loss rate} = 1 - \frac{m_2}{m_0 (1 - m)} \times 100\% \quad (2)$$

$$\text{Rehydration ratio} = \frac{m_1 - m_0}{m_0} \times 100\% \quad (3)$$

Where  $m$ : the amount of water in semi-dried rice noodles;  $m_0$ : weight of uncooked semi-dried rice noodles;  $m_1$ : weight of cooked semi-dried rice noodles;  $m_2$ : dry weight of cooked semi-dried rice noodles.

### 2.10.3. Iodine blue value

With a few modifications from Nagano et al. (24) methods, the turbidity of rice soup with semi-dried rice noodles was measured. We selected 5 semi-dried rice noodles of about 10 cm in length into a beaker, added boiling water, and heated them for 3 min. then rapidly removed the rice noodles, cooled the rice soup, and centrifuged for 5 min at a high-speed refrigerator centrifuge (Centrifugal force of 2,650 g). Take 5 mL of supernatant, add 50 mL of distilled water, 1 mL each of 1 mol/L hydrochloric acid, and 1 mL of 0.1 mol/L iodine reagent, and fix the volume. At 620 nm, the absorbance of rice soup was quantified. Add 1 mL of 1 mol/L hydrochloric acid, 1 mL of 0.1 mol/L iodine reagent, and a set volume for the control group.

## 2.11. Textural properties

We examined the texture properties of semi-dried rice noodles samples with a texture analyzer (TA.XT plus C, Stable Micro Systems, London, United Kingdom) following the description given by Li et al. (25) with a few modifications. A total of 15 semi-dried rice noodles were selected, each measuring around 20 cm in length. They were steamed for the optimal steaming time (2 min and 30 s) and then allowed to sit in the test sieve for 5 min. Five semi-dried rice noodles, about 5 cm long, were selected and placed on the texture meter. The settings were model type P/36R, pre-test rate of 2 mm/s, mid-test rate of 1 mm/s, post-test rate of 1 mm/s, a compression ratio of 50%, and compression interval of 3 s.

## 2.12. Color changes

We examined the color changes of semi-dried rice noodles samples with a colorimeter (UltraScan PRO instrument, HunterLab Instruments Inc., USA). According to the method of Wang et al. (26) with minor modifications, we selected 15 semi-dried rice noodles that were about 20 cm long, arranged them neatly, and put them in the colorimeter for photography, mostly referring to  $L^*$  values and  $b^*$  values.

## 2.13. Sensory evaluation

The sensory evaluation of semi-dried rice noodles was evaluated according to the method of Aydin et al. (27) with minor modifications. By inviting 10 trained panelists (5 male and 5 female) from the Food Science and Technology Institute were selected for sensory testing. The sensory panelists were trained in the ISO sensory analysis standard (ISO 8586:2012) and pretested using the method described in ISO 11132:2021. A lunch box containing distilled water and 10 semi-dried rice noodles from the sample was filled with the rice noodles after they had been steamed following the optimal steaming time and collected in a beaker. In **Supplementary Table 1**, the semi-dried rice noodle sensory assessment standard is presented.

## 2.14. X-ray diffraction

An X-ray diffractometer (D8 Advance, Bruker AXS Inc., Karlsruhe, Germany) was used to evaluate the crystallinity of semi-dried rice noodles samples. The diffraction scan region was set at  $5^\circ$  to  $50^\circ$ , the voltage was set at 40 kV, the current was set at 40 mA, and the scan speed was set at  $2^\circ/\text{min}$  by the approach given by Tao et al. (15) with minor modifications. Additionally, samples of semi-dried rice noodles were dried at  $50^\circ\text{C}$  for 7 h before being pulverized and sieved through sieves with a mesh size of 200.

## 2.15. Moisture distribution

Semi-dried rice noodles samples were subjected to moisture distribution analysis using an NMR analyzer (NMI20, Newmax Analytical Instruments, Suzhou, China), with minor changes to the procedure outlined by Sangpring et al. (28). Before inserting the test

tube into the NMR analyzer, we take 10 semi-dried rice noodles, each measuring about 3 cm in length, but then in the test tube to prevent moisture evaporation. The parameters were sampling points TD = 150030, a number of repetitions NS = 32, and TW = 2,000 ms.

## 2.16. Scanning electron microscope (SEM)

The morphological structure of the cross-section of the semi-dried rice noodles samples was examined using a scanning electron microscope (MIRA LMS, Teescan Inc., Brno, Czechia). Semi-dried rice noodles were freeze-dried following the Geng et al. (29) with minor modifications. The samples were then fastened to a sample holder with double-sided carbon tape, coated with gold for 120 s using a sputter coater, and pictures were captured at 3.0 kV accelerating voltage and  $1,200\times$  magnification.

## 2.17. Statistical analysis

Using SPSS 20.0, we performed a one-way analysis of variance (ANOVA) (SPSS Inc., Chicago, USA). The measurement for statistical significance was  $p < 0.05$ . Data were presented using the mean  $\pm$  standard deviation ( $n = 3$ ). ORIGIN 2018 (Northampton, MA, USA) and GraphPad Prism 8 were used to analyze spectral pictures (GraphPad Software, San Diego, USA).

# 3. Results and discussion

## 3.1. Basic physicochemical composition

**Table 1** showed the effect of sodium bicarbonate on the basic physicochemical composition of rice flour. The pH increased with increasing sodium bicarbonate addition, whereas lipid and protein levels decreased. The pH increased from 4.28 to 9.43, while the lipid content and protein content decreased from 0.57 and 7.64 to 0.46 and 5.71%, respectively. The decreased in lipid content was similar to the extraction from soap, and alkali and lipids may interact to generate soap through a process called saponification (7). The decreased in protein content was comparable to the starch extraction that used alkali to remove proteins, and the proteins that were partially eliminated were albumin and globulin, which are soluble in water and alkali solutions, respectively (30). With the addition of sodium bicarbonate from 0 to 0.2%, the amylose content increased, this might be due to the increased removal of protein-bound by starch granules, which increased amylose content (31). With more addition (0.2~0.5%), the amylose content decreased. This might be because the pH was weakly alkaline, which made the starch and protein partially negatively charged, and the ionic repulsion between negative charges would be broken the hydrogen bond between starch molecules and resulted in the decrease of amylose content (32).

## 3.2. Farinograph properties

**Table 2** showed the effect of sodium bicarbonate on the farinograph properties of rice flour. With the addition of sodium bicarbonate was increased, the WA, DDT, and DST of rice flour

**TABLE 1** Effect of sodium bicarbonate on the basic physicochemical composition of rice flour.

Addition/%	pH value	Lipid content/%	Protein content/%	Amylose content/%
0	4.28 ± 0.03 <sup>h</sup>	0.57 ± 0.01 <sup>a</sup>	7.64 ± 0.19 <sup>a</sup>	20.04 ± 0.15 <sup>e</sup>
0.02	4.53 ± 0.02 <sup>g</sup>	0.54 ± 0.01 <sup>b</sup>	7.17 ± 0.10 <sup>b</sup>	20.43 ± 0.08 <sup>d</sup>
0.06	4.78 ± 0.05 <sup>f</sup>	0.53 ± 0.01 <sup>bc</sup>	7.06 ± 0.05 <sup>b</sup>	20.69 ± 0.03 <sup>c</sup>
0.1	5.26 ± 0.05 <sup>e</sup>	0.52 ± 0.01 <sup>c</sup>	6.96 ± 0.04 <sup>b</sup>	21.23 ± 0.10 <sup>b</sup>
0.2	6.29 ± 0.05 <sup>d</sup>	0.51 ± 0.00 <sup>d</sup>	6.66 ± 0.20 <sup>c</sup>	21.90 ± 0.12 <sup>a</sup>
0.3	7.49 ± 0.08 <sup>c</sup>	0.50 ± 0.01 <sup>d</sup>	6.41 ± 0.02 <sup>d</sup>	19.48 ± 0.13 <sup>f</sup>
0.4	8.36 ± 0.10 <sup>b</sup>	0.47 ± 0.01 <sup>e</sup>	6.22 ± 0.13 <sup>d</sup>	18.75 ± 0.29 <sup>g</sup>
0.5	9.43 ± 0.07 <sup>a</sup>	0.46 ± 0.00 <sup>f</sup>	5.71 ± 0.20 <sup>e</sup>	17.80 ± 0.12 <sup>h</sup>

Values are presented as the mean ± SD of three replicate samples. This means in a column that shares the same letters do not significantly differ ( $p < 0.05$ ).

**TABLE 2** Effect of sodium bicarbonate on the farinograph properties of rice flour.

Addition/%	WA/%	DDT/min	DST/min
0	55.33 ± 0.58 <sup>h</sup>	0.73 ± 0.06 <sup>f</sup>	0.40 ± 0.00 <sup>f</sup>
0.02	59.67 ± 1.15 <sup>g</sup>	0.90 ± 0.10 <sup>e</sup>	0.43 ± 0.06 <sup>ef</sup>
0.06	63.00 ± 1.00 <sup>f</sup>	1.13 ± 0.06 <sup>d</sup>	0.47 ± 0.06 <sup>ef</sup>
0.1	65.00 ± 1.00 <sup>e</sup>	1.23 ± 0.06 <sup>d</sup>	0.58 ± 0.06 <sup>de</sup>
0.2	69.67 ± 1.15 <sup>d</sup>	1.53 ± 0.06 <sup>c</sup>	0.63 ± 0.06 <sup>cd</sup>
0.3	72.67 ± 1.15 <sup>c</sup>	1.73 ± 0.12 <sup>b</sup>	0.77 ± 0.06 <sup>bc</sup>
0.4	75.33 ± 0.58 <sup>b</sup>	1.83 ± 0.06 <sup>b</sup>	0.83 ± 0.06 <sup>b</sup>
0.5	78.33 ± 0.58 <sup>a</sup>	2.17 ± 0.15 <sup>a</sup>	1.30 ± 0.20 <sup>a</sup>

Values are presented as the mean ± SD of three replicate samples. This means in a column that shares the same letters do not significantly differ ( $p < 0.05$ ). WA, dough water absorption; DDT, dough development time; DST, dough stability time.

increased from 55.33%, 0.73 and 0.40 min to 78.33%, 2.17 and 1.30 min, respectively. Consistent with the results of Guo et al. (33), the addition of alkali constantly enhanced dough water absorption. This is due to the fact that aqueous alkali solutions are potent electrolytes and improve the solubility of proteins by exposing their hydrophilic groups, which causes an increase in the water absorption of dough (34). The increase in DDT and DST indicated that the addition of alkali strengthened and increased the stability of the dough, reducing the likelihood that it would break while being mixed (35).

**TABLE 3** Effect of sodium bicarbonate on the pasting properties of rice flour.

Addition/%	Peak viscosity/cp	Trough viscosity/cp	Final viscosity/cp	Breakdown/cp	Setback/cp
0	1266.67 ± 38.08 <sup>de</sup>	849.33 ± 20.43 <sup>bc</sup>	1641.67 ± 60.19 <sup>d</sup>	417.33 ± 17.67 <sup>b</sup>	792.33 ± 40.05 <sup>cd</sup>
0.02	1311.33 ± 12.34 <sup>cd</sup>	867.00 ± 13.08 <sup>bc</sup>	1703.33 ± 40.61 <sup>c</sup>	444.33 ± 5.13 <sup>ab</sup>	836.33 ± 27.97 <sup>c</sup>
0.06	1372.67 ± 31.90 <sup>b</sup>	893.67 ± 17.56 <sup>b</sup>	1777.00 ± 5.57 <sup>b</sup>	479.00 ± 22.11 <sup>a</sup>	883.33 ± 12.01 <sup>b</sup>
0.1	1463.00 ± 28.16 <sup>a</sup>	975.00 ± 47.84 <sup>a</sup>	1908.33 ± 34.79 <sup>a</sup>	488.00 ± 19.70 <sup>a</sup>	933.33 ± 27.50 <sup>a</sup>
0.2	1321.67 ± 33.13 <sup>c</sup>	890.33 ± 31.37 <sup>b</sup>	1722.33 ± 29.14 <sup>bc</sup>	431.33 ± 47.61 <sup>b</sup>	832.00 ± 29.31 <sup>c</sup>
0.3	1281.33 ± 6.11 <sup>cde</sup>	855.67 ± 10.79 <sup>bc</sup>	1628.67 ± 4.73 <sup>d</sup>	425.67 ± 14.01 <sup>b</sup>	773.00 ± 6.08 <sup>d</sup>
0.4	1243.67 ± 2.08 <sup>e</sup>	825.67 ± 6.43 <sup>cd</sup>	1487.33 ± 19.63 <sup>e</sup>	418.00 ± 4.58 <sup>b</sup>	661.67 ± 24.19 <sup>e</sup>
0.5	1165.67 ± 34.43 <sup>f</sup>	799.00 ± 11.53 <sup>d</sup>	1417.33 ± 34.43 <sup>f</sup>	366.67 ± 35.53 <sup>c</sup>	618.33 ± 27.10 <sup>e</sup>

Values are presented as the mean ± SD of three replicate samples. This means in a column that shares the same letters do not significantly differ ( $p < 0.05$ ).

**TABLE 4** Effect of sodium bicarbonate on the thermal properties of rice flour.

Addition/%	T <sub>0</sub> /°C	T <sub>p</sub> /°C	T <sub>c</sub> /°C	ΔH/J·g <sup>-1</sup>
0	70.14 ± 0.09 <sup>g</sup>	76.70 ± 0.00 <sup>g</sup>	80.95 ± 0.05 <sup>h</sup>	2.69 ± 0.13 <sup>f</sup>
0.02	71.23 ± 0.16 <sup>f</sup>	76.95 ± 0.00 <sup>f</sup>	81.40 ± 0.05 <sup>g</sup>	3.18 ± 0.00 <sup>e</sup>
0.06	72.28 ± 0.05 <sup>e</sup>	77.10 ± 0.12 <sup>ef</sup>	81.83 ± 0.00 <sup>f</sup>	3.91 ± 0.02 <sup>b</sup>
0.1	72.68 ± 0.09 <sup>d</sup>	77.16 ± 0.03 <sup>e</sup>	82.10 ± 0.00 <sup>e</sup>	4.44 ± 0.07 <sup>a</sup>
0.2	72.95 ± 0.00 <sup>c</sup>	77.37 ± 0.03 <sup>d</sup>	82.58 ± 0.05 <sup>d</sup>	3.99 ± 0.02 <sup>b</sup>
0.3	73.22 ± 0.00 <sup>b</sup>	77.53 ± 0.05 <sup>c</sup>	82.82 ± 0.09 <sup>c</sup>	3.78 ± 0.04 <sup>c</sup>
0.4	73.34 ± 0.05 <sup>b</sup>	77.76 ± 0.15 <sup>b</sup>	83.10 ± 0.00 <sup>b</sup>	3.67 ± 0.03 <sup>d</sup>
0.5	73.70 ± 0.10 <sup>a</sup>	78.12 ± 0.20 <sup>a</sup>	83.44 ± 0.12 <sup>a</sup>	3.09 ± 0.02 <sup>e</sup>

Values are presented as the mean ± SD of three replicate samples. This means in a column that shares the same letters do not significantly differ ( $p < 0.05$ ). T<sub>0</sub>, onset temperatures of thermal; T<sub>p</sub>, peak temperatures of thermal; T<sub>c</sub>, conclusion temperatures of thermal; ΔH, enthalpy changes of thermal.

### 3.3. Pasting properties

**Table 3** showed the effect of sodium bicarbonate on the pasting properties of rice flour. Pasting viscosity reflects the degree of swelling of starch granules during pasting (36). With the addition of sodium bicarbonate from 0 to 0.1%, the peak, trough, and final viscosity of semi-dried rice noodles increased; at 0.1 to 0.5%, it decreased. These are due to the breakage of the starch molecular chains brought on by the adsorption of sodium bicarbonate in the amorphous region of the starch granules and the increased swelling of the starch granules (37). The decrease in pasting viscosity was attributable to the further addition of sodium bicarbonate (0.1~0.5%), since the interaction of sodium ions with hydroxyl groups in starch weakened hydrogen bonds between starch molecules and prevented starch granule expansion (38). A higher peak, trough, and final viscosity contributed to a smooth surface and a good flavor of cooked rice noodles (39).

### 3.4. Thermal properties

**Table 4** showed the effect of sodium bicarbonate on the thermal properties of rice flour. The T<sub>0</sub>, T<sub>p</sub>, and T<sub>c</sub> increased with the addition of sodium bicarbonate. T<sub>0</sub>, T<sub>p</sub>, and T<sub>c</sub> increased from 70.14, 76.70, and 80.95 to 73.70, 78.12, and 83.44, respectively. These were probably caused by the rearrangement of the starch chains following



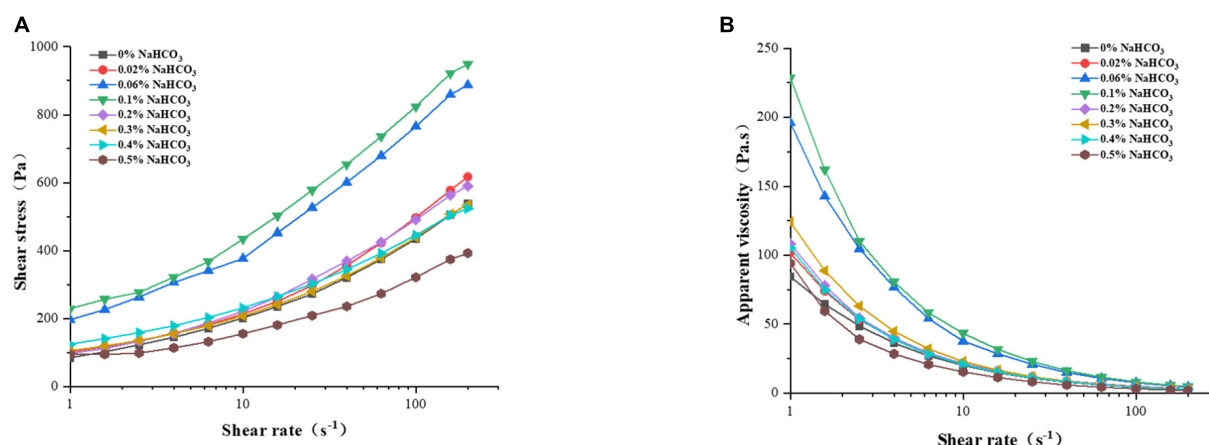


FIGURE 1  
Effect of sodium bicarbonate on shear stress (A) and apparent viscosity (B) of rice flour.

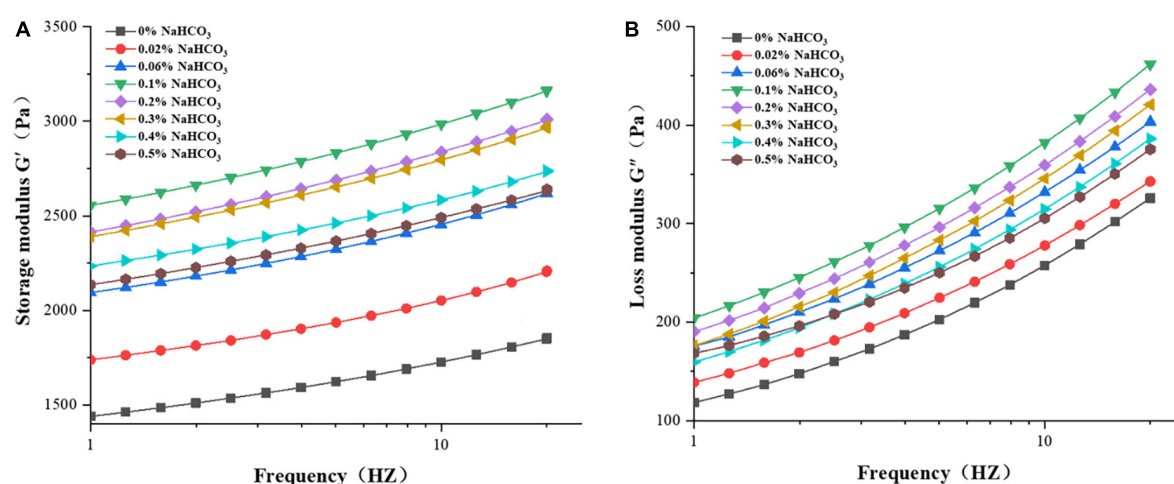


FIGURE 2  
Effect of sodium bicarbonate on storage modulus (A) and loss modulus (B) of rice flour.

the addition of sodium bicarbonate, which produced a more ordered structure of the starch molecules and helped the thermal stability of crystals, raising the pasting temperature of rice flour (40). Studies showed that the enthalpy of thermal absorption ( $\Delta H$ ) is directly proportional to the degree of starch aging (41). With the addition of sodium bicarbonate from 0 to 0.1%, the  $\Delta H$  increased; at 0.1 to 0.5%, it decreased. These were most likely attributable to the fact that sodium bicarbonate disrupted the amorphous region of starch, and reduced the inhibition of straight-chain starch, it would have contributed to the short-term aging of some straight-chain starch in rice flour (42). With more addition (0.1~0.5%), the starch's hydroxyl groups interacted with sodium ions to decrease water mobility in the starch-water system and inhibited the aging of starch (43).

## 3.5. Rheological properties

### 3.5.1. Static rheological

The effect of sodium bicarbonate on the static rheological properties of rice flour was shown in Figure 1. As shown in

Figure 1A, as the addition of sodium bicarbonate was from 0 to 0.1%, the shear stress of rice flour increased; and it decreased at 0.1 to 0.5%. Chen reported that the higher shear stress of rice flour indicates the higher gel strength and more stable gel structure of rice noodles (44). The maximum shear stress of rice flour at 0.1% addition of sodium bicarbonate indicated the maximum gel strength and the most stable gel structure of semi-dried rice noodles. As shown in Figure 1B, the apparent viscosity of rice flour gradually decreased with the increased shear rate, which has the characteristic of shear thinning and typical of non-Newtonian fluids (45).

### 3.5.2. Dynamic rheological

The effects of sodium bicarbonate on the dynamic rheological properties of rice flour were shown in Figure 2. The storage modulus ( $G'$ ) and loss modulus ( $G''$ ) of rice flour increased with the increased frequency, and  $G'$  was higher than  $G''$  it demonstrated that more elastic characteristics were exhibited of rice flour. As the addition of sodium bicarbonate was from 0 to 0.1%, the  $G'$  and  $G''$  increased; at 0.1 to 0.5%, it decreased. According to Meerts et al. (46), the rheological properties of dough were significantly impacted by the interaction between starch and molecules. With the addition of a



**TABLE 5** Effect of sodium bicarbonate on the cooking properties of semi-dried rice noodles.

Addition/%	Cooked broken rate/%	Cooking loss rate/%	Rehydration ratio/%	Iodine blue value
0	2.56 ± 0.28 <sup>e</sup>	8.18 ± 0.44 <sup>g</sup>	69.14 ± 1.79 <sup>h</sup>	0.281 ± 0.003 <sup>g</sup>
0.02	1.86 ± 0.41 <sup>f</sup>	8.79 ± 0.03 <sup>f</sup>	72.06 ± 0.93 <sup>g</sup>	0.285 ± 0.002 <sup>g</sup>
0.06	1.21 ± 0.14 <sup>g</sup>	9.11 ± 0.10 <sup>ef</sup>	74.55 ± 0.54 <sup>f</sup>	0.290 ± 0.003 <sup>f</sup>
0.1	1.02 ± 0.12 <sup>g</sup>	9.31 ± 0.04 <sup>e</sup>	76.07 ± 0.24 <sup>e</sup>	0.296 ± 0.002 <sup>e</sup>
0.2	3.76 ± 0.26 <sup>d</sup>	10.19 ± 0.16 <sup>d</sup>	78.20 ± 0.16 <sup>d</sup>	0.316 ± 0.003 <sup>d</sup>
0.3	5.38 ± 0.18 <sup>c</sup>	10.64 ± 0.21 <sup>c</sup>	80.75 ± 0.22 <sup>c</sup>	0.477 ± 0.001 <sup>c</sup>
0.4	6.59 ± 0.04 <sup>b</sup>	12.23 ± 0.11 <sup>b</sup>	84.43 ± 1.13 <sup>b</sup>	0.487 ± 0.005 <sup>b</sup>
0.5	8.47 ± 0.44 <sup>a</sup>	13.51 ± 0.30 <sup>a</sup>	88.70 ± 0.35 <sup>a</sup>	0.532 ± 0.004 <sup>a</sup>

Values are presented as the mean ± SD of three replicate samples. This means in a column that shares the same letters do not significantly differ ( $p < 0.05$ ).

moderate amount of sodium bicarbonate (0~0.1%) might increase the interaction between sodium ions and starch molecules, and that would contribute to an increase in  $G'$  and  $G''$ . This result was in agreement with Beck et al. (47). With more addition (0.1~0.5%), with increased addition, excessive sodium ions affected on gel structure of rice flour and resulted in decreased  $G'$  and  $G''$  (48).

### 3.6. Cooking properties

**Table 5** showed the effect of sodium bicarbonate on the cooking properties of semi-dried rice noodles. Cooking properties were influenced by cooked broken rate, cooking loss, and rehydration. The turbidity of the cooked rice soup was represented in the iodine blue value. Cooking loss, the ratio of rehydration, and the value of iodine blue all rose with the addition of more sodium bicarbonate, whereas cooked broken rate initially decreased and subsequently increased. The cooked broken rate of semi-dried rice noodles decreased to the lowest rate of 1.02% with the addition of sodium bicarbonate at a rate of 0.1%. These are most likely attributed by sodium bicarbonate causing hydrogen bonds between starch molecules to break, which made the gel structure of semi-dried rice noodles more stable and decreased the cooked broken rate. As the amount added increased (0.1~0.5%), the interaction of sodium ions with hydroxyl groups in starch reduced the interaction of water with starch, and made the gel structure of

**TABLE 7** Effect of sodium bicarbonate on the color changes of semi-dried rice noodles.

Addition/%	Appearance	$L^*$	$a^*$	$b^*$
0		81.71 ± 0.67 <sup>a</sup>	0.07 ± 0.02 <sup>e</sup>	8.10 ± 0.51 <sup>f</sup>
0.02		80.13 ± 0.47 <sup>b</sup>	0.10 ± 0.01 <sup>d</sup>	8.89 ± 0.16 <sup>e</sup>
0.06		78.19 ± 0.16 <sup>c</sup>	0.12 ± 0.01 <sup>d</sup>	9.88 ± 0.72 <sup>d</sup>
0.1		76.71 ± 0.21 <sup>d</sup>	0.16 ± 0.03 <sup>c</sup>	11.55 ± 0.13 <sup>c</sup>
0.2		76.35 ± 0.73 <sup>d</sup>	0.22 ± 0.00 <sup>b</sup>	11.99 ± 0.12 <sup>bc</sup>
0.3		75.96 ± 0.51 <sup>de</sup>	0.23 ± 0.01 <sup>ab</sup>	12.23 ± 0.19 <sup>b</sup>
0.4		75.39 ± 0.12 <sup>e</sup>	0.23 ± 0.00 <sup>ab</sup>	12.59 ± 0.14 <sup>ab</sup>
0.5		72.64 ± 0.37 <sup>f</sup>	0.25 ± 0.01 <sup>a</sup>	12.85 ± 0.11 <sup>a</sup>

Values are presented as the mean ± SD of three replicate samples. This means in a column that shares the same letters do not significantly differ ( $p < 0.05$ ).

semi-dried rice noodles looser, and caused increased cooked broken rate (40, 43). Cooking loss and iodine blue value increased with the addition of sodium bicarbonate from 8.18% and 0.281 to 13.51% and 0.532, respectively. This could be explained by sodium bicarbonate's disruption of the amorphous region of starch molecules, which promoted starch dissolution and led to some straight-chain starch inside the starch dissolving out and dissolving in rice soup when semi-dried rice noodles were steamed (23). In addition to the fact that the addition of sodium bicarbonate increased the rehydration ratio of semi-dried rice noodles, it is likely that this phenomenon was caused by the breaking of hydrogen bonds in

**TABLE 6** Effect of sodium bicarbonate on the textural properties of semi-dried rice noodles.

Addition/%	Hardness/g	Adhesiveness/g·s	Resilience/%	Cohesion	Springiness/%	Chewiness/g
0	3140.56 ± 85.26 <sup>bc</sup>	-32.90 ± 6.64 <sup>b</sup>	46.86 ± 2.94 <sup>ab</sup>	0.70 ± 0.04 <sup>ab</sup>	87.91 ± 1.80 <sup>ab</sup>	1932.89 ± 142.86 <sup>a</sup>
0.02	3166.16 ± 121.63 <sup>b</sup>	-19.57 ± 9.34 <sup>a</sup>	49.31 ± 1.45 <sup>a</sup>	0.74 ± 0.02 <sup>a</sup>	86.40 ± 1.62 <sup>b</sup>	1957.67 ± 44.04 <sup>a</sup>
0.06	3258.59 ± 158.38 <sup>b</sup>	-24.53 ± 7.02 <sup>ab</sup>	45.39 ± 2.31 <sup>b</sup>	0.72 ± 0.01 <sup>a</sup>	86.54 ± 3.16 <sup>b</sup>	1972.68 ± 63.42 <sup>a</sup>
0.1	3470.86 ± 128.15 <sup>a</sup>	-27.49 ± 7.09 <sup>ab</sup>	44.44 ± 1.59 <sup>bc</sup>	0.67 ± 0.02 <sup>bc</sup>	86.80 ± 1.47 <sup>b</sup>	2010.31 ± 38.60 <sup>a</sup>
0.2	2958.31 ± 104.32 <sup>cd</sup>	-16.48 ± 7.32 <sup>a</sup>	41.71 ± 1.07 <sup>c</sup>	0.64 ± 0.02 <sup>c</sup>	86.48 ± 2.66 <sup>b</sup>	1861.72 ± 67.19 <sup>a</sup>
0.3	2777.18 ± 106.16 <sup>de</sup>	-17.05 ± 3.77 <sup>a</sup>	43.65 ± 0.79 <sup>bc</sup>	0.73 ± 0.00 <sup>a</sup>	91.68 ± 0.70 <sup>a</sup>	1683.17 ± 134.48 <sup>b</sup>
0.4	2594.64 ± 38.33 <sup>e</sup>	-15.66 ± 2.25 <sup>a</sup>	44.49 ± 1.66 <sup>bc</sup>	0.74 ± 0.03 <sup>a</sup>	87.52 ± 3.23 <sup>b</sup>	1639.24 ± 92.04 <sup>b</sup>
0.5	2361.53 ± 109.23 <sup>f</sup>	-26.78 ± 4.04 <sup>ab</sup>	37.73 ± 2.27 <sup>d</sup>	0.64 ± 0.03 <sup>c</sup>	85.78 ± 1.94 <sup>b</sup>	1288.97 ± 48.67 <sup>c</sup>

Values are presented as the mean ± SD of three replicate samples. This means in a column that shares the same letters do not significantly differ ( $p < 0.05$ ).

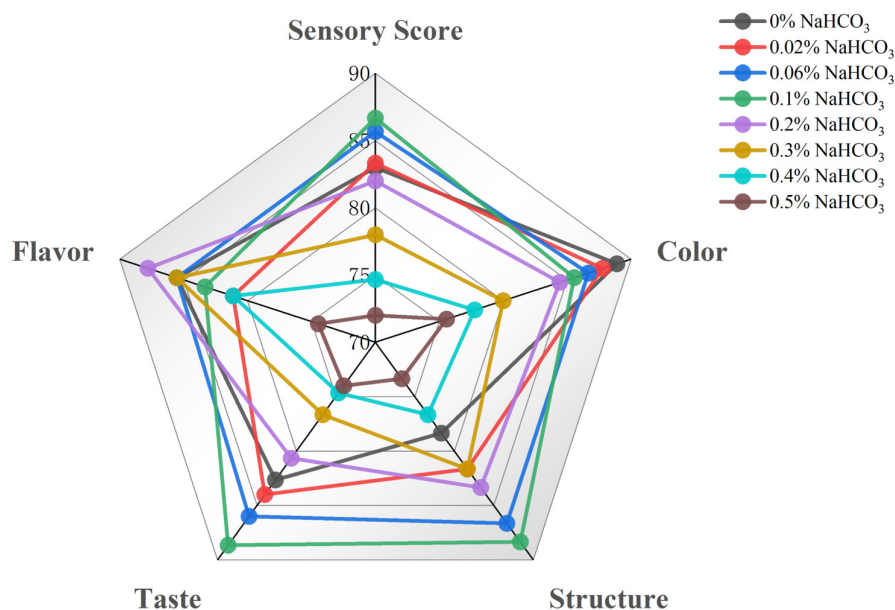


FIGURE 3  
Effect of sodium bicarbonate on the sensory evaluation of semi-dried rice noodles.

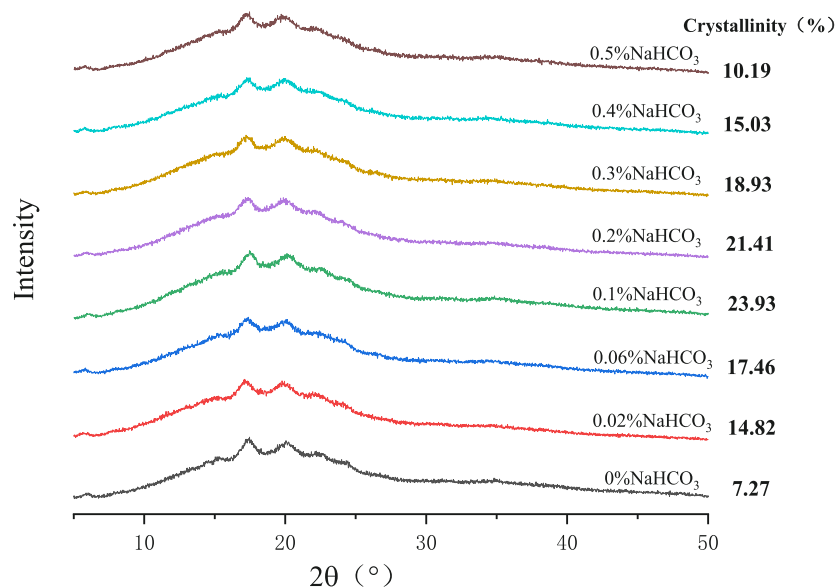


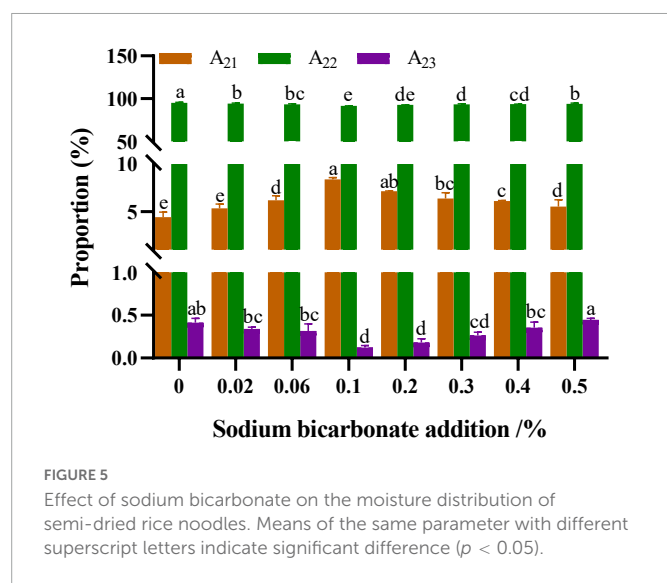
FIGURE 4  
Effect of sodium bicarbonate on the crystallinity of semi-dried rice noodles.

the amorphous region, which led to slow and irreversible water absorption (42).

### 3.7. Textural properties

Table 6 showed the effect of sodium bicarbonate on the textural properties of semi-dried rice noodles. Hardness is a vital parameter for cooking properties and chewiness affects consumer preferences (49). With the addition of sodium bicarbonate from 0 to 0.1%, the hardness and chewiness of semi-dried rice noodles increased; at 0.1 to 0.5%, it decreased. According to Tang et al. (50), the aging of

starch was positively connected with the hardness of rice noodles. These could be attributed to sodium bicarbonate disrupting the amorphous region of starch, and the reduction of the amorphous region accelerated the short-term aging of some straight-chained starches, increased the orderly structure, and recrystallization formed by starch molecules, and increased the hardness of semi-dried rice noodles (42). With more addition (0.1~0.5%), the interaction of too many sodium ions with the hydroxyl groups in starch decreased the interaction between water and starch, prevented the aging of starch, and disorganized the microcrystalline structure formed during the recrystallization of starch, resulting in a decrease in the hardness of semi-dried rice noodles (43). According to studies, the chewiness and



hardness of rice noodles have a significant impact on their taste, with moderate hardness and high chewiness producing the tastiest rice noodles (51).

### 3.8. Color changes

**Table 7** showed the effect of sodium bicarbonate on the color of semi-dried rice noodles. The  $L^*$  values decreased from 81.71 to 72.64 and  $b^*$  values increased from 8.10 to 12.85 as the amount of sodium bicarbonate added increased. This demonstrated that the semi-dried rice noodles had a yellow color when made with the addition of sodium bicarbonate and that the color of the semi-dried rice noodles grew with the addition of sodium bicarbonate. This modification might be explained by the fact that the raw materials' flavonoid compounds are released with the increasing addition of sodium bicarbonate, giving semi-dried rice noodles their yellow appearance (52).

### 3.9. Sensory evaluation

The effect of sodium bicarbonate on the sensory evaluation of semi-dried rice noodles was shown in **Figure 3**. The color of the semi-dried rice noodles made with the addition of sodium bicarbonate was slightly less pleasing, indicating that the addition of sodium bicarbonate produced semi-dried rice noodles with a yellowish tint. The overall sensory evaluation score was higher for semi-dried rice noodles as they displayed superior structural integrity and flavor when sodium bicarbonate was added in the proper proportion. Semi-dried rice noodles had the highest total sensory evaluation score of 86.67 in addition to the 0.1% sodium bicarbonate. This outcome could be explained by the important roles that rice noodle structure and flavor played.

### 3.10. Crystallinity

The effect of sodium bicarbonate on the crystallinity of semi-dried rice noodles was shown in **Figure 4**. All of the semi-dried rice

noodle samples had typical B-type crystals with typical diffraction peak sites at around  $5.6^\circ$ ,  $17^\circ$ ,  $20^\circ$ , and  $22^\circ$ . Since these peak locations corresponded to the normal peaks of starch aging, it was clear that the aging of the semi-dried rice noodle samples exhibited aging of starch. The outcomes demonstrated that the addition of sodium bicarbonate would not change the starch's crystal structure, which was consistent with Wang and Tao's (15, 53) report that the alkali treatment did not affect starch's crystal structure. With the addition of sodium bicarbonate from 0 to 0.1%, the crystallinity increased; at 0.1 to 0.5%, it decreased. These might be related to the sodium bicarbonate-induced breakdown of the amorphous sections of the starch molecules and the orderly stacking of double helices of starch chains to generate more ordered structures and increase crystallinity (54). The decreased crystallinity was due to the further addition of sodium bicarbonate (0.1~0.5%), the interaction of sodium ions with hydroxyl groups in starch prevented the formation of hydrogen bonds between them, which resulted in the disordering of starch microcrystals and the reduction or unraveling of the tightness in the double helix (28). According to studies, starch-based foods' crystallinity is a key measure of their quality, and it is directly correlated with the products' hardness, and moisture distribution (55).

### 3.11. Moisture distribution

The effect of sodium bicarbonate on the moisture distribution of semi-dried rice noodles was shown in **Figure 5**. As shown in **Figure 4**, the bound water, weakly bound water, and free water contents in semi-dried rice noodles were  $A_{21}$ ,  $A_{22}$ , and  $A_{23}$ , respectively. With the addition of sodium bicarbonate from 0 to 0.1%,  $A_{21}$  increased,  $A_{22}$  and  $A_{23}$  decreased in semi-dried rice noodles; at 0.1 to 0.5%,  $A_{21}$  decreased, and  $A_{22}$  and  $A_{23}$  increased. These could be attributed to sodium bicarbonate disrupting the amorphous region of starch, which facilitates some straight-chain starch recrystallizing with water molecules and promoted the interaction between starch chains and water molecules, resulting in an increase in the amount of bound water in the semi-dried rice noodles (42). With more being added (0.1~0.5%), the sodium ion concentration increased. The interaction of sodium ions with the hydroxyl groups in starch inhibited the recrystallization of starch and water molecules, decreased the quantity of water diffusing from the amorphous to the crystalline area, and increased the mobility of water in semi-dried rice noodles (43). Singh said that higher amounts of bound water meant less water that wasn't bonded firmly and had a higher water-holding capacity (56).

### 3.12. Morphological characteristics

The effect of sodium bicarbonate on the microscopic morphological structure of semi-dried rice noodles was shown in **Figure 6**. With the addition of sodium bicarbonate from 0 to 0.1%, the starch-protein combination increased, starch granules were embedded in the protein network structure, and starch and protein were formed into an orderly and stable network structure. With the further addition of sodium bicarbonate (0~0.5%), there were fewer agglomerated structures, the starch-protein network structure was distorted, and starch granules could not be properly

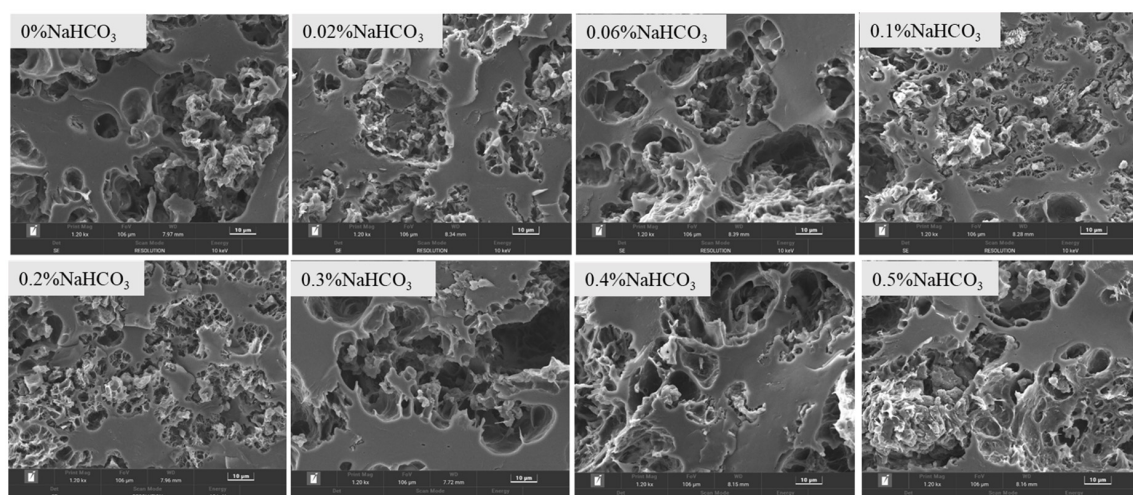


FIGURE 6  
Effect of sodium bicarbonate on the microscopic morphology of semi-dried rice noodles.

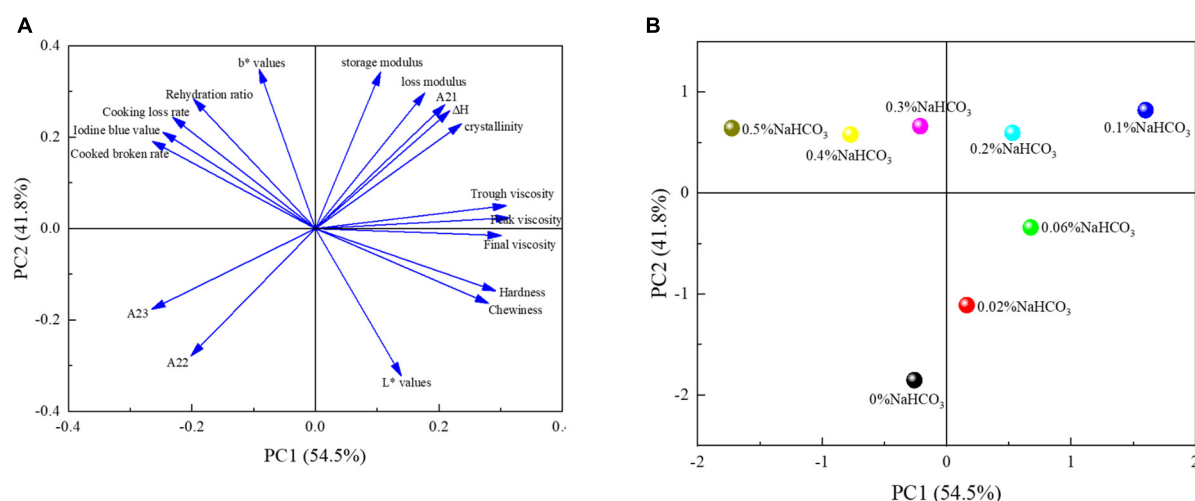


FIGURE 7  
Principal component analysis of semi-dried rice noodles with different sodium bicarbonate additions. Loading plot of the variables of samples (A). Score plot of the different samples (B).

embedded in the protein network structure. This showed that lower sodium bicarbonate concentrations caused greater interaction between the starch and protein in semi-dried rice noodles and totally contained the starch granules within the protein network structure. However, excessive sodium bicarbonate would make the starch-protein network structure lose and discontinuous, and result in the separation of starch granules from the network structure.

### 3.13. Principal component analysis (PCA)

The principal component analysis of semi-dried rice noodles with different sodium bicarbonate additions was shown in Figure 7. As shown in Figure 7A, the loading plots clearly demonstrated that PC1 and PC2 contributed 96.3% of the variance, with respective variance contributions of 41.8 and 54.5%. Therefore, the PC1-PC2 plane could represent the response variables' primary contribution. With various

amounts of sodium bicarbonate, PCA score plots showed that the quality of semi-dried rice noodles dramatically altered. As shown in Figure 7B, the addition of 0.1% sodium bicarbonate produced semi-dried rice noodles with the best quality and overall scores. In light of this, it may be said that adding a small amount of sodium bicarbonate could enhance the chewiness, flavor, and edible quality of semi-dried rice noodles.

## 4. Conclusion

The addition of sodium bicarbonate had a significant effect on the physicochemical properties of rice flour and the quality characteristics of semi-dried rice noodles. With the increase of sodium bicarbonate addition, the pH value was increased, and lipid and protein content were decreased in rice flour. Meanwhile, Thermal and farinograph properties showed that the pasting temperature,



dough water absorption, dough development time, and dough stability time of rice flour increased with the addition of sodium bicarbonate. Pasting and rheological properties of rice flour revealed that a modest amount of sodium bicarbonate could be increased the pasting viscosity, storage modulus ( $G'$ ), and loss modulus ( $G''$ ), and that the  $G'$  were more than  $G''$  for all samples, it demonstrated that rice flour showed more elastic characteristics. Additionally, with the addition of sodium bicarbonate from 0 to 0.1%, the cooked broken rate decreased, and the hardness and chewiness of semi-dried rice noodles increased. With the addition of a small amount of sodium bicarbonate, X-ray diffraction showed that it could be increased the crystallinity of semi-dried rice noodles, which increased from 7.27 to 23.93%, it demonstrated that the addition of sodium bicarbonate could increase the short-term aging of starch. Low-field nuclear magnetic resonance showed that  $A_{21}$  increased,  $A_{22}$  and  $A_{23}$  decreased in semi-dried rice noodles,  $A_{21}$  increased from 4.44 to 8.39%,  $A_{22}$  and  $A_{23}$  decreased from 95.16 and 0.41 to 91.48 and 0.12%, respectively. Scanning electron microscope showed that it could increase the starch-protein interaction and result in the formation of an ordered and stable network structure of starch-protein. Finally, the principal component analysis showed that the chewiness, texture and eating quality of semi-dried rice noodles were the best with the addition of sodium bicarbonate at 0.1%. Although this study elucidated the significant effects of sodium bicarbonate on the physicochemical properties of fermented rice flour and the quality characteristics of fermented semi-dried rice noodles, the variation of acidic taste in fermented semi-dried rice noodles was not specifically analyzed by instrumentation. Further studies are needed to accurately analyze the dynamics of acidic taste and flavor in fermented semi-dried rice noodles made with different sodium bicarbonate additions using electronic nose or gas chromatography-mass spectrometry (GC-MS).

## Data availability statement

The original contributions presented in this study are included in this article/**Supplementary material**, further inquiries can be directed to the corresponding author.

## References

- Li Y, Liang J, Yang M, Chen J, Han B. Traditional Chinese rice noodles: history, classification, and processing methods. *Cereal Foods World*. (2015) 60:123–7. doi: 10.1094/CFW-60-3-0515
- Tong L, Gao X, Lin L, Liu Y, Zhong K, Liu L, et al. Effects of semidry flour milling on the quality attributes of rice flour and rice noodles in China. *J Cereal Sci*. (2015) 62:45–9. doi: 10.1016/j.jcs.2014.12.007
- Lu Z, Li L, Cao W, Li Z, Tatsumi E. Influence of natural fermentation on physicochemical characteristics of rice noodles. *Int J Food Sci Technol*. (2003) 38:505–10. doi: 10.1046/j.1365-2621.2003.00701.x
- Li Y, Zheng X, Chen J, Liang J, Yu S, Han B. Lactic acid bacteria diversity of fresh rice noodles during the fermentation process, revealed by culture-dependent and culture-independent methods. *Biotechnol Biotechnol Equip*. (2015) 29:915–20. doi: 10.1080/13102818.2015.1051494
- Yi C, Yang Y, Zhou S, He Y. Role of lactic acid bacteria in the eating qualities of fermented rice noodles. *Cereal Chem*. (2017) 94:349–56. doi: 10.1094/CHEM-07-16-0187-R
- Li N, Zhang B, Zhao S, Niu M, Jia C, Huang Q, et al. Influence of *Lactobacillus/candida* fermentation on the starch structure of rice and the related

## Author contributions

LL and WX devised and planned the experiments. YD, WX, and YC carried out the experiments. WX, YC, and SX examined the data. WX and YD wrote the manuscript. All authors have been reviewed and approved the final draft.

## Funding

This research was supported by the Hunan Provincial Natural Science Foundation (No. 2020JJ4137) and Hunan Provincial Education Department's Scientific Research Foundation (No. 19B594).

## Conflict of interest

The authors declare that the research was conducted in the absence of any commercial or financial relationships that could be construed as a potential conflict of interest.

## Publisher's note

All claims expressed in this article are solely those of the authors and do not necessarily represent those of their affiliated organizations, or those of the publisher, the editors and the reviewers. Any product that may be evaluated in this article, or claim that may be made by its manufacturer, is not guaranteed or endorsed by the publisher.

## Supplementary material

The Supplementary Material for this article can be found online at: <https://www.frontiersin.org/articles/10.3389/fnut.2023.1100422/full#supplementary-material>

- noodle features. *Int J Biol Macromol*. (2019) 121:882–8. doi: 10.1016/j.ijbiomac.2018.10.097
- Fu B. Asian noodles: history, classification, raw materials, and processing. *Food Res Int*. (2008) 41:888–902. doi: 10.1016/j.foodres.2007.11.007
- Uzogara S, Morton I, Daniel J. Quality changes and mineral content of cowpea (*Vigna unguiculata* L. Walp) seeds processed with 'kanwa'alkaline salt. *Food Chem*. (1988) 30:1–18. doi: 10.1016/0308-8146(88)90019-2
- Lai L, Karim A, Norziah M, Seow C. Effects of Na<sub>2</sub>CO<sub>3</sub> and NaOH on pasting properties of selected native cereal starches. *J Food Sci*. (2004) 69:FCT249–56. doi: 10.1111/j.1365-2621.2004.tb06324.x
- Pedcharat K, Jangchud K, Prinyawiwatkul W. Physicochemical properties of rice flour as affected by alkaline soaking and washing treatments. *Int J Food Sci Technol*. (2021) 56:2539–47. doi: 10.1111/ijfs.14892
- Kim SK. Instant noodle. In: Kruger J, Matsuo R, Dick J editors. *Pasta and Noodle Technology*. (Saint Paul, MN: American Association of Cereal Chemist. Inc) (1996).



13. Shiau S, Yeh A. Effects of alkali and acid on dough rheological properties and characteristics of extruded noodles. *J Cereal Sci.* (2001) 33:27–37. doi: 10.1006/jcrs.2000.0344
14. Suwannaporn P, Wiwattanawanich K, Tester R. Effect of water requirement and alkali on wheat-riced noodle quality. *Starch Starke* (2014) 66:475–83. doi: 10.1002/star.201300124
15. Tao H, Li M, Deng H, Ren K, Zhuang G, Xu X, et al. The impact of sodium carbonate on physico-chemical properties and cooking qualities of starches isolated from alkaline yellow noodles. *Int J Biol Macromol.* (2019) 137:697–702. doi: 10.1016/j.ijbiomac.2019.07.008
16. Fan H, Ai Z, Chen Y, Fu F, Bian K. Effect of alkaline salts on the quality characteristics of yellow alkaline noodles. *J Cereal Sci.* (2018) 84:159–67. doi: 10.1016/j.jcs.2018.10.007
17. Xiao W, Ding Y, Cheng Y, Xu S, Lin L. Understanding the changes in quality of semi-dried rice noodles during storage at room temperature. *Foods.* (2022) 11:2130. doi: 10.3390/foods11142130
18. AOAC. *Official Methods of Analysis*. Washington, DC: AOAC (1990).
19. Yeoh S, Lubowa M, Tan T, Murad M, Easa A. The use of salt-coating to improve textural, mechanical, cooking and sensory properties of air-dried yellow alkaline noodles. *Food Chem.* (2020) 333:127425. doi: 10.1016/j.foodchem.2020.127425
20. American Association for Clinical Chemistry. *Approved Methods of the AACC*. Washington, DC: American Association for Clinical Chemistry (2000).
21. Rombouts I, Jansens K, Lagrain B, Delcour J, Zhu K. The impact of salt and alkali on gluten polymerization and quality of fresh wheat noodles. *J Cereal Sci.* (2014) 60:507–13. doi: 10.1016/j.jcs.2014.09.003
22. Xu M, Hou G, Ding J, Du X. Comparative study on textural and rheological properties between dry white salted noodle and yellow alkaline noodle as influenced by different tea extracts. *J Food Process Preserv.* (2020) 44:e14981. doi: 10.1111/jfpp.14981
23. Cham S, Suwannaporn P. Effect of hydrothermal treatment of rice flour on various rice noodles quality. *J Cereal Sci.* (2010) 51:284–91. doi: 10.1016/j.jcs.2010.01.002
24. Nagano K, Sasaki K, Endo T. Breeding of new rice cultivar 'Tohoku 194' with 'Sasanishiki'-type good eating quality of cooked rice. *Breed Sci.* (2013) 63:233–7. doi: 10.1270/jsbbs.63.233
25. Li M, Zhu K, Sun Q, Amza T, Guo X, Zhou H. Quality characteristics, structural changes, and storage stability of semi-dried noodles induced by moderate dehydration. Understanding the quality changes in semi-dried noodles. *Food Chem.* (2016) 194:797–804. doi: 10.1016/j.foodchem.2015.08.079
26. Wang J, Li A, Hu J, Zhang B, Liu J, Zhang Y, et al. Effect of frying process on nutritional property, physicochemical quality, and in vitro digestibility of commercial instant noodles. *Front Nutr.* (2022) 9:823432. doi: 10.3389/fnut.2022.823432
27. Aydin E, Gocmen D. Cooking quality and sensorial properties of noodle supplemented with oat flour. *Food Sci Biotechnol.* (2011) 20:507–11. doi: 10.1007/s10068-011-0070-1
28. Sangpring Y, Fukuoka M, Ratanasumawong S. The effect of sodium chloride on microstructure, water migration, and texture of rice noodle. *LWT Food Sci Technol.* (2015) 64:1107–13. doi: 10.1016/j.lwt.2015.07.035
29. Geng D, Zhou S, Wang L, Zhou X, Liu L, Lin Z, et al. Effects of slight milling combined with cellulase enzymatic treatment on the textural and nutritional properties of brown rice noodles. *Lwt Food Sci Technol.* (2020) 128:109520. doi: 10.1016/j.lwt.2020.109520
30. Zhou Z, Robards K, Helliwell S, Blanchard C. Composition and functional properties of rice. *Int J Food Sci Technol.* (2002) 37:849–68. doi: 10.1046/j.1365-2621.2002.00625.x
31. Wang L, Yang-Yang X, Zhu Y, Jiao R, Cao X, Han L. Effects of sodium hydroxide solutions physical on properties and structure of buckwheat starch. *Sci Technol Food Industry.* (2017) 38:79–83.
32. Israkarn K, Nakornpanom N, Hongsprabhas P. Physicochemical properties of starches and proteins in alkali-treated mungbean and cassava starch granules. *Carbohydr Polym.* (2014) 105:34–40. doi: 10.1016/j.carbpol.2014.01.054
33. Guo X, Wei X, Zhu K. The impact of protein cross-linking induced by alkali on the quality of buckwheat noodles. *Food Chem.* (2017) 221:1178–85. doi: 10.1016/j.foodchem.2016.11.041
34. Rui, L, Xiao-Jun M. Composition of instant soluble peng gray and its mechanisms in improving dough quality. *Food Sci.* (2011) 32:89–94. doi: 10.1111/j.1759-6831.2010.00113.x
35. Alaunyte I, Stojceska V, Plunkett A, Ainsworth P, Derbyshire E. Improving the quality of nutrient-rich Teff (*Eragrostis tef*) breads by combination of enzymes in straight dough and sourdough breadmaking. *J Cereal Sci.* (2012) 55:22–30. doi: 10.1016/j.jcs.2011.09.005
36. Karim A, Nadiha M, Chen F, Phuah Y, Chui Y, Fazilah A. Pasting and retrogradation properties of alkali-treated sago (*Metroxylon sagu*) starch. *Food Hydrocoll.* (2008) 22:1044–53. doi: 10.1016/j.foodhyd.2007.05.011
37. Rafiq S, Singh S, Saxena D. Effect of alkali-treatment on physicochemical, pasting, thermal, morphological and structural properties of Horse Chestnut (*Aesculus indica*) starch. *J Food Meas Charact.* (2016) 10:676–84. doi: 10.1007/s11694-016-9351-y
38. Lim S, Lee J, Shin D, Lim H. Comparison of protein extraction solutions for rice starch isolation and effects of residual protein content on starch pasting properties. *Starch Stärke.* (1999) 51:120–5. doi: 10.1002/(SICI)1521-379X(199904)51:4<120::AID-STAR120>3.0.CO;2-A
39. Li M, Luo L, Zhu K, Guo X, Peng W, Zhou H. Effect of vacuum mixing on the quality characteristics of fresh noodles. *J Food Eng.* (2012) 110:525–31. doi: 10.1016/j.jfoodeng.2012.01.007
40. Lai L, Abd Karim A, Norziah M, Seow C. Effects of Na<sub>2</sub>CO<sub>3</sub> and NaOH on DSC thermal profiles of selected native cereal starches. *Food Chem.* (2002) 78:355–62. doi: 10.1016/S0308-8146(02)00097-3
41. Satmalee P, Charoenrein S. Acceleration of ageing in rice stick noodle sheets using low temperature. *International J Food Sci Technol.* (2009) 44:1367–72. doi: 10.1111/j.1365-2621.2009.01966.x
42. Fan D, Wang L, Ma S, Ma W, Liu X, Huang J, et al. Structural variation of rice starch in response to temperature during microwave heating before gelatinisation. *Carbohydr Polym.* (2013) 92:1249–55. doi: 10.1016/j.carbpol.2012.10.053
43. Li Z, Wang L, Chen Z, Yu Q, Feng W. Impact of protein content on processing and texture properties of waxy rice flour and glutinous dumpling. *J Cereal Sci.* (2018) 81:30–6. doi: 10.1016/j.jcs.2018.03.005
44. Chen P, Yu L, Kealy T, Chen L, Li L. Phase transition of starch granules observed by microscope under shearless and shear conditions. *Carbohydr Polym.* (2007) 68:495–501. doi: 10.1016/j.carbpol.2006.11.002
45. Marcotte M, Hoshahili A, Ramaswamy H. Rheological properties of selected hydrocolloids as a function of concentration and temperature. *Food Res Int.* (2001) 34:695–703. doi: 10.1016/S0963-9969(01)00091-6
46. Meerts M, Cardinaels R, Oosterlinck F, Courtin C, Moldenaers P. The impact of water content and mixing time on the linear and non-linear rheology of wheat flour dough. *Food Biophys.* (2017) 12:151–63. doi: 10.1007/s11483-017-9472-9
47. Beck M, Jekle M, Becker T. Impact of sodium chloride on wheat flour dough for yeast-leavened products. I. Rheological attributes. *J Sci Food Agric.* (2012) 92:585–92. doi: 10.1002/jsfa.4612
48. Yu S, Ma Y, Sun D. Impact of amylose content on starch retrogradation and texture of cooked milled rice during storage. *J Cereal Sci.* (2009) 50:139–44. doi: 10.1016/j.jcs.2009.04.003
49. Janve M, Singhal R. Fortification of puffed rice extrudates and rice noodles with different calcium salts: physicochemical properties and calcium bioaccessibility. *LWT.* (2018) 97:67–75. doi: 10.1016/j.lwt.2018.06.030
50. Tang A, Li M, Wang R, Dhital S, Lu D. Manipulating raw noodle crystallinity to control the hardness of cooked noodle. *Lwt Food Sci Technol.* (2019) 109:305–12.
51. Roberts T. Cadmium and phosphorous fertilizers: the issues and the science. *Proc Eng.* (2014) 83:52–9. doi: 10.1016/j.proeng.2014.09.012
52. Asenstorfer R, Wang Y, Mares D. Chemical structure of flavonoid compounds in wheat (*Triticum aestivum* L.) flour that contribute to the yellow colour of Asian alkaline noodles. *J Cereal Sci.* (2006) 43:108–19.
53. Wang S, Copeland L. Effect of alkali treatment on structure and function of pea starch granules. *Food Chem.* (2012) 135:1635–42. doi: 10.1016/j.foodchem.2012.06.003
54. Spier F, Zavareze Eda R, Marques e Silva R, Elias M, Dias A. Effect of alkali and oxidative treatments on the physicochemical, pasting, thermal and morphological properties of corn starch. *J Sci Food Agric.* (2013) 93:2331–7. doi: 10.1002/jsfa.6049
55. Dome K, Podgorbunskikh E, Bychkov A, Lomovsky O. Changes in the crystallinity degree of starch having different types of crystal structure after mechanical pretreatment. *Polymers.* (2020) 12:641. doi: 10.3390/polym12030641
56. Singh N, Singh J, Kaur L, Sodhi N, Gill B. Morphological, thermal and rheological properties of starches from different botanical sources. *Food Chem.* (2003) 81:219–31. doi: 10.1016/S0308-8146(02)00416-8



## OPEN ACCESS

EDITED BY  
Baoguo Xu,  
Jiangsu University,  
China

REVIEWED BY  
Teodora Coldea,  
University of Agricultural Sciences and  
Veterinary Medicine of Cluj-Napoca,  
Romania  
Tao Feng,  
Shanghai Institute of Technology, China

\*CORRESPONDENCE  
Guoquan Zhang  
✉ zhanggq98@nwsuaf.edu.cn

SPECIALTY SECTION  
This article was submitted to  
Nutrition and Food Science Technology,  
a section of the journal  
Frontiers in Nutrition

RECEIVED 14 November 2022  
ACCEPTED 09 February 2023  
PUBLISHED 02 March 2023

CITATION  
Zheng Q, Wang Z, Xiong F and Zhang G (2023)  
Enzyme inactivation induced by thermal  
stabilization in highland barley and impact on  
lipid oxidation and aroma profiles.  
*Front. Nutr.* 10:1097775.  
doi: 10.3389/fnut.2023.1097775

COPYRIGHT  
© 2023 Zheng, Wang, Xiong and Zhang. This is  
an open-access article distributed under the  
terms of the [Creative Commons Attribution  
License \(CC BY\)](#). The use, distribution or  
reproduction in other forums is permitted,  
provided the original author(s) and the  
copyright owner(s) are credited and that the  
original publication in this journal is cited, in  
accordance with accepted academic practice.  
No use, distribution or reproduction is  
permitted which does not comply with these  
terms.

# Enzyme inactivation induced by thermal stabilization in highland barley and impact on lipid oxidation and aroma profiles

Qianna Zheng, Zheng Wang, Feiyang Xiong and  
Guoquan Zhang\*

College of Food Science and Engineering, Northwest A&F University, Xianyang, Shaanxi, China

Thermal stabilization is efficient for slowing lipid degradation and prolonging the shelf life of highland barley, but the impacts of different thermal stabilized treatments on highland barley and possible chemical reactions remain unclear. The effects of thermal stabilization treatments (bake, far-infrared, fry, microwave and steam) on the enzymes, lipids and aroma profiles of highland barley flour (HBF) were investigated in this study. Thermal stabilization significantly decreased the contents of ash and GABA. Baked HBF exhibited the lowest fatty acid value and peroxide value. Untreated HBF had higher lipase and lipoxygenase activities and fried mostly inactivated these enzymes. All thermal stabilization treatments increased the catalase activities and fried showed the higher level. Thus, fried might be an effective method to stabilize the HBF. The high temperatures during stabilizing triggered the complex reactions, leading to the loss of some volatile compounds, and in the meantime the formation of others such as furans and aldehydes. These productions contributed to the unique aroma profiles of different HBFs. Furthermore, a chemometric approach was used to analyze the changes of thermal stabilized treated HBFs and to identify six key volatile compounds, which provided important knowledge on possible chemical reactions caused by thermal stabilization. Overall, these results provide the theoretical basis for the wider application of thermal stabilization technologies in highland barley processing.

## KEYWORDS

highland barley, thermal stabilization, enzymatic activities, volatile compounds, PLS-DA

## 1. Introduction

Highland barley, the most distinctive crop produced in Qinghai Tibet Plateau, which has gained much attention in recent years due to its unique nutritional values (1). Highland barley is abundant in  $\beta$ -glucan, arabinoxylan, dietary fiber, vitamins, polyphenols, and GABA, which endow highland barley with the functions of preventing cancer and controlling cholesterol and blood glucose levels (2).

Highland barley has a thick and organizational outer layer structure, including seed coat, pericarp and aleurone layer. The main bioactive components in highland barley, such as  $\beta$ -glucan and phenolic compounds, are mainly distributed in the outer layer structure (3). Due to the short of advanced milling technology and the demand on nutrition, most of the aleurone layer and germ are retained in the highland barley flour. The lipase existing in aleurone layer and germ may induce deplete of lipids through enzymatic oxidation and hydrolysis, resulting in the

deterioration of the flour and the short shelf life (4). The oxidative rancidity of lipids causes the deterioration of product sensory quality and the loss of nutritional properties (5). Therefore, inactivation of enzyme activities may be an appropriate strategy for preventing or slowing lipid degradation and prolonging the shelf life.

Many researchers have utilized high temperature to destroy the structure of enzyme, resulting in the inactivation of enzyme activity, the good storage stability and better flavor. In general, the thermal stabilization technologies mainly include bake, far-infrared, microwave, fry and steam and other technologies such as superheated steam and ultrasound. Baking, frying and steaming are traditional methods of cereal processing, and they have the advantages of simple operation and low equipment cost (6). Zhao et al. (7) found that roasting treatment of highland barley decreased the lipase activity by 81.1% with the moisture content 20%. Microwave and infrared heating are commonly recognized as hopeful alternative methods to traditional methods because of the short time taken and an efficient energy provided (8). Rose et al. (9) determined the effectiveness of steam and microwave treatments of stabilization in whole wheat flour, the lipase activity decreased by 93 and 96% of microwave and steam treatments only for 1 min. Dang et al. (10) found that the moisture content and lipase activity of the whole grain highland barley flour after thermal treatment remained at a low level, and the fatty acid value, peroxide value, and malondialdehyde value increased. It has been reported that superheated steam processing improved storage properties of highland barley by improving the stability of lipid (11). Li et al. (12) examined the enzymolysis kinetics of rice protein pretreated with ultrasound. They found that the ultrasound assisted alkali caused the less active enzyme for lower enzyme loading, resulted in the initial rate declination of enzyme catalytic reaction kinetics. The contribution of ultrasound effects to improve the enzymolysis reaction rate constant was more significant at lower temperatures than at higher temperatures (13).

The volatile compounds of highland barley are complex and diverse, which has an important impact on the sensory quality of highland barley products and directly determines the acceptance of consumers (14). Thermal stabilization has a certain impact on highland barley flavor due to the enzymatic oxidation, maillard reaction and thermally induced lipid oxidation will change the flavor. In other words, aldehydes and ketones produced in the lipid degradation will interact with amino acids or reducing sugars which produced in maillard reaction (15). At present, the research on volatile compounds changes during processing is mostly concentrated on other cereals such as wheat, rice and oat, while little in highland barley. Lampi et al. (16) studied the stability of heat-treated oat grains, and extensive lipid oxidation occurred once the temperature reached 130°C. Wei et al. (17) investigated the aroma deteriorations of rice bran by infrared radiation heating. They found that the contents of esters, aldehydes, and phenols in the infrared radiation-treated group were significantly higher than those in the control group.

In summary of the literatures, the majority of existing literatures on the properties of highland barley by thermal stabilization have been performed with a single processing technology, whereas there are few with respect to the comparison of bake, far-infrared, microwave, fry and steam. The effects of thermal treatments on the

structure and physicochemical characteristics of HBF are currently being investigated from the standpoint of the enzyme-destroying effect, and all these studies have concentrated on the effect of thermal stabilization on the structure of starch and protein. Nonetheless, no study has further contrastive analysis of the lipids and flavor properties of HBF after these thermal stabilization technologies inactivate enzymes. Only by clarifying these properties and possible chemical reaction can the appropriate treatment method be selected in accordance with the demands of various products for raw materials.

Overall, highland barley thermal stabilization provokes the occurrence of complex biochemical reactions, leading to the changes of nutrients, enzymes activities and volatile flavor compounds. At present, the researches on the thermal stabilization of highland barley flour mainly focus on the structural properties, and few studies have clarified and compared the effects of different thermal stabilization techniques on enzyme activity and storage stability. At the meantime, this paper preliminarily speculated the possible chemical reactions in the thermal stabilization technology and marked the key compounds, which is of great significance to further study and better apply the thermal stabilization technology to highland barley products for improving storage stability and reducing the undesirable odor.

## 2. Materials and methods

### 2.1. Materials

Highland barley grains were provided by Tibet Academy of Agriculture and Animal Husbandry Sciences. The moisture content of highland barley was adjusted to 5% after sieving and removing impurities. After different thermal stabilization, five kinds of highland barley flour (HBF) with 4% pearling were obtained using a cyclone mill (FW-400 AD, XINBODE, China).

### 2.2. Thermal stabilization processing

About 1 kg of HBF was prepared for experiment, of which 200 g was used for the control group and each experiment group, respectively. The HBF was steamed, baked, fried, microwaved and infrared as follows.

#### 2.2.1. Steam processing

Distilled water was put into a household electric cooker (MZ-ZG28W4-001, Media, China) and the water was heated. When the water was boiled and the hot steam was filled in the cooker, and the HBF was put on the steam grid. The HBF was steamed for 30 min at 900 w and then taken out.

#### 2.2.2. Baked processing

The HBF was treated in hot air oven (101-1AB, Taisite, Tianjin, China) for 30 min at 155°C.

#### 2.2.3. Fried processing

A household electric oven (C22-WT2202, Media, Guangdong Province, China) was used and the oven was adjusted to 100°C at 900 W. After 30 min, the HBF was taken out.

### 2.2.4. Microwaved processing

The HBF was put near the center position in microwave oven (X3-233A, Media, Guangdong Province, China) for 3 min at 560 W.

### 2.2.5. Infrared processing

A far-infrared electric oven (KWS1530X-H7R, Galanz, Guangdong Province, China) was used and the HBF was treated for 3 min at 900 W, 210°C. The non-treated HBF was used as control.

## 2.3. Proximate composition

The HBF samples were estimated for their moisture (44–01), crude protein ( $N \times 6.25$ ) (46–11A), crude fat (30–10), ash (08–01), and mineral elements (40–70) were analyzed according to AACC methods. Dietary fiber, total starch, amylose content and  $\beta$ -glucan contents were determined using the megazyme mixed-linkage assay kit (Megazyme International Ltd., Ireland).  $\gamma$ -aminobutyric acid (GABA) was measured as described by Kitaoka (18).

## 2.4. Analysis of fatty acid value

Firstly, the HBF (10 g) was mixed with 50 ml petroleum ether, shook for 10 min, and filtered and collected the filtrate. The filtrate (25 ml) was mixed with 75 ml 50% ethanol solution and titrated with 0.01 M KOH. Added five drops of phenolphthalein, until a pink color appeared and persisted for 30 s. The sample was replaced with petroleum ether for a blank test. The phenolphthalein (1%, w/v) was used as an indicator and the fatty acid value (mg KOH/100 g) was calculated according to the Eq (1).

$$\text{Fatty acid value} = (V_1 - V_2) \times c \times 56.1 \times \frac{50}{25} \times \frac{100}{m \times (100 - w)} \quad (1)$$

where  $V_1$  = volume of sample titration (mL),  $V_2$  = volume of blank titration (mL),  $c$  = normality of titrant (mol/L),  $m$  = weight of sample (g), and  $w$  = moisture of sample (%).

## 2.5. Analysis of peroxide value and catalase activity

Peroxide value (PV) was determined according to AOCS method (19). The catalase (CAT) activity was determined according to GB/T 5522–2008 (20).

## 2.6. Determination of lipase activity

Lipase (LIP) activity of HBF was measured as follows: about 2 g HBF was mixed with 1 ml pure oil and phosphate buffer solution (5 ml, pH 7.4, 0.1 M) and the mixture was allowed to react at 30°C for 24 h. After that, 50 ml of a mixture of ethanol and ether was added, shook well and stood for 1–2 min. This was followed by filtration and pipetting 25.0 ml of filtrate. Phenolphthalein indicator was added and

titrated with 0.05 M potassium hydroxide solution until it was reddish and colorless for 30 s.

## 2.7. Determination of lipoxygenase activity

Lipoxygenase (LOX) activity was determined according to method described by Cato (21) with slight modification.

To prepare the linoleic acid substrate: 0.5 ml Tween-20 was dissolved in borate buffer (10 ml, pH 9.0, 0.05 M) and mixed well. 0.5 ml linoleic acid was added dropwise to emulsion, and then NaOH (1.3 ml, 1 M) solution was added until the solution was clarified. Finally, 90 ml of the borate buffer was added, and the volume was fixed to 200 ml with distilled water, and 1 M HCl was used to adjust the pH to 7.0.

To extract the enzyme, 0.5 g HBF was added with 2.5 ml phosphate buffer (0.05 M, pH 7.5) and incubated at 4°C for 30 min. After that, the mixture was centrifuged with a speed of 8,000 r/min at 4°C for 10 min.

Reaction system: Sodium acetate buffer (9.5 ml, 0.05 M, pH 5.6) and 0.3 ml linoleic acid substrate were mixed with 60  $\mu$ l enzyme extract, and then the absorbance was measured at 234 nm using a spectrophotometer (TU-1810, Puxi General Instrument Co., Ltd., Beijing, China). The enzyme extract in the reaction system was replaced by the inactivated enzyme extract as the substrate control. One LOX activity unit was defined as an increase in absorbance of 0.01 at 234 nm within 1 min.

## 2.8. Determination of volatile compounds

Volatile compounds were extracted with a headspace solid phase micro-extraction (HS-SPME) coated with a divinylbenzene/carboxen/polydimethylsiloxane (DVB/CAR/PDMS, 50/30  $\mu$ m) film and analyzed on a gas-chromatography/mass spectrometry (GC/MS) (QP2010 Ultra, Shimadzu, Japan). Two grams of HBF were weighed in a 20 ml headspace vial. The SPME sampling was performed by inserting the SPME fiber into the headspace with heating (45°C) and continuous stirring for 50 min. After extraction, it was injected into the GC–MS and desorbed the volatile compound at 250°C for 5 min. The volatile compounds were separated on a Restek fused silica capillary column (30 m  $\times$  0.25 mm  $\times$  0.25  $\mu$ m) and helium was used as the carrier gas with a constant flow rate of 1 ml/min in a splitless injection mode. The temperature program was set as follows: The oven temperature was held at 40°C for 3 min, then increased to 120°C at a rate of 4°C/min and finally increased to 240°C at a rate of 6°C/min. The MS detector was conducted by electron impact (EI) source at the following conditions: electron energy 70 eV; ionization temperature, 230°C; the transfer line temperature was 220°C; scan range 35–500 m/z. The reference mass spectra of National Institute of Standards and Technology (NIST) was used for the identification of the volatiles by comparing their programmed temperature retention indices (RI) in two different phases of gas chromatograph column, molecular weights, and mass fragmentation patterns. The relative contents of each volatile



compound were quantified by peak area normalization. The analysis was carried out in triplicate.

## 2.9. Data processing and multivariate analyses

Statistical analyses were performed using Minitab 8.0. The mean values were compared *via* one-way and Tukey's *post hoc* test was used to detect significant differences of different stabilized HBF samples ( $p \leq 0.05$ ). Results were presented as the means  $\pm$  standard deviations of triplicate samples. The figures were plotted using Origin 8.0.

To investigate the effect of thermal stabilized treatments on the integrated data of volatiles compounds (VOC), a regression-based supervised classification technique, which called partial least squares discriminant analysis (PLS-DA) was applied. Score-plots were generated using the PLS-DA model to visualize the contributions and changes of VOCs. Variable importance in projection (VIP) scores were calculated to estimate the importance of each variable in the PLS projection. Variables with VIP >1 were the most relevant variable for explaining Y-variables (SIMCA 14.1 software).

## 3. Results and discussion

### 3.1. Effect of thermal stabilization on proximate composition

There were great diversities in proximate composition (moisture, ash, amylose, GABA and mineral elements) of HBF affected by thermal stabilization (Table 1). When steamed, the moisture content of HBF was higher than that of the control group, while other treatment groups were lower than that. In all thermal stabilized treated samples, a decreasing tendency of the ash contents was observed, thereby improving the color and smoothness of HBFs. Table 1 showed that fat, protein, total dietary fiber and  $\beta$ -glucan contents of thermal stabilized treated groups did not show any significant variation. Microwave treatment significantly decreased the total starch content whereas increased the amylose content. The  $\gamma$ -aminobutyric acid content was reduced significantly after microwave and infrared treatment. Different stabilizing treatments had significant effects on calcium content of HBF, which may be due to the oxidation reaction of calcium. The statistical analysis showed significant increase in zinc content of microwaving, frying and baking, whereas it is not significant for infrared and steaming treatments, which may be related to the state of binding and solubility of minerals; (22). Iron content was significantly decreased in steaming treatment group, while the other treatments significantly increased the iron content. Copper content of steamed HBF was significantly lower than the control group but there was no difference after other treatments, which may be attributed to the oxidation reaction occurred in humid air. Baking treatment significantly reduced phosphorus content of HBF, while steamed, microwaved and infrared technologies significantly increased phosphorus content. Selenium content of fried HBF was significantly higher than the raw HBF and other treatments had no significant effects.

### 3.2. Effect of thermal stabilization on fatty acid value and peroxide value

Changes of lipid properties were usually used for monitoring the quality deterioration of flour because lipid was more prone to degradation rapidly than that of protein and starch (23). Fatty acids value was used as an indicator of the degree of lipid hydrolysis (24). Figure 1A portrayed the free fatty acid content changes of HBF with respect to different treatments. The fatty acid value of raw HBF was 23.11 mg/100 g and the HBFs after infrared, baked, microwaved, fried, and steamed were 23.73, 20.67, 27.00, 23.21, and 23.79 mg/100 g, respectively. This result indicated that hydrolytic rancidity of HBF not obviously occurred during thermal stabilization. Rose et al. (9) also reported that microwave treatment or steam treatment had no obvious effect on the fatty acid value of wheat flour.

The peroxide value (PV) provides a measure of the initial oxidative rancidity of lipid during storage (25). Peroxide values of infrared and baked HBF had no obvious difference with the raw HBF (Figure 1B). The peroxide value of raw HBF was 0.34 meq/kg. After microwaved, fried and steamed, the PV of HBF were 1.77, 1.81, and 0.94 meq/kg, respectively, indicating that lipid oxidation (both enzymatic and non-enzymatic) occurred during stabilization treatments of HBF. The reason might be microwaved, fried and steamed treatments induced deformation of outer layers structure and disruption of endosperm cell walls, and thus increased the fat-soluble components (1).

### 3.3. Inactivation of lipase and lipoxygenase

Lipases hydrolyzed the ester bonds of triacylglycerols, contributing to the aging flavor, so it was important to inactivate the lipase for longer storage. All thermal stabilized treatments effectively reduced the LIP activity (Figure 1C). The raw HBF had the highest LIP activity (1.59 mg/g). The infrared, baked, microwaved, fried, steamed HBF lipase activities were significantly reduced by 30.2, 13.2, 25.8, 40.9, and 25.8%, respectively. The different reduction percentage of LIP activity employed thermal stabilization was expected, since previous report have indicated that microwave, steam, infrared, and other thermal stabilization exert a good effect on lipase inactivation (6). Our results suggested that the lipase activity was more stable to bake treatment than the other treatments. Meanwhile, fried HBF was more efficient at decreasing lipase activity than others, which meant fried treatment mostly enhanced the HBF storage stability by reducing enzymatic oxidation reactions. Whereas LIP could not be completely inactivated which might be explained by the fact that LIP was relatively stable compared with other enzymes and the activity was too low to be reduced. This result was kept in with the reports of Li et al. (26), who found that the inactivation rates of lipase in microwaved or roasted HB grain and flour were 50 or 60%.

The LOX activities declined sharply for all the treatments, and the decrease rates were more apparent compared with lipase (Figure 1D). This result was consistent with Xu et al. (27), who found that lipase activity was more heat-stable than the lipoxygenase. There were no significant difference among different thermal stabilized treatments (31–46%). Baked and fried were found to be most effective in inactivating lipoxygenase ( $p > 0.5$ ). These results are in accord with recent studies indicating that the LOX decreased rate was 60.2% when the flours were subjected to treatments of thermal infrared rays (28).



TABLE 1 Proximate composition of the highland barley flour.

Sample	Moisture (%)	Ash (%)	Fat (%)	TS (%)	Protein (%)	Amylose content (%)	TDF (%)	$\beta$ -glucan (%)	GABA (%)	Calcium (mg/kg)	Zinc (mg/kg)	Iron (mg/kg)	Copper (mg/kg)	Phosphorus (mg/100g)	Selenium (mg/kg)	Total mineral (mg/kg)
Raw	9.06 ± 0.04b	2.34 ± 0.35a	1.92 ± 0.32a	69.09 ± 0.45a	10.74 ± 0.09a	18.17 ± 1.08bc	19.72 ± 1.20a	4.03 ± 1.24a	1.98 ± 0.10a	439 ± 1d	16.00 ± 0.14c	39.65 ± 0.35c	4.72 ± 0.04a	347 ± 3c	0.0056 ± 0.0004b	533.58 ± 1.53d
Infrared	8.31 ± 0.97b	0.66 ± 0.11b	2.26 ± 0.24a	70.73 ± 6.07a	10.35 ± 0.00a	23.01 ± 2.11b	20.35 ± 1.02a	5.67 ± 0.77a	1.22 ± 0.16c	419 ± 1e	16.30 ± 0.14c	41.90 ± 0.42b	4.74 ± 0.08a	370 ± 1b	0.0057 ± 0.0001b	518.89 ± 1.55e
Baked	5.49 ± 0.31c	0.72 ± 0.23b	2.25 ± 0.27a	63.06 ± 1.07ab	10.92 ± 0.27a	20.02 ± 2.11bc	20.39 ± 0.15a	4.94 ± 0.95a	1.77 ± 0.17ab	468 ± 1b	19.40 ± 0.28a	43.70 ± 0.14a	4.92 ± 0.06a	78.65 ± 1d	0.0064 ± 0.0001ab	543.391 ± 0.276c
Microwaved	5.60 ± 0.73c	0.80 ± 0.11b	2.20 ± 0.16a	53.68 ± 1.02b	10.59 ± 0.33a	35.72 ± 1.06a	18.89 ± 0.33a	4.83 ± 0.39a	1.48 ± 0.04bc	457 ± 0c	17.45 ± 0.21b	43.60 ± 0.57a	4.92 ± 0.01a	389 ± 2a	0.0065 ± 0.0002ab	561.826 ± 0.552b
Fried	3.61 ± 0.32c	0.30 ± 0.06b	2.21 ± 0.13a	64.09 ± 0.46ab	11.04 ± 0.80a	22.21 ± 1.05bc	20.09 ± 0.16a	4.02 ± 1.11a	1.98 ± 0.10a	543 ± 0a	17.90 ± 0.14b	44.40 ± 0.28a	4.85 ± 0.08a	347 ± 4c	0.0076 ± 0.0006a	644.853 ± 0.771a
Steamed	13.11 ± 0.02a	0.50 ± 0.00b	2.58 ± 0.06a	65.63 ± 1.91a	9.85 ± 0.016a	16.65 ± 1.08c	20.81 ± 0.35a	3.85 ± 0.14a	1.72 ± 0.05ab	376 ± 2f	15.85 ± 0.35c	36.15 ± 0.07d	4.17 ± 0.04b	373 ± 1b	0.0053 ± 0.0003b	468.93 ± 1.81f

TS, total starch; TDF, total dietary fiber; GABA,  $\gamma$ -aminobutyric acid. Data are the mean  $\pm$  standard deviation of triplicates. Different lowercase letters within a column indicate statistical differences ( $p \leq 0.05$ ).

Moreover, the result clearly outlined again that fried followed by other thermal stabilization reduced the occurrence of enzymatic oxidation reactions.

### 3.4. Effect of thermal stabilization on catalase activity

Hydrogen peroxide in living organisms was catalyzed by catalase to form oxygen and water, which protected organisms from damage caused by reactive oxygen species (29). Study has shown that the catalase activity was closely related to the vigor of seeds and could be used as a judge index of grain freshness (30). The changes in catalase activity of HBF were shown in Figure 1E. Catalase activities were found to be the highest in fried HBF and the increase rate was 14.8%. The other treatments increased the catalase activity but the results were not significant. The possible reason might be that the differences in moisture and temperature in different treatments. Gili et al. (31) reported that water activity improved the sensitivity of enzymes to heat, and water could be used as a good transfer medium of heat.

### 3.5. Determination of volatile compounds

Using the SPME-GC-MS method, there were 36 volatile compounds detected in HBFs (Table 2). In terms of categories, VOCs were divided into eight classes including alcohols, aldehydes, alkanes, esters, hydrocarbon, ketones, furans, and others. These compounds are generally considered to be derived from the photosynthesis and metabolism of proteins, free amino acids, carbohydrates, triglycerides or their derivatives, as well as vitamins and minerals (32).

The numbers of VOCs in raw and stabilized processed samples were different (Figure 2A), including 24 in raw HBF (seven alcohols, six aldehydes, three alkanes, two hydrocarbon, and six other compounds), 14 in infrared HBF (five aldehydes, three hydrocarbons, two esters, and four other compounds), 10 in baked HBF (three aldehydes, three hydrocarbons, two alkanes, and two other compounds), 13 in microwaved HBF (four hydrocarbons, three aldehydes, two alkanes, two esters, and two other compounds), 13 in fried HBF (four aldehydes, three alcohols, two hydrocarbons, two alkanes, and two other compounds), and 18 in steamed HBF (five aldehydes, four hydrocarbons, three alkanes, two alcohols, two esters, and two other compounds).

Aldehydes were the dominant compounds of raw (Figure 2B), infrared and steamed HBF which may be due to the low sensory threshold (33). The straight-chain aldehydes such as hexanal were derived from the linoleic acid oxidation, which are considered safe and could be used as flavor substances in food (34). It was worth mentioning that steamed treatment remarkable increase the strecker aldehydes such as 3-Methyl butanal and 2-Methyl butanal. Strecker degradation is one of side reactions of the Maillard reaction. The first step of Maillard reaction was a condensation involving an amino acid and a reducing sugar with a carbonyl group. The result of this condensation was a not thermostable Amadori compound, which could be demolished and produced the rearranged sugars due to the prolonged storage periods (35). The sugars then could be split into dicarbonyl and degraded the amino acids, leading to the deamination

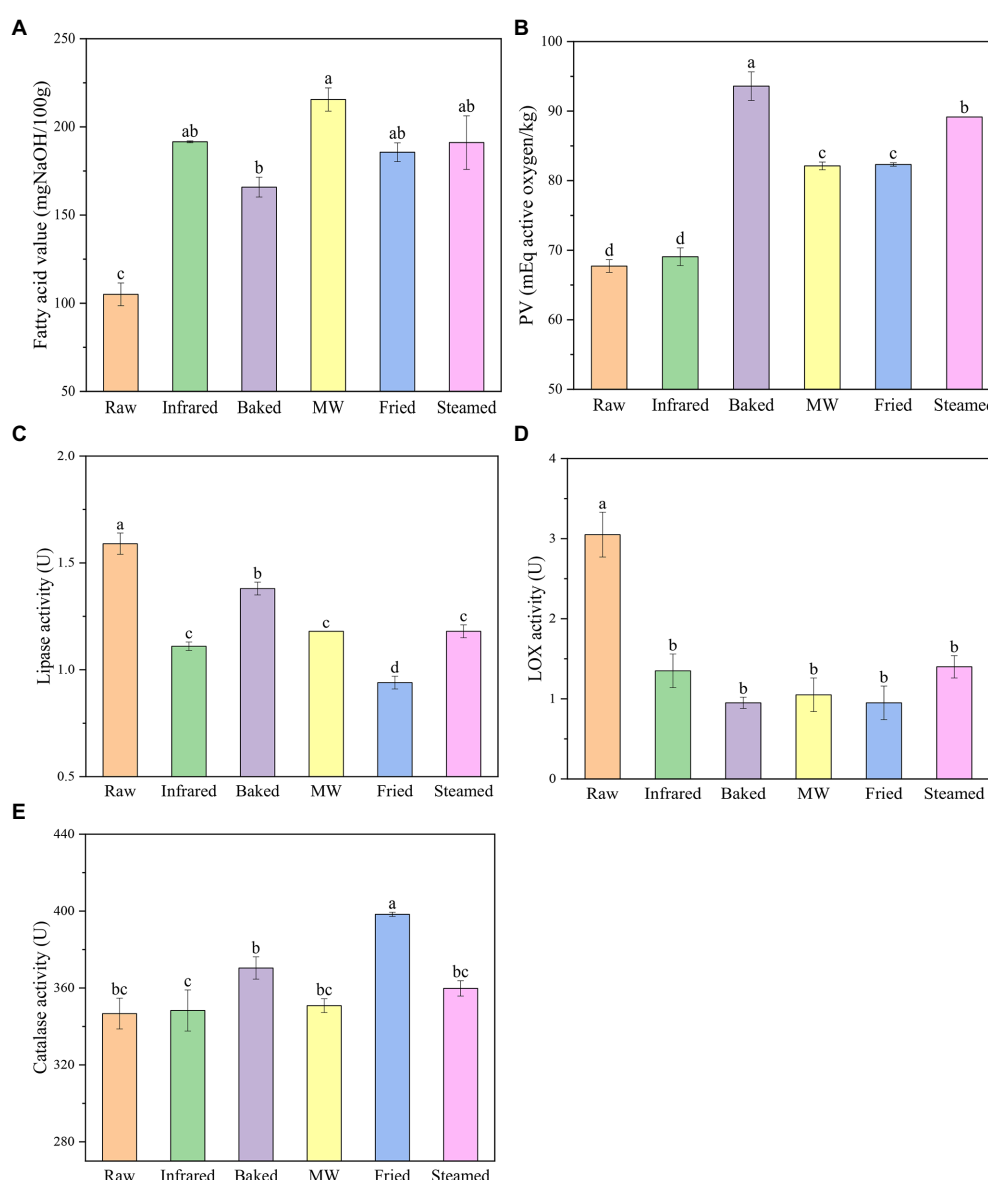


**FIGURE 1**  
Fatty acid value (A), peroxide value (B), lipase (C), lipoxygenase (D), and catalase (E) activities of highland barley flour. Different lowercase letters indicate significantly different at level  $p \leq 0.05$ .

and decarboxylation, which were called Strecker degradation. The Strecker aldehydes were closely related to flavor formation (36). The formation of these compounds was triggered during steaming and the process seemed to have a combined effect of Maillard reaction and non-enzymatic oxidation. These aldehydes gave the unique aroma of fat, grass, caramel of HBF. The highest contents in baked, microwaved and fried HBF were esters (Figure 2B), which might come from the raw material or the esterification reaction of alcohols and acids and contribute to the sweet and fruity aroma of the HBF samples, which indicated that thermal stabilization changed the mainly aromatic substances. As occurs in aldehydes, steamed HBF presented the highest contents than others. The volatile compound present at the highest level in all treatments was hexanal followed by acetaldehyde. This finding was consistent with some studies that reported the hexanal was the major compound in cereal flour (37). As occurs in

esters, fried showed the highest value, and ethyl acetate was the dominant VOC.

### 3.6. Partial least squares-discriminant analysis

To deeply highlight the differences of aroma compounds in raw and stabilized HBF, the PLS-DA was applied to investigate the contributions and changes of aroma compounds of stabilized treatment. The differences among six HBF samples had been distinctly identified in the PLS-DA score plots as shown in Figure 3A, which exhibited a total variance of 68.4% (PLS1, 46.5%; PLS2, 21.9%). The permutations plot helped to assess the risk that the current PLS-DA model was spurious (Figure 3B). The idea of this validation was to

TABLE 2 Comparisons of the detected VOCs in highland barley flour by SPME-GC-MS.

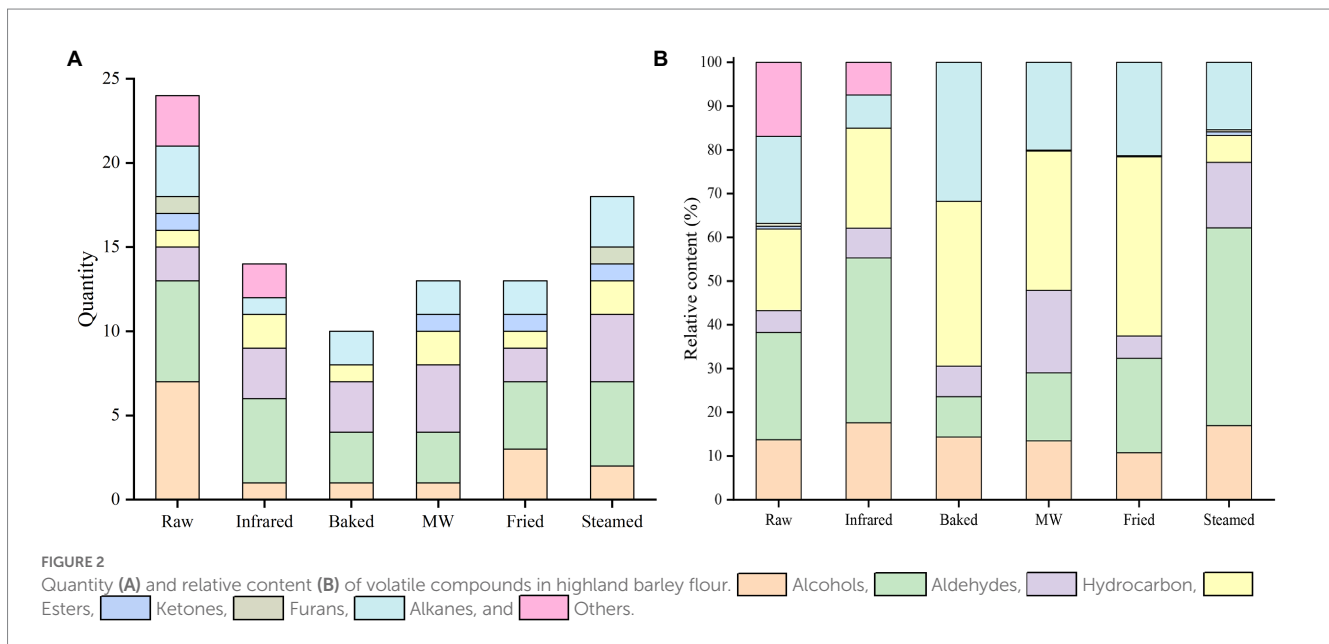
Compounds	Formula	CAS	Molecular weight	Retention index	Highland barley flour relative content (%)					
					Raw	Infrared	Baked	Microwaved	Fried	Steamed
Aldehydes										
Acetaldehyde	C2H4O	75-07-0	44	408	2.183 ± 0.661c	13.747 ± 1.592a	7.840 ± 0.820b	ND	ND	ND
2-Methylpropanal	C4H8O	78-84-2	72	543	0.5350 ± 0.4010bc	0.2548 ± 0.0534c	0.8262 ± 0.0292b	0.3988 ± 0.0279bc	0.6359 ± 0.1374bc	1.7607 ± 0.1702a
Butanal	C4H8O	123-72-8	72	607	ND	0.2518 ± 0.0581a	ND	ND	ND	ND
3-Methylbutanal	C5H10O	590-86-3	86	643	0.3820 ± 0.2130b	ND	ND	ND	0.7611 ± 0.1165b	4.370 ± 0.491a
2-Methylbutanal	C5H10O	96-17-3	86	643	0.2065 ± 0.1542c	0.4235 ± 0.0849bc	0.6127 ± 0.0414b	0.5126 ± 0.0327b	0.5158 ± 0.0166b	2.695 ± 0.145a
Pentanal	C5H10O	110-62-3	86	707	ND	ND	ND	ND	ND	1.8204 ± 0.09a
Hexanal	C6H12O	66-25-1	100	806	20.27 ± 0.99bc	26.40 ± 1.35b	ND	16.59 ± 1.70c	18.37 ± 6.93bc	36.55 ± 1.10a
Nonanal	C9H18O	124-19-6	142	1,104	2.811 ± 0.469a	ND	ND	ND	ND	ND
Alcohols										
2,5-Cyclooctadien-1-ol	C8H12O	10,054-74-7	124	1,112	0.7354 ± 0.0702a	ND	ND	ND	ND	ND
Ethanol	C2H6O	64-17-5	46	463	5.965 ± 0.778d	18.574 ± 0.995a	15.277 ± 0.797b	13.678 ± 0.196b	8.164 ± 0.625c	13.421 ± 0.388b
1-Penten-3-ol	C5H10O	616-25-1	86	671	0.6386 ± 0.0877a	ND	ND	ND	ND	ND
1-Pentanol	C5H12O	71-41-0	88	761	2.729 ± 0.280b	ND	ND	ND	ND	4.337 ± 0.445a
1-Heptacosanol	C27H56O	2004-39-9	396	2,948	0.4895 ± 0.1353a	ND	ND	ND	ND	ND
P-Mentha-1,8-Dien-7-ol	C10H16O	536-59-4	152	1,261	2.771 ± 0.719a	ND	ND	ND	1.504 ± 0.130b	ND
1-Hexanol	C6H14O	111-27-3	102	860	3.067 ± 0.733a	ND	ND	ND	1.7914 ± 0.1478b	ND
Hydrocarbon										
Dimethyl-Diazene	C2H6N2	503-28-6			ND	ND	ND	14.951 ± 0.639a	ND	ND
Benzene	C6H6	71-43-2	78	680	3.284 ± 0.196b	2.854 ± 0.170bc	2.567 ± 0.100c	1.484 ± 0.382d	2.989 ± 0.185bc	6.507 ± 0.200a
Toluene	C7H8	108-88-3	92	794	1.797 ± 0.041d	2.705 ± 0.131bc	3.142 ± 0.304b	1.735 ± 0.052d	2.454 ± 0.129c	5.819 ± 0.238a
(E)-2-Octen-1-ol	C8H16O	18,409-17-1	128	1,067	ND	ND	ND	ND	ND	0.7242 ± 0.1125a
D-Limonene	C10H16	5,989-27-5	136	1,018	ND	1.563 ± 0.067b	1.651 ± 0.054b	1.316 ± 0.377b	ND	3.772 ± 1.222a
Others										
Dimethyl peroxide	C2H6O2	690-02-8	62	372	ND	2.197 ± 0.222a	ND	ND	ND	ND
Dimethyl sulfide	C2H6S	75-18-3	62	471	0.4154 ± 0.1339a	ND	ND	ND	ND	ND
Ammonium acetate	C2H7NO2	631-61-8	77	630	ND	6.269 ± 0.709a	ND	ND	ND	ND
Acetic acid	C2H4O2	64-19-7	60	576	7.222 ± 0.769a	ND	ND	ND	ND	ND
2,4-Di-tert-butylphenol	C14H22O	96-76-4	206	1,555	10.29 ± 0.01a	ND	ND	ND	ND	ND

(Continued)

TABLE 2 (Continued)

Compounds	Formula	CAS	Molecular weight	Retention index	Highland barley flour relative content (%)					
					Raw	Infrared	Baked	Microwaved	Fried	Steamed
Alkanes										
2,2,4,6,6-Pentamethyl heptane	C12H26	13,475-82-6	170	981	17.18 ± 1.58 cd	7.696 ± 0.104e	30.18 ± 0.20a	19.92 ± 0.68c	23.76 ± 2.59b	13.70 ± 1.03d
2,2,4,4-Tetramethyloctane	C12H26	62,183-79-3	170	1,045	1.475 ± 0.0829b	ND	2.125 ± 0.386a	0.7854 ± 0.0572c	ND	ND
Dodecane	C12H26	112-40-3	170	1,214	0.6004 ± 0.065b	ND	ND	ND	0.4958 ± 0.025b	1.413 ± 0.265a
Tetradecane	C14H30	629-59-4	198	1,413	ND	ND	ND	ND	ND	0.3832 ± 0.0323a
Esters										
Ethyl acetate	C4H8O2	141-78-6	88	586	16.83 ± 1.70e	21.28 ± 0.92d	36.902 ± 0.93b	32.69 ± 1.338c	42.8 ± 1.75a	ND
2-Methyl ethoxyacetate	C5H10O3	0-00-0	118	761	ND	ND	ND	ND	ND	3.683 ± 1.143a
Formic acid hexyl ester	C7H14O2	629-33-4	130	981	ND	1.703 ± 0.351b	ND	0.6552 ± 0.0312c	ND	3.697 ± 0.488a
Furans										
Tetrahydrofuran	C4H8O	109-99-9	72	589	ND	ND	ND	ND	ND	0.5381 ± 0.0786a
2-Pentylfuran	C9H14O	3,777-69-3	138	1,040	0.7486 ± 0.0675a	ND	ND	ND	ND	ND
Ketones										
2-Butanone	C4H8O	78-93-3	72	555	0.6314 ± 0.0266a	ND	ND	0.2521 ± 0.0316b	0.3146 ± 0.0723b	ND
Acetoin	C4H8O2	513-86-0	88	717	ND	ND	ND	ND	ND	1.047 ± 0.300a

ND, not detected or value below the detection threshold. Different lowercase letters in the same row are significantly different ( $P \leq 0.05$ ).



compare the goodness of fit ( $R^2$  and  $Q^2$ ) of the original model with the goodness of fit of several models based on data where the order of the Y-observations has been randomly permuted, while the X-matrix has been kept intact. Result demonstrated that the PLS-DA model was valid and not overfitted, therefore validated the VIP values obtained from this model (Figure 3B).

A heatmap was generated (Figure 3C) based on the contents of VOCs. Taking the estimated concentrations of the identified 36 VOCs as variables, each variable was normalized by sum. The row comparison showed the distribution frequency of each substance in the six samples. Color coding was graded on the basis of the scale with the relative intensity increasing from low (purple) to high (red) for one volatile compound. Comparing the different treatments, raw HBF displayed higher content of 2, 5-cyclooctadien-1-ol, dimethyl sulfide, 2-butanone, acetic acid, 1-penten-3-ol, 1-hexanol, p-mentha-1, 8-dien-7-ol, nonanal, 1-heptacosanol and 2, 4-di-tert-butylphenol. The profile of VOCs was changed after treatments. For example, dimethyl peroxide, butanal and ammonium acetate were only detected in infrared group and dimethyl-diazene only in microwaved HBF. Most VOCs were produced after steaming such as 2-methylethoxy acetate, tetrahydrofuran, pentanal, (E)-2-octen-1-ol, tetradecane, et al.

Variable importance in projection scores were calculated to select compounds driving the classification and that were significantly affected by the treatments. All the variables presenting a  $VIP > 1$  were considered relevant for the discrimination of raw samples HBF from thermal stabilized processed HBFs. According to the literature reported and the VIP values, 6 common VOCs were selected as key VOCs for further analysis (Figure 3C). The treatment that the compound was selected as a discriminant marker was marked with red color circle (Figure 3D). Among these VOCs, there were two hydrocarbons (Dimethyl-diazene and 2, 2, 4, 6, 6-Pentamethyl heptane), an esters (ethyl acetate), an aldehydes (hexanal), an alcohols (ethanol) and an acids (acetic acid). The hydrocarbons could be generated by decarboxylation and cleavage of carbon chains of fatty acids, thus they might be produced by the oxidation and

decomposition of HBF during high temperature treatment (38). Dimethyl-diazene showed the highest content in microwaved and baked group. These VOCs were considered could provide fatty, fruity and green aroma characters depending on their concentration. Hexanal was the basic product of linoleic acid oxidation. The oxidation of linoleic acid produced the 13-hydroperoxide, which could cleaved to hexanal and gave HBF the aroma of fatty, grass, and caramel (39). Acetic acid was a volatile component found in almost all crops, and its content decreased significantly after all thermal stabilization. Alcohols had a higher threshold, which contributed to the aroma of light, sweet, fruity, floral, and other mellow notes and infrared significantly increased the ethanol content. Compared with other HBFs, fried and baked HBFs showed the higher contents of ethyl acetate, which gave them the characteristic flavor of sweet and fruity.

## 4. Conclusion

This study gave a comprehensive insight into the effect of thermal stabilization technologies on the enzymes, lipids and volatile compounds of highland barley. The results demonstrated that thermal stabilization had no obvious effects on the contents of fat, protein, total dietary fiber and  $\beta$ -glucan. The activities of lipase and lipoxygenase in HBF were significantly decreased by the thermal stabilization and frying seemed to be the most effective method to inactivate the enzyme activities. While the catalase activity was improved in all groups which might be caused by the sensitivity differences of enzymes. Baking significantly inhibited the increase of fatty acid value in HBF. Five types of thermal stabilized technologies had obviously different effects on the aroma profiles. Aldehydes acted as the dominant compounds of raw, infrared and steamed HBF while the highest relative contents in baked, microwaved and fried HBF were esters. Non-enzymatic oxidation could be promoted and played a key role when the thermal stabilized treatments were applied. After thermal stabilizing, six



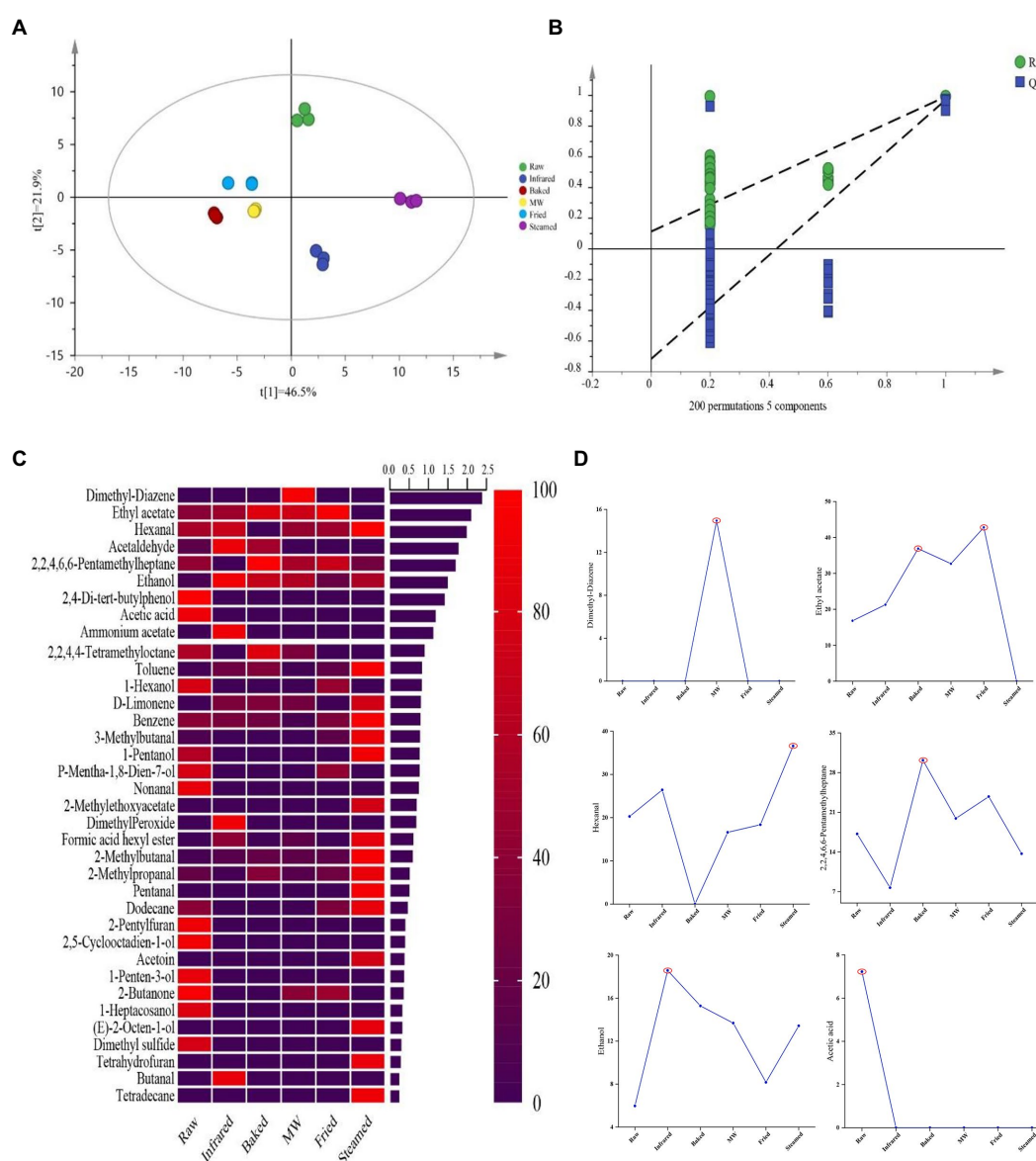


FIGURE 3

Partial least squares discriminant analysis (PLS-DA) score plots (A), permutations plots (B), heatmaps (C), and discriminant markers (D) analysis of the volatile aroma compounds identified in highland barley flour. The treatment that the compound was selected as a discriminant marker was marked with red color circle.

volatile compounds (Dimethyl-diazene, 2, 2, 4, 6, 6-pentamethyl heptane, ethyl acetate, hexanal, ethanol, and acetic acid) were identified through PLS-DA. These results of this study could be further used to investigate the effects of thermal stabilization on highland barley in order to obtain better products with longer shelf life. Even though this study provides a broader perspective on complicated chemical interactions, further research is required in order to fully comprehend how thermal stabilization affects the qualities of highland barley products. First, the standard sample needs to be used to confirm and measure the volatile compounds. The next are that verification experiments should be carried out. Finally is that the thorough reaction kinetic is needed to be deeply studied to gain more understanding and to regulate a specific reaction. In the future, stabilized technologies should be deeply

studied because it is of great significance to the development stable HB product.

## Data availability statement

The original contributions presented in the study are included in the article/supplementary material, further inquiries can be directed to the corresponding author.

## Author contributions

QZ carried out the experiments, wrote the main manuscript, and corrected the manuscript. ZW carried out the experiments and corrected the manuscript. FX corrected the manuscript. GZ

conceived the idea and supervised the work. All authors reviewed the manuscript.

## Conflict of interest

The authors declare that the research was conducted in the absence of any commercial or financial relationships that could be construed as a potential conflict of interest.

## References

- Bai, YP, Zhou, HM, Zhu, KR, and Li, Q. Effect of thermal treatment on the physicochemical, ultrastructural and nutritional characteristics of whole grain highland barley. *Food Chem.* (2021) 346:128657. doi: 10.1016/j.foodchem.2020.128657
- Obadi, M, Sun, J, and Xu, B. Highland barley: chemical composition, bioactive compounds, health effects, and applications. *Food Res Int.* (2021) 140:110065. doi: 10.1016/j.foodres.2020.110065
- Li, Q, Yang, SH, Li, YQ, Huang, YH, and Zhang, JP. Antioxidant activity of free and hydrolyzed phenolic compounds in soluble and insoluble dietary fibres derived from hullless barley. *LWT-Food Sci Technol.* (2019) 111:534–40. doi: 10.1016/j.lwt.2019.05.086
- Liu, L, Wen, W, Zhang, RF, Wei, ZC, Deng, YY, Xiao, J, et al. Complex enzyme hydrolysis releases antioxidative phenolics from rice bran. *Food Chem.* (2017) 214:1–8. doi: 10.1016/j.foodchem.2016.07.038
- McGorin, RJ. Key aroma compounds in oats and oat cereals. *J Agric Food Chem.* (2019) 67:13778–89. doi: 10.1021/acs.jafc.9b00994
- Wang, LJ, Wang, LB, Qiu, J, and Li, ZG. Effects of superheated steam processing on common buckwheat grains: lipase inactivation and its association with lipidomics profile during storage. *J Cereal Sci.* (2020) 95:103057. doi: 10.1016/j.jcs.2020.103057
- Zhao, B, Shang, JY, Liu, LY, Tong, LT, Zhou, XR, Wang, SS, et al. Effect of roasting process on enzymes inactivation and starch properties of highland barley. *Int J Biol Macromol.* (2020) 165:675–82. doi: 10.1016/j.ijbiomac.2020.09.180
- Berk, Z. *Food Process Engineering and Technology*. 3rd ed Academic Press (2018).
- Rose, DJ, Ogden, LV, Dunn, ML, and Pike, OA. Enhanced lipid stability in whole wheat flour by lipase inactivation and antioxidant retention. *Cereal Chem.* (2008) 85:218–23. doi: 10.1094/cchem-85-2-0218
- Dang, B, Zhang, WG, Zhang, J, Yang, XJ, and Xu, HD. Effect of thermal treatment on the internal structure, physicochemical properties and storage stability of whole grain highland barley flour. *Foods.* (2022) 11:2021. doi: 10.3390/foods11142021
- Wang, HR, Cui, SW, Wang, AL, Li, ZG, and Qiu, J. Influence of superheated steam treatment with tempering on lipid oxidation and hydrolysis of highland barley during storage. *Food Control.* (2021) 127:108133. doi: 10.1016/j.foodcont.2021.108133
- Li, S, Yang, X, Zhang, Y, Ma, H, Qu, W, Ye, X, et al. Enzymolysis kinetics and structural characteristics of rice protein with energy-gathered ultrasound and ultrasound assisted alkali pretreatments. *Ultrason Sonochem.* (2016) 31:85–92. doi: 10.1016/j.ulsonch.2015.12.005
- Li, Q, Yang, H, Coldea, TE, Andersen, ML, Li, W, and Zhao, H. Enzymolysis kinetics, thermodynamics and structural property of brewer's spent grain protein pretreated with ultrasound. *Food Bioprod Process.* (2022) 132:130–40. doi: 10.1016/j.fbp.2022.01.001
- Zhang, KZ, Yang, JG, Qiao, ZW, Cao, XZ, Luo, QC, Zhao, JS, et al. Assessment of beta-glucans, phenols, flavor and volatile profiles of hullless barley wine originating from highland areas of China. *Food Chem.* (2019) 293:32–40. doi: 10.1016/j.foodchem.2019.04.053
- Wei, CK, Ni, ZJ, Thakur, K, Liao, AM, Huang, JH, and Wei, ZJ. Aromatic effects of immobilized enzymatic oxidation of chicken fat on flaxseed (*Linum usitatissimum* L.) derived Maillard reaction products. *Food Chem.* (2020) 306:125560. doi: 10.1016/j.foodchem.2019.125560
- Lampi, AM, Damerau, A, Li, J, Moisio, T, Partanen, R, Forsell, P, et al. Changes in lipids and volatile compounds of oat flours and extrudates during processing and storage. *J Cereal Sci.* (2015) 62:102–9. doi: 10.1016/j.jcs.2014.12.011
- Yan, W, Liu, Q, Wang, Y, Tao, TT, Liu, B, Liu, J, et al. Inhibition of lipid and aroma deterioration in Rice bran by infrared heating. *Food Bioprocess Technol.* (2020) 13:1677–87. doi: 10.1007/s11947-020-02503-z
- Kitaoka, S, and Nakano, Y. Colorimetric determination of omega-amino acids. *J Biochem.* (1969) 66:87–94. doi: 10.1093/oxfordjournals.jbchem.a129124
- AOCS. *Official Methods and Recommended Practices*. Champaign, IL: American Oil Chemists Society (2003).
- According to Chinese National Standard GB/T 5522–2008. A: *Inspection of grains and oils—Determination of hydrogen peroxidase activity of grain and oilseeds*.
- Cato, L, Halmos, AL, and Small, DM. Measurement of lipoxigenase in Australian white wheat flour: the effect of lipoxigenase on the quality properties of white salted noodles. *J Sci Food Agri.* (2006) 86:1670–8. doi: 10.1002/jsfa.2539
- Wang, M, Kong, FM, Liu, R, Fan, QQ, and Zhang, XC. Zinc in wheat grain, processing, and food. *Front Nutr.* (2020) 7:7. doi: 10.3389/fnut.2020.00124
- Poudel, R, and Rose, DJ. Changes in enzymatic activities and functionality of whole wheat flour due to steaming of wheat kernels. *Food Chem.* (2018) 263:315–20. doi: 10.1016/j.foodchem.2018.05.022
- Hu, YM, Wang, LJ, and Li, ZG. Superheated steam treatment on wheat bran: enzymes inactivation and nutritional attributes retention. *LWT-Food Sci Technol.* (2018) 91:446–52. doi: 10.1016/j.lwt.2018.01.086
- Wu, JY, McClements, DJ, Chen, J, Liu, W, Luo, SJ, and Liu, CM. Improvement in storage stability of lightly milled rice using superheated steam processing. *J Cereal Sci.* (2016) 71:130–7. doi: 10.1016/j.jcs.2016.08.006
- Li, MJ, Wang, HR, Tong, LT, Fan, B, Yang, XJ, Sun, RQ, et al. A comparison study of three heating assisted enzyme inactivation pretreatments on the physicochemical properties and edible quality of highland barley grain and flour. *J Cereal Sci.* (2022) 104:103404. doi: 10.1016/j.jcs.2021.103404
- Xu, B, Wang, LK, Miao, WJ, Wu, QF, Liu, YX, Sun, YL, et al. Thermal versus microwave inactivation kinetics of lipase and lipoxigenase from wheat germ. *J Food Process Eng.* (2016) 39:247–55. doi: 10.1111/jfpe.12216
- Vinutha, T, Kumar, D, Bansal, N, Krishnan, V, Goswami, S, Kumar, RR, et al. Thermal treatments reduce rancidity and modulate structural and digestive properties of starch in pearl millet flour. *Int J Biol Macromol.* (2022) 195:207–16. doi: 10.1016/j.ijbiomac.2021.12.011
- George, P. Reaction between catalase and hydrogen peroxide. *Nature.* (1947) 160:41–3. doi: 10.1038/160041a0
- Sharma, I, and Ahmad, P. *Catalase-Chapter 4: A Versatile Antioxidant in Plants*. (2014).
- Gili, RD, Penc, MC, Irigoyen, MRT, Giner, SA, and Ribotta, PD. Effect of wheat germ heat treatment by fluidised bed on the kinetics of lipase inactivation. *Food Bioprocess Technol.* (2018) 11:1002–11. doi: 10.1007/s11947-018-2069-6
- Zhao, QY, Xue, Y, and Shen, Q. Changes in the major aroma-active compounds and taste components of jasmine rice during storage. *Food Res Int.* (2020) 133:109160. doi: 10.1016/j.foodres.2020.109160
- Zhang, MN, Li, LQ, Song, GS, Wang, HH, Wang, HX, and Shen, Q. Analysis of volatile compound change in tuna oil during storage using a laser irradiation based HS-SPME-GC/MS. *LWT-food. Sci Technol.* (2020) 120:108922. doi: 10.1016/j.lwt.2019.108922
- Lehtonen, M, Kekalainen, S, Nikkila, I, Kilpelainen, P, Tenkanen, M, and Mikkonen, KS. Active food packaging through controlled in situ production and release of hexanal. *Food Chemistry-X.* (2020) 5:100074. doi: 10.1016/j.fochx.2019.100074
- Salvatore, P, and Luo, W. “Maillard reaction in processed foods—reaction mechanisms,” in *Springer Briefs in Molecular Science*. ed. S. Parisi Cham: Springer International Publishing (2018). 39–51.
- Van Boekel, M. Formation of flavour compounds in the Maillard reaction. *Biotechnol Adv.* (2006) 24:230–3. doi: 10.1016/j.biotechadv.2005.11.004
- Gao, C, Li, Y, Pan, QF, Fan, MC, Wang, L, and Qian, HF. Analysis of the key aroma volatile compounds in rice bran during storage and processing via HS-SPME GC/MS. *J Cereal Sci.* (2021) 99:103178. doi: 10.1016/j.jcs.2021.103178
- Molteberg, EL, Magnus, EM, Borge, JM, and Nilsson, A. Sensory and chemical studies of lipid oxidation in raw and heat-treated oat flours. *Cereal Chem.* (1996) 73:579–87.
- Lehto, S, Laakso, S, and Lehtinen, P. Enzymatic oxidation of hexanal by oat. *J Cereal Sci.* (2003) 38:199–203. doi: 10.1016/s0733-5210(03)00028-6

## Publisher's note

All claims expressed in this article are solely those of the authors and do not necessarily represent those of their affiliated organizations, or those of the publisher, the editors and the reviewers. Any product that may be evaluated in this article, or claim that may be made by its manufacturer, is not guaranteed or endorsed by the publisher.

# Frontiers in Nutrition

Explores what and how we eat in the context of health, sustainability and 21st century food science

A multidisciplinary journal that integrates research on dietary behavior, agronomy and 21st century food science with a focus on human health.

## Discover the latest Research Topics

[See more →](#)

### Frontiers

Avenue du Tribunal-Fédéral 34  
1005 Lausanne, Switzerland  
[frontiersin.org](https://frontiersin.org)

### Contact us

+41 (0)21 510 17 00  
[frontiersin.org/about/contact](https://frontiersin.org/about/contact)

